Richard Andrew Staff

(Linacre College, University of Oxford)

Research on Radiocarbon Calibration Records, Focussing on New Measurements from Lake Suigetsu, Japan

(Volume 1)

Thesis submitted for DPhil in Archaeological Science, Trinity Term 2011

Research on Radiocarbon Calibration Records, Focussing on New Measurements from Lake Suigetsu, Japan

Richard Andrew Staff
(Linacre College, University of Oxford)

Thesis submitted for DPhil in Archaeological Science, Trinity Term 2011

Abstract:

Radiocarbon calibration is a fundamental stage of the radiocarbon dating process if meaningful calendar ages are to be derived from samples' radiocarbon determinations. However, the present limit of direct, non-reservoir-corrected, atmospheric radiocarbon calibration is 12,550 calibrated years before present (Reimer *et al*. 2009), leaving approximately three quarters of the radiocarbon timescale to be necessarily calibrated via less secure marine records.

The sediment profile of Lake Suigetsu, Honshu Island, central Japan, offers an ideal opportunity from which to derive an extended, 'wholly terrestrial' and continuous record of atmospheric radiocarbon back to the limits of radiocarbon detection (*circa* 60,000 years before present). The presence of well-defined, annually-deposited laminae (varves) throughout this extended time period provides an independent, high resolution chronometer against which radiocarbon measurements, performed upon plant macrofossil samples retrieved from the sediment column, can be directly related. This site was first exploited for radiocarbon calibration purposes by Kitagawa and van der Plicht (1998a, 1998b), however, issues pertaining to the reliability of the calendar age scale of this work precluded the widespread uptake of this dataset.

The work presented in this DPhil thesis represents a significant contribution to the broader, 'Suigetsu Varves 2006' project – an international collaboration centring on the re-coring of Lake Suigetsu, which was undertaken in summer 2006 to improve upon the shortcomings of the previous project and, thereby, to fully exploit the site's potential for both radiocarbon calibration and multi-proxy palaeoenvironmental study (Nakagawa *et al*. 2011).

This DPhil thesis describes the generation of the revised ('SG06') terrestrial radiocarbon calibration dataset from Lake Suigetsu, comprising 647 accelerator mass spectrometry (AMS) radiocarbon determinations, and extending across the complete range of the radiocarbon dating method. Furthermore, visual matching of archive SG93 core sections to the continuous SG06 sediment profile was undertaken, allowing the integration of the ≈ 300 radiocarbon determinations from the original Lake Suigetsu project into a higher resolution (≈ 900 radiocarbon measurements), combined Lake Suigetsu radiocarbon calibration dataset, providing a unique reconstruction of atmospheric radiocarbon across the entire radiocarbon dating timescale.

Kitagawa H and van der Plicht J (1998a) *Science* **279**, 1187-1190.
Kitagawa H and van der Plicht J (1998b) *Radiocarbon* **40** (1), 505-515.
Nakagawa T *et al*. (2011) *Quaternary Science Reviews*, in press.
Reimer PJ *et al*. (2009) *Radiocarbon* **51** (4), 1111-1150.

Acknowledgements:

Firstly, I would like to thank Professor Hiroyuki Kitagawa (Institute for Hydrospheric-Atmospheric Sciences, Nagoya University, Japan) and Professor Johannes van der Plicht (Centre for Isotope Research, Groningen University, the Netherlands), both for use of their original data from the Suigetsu '93 study, and for the inspiration for the re-coring of Lake Suigetsu undertaken by 'Suigetsu Varves 2006' project members. Additionally, I would like to thank Prof. Kitagawa for being such a wonderful host of a two week visit to his lab in Nagoya, undertaken during the course of this DPhil project.

I especially thank my two supervisors, Professor Christopher Bronk Ramsey (Research Laboratory for Archaeology and the History of Art, RLAHA, University of Oxford) and Professor Takeshi Nakagawa (Department of Geography, University of Newcastle-upon-Tyne), for simply being two fantastic, inspiring supervisors, constant sources of enthusiasm towards the project, and always there to assist whenever required.

My thanks to my on-going 'Suigetsu Varves 2006' project colleagues, namely: Dr. Achim Brauer, Dr. Fiona Brock, Dr. Charlotte Bryant, Dr. Dieter Demske, Dr. Annette Kossler, Dr. Henry Lamb, Dr. Michael Marshall, Rebecca Payne, Dr. Emma Pearson, Dr. Megumi Saito-Kato, Gordon Schlolaut, Dr. Pavel Tarasov, Dr. Jonathan Tyler and Prof. Yusuke Yokoyama.

I thank the C14 group at RLAHA for all their various assistance throughout the progress of my DPhil, namely: Diane Baker, Angela Bowles, Dr. David Chivall, Jane Davies, Dr. Michael Dee, Dr. Peter Ditchfield, Dr. Katerina Douka, Barbara Emery, Stephen Hick, Dr. Tom Higham, Sharen Lee, Anat Marom-Rotem, Hayley Sula, Christine Tompkins and Dr. Rachel Wood.

Thanks to the staff at the NERC Radiocarbon Facility-Environment (NRCF-E), East Kilbride for processing of radiocarbon samples, and specifically Margaret Currie, Frank Elliott, Callum Murray and Liam Chalmers.

Thanks also to the Physical Geography cluster at the University of Newcastle-upon-Tyne, especially: Priscilla Crumrine and Dr. Chris Stemerdink.

I thank RLAHA and the Natural Environment Research Council (NERC) for individual- and project funding (grant: NE/F003048/1), respectively. I additionally thank the 'Pan-Pacific Environmental Changes and Civilization' (PPECC) project, under the leadership of Professor Yoshinori Yasuda (International Research Center for Japanese Studies, Kyoto, Japan) and Dr. Hitoshi Yonenobu (Naruto University of Education, Japan) for funding my flights to Japan, and accommodation at the University of Nagoya, to work with the original Suigetsu '93 sediment core.

I thank my two examiners, Professor Paula Reimer (Queens University, Belfast) and Professor Tom Higham (RLAHA), for having the patience to read through the entirety of this tome!

Finally, I thank my family for their continued love and support. Thanks to Mum, Dad and Rachel, and to my wife Sarah, who married me during the course of this DPhil, and more than anybody else has accompanied me on the 'ups' and the 'downs' of this DPhil adventure.

This thesis is dedicated to my
Nanna and Grandad,
Connie and Vin Pearson

Table of Contents:

VOLUME 1

VOLUME 2

List of Figures:

List of Tables:

1. Introduction

The development of radiocarbon dating through the latter half of the twentieth century has provided an invaluable tool in such fields as archaeology and palaeoclimatology that seek robust chronological information from the samples that they study. Radiocarbon calibration is a vital component in this dating process in terms of generating meaningful calendar ages from samples' initial radiocarbon determinations and, for this stage, measurements must be compared with radiocarbon-dated material of known absolute age.

There are many useful archives from which radiocarbon calibration datasets can be developed. Tree-ring records provide an important repository of such information since their annual growth bands provide an 'almost perfect' calendar year age ('almost perfect' since these records need to be reliably cross-matched to produce extended records beyond the lifetime of an individual tree; section 2.5.1), whilst the same material can be directly analysed for their radiocarbon measurements. However, this dendrochronological record is limited further back in time by the availability of suitable fossil wood and, at present, the limits of this continuous tree-ring-based age scale for radiocarbon calibration is only 12,593 calendar years before present (Schaub *et al*. 2008b).

Accordingly, other sources must therefore be examined to extend radiocarbon calibration further back in time. Chief amongst these alternative archives is the partially varved (annually laminated) sedimentary record from the Cariaco Basin, tropical North Atlantic Ocean (Hughen *et al*. 2004b, 2006; section 2.5.4d). Another such archive is provided by uranium series-dated corals (e.g. Fairbanks *et al*. 2005, working on sites in the Bahamas; section 2.5.2). Whilst extremely useful, such records provide information on radiocarbon calibration in the oceans, rather than the atmosphere. Although atmospheric radiocarbon concentration can be approximated from such marine data, a correction factor for the 'marine reservoir effect' must necessarily be applied (section 2.2.1). Since the marine reservoir age is

known to vary both temporally and spatially (Stuiver and Braziunas 1993a; Reimer and Reimer 2001), such approximations for atmospheric radiocarbon therefore contain an additional tier of uncertainty.

Similarly, radiocarbon calibration data can be obtained from independently uranium series-dated speleothems (re-precipitated cave calcite; e.g. Beck *et al*. 2001, working on a submerged cave site in the Bahamas; section 2.5.3), but correction assumptions must again be made. In this instance, the relative offset in radiocarbon age between the newly precipitated speleothem layering and that of the contemporaneous atmosphere is the result of the 'dead carbon fraction' (DCF) contained within this calcium carbonate. As with the marine reservoir correction, assumptions must be made about the continuity of the DCF contribution to speleothem calcite through time.

To avoid such uncertainties, a more direct record of atmospheric radiocarbon is required, therefore. The varved sediments of Lake Suigetsu, Honshu Island, central Japan (chapter 3) provide an ideal sequence from which to derive such a 'wholly terrestrial' record for radiocarbon calibration, through dating of plant macrofossils identified from within its independently varve-counted, sedimentary strata. Such data were previously presented by Kitagawa and van der Plicht (1998a, 1998b, 2000), however, comparison with the aforementioned, alternative calibration datasets yielded unexplained discrepancies, particularly so further back in time. It is unlikely that such a systematic divergence between the Lake Suigetsu data and the alternative radiocarbon calibration datasets could represent a 'real' offset between these respective archives. The more likely causes of divergence therefore lie in the 'absolute age' chronology derived for the Lake Suigetsu record, either in the accuracy of the varve counting itself, or as a result of the core drilling methodology applied (van der Plicht *et al*. 2004). Both of these issues are not due to the nature of the

Suigetsu sediments themselves, but, rather, they are the result of the methodologies applied in the original study.

This DPhil thesis forms a major component of the broader, international, collaborative 'Suigetsu Varves 2006' research project, which seeks to reproduce the Lake Suigetsu radiocarbon calibration dataset, but without the problems of the former study. To this end, a series of ≈ 600 new accelerator mass spectrometry (AMS) radiocarbon determinations have been obtained from terrestrial plant macrofossil remains, sub-sampled from a new, annually-laminated and "perfectly continuous" sediment core ('SG06') collected from Lake Suigetsu (Nakagawa *et al*. 2011). It is these new measurements that form the central corpus of this present work.

1.1 Structure of the Present Document

The remainder of chapter 1 describes the practical conventions adopted in producing this DPhil thesis, as well as states the overarching aim of this present work.

Chapter 2 provides a basic introduction to radiocarbon dating, before discussing in greater detail the need for calibration of radiocarbon measurements, and documenting a summary of the existing radiocarbon calibration datasets produced from a range of sites, utilising different palaeo-archives, worldwide.

Chapter 3 describes the characteristics of the study site, Lake Suigetsu, Honshu Island, central Japan, from which the sediment core was collected for the present study, noting in particular those attributes of Lake Suigetsu that make it so favourable in terms of developing a robust radiocarbon calibration dataset. A more thorough précis of the previous study undertaken at the site (herein, referred to as the "Suigetsu '93" project) is given, and the present, 'Suigetsu Varves 2006', project is introduced.

Chapter 4 sequentially describes the field and laboratory methods utilised in the present study, beginning with the sediment coring process undertaken at Lake Suigetsu, working through macrofossil sub-sampling, radiocarbon pre-treatment methodologies and accelerator mass spectrometry (AMS). Chapter 5 then continues with a discussion of the statistical methodologies applied in the present work, focussing specifically on Bayesian modelling approaches, and introduces the Bayesian calibration software 'OxCal' (Bronk Ramsey 1995).

Chapter 6 presents a two-part re-analysis of the previous radiocarbon dataset obtained from Lake Suigetsu (Kitagawa and van der Plicht 1998a, 1998b, 2000). The first part details a purely statistical comparison of this dataset with that of the international consensus calibration curve, IntCal09 (Reimer *et al*. 2009), whilst the second part describes a physical comparison of the previous project's sediment cores with the composite core obtained from the present project, and the resultant implications of this matching on the original radiocarbon dataset.

The main results of this thesis, the data constituting the 'Suigetsu Varves 2006' radiocarbon calibration dataset, are presented in chapter 7, with a more detailed discussion of the principal findings and implications of this dataset provided in chapter 8. Finally, the totality of this work is summarised in the concluding chapter, 9.

1.2 Conventions Adopted

Since the present study deals with several different timescales (principally, 'true' calendar age, uncalibrated radiocarbon age, calibrated radiocarbon age, and 'Suigetsu varve years'), it is important to be aware of which timescale one is referring to, and to be consistent with the notation applied to each. In the present study, the following notation is applied: (i) following the conventions of the radiocarbon dating community (Mook 1986), radiocarbon ages (based upon a radiocarbon half-life of 5,568 years; section 2.1) are given the notation

'BP' ('radiocarbon years before present') or 'ka BP' ('thousand radiocarbon years before present'); (ii) calibrated radiocarbon ages are given the notation 'cal. BP' ('calibrated years before present') or 'cal. ka BP' ('thousand calibrated years before present'); and (iii) ages according to the 'Suigetsu varve year' chronologies of either the previous- (1993 coring) or present- (2006 coring) Lake Suigetsu projects are given the notation 'SG93 vyr BP' or 'SG06 vyr BP', respectively. In *sensu stricto*, the 'cal. BP' notation should only be applied to calibrated radiocarbon ages, but this notation is also applied herein to represent the conceptual 'absolute age' timescale (i.e. the 'real', calendar age scale, which, theoretically, should be equivalent to calibrated radiocarbon ages in any case), both within- and beyond the range of the radiocarbon dating method. In all instances, 'before present' ('BP') means 'before AD 1950', again following the conventions of radiocarbon dating literature. Where calibrated ages are given, it should be clear from the context which calibration dataset has been utilised to produce these ages from the raw radiocarbon determinations. One additional timescale that is occasionally referred to in this thesis is that of the North Greenland Ice Core Project ('NGRIP') 'cal. yr b2k' timescale (Rasmussen *et al*. 2006), which is equivalent to the 'cal. BP' chronology, but with the datum shifted from 'before AD 1950' to 'before AD 2000'. Except for specifically citing events within NGRIP, the cal. yr b2k notation is not applied elsewhere within this thesis, and in all instances where it is cited, the equivalent cal. BP value will also be given for clarity.

Following the same convention as that adopted by Bowman (1990, p.10), '^{14}C' is used only when referring to the radioisotope carbon-14 specifically, whereas 'radiocarbon' is used to discuss the dating technique more broadly.

Due to the high precision possible with the Suigetsu Varves 2006 sediment core, depth information is generally given in cm, rather than the standard SI (*Système international d'unités*; International System of Units) unit of depth, m. The depth units of this core are

described more thoroughly in section 4.1, but it will be noted from the outset that there are three differing depth units used throughout the Suigetsu Varves 2006 project. Specifically, these depth units are: (i) drilling depth; (ii) composite depth; and (iii) event-free depth; and it is the second of these that is most readily used. Again, it should be made clear at all times which depth unit is being referred to. Both composite depth and event-free depth models do have the potential to change over the course of the Suigetsu Varves 2006 project, as additional information becomes available, although such changes would be expected to only be very minor (as have been previous revisions to these depth scales; Nakagawa *et al*. 2011). Throughout this DPhil thesis, the version of 24th August 2009 is used for composite depth and the version of 2nd January 2009 is used for event-free depth. At the time of submission of the present work, these versions reflect the latest revisions to the respective SG06 depth models.

Abbreviations used throughout this thesis are written out in full upon their first usage, but a comprehensive list is provided for reference in appendix 1.

Terms specific to the Bayesian radiocarbon calibration program OxCal (*inter alia* Bronk Ramsey 2008a) are introduced from chapter 5 onwards, and for these the `Lucida Console` font is applied.

The nine chapters of this thesis are subdivided into successive levels of sections and sub-sections (e.g. '2.5.4d' refers to sub-section 4d of the fifth section of chapter 2). Both figures and tables are numbered successively according to the order in which they are first mentioned in the text, and according to the chapters in which they are first cited (e.g. '**Figure 4.3**' refers to the third figure of chapter 4). Similarly, equations within the text are numbered according to their order within individual chapters (e.g. '[2.1]' refers to the first equation of chapter 2). Specific model specifications in the radiocarbon calibration OxCal are

also listed successively according to their order within the particular chapters that they are first referred to (e.g. 'OCM-7.2' refers to the second 'OxCal Model' of chapter 7).

1.3 Overarching DPhil Aim

As introduced above, the annual laminations of the Lake Suigetsu sedimentary régime provide a high resolution archive from which to extend the terrestrial radiocarbon calibration curve beyond that of the current dendrochronologically-based data, continuing through to the limits of radiocarbon detection (*circa* 60 ka BP). The principal aim of my DPhil research is therefore to produce this wholly terrestrial radiocarbon calibration dataset as part of the broader 'Suigetsu Varves 2006' project. Additional, more specific, subsidiary aims to this broader goal are listed in section 3.7, after the theoretical context (chapter 2) and study site (chapter 3) have been more thoroughly described.

2. Radiocarbon Calibration

2.1 Radiocarbon Dating

The discovery of the radiocarbon dating technique in the mid-twentieth century by Willard Libby and colleagues (Libby *et al*. 1949; Arnold and Libby 1949, 1951; Libby 1951, 1955) revolutionised such fields as archaeology and palaeoclimatology that require robust chronological information to inform their study. Any sample yielding sufficient quantities of carbon could be dated in this manner, with the older age limit of the method (currently *circa* 50 to 60 ka BP) having been pushed back significantly since its inception.

The underlying basis of radiocarbon dating is the radioactive decay of the radioisotope carbon-14 (^{14}C) to stable nitrogen-14 (^{14}N) through beta (β) decay:

[2.1] $$^{14}C \rightarrow {}^{14}N + e^{-} + \bar{\nu}_e$$

where: e- is an electron and $\bar{\nu}_e$ is an electron antineutrino. This is an entirely stochastic process, with the spontaneous decay of individual ^{14}C atoms occurring entirely at random. However, as with all radioactive decay, the rate of decay of the radioactive atoms in the entire sample does behave predictably, with 1% of all ^{14}C atoms decaying every 83 years, irrespective of climate or environment. This produces an exponential decay curve for ^{14}C (figure 2.1) with a half-life ($T_{½}$) of ≈ 5,730 years (Godwin 1962). This means that after 5,730 years, the number of ^{14}C atoms remaining in a sample will be half that of the initial activity. After a further 5,730 years this number will be halved again, and so on until the number of remaining ^{14}C atoms is statistically indistinguishable from zero.

Figure 2.1: The exponential decay curve of ^{14}C, where A_0 is the initial number of ^{14}C atoms in the sample at equilibrium with the carbon exchange reservoir. After each successive half-life ($T_{½}$; 5,730 years) the number of remaining ^{14}C atoms remaining is halved.

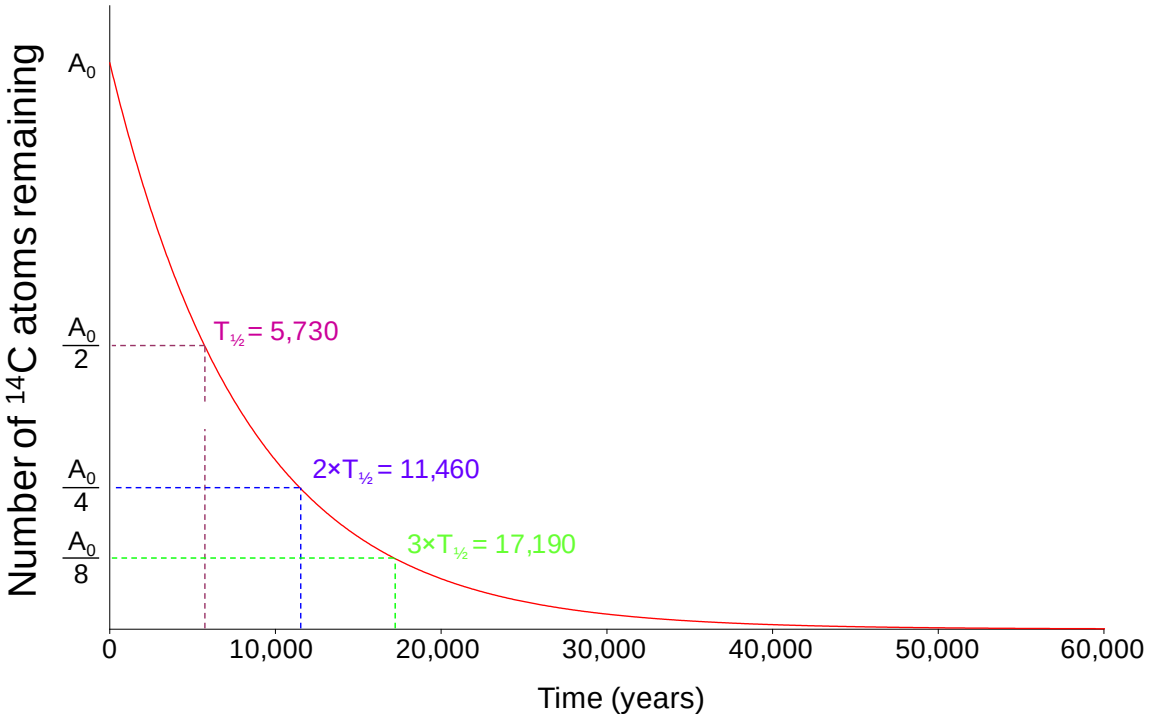

Carbon-14 represents approximately one in a million million (10^{12}) atoms of naturally occurring carbon, with the majority of carbon atoms being composed of the two stable isotopes carbon-12 (^{12}C) and carbon-13 (^{13}C). These stable isotopes constitute approximately 98.9% and 1.1% of naturally occurring carbon, respectively. Therefore, the measurement of ^{14}C atoms remaining in a sample has to take account of such low abundances.

Levels of ^{14}C are kept essentially constant in the Earth's system through a dynamic equilibrium between the loss through exponential radioactive decay described above, and the formation in the upper atmosphere (concentrated in the lower stratosphere and upper troposphere; Lingenfelter 1963; Bronk Ramsey *et al.* 2007) of ^{14}C from ^{14}N due to the interaction of cosmic ray neutrons, reaching the Earth's atmosphere from deep space, with

nitrogen atoms. Specifically, this involves neutron (n) capture by ^{14}N, with the associated loss of a proton (p):

[2.2] $^{14}N + n \rightarrow {}^{14}C + p$

(Montgomery and Montgomery 1939). The ^{14}C atoms thus produced are rapidly oxidised to form 'heavy' carbon monoxide (^{14}CO), and, subsequently, heavy carbon dioxide ($^{14}CO_2$), which becomes thoroughly mixed through the atmospheric reservoir of 'ordinary', stable carbon dioxide ($^{12}CO_2$ and $^{13}CO_2$) and thence may be assimilated into the biosphere through photosynthesis, or dissolved into the oceans. The combined stores of atmospheric, biospheric and oceanic carbon are known collectively as the 'carbon exchange reservoir'.

Whilst an organism is alive, its ^{14}C content remains in equilibrium with that of the carbon exchange reservoir (although with potential fractionation offsets from it; section 2.2.2, below), but after death this exchange ceases, and thus the 'radiocarbon clock' begins counting down, with radioactive decay continuing in the absence of replenishment. Thus, the time elapsed since equilibrium with the carbon exchange reservoir can be calculated through comparison of the ratio of ^{14}C:^{12}C in a sample with that of the ambient atmospheric level:

[2.3] $t = -8{,}033 \ln(A/A_0)$

where: t is the time elapsed since equilibrium (i.e. the time since death), measured in 'conventional radiocarbon years' (Stuiver and Polach 1977); A is the number of ^{14}C atoms remaining in the sample; A_0 is the initial number of ^{14}C atoms in the sample at equilibrium with the carbon exchange reservoir; and 8,033 describes the mean-life (τ) of a ^{14}C atom in radiocarbon years if the 'Libby half-life' of 5,568 years is applied (see section 2.3, below). Following the laws of exponential decay, τ is related to half-life ($T_{½}$) by the equation:

[2.4] $T_{½} = (\ln 2)\, \tau$

and so indeed:

[2.5] 5,568 years = (ln2) 8,033 years.

2.2 Reservoir Effects, Fractionation and Regional Radiocarbon Offsets

In Libby's initial radiocarbon studies he found a general uniformity for ^{14}C activity measurements worldwide (Libby *et al*. 1949), including both atmospheric and biospheric (i.e. living organic tissue) carbon sources. He therefore argued for a rapid mixing of $^{14}CO_2$ throughout the atmosphere, hydrosphere and biosphere systems to maintain this global uniformity. As the technique became more precise, however, it emerged that such assumptions were not wholly true. Reservoir effects and fractionation effects both produce divergence in the ^{14}C signal of the biosphere and hydrosphere from that of the ambient atmosphere, and even within the atmospheric ^{14}C reservoir, more recent work has shown that the assumption of global uniformity of the ^{14}C:^{12}C ratio might also differ. These issues will be discussed in turn below.

2.2.1 Radiocarbon Reservoir Effects

Through exchange reactions, atmospheric CO_2, and hence ^{14}C, is incorporated into surface ocean waters in the form of dissolved carbonates. However, the mixing rate of ocean surface- and ocean deep-waters is very slow, and so the radiocarbon signal of deep ocean waters becomes depleted, relative to the atmosphere, since radioactive decay of ^{14}C within this reservoir significantly outweighs replenishment. Accordingly, sea water bears an 'apparent age', with the difference in ^{14}C:^{12}C between the atmosphere and ocean water described as the 'marine reservoir effect' (Suess 1955; Mangerud 1972; Stuiver *et al*. 1986b; Reimer and Reimer 2001). For the deep ocean, this apparent age may be of the order of

several millennia. Marine-dwelling organisms (such as foraminifera, molluscs etc.) therefore take on such ages as they assimilate dissolved carbonate into their skeletal structures. Surface ocean waters also bear an apparent age, which reflects a mixture of both atmospheric- and deep ocean radiocarbon signals. The globally averaged (pre-industrial) surface ocean radiocarbon reservoir age (R) is approximately 400 years (Stuiver and Braziunas 1993a). However, there is considerable spatial variability in this apparent age of ocean water around the world due to, *inter alia*, the pattern of surface current movements, thermohaline circulation (THC), and upwelling. These local variations in R are given the notation 'ΔR', and may be up to several hundred years in magnitude (Reimer and Reimer 2001; www.calib.org). Furthermore, due to changes through time of these aforementioned processes, the apparent age of ocean waters also changes through time (Reimer and Reimer 2001). It is this temporal variability that makes radiocarbon calibration from marine archives (section 2.5, below) particularly problematic, since the appropriate marine reservoir correction must be made to generate the equivalent, contemporaneous atmospheric ^{14}C signal.

Further to this marine reservoir effect, apparent aging may also occur in terrestrial water bodies. Again, relatively slow exchange between atmospheric- and lake water carbon would generate such an offset, but there might additionally be seepage into lakes of dissolved carbonates (from depleted ^{14}C sources) in groundwater. This process, termed the 'hard-water effect' (Deevey *et al*. 1954), again produces a depleted ^{14}C signal and yields an apparent age that is hard to quantify due to particular local geological and hydrological features that are likely to change through time. Since aquatic plants photosynthesise sub-aquatically, their carbon is drawn from dissolved inorganic carbon (DIC), rather than directly from the atmosphere, and so these species also reflect the ^{14}C:^{12}C of the water body. Similarly, any heterotrophs feeding on these aquatic plants will carry such a depleted ^{14}C signal up the food-chain.

2.2.2 Radiocarbon Fractionation

Although the three isotopes of carbon (^{12}C, ^{13}C and ^{14}C) are chemically indistinguishable, there is a tendency in any biological pathway towards uptake of the lighter isotopes. Therefore, in photosynthesis ^{12}C is preferentially assimilated as compared to ^{13}C (Craig 1953), which in turn is preferentially assimilated as compared to the heavier ^{14}C. The resulting plant tissue laid down by this process is therefore depleted in ^{14}C relative to that of the contemporaneous atmosphere. This picture is complicated further since relative carbon isotopic uptake by plants also varies according to species, and so different parts of the biosphere bear differing apparent radiocarbon ages.

Fractionation has the opposite effect in ocean waters, since, in equilibrium, gas exchange favours the release of lighter isotopes to the atmosphere from the ocean surface. Thus, marine-dwelling species would exhibit relatively younger ^{14}C ages than the ambient atmosphere, were it not for the counter-acting marine reservoir effects described above.

Fortunately, such fractionation effects are relatively easy to correct for since it is assumed that, as a first order approximation, relative depletion in ^{14}C is twice that of ^{13}C (reflecting the mass differences between the respective isotopes). Therefore, the ratio of stable ^{13}C:^{12}C in a sample, determined by mass spectrometry, can be used to derive the relevant corrections to provide the initial (time of death) ^{14}C activity of a sample. This measured ^{13}C:^{12}C ratio is compared to that of the Vienna PDB (VPDB) limestone (belemnite carbonate from the Cretaceous Peedee Formation in South Carolina, USA) international standard, with the relative deviation of a sample's ^{13}C:^{12}C from that of VPDB limestone given by $\delta^{13}C$ where:

$$[2.6] \quad \delta^{13}C\ (‰) = \left[\frac{\left(^{13}C/^{12}C\right)_{sample}}{\left(^{13}C/^{12}C\right)_{VPDB}} - 1 \right] \times 1000$$

(Coplen 1994). As already noted, $\delta^{13}C$ differs between species, however, the mean isotopic composition of wood is approximately -25‰. Convention dictates that it is to this value (-25‰) that ^{14}C activity is fractionation-corrected before a conventional radiocarbon date is published (Stuiver and Polach 1977). This fractionation-corrected ^{14}C value of a sample (A_c) can be approximated from the measured ^{14}C activity (A_m) by:

$$[2.7] \quad \frac{A_c}{A_m} = \left[\frac{1+(-25/1000)}{1+(\delta^{13}C/1000)}\right]^2$$

2.2.3 Regional Radiocarbon Offsets

Early work by Libby and colleagues (1949) showed the atmospheric ^{14}C signal to be approximately constant on a global basis, thus providing one of the underlying assumptions of the method upon which radiocarbon dating was reliant. However, as measurements have become increasingly precise, it has been demonstrated that this assumption only holds for intra-hemispheric atmospheric ^{14}C concentrations, with an offset between the two hemispheres such that ages from the Southern Hemisphere (defined with respect to the thermal equator) appear to lag those of the Northern Hemisphere by approximately 30 years (Lerman *et al*. 1970; Vogel *et al*. 1986, 1993; McCormac *et al*. 1998a; Stuiver and Braziunas 1998; Hogg *et al*. 2002, 2009; Zimmerman *et al*. 2010). This is believed to be a result of the greater surface area of the Southern Hemisphere covered by oceans, as well as slightly higher wind speeds, which result in a greater mixing of CO_2 from the ^{14}C-depleted deep oceans with that of the atmosphere (Cain and Suess 1976).

Investigations have been carried out to investigate whether additional, intra-hemispheric regional radiocarbon offsets are evident but, at present, data regarding the existence of such offsets remain equivocal (Suess 1970; Stuiver and Quay 1981; Stuiver

1982; McCormac *et al*. 1995). Braziunas *et al*. (1991, 1995) provide general circulation modelling (GCM) support for the zonal homogeneity of Northern Hemisphere (NH) ^{14}C concentration, with minimal deviation (≈ 1‰) found in the mid-latitudes (from whence the dendrochronologically-derived terrestrial calibration datasets derive; section 2.5.1, below). Those effects that have been noted are relatively small, and are ascribed to a differing growth season of plants in certain regions (Kromer *et al*. 2001, 2010; Dee *et al*. 2009; Bronk Ramsey *et al*. 2010b), or proximity to large scale ^{14}C-deficient carbon sources, such as intense ocean upwelling (Stuiver and Braziunas 1998; Sakamoto *et al*. 2003), thawing permafrost (Damon *et al*. 1992) or volcanic emissions (Bruns *et al*. 1980; section 3.4). I.e., data demonstrating 'real', concomitant intra-hemispheric, geographical offsets are seemingly lacking, whereas demonstrable intra-hemispheric radiocarbon age offsets can be attributed to sample or site-specific physical (not strictly geographical) causes. Each of these potential causes of offsets would produce temporally-variable effects, which would necessitate site-specific calibration datasets if reliable calibrated ages were required from such sites..

2.3 The Need for Radiocarbon Calibration

For a number of contributing reasons, the raw, fractionation- and reservoir-corrected, radiocarbon dates produced for samples through laboratory analysis are not the same as their 'true', calendar age. Firstly, the original radiocarbon half-life (the 'Libby half-life' of 5,568 ± 30 years; Anderson and Libby 1951; Arnold and Libby 1951) used in calculating a sample's conventional radiocarbon age from its ^{14}C activity has long been known to have been an under-estimate of the 'real' ^{14}C decay rate. The presently accepted, consensus value of the true ^{14}C half-life (the 'Cambridge half-life', as given by Godwin 1962) is 5,730 ± 40 years. (This value remains disputed, however, with Chiu *et al*. 2007, for example, suggesting that a value as high as 6,000 years might better reflect the true value. Conversely,

Roberts and Southon 2006 derived a value in good agreement with the original Libby half-life.) So as to maintain consistency with the previously published data, as well as to avoid any additional confusion related to any future revision of the ^{14}C half-life, it is the convention of the radiocarbon dating community to continue giving radiocarbon 'dates' as those calculated from the original Libby half-life (Mook 1986).

Were this to be the only source of divergence between radiocarbon and calendar timescales, the conversion of radiocarbon ages into real time would be straightforward. However, a second complication in calendar age determination from radiocarbon dates introduces non-linearity into this conversion. Libby's premise that the atmospheric radiocarbon concentration remained constant through time (Anderson and Libby 1951) has also been shown not to be the case (de Vries 1958; Willis *et al*. 1960; Suess 1965, 1970; Damon *et al*. 1966, 1978). There are two major reasons for such changes: firstly, the global production rate of ^{14}C in the upper atmosphere has not remained constant through time (Lal and Peters 1967); and secondly, internal changes between the respective reservoirs of the Earth's carbon cycle system have taken place to alter global distribution of relatively older and younger carbon sources through time (Broecker *et al*. 1960; Siegenthaler *et al*. 1980). Furthermore, anthropogenic influence over recent centuries has added to the natural sources of atmospheric ^{14}C variation. These three issues will be discussed below.

2.3.1 Changing ^{14}C Production Rate

As already noted, ^{14}C is formed in the upper atmosphere due to the interaction of secondary neutrons, produced by cosmic ray spallation, with ^{14}N. The rate of ^{14}C production is therefore modulated, over both long and short timescales, by any changes in the cosmic ray flux reaching the Earth's atmosphere. Such changes may be the result of changes in the Earth's geomagnetic field (the geomagnetic moment), which, when weakened, reduces its

shielding effect and therefore allows increased ^{14}C production with increased entry of cosmic rays into the Earth's atmosphere (Elsasser *et al*. 1956; Bard *et al*. 1990a; Guyodo and Valet 1999; Laj *et al*. 2000). Conversely, at times of strengthened geomagnetic field intensity, ^{14}C production in the upper atmosphere decreases, as cosmic rays are increasingly deflected away from the Earth.

Changes in the intensity of solar activity are also known to play a rôle in ^{14}C production over short time scales (Stuiver 1961; Suess 1965; Damon *et al*. 1966; Stuiver and Quay 1980; Stuiver *et al*. 1991; Stuiver and Braziunas 1993b), with a reduction in solar activity, and specifically in the 'solar wind', again allowing increased ^{14}C production by allowing an increased cosmic ray flux into the upper atmosphere (van Geel *et al*. 2003).

Additionally, changes in the interstellar galactic cosmic ray flux would directly impact on ^{14}C production rate in the upper atmosphere. Such a cause has been postulated by some authors (Sonnett *et al*. 1987; McHargue *et al*. 1995) as being responsible for the most marked episode of atmospheric ^{14}C concentration over the radiocarbon timescale – the 'Laschamp event' (section 2.7, below).

2.3.2 Internal Changes Within the Global Carbon Cycle System

As well as the factors cited above in altering ^{14}C production rate, the atmospheric ^{14}C:^{12}C ratio is affected by changes internal to the Earth's climatic system (Siegenthaler *et al*. 1980; Edwards *et al*. 1993; Hughen *et al*. 2000). Of paramount importance in this regard are changes through time in the strength of the global thermohaline 'conveyor' (*sensu* Broecker 1991). A reduction in thermohaline circulation (THC), leading to decreased upwelling of ^{14}C-depleted deepwaters and reduced draw-down of relatively ^{14}C-enhanced atmospheric carbon, would produce a relative increase in atmospheric ^{14}C concentration since ocean deepwaters represent a reservoir of old carbon (section 2.2.1, above). Similarly, an increase in the

strength of THC, with associated increase in deepwater upwelling and increased draw-down of relatively ^{14}C-enhanced atmospheric carbon, would release large quantities of ^{14}C-depleted CO_2 back into the atmosphere, making the atmospheric ^{14}C:^{12}C ratio appear relatively older. Such changes in ocean circulation patterns were especially significant at transitions from glacial to interglacial conditions, but would also affect the atmospheric radiocarbon signal over shorter timespans, such as the Younger Dryas cold reversal, where THC was suddenly interrupted (Broecker *et al*. 1989).

2.3.3 Anthropogenic Effects

Over the last 200 to 300 years, the anthropogenic burning of fossil fuels has liberated large quantities of ^{14}C-depleted CO_2 into the atmosphere through the burning of fossil fuels. Atmospheric ^{14}C has therefore been diluted through the addition of this 'dead carbon' and therefore produces apparently older radiocarbon dates over this period than would otherwise be expected. This is termed the 'fossil fuel-', 'industrial-' or 'Suess effect' (after its discoverer, Hans Suess 1955).

A second anthropogenic impact on ^{14}C levels is the effect of nuclear weapons testing in the mid 20th century. The neutrons released by such explosions promoted the formation of ^{14}C from ^{14}N in the same manner as with the neutrons reaching the atmosphere naturally from cosmic rays. This 'bomb effect' doubled the atmospheric ^{14}C concentration of the Northern Hemisphere, peaking around 1963, resulting in radiocarbon determinations from the latter half of the 20th century giving data well in excess of 100% 'modern' values. Radiocarbon measurements of samples dating to this period (1950 onwards) are therefore reported in terms of their percentage of modern carbon (pMC; or, preferably, as 'fraction modern carbon' – $F^{14}C$; Reimer *et al*. 2004b), rather than as 'conventional radiocarbon years before present'. Atmospheric ^{14}C levels have subsequently been declining (due to the continual removal of

atmospheric carbon into the oceans), and will soon re-pass 100% modern, with an over-shoot to depleted atmospheric levels due to the continuing release of fossil fuels into the atmosphere. The Southern Hemisphere 'bomb pulse' was smaller (increasing atmospheric ^{14}C concentrations by ≈ 60%) and slightly lagging that of the Northern Hemisphere, due to the geographic distribution of nuclear testing (almost entirely performed in the Northern Hemisphere; Hua 2009), and the relative resistance of atmospheric circulation patterns to inter-hemispheric exchange. The bomb pulse actually contributed greatly to scientific understanding of the global carbon cycle, as well as atmospheric and ocean circulation dynamics, since the ^{14}C signal provided such a clearly observable tracer.

2.4 Radiocarbon Detection Limit

The nature of the exponential radiocarbon decay curve (figure 2.1) is such that after approximately ten half lives, the ^{14}C activity of a sample is statistically indistinguishable from 'background' ^{14}C values (i.e. those measurements from sample standards known to date considerably older than this). Such samples dated to beyond this 'detection limit' are defined as being of 'infinite age', with dates generally expressed as 'greater than' ages (e.g. > 57,000 years). To be presented as a 'finite age' (e.g. 45,800 ± 800 years), background-corrected results must be greater than two standard deviations from zero (Stuiver and Polach 1977).

Since the Lake Suigetsu sediment profile dates back right through the last interglacial to at least 150 cal. ka BP (Nakagawa *et al*. 2011; section 3.2), the limit of the radiocarbon calibration dataset constructed from the present study is provided by the ^{14}C detection limit alone.

2.5 Palaeoenvironmental Archives Utilised for Radiocarbon Calibration

The long- and short-term factors discussed in section 2.3 necessitate a calibration stage against material of known age if conventional radiocarbon dates are to be converted into a more meaningful calendar age. Over recent decades, considerable effort has been made to derive calibration datasets from a range of natural palaeoenvironmental archives, which act as records of natural atmospheric radiocarbon concentration variation ($\Delta^{14}C$) through time. Fundamental to this effort is that the archives in question demonstrate a reliable, independent means of deriving calendar age, against which the radiocarbon determinations can be directly compared. Over the last decade or so, there has been a "spectacular growth" of new calibration data (van der Plicht *et al*. 2004), which now cover the entirety of the radiocarbon dating range. These efforts are demonstrated by a number of dedicated calibration volumes of the journal *Radiocarbon* (Stuiver and Kra 1986; Stuiver *et al*. 1993; Stuiver and van der Plicht 1998; Reimer 2004, 2009), as well as a separate varve comparison issue (van der Plicht 2000a).

Section 2.5 discusses the range of different palaeoenvironmental archives from which radiocarbon calibration data have been obtained, with a summary of the advantages and disadvantages of each given in section 2.5.6. The publications cited are not exhaustive, but provide examples of the different archives thus far exploited for radiocarbon calibration purposes, and includes the datasets that are applied for comparison purposes in later chapters of this DPhil thesis. The following section, 2.6, introduces the international consensus (IntCal) calibration curves, which draw together the present best estimates of the 'true' calibration curve, based upon the concomitant state-of-knowledge of the radiocarbon dating community, as derived from the various individual, contributing calibration datasets. Key features of these calibration datasets are described in section 2.7.

2.5.1 Dendrochronological Records

Ever since the discovery of the need to calibrate radiocarbon dates (de Vries 1958), dendrochronological records have, understandably, been central to developing robust calibration datasets, since a direct comparison can be made between the wood's radiocarbon- and dendrochronological (annual tree-ring-counted) ages, based upon analysis of the same sample material. Testing has shown that once laid down, tree-rings do not exchange their carbon with other rings (at least for the non-mobile cellulose fraction; section 4.3.2), and therefore they provide an accurate, high resolution, direct record of changing atmospheric ^{14}C concentration through time. Both calendar ages and radiocarbon measurements can be made with high precision and accuracy, and provide readily reproducible measurements.

Continuous dendrochronological records, obtained from thousands of overlapping tree-ring series, are now available through the entirety of the Holocene, and provide an absolute calendar timescale to within the bounds of dendrochronological error, with this being minimised through rigorous internal replication and external cross-checking of datasets (Douglass 1941; Fritts 1976).

In general, the dendrochronological datasets are comprised of data representing decadal or bidecadal spans of calendar time, although the potential of the tree-ring record does allow for greater levels of precision, and, indeed, single year results have now been performed (Stuiver and Braziunas 1993b; Stuiver *et al*. 1998b). Vogel and van der Plicht (1993) provided a high-precision calibration dataset (between one and four tree-rings per sample) from the German oak (*Quercus robur* and *Q. petraea*) dendrochronology over the fifth and sixth millennia BP, demonstrating, through comparison with other datasets, that little detail of the calibration curve is lost through decadal averaging.

Early dendrochronological radiocarbon calibration centred upon US sequoia (*Sequoia gigantea*; e.g. Willis *et al*. 1960) and bristlecone pine (*Pinus longaeva*, from the White

Mountains, California, USA; e.g. Ralph and Michael 1970; Damon *et al*. 1974; Ferguson and Graybill 1983) chronologies, due to the exceptional ages reached by these species (> 2,000 years, and up to 5,000 years for specific examples of bristlecone pine). In addition to these US measurements, two extensive dendrochronological datasets central to radiocarbon calibration curve development have been provided by the Irish oak, and central European (German and Swiss) oak and pine dendrochronologies. The Irish data are obtained from sub-fossil oaks (*Q. robur* and *Q. petraea*), retrieved from Northern Irish bogs, and extend back in time across the last seven millennia (Pearson and Baillie 1983; Pilcher *et al*. 1984; Pearson *et al*. 1986). The German (Hohenheim) oak chronology is also composed of sub-fossil *Q. robur* and *Q. petraea* (> 4,000 trees), obtained from the Upper Rhine, Main and Danube valleys (Becker 1980, 1993; Kromer *et al*. 1986). By 1993, this absolute dendrochronology had been extended to 9,888 cal. BP (Becker 1993). To extend this central European dendrochronology further back in time, however, other species needed to be exploited, since oak only re-migrated to the region at the Preboreal/Boreal transition (*circa* 10,000 BP). To this end, Kromer and Becker (1993) presented a 1,784 year German pine (*Pinus sylvestris*) chronology, which they tentatively linked to the oak chronology, producing an extended dataset back to 11,388 cal. BP.

A key early finding of radiocarbon calibration using dendrochronologically-dated wood, was the demonstration of characteristic 'wiggles' in the calibration curve, produced by variations in the atmospheric ^{14}C:^{12}C ratio over time (Suess 1965, 1970; Stuiver and Suess 1966). These 'wiggles' were initially questioned by other authors (e.g. Clark 1975; Pearson *et al*. 1977; Damon *et al*. 1978; Pearson and Pilcher 1978), and were ascribed to imprecision of the experimental method. As further data were produced, however, Suess' wiggles were shown to represent an authentic signal (Suess 1978, 1980; Stuiver 1982).

Pearson and Stuiver (1986) and Stuiver and Pearson (1986) gave extensive, high-precision measurements of both European (Irish and German) oak, and US Douglas fir (*Pseudotsuga menziesii*) and sequoia samples back to 4,450 cal. BP, with measurements obtained from the Belfast (Pearson) and Seattle (USA; Stuiver) laboratories. Significantly, these datasets demonstrated no significant geographic offsets between the US and European samples for this time period.

By 1993, Pearson and Stuiver were able to extend their trans-Atlantic dendrochronological calibration datasets across the last 8,000 cal. years, combining the decadal Seattle data of Stuiver and Becker (1993) and bidecadal Belfast data of Pearson and Qua (1993) and Pearson *et al*. (1993). These datasets included slight correction of both the Seattle (Stuiver and Becker 1993) and Belfast (Pearson and Qua 1993) datasets, although these corrections were subsequently questioned by van der Plicht *et al*. (1995) and McCormac *et al*. (1995).

Kromer *et al*. (1996) demonstrated, through comparison with a second German (Göttingen) oak chronology (back to 9,147 cal. BP, based upon sub-fossil river and bog oaks; Leuschner 1992) that the Hohenheim oak dataset of Becker (1993) contained an important dendrochronological error. Forty one previously missing calendar years were therefore inserted into the Hohenheim chronology at 7,190 cal. BP, enabling "perfect synchronisation" of the two, independent German dendrochronologies back to 9,147 cal. BP (Spurk *et al*. 1998). This error explained the discrepencies pointed out in the 1993 calibration curve (Pearson and Stuiver 1993; Stuiver and Pearson 1993; McCormac *et al*. 1995). A further 54 years were also inserted at 9,741 cal. BP, and additional dendrochronological data added, such that the continuous German oak chronology was extended back to 10,429 cal. BP (Spurk *et al*. 1998). Additionally, the tentative placement of the floating German pine chronology of Becker (1993) was further pushed back in time (Spurk *et al*. 1998), with a new, tentative link

(obtained by radiocarbon 'wiggle matching', rather than firm, dendrochronological means; section 5.3.2a) placing the older limit of this total chronology at 11,871 ± 20 cal. BP (Kromer and Spurk 1998).

Friedrich *et al*. (2004) presented a revised version of the continuous Hoheneim oak chronology (extending back to 10,429 cal. BP). This paper noted the removal of trees from previous versions of the chronology, which had suffered from cockchafer beetle (*Melolontha melolontha* and *M. hippocastrani*) damage. Additionally, these authors presented a revised and extended central European (German and Swiss) pine chronology, which could now be firmly, dendrochronologically-linked to the oak chronology, requiring only an eight year shift as compared to the radiocarbon wiggle-matched method of Kromer and Spurk (1998). The absolute dendrochronologically-derived calibration dataset thus produced, extended back to 12,410 cal. BP (i.e. the mid-Younger Dryas). This central European pine chronology has since been extended yet further by Schaub *et al*. (2008b), such that absolute dendrochronological radiocarbon calibration data now extend back to 12,593 cal. BP.

Further, currently 'floating' (i.e. not yet reliably dendrochronologically-connected to the continuous tree-ring record), European tree-ring datasets (sub-fossil pines from the Bølling/Allerød interstadial and early Younger Dryas) should be linked to the absolute dendrochronological timescale in the near future, providing dendro-calibration back to approximately 14,000 cal. BP (Friedrich *et al*. 2004; Kromer *et al*. 2004; Schaub *et al*. 2008a, 2008b).

An important Southern Hemisphere tree-ring record was provided by Hua *et al*. (2009), which is composed of a 617 year Tasmanian (Australia) Huon pine (*Lagorostrobos franklinii*) dataset and spans the early Younger Dryas. By wiggle matching (section 5.3.2) the Huon pine data to the European absolute and floating oak and pine chronologies (implementing a necessary SH correction), these authors were able to bridge the gap in the European

dendrochronology, thus producing a combined dendro-calibration dataset back to *circa* 14,000 cal. BP, though, of course, this dataset was not firmly, dendrochronologically-linked.

Whilst the European dendrochronology is currently being extended back into the Late Glacial, it is unlikely that this region will yield suitable trees before the Last Glacial Maximum (LCM, *circa* 18,000 cal. BP) because of the extent of Northern Hemisphere glaciation at that time, limiting tree populations and destroying previously deposited dendro-material (Turney *et al*. 2007). However, Southern Hemisphere data derived from New Zealand kauri (*Agathis australis*) tree-rings offer considerable potential to extend dendro-calibration across the entire range of the radiocarbon method (Hogg *et al*. 2006; Palmer *et al*. 2006; Turney *et al*. 2007; Bronk Ramsey *et al*. 2010a), but will potentially take several decades to achieve, if at all (Bronk Ramsey *et al*. 2006). Extracted trees have already been obtained for sporadic periods back to the limits of the radiocarbon method, with individual trees exhibiting chronologies of > 2,000 calendar years (Turney *et al*. 2007). Until such extension of the dendrochronological radiocarbon calibration data is achieved, however, alternative archives must be examined to extend radiocarbon calibration beyond its current absolute limit of 12,593 cal. BP.

2.5.2 Coral Records

Beyond the high-precision timescale of the dendrochronologically-dated tree-ring record, fossil shallow water tropical corals can provide an alternative archive suitable for radiocarbon calibration purposes, since they can be independently dated by both uranium series- (^{234}U-^{230}Th) and radiocarbon dating techniques. Kaufman and Broecker (1965) first attempted ^{234}U-^{230}Th dating of carbonates for calibration of the radiocarbon timescale, but limitations in the α-counting ^{234}U-^{230}Th methodology meant that the calendar timescale was insufficiently precise. The later development of thermal ionisation mass spectrometry (TIMS)

allowed ^{234}U-^{230}Th dating at significantly improved levels of precision (equivalent to those of the radiocarbon dating method) and reproducibility (Edwards *et al*. 1987a, 1987b). Bard *et al*. (1990a, 1990b) were the first to exploit this technique for generating radiocarbon calibration data from corals, and demonstrated that the radiocarbon timescale was "significantly compressed" during the Younger Dryas. Subsequent studies of note include those of Bard *et al*. (1993, 1998), Edwards *et al*. (1993), Burr *et al*. (1998, 2004), Yokoyama *et al*. (2000) and Cutler *et al*. (2004). The studies of Burr *et al*. (1998, 2004) are particularly noteworthy, since the coral species sampled (*Diploastrea heliopora* and *Goniastrea favulus*, respectively) exhibited annual growth bands. Thus, annual resolution reconstruction of past radiocarbon fluctuations was possible (equivalent to the precision of the tree-ring archives), with the chronology of these archives tied to the absolute age scale by ^{234}U-^{230}Th. The former of these two studies was the first to provide fine structure of the radiocarbon signal into the Younger Dryas (between *circa* 12,400 and 11,700 cal. BP), whilst the latter (covering *circa* 13,100 to 13,000 cal. BP) was able to demonstrate high frequency (intra-decadal) radiocarbon oscillations, equivalent to those seen in modern corals (e.g. Brown *et al*. 1993; Guilderson *et al*. 1998).

The most extensive, and arguably the most robust, coral-derived radiocarbon calibration dataset produced to date is that of Fairbanks *et al*. (2005). These data, based upon offshore coral samples from Barbados (western tropical Atlantic Ocean), Kirimati Atoll (central equatorial Pacific Ocean) and Araki Island (south-western Pacific), provided an extension to the dendrochronological radiocarbon calibration curve back to 50,000 cal. BP (i.e. spanning the entire range of the radiocarbon dating technique), and included re-analysis of all Barbados samples from the group's previous studies (Fairbanks 1989, 1990; Bard *et al*. 1990a, 1993, 1998; Stuiver *et al*. 1998a, 1998b). The authors used rigorous pre-treatment and screening protocols for inclusion of data into their "calibration curve" [*sic*], to minimise any

of the uncertainties that they believed remained in the coral data included within the IntCal04 curve (Reimer *et al*. 2004a; section 2.6.5, below). Uranium series data were obtained by multi-collector inductively-coupled plasma mass spectrometry (MC-ICPMS), which provides practical advantages over the TIMS method (Fairbanks *et al*. 2005; Chiu *et al*. 2006). The dataset itself is composed of 250 radiocarbon ages (representing 180 separate calendar ages), combined with 209 ^{234}U-^{230}Th ages. Although covering the majority of the radiocarbon dating range, there are several gaps present within the dataset, due to the lack of availability of suitable corals, which require resultant interpolation. Such notable gaps include those between 33,677 and 31,366 cal. BP, 29,540 and 26,136 cal. BP, and 17,580 and 14,685 cal. BP.

There are several potential problems associated with using corals for radiocarbon calibration. Firstly, it is difficult in practice to acquire fossil corals from the appropriate timeframe, both for logistical reasons, and the rare geological setting required for their preservation (Burr *et al*. 2004; Fairbanks *et al*. 2005). As with varved sediment records (section 2.5.4, below), there might be hiatuses present within the coral sequences. For example, Burr *et al*. (1998) describe three such hiatus events in their Vanuatu record, representing times at which the coral died off for some period, perhaps attributable to sudden changes in isostatic sea level, or changes in ambient water temperature. Secondly, corals are susceptible to diagenetic alteration or uranium exchange subsequent to skeletal growth. The formation of secondary calcite on subaerially-exposed aragonitic corals (which can generate both older or younger radiocarbon determinations; Reimer *et al*. 2006) is a particular problem, as is the presence in some instances of marine cements (Fairbanks *et al*. 2005), and potential organic contamination (Chiu *et al*. 2005). In order to avoid the sampling of corals that have been sub-aerially-exposed requires the avoidance of time intervals during which the sea level fell rapidly (faster than any concomitant tectonic depression at the site). Such conditions occurred immediately prior to the LGM, for example, and so a slightly biased

dataset (lacking in particular time periods) is produced. Finally, an over-riding issue with radiocarbon dating of corals is that, as with other organisms deriving their carbon from the ocean rather than directly from the atmosphere, a site-specific marine reservoir correction (ΔR) must be applied (section 2.2.1). However well this correction is defined from modern (pre-industrial) samples, or from comparison of older data overlapping the dendrochronologically-derived atmospheric radiocarbon calibration curve, the fact that this reservoir correction may have varied over the course of such records results in the incorporation of additional uncertainties in the datasets produced, which are hard to define.

2.5.3 Speleothem Records

Speleothems are re-precipitated carbonate deposits (including stalagmites, stalactites and flowstones) found in caves in limestone regions, and formed by de-gassing of CO_2 from cave seepage waters. As with corals, speleothems can be utilised for paired radiocarbon and ^{234}U-^{230}Th dates to provide radiocarbon calibration beyond the dendrochronological limits.

As with coral samples, speleothems must be carefully analysed for any post-depositional re-crystallisation or detrital contamination. Although not incorporating the marine reservoir effect, there is nevertheless an analogous reservoir offset generated through the incorporation of 'old' carbonate into the speleothem deposits from percolation of water through the host limestone (Genty *et al*. 1999). This 'old' carbonate is of geological age (i.e. contains minimal remaining ^{14}C), and therefore the proportion that this old carbonate contributes to the total carbonate of the speleothem is described as the 'dead carbon fraction' (DCF). The remainder of the precipitated carbon, which is close to equilibrium (within approximately ten years) with the contemporaneous atmospheric concentration (Beck *et al*. 2001), is primarily sourced from dissolved inorganic carbon (DIC), obtained as the water seeps through soil. As with the estimation of a site-specific marine reservoir correction, DCF

must be estimated through comparison of the radiocarbon data from speleothem samples with the existing calibration curve, or from observation of 'modern' values. In the absence of additional information, a necessary assumption of constant DCF over the speleothem's existence must be made, which, in reality, may be far from accurate (e.g. Genty *et al*. 1999), particularly during time periods of markedly differing climatic conditions. Changes in vegetation, hydrology, and geochemistry of the soil and unsaturated zone may all influence DCF (Genty *et al*. 1999).

Twenty paired ^{234}U-^{230}Th (α-counting) and radiocarbon (gas proportional-, β-counting; section 4.4) measurements of a stalagmite from the Cango Caves, South Africa, were presented by Vogel (1983) and Vogel and Kronfeld (1997), intermittently covering the last 50,000 years. This record demonstrated the large (> 5,000 'year' divergence of the conventional radiocarbon- and calendar timescales for the time period 45 to 35 cal. ka BP. However, the resolution of the record was very sparse, and the calendar age-scale uncertainties were relatively large due to the α-counting ^{234}U-^{230}Th technique implemented.

Beck *et al*. (2001) provided the first extensive, high resolution speleothem record for radiocarbon calibration, with a stalagmite record ('GB-89-24-1') collected from a submerged cave site in the Bahamas (Sagittarius Blue Hole, Grand Bahama), composed of 278 radiocarbon measurements, covering the period 45 to 11 cal. ka BP. The calendar timescale was provided by 81 ^{234}U-^{230}Th (TIMS) measurements (and necessary interpolation between these dated points), demonstrating a mean growth rate of 0.019 mm/year and a hiatus between 28 and 26 cal. ka BP. When compared to IntCal98 (Stuiver *et al*. 1998a; section 2.6.4, below) over the period 15.5 to 11.1 cal. ka BP, a reasonably constant DCF of 1,450 ± 470 (2σ) years (16.5 ± 4.7%, 2σ) was obtained. This value was therefore applied to radiocarbon data from the remainder of the record. A key finding of this study was highly

elevated (> 1000‰) and variable $\Delta^{14}C$ in the time period 45 to 33 cal. ka BP (and especially so for the period prior to 40 cal. ka BP).

Hoffmann *et al*. (2010) presented a second stalagmite record ('GB-89-25-3') from the same Bahamian cave as that of Beck *et al*. (2001), giving high resolution $\Delta^{14}C$ for the period 44 to 28 cal. ka BP. A constant DCF correction of 2,075 ± 540 (2σ) years (22.7 ± 5.9%, 2σ) was applied to this older section, as generated from comparison of the uppermost part of the same stalagmite with the IntCal04 dataset (Reimer *et al*. 2004a; section 2.6.5, below) over the period of overlap, 15 to 11 cal. ka BP. This relatively large DCF uncertainty value was the result of some "non-random structure" in the DCF-corrected stalagmite data, compared to IntCal04 (Hoffmann *et al*. 2010). ^{234}U-^{230}Th (MC-ICPMS) determinations were performed to derive the calendrical timescale: 35 from the uppermost section (15 to 11 cal. ka BP; mean growth rate 0.09 mm/year), and 44 in the lower section (mean growth rate 0.05 mm/year).

The newer stalagmite study of Hoffmann *et al*. (2010) also demonstrated errors in the older section (44 to 41 cal. ka BP) of the previously published Bahamian speleothem dataset (Beck *et al*. 2001), cited as being the result of analytical ^{14}C background subtraction issues. As a result, the more extreme $\Delta^{14}C$ shifts demonstrated by the original dataset were shown to be much smaller than previously suggested.

As well as the missing mid-section of GB-89-25-3, Hoffmann *et al*. (2010) noted a hiatus close to the top of the lower stalagmite section (from *circa* 27.7 ± 0.2 to 23.8 ± 0.2 cal. ka BP). The Cango Caves stalagmite (Vogel and Kronfeld 1997) also demonstrated a significant hiatus, covering the time period 17 to 7 cal. ka BP.

One final speleothem record noted here is the 'Arabian speleothem' of Weyhenmeyer *et al*. (2003) from Socotra Island in the Indian Ocean, off the Arabian coast. This record provided radiocarbon measurements between 55 and 42 cal. ka BP, with calendar ages

obtained by nineteen ^{234}U-^{230}Th ages and DCF (1,237 ± 300 years) estimated from variations in $\delta^{13}C$ values.

2.5.4 Varved Sediment Records

'Varves' are laminated sediments in which the deposited layers have been shown to represent an annual deposition sequence. The word 'varve', originally from the Swedish '*varv*', meaning 'revolution', 'circular', or 'in layers', was thus re-defined by Gerard de Geer (1912) as "an annual sedimentary layer". Although initially limited to pro-glacial laminations, the term 'varve' was later extended to incorporate all annually-laminated sediments, irrespective of the formation mechanism. Non-glacial varves are formed from the cyclic deposition of biogenic materials (such as diatom frustrules; e.g. Simola 1979) and/or minerogenic material (e.g. Calvert 1966), together comprising an annual sedimentary signal.

In general, varve formation requires marked seasonal climate (temperature and precipitation) variation, generating a cyclic succession of different physical, chemical, or biological processes within water bodies (both lacustrine and marine), or their catchments (Zolitschka 2007). The preservation of varves, once initially formed, requires anoxic sedimentary conditions to eliminate the potential for bioturbation of the sediments by benthic-dwelling organisms (Kato *et al*. 2004). Basal morphometry is also important in preventing disturbance of the deposited sediments through the action of the wind or currents (Hughen and Zolitschka 2007). Deep water bodies, with relatively flat basal topographies provide ideal conditions, whilst strong, seasonal, semi-permanent water stratification (meromixis) is also advantageous to varve formation in lake sediments (O'Sullivan 1983). Preservation of marine varves requires physical isolation of bottom waters, such as in deep fjords (e.g. Saanich Inlet, British Columbia, Canada; Blais-Stevens *et al*. 1997), or tectonic basins (e.g. the Cariaco Basin, Venezuela; Peterson *et al*. 2000; section 2.5.4d, below).

A varve chronology should only be established if the structure of the varve year- and underlying causal mechanisms of varve formation are clear (Zolitschka 2007; Kitagawa, forthcoming). As with tree-ring counting, varve counting is subject to the issues of missing layers (leading to under-counting), or multiple intra-annual layers (over-counting). If possible, replicate counts from multiple, contemporaneous sediment exposures/sediment cores should be undertaken to aid the identification of such issues, and help in estimating counting error. Hiatuses within the varve profile are particularly problematic, since they provide chronological gaps, which are hard to quantify. Varve chronologies only provide an absolute age scale if the annual layering continues through to the present day, otherwise 'floating' varve chronologies are produced and need to be tied to the absolute age scale by some other means. Today, varve counting is usually performed by either micro-stratigraphical (optical- and electron microscopy) analysis, or by quicker, automated image analysis techniques (Hughen and Zolitschka 2007).

Varved sediments provide an excellent archive for palaeoenvironmental studies because of the degree of precision enabled by such material (Fukusawa 1995; Walker 2005, p.136). Such applications include studies of: geochronology, palaeoclimate, vegetation change, sedimentation changes, anthropogenic processes (e.g. pollution studies), and recurrence intervals of natural hazards (such as floods, volcanic eruptions and earthquakes). Similarly, the annually-resolved, independent chronology provided by varves offers an ideal archive for extending the dendrochronological radiocarbon calibration curve (van der Plicht 2000a). Principal examples of the use of varves for radiocarbon calibration are introduced below, with the most extensive varved record for radiocarbon calibration produced to date, that of Lake Suigetsu, central Japan (Kitagawa and van der Plicht 1998a, 1998b, 2000), which is the principal study site of this DPhil thesis, described in considerably more detail in the following chapter, 3.

2.5.4a The Scandinavian Varve Chronology

The potential of varved sediments to extend the radiocarbon calibration curve was realised over 40 years ago (Olsson 1970; Tauber 1970), with the lengthy Scandinavian varve chronology seen as offering a prime opportunity to provide such a dataset. As the Fennoscandian ice sheet retreated during the termination of the Weichselian (the Last Glacial of northern Europe), glacio-lacustrine clastic varves formed in the pro-glacial 'Baltic Ice Lake', close to the ice margins. The varves consist of alternating light, sandy layers, and darker, clay layers. The former, larger particles were preferentially deposited through spring and summer ice melt, whereas the latter, finer particles remained in suspension, before settling during the winter months whilst the pro-glacial lake was frozen over (Wohlfarth *et al*. 1995). As the ice retreated further northwards, additional varve sequences were deposited, mainly as deltaic sediments in estuaries of large rivers (Tauber 1970; Wohlfarth *et al*. 1994), and varve formation continues up to the present day (Cato 1985). Through matching of distinct horizons in adjacent varve sequences, a master Scandinavian varve chronology was established. Following on from the pioneering work of de Geer (1912) in this region, numerous revisions of the original varve chronology have been made (e.g. Cato 1985, Strömberg 1985). The entire sequence, based upon matching of varve sequences across numerous sites, was believed to represent the last ≈ 13,300 years continuously (Wohlfarth *et al*. 1993).

Initial comparison of radiocarbon determinations associated with the varve chronology (via synchronisation of the climate signal from other sites), demonstrated that there must be errors in the overall chronology (Fromm 1970). With the development of AMS (section 4.4) allowing significantly smaller samples to be reliably radiocarbon-dated, terrestrial plant macrofossils extracted directly from the varved clays (rather than the more tenuous linkages via palynological association) were enabled (Björck *et al*. 1995). Additionally, these

measurements from the Swedish varves also demonstrated the offset between radiocarbon ages of macrofossil samples and the non-carbonate fraction of bulk sediment (i.e. a non-'hard water' lake reservoir effect), of 200 to 400 years (Wohlfarth *et al*. 1993). This reservoir effect is caused by re-deposition of older organic carbon material, as well as direct, dissolved carbon with a long residence time in the lake (and melting ice) waters.

More recent comparison with alternative, dendrochronological- and ice core records, via radiocarbon wiggle-matching (section 5.3.2) or climatic synchronisation, suggests that several hundreds of varve years remain missing from the composite varve chronology, both in the older (Björck *et al*. 1996; Wohlfarth 1996) and younger (Wohlfarth *et al*. 1997) time periods. These methods suggest at least 800 missing varves in the early Holocene, ≈ 500 more missing varves between the Bølling/Older Dryas and Younger Dryas/Holocene boundaries, and a further ≈ 700 missing varves during the Bølling, such that the total offset between the Scandinavian varve chronology and real, calendar time is > 2,000 years for the oldest part of the chronology (Wohlfarth and Possnert 2000). It is most likely that these errors lie in less secure correlations between separate, individually-reliable sections of the varve chronology (Wohlfarth and Possnert 2000). Contrary to previous publications, individual, robust sections of the Scandinavian varve chronology must, therefore, be regarded as only providing floating varve sequences (Wohlfarth and Possnert 2000).

2.5.4b Central European Varve Chronologies

Amongst the first attempts to extend the calibration curve through direct AMS dating of terrestrial macrofossils identified from within varved lake records were those of the Soppensee (Switzerland) and Holzmaar (Germany) sediment profiles (Hajdas *et al*. 2000). Soppensee provides a floating varve chronology, which was tied to the dendrochronologically-derived calibration curve by wiggle-matching (section 5.3.2) over the

period ≈ 10,000 to 7,000 BP of 50 AMS radiocarbon determinations, obtained from terrestrial macrofossils identified from within the varved sediment profile. A further 31 radiocarbon determinations extended this calibration dataset back into the Late Glacial (Hajdas *et al*. 1993). Agreement of radiocarbon data over the first ≈ 3,000 years of the Holocene remains good, but there are problems evident in the chronology of the Younger Dryas period (Hajdas *et al*. 1995b, 2000). Corrections, necessarily applied for unlaminated sections within the sediment profile, had been initially made by assumptions of sedimentation rate (Hajdas *et al*. 1993), but more recent comparative data suggests that this correction underestimated the missing varves by a further 500 to 600 years (Hajdas *et al*. 2000).

Unlike Soppensee, the Holzmaar sediments are laminated through to the present, but comparison of the radiocarbon dataset (from AMS-dated terrestrial macrofossils) with the calibration curve demonstrated the need for an additional 878 varve years to be added between 3,838 and 2,000 cal. BP (Hajdas *et al*. 1995c). The remainder of the Holocene demonstrates good agreement with the tree-ring calibration data (Hajdas *et al*. 1995c). As with Soppensee, however, additional varves were seemingly missing in the Younger Dryas, with Leroy *et al*. (2000) suggesting a correction of 320 varve years beyond 12,025 cal. BP, based upon synchronisation of palynological data, a value that Hajdas *et al*. (2000) suggests is still somewhat conservative based upon comparison of the Soppensee radiocarbon data with IntCal98 (Stuiver *et al*. 1998a; section 2.6.4, below).

A further, significant central European varve chronology exploited for radiocarbon calibration was provided by Goslar *et al*. (1989, 1992, 1993, 1995, 2000a, 2000b; Hajdas *et al*. 1995a), utilising terrestrial plant macrofossils retrieved from the varved sediments of Lake Gościąż, central Poland. The floating 9,662 (± 90) varve year chronology covers the time period *circa* 13,000 to 3,000 cal. BP (Goslar *et al*. 1992, 1995), and is replicated across ten separate sediment cores, but is separated into four segments by three hiatus events. Although

aided by this ‘varve-to-varve synchronisation’ across sediment cores, the accuracy of the combined varve chronology is ultimately limited by layers that are unclear across all sediment cores. The annual lamination was confirmed by observation of seasonality of deposition of diatoms, authigenic calcite (summer deposition) and organic detritus (autumn/winter deposition; Goslar *et al*. 1992). The plant macrofossils themselves were “rather rare” and “small”, necessitating the mixing of samples from adjacent varve years for AMS dating (Goslar *et al*. 1993). The sampling resolution was therefore not optimal, with sediment combined from samples containing approximately 100 varves (Hajdas *et al*. 1995a). One hundred radiocarbon determinations were thus obtained for the time period 12,950 to 10,500 cal. BP (Goslar *et al*. 1995, 2000a), with the absolute age of the floating varve chronology obtained through wiggle-matching of the Lake Gościąż radiocarbon determinations (Goslar and Madry 1998) to the dendrochronological calibration curve (Kromer and Spurk 1998).

The Gościąż record was supplemented by 56 additional radiocarbon determinations from seven separate sediment cores collected from the partially-varved Lake Perespilno, eastern Poland (Goslar *et al*. 2000a, 2000b). Perespilno is annually-laminated for ≈ 3,100 years, separated into two sections by a hiatus event, ≈ 10 cm below the onset of the Younger Dryas (Goslar *et al*. 2000b). The older section covers the time period 14,455 to 13,645 (± 50) cal. BP, as attained by wiggle-matching to the coral data of Edwards *et al*. (1993) and Bard *et al*. (1996, 1998). In both Lakes Gościąż and Perespilno, only large, non-mechanically-damaged or decomposing macrofossil samples were selected for dating, so as to minimise the probability of dating re-worked material (Goslar *et al*. 2000b).

2.5.4c Palaeolake Lisan

A sedimentary formation of deposits from Palaeolake Lisan (the Last Glacial precursor of the modern Dead Sea) represents the time period of *circa* 70.0 to 17.4 cal. ka BP (Haase-Schramm *et al*. 2004). The formation consists of three distinct units, coinciding with each of marine isotope stages- (MIS) 2 to 4 (Schramm *et al*. 2000). Both the upper and lower units demonstrate annual lamination (≈ 0.5 to 1.0 mm thickness per year), consisting primarily of authigenic, inorganic aragonite (precipitated during dry seasons) and fine, silty detritus (during wet seasons). The middle unit is composed mostly of sand and clay layers, reflecting lower lake water conditions. Initially, the calendar age scale of these sediments was provided by ^{234}U-^{230}Th (TIMS) dating of the aragonitic layers (Schramm *et al*. 2000). This U-series dating is more problematic than with the dating of corals, since there is an increased likelihood of non-authigenic U and Th being present, which needs to be corrected for (Stein *et al*. 2000; Haase-Schramm *et al*. 2004). Additionally, Prasad *et al*. (2009) provided a varve-counted chronology over the time period 22.0 to 17.4 cal. ka BP, with Bayesian wiggle-match modelling (section 5.3.2) to IntCal04 (Reimer *et al*. 2004a; section 2.6.5, below) suggestive of ≈ 79 'missing years' across ≈ 3,000 cal. years of this record (i.e. < 3% 'error').

Similar to the DCF correction of the speleothem records (section 2.5.3, above), the radiocarbon-dated Lake Lisan calcium carbonate samples required a reservoir correction (due to the lake hardwater effect; section 2.2.1, above). This correction was determined by Schramm *et al*. (2000) to be ≈ 1,000 radiocarbon years, based upon analysis of the modern lake water reservoir age of the Dead Sea, a value that was updated to ≈ 1,200 radiocarbon years (Haase-Schramm *et al*. 2004) by comparison of older radiocarbon measurements with calibration data from coral records. However, high resolution data from the youngest part of the record (36.0 to 17.4 cal. ka BP; van der Borg *et al*. 2004; Prasad *et al*. 2009) suggested that the DCF at the site might actually have varied considerably, with values of between

≈ 200 and 2,000 radiocarbon years obtained, seemingly related to varying lake water levels through time. Unfortunately, the realisation of such a significant, temporally variable DCF correction makes the Lake Lisan record impractical for producing high precision radiocarbon calibration data.

2.5.4d Cariaco Basin Marine Sedimentary Record

One of the most important archives for extending the radiocarbon calibration curve back beyond the limits of the dendrochronological data is provided by the partially varved marine sediment sequence of the Cariaco Basin (sited in the tropical North Atlantic on the northern continental margin of Venezuela). The bathymetry is such that shallow (< 146 m) sills protect the Cariaco Basin from the open Caribbean Sea, enabling basal water anoxia, which facilitates varve preservation (Hughen *et al*. 1998a). These varves are composed of alternating light- (plankton-rich) and dark (mineral-rich) layers. The former are associated with winter and spring trade-wind-induced upwelling, and the resultant increased bio-productivity thus induced; the latter are composed of terrestrial material from summer and autumn run-off from the rainy season of northern South America (Peterson *et al*. 1991, 2000; Hughen *et al*. 1996a). The varved section of the Cariaco Basin sediments represents the time period from 14,553 to 9,051 cal. BP (≈ 12,700 to 8,200 BP), with less distinct lamination continuing above (Hughen *et al*. 1998b). Radiocarbon dates were obtained on mono-specific planktonic foraminifera (*Globigerina bulloides*) samples, hand-picked from 1.5 to 2.0 cm thick (10 to 15 varve year) sediment sections (Hughen *et al*. 1998a). An average marine reservoir correction of 420 years was subtracted from all radiocarbon dates (Hughen *et al*. 1996a). The floating varve chronology was wiggle-matched (section 5.3.2) to the absolute timescale provided by the dendrochronological dataset of Kromer and Becker (1993; utilised by Hughen *et al*. 1998b).

Since the annually-resolved laminae at Cariaco are limited to only a short section of the sediment sequence, the chronological control for the majority of the Cariaco radiocarbon calibration curve was achieved through 'tuning' of the Cariaco palaeoclimatic record with those of the annual layer-counted chronologies of: (i) the Greenland Ice Sheet Project 2 (GISP2) ice core (Meese *et al*. 1997; utilised by Hughen *et al*. 2004b); and (ii) the Hulu cave (China) speleothem ^{234}U-^{230}Th record (Wang *et al*. 2001; utilised by Hughen *et al*. 2006). The Cariaco sediment parameter utilised for this purpose was 'grey-scale' (550 nm wavelength relative reflectance), with the thickness of the lighter laminae interpreted as being a proxy for upwelling intensity, and thereby North Atlantic trade-wind intensity (Hughen *et al*. 1996b). Of course, the matching of the Cariaco dataset to these alternative records results in the loss of independence in the former record, and introduces the circular assumption of contemporaneity of palaeoclimatic events across these widespread geographical ranges, which could, in reality, be time transgressive. Additional calibrated age scale uncertainties are therefore present in the Cariaco radiocarbon calibration datasets through both the matching of the respective timescales, as well as the original uncertainties present within the GISP2 and Hulu Cave timescales themselves. The former matched timescale has uncertainties of ±2% at 39.9 cal. ka BP, increasing to ±5% at 44.6 cal. ka BP (Meese *et al*. 1997). The latter matched timescale is based on 59 ^{234}U-^{230}Th dates from five individual stalagmites, two of which having the additional age control of annual banding (Wang *et al*. 2001). The quoted 1σ uncertainties on the Hulu Cave timescale are ±50 years at 10 cal. ka BP and ±50 years at 50 cal. ka BP, i.e. substantially more precise than with those for the calendar timescale produced from the previous match to GISP2.

The full Cariaco Basin calibration datasets (Hughen *et al*. 2004b, 2006) provide high resolution data back to 50,000 cal. BP (280 AMS radiocarbon determinations in Hughen *et al*. 2004b, expanded to 467 determinations by Hughen *et al*. 2006).

Support for the temporal invariance of the 420 year marine reservoir correction applied is provided by coherence between the Cariaco Basin dataset and the German pine tree-ring record (Hughen *et al*. 2006), though the floating extension to this tree-ring record (Kromer *et al*. 2004) suggests that this may not have been the case back into the Allerød.

2.5.5 Non-Varved Sediment Records

Although lacking in the annual temporal resolution provided by varved sediment records, non-varved sediments have also been utilised for calibration of the radiocarbon timescale – one such example being the non-varved portion of the Cariaco Basin sediment profile (Hughen *et al*. 2004b, 2006), described above. In the absence of a layer-counted age scale, the calendar age of such sediments must be derived by alternative means.

Voelker *et al*. (1998, 2000) presented relatively high resolution radiocarbon calibration data (80 radiocarbon determinations) between 53.3 and 11.4 cal. ka BP, obtained from two North Atlantic (Iceland and Norwegian Seas) marine sediment cores. The calendar timescale was derived from cross-correlation of stable isotope ratios of planktonic foraminifera (*Neogloboquadrina pachyderma*) from the marine cores with the GISP2 ice-core (Meese *et al*. 1997) $\delta^{18}O$ record (both representing proxies of palaeo-temperature). Such chronological synchronisation requires the assumption that the reconstructed climate variable represents the same climatic events (assumed for these two sites to be propagated through the North Atlantic by THC), and that the climatic events occurred contemporaneously at the two sites. Regrettably, these high latitude North Atlantic sites exhibit large, rapid variations in the local marine reservoir correction (Voelker *et al*. 2000), rendering their data unsuitable for radiocarbon calibration curve construction.

A similar, non-varved sediment core (‘MD95-2042’) for radiocarbon calibration purposes was provided by Bard *et al*. (2004a, 2004c) and Shackleton *et al*. (2004), from the

North Atlantic Iberian margin. Samples for radiocarbon dating were obtained from monospecific planktonic foraminifera (*G. bulloides*), with ≈ 2,000 shells in each sample. A local sea surface marine reservoir age of 500 ± 100 years was applied, based upon 'modern' (pre-bomb) mollusc measurements, and a broader assessment of the hydrological conditions at the site. The calendar age chronology was obtained via tuning of climate proxies to both GISP2 (Meese *et al*. 1997) and GRIP (Johnsen *et al*. 2001) Greenland Summit ice-cores (using $U_{37}^{K'}$ alkenone data from MD95-2042 and $\delta^{18}O$ from the ice cores), shown by modelling to vary synchronously between both areas. Being geographically situated away from the higher latitude zones of high and varying marine reservoir changes (Bard *et al*. 2004a, 2004c), the reservoir-corrected radiocarbon data should be far more reliable than those of the Nordic Seas, described above (Voelker *et al*. 1998, 2000).

2.5.6 Summary of the Advantages and Disadvantages of the Different Palaeoenvironmental Archives Utilised for Radiocarbon Calibration

As has been described through section 2.5, there is a variety of potential natural archives from which past changes in atmospheric radiocarbon concentration ($\Delta^{14}C$) can be reconstructed. In *sensu stricto*, a calibration curve should be composed of radiocarbon data obtained directly from the reservoir of interest (i.e. for the majority of users who date terrestrial material, an atmospheric source), and with an independent calendar age that is known exactly (Bronk Ramsey *et al*. 2006; Reimer *et al*. 2009). Such data are only truly demonstrated by the absolutely-, dendrochronologically-dated tree-ring archives, which provide the highest quality calibration data. However, despite decades of research, the scarcity of fossil trees dating from the Last Glacial period means that dendro-calibration data

only presently extend to 12,593 cal. BP (Schaub *et al*. 2008b), representing approximately the final quarter of the radiocarbon dating age range.

Beyond tree-rings, calibration has been "difficult and contentious" (Bronk Ramsey *et al*. 2006; Mellars 2006a, 2006b; Turney *et al*. 2006; Blockley and Housley 2009), with significant disagreements exhibited between certain datasets. Although there is potential for extending the dendro-calibration curve further back in time, particularly through use of the Southern Hemisphere records (Turney *et al*. 2007; Hua *et al*. 2009), other archives must necessarily be utilised at present to extend the radiocarbon calibration curve across the entire range of the radiocarbon method.

Whilst extremely useful, the above marine-derived datasets (most extensively demonstrated by Hughen *et al*. 2004b, 2006 and Fairbanks *et al*. 2005) provide information on radiocarbon calibration in the oceans, rather than the atmosphere, and so these data must necessarily be corrected for the marine reservoir effect (section 2.2.1) if the contemporaneous atmospheric radiocarbon concentration ($\Delta^{14}C$) is to be approximated from these archives. As has already been noted, the marine reservoir effect is known to vary both temporally and spatially (Reimer and Reimer 2001) and so such approximations for $\Delta^{14}C$ therefore contain an additional tier of uncertainty. Similarly, speleothem data (demonstrated most extensively by Beck *et al*. 2001 and Hoffmann *et al*. 2010), require a reservoir correction (for 'dead carbon fraction', DCF), which, like the marine correction, necessitates the assumption of temporal invariance, and therefore incorporates similar uncertainties.

Errors in the absolute, dendrochronological age scale are assumed to be negligible (on the order of only one to two years; McCormac *et al*. 2004), however, as exemplified in section 2.5.1 (Kromer *et al*. 1996), errors in cross-matching are certainly possible. Friedrich *et al*. (2004) note the increased tendency of pines to miss occasional rings, which therefore requires higher levels of replication than with the oak chronologies. Increased replication

leads to increased confidence in the dendro- data, for example 96% of individual calendar years within the lengthy Hohenheim oak chronology is represented by at least 20 separate, cross-dated trees, and the central European pine chronology demonstrates a mean replication of 30 trees per year (Friedrich *et al*. 2004). The only confirmation of absolute dendrochronology is external replication by significant cross-dating of independently-derived chronologies (Becker 1993), or the identification of specific volcanic events within the dendrochronologies that can be tied to independently-dated eruptions, or correlated to alternative chronologies via tephra.

Alternative datasets based upon incremental layer counting (varves, or ice cores) incorporate correlated uncertainties, produced from counting errors or deposition modelling uncertainties. Since their uncertainties are cumulative, total uncertainty in the calendar age at the older end of the timescale is significantly greater (in the absence of any, independent age verification). Such methodologies are generally reliable for providing relative chronological information over more temporally-limited sections of the total chronologies, however. Wiggle-matching data to the pre-existing absolutely-dated calibration curve additionally incorporates correlated error into its data points.

The problems related to the calendar age scales of varved records, and particularly the presence of hiatuses within these sequences, has limited the utilisation of such records for radiocarbon calibration, with a short period of the Cariaco Basin record being the only varved archive represented in the present international consensus calibration curve ('IntCal09'; Reimer *et al*. 2009; section 2.6.9, below). To reduce the uncertainty in the calendar timescale (and to aid identification of hiatuses), sediment- (or ice-) core records should be produced from multiple, replicate cores from a site, ideally with independent tie points (such as tephra) to alternative, comparison chronologies. Likewise, substantiation for the absence of hiatuses in coral or speleothem records is preferable, via measurement of alternative material from the

site. However, larger-scale events that have influenced the entire dataset of a given site (e.g. lake-wide hiatuses in sediment profiles derived from large, tectonically-driven turbidite events, or isostatic sea level change that has interrupted the growth of coral colonies at a site) would not be identified by such an approach, and comparison with data from alternative, more distant, sites would be required for the identification and quantification of such gaps.

A specific issue related to the radiocarbon dating of macrofossils retrieved from varved sediments, rather than direct dating of the contributory material forming the varves themselves (e.g. the aragonite laminae of Palaeolake Lisan), is that one can never be certain that the dated macrofossil samples reflect the concomitant atmospheric radiocarbon concentration at the time that the specific varve was deposited (Goslar *et al*. 1992). I.e., the macrofossils might reflect an inbuilt age as compared to the calendar age that they are supposed to represent.

Despite advances in the identification and counting of varves, varve counting remains a somewhat subjective process, dependent upon varve type, quality, and preservation, as well as additional human complications such as analyst bias, or availability of resources (Kitagawa, forthcoming). Counting by multiple analysts and multiple techniques, on cross-dated cores, with a mechanistic understanding of varve formation is necessary if reliable varve count chronologies are to be obtained. Even then, it may not be possible to remove varve count errors entirely, with the vagaries of less clearly deposited/preserved laminae providing one crucial problem, as well as the ever-present risk of sedimentary hiatuses described above (Kitagawa, forthcoming).

Having discussed these drawbacks of varve-counted archives, however, it must be emphasised that lacustrine varves nevertheless have the potential to provide a continuous record of direct atmospheric radiocarbon concentration across the entire span of the

radiocarbon method. Lake Suigetsu provides such an archive, and is described thoroughly in the following chapter.

Transferred timescales are "not ideal" (Reimer *et al*. 2009). Those that are applied require a fully understood physical mechanism linking the respective proxy climate signals, but nevertheless include circularities pertaining to assumptions of contemporaneous regional climate, if palaeoclimatic proxies are utilised for this purpose. Chronologies built upon such assumptions incorporate propagated errors from this matching process, as well as uncertainties present in the original correlative timescale. Reconstructed $\Delta^{14}C$ values may be altered dramatically if the chronology of the correlated record is subsequently amended (Hoffmann *et al*. 2010, citing the Cariaco Basin dataset of Hughen *et al*. 2006). Additionally, interpolation between the matched chronological tie-points may distort the true amplitude and shape of the calibration record produced (Chiu *et al*. 2007).

Both marine coral- and speleothem archives can be dated by direct radiometric (i.e. ^{234}U-^{230}Th) means, which provide independent uncertainties for each measurement of the calendar age scale (Chiu *et al*. 2006). (This is not the case if uranium series dating is not obtained at the same temporal resolution as radiocarbon analyses, however, since the calendar timescale will resultantly incorporate additional uncertainties if interpolated between more temporally distant ^{234}U-^{230}Th measurements; e.g. Beck *et al*. 2001.) However, both uranium series- and radiocarbon dating methods require an assumption of closed system behaviour (Yokoyama *et al*. 2000), and must not have suffered from secondary alteration, mineral growth, or organic contamination.

Corals, as with alternative archives that have derived their carbon from the ocean, rather than directly from the atmosphere, incorporate a marine reservoir effect, which must be accounted for. These corrections can be made using modern (pre-industrial) data, or by comparison of the dataset through time as compared with a wholly reliable record of

atmospheric radiocarbon concentration (i.e. the terrestrial tree-ring record). The latter approach is arguably preferable, as it better demonstrates the range of temporal variability of the reservoir offset at a given site. However, extrapolation of comparison with the tree-ring data (mostly from the Holocene) will not necessarily account for the full range of variation across the dramatically different climatic régime of the Last Glacial. Strictly speaking, short-term fluctuations in local marine reservoir make individual marine-derived data only fit for their own sites, however, uncertainty of reservoir corrections does become less significant further back in time, because of the reduced proportional effect of potential errors in this correction as compared to the overall measurement uncertainty of the raw radiocarbon data (especially beyond ≈ 35,000 cal. BP; Chiu *et al*. 2007).

$\Delta^{14}C$ reconstructed from marine archives represents a 'smoothed' (time-integrated) signal, as compared to direct atmospheric archives, due to the residence time of ^{14}C in ocean waters. Additional smoothing of marine sediments might result from bioturbation where the sediment/water interface is not anoxic. This would further reduce the temporal resolution possible for radiocarbon calibration data from such records. A similar temporal smoothing effect is also achieved through sampling of material for radiocarbon dating from across a range of calendar years (such as the decadal or bidecadal determinations from tree-rings, the integrated terrestrial macrofossil samples combined across varves by, *inter alia*, Hajdas *et al*. 1995a, or the integrated foraminifera samples across the Cariaco Basin varves by Hughen *et al*. 1998a).

As with correction for the marine reservoir effect, DCF corrections of speleothems are achieved through comparison with modern (pre-bomb) radiocarbon determinations (e.g. Genty *et al*. 1999), comparison with data overlapping the dendro-derived portion of the calibration curve (e.g. Beck *et al*. 2001), or estimation through $\delta^{13}C$ modelling (e.g. Weyhenmeyer *et al*. 2003).

Across all of the potential archives, there are increased problems at the older end of the timescale, with more marked effects of ^{14}C contamination from more modern carbon sources due to the extremely low residual ^{14}C concentration present in samples (Bard *et al*. 2004b; section 4.3.1). Furthermore, there are increased uncertainties and errors with the calendar timescale, as a result of recognised/unrecognised hiatuses, cumulative counting errors, ambiguities in cross correlations, diagenetic alterations etc.

The problems of individual datasets can lie in both the absolute age scale, and the degree of fidelity with which archives represent the concomitant atmospheric carbon reservoir. Ultimately, however, agreement in findings obtained by differing methods is needed to demonstrate credibility in the calibration data produced (Schramm *et al*. 2000).

2.6 The International Consensus Radiocarbon Calibration Curve, IntCal

In response to the many differing calibration datasets produced over the last three decades or so, the radiocarbon dating community has produced an 'international standard' calibration curve, enabling consistent, meaningful intercomparison of calibrated radiocarbon dates. IntCal09 (Reimer *et al*. 2009) is the latest incarnation of this international consensus calibration programme, and builds upon the previous IntCal04 (Reimer *et al*. 2004a) and IntCal98 (Stuiver *et al*. 1998a) calibration models. In *sensu stricto*, only this international consensus dataset should be referred to as 'the calibration curve', with alternative calibration datasets representing 'comparison curves' (van der Plicht 2000b; van der Plicht *et al*. 2004; Bronk Ramsey *et al*. 2006). This recent convention, as well as the very purpose of IntCal, has been adopted to clarify to users of radiocarbon data just how to calibrate their data to the calendar age scale, given the concurrent state of knowledge of the radiocarbon dating community. The data included within the consensus calibration curve are carefully screened and statistically robust, providing a clear, single dataset with which radiocarbon users can

calibrate their data (Reimer *et al*. 2009). The evolution of the calibration curve (described chronologically below) represents the joint efforts of many laboratories, and is ratified by the international radiocarbon dating community. The fact that Fairbanks *et al*. (2005) released their own, "stand alone coral calibration curve" was not well received by the IntCal group (Reimer *et al*. 2006), since this demonstrated exactly the kind of problems that the IntCal group was set up to prevent (Reimer *et al*. 2004a).

2.6.1 The 1982 Calibration Curve

In 1982, Klein *et al*. published "the first in a series of 'consensus' calibrations, [to be] updated as warranted by improvements in the database". This calibration dataset comprised 1,154 radiocarbon determinations over the period 8,000 to 0 cal. BP, principally obtained from dendrochronologically-dated bristlecone pine and sequoia samples, and updating previously published datasets produced from the individual contributing laboratories. All measurements were obtained on integrated samples of 20 contiguous tree-rings, or fewer, so as to minimise any resultant attenuation of any short-term $\Delta^{14}C$ variations.

2.6.2 The 1986 Calibration Curve

The internationally-ratified 1986 calibration curve (Stuiver and Reimer 1986) consisted of bidecadal-resolution, dendrochronologically-dated (Irish, German and US) tree-ring samples over the time period back to 4,450 cal. BP (Stuiver and Pearson 1986; Pearson and Stuiver 1986). A number of other records were used to extend this dataset back to 9,160 cal. BP, including those of Linick *et al*. (1985; German oak data between 9,149 and 7,169 cal. BP), Kromer *et al*. (1986) and Stuiver *et al*. (1986a; German oak and US

bristlecone pine data between 9,157 and 7,179 cal. BP), and Linick *et al*. (1986; US bristlecone pine data between 8,504 and 8,034 cal. BP and between 7,770 and 7,300 cal. BP).

2.6.3 The 1993 Calibration Curve

In 1993, the internationally-ratified calibration curve was extended to cover the last 22,000 cal. years (Stuiver and Reimer 1993). This dataset comprised the bidecadal dendrochronological data of Stuiver and Pearson (1993) and Pearson and Stuiver (1993) over the last 8,000 cal. years. Further back in time, these data were supplemented by the bristlecone pine data of Linick *et al*. (1986), and the German oak data of Linick *et al*. (1985), Kromer *et al*. (1986) and Kromer and Becker (1993). Beyond the 11,390 cal. BP limit of these dendrochronological data, the marine corals data of Bard *et al*. (1993) were utilised (with an assumed 400 year marine reservoir correction applied), extending back in time to 21,950 cal. BP.

Additionally, Stuiver and Braziunas (1993a) provided a marine calibration dataset (for a theoretical, 'global average' ocean signal), which, back to 11,400 cal. BP, was produced through application of an ocean-atmosphere box model (adapted from Oeschger *et al*. 1975), using the tree-ring data as the input.

2.6.4 IntCal98

The IntCal98 calibration curve (Stuiver *et al*. 1998a) was the first publication to officially use the 'IntCal' title. Decadally-averaged tree-ring data (provided by: Kromer *et al*. 1986; Pearson *et al*. 1993; Vogel and van der Plicht 1993; Kromer and Spurk 1998; McCormac *et al*. 1998a, 1998b; and Stuiver *et al*. 1998b) were used to build the calibration curve back to 11,855 cal. BP. These were supplemented by the coral data of Bard *et al*.

(1990a, 1993, 1996, 1998), Edwards *et al*. (1993), and Burr *et al*. (1998), which extended these calibration data back to the 24,000 cal. BP limit of IntCal98 (although, the data were sparse before 15,585 cal. BP). The varved section of the Cariaco Basin marine sediment record (Hughen *et al*. 1998b) was used to add credence to the younger portion of the purely coral-derived dataset (11,700 to 14,500 cal. BP). The lack of agreement between datasets beyond 24,000 cal. BP at the time of publication precluded extension of the radiocarbon calibration curve further back in time (van der Plicht *et al*. 2004).

Rather than using the marine reservoir corrections provided by the original authors of the individual contributing sampling sites (i.e. 300 years for Tahiti and Mururoa, and 400 years for Barbados, Bard *et al*. 1998; and 400 years for Papua New Guinea, Edwards *et al*. 1993), however, Stuiver *et al*. (1998a) applied a uniform (temporally variable) correction across the entire tropical ocean (i.e. 500 years for samples older than 11,000 cal. BP, and 400 years for younger samples). Such an assumption was criticised by Goslar *et al*. (2000b), for example, and was not adopted for the succeeding IntCal04 (Reimer *et al*. 2004a) calibration curve (below).

2.6.5 IntCal04

The IntCal04 calibration curve (Reimer *et al*. 2004a) was explicitly provided for Northern Hemisphere, terrestrial radiocarbon age calibration, with sister curves 'Marine04' (Hughen *et al*. 2004a; section 2.6.6, below) and 'SHCal04' (McCormac *et al*. 2004; section 2.6.7, below) for marine- and Southern Hemisphere calibration, respectively.

The IntCal04 calibration curve itself extended back to 26,000 cal. BP, and was composed of high resolution, dendrochronologically-dated tree-ring samples through the period 12,410 to 0 cal. BP (Friedrich *et al*. 2004). Before this time, the tree-ring data were supplemented by marine records back to the 26,000 cal. BP IntCal04 limit. These marine data

were provided by corals (to 26 cal. ka BP; Bard *et al*. 1998; Burr *et al*. 2004; Cutler *et al*. 2004; Fairbanks *et al*. 2005) and the varved portion of the Cariaco Basin marine sediments (to ≈ 14.7 cal. ka BP; Hughen *et al*. 2004b), corrected for site-specific (temporally invariant) marine reservoir offsets. Beyond this 26,000 cal. BP limit, disparities between the individual radiocarbon datasets (including that of the initial Lake Suigetsu study; Kitagawa and van der Plicht 1998a, 1998b, 2000) were so substantial (at the time of IntCal04's publication) that no calibration data were included prior to this time (van der Plicht *et al*. 2004).

Strict quality assurance protocols were applied by the IntCal working group (Reimer *et al*. 2002) to determine those datasets that were suitable for inclusion into the consensus calibration curve. Such criteria included the necessity for reliably quantified uncertainties in both radiocarbon- and calendar timescales. Specific selection criteria for individual archive types included:

- tree-rings: dendrochronological dating with robust cross-checking;
- aragonitic corals: a < 1% calcite cut-off, assessed by X-ray diffraction (XRD) measurement; a realistic uranium concentration; belief in 'closed-system' behaviour; a site-specific marine reservoir correction, with uncertainty (and, ideally, minimal temporal variability);
- varve-counted chronologies: replicate sediment coring to limit the potential for hiatuses; replicate counts performed by 'experienced individuals'; ideally, a multi-proxy approach to varve counting; confirmation of the chronology through independent means (e.g. tephra, or radiometric methods); minimal potential for re-working of material or delayed transport to deposition (i.e. minimal inbuilt age);
- where calendar age scale is derived from correlation to a secondary site, it is critical to identify the physical (climatic/ocean circulation) mechanism linking the respective proxy data of the two sites.

The contributing datasets that passed these selection criteria were combined statistically using a Bayesian random walk model (Buck and Blackwell 2004). This model reduced the overall scatter around the 'true' calibration curve, producing a more 'smoothed' curve as compared to IntCal98.

2.6.6 SHCal04

Minimal intra-hemispheric radiocarbon offsets make application of the calibration curve much more useful than if many, separate, regional curves were required. However, as identified in section 2.2.3, the atmospheric radiocarbon concentration of the Southern Hemisphere (SH) does differ from that of the Northern Hemisphere (NH). Differences in the structural form of calibration data from the respective hemispheres mean that it is preferable for high precision SH calibration to have a specific calibration curve produced directly from SH samples, rather than simply applying an assumed correction from the NH calibration curve (McCormac *et al*. 1998a, 2002; Hogg *et al*. 2002; Zimmerman *et al*. 2010). SHCal04 (McCormac *et al*. 2004) is this SH-specific atmospheric calibration curve, produced alongside IntCal04, and extended to 1,000 cal. BP based upon SH dendrochronologically-dated samples. Beyond 1,000 cal. BP, back to the 11,000 cal. BP limit of SHCal04, a modelled correction to the NH (IntCal04) dataset was, nevertheless, applied. The inter-hemispheric offset in the radiocarbon concentration applied varies over time between 8 and 80 radiocarbon years (≈ 1 to 10‰; McCormac *et al*. 2004). Rather than applying a simple average correction, SHCal04 utilised a random effects model (Buck and Blackwell 2004), which accounted for the potential variation of this offset through time. The modelled offset only varied between 55 and 58 years, but the uncertainty increased from ±7.9 radiocarbon years at 1,000 cal. BP to ±25 at 11,000 cal. BP (McCormac *et al*. 2004).

At the time of writing, SHCal04 remains the most up-to-date SH calibration curve, but does not extend further back in time beyond 11,000 cal. BP due to potentially heightened inter-hemispheric offsets (due to larger scale alterations of the respective carbon reservoirs back into the Late Glacial), which would dramatically increase the uncertainties of reconstructed SH $\Delta^{14}C$ if based upon corrected values from the concomitant NH. It should also be noted that additional inter-hemispheric comparison data (Hogg *et al*. 2009) suggest that the mean offset value applied for SHCal04 might be an over-estimation, with their data (and other datasets: McCormac *et al*. 2002; Zimmerman *et al*. 2010) suggesting more likely mean offsets of between 23 and 41 years. A tentative, as yet not formally-ratified, extension to the SH calibration dataset has recently been provided by Zimmerman *et al*. (2010) based upon dendrochronologically-dated Tasmanian Huon pine, extending back to 2,120 cal. BP.

2.6.7 Marine04

As with the 1993 and 1998 consensus calibration curves above, IntCal04 was produced alongside a separate calibration dataset that was explicitly provided for calibration of samples that drew their carbon from the surface mixed ocean layer. This dataset, Marine04 (Hughen *et al*. 2004a), was composed of coral (Edwards *et al*. 1993; Bard *et al*. 1998; Burr *et al*. 1998, 2004; Cutler *et al*. 2004; Fairbanks *et al*. 2005) and foraminifera (Hughen *et al*. 2000) radiocarbon measurements over the time period 26.0 to 10.5 cal. ka BP, normalised to give values for the theoretical 'global ocean' mixed layer (following Stuiver *et al*. 1986b). The later time period, 10.5 to 0 cal. BP, was composed of the terrestrial tree-ring data of IntCal04 (Reimer *et al*. 2004a), converted with a box diffusion model (Stuiver and Braziunas 1993a) to produce approximate equivalent values for the global ocean mixed layer. Throughout the dataset, application of specific ΔR corrections is necessary to calibrate data from individual sites.

2.6.8 NotCal04

At the time of publication of IntCal04 (Reimer *et al*. 2004a), disparities between the individual radiocarbon calibration datasets prior to 26,000 cal. BP were so large as to preclude the identification of any single calibration curve through this older time period. To demonstrate the range of these disparities to radiocarbon users, van der Plicht *et al*. (2004) published the 'NotCal04' dataset (with the 'Not-' prefix making it clear that this was 'not a calibration curve' that should be used to calibrate real radiocarbon measurements). The NotCal04 data clearly demonstrated the broad scatter of radiocarbon measurements obtained for this time period, as well as offsets between the individual contributing datasets. The scatter was perhaps the result of inadequate sample screening or pre-treatment protocols, whilst the offsets perhaps represented poorly determined calendar age scales or reservoir corrections (Reimer *et al*. 2006). These individual datasets must include errors, since, by definition, there can only be one true atmospheric radiocarbon calibration curve (van der Plicht 2004; van der Plicht *et al*. 2004)

2.6.9 IntCal09 and Marine09

IntCal09 (Reimer *et al*. 2009) represents the latest version of the international consensus calibration curve and, for the first time, provides an internationally-ratified calibration dataset across approximately the entire range of the radiocarbon dating method (50,000 to 0 cal. BP). This latest draft of IntCal represents advances in the available contributing datasets, which have begun to demonstrate greater coherence beyond the previous 26,000 cal. BP IntCal04 limit.

For the period 12,000 to 0 cal. BP, no changes were made to the IntCal04 dendrochronological data, except that a small (19 calendar year) error was corrected in two of the three oldest German pines that had been utilised in IntCal04. The extension of the absolute European pine chronology to 12,594 cal. BP using Swiss pines (Shaub *et al*. 2008b) was additionally utilised in IntCal09, but only including measurements back to 12,550 cal. BP due to the lack of replication of the earliest samples of the Swiss record.

The independently ^{234}U-^{230}Th-dated corals included in IntCal09 were those of Edwards *et al*. (1993), Bard *et al*. (1998), Burr *et al*. (1998), Cutler *et al*. (2004) and Fairbanks *et al*. (2005), with assumed temporally-constant, site-specific marine reservoir corrections applied. In many cases, these corrections were updated from their previously-published values, derived from comparison with the updated dendrochronological record for the periods of overlap (Reimer *et al*. 2009).

In addition to the data provided by the varved section of the Cariaco Basin dataset that were included in IntCal98 and IntCal04, IntCal09 additionally included data from the non-varved portion of the sediment profile, as matched to the Hulu Cave timescale (Hughen *et al*. 2006). An updated marine reservoir correction of 430 ± 50 years was applied, as derived from the same method of overlap with the tree-ring data as were the coral samples (Reimer *et al*. 2009).

A total of 43 measurements were included from the Iberian margin marine sediment dataset of Bard *et al*. (2004a, 2004c) and Shackleton *et al*. (2004). As with the Cariaco Basin data, the tuning of this site's climatic record was updated to that of Hulu Cave (Wang *et al*. 2001).

Due to evidence that the marine reservoir of the western sub-tropical Atlantic may have been significantly reduced during the early Younger Dryas (Kromer *et al*. 2004; Muscheler *et al*. 2008; Schaub *et al*. 2008a, 2008b; Singarayer *et al*. 2008), the data from this region

(i.e. both the Barbados corals of Fairbanks *et al*. 2005 and the varved Cariaco Basin data of Hughen *et al*. 2004b) were removed from the calibration curve over the time period 12,900 to 12,550 cal. BP. Such findings are hypothesised as being the result of reduced- (or complete shutdown of-) North Atlantic Deep Water (NADW) formation through this period (Singarayer *et al*. 2008).

Although not included in IntCal09, the Bahamas speleothem data of Hoffmann *et al*. (2010) and preliminary data from the present, Suigetsu Varves 2006, project (Staff *et al*. 2009) provided supporting evidence to the IntCal working group that the data included within the calibration curve for the period older than the previous 26,000 cal. BP limit were not unreasonable. However, the fact that the majority of the older portion of IntCal09 remains based upon the marine Cariaco Basin and coral records, means that high resolution atmospheric radiocarbon concentration variability may not be fully represented in IntCal09 (Reimer *et al*. 2009).

As with previous incarnations of the calibration curve, IntCal09 represents a 'work-in-progress' model, which will be improved over coming years (and decades) as ever more robust calibration data are obtained.

An updated marine calibration curve, 'Marine09', was also provided by Reimer *et al*. (2009). Again, this represents a generalised curve for the 'globally-averaged' surface oceans and makes the assumption of constant reservoir corrections. Therefore, for the period 50 to 12.5 cal. ka BP, Marine09 is generated simply from the IntCal09 dataset (produced entirely from marine records over this period), plus a constant reservoir correction of 405 years. The authors admit that this is an obvious over-simplification, but that, in the absence of better data, demonstrates the best present state-of-knowledge of marine records.

For both IntCal09 and Marine09 calibration curves, an improved Markov Chain Monte Carlo (MCMC) implementation of the Bayesian random walk model (used for IntCal04 and

Marine04) was applied (Heaton *et al*. 2009). Such an approach enables potential realisations of plausible, complete calibration curves to be produced simultaneously, rather than the point-wise methodology applied previously (Buck and Blackwell 2004). This offers increased flexibility over the previous methodology, and is able to incorporate covariance of related data, and is also able to explicitly include known ordering constraints.

As the most up-to-date consensus atmospheric radiocarbon calibration curve, IntCal09 therefore provides the primary dataset for comparison/calibration of the Lake Suigetsu radiocarbon determinations discussed later in this DPhil thesis. Nevertheless, this extension remains comprised of radiocarbon measurements from marine sources, and so the additional complexity of varying marine reservoir offsets through time must be considered. A wholly terrestrial sequence of radiocarbon data through the entire radiocarbon calibration period, beyond the existing limits of dendrochronologically-dated wood, would remove the persisting uncertainties associated with the additional layer of complexity associated with the marine records, and therefore remains a fundamental aim of the radiocarbon dating community.

2.7 Key Features of the Existing Radiocarbon Calibration Datasets

The long-term trend of the radiocarbon calibration curve is of systematically younger conventional radiocarbon ages compared to their equivalent calendar ages, for all but a fleeting period (*circa* 2500 to 500 cal. BP) of the radiocarbon method (Bard *et al*. 1993). This is the result of a long-term decrease in $\Delta^{14}C$, generally attributed to concomitant long-term increase of the intensity of the Earth's geomagnetic field (Bard *et al*. 1990a, Bard 1997, Stuiver *et al*. 1991). The highly elevated $\Delta^{14}C$ observed between 45 and 15 cal. ka BP might also be attributable to very different distributions of ^{14}C between the surface and deep ocean reservoirs of the Late Glacial as compared to the situation today (Hughen *et al*. 2006). Alternatively, Chiu *et al*. (2007) suggest that this long-term trend in $\Delta^{14}C$ might be biased by

uncertainties in the ^{14}C half-life. Although not affecting the calibration of radiocarbon determinations (between conventional radiocarbon and calendar ages), an incorrect half-life does influence any conclusions drawn from such data regarding past geophysical processes.

As has been noted above (section 2.3), the relationship between radiocarbon 'time' and the passing of true, calendrical time is not a linear one. As Suess (1965, 1970) first described, the calibration curve exhibits distinct decadal to millennial structure ('wiggles'), super-imposed upon the longer-term trend. If such features are observed across multiple calibration datasets, support is provided for the authenticity of these structures, rather than their being simple artifacts of methodological uncertainty, as was initially postulated by Suess' doubters (e.g. Clark 1975; Pearson *et al*. 1977; Damon *et al*. 1978; Pearson and Pilcher 1978).

Marine archives represent a regional record of surface ocean ^{14}C concentration, with atmospheric radiocarbon concentration approximated through application of a marine reservoir correction (R). Even if R is (hypothetically) corrected perfectly at a site, short-term atmospheric variability is attenuated in these marine datasets, since their ^{14}C in any case represents a time-integrated signal due to the residence time of ^{14}C in the ocean reservoir. Additional 'over-printing' might be caused by changes to ocean circulation patterns (i.e. causing temporal variations in R), which would mask the authentic temporal changes in radiocarbon concentration (Stuiver *et al*. 1986b).

Characteristic features of the radiocarbon calibration curve include numerous plateaux, or 'flat spots' (*sensu* Clark 1975; figure 2.2a). These plateaux reflect times when the rate that the concentration of ^{14}C in the atmosphere declined over time approximately matched the rate of radioactive decay of isolated samples. Such plateaux identified from the terrestrial radiocarbon archives include those at *circa* 2,500 BP and 7,950 BP (Reimer *et al*. 2004a), 8,750 BP and 9,600 BP (Hajdas *et al*. 2000), 10,000 BP (which coincides with the transition

from the Younger Dryas into the present interglacial, the Holocene, and so complicates the precise dating of this event in calendar time via the radiocarbon method; Kromer and Becker 1993), 10,400 BP (Goslar *et al*. 1995, 2000a), 11,000 BP, 11,550 BP and 11,800 BP (Kromer *et al*. 2004). Even more extreme circumstances produce short-term 'inversions' ('reversals') in the calibration curve (where the rate that the concentration of ^{14}C in the atmosphere declined over time exceeded the rate of radioactive decay in isolated samples; figure 2.2b). Prominent examples of these include those at *circa* 5,400 cal. BP and 5,550 cal. BP (Reimer *et al*. 2004a), and 13,200 cal. BP (according to the floating Late Glacial pine chronology of Kromer *et al*. 2004, as adjusted by Hua *et al*. 2009). Conversely, there are periods where the concentration of ^{14}C in the atmosphere rose rapidly over time, producing steep gradients in the calibration curve (figure 2.2c). Notable examples include those at *circa* 300 cal. BP, 2,350 cal. BP, 4,850 cal. BP, 9,550 cal. BP, 10,250 cal. BP and 11,200 cal. BP (Reimer *et al*. 2004a). Similar features are also evident in the preceding time periods, as demonstrated by the marine and speleothem datasets, but potential variations in the marine- or DCF reservoir corrections applied to these data make such features 'less permanent fixtures' of the calibration curve.

The "most prominent feature" of the calibration curve over the last 20,000 years (Edwards *et al*. 1993) is a rapid decline in $\Delta^{14}C$ evident at the onset of the Younger Dryas, as demonstrated, *inter alia*, by the Lake Gościąż data (Goslar *et al*. 1995, 2000a), the coral datasets of Bard *et al*. (1990a, 1993) and Edwards *et al*. (1993), and the Late Glacial pine chronology of Kromer *et al*. (2004). This decrease in $\Delta^{14}C$ is associated with significant ocean circulation changes during the Younger Dryas cold reversal (Edwards *et al*. 1993).

As identified in section 2.6.9, the reservoir-corrected marine data from the western sub-tropical Atlantic are now believed to erroneously represent the authentic atmospheric signal through the Younger Dryas, due to significant deviation through this period from the constant R value applied (Singarayer *et al*. 2008). It is also possible that similar changes to THC

would have occurred during previous Heinrich events and cold stadial phases of Dansgaard/ Oeschger (D/O) cycles (Clark *et al*. 2002), and would therefore affect the western Atlantic calibration data from these periods. Supporting this idea is the disagreement of the Cariaco Basin record (Hughen *et al*. 2006) from the Bahamas speleothem (Beck *et al*. 2001) and Iberian margin (Bard *et al*. 2004c) datasets during Heinrich event 1 (H1; ≈ 17.5 to 15 cal. ka BP).

Figure 2.2: Characteristic features of the radiocarbon calibration curve (IntCal09; Reimer *et al*. 2009): **(a)** plateaux (example shown at *circa* 7,950 BP); **(b)** inversions (examples shown at *circa* 5,400 and 5,550 cal. BP); and **(c)** periods of steeper gradient (example shown at *circa* 9,550 cal. BP).

(a):

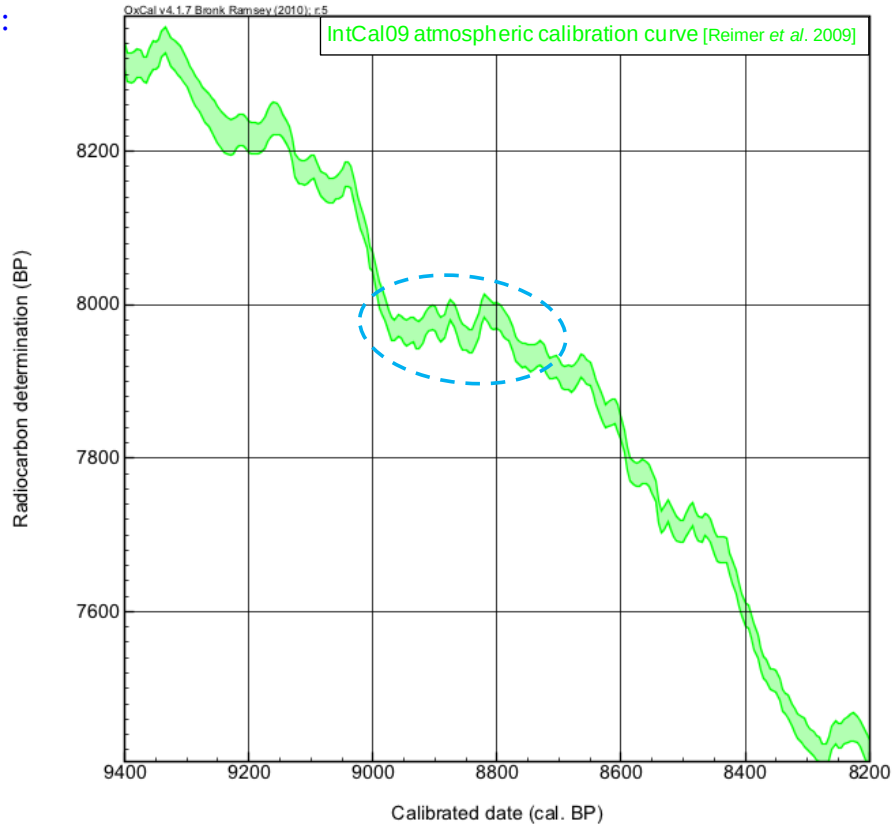

Figure 2.2 (continued):

(b):

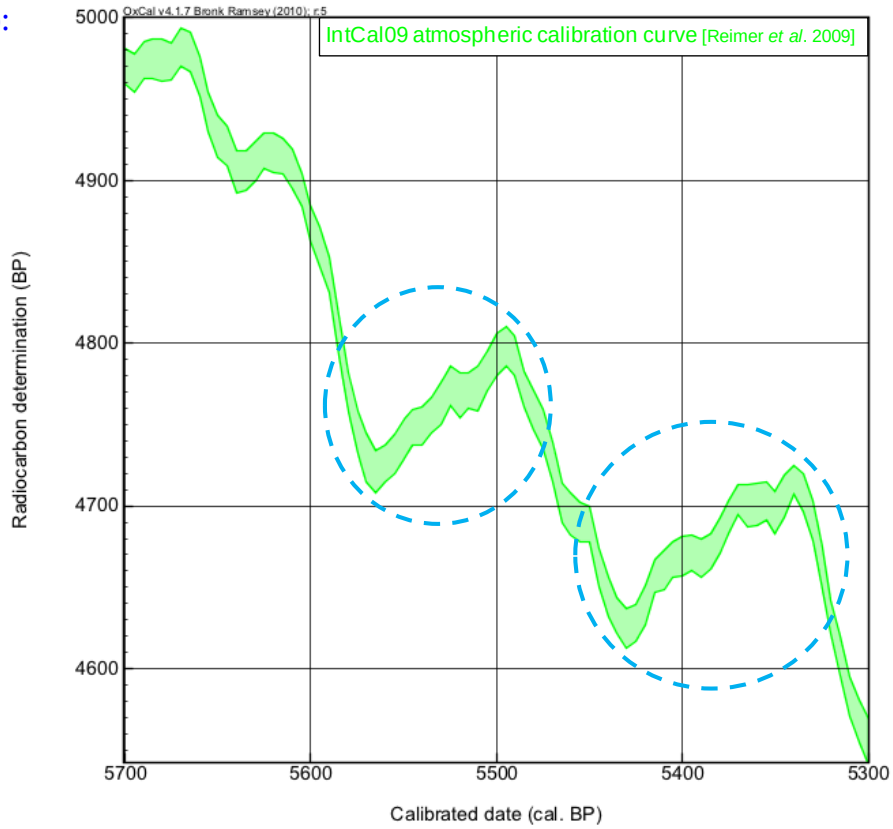

(c):

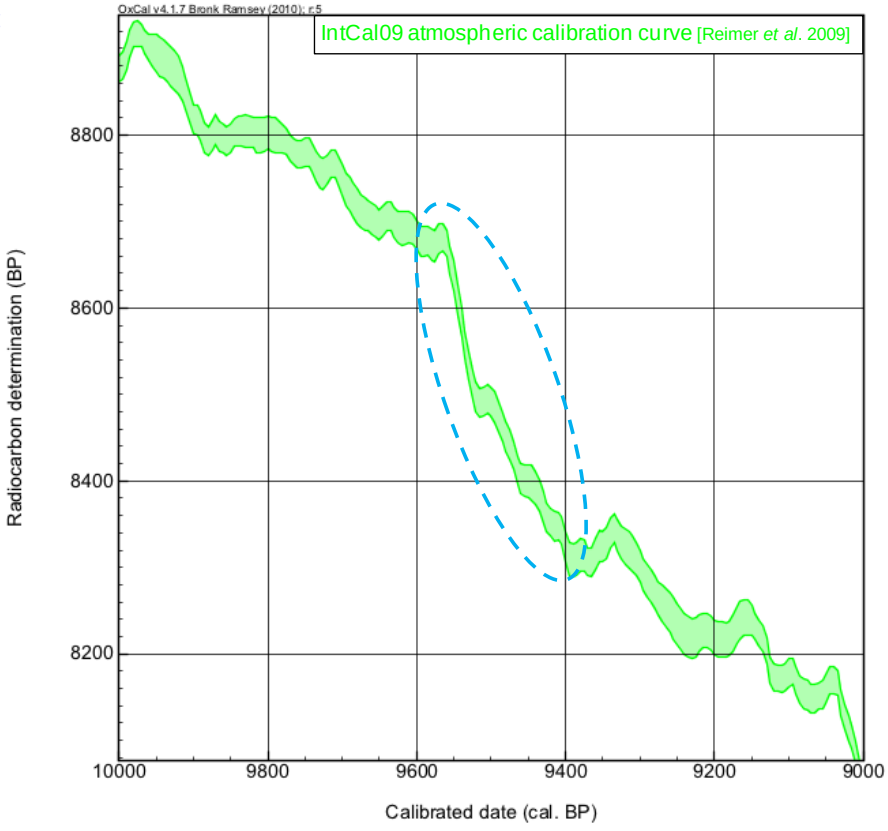

Another distinctive feature of the calibration curve further back in time is likely to be associated with the 'Laschamp' geomagnetic excursion. The most reliable radiometric dating yet obtained for this event places it at 40.4 ± 2.0 cal. ka BP, as obtained by argon-argon (^{40}Ar-^{39}Ar) dating of lava flows from the type locality in the Massif Central, France (Guillou *et al*. 2004). The Laschamp event is associated with an abrupt increase in cosmogenic nuclide production, and has been found in both ice cores (e.g. Yiou *et al*. 1997; Muscheler *et al*. 2005; and Raisbeck *et al*. 2007) and marine sediment cores (e.g. McHargue *et al*. 1995; Robinson *et al*. 1995; Carcaillet *et al*. 2004; and Leduc *et al*. 2006). Thus, the Laschamp event provides a critical, globally-synchronous, 'absolute' tie-point at the older end of the radiocarbon dating range, potentially allowing reliable, independent correlation between geographically-distant sites (section 3.6.4). The underlying cause of the Laschamp event remains somewhat equivocal, however (Bard 1997), with suggested causes including: the geomagnetic field no longer being dipolar and dramatically reduced in intensity at this time (Guyodo and Valet 1996); extreme solar modulation (Raisbeck *et al*. 1987); the shockwave from a supernova (Sonnett *et al*. 1987); or a combination of these factors (McHargue *et al*. 1995; Robinson *et al*. 1995).

The Laschamp event is evidenced in the Cariaco Basin record by dramatic increases in Δ^{14}C at *circa* 42 to 40 cal. ka BP, with nearly 7,000 radiocarbon years elapsing over ≈ 2,000 calendar years (Hughen *et al*. 2004b). The event is also identified by Voelker *et al*. (1998; between 41.7 and 40.3 cal. ka BP), amongst others.

Other geomagnetic excursions over the radiocarbon timescale, such as the 'Mono Lake event', remain more "controversial" (Guillou *et al*. 2004). The Mono Lake event is dated at *circa* 32 cal. ka BP by McHargue *et al*. (1995; using ^{10}Be from a marine sediment core from the Gulf of California, USA) and between 33.3 and 31.5 cal. ka BP by Benson *et al*. (2003; based on radiocarbon measurements at the type-site, Mono Basin, California, USA). The

speleothem record of Hoffmann *et al*. (2010) also picks up a steep rise in $\Delta^{14}C$ at about 35 cal. ka BP (matched by drops in the 'GLOPIS' geomagnetic intensity record of Laj *et al*. 2004), and an excursion ascribed to Mono Lake is also present in the Cariaco Basin (*circa* 34 cal. ka BP; Hughen *et al*. 2004b, 2006) and Nordic Seas (34.5 to 33.5 cal. ka BP; Voelker *et al*. 1998) datasets.

Additional dramatic increases in $\Delta^{14}C$ have been identified at *circa* 30 cal. ka BP (by Hughen *et al*. 2006 and Hoffmann *et al*. 2010), as well as deep minima at *circa* 50 to 45 cal. ka BP (Hughen *et al*. 2006), 36 cal. ka BP, and 33 to 31 cal. ka BP, seemingly reflecting geomagnetic modulations to ^{14}C production rate, amplified by reduced ^{14}C sinks during full glacial conditions (Hughen *et al*. 2004b).

In terms of the dominant forcing mechanisms, Mazaud *et al*. (1991) determined by box modelling that the geomagnetic dipole field strength is the main factor governing ^{14}C production rate over time. Over shorter time-scales, major carbon cycle re-organisations and solar modulation exert influence over the structure of the radiocarbon calibration curve. Central to all such interpretation, however, is that the atmospheric radiocarbon calibration curve itself is reliably defined. The remainder of this DPhil thesis will describe new radiocarbon measurements obtained from the varved sediments of Lake Suigetsu, central, Japan, which will seek to substantiate this atmospheric calibration curve across the entire range of the radiocarbon method.

3. Study Site: Lake Suigetsu, Central Japan

Chapter 3 introduces the principal study site of the present DPhil thesis, that of Lake Suigetsu, central Japan, and commences with the basic geographical details of the site, noting the catchment hydrology, regional climate, and sediment profile, before discussing the factors that make Suigetsu so suitable for developing a radiocarbon calibration dataset. The chapter continues with a discussion of the previous ("Suigetsu '93") project performed at Lake Suigetsu (which focussed on a ≈ 75 m sediment core, 'SG93' collected from the lake bottom), before introducing the present 'Suigetsu Varves 2006' project (based around a new, ≈ 73 m composite sediment core, 'SG06'), to which this DPhil thesis forms a major contribution.

3.1 Situation and Site Characteristics

Lake Suigetsu ('*Suigetsu-ko*') is situated in the north-west of Mikata district ('*Mikata-gun*'), southern Fukui prefecture, Honshu Island, central Japan at 35° 35' N, 135° 53' E (figure 3.1), 0 m above present sea level (a.s.l.), proximal to the Sea of Japan coast (clearly evident in figure 3.2) at Wakasa Bay. Suigetsu is a tectonic lake, located on the western side of the active Mikata fault line, and lying at the northern apex of the triangular neotectonic province known as the 'Kinki Triangle'. The lake covers an area of ≈ 4.3 km^2, has a perimeter of ≈ 10 km, and a diameter of ≈ 2 km in both N/S and E/W directions. Suigetsu is a kettle-type lake and has an approximately flat bed at the centre, ≈ 34 m deep. The lake is surrounded by a ring of Palaeozoic hills (maximum elevation 400 m), which provide natural protection from the wind (Matsuyama 1973c; Kitagawa *et al*. 1995; Kawakami *et al*. 1996; Kitagawa and van der Plicht 1998a; Nakagawa *et al*. 2005, 2011).

Figure 3.1: The location of Lake Suigetsu, Honshu Island, central Japan (latitude 35˚ 35' N, longitude 135˚ 53' E). (Source: Nakagawa *et al*. 2011.)

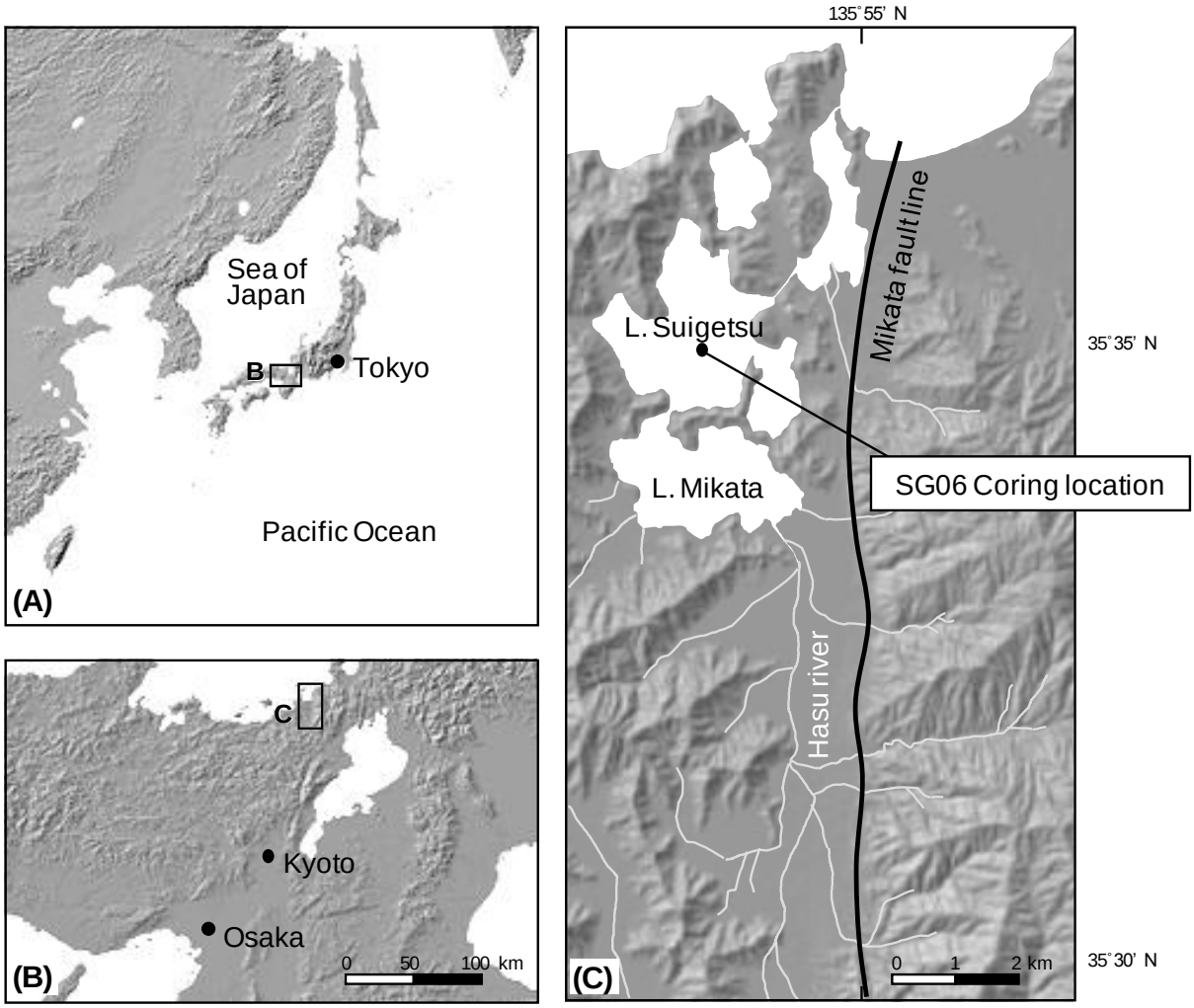

Figure 3.2: The situation of Lake Suigetsu, proximal to the Sea of Japan coast. Suigetsu is part of a five lake system (the '*Mikata-goko*'), the others being Mikata, Suga, Hiruga and Kugushi (all pictured).

3.1.1 Hydrology

As illustrated in figures 3.2 and 3.3, Suigetsu constitutes one of the '*Mikata-goko*' (Mikata five lakes), the others being Hiruga, Kugushi, Mikata, and Suga. Table 3.1 provides details of the hydrological information pertaining to the *Mikata-goko*. Suigetsu is the largest of the five lakes, with- or without the inclusion of Lake Suga, which is effectively a side branch of Suigetsu.

Figure 3.3: The contemporary hydrological system of the *Mikata-goko*. Anthropogenically-altered/added watercourses are indicated in purple; natural/former hydrological features are indicated in blue. (Sources: Shigematsu *et al*. 1961; Matsuyama 1974; Masuzawa and Kitano 1982a; Kawakami *et al*. 1996; K. Takemura, personal communication.)

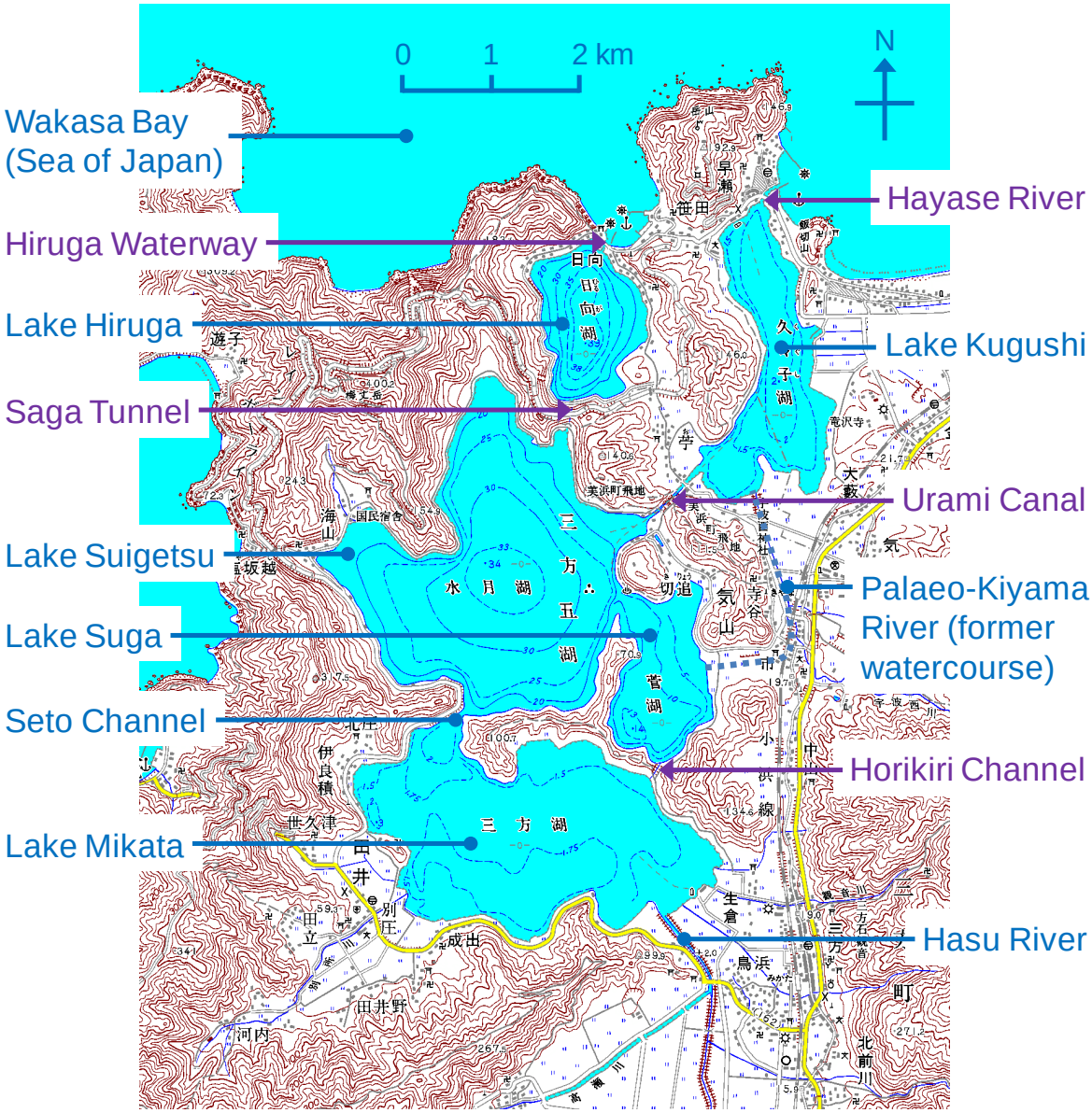

Table 3.1: Hydrological information of the *Mikata-goko*. (Sources: Shigematsu *et al*. 1961; Matsuyama and Saijo 1971; www.wakasa-mikatagoko.jp).

Lake	Surface Area (km^2)	Perimeter (km)	Maximum water depth (m)	Average water depth (m)	Volume (km^3)	Quality
Mikata	3.45	9.60	5.80	1.33	0.00484	Shallow, eutrophic lake
Suigetsu	4.06	9.85	34.00	14.33 (combined)	0.07165 (combined)	Deep, brackish lake
Suga	0.95	4.20	14.50			
Kugushi	1.25	7.00	2.50	0.83	0.00117	Shallow, haline lake
Hiruga	0.92	3.60	38.50	14.33	0.04085	Deep, polyhaline lake

The majority of water feeding into Lake Suigetsu comes via the Seto Channel from Lake Mikata. The total catchment area for Suigetsu (including the area feeding into Lake Mikata) is relatively small (≈ 49 km^2; Matsuyama 1973c), with Suigetsu representing ≈ 6% of this total surface area. Of the catchment area that feeds Lake Suigetsu directly (i.e. that which does not enter Suigetsu from Lake Mikata), however, ≈ 54% of the surface area is comprised by Suigetsu itself. There are two small rivers that feed into the Mikata-Suigetsu Lakes, one being ≈ 10 km in length (the Hasu River, visible in figure 3.2) and the other of negligible length. The hydrological linkage between Lakes Suigetsu and Mikata is critical to the sediment régime of the former. Since the shallow (≈ 2m deep) Seto Channel provides the only (significant) inflow of water into Suigetsu, there is no deposition of coarse material in the lake (Nakagawa *et al*. 2005); only fine, suspended material is borne across Lake Mikata into Suigetsu, with any coarser material entering Mikata from the Hasu River deposited in Mikata before reaching Suigetsu.

Previously, all of the Mikata five lakes were freshwater bodies. However, anthropogenic influence over historical times has significantly altered the hydrology of the lake system (Shigematsu *et al*. 1961; Matsuyama and Saijo 1971; Matsuyama 1973c;

Masuzawa and Kitano 1982a, 1982b). In AD 1630, Lake Hiruga became joined to the Sea of Japan through the construction of the Hiruga waterway, and thus became saline. Lake Kugushi also became saline, due to the anthropogenic deepening of the Hayase river, which links it to the sea. A major earthquake in AD 1662 (the Kanbun earthquake, estimated magnitude 7.5) uplifted the Kiyama River, which had formerly drained Lake Suigetsu into Lake Kugushi, causing resultant flooding of fields and villages around Suigetsu and Mikata (Kawakami *et al*. 1996). In response to this, Lakes Suigetsu and Kugushi were joined by the Urami Canal in AD 1664, at which point the surface water level of Lake Suigetsu dropped to equalise with sea level (from its pre-earthquake level of ≈ 3.0 to 3.5 m a.s.l.) and seawater began to enter Suigetsu, turning the previously freshwater lake to brackish, meromictic conditions. Suigetsu was later linked to Lake Hiruga in AD 1801 with the construction of the Saga Tunnel (which was subsequently re-built in AD 1848). Both the Urami Canal (380 m long, 14 m wide, 1.8 m deep) and Saga Tunnel (145 m long, 5.5 m wide, 1.8 m deep) were dredged and widened in AD 1934 to 1935 for the dual purposes of improved flood prevention and of facilitating transportation. This enabled additional saltwater to enter into Lake Suigetsu, increasing hydrogen sulphide levels in the lake, increasing bottom water chlorine concentration, and causing the chemocline to rise from ≈ 15 m to ≈ 7 m (Matsuyama 1973c). Thus, Lake Suigetsu is today a "typical" meromictic lake (Matsuyama 1973a, 1973b), with a permanent chemocline (at a water depth of between ≈ 3 m and 8 m) separating the oxic freshwater mixolimnion from the deeper, anoxic, saline, sulphidogenic, monimolimnion extending to the lake bottom at 34 m (Takahashi and Ichimura 1968; Kondo *et al*. 2000, 2006, 2009; Kondo and Butani 2007; Okada *et al*. 2007).

Due to the marked anthropogenic intervention of the past ≈ 400 years, the conditions of the lake prior to this time are not fully known (Tyler *et al*. 2011). However, the presence of well preserved laminae down the sediment profile (section 3.2, below) is suggestive of

persistent hypolimnetic- and sediment anoxia for at least the last ≈ 50,000 years (Kitagawa and van der Plicht 1998a, 1998b, 2000; Yasuda *et al*. 2004).

3.1.2 Climate

Lake Suigetsu is situated in the mid-latitude western Pacific region, within the area between which the Asian monsoon front seasonally migrates. Thus, the climate of the Lake Suigetsu region exhibits clear seasonality, being typically characterised by both summer and winter monsoons (Fukui 1977; Nakagawa *et al*. 2005, 2006). During summer months, preferential heating over continental eastern Eurasia, as compared to the Pacific Ocean, generates an atmospheric pressure gradient that drives the predominant south-easterly winds over the Japanese archipelago (figure 3.4a). This results in intense summer precipitation of moisture entrained by this air mass from the warm surface waters of the Pacific Ocean. During winter months, the situation is reversed such that the eastern Eurasian continent cools more rapidly than the Pacific Ocean, producing an atmospheric pressure gradient that drives the dominant wind direction over the Japanese archipelago from the north-west (figure 3.4b). The air mass being borne over Japan, originating from the Siberian continental interior, is cold, but not dry; rather, moisture is entrained from the relatively warm surface waters of the Sea of Japan and provides heavy winter precipitation over Japan, particularly along the Sea of Japan coastal regions (including the *Mikata-goko*; Nakagawa *et al*. 2011). The location of Lake Suigetsu with respect to this important geoclimatic boundary of the Asian monsoon front makes it ideally situated to provide an important repository of palaeoclimatic information pertaining to any changes in this boundary back in time (section 3.5.4; Nakagawa *et al*. 2006, 2011). For reference, present day climatic data from the nearby Tsuruga meteorological observatory (35°39’00” N, 136°03’54” E, 16 m a.s.l., approximately 15 km ENE of Lake Suigetsu) are provided in table 3.2.

Figure 3.4: Atmospheric circulation over Japan during: **(a)** July; and **(b)** January. The arrows show the predominant wind directions and the bold line plots the average position of the Asian monsoon front during: **(a)** the summer-; and **(b)** the winter months, respectively. (Source: Nakagawa *et al*. 2011.)

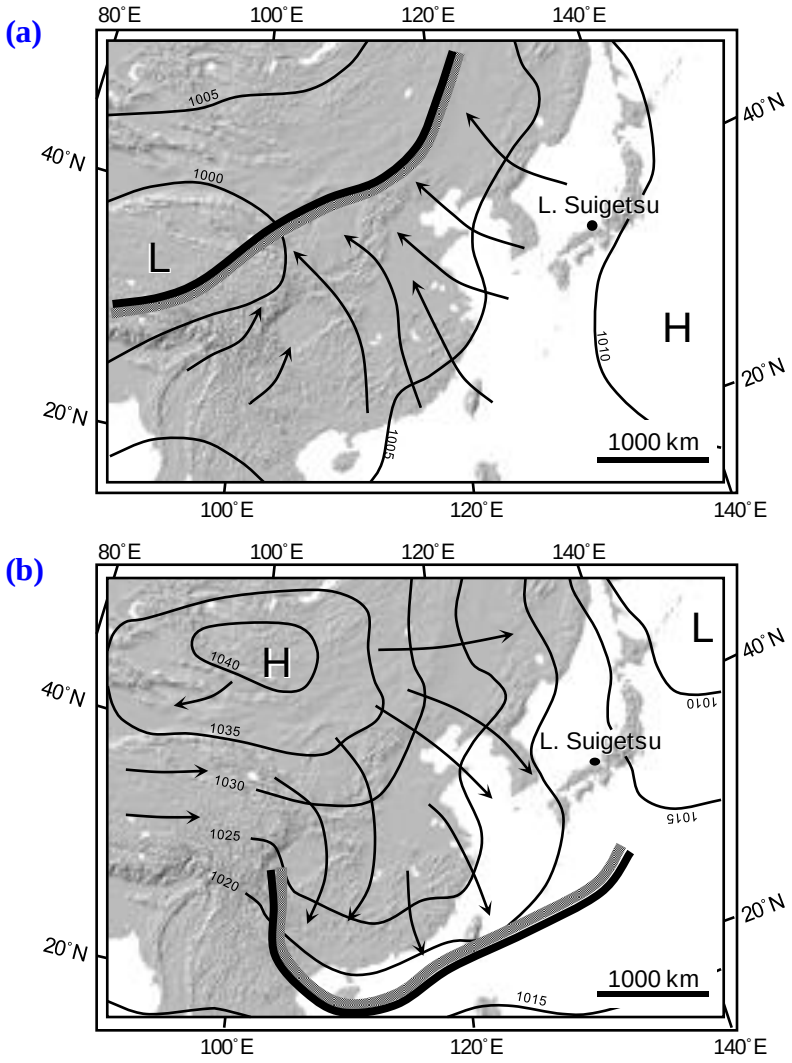

Table 3.2: Modern climatic data (30 year average data, covering the period 1961-1990) observed at the Tsuruga meteorological observatory, approximately 15 km ENE of Lake Suigetsu. (Source: Japan Meteorological Agency 1998a, 1998b, cited by Nakagawa *et al*. 2011.)

Mean annual temperature:	14.8 °C
Mean temperature of the warmest month:	27.0 °C
Mean temperature of the coolest month:	3.3 °C
Annual precipitation:	2,419 mm
Precipitation from April to September:	1,081 mm
Precipitation from October to March:	1,338 mm

3.2 Sediment Stratigraphy

Based upon observation of the SG93 core, the stratigraphy of the Lake Suigetsu sediments was divided into five primary units by Takemura *et al*. (1994; figure 3.5). The upper three of these units ('SG-I', 'SG-II' and 'SG-III') were described by Kitagawa *et al*. (1995) as displaying "distinct lamination" and correspond to the upper 4601.4 cm of the SG06 core (Nakagawa *et al*. 2011). The sediment between SG06 composite core depths 4601.4 cm and 6375.2 cm is not laminated. This core section (equivalent to unit 'SG-IV' of the SG93 stratigraphy) represents a period when Suigetsu was not deep enough to maintain abiotic basal water conditions (Takemura *et al*. 1994; Nakagawa *et al*. 2011). Below SG06 composite depth 6375.2 cm, down to the base of the retrieved SG06 core, the sediment is composed of alternating peat, inorganic clay layers, and occasionally finely laminated organic clays. This core section (equivalent to unit 'SG-V' of the SG93 stratigraphy)

represents a time period of alternating fluvial- and shallow water lacustrine environments that occurred after the initial tectonic formation of the basin (Nakagawa *et al*. 2011).

Figure 3.5: Stratigraphy of the SG93 sediment core. The five primary sedimentary units (I to V) defined by Takemura *et al*. (1994) are shown, as are the tephra horizons (preliminarily) identified by the same authors. (Adapted from: Takemura *et al*. 1994.)

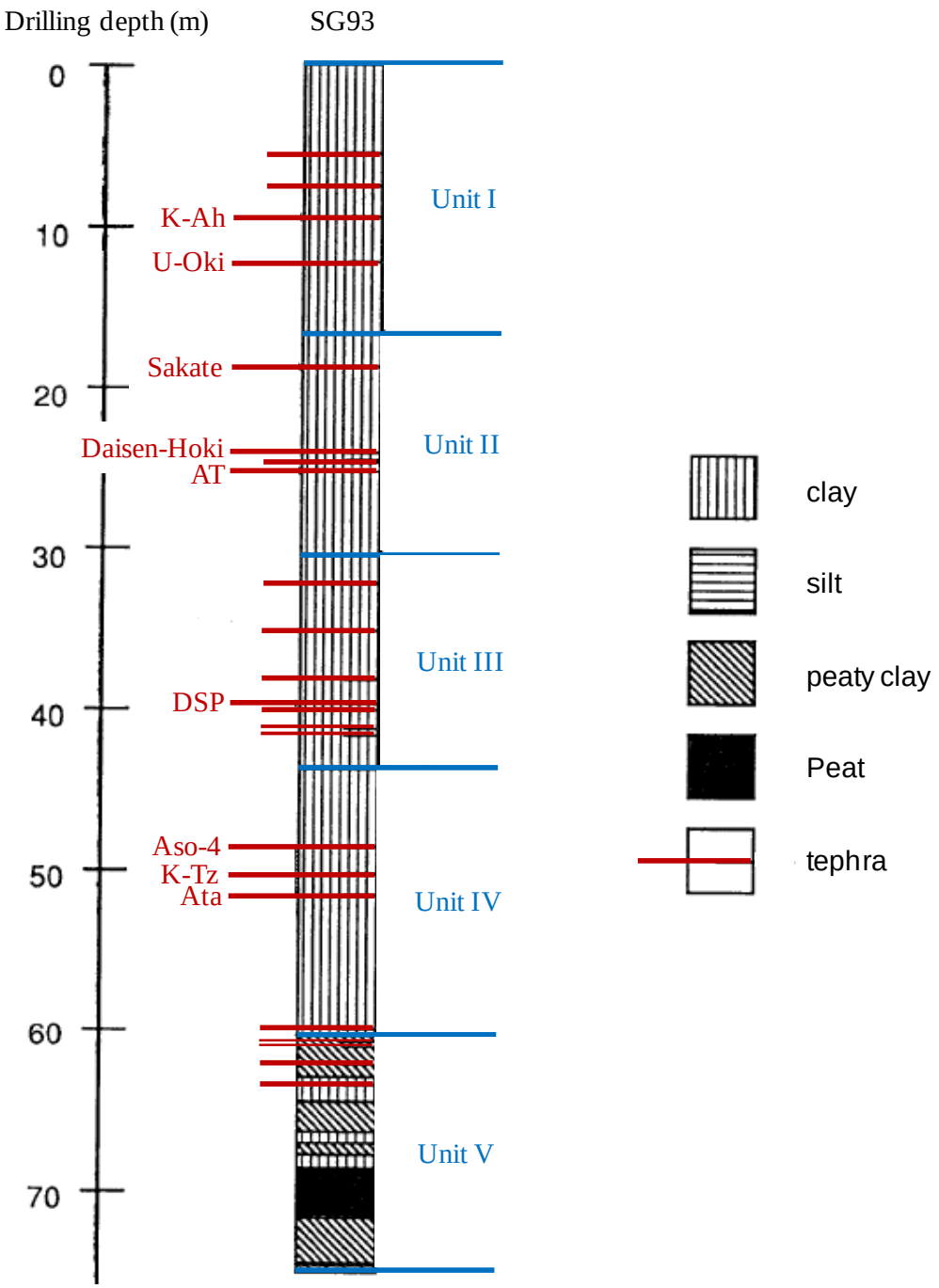

Kitagawa and van der Plicht (1998a) estimated the base of SG93 to be in excess of 100,000 cal. BP, "close to the beginning of the last interglacial period" (equivalent to the Eemian of North-Western Europe). However, utilising the SG06 core, this date is pushed back significantly by Nakagawa *et al*. (2011), putting the base of the Lake Suigetsu sedimentary profile at, conservatively, 150,000 cal. BP (potentially, being as old as 200,000 cal. BP). This date is achieved through extrapolation of sedimentation rate below the previously- (potassium-argon-, ^{40}K-^{40}Ar-) dated Aso-4 and Ata tephras (section 3.2.3, below), as well as examination of low resolution palynological data gathered from the SG06 core (by project colleague R. Payne). Thus, the Lake Suigetsu sediments provide a continuous palaeoenvironmental record back in time since marine isotope stage- (MIS-) 6 (well before the previous interglacial).

3.2.1 Varve Structure

The most important sedimentological feature at Lake Suigetsu is the presence of annually-deposited laminae (varves) throughout much of its sediment profile. This layering is the result of the strong seasonality at the site, which causes differential deposition of material throughout the seasons and produces the sub-annual stratigraphic structure that comprises the Lake Suigetsu varve sequence (Nakagawa *et al*. 2011). The lake bottom is a very stable environment, being protected from physical disturbance by the surrounding ring of hills and the deep water column, which, in combination with the anoxic benthic conditions that prevent bioturbation by basal-dwelling organisms, enable the annual laminations initially formed to be perfectly preserved in the sedimentary record (Kato *et al*. 2004).

The annual nature of these laminae was confirmed by Kitagawa *et al*. (1995) through: (i) study of seasonal changes in diatom and mineral compositions; (ii) thin section

microscopy; and (iii) scanning electron microscopy (SEM) of selected layers. The average varve thickness is relatively uniform, typically 0.61 mm/year during the Glacial, increasing to 1.2 mm/year during the Holocene (Kitagawa and van der Plicht 1998a).

Although the upper three units of the SG93 core were described as displaying this "distinct lamination" by Kitagawa *et al*. (1995), 'countable' varves are only present across the SG06 composite depth range ≈ 1250 cm to ≈ 4600 cm (and, in actuality, varve counting from SG93 was only undertaken from 1042 cm and below; Kitagawa and van der Plicht 2000), with varve formation/preservation being poor for the uppermost core section. This, presumably, is the result of altered lake water conditions for this more recent time period (covering the majority of the Holocene), perhaps associated with reduced lake bottom anoxia.

The varves themselves (illustrated in figure 3.6) consist of grey and dark grey clays, interbedded with lighter layers. The darker layer (representing autumn and winter deposition, i.e. from October to March) is composed of organic matter, diatoms, clay, and aeolian dust (including Chinese loess, from February to March); and the lighter layer (representing spring and summer deposition, i.e. April through to September) is composed of clay (the typhoon floods being from July to September) and more abundant diatom species; a siderite ($[Fe,Mn]CO_3$) layer is precipitated during lake overturn in late summer/early autumn, and provides the dominant annual signal for varve counting (Fukusawa 1995, 1999; Kitagawa *et al*. 1995; Marshall and Schlolaut 2010). The presence of different diatom taxa are associated with the annual layering, providing critical additional evidence for the seasonal timings of these events. *Encyonema* species, associated with precipitation of the primary siderite layer, demonstrate that the latter must occur during autumnal lake overturn; below, additional, occasional siderite layers can be associated with *Fragilaria ulna*, along with light amorphous organic (LAO) material, indicative of summer deposition; furthermore, additional siderite layers can also be associated with the dominant *Aulocoseira* diatom species and clay,

demonstrating winter deposition (Schlolaut *et al*. forthcoming). Obviously from the above, there might often be more than one siderite layer precipitated within an annual deposition sequence, necessitating rigorous varve counting protocols (sections 3.5.1 and 3.6.3) to minimise the possibility of over-counting (inclusion of these intra-annual laminations as 'whole years').

The formation of siderite layers is induced by changes in the redox (reduction/ oxidation) conditions of the lake water (figure 3.7; Bahrig 1988; Fukusawa *et al*. 2002; Marshall *et al*. 2009). Siderite forms when oxidised iron ions (Fe^{3+}, precipitated as iron hydroxides during lake overturn) become reduced (to Fe^{2+}, by decomposition of organic matter during subsequent lake stratification) at the sediment-water interface, and bond with available bicarbonate ions (CO_3^{2-}). Manganese (Mn^{2+}) is also precipitated in this way, generally substituting for iron in the $FeCO_3$ lattice.

Figure 3.6: Magnified view of a section of the Lake Suigetsu sediment core from the present study (SG06 core section B-18, composite core depth 3593.1 to 3596.7 cm), demonstrating the clear laminations present throughout the sediment profile.

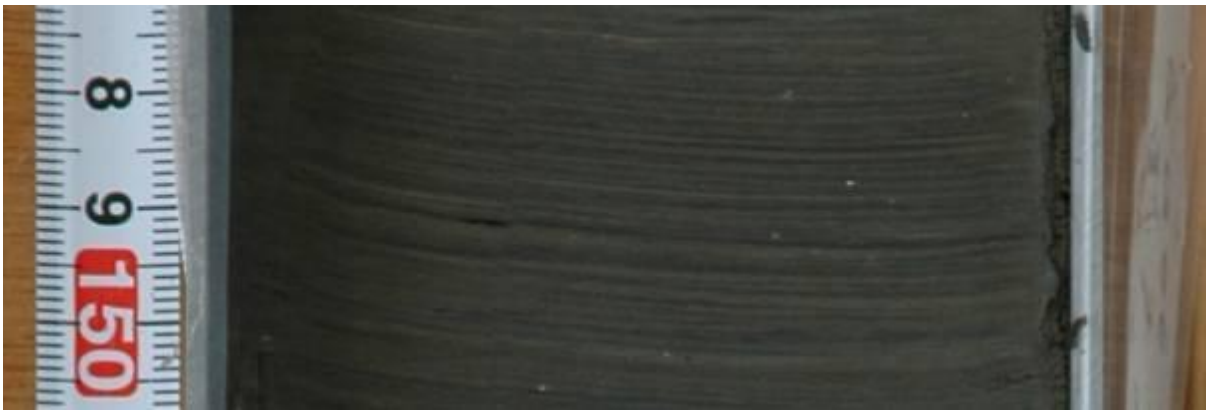

Figure 3.7: Siderite formation in Lake Suigetsu. Reduced iron (Fe^{2+}) bonds with bicarbonate (CO_3^{2-}) ions at the sediment-water interface. (Simplified from Fukusawa *et al*. 2002).

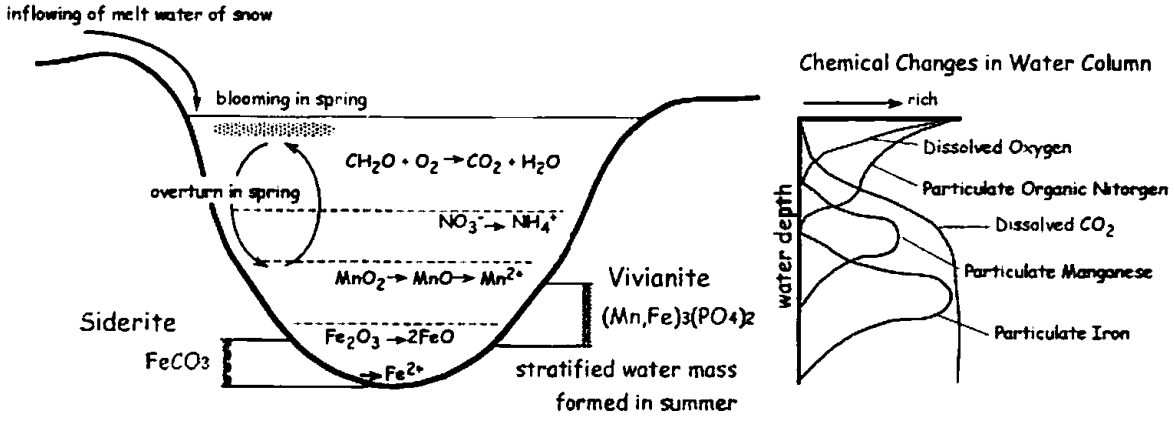

3.2.2 Event Layers

The laminated sections of the Lake Suigetsu sediment profile (units I to III of the SG93 core; Takemura *et al*. 1994; Kitagawa *et al*. 1995) include occasional thicker 'event layer' intercalations that are lacking in such fine structure. These event layers provide the distinctive horizons that enable reliable cross-correlation of core segments from the respective projects' bore-holes (sections 3.5.1, 4.1 and 6.2, below). The event layers are empirically divided into three categories (Nakagawa *et al*. 2011): (i) visible tephra (volcanic ash) layers (figure 3.8a); (ii) relatively light-coloured, massive clay layers that directly over-lie regularly-deposited varved laminae (figure 3.8b); and (iii) a similarly light-coloured, often thicker, clay layer accompanied by an underlying darker coloured and slightly coarser layer (figure 3.8c). The second and third of these event layers are preliminarily hypothesised (in the present project) as representing large flood events in the former instance and small-scale turbidite layers (perhaps related to the earthquake events of such a tectonically active area) in the latter. The sediments attributed to flood events are lacking in underlying coarser material (which might be expected during such flood events from other sites) because, as with the regular

sedimentation process in the lake system, these are preferentially deposited in Lake Mikata before reaching Lake Suigetsu. The layers attributed to turbidite events are composed of coarser material at the bottom, with finer material grading towards the top. These sediments would be sourced from re-worked material from the littoral zone, originally entering the lake from much more localised surface run-off from the surrounding slopes, rather than via the Hasu River, Lake Mikata and Seto Channel.

Kitagawa and colleagues (Fukusawa *et al*. 1994; Kitagawa *et al*. 1995) also attributed the "many spike-like muddy turbidite layers" to historical earthquake and flood events. Through comparison of the distribution of the more recent event layers with documented historical records, these authors attributed one such turbidite layer (at ≈ 29 cm depth) to the known historical Kanbun earthquake of AD 1662.

Figure 3.8: Event layers from the Lake Suigetsu sediment profile (SG06 core) preliminarily identified by Nakagawa *et al*. (2011) as representing: **(a)** a tephra horizon (the example shown being the 'U-Oki' tephra, event layer A-07-16, at a composite core depth of 1286.1 to 1288 cm); **(b)** flood layers (examples shown are A-18, 73.6 cm and 77.1 cm, composite core depths 3455.3 cm and 3458.8 cm); and **(c)** a turbidite layer (example shown is event layer B-07-11, composite core depth 1431.2 to 1433.5 cm).

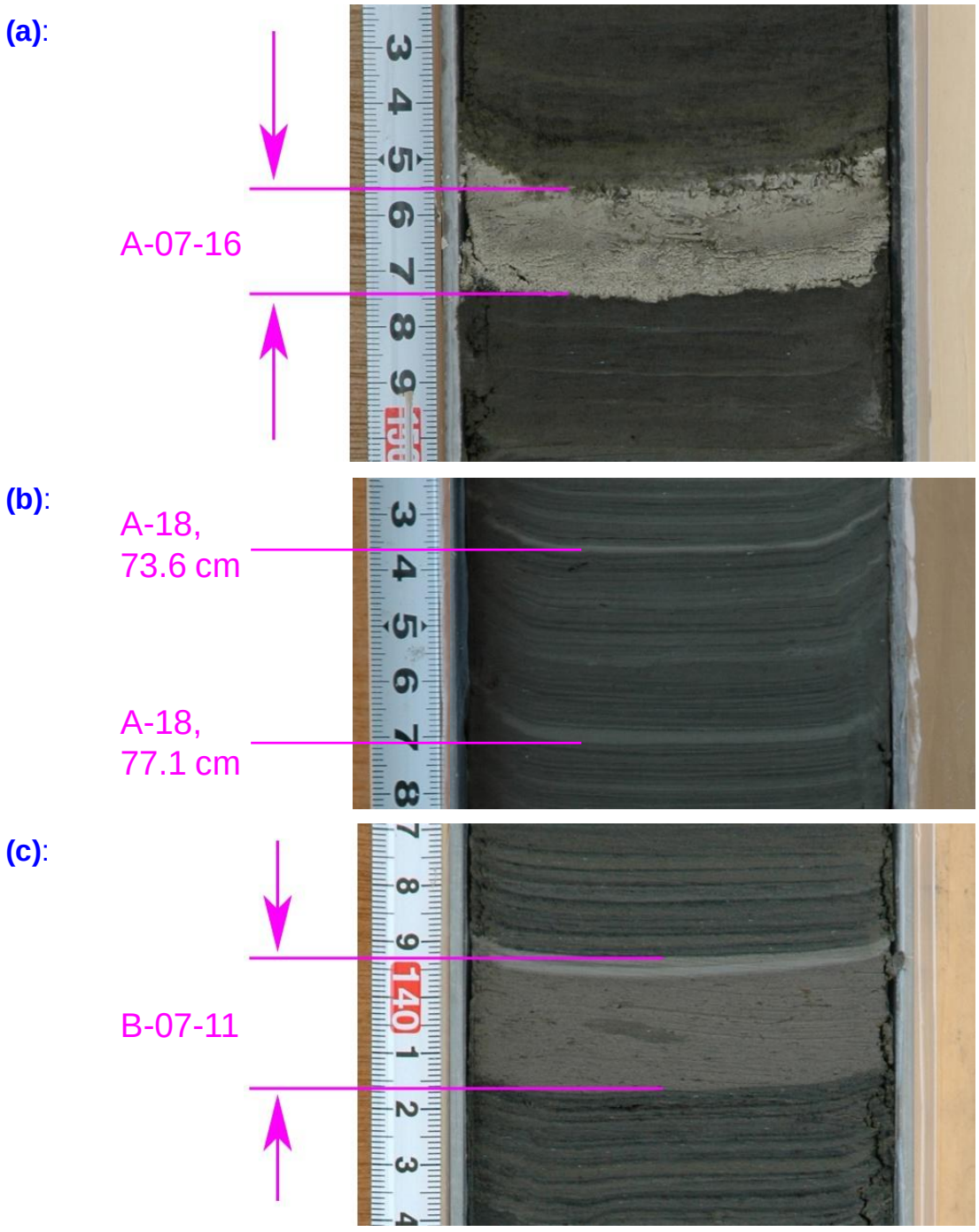

3.2.3 Tephrostratigraphy

Some 30 visible tephra (volcanic ash) horizons have been identified from the entire SG06 core (fourteen of which being from the time period represented by the radiocarbon dating method; Nakagawa *et al*. 2011), which will be further supplemented by many more cryptotephra horizons (not visible to the naked eye, and also referred to as 'microtephras'; Lowe 2011). Preliminary work to this end is being carried out by project colleagues (S. Blockley and A. MacLeod) and will be tied to specific eruptions of volcanoes in the broader region (mainly from Japan and Korea) through robust geochemical analyses of both the glass material within SG06, and proximal volcanic deposits (by project colleague V. Smith). The down-core distribution of these visible tephra horizons, as well as their tentative identifications at present, and any known age information provided for these events from other publication sources, is given in table 3.3. In general, the 'known ages' given for the particular eruption events of table 3.3 that have occurred during the time period represented by the Suigetsu varve chronology will not be as reliable as the dating to be obtained from the present project. Eventually, it is hoped that the SG06 chronology will provide a regional type-site for tephrochronological comparison (cf. the varved Lago Grande di Monticchio for the central Mediterranean region; Wulf *et al*. 2004, 2008), enabling other terrestrial sites and sediments to be tied into the high precision Lake Suigetsu chronology through use of these isochronous (tephra) events. In the meantime, and for this present DPhil thesis, the ages of these tephra events provide comparative information for the radiocarbon- and varve count chronologies constructed, but will not be built into the prior information fed into the age-depth modelling process of the present work (chapter 5). The reason for the exclusion of these data is that the 'known age' information for these events is not wholly reliable (being based on a small number of radiocarbon measurements of material – often of bulk sediment – from horizons above and below distal tephra horizons, rather than of proximal material

directly dating the eruption source), and the tephra horizons themselves are also poorly characterised (i.e. not robustly geochemically correlated between differing distal sites, nor to proximal erupted material – *cf.* Smith *et al*. 2011), therefore not necessarily even representing the same presumed eruptions.

Finally for this section, I draw the reader's attention to the tephra identified as representing the Uzuryo-Oki ('U-Oki') eruption at a composite depth in SG06 of 1286.1 to 1288.0 cm (illustrated in figure 3.8a). This tephra layer, dated to between 10,250 and 10,200 SG93 vyr BP (H. Kitagawa, personal communication; and therefore occurring a few centuries after the onset of the Holocene), lies very close to the top of the annually-laminated portion of the Lake Suigetsu sediments (approximately 1250 cm composite depth in SG06). Since this provides such an obvious marker horizon, it was deemed logical to start the floating SG06 varve chronology from this event (i.e. the U-Oki tephra is at an age of 0 'SG06 floating vyr').

Table 3.3: Selected tephrostratigraphy of the Lake Suigetsu sediment profile. Only those tephra horizons preliminarily identified to specific volcanic eruptions (though subject to change with the performance of more detailed geochemistry in the future by project colleagues S. Blockley, A. MacLeod and V. Smith) are included.

Tephra Horizon	SG93 Core Depth (cm) (Takemura *et al*. 1994)	SG06 Composite Core Depth (cm) (Nakagawa *et al*. 2011)	Age Information from Previous Publications
Kikai-Akahoya (K-Ah) tephra	930	964.5 to 967.3	6,500 BP, 7,300 cal. BP (Machida and Arai 1992; Machida 2002); 7,283 SG4 vyr BP (Kitagawa *et al*. 1995; see section 3.5.1, below)
Uzuryo-Oki (U-Oki) tephra	1240	1286.1 to 1288.0	9,551 ± 73 BP, 10,650 ± 250 cal. BP (Machida and Arai 1992; Kitagawa *et al*. 1995); < 11,200 cal. BP (Okuno *et al*. 2010); 10,226 SG93 vyr BP (H. Kitagawa, personal communication)
Sakate ash	1867	1963.8 to 1964.5	18,790 SG93 vyr BP (H. Kitagawa, personal communication)
DMs		2503.4	
Daisen-Hoki (DHg)	2400	2534.4	27,630 SG93 vyr BP (H. Kitagawa, personal communication)
DSs	2470	2600.6 to 2601.5	28,840 SG93 vyr BP (H. Kitagawa, personal communication)
Aira-Tn (AT) Ash	2500	2615.2 to 2650.3	24,330 ± 225 BP (Murayama *et al*. 1993) 29,000 SG93 vyr BP (H. Kitagawa, personal communication)
SI		3668.1	
DSP	4130		
Aso-4	4850	4959.1 to 4962.6/ 4978.6	85-90 cal. ka BP (MIS-5b/5a boundary; Machida 2002; Machida and Arai 2003)
Kikai-Tozurahara (K-Tz)	5030	5178.1 to 5180.5	95 cal. ka BP (early MIS-5b; Machida and Arai 1992, 2003)
Aso-ABCD		5282.9 to 5286.9	
Ata	5180	5351.1 to 5352.6	105 to 110 cal. ka BP (Machida and Arai 1992); 108 ± 3 cal. ka BP (Matsumoto and Ui 1997)

3.2.4 Macrofossil Remains

Present within the Lake Suigetsu sediment profile are occasional macrofossil remains, quasi-evenly distributed down the sediment column according to the vicissitudes of chance deposition (Nakagawa *et al*. 2011). Of specific importance to the development of a radiocarbon calibration dataset from the site (sections 3.5.2 and 3.7) are the presence of leaves, needles, twigs and bark from terrestrial tree species, providing a faithful record of past changes in $\Delta^{14}C$. Additional remains of aquatic plant species and, very occasional, insect fragments are also present. The *Mikata-goko* region was never covered by Quaternary ice sheets, and was always surrounded by forest, even during the last glacial maximum (LGM; Gotanda *et al*. 2002, 2008; Gotanda and Yasuda 2008), allowing for the continuous transferral of the remains of these species into Suigetsu's basal sediments throughout the entire period of the lake's being.

3.3 Favourable Site Attributes for Radiocarbon Calibration Purposes

The key factor in determining Lake Suigetsu's importance for both radiocarbon calibration- and palaeoenvironmental reconstruction purposes is the independent, high precision chronology provided by the presence of the annually-deposited laminae (varves) throughout much of its sedimentary profile. Significantly for radiocarbon calibration purposes, these varves cover the entire period of interest for extending the terrestrially-based atmospheric radiocarbon calibration curve across the remainder of the radiocarbon dating method (i.e. from the early Holocene, several millennia after the present terrestrial limit of the IntCal calibration curve, through to beyond 60 cal. ka BP). These varves serve as an independent chronometer against which radiocarbon determinations from plant macrofossils,

retrieved from within these sedimentary layers, can be directly compared (Kitagawa *et al*. 1995).

As identified above, the hydrological features of the *Mikata-goko* (prior to anthropogenic intervention), contribute largely to the exceptionally well preserved palaeoenvironmental record exhibited in the sediment profile of Lake Suigetsu. As well as enabling the preservation of the varve structure of the basal sediments, the anoxic benthic conditions of Suigetsu prevent the microbial decay of the macrofossil samples deposited, allowing their preservation for radiocarbon analysis. The fact that only finer sediments are borne through the Seto Channel into Suigetsu from Lake Mikata means that the more abrasive, larger sediment particles are not represented significantly in the depositional régime of Suigetsu, which might otherwise also inhibit macrofossil preservation.

The Suigetsu sediment cores apparently maintain stratigraphic integrity throughout (section 4.1), with no obvious evidence of sedimentary hiatuses or inversions, which would otherwise severely impair the site's independent chronology and, therefore, markedly reduce the attractiveness of the site for radiocarbon calibration purposes.

As already emphasised in section 2.5, the major advantage over existing marine-based radiocarbon calibration datasets is that the Lake Suigetsu study, making measurements only on terrestrial material (i.e. terrestrially-growing plant macrofossils), is free from the added complication of marine reservoir effects or dead carbon fraction (DCF) corrections.

The small catchment size (identified above) is another advantage of the site, as this limits the residence time of samples within the catchment system prior to deposition in the Lake Suigetsu sediments. This is important for radiocarbon calibration development since the samples for radiocarbon measurement should be representing an atmospheric radiocarbon signal as contemporaneous as possible with the formation of the lake varves. Therefore, any inbuilt age of macrofossil samples in the Lake Suigetsu core should be minimised (albeit with

the caveats noted in section 4.2). The small catchment area has also remained (relatively) hydrologically stable through time, with any changes in the catchment (caused by past earthquake activity, and potentially affecting the varve thickness and/or structure) more easily recognisable than were the catchment significantly larger.

The presence of numerous tephra horizons throughout the sediment profile (section 3.2.3) provide isochronous markers that will enable the Lake Suigetsu sediments to be correlated to nearby (Sea of Japan and western Pacific) marine sediment cores. These correlations will provide the reliable chronological comparison to palaeoenvironmental data from the marine realm. More importantly for radiocarbon calibration purposes, it is possible to derive independent age measurements for the tephras originating from Korean source volcanoes (which, unlike their counterparts from the Japanese archipelago, erupt material derived from alkali-rich magmas) throughout the period covered by the radiocarbon calibration dataset via the argon-argon (^{40}Ar-^{39}Ar) dating method. (Only crystals from alkali-rich volcanic deposits, such as alkali feldspar, sanidine, [Na,K]$AlSi_3O_8$, can be reliably dated by the ^{40}Ar-^{39}Ar method. Volcanic material low in potassium content cannot be reliably dated, since the quantities of argon, arising from the decay of K, in such samples fall below the limit of reliable measurement.) These tie-points to the absolute timescale will be used to constrain the cumulative SG06 vyr counting uncertainty necessarily incorporated in any such layer counting methodology (section 3.6.6). Moreover, ^{40}Ar-^{39}Ar dates from lower down the core (below the annually-laminated portion of the sediment profile) can aid the age-depth modelling for palaeoenvironmental purposes at this older end of the Suigetsu timescale.

3.4 Potential Disadvantages for Radiocarbon Calibration Purposes

As was the case with the Suigetsu ’93 project (section 3.5, below), the main difficulty in generating a radiocarbon calibration curve from varved sediment is the ability to derive the

calendar timescale against which the radiocarbon determinations are plotted. These problems can be summarised into two categories: (i) the ability to reliably count the annual laminations; and (ii) the potential for there being hiatuses within the sediment column. The most likely cause of the latter issue in such a tectonically active region, would be disturbances to the benthic sediments caused by earthquake-generated turbidites. Such interruptions to the sediment profile might remove an unknown number of annually-deposited layers, severely inhibiting the construction of a calendar age scale. The former issue might vary with depth as the quality of varve preservation differs down the sediment profile, most likely caused by variations in the chemistry of lake basal water (specifically, the degree of anoxia) over time. As with the counting of other annually-layered palaeoenvironmental archives (e.g. tree-rings or ice cores), issues of multiple layers within a particular annual cycle, as well as that of particular missing annual layers, further complicate varve counting. Whereas dendrochronologies tend to be built up from extensive cross-matched records from many different trees, the varved sediment utilised herein is necessarily limited to a single lake site. Although the collection of sediment from multiple bore-holes (section 4.1) aids the identification of missing/within year laminations where particular depth horizons are duplicated between cores, any larger-scale events/factors affecting the whole of the lake bottom (e.g. from broader-scale turbidite events) would not be so easily recognised. Rigorous varve examination and counting by Suigetsu Varves 2006 project colleagues is seeking to identify any examples of potential hiatus events (specifically, by the thin-section microscopy approach) and, through a robust statistical interpolation approach (section 3.6.3, below), to minimise the uncertainties caused by poorly-preserved annual layers, or multiple intra-annual layers.

In terms of the radiocarbon signal provided by plant macrofossil samples retrieved from the Lake Suigetsu sediments, the most important issue is to ensure that the

determinations provide a reliable representation of the atmospheric radiocarbon concentration as contemporaneous as possible with the annually-deposited sediment laminae (calendar age) that their measurements relate to. As is detailed in section 4.2, careful sample selection is required for this purpose.

The Japanese island arc is subject to frequent volcanic activity. Volcanic degassing is associated with emission of 'old carbon', relatively depleted in ^{14}C. Thus, biota living in close proximity to volcanic vents would incorporate this signal into their tissue and yield apparent dates significantly older than their true values (e.g. Pasquier-Cardin *et al*. 1999; Beavan-Athfield *et al*. 2001; Cook *et al*. 2001). Such effects can be highly temporally variable. However, such signals fortunately tend to be very localised and short-term in their effects (Bruns *et al*. 1980), and so should not be an issue at Suigetsu.

3.5 The Suigetsu '93 Project

Four short sediment cores were obtained from the centre of Lake Suigetsu by Yasuda and co-workers (Takemura *et al*. 1994; Kitagawa *et al*. 1995, Yasuda *et al*. 2004) using piston-corers: cores 'SG1' (4 m long) and 'SG2' (11 m long) being collected in 1991, and cores 'SG3' and 'SG4' (both 16 m long) being collected in 1993. A longer, ≈ 75 m core ('SG93', also referred to as simply 'SG' in previous publications) was also obtained in 1993 using a drilling machine, and reached the base of the lake's sediment profile.

The Suigetsu '93 project was highly significant, as it was the first to identify varved sediments ('*nenko*') in Japan (Yasuda *et al*. 2004; Nakagawa *et al*. 2011), and had a number of important publications produced from it. Establishing a high precision independent chronology for the SG93 core through varve counting, Kitagawa and van der Plicht (1998a, 1998b, 2000) produced a terrestrially-based atmospheric radiocarbon calibration dataset from *circa* 8,800 to 37,400 cal. BP using > 300 radiocarbon determinations from plant macrofossil

samples obtained from the sediment core. High resolution palaeoenvironmental data were also obtained from the SG93 core spanning the late glacial to interglacial transition (LGIT; Nakagawa *et al*. 2003, 2005, 2006). However, suspected problems with the independent chronology of SG93 have limited the impact of these studies. The remainder of section 3.5 will provide more detail of the principal outcomes of the Suigetsu '93 project, as such matters, especially the potential problems identified from it, are of critical importance to the research objectives and overall success of the present Suigetsu Varves 2006 project (section 3.6). The radiocarbon- and palaeoclimatic findings of this original project are necessarily dwelt upon, since their conclusions will be re-interpreted (chapter 6) in light of revisions made to the original Suigetsu '93 chronology in this present DPhil thesis.

3.5.1 Suigetsu '93 Varve Chronology

As with the different bore-holes from the present project (section 4.1), Kitagawa and colleagues (1995) were able to tie together the SG2, SG4 and (upper portion of) SG93 sediment cores through correlation of characteristic event horizons (section 3.2, above). As reproduced in figure 3.9, the upper and lower segments ('I' and 'III') of the cores could be reliably correlated, whereas the middle segment ('II'), between the Kikai-Akahoya ('K-Ah') and U-Oki tephras, demonstrated a potential hiatus(es) in the SG4 core. The upper ≈ 29 cm of the sediments could not be counted because of the flocculent and disturbance of these layers. The floating varve chronology thus obtained for segment I was tied to the absolute timescale on the assumption that the turbidite layer at ≈ 29 cm was that caused by the historically known AD 1662 Kanbun earthquake (sections 3.1.1 and 3.2.2; Fukusawa *et al*. 1994; Kitagawa *et al*. 1995).

Initial varve counting of segments I and III (Kitagawa *et al*. 1995) was undertaken principally on the short piston cores under a microscope using ultraviolet (UV) light, which

picked out the lighter, diatom- and siderite-rich layers. An initial varve chronology of 6,995 and 5,489 varves (for segments I and III, respectively) was thus generated, placing the K-Ah tephra at 7,283 SG4 vyr BP, a date in very close agreement with the previously reported age of *circa* 7,300 cal. BP (derived from calibration according to the then dendrochronological calibration curve of a mean radiocarbon age of ≈ 6,500 BP from ≈ 100 radiocarbon determinations from across Japan; Machida and Arai 1992; Kitagawa *et al*. 1995), providing additional support for the annual nature of the laminations.

Originally, Kitagawa *et al*. (1995) anchored their lower floating varve chronology (segment III of figure 3.9) to the absolute timescale using the calibrated age (10,650 ± 250 cal. BP, according to the then dendrochronological calibration curve of Kromer and Becker 1993) for the weighted mean value of four reported radiocarbon ages of the U-Oki tephra (9,551 ± 73 BP; Machida and Arai 1992).

This initial varve chronology (Kitagawa *et al*. 1995) was subsequently revised (Kitagawa and van der Plicht 1998a, 1998b) because of: (i) the ability to derive a more precise wiggle-match of the floating Suigetsu varve chronology to the dendrochronologically-derived calibration dataset using the higher resolution radiocarbon data produced from SG93; and (ii) "previous miscounting of varve numbers". The previous varve counting method of UV light microscopy was found to under-count the less distinct varving of some intervals during the deglaciation and Pleniglacial (Kitagawa and van der Plicht 1998b). Therefore, a revised varve counting methodology was undertaken involving greyscale image analysis of digital core photographs. The deviation in varve counts between the former- and revised counting methodologies was on the order of ≈ 5% (Kitagawa, forthcoming) – significantly larger than the quoted ≈ 1.5% counting error, which was based upon replicate varve counts of selected SG93 core sections (Kitagawa and van der Plicht 1998a, 1998b). Using this revised varve counting protocol, a 29,100 year floating varve chronology was constructed for the

SG93 core between depths of 10.43 and 30.45 m (Kitagawa and van der Plicht 1998a, 1998b).

Figure 3.9: Correlation of the Suigetsu '93 piston cores SG2 and SG4 and upper portion of the longer SG93 core based on observation of characteristic event horizons. Initial varve count data according to Kitagawa and colleagues are also given. (Source: Kitagawa *et al*. 1995.)

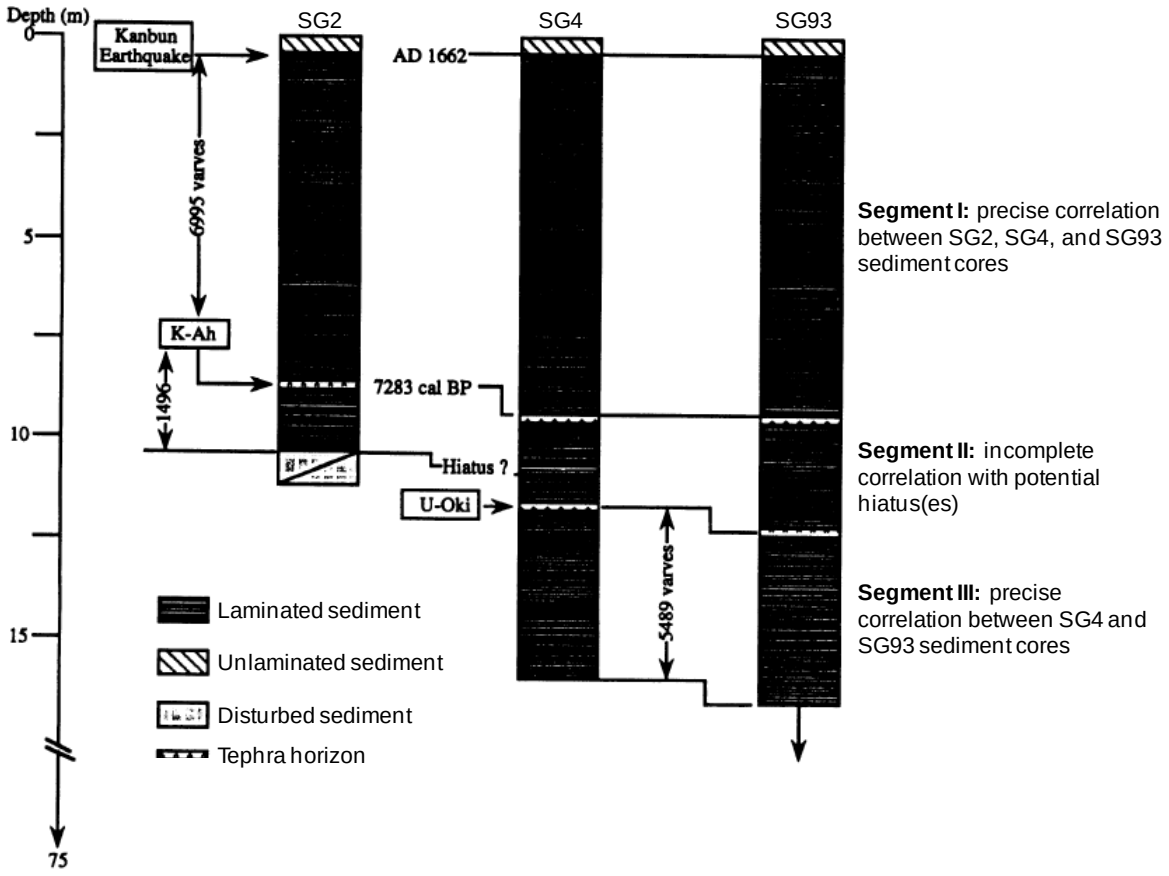

This floating SG93 varve chronology was tied to the absolute calendar timescale through least squares minimisation ('wiggle matching', section 5.4) of the radiocarbon data obtained from the core (section 3.5.2, below) to the absolute German oak- and floating German pine chronologies of Kromer *et al*. (1996) and Kromer and Becker (1993),

respectively. Twenty two SG93 radiocarbon determinations (spanning a period of ≈ 3000 years common to both records) were used for this match. This process provided 'absolute' calendar ages of 8,830 to 37,930 SG93 vyr BP for the SG93 varves. (For core depths below 30.45 m for which additional radiocarbon dates were obtained, i.e. 30.45 to 35.00 m, an approximation for the SG93 varve age was obtained through assuming a constant Glacial sedimentation rate.)

3.5.2 Suigetsu '93 Radiocarbon Calibration Dataset

Initial (Kitagawa *et al*. 1995), radiocarbon determinations were obtained for 46 terrestrial macrofossil samples (single pieces of leaves, twigs and insect fragments) from ≈ 7 m (969.5 to 1580 cm) of the SG4 core (i.e. segments II and III identified in figure 3.9). A standard acid-base-acid (ABA) pre-treatment methodology (section 4.3) was performed on all samples (with an additional protocol followed to produce holocellulose from the largest samples, i.e. those > 5 mg starting weight). Radiocarbon determinations were obtained on the Dating and Materials Research Centre, Nagoya University (Japan) Tandetron accelerator mass spectrometer (AMS). The ages of these samples ranged between 6,565 ± 70 and 14,665 ± 120 BP (appendix 2).

Following on from this initial study, Kitagawa and van der Plicht (1998a, 1998b) produced > 250 AMS radiocarbon determinations of terrestrial macrofossil samples from the longer SG93 sediment core. For the upper core sections (down to 19.3 m depth), samples were obtained through splitting of the core into ≈ 3 cm thick sections (corresponding to a sampling resolution of ≈ 20 to 50 years), and washing out of samples from the resulting ≈ 60 cm^3 of sediment. For the deeper core sections (down to 35 m depth), larger macrofossils were picked by hand (Kitagawa and van der Plicht 1998b). A strong ABA pre-treatment methodology was again applied to samples, and radiocarbon determinations obtained at the

Groningen AMS facility (the Netherlands). A large number (> 50) of 'reference blanks' were obtained from ^{14}C-free plant material picked from lower down the SG93 core (corresponding to an age of *circa* 90 to 100 cal. ka BP) and processed alongside the regular samples. The blank correction thus obtained for larger samples (yielding > 0.7 mg carbon) was 0.28 ± 0.03 (1σ) percent modern carbon (pMC), giving a 'background' age of 47,000 BP. This blank correction, and its scatter, increased with decreasing sample size below this value (Kitagawa and van der Plicht 1998b).

This SG93 radiocarbon calibration dataset was extended somewhat by Kitagawa and van der Plicht (2000), increasing the total number of radiocarbon determinations in the combined dataset to 333, however, the varve counting (performed for the earlier publications; Kitagawa and van der Plicht 1998a, 1998b) was not revised. (Using the improved tree-ring records of Spurk *et al*. 1998 and Kromer and Spurk 1998 did not affect the wiggle-match of the SG93 timescale on to the absolute timescale; Kitagawa and van der Plicht 2000.)

The final SG93 radiocarbon calibration dataset (as published by Kitagawa and van der Plicht 2000) is illustrated in figure 3.10, with the full dataset provided in appendix 3. These authors noted that the data younger than *circa* 12,500 cal. BP agreed well with IntCal98 (Stuiver *et al*. 1998a), but began to diverge systematically prior to this time (figure 3.10a). The older part of the Lake Suigetsu record was shown to agree well with the uranium-thorium (^{234}U-^{230}Th)-dated corals of Bard *et al*. (1998) between 24,000 and 15,000 cal. BP, but with potential divergence suggested for the preceding time period (figure 3.10b).

Figure 3.10: The original Suigetsu '93 radiocarbon calibration dataset, as presented by Kitagawa and van der Plicht (2000) covering the time periods: **(a)** 16,000 to 8,000 SG93 vyr BP/cal. BP (compared to the IntCal98 dataset of Stuiver *et al*. 1998a); and **(b)** 45,000 to 15,000 SG93 vyr BP/cal. BP (compared to the ^{234}U-^{230}Th dated corals of Bard *et al*. 1998).

(a):

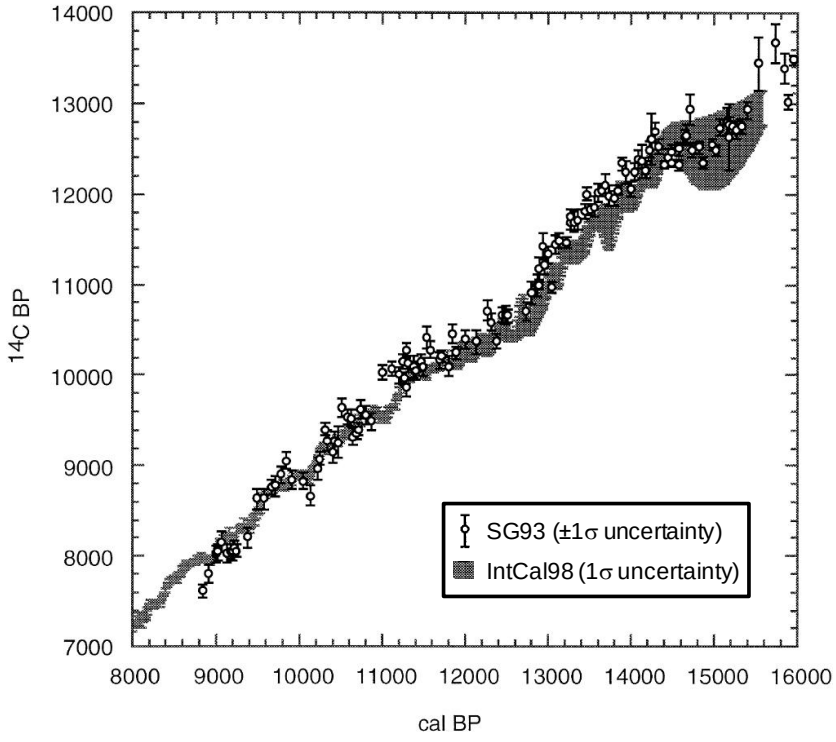

(b):

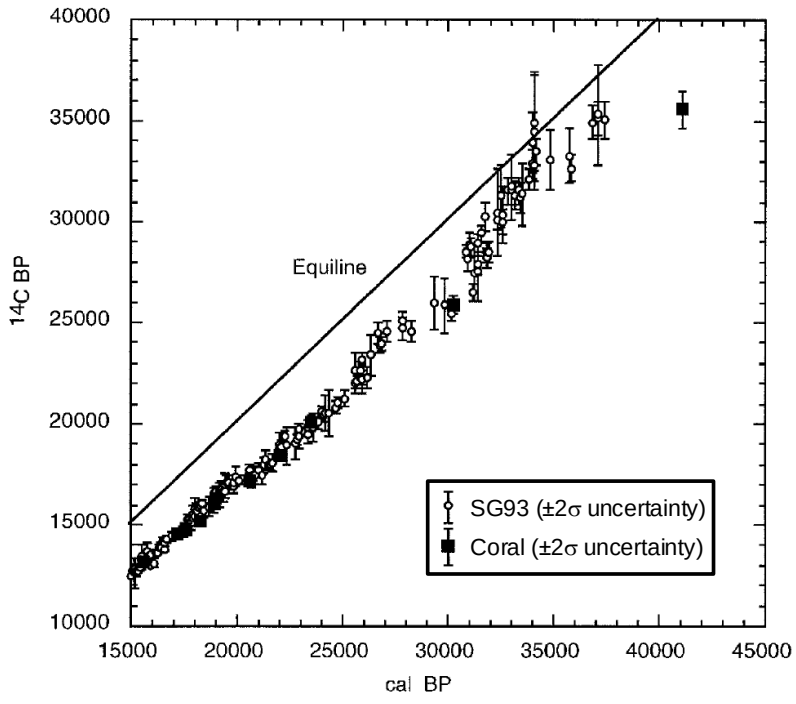

3.5.3 Chronological Problems

Kitagawa and van der Plicht (1998b, 2000) themselves identified the chief causes of uncertainty in their varve chronology as being: (i) the core sampling methodology; (ii) the varve counting itself; and (iii) the anchoring of their record on to the absolute age scale through wiggle-matching to the dendro- curve. With regard to the first of these issues, the SG93 core was retrieved in 90 cm-long sections from a single bore-hole. Thus, there was the potential for the loss of sediment (representing an unknown number of varves) between successive core sections. Comparison of the uppermost 16 m of the SG93 core with the two longest piston cores (SG3 and SG4), suggested that this sampling strategy did not cause "significant loss of varves" ("typically 0 to 2 cm to a maximum of 3 cm", representing ≈ 20 to 30 years in the Holocene and ≈ 50 years in the Glacial; Kitagawa and van der Plicht 1998b). In terms of the reliability of the varve counting, Kitagawa and van der Plicht (1998b, 2000) cited the varying quality of lamination through the sediment (and its preservation since coring) as limiting the detectability of the varves and, therefore, the accuracy of the varve counting. Based purely on duplicate counting of selected sections of core (≈ 10% of the entire 29,100 SG93 vyr chronology), and independent counting of core sections covering the same horizons, these authors estimated their counting error at < 1.5% (i.e. 150 years in 10,000 varve years). Below 16 m, down to 30.45 m, varve counting was performed on the single, longer, SG93 core, and so Kitagawa and van der Plicht (2000) therefore stated that their quoted varve ages beyond *circa* 18,800 SG93 vyr BP must be "considered as minimum ages", with cumulative error increasing with depth. The combination of these error sources leads the oldest part of the SG93 profile (at *circa* 40,000 cal. BP) to yield an estimated absolute timescale error of ≈ 2000 years, therefore precluding the use of this dataset as a reliable calibration curve (van der Plicht *et al*. 2004).

Sure enough, publication of alternative, high resolution radiocarbon calibration datasets (e.g. Hughen *et al*. 1998a, 1998b, 2004; Beck *et al*. 2001) released soon after the SG93 studies revealed significant divergence from the Lake Suigetsu record. This divergence is demonstrated in figure 3.11, with the Suigetsu '93 data (Kitagawa and van der Plicht 2000) plotted against the more recent (and seemingly more reliable) marine-derived calibration datasets of Fairbanks *et al*. (2005) and Hughen *et al*. (2006), along with the present consensus curve, IntCal09 (Reimer *et al*. 2009). It can be seen that this divergence becomes increasingly pronounced further back in time, especially before *circa* 25,000 cal. BP.

Figure 3.11: The SG93 radiocarbon calibration dataset (Kitagawa and van der Plicht 2000) as compared with the alternative calibration data of IntCal09 (Reimer *et al*. 2009), Hughen *et al*. (2006), and Fairbanks *et al*. (2005). All curves are plotted with 1σ uncertainties.

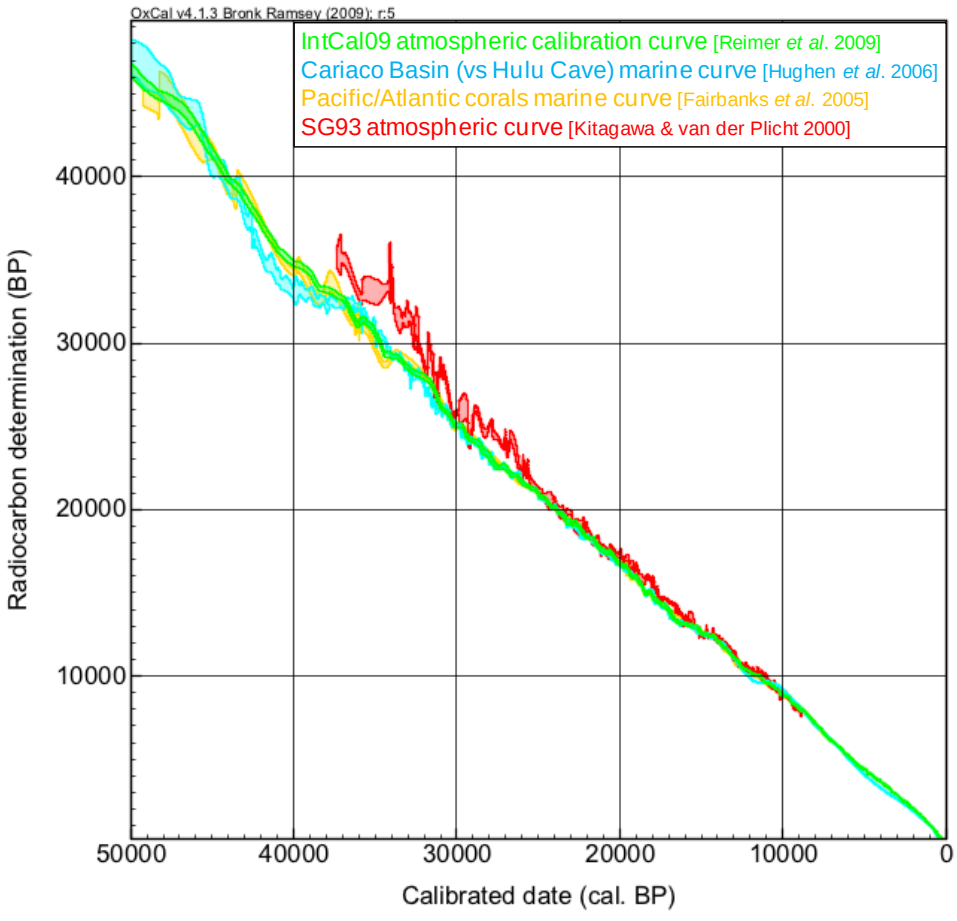

It is unlikely that such a systematic divergence between the Lake Suigetsu dataset and these alternative datasets represents a 'real' offset between the respective reservoirs from which the dated samples drew their ^{14}C. Whilst short-term (annual to millennial) deviations between the marine- and terrestrial data might be caused by unreliable correction for the marine reservoir effect, there is no feasible mechanism that would allow an increasing divergence (as indicated by figure 3.11) further back in time. The more likely causes of divergence therefore lie in the 'absolute age' profile generated for the Lake Suigetsu record caused by the reasons identified above.

Despite these problems with the Suigetsu '93 study, the work of Kitagawa and van der Plicht (1998a, 1998b, 2000) remains the only high resolution, terrestrially-based atmospheric radiocarbon calibration dataset that is both free from DCF correction (as is the case with speleothem archives; e.g. Beck *et al*. 2001) and that extends close to the limits of the radiocarbon dating method (Nakagawa *et al*. 2011). The Suigetsu '93 study therefore provides an "opportunity to learn what needs to be done to improve the accuracy and precision of varve chronology" with "lessons learned" (Kitagawa, forthcoming) for the present, Suigetsu Varves 2006 project. A principle aim of the Suigetsu Varves 2006 project, and the overall aim of my own DPhil research, is to improve upon the shortcomings of this previous project, and thereby fully exploit the site's potential for high resolution radiocarbon calibration.

3.5.4 Suigetsu '93 Palaeoenvironmental Reconstruction

Utilising the exceptional precision of the SG93 sediment profile, Nakagawa *et al*. (2003, 2005, 2006) produced a high resolution (average sampling interval 14.86 years from 386 sediment horizons), quantitative, palynologically-derived, palaeoclimatic reconstruction across the deglacial to early Holocene ('Last Termination'; 15,701 to 10,217 SG93 vyr BP)

sections of the core. The authors made the high impact claim that, whilst the sequence of climatic changes in Japan during the Last Termination closely resembled those of the circum-North Atlantic region (specifically, those of the Greenland ice cores, e.g. Alley *et al*. 1993 and Dansgaard *et al*. 1993, and the Cariaco Basin record, e.g. Hughen *et al*. 1996b), the timings of important climatic transitions were significantly asynchronous. The key findings of Nakagawa and colleagues (2003, 2005) were that: (i) an interstadial interval (Suigetsu pollen interstadial-, SGPI-, 1) commenced at *circa* 15,000 SG93 vyr BP in Japan, leading its counterpart in the North Atlantic (the Bølling, or Greenland Interstadial-, GI-, 1) by several centuries (≈ 300 years relative to Cariaco; ≈ 500 years relative to the GRIP ice core); (ii) conversely, a cold reversal in Japan (Suigetsu pollen stadial-, SGPS-, 1; from *circa* 12,300 to 11,250 SG93 vyr BP) lagged its North Atlantic counterpart (the Younger Dryas, YD, or Greenland Stadial-, GS-, 1) by several centuries (≈ 250 to 400 years); and (iii) the onset of the Suigetsu pollen Holocene (SGPH) biozone led the North Atlantic Holocene onset by ≈ 250 years. Furthermore, the amplitude of the cooling associated with the SGPS-1 event was much reduced as compared to its North Atlantic equivalent. Table 3.4 summarises the principal palaeoclimatic episodes identified from the SG93 core, as well as their "phenomenal-" (though "not chronological-"; Nakagawa *et al*. 2005) equivalent events in the North Atlantic.

Table 3.4: Summary table of the palynologically-derived event stratigraphy/palaeoclimatic data obtained from the SG93 core (Nakagawa *et al*. 2003, 2005). The minimum and maximum of the reconstructed T_{ann} (mean annual temperature) are given at the 68.2% confidence interval (and compare with a value of 14.8 ˚C today, section 3.1.2).

Name: Suigetsu Pollen-	**Duration (SG93 vyr BP)**	**Reconstructed climatic signal and dominant vegetation type**	**T_{ann} (min. to max.)**	**Equivalent North Atlantic event (in type, not timing)**	
stadial-2 (SGPS-2)	until 15,000	cold conditions, though long-term warming trend (T_{ann} reaching ≈ 10 ˚C by 15,000 SG93 vyr BP); cool mixed (COMX) forest	4 to 8 ˚C	GS-2	Oldest Dryas
interstadial-1c (SGPI-1c)	15,000 to 13,950	relatively warm temperature (T_{ann} ≈ 5˚C warmer than during Pleniglacial conditions; ≈ 5˚C cooler than at present); temperate deciduous (TEDE) forest, though centennial-scale fluctuations in dominant taxa	8 to 12 ˚C	GI-1e	Bølling/ Allerød
interstadial-1b (SGPI-1b)	13,950 to 13,750	sharp cooling spike within the broader interstadial (SGPI-1) period; continued centennial-scale fluctuations in dominant taxa	4 to 8 ˚C	GI-1b to GI-1d?	
interstadial-1a (SGPI-1a)	13,750 to 12,300	return to interstadial conditions following previous short-term cooler period; continued centennial-scale fluctuations in dominant taxa	8 to 12 ˚C	GI-1a	
stadial-1 (SGPS-1)	12,300 to 11,250	abrupt cold reversal (≈ 3 to 5˚C cooling), though climate unstable; “noisy” signals of major taxa	4 to 8 ˚C	GS-1	Younger Dryas
Holocene (SGPH)	11,250 onwards	warming conditions; TEDE forest, only later (sometime after 10,000 SG93 vyr BP) becoming warm mixed (WAMX) forest	8 to 12 ˚C	early Holocene	

The identification of such leads and lags in the global climatic system enables better understanding of the mechanisms of climate change and is a primary aim of the Quaternary

science community (e.g. Blunier *et al*. 1998). However, the conclusions drawn from such inter-regional comparisons are necessarily reliant upon the chronologies of each of the datasets involved, which need to be both accurate and highly precise to reveal the true pattern of spatial synchronisms/diachronisms, with any spatio-temporal offsets potentially taking place over relatively short time intervals. Furthermore, these chronologies need to be independent (rather than those based on the circular logic of tying to other sites' chronologies based upon assumptions of event synchronicities). As has been spelt out in the preceding section, the chronology of SG93 has been shown to be suspect and, as such, the palaeoenvironmental conclusions discussed above cannot be regarded as authentic without more robust chronological control.

Further to these issues of spatio-temporal leads and lags in the global climate system, the palaeoenvironmental record of Lake Suigetsu was also utilised to reveal seasonally-specific information pertaining to the Asian monsoon front. Nakagawa *et al*. (2006) showed that whilst the YD equivalent in Japan (SGPS-1) brought significantly cooler temperatures and increased precipitation (compared to the preceding interglacial period, SGPI-1) during winter months, the impact on summer climate was far less marked. The anomaly between the reconstructed stadial- and interstadial mean temperature of the coldest month (MTCO) was ≈ 2 to 4 ˚C, whereas that of the mean temperature of the warmest month (MTWA) was significantly smaller (≈ 0 to 2 ˚C). Winter precipitation (defined as the cumulative precipitation between October and March; P_{win}) was shown to increase markedly into the stadial (≈ 900 mm in SGPS-1, compared to ≈ 400 mm in SGPI-1), whereas there was no change to summer precipitation (cumulative precipitation between April and September; P_{sum}), remaining at ≈ 700 mm. Conversely, these authors found that at the onset of the interstadial (SGPI-1), both winter and summer temperatures responded by a similar magnitude (≈ 5 ˚C warming), with P_{win} remaining unchanged and P_{sum} decreasing. The

conclusions drawn by Nakagawa *et al*. (2006) from this dataset were that the response of the Siberian air mass (represented by winter temperature reconstruction at Lake Suigetsu) to YD cooling was far more marked than that of the Pacific air mass (represented in the Lake Suigetsu record by summer temperature reconstruction); severe winter cooling of the Siberian air mass would create the stronger temperature gradient responsible for an intensified winter monsoon (increase in P_{win}), whereas there was no change to the summer temperature gradient (and therefore no change to P_{sum}). The mechanism therefore envisaged by Nakagawa *et al*. (2006) as being responsible for driving climate change into the interstadial (SGPI-1) would be global (e.g. insolation changes), affecting both Siberian- and Pacific air masses equally, whereas there was a more regional causation of the YD-like cold reversal (e.g. THC interruption in the North Atlantic being propagated to the Siberian air mass far more effectively than to the Pacific region). The conclusions of this latest work would not be expected to be affected in light of subsequent revisions to the chronology of the study.

3.6 The Suigetsu Varves 2006 Project

The Suigetsu Varves 2006 project is a multi-national, multi-disciplinary project under the leadership of Professor Takeshi Nakagawa (Newcastle University, UK). The two over-riding aims of the project are: (i) to provide high resolution palaeoenvironmental data, coupled with an excellent chronology, to facilitate the understanding of spatial leads and lags in climate change across the global climate system; and (ii) through comparison of radiocarbon dating and the independent varve count chronology, to extend the purely terrestrially-based atmospheric radiocarbon calibration curve to the detection limits of the radiocarbon dating method. It is this latter project aim that my own DPhil research is fundamentally addressing.

3.6.1 Suigetsu Varves 2006 Palaeoenvironmental Reconstruction

Recognition of the global significance of Lake Suigetsu in terms of its palaeoenvironmental record is demonstrated by its recent acceptance as an 'auxiliary Global Stratotype Section and Point' (GSSP) for the onset of the present interglacial, the Holocene (Walker *et al*. 2009). The principal GSSP is provided by the North Greenland Ice Core Project (NGRIP; Dahl-Jensen *et al*. 2002; North Greenland Ice Core Project Members 2004; Andersen *et al*. 2006; Rasmussen *et al*. 2006; Svensson *et al*. 2006, 2008; Vinther *et al*. 2006), which places the Holocene base (Pleistocene/Holocene boundary) at 11,700 cal. yr b2k (i.e. 11,650 cal. BP, at a depth of 1492.45 m within the NGRIP ice core). In contrast to most GSSPs, which are based upon biological (fossil) evidence from the geological record, the NGRIP stratotype is defined by climatically-driven physical and chemical parameters within the ice core. For this reason, as well as the chronological precision possible for this most recent transition in geological time, which allows the identification of spatio-temporal variations in the onset of such recent events, five auxiliary, more conventional, stratotypes, based on biostratigraphic evidence, have been identified. Lake Suigetsu is one of these five auxiliary stratotypes, the others being: the Eifelmaar lakes (Holzmaar and Meerfelder Maar), Germany; Splan Pond, Canada; Lake Maratoto, New Zealand; and the Cariaco Basin, Venezuela (see Walker *et al*. 2009 for specific references for these four sites).

Suigetsu also offers the potential to contribute greatly to the aims of the 'INTIMATE' group ('INTegration of Ice core, MArine, and TErrestrial records, 60,000 to 8,000 years ago'; e.g. Björck *et al*. 1998; Walker *et al*. 2001; Lowe *et al*. 2001, 2008); as well as providing an extension to the terrestrial radiocarbon calibration curve, the Suigetsu Varves 2006 project will provide a high resolution, multi-proxy archive of past changes in palaeoenvironment, with excellent chronological control, and that can be correlated intra- and inter-regionally (with the aid of the site's tephrostratigraphy) to greatly enhance the identification of leads and

lags of changes in the global climate system, which can ultimately facilitate the better understanding of the causal mechanisms of global climate change (Nakagawa *et al*. 2011).

The methods of palaeoenvironmental reconstruction are, as has previously been introduced, multi-disciplinary, with a "wealth" of palaeoenvironmental indicators presently under investigation (Nakagawa *et al*. 2011), including: aeolian dust flux and origin analysis; biomarker analysis; compound-specific stable isotope analysis; diatom analysis; microbial DNA analysis; thin-section microfacies analysis; X-ray fluorescence (XRF) elemental and major component analysis; and pollen analysis and pollen-based quantitative climate reconstruction. It is this final proxy that will provide perhaps the most rigorous palaeoenvironmental dataset from SG06. As with the previous (Suigetsu '93) project (cf. Nakagawa *et al*. 2006), conventional pollen data are converted to a range of (palaeo-)climatic indices including: mean annual temperature (T_{ann}); mean temperature of the coldest month (MTCO); mean temperature of the warmest month (MTWA); winter precipitation (cumulative precipitation from October to March; P_{win}); summer precipitation (cumulative precipitation from April to September; P_{sum}); and the temperature difference between the warmest and coldest months (T_{var}). These various indices are obtained through performing the best modern-analogues technique (MAT; Nakagawa *et al*. 2002, 2003, 2005, 2006) and requires a vast training set to achieve reliable climatic reconstruction.

3.6.2 Project Collaborators

Up-to-date information on the progress of the Suigetsu Varves 2006 project, as well as the full details of team members, may be found at the project's external website: www.suigetsu.org. A summary of the existing project disciplines, and collaborating group members (and their institutions) at the time of writing, is also provided in table 3.5. A more

detailed account of pertinent work by project colleagues that will be referred to specifically in later parts of this DPhil thesis is given below.

Table 3.5: The multiple disciplines being undertaken as part of the Suigetsu Varves 2006 project (as of June 2011), along with the details of the team members responsible. (* indicates 'associate members' – i.e. not formal members of the Suigetsu Varves 2006 project; † indicates "now at the Department of Earth Sciences, University of Oxford, UK".)

Technique	Personnel	Institution
Radiocarbon dating	Prof. Christopher Bronk Ramsey, Dr. Fiona Brock, Richard Staff	Oxford Radiocarbon Accelerator Unit (ORAU), University of Oxford, UK
	Dr. Charlotte Bryant	NERC Radiocarbon Facility-Environment (NRCF-E), East Kilbride, UK
Varve counting	Dr. Henry Lamb, Dr. Michael Marshall	Institute of Geography and Earth Sciences, Aberystwyth University, UK
	Dr. Achim Brauer, Gordon Sclolaut	GeoForschungsZentrum (GFZ), Potsdam, Germany
Beryllium-10	Prof. Yusuke Yokoyama	Department of Earth and Planetary Sciences, University of Tokyo, Japan
Tephrochronology	Dr. Victoria Smith *	Research Laboratory for Archaeology and the History of Art (RLAHA), University of Oxford, UK
	Dr. Simon Blockley *, Dr. Alison MacLeod *	Department of Geography, Royal Holloway, University of London, UK
Optically stimulated luminescence (OSL)	Dr. Jean-Luc Schwenninger *	Research Laboratory for Archaeology and the History of Art (RLAHA), University of Oxford, UK
Palynology	Prof. Takeshi Nakagawa, Rebecca Payne	School of Geography, Politics and Sociology, University of Newcastle, UK
	Dr. Pavel Tarasov, Dr. Dieter Demske	Department of Earth Sciences, Freie Universität Berlin, Germany
Biomarkers	Dr. Emma Pearson	School of Geography, Politics and Sociology, University of Newcastle, UK
Organic chemistry	Dr. Jonathan Tyler	Department of Earth and Planetary Sciences, University of Tokyo, Japan †
Diatoms	Dr. Annette Kossler	Department of Earth Sciences, Freie Universität Berlin, Germany
	Dr. Megumi Saito-Kato	National Museum of Nature and Science, Tokyo, Japan

3.6.3 Suigetsu Varves 2006 Varve Chronology

Varve counting for the Suigetsu Varves 2006 project is being undertaken by two complementary methodologies, those of: (i) thin section microscopy (microfacies analysis; by project colleagues A. Brauer and G. Schlolaut); and (ii) ultra-high resolution XRF and X-radiography (by H. Lamb and M. Marshall). Although these methodologies have been combined previously to quantitatively assess micro-facies change through varved sediment, the Suigetsu Varves 2006 project is the first to utilise such an approach directly for varve counting (Marshall *et al*. forthcoming).

The XRF and X-radiography are carried out on an Itrax™ core scanner (Francus *et al*. 2009) with elemental scans carried out at 60 μm intervals throughout the SG06 core profile (i.e. at least ten measurements per annual cycle). This rapid, non-destructive methodology is performed on 1 m by 1 cm by 1 cm 'double-L channel' core sections (Nakagawa 2007), sub-sampled from SG06 immediately after extraction from their respective sampling tubes (section 4.1). The Itrax™ scanner has a flat X-ray beam, with a measurement area of 100 μm by 2 cm, which allows the averaging of grain-to-grain variance parallel to the sediment lamination, reducing 'noise', and facilitating clearer interpretation of the annual geochemical varve signal (Marshall *et al*. forthcoming). The freely available 'PeakCounter' software (http://dendro.naruto-u.ac.jp/~nakagawa; produced by T. Nakagawa), designed specifically for the Suigetsu Varves 2006 project to count varves from the Itrax™ instrument, aids manual interpretation of the annual lamination signal from the multi-parameter data from SG06. Each 'varve' identified by this approach is subjectively categorised from 1 ('extremely clear') to 4 ('extremely unclear'), which will be further discussed in chapter 7 (where radiocarbon data are used to independently assess the reliability of the project's varve counting). Replicate varve counts from overlapping double-L channels, as well as parallel bore-holes, have been

compared and demonstrate a < 1% error on the individual XRF and X-radiography counting method (Marshall *et al*. forthcoming).

Thin section microscopy is performed on 10 cm-long slices of SG06 core that have been freeze-dried, impregnated with synthetic resin under vacuum, and finely polished (Schlolaut *et al*. forthcoming). This, more classical varve counting approach, allows studying and characterising of the sediment (varve) composition and facilitates understanding of the processes of deposition, for which there is no automated substitution. As with the XRF and X-radiography approach, replicate counting of overlapping core sections, within- and between boreholes, suggests a < 1% error on the raw count data from the thin section microscopy approach (Marshall *et al*. forthcoming).

Throughout the sediment profile, an interpolation algorithm is implemented to supplement the raw count data (from each of the complementary varve counting methodologies) from core depths where the quality of varve preservation is less optimal. This automated interpolation algorithm is based upon the frequency distributions of varve thickness across proximal core depths, providing a more realistic, objective approach than simple manual interpolation (Schlolaut *et al*. forthcoming). Since only adjacent sections of core are utilised in this approach, interpolation is unbiased by the sedimentation rate of more distant core sections.

Comparisons of the multiple criteria for varve identification between the respective varve counting methodologies allows both quantification of- and dramatic reduction of internal error (Francus *et al*. 2009), with any differences between the respective methods accounted for. The finalised, complete SG06 varve count will involve combination of the mean (interpolated) data from both of the separate methodologies, with the maximum differences between the two counts used to provide the envelope of uncertainty (Marshall *et al*. forthcoming). For the SG06 core sections (1250 to 1814.6 cm composite depth) for which

varve counting has been provisionally completed, this maximum uncertainty range (different from the raw counting error, or repeatability, of the individual counting methods, described above) is ± 4% (G. Schlolaut and M. Marshall, personal communication), although this is likely to be a conservatively large estimate of the 'true' total varve count error.

As noted above, only the upper, annually laminated SG06 core sections (1250 to 1814.6 cm composite depth) presently provide provisionally completed varve count data, with the extension of this combined count, to the limits of radiocarbon detection, yet to be finished. Therefore, at the time of writing, the remainder of the required SG06 core depths for radiocarbon calibration purposes is necessarily reliant on the data from the XRF and X-radiography counting technique only, and, as such, the radiocarbon calibration data presented in chapter 7 are only preliminary and must accordingly be treated as such. The combined varve counting for the entirety of the radiocarbon dating method is expected to be completed within ≈ 9 months from the submission of this thesis (i.e. early 2012), at which point the data contained herein will be updated for publication (and hopeful inclusion into the international consensus, IntCal, calibration curve).

3.6.4 Beryllium-10

Like ^{14}C, beryllium-10 (^{10}Be) is a radioactive (half-life, $T_{½}$ = 1.50 × 10^6 years), cosmogenic nuclide formed in the upper atmosphere through high-energy cosmic ray spallation (of oxygen and nitrogen, in the latter instance; McHargue and Damon 1991). As with ^{14}C production, ^{10}Be production rate is affected by variations in solar activity and changes in the Earth's geomagnetic field intensity, which modulate these incoming galactic cosmic rays (Raisbeck *et al*. 1981; Muscheler *et al*. 2008). Unlike ^{14}C, which becomes incorporated into the global carbon cycle, ^{10}Be is rapidly precipitated out of the atmosphere (with a mean residence time of one to two years; McHargue and Damon 1991). ^{10}Be can

therefore be utilised to demonstrate past changes in upper atmosphere radionuclide production.

It was hoped that through identification of the Laschamp geomagnetic excursion (section 2.5.6), and other notable ^{10}Be signals in SG06, direct tie points with the Greenland and Antarctic ice core records would be established (cf. Raisbeck *et al*. 2007). The Laschamp event is particularly relevant as, being temporally relatively close to the limits of the radiocarbon dating method, this would provide an important isochronous marker with the ice core datasets (Bard *et al*. 2004b), reducing the issues of cumulative varve/ice layer counting errors that would limit the identification of geographic leads and lags between these respective palaeoenvironmental records. Whilst reconstructed Δ^{14}C can also serve this purpose, the radiocarbon signal is also affected by the changing partitioning of carbon between the different global carbon reservoirs, whereas the ^{10}Be signal provides a direct indication of atmospheric production rates (Muscheler *et al*. 2000, 2004, 2008).

Importantly for this DPhil thesis, having a reliable, independent chronological constraint towards the older limit of the radiocarbon method would significantly improve the robustness of the varve age scale against which the radiocarbon determinations are directly compared. However, as will be discussed more fully in section 8.1.4, low resolution ^{10}Be analysis of the SG06 core (performed by project colleague Y. Yokoyama) has yielded equivocal findings, thus far preventing the use of ^{10}Be in achieving this aim.

3.6.5 Radiocarbon Dating of Pollen

Project colleague F. Brock has received funding (from the John Fell OUP Research Fund, University of Oxford) to undertake a pilot study to radiocarbon date pollen grains extracted from sediments using flow cytometry (with collaborator R. Jones from the University of Exeter). This novel approach to pollen extraction aims to minimise the potential

for modern ^{14}C contamination that more regular- (density separation) techniques necessarily introduce, as well as significantly reducing the time required to prepare each sample. Specifically, this project includes samples from four horizons down the SG06 sediment core. Comparison of the data obtained from the dating of pollen with that obtained from the macrofossil samples (performed herein) will demonstrate how successful this technique will have been. A potential future ramification of a successful outcome to this pilot study would be the opportunity to radiocarbon date many more horizons from the SG06 core using pollen. In this way, the distribution of radiocarbon data in the Suigetsu Varves 2006 calibration dataset would no longer be constrained to the punctuated distribution of plant macrofossil samples down the sediment profile but, rather, would become an effectively continuous archive from which radiocarbon samples could be drawn, as is the case with the tree-ring record. Conversely, a limiting factor to this would be the number of pollen grains available from a given depth horizon necessary to give a sufficient carbon mass to yield a reliable radiocarbon determination; low density of pollen samples at a given depth might require the integration of samples from a broader depth range. Thus, there would be a trade-off between the ability to date sections of sediment lacking macrofossils, with the possible loss of sampling resolution achieved through dating of the pollen grains (as compared to the single year resolution of dating macrofossils).

3.6.6 ^{40}Ar-^{39}Ar Dating of the U-Oki Tephra

As noted in section 3.2.3, the reference year for the floating SG06 varve chronology will be the U-Oki tephra horizon at a composite depth of 1286.1 to 1288.0 cm. Pilot work undertaken by project colleague V. Smith (also funded by the John Fell OUP Research Fund, University of Oxford) has geochemically correlated this tephra layer with the proximal material from its source volcano (deposit ‘U4’ of the Ulleung-do volcano, South Korea,

< 500 km distant from Lake Suigetsu). This proximal material can be directly dated by the ^{40}Ar-^{39}Ar method and, for the time being, will provide the only reliable, independent comparison for the fixing of the floating varve chronology to the IntCal09 calibration curve via wiggle matching of the SG06 radiocarbon dataset (section 7.4). It is hoped that future grant money will be obtained to perform similar analysis for other tephra layers (of Korean origin) down the SG06 core (section 8.2.2).

3.7 Specific DPhil Aims and Objectives

As noted previously, the overarching aim of my DPhil research is to produce the SG06 radiocarbon calibration curve on behalf of- and in collaboration with other Suigetsu Varves 2006 project members. There are, however, a number of subsidiary aims that lead to this overall objective:

(i) to produce an initial statistical re-analysis of the original Suigetsu '93 dataset, thereby providing a predictive model for the likely fit of the SG06 calibration dataset, as compared to IntCal. This exercise was performed using the latest Bayesian statistical methods (chapter 5) to assess this original data. A thorough description- and the results of this exercise are provided in section 6.1 (and have also been published by Staff *et al*. 2010; appendix 7).

(ii) to refine the specific laboratory methodologies required for the production of reliable AMS radiocarbon determinations from the smaller than usual sample sizes (submitted to ORAU; i.e. samples of < 0.7 mg C) of the small macrofossil samples throughout the SG06 sediment profile. The most significant stage in this methodological development involved enhancement of the graphitisation process. Although not included in the main body of this thesis, these issues, and the empirical findings of the experiments performed, are provided in appendix 4.

(iii) to sub-sample sufficient terrestrial plant macrofossils from the SG06 sediment core to yield the ≈ 600 radiocarbon determinations for which funding was secured (UK Natural Environment Research Council, NERC, grant NE/D000289/1) for the Suigetsu Varves 2006 project. To this end, more than the required number of ≈ 600 samples needed to be collected, since a sizable proportion of the samples collected were either too small (to provide reliable radiocarbon determinations), or were in too close proximity to other samples (in terms of composite depth) to make it worthwhile in dating these samples. I.e., since the ≈ 600 radiocarbon data points should be spread as evenly as possible throughout the radiocarbon dating range (0 to ≈ 60,000 BP), some more problematic samples (smaller, or less reliable sample types) needed to be processed to avoid some larger gaps down the SG06 depth profile than would be achieved through simply dating the best (largest) samples selected. An overview of all of the samples collected is given in section 7.1, whilst a more thorough inventory is provided in appendices 10 and 11.

(iv) in combination with the NERC Radiocarbon Facility-Environment (NRCF-E), East Kilbride (specifically involving project colleague C. Bryant), to produce the ≈ 600 radiocarbon determinations for which funding was secured for the Suigetsu Varves 2006 project. These ≈ 600 determinations were divided equally between the two laboratories, which included a number (approaching 10%) of duplicate measurements (from splitting of larger, individual entities) down SG06 to demonstrate inter-laboratory dating consistency. A comprehensive table of these radiocarbon data are provided in appendix 12, whilst detailed summaries and interpretations are provided throughout chapter 7.

(v) to anchor the floating SG06 varve chronology (with the datum year at the U-Oki tephra, 1286.1 to 1288.0 cm composite depth) to the absolute timescale through wiggle matching of radiocarbon data to the international consensus calibration curve, IntCal09

(Reimer *et al*. 2009). A discussion of the statistical techniques for performing this exercise is presented in sections 5.3 and 5.4.1, and the outcomes are presented in section 7.4.

(vi) to physically examine the archive material from the SG93 core and, through comparison with the composite SG06 core, to tie the former, problematic depth profile on to that of the latter. This process provides an empirical test of the accuracy of the findings of the statistical exercise described in aim (i). More significantly, this process enables the integration of the ≈ 300 data points from the Suigetsu '93 study (Kitagawa and van der Plicht 1998a, 1998b, 2000) into a combined Lake Suigetsu radiocarbon calibration dataset, significantly enhancing the resolution of the overall dataset thus achieved (to nearly 900 data points, i.e. ≈ 300 data points from SG93 and ≈ 600 from SG06). Simple mathematics would suggest that the average dating interval of such a dataset is well under 100 years (i.e. ≈ 900 data points covering the radiocarbon dating range, 0 to ≈ 60,000 BP; Nakagawa *et al*. 2011). This physical matching of the respective Suigetsu cores is described in section 6.2, with additional figures demonstrating the matching given in appendix 9. The comparison of the re-modelled SG93 dataset with the SG06 dataset is provided in section 7.6.1, and the two datasets combined in section 7.6.2.

(vii) using the varve chronology provided by project colleagues (A. Brauer, H. Lamb, M. Marshall and G. Schlolaut), to provide the finalised Suigetsu Varves 2006 radiocarbon calibration dataset. Unlike the previous Suigetsu study, it is hoped that this dataset will be suitable for forming a major contribution to a future revision of the international consensus calibration curve (IntCal). The preliminary Suigetsu Varves 2006 radiocarbon calibration curve (in the absence of completed varve counting by project colleagues) is provided in chapter 8.

(viii) to compare the Suigetsu Varves 2006 radiocarbon calibration dataset with those derived from marine sources (notably the high resolution Cariaco Basin dataset of Hughen *et*

al. 2004b, 2006, and the Bahamas coral data of Fairbanks *et al*. 2005). Whilst the long-term trends of these datasets should be in good agreement (assuming the calendar timescales of these respective datasets to be broadly coherent), any shorter-term (centennial to millennial) departures of the marine data might reveal significant information on the changing marine reservoir correction at these sites over time, which in turn has major implications for changing marine circulation patterns (with a presumed linkage to major climatic events; Nakagawa *et al*. 2011). Initial data comparison of these respective radiocarbon calibration datasets, as well as their implications, is provided through chapter 8.

Inevitably in such a collaborative project, there is a significant degree of sharing of ideas and data, which will have fed into the work presented herein. Throughout this thesis, it should be made clear which aspects of the broader project that are being referred to have been performed by project colleagues, rather than by myself. As has been emphasised, my responsibility on the Suigetsu Varves 2006 project was the development of the radiocarbon dataset, to be combined with the data from varve counting colleagues to produce the Suigetsu Varves 2006 radiocarbon calibration dataset. The sediment coring (described in section 4.1) was undertaken prior to my involvement on the project, as was the collection of the first 326 macrofossil samples from the core (which was carried out by project colleagues T. Nakagawa and R. Payne), and ≈ 60 pilot radiocarbon determinations performed between the ORAU and NRCF-E AMS facilities (performed by project colleagues C. Bryant and F. Brock). The remainder of macrofossil sub-sampling (section 4.2), chemical pre-treatment and preparation for AMS at ORAU (section 4.3), and sample selection for submission to NRCF-E was performed by myself, and the data analysis is my own (although, of course, with input from project colleagues).

4. Field and Laboratory Methods

The methodologies applied in developing the Suigetsu Varves 2006 radiocarbon calibration curve are summarised in figure 4.1. Each of the field and laboratory stages will be discussed sequentially through chapter 4, with the final stage, that of statistical methods and interpretation, being described in chapter 5. An additional discussion of the specific laboratory methodological refinements necessarily developed for dealing with the smaller than usual plant macrofossil samples collected from the SG06 sediments is provided in appendix 4.

Figure 4.1: Flow diagram demonstrating schematically the methodological stages applied in developing the Suigetsu Varves 2006 radiocarbon calibration curve.

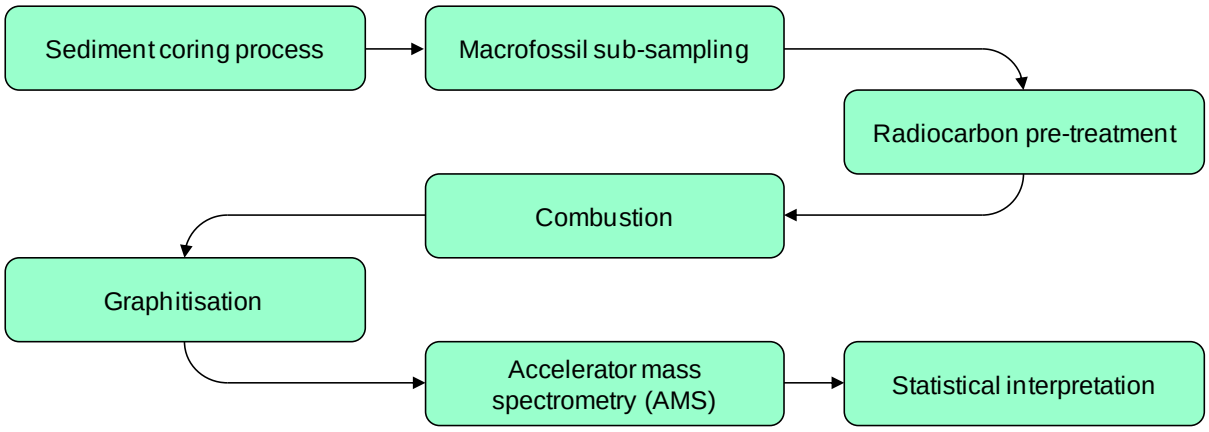

4.1 Sediment Coring Process

A significant improvement of the Suigetsu Varves 2006 project upon that of the previous study undertaken at Lake Suigetsu (the Suigetsu '93 project; section 3.5) was the sediment coring methodology applied. Specifically, this involved collection of material from four separate bore-holes (A, B, C and D) overlapping such that material from any given Lake

Suigetsu sedimentary horizon would be represented by at least one of these individual sediment cores (figure 4.2). The sediment coring was undertaken by SEIBUSHISUI CO. LTD. (Nagasaki, Japan) over a six week period from 3rd July to 11th August 2006 using a hydro-pressure thin-walled piston sampler installed on a floating drilling platform (Nakagawa *et al*. 2011; figure 4.3). Bore-hole A was drilled at 35˚35'08"N, 135˚52'57"E at the lake's depocentre of 34 m, with the three further bore-holes, B to D, drilled within a 20 m radius of bore-hole A. Core sections from each bore-hole were numbered successively from the top: 46 core sections were retrieved from bore-hole A, down to a drilling depth of 71.0 m; 47 from bore-hole B (although four of which were 'wholly disturbed'), to a drilling depth of 71.5 m; 21 core sections were attempted from bore-hole C (although two of which were not successfully retrieved), to a drilling depth of 51.9 m; and three core sections were obtained from bore-hole D, to a drilling depth of 7 m (figure 4.2).

The inner diameter of the sampling tube (and therefore the diameter of each of the retrieved sediment core sections) was 7.8 cm. Each of these sediment core sections was extracted from its sampling tube within a few days (at most) of its recovery from the lake bottom. A mechanical piston was used for this extraction process, inevitably resulting in a compaction and/or disturbance of the upper $\leq$ 5 cm of each core section. No significant disturbance was evident beyond this upper 5 cm region. These, and other aspects of the sediment coring process, are described more fully in Nakagawa *et al*. 2011 (produced *in toto* in appendix 5).

Figure 4.2: Schematic diagram of the generation of the composite 73.19 m Suigetsu Varves 2006 core ('SG06') generated from the four separate sediment cores, A to D. The primarily grey in appearance core sections are miniaturised core photographs, whilst the brown core sections are those that were disturbed during coring. The solid red horizontal lines (along with 'K-' label) are the 'key correlation layers' between the respective bore-holes, whilst the hashed red lines reflect less secure correlations. (Adapted from: Nakagawa *et al*. 2011.)

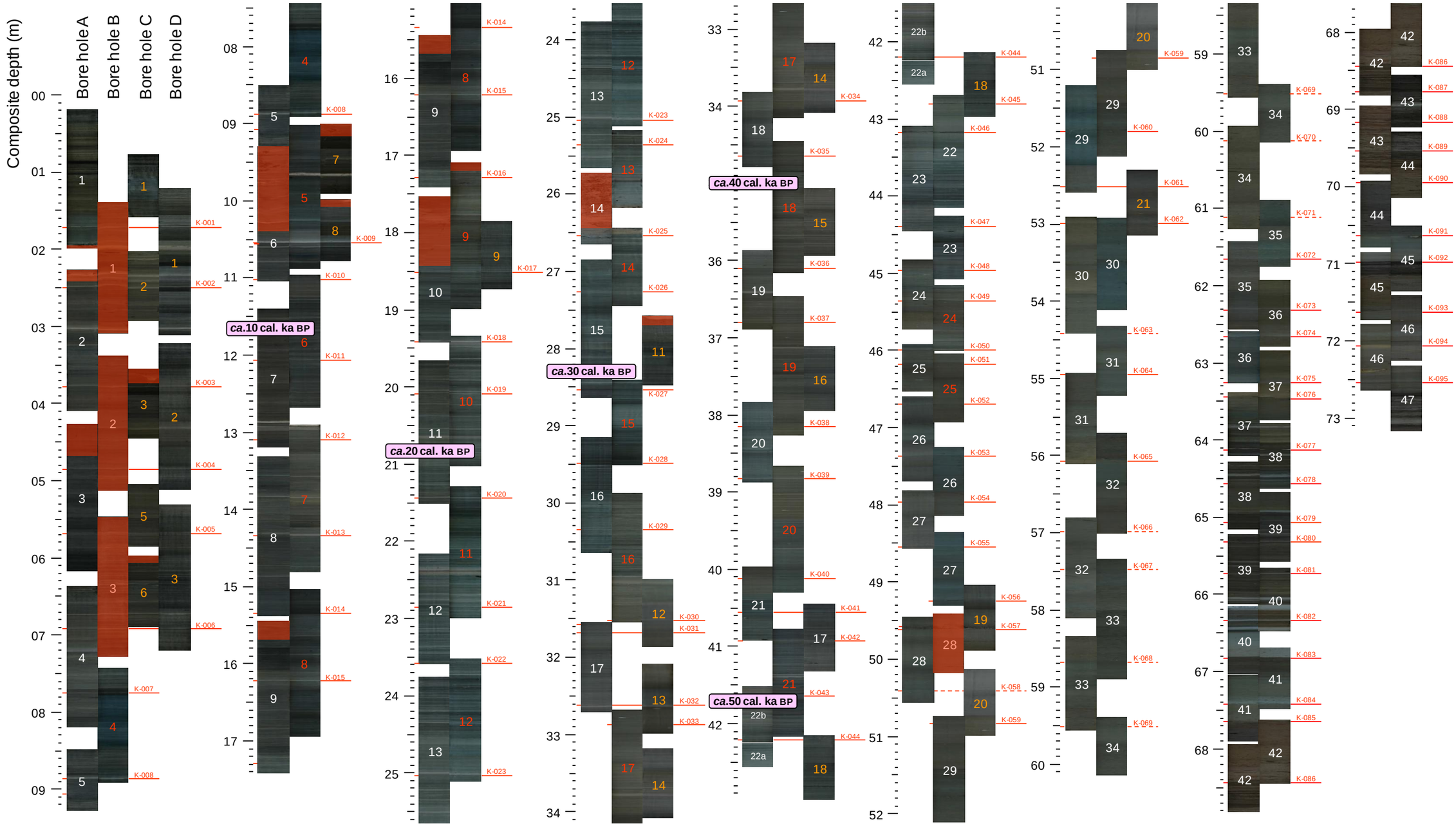

Figure 4.3: Drilling platform for the coring of the SG06 sediment core. (Source: K. Takemura, personal communication.)

Continuity of sedimentary facies can clearly be seen through visual comparison of characteristic event layers (including tephras, flood layers, turbidite layers and laminae with distinct colouration) from equivalent depths across the separate cores. On-going thin-section micromorphological analysis (performed by project colleagues A. Brauer and G. Schlolaut) has yet to identify the presence of any significant discontinuities within the sequence (at least for the time period of interest to the present study – that of the varved core sections), as might be generated from earthquake events, for example, which might be suspected for such a tectonically active area.

Through visual comparison of the major event horizons between core sections from the four separate bore-holes, a composite core ('SG06') of 73.19 m length was produced (figure 4.2), seemingly lacking any of the age gaps down the depth profile that so significantly affected the Suigetsu '93 study.

4.1.1 Composite Depth and 'Event-free' Depth Units

Upon extraction of each of the SG06 core sections from their sampling tubes, the cores were immediately split into two half cylinders (designated 'North', 'N', or 'South', 'S', according to the orientation of the core sections within the sediment profile) and the freshly-exposed sediment surface digitally photographed (Inoue *et al*. 2007), along with a 'quasi-real' depth scale, before any colour changes through oxidation could occur (i.e. within a minute of splitting). Within each core section, layers with clearly identifiable characteristics were numbered (from the top), ideally at 10 to 20 cm intervals. These layers were defined at 1 mm precision using the depth scale of the digital images (Nakagawa *et al*. 2011).

The red horizontal lines (along with 'K-' label) on figure 4.2 are the 'key correlation layers' between core sections of the respective four bore-holes, between which the depth scale (according to the digital core images) of only one of the core sections contributes to the master depth scale of the composite SG06 core. Thus, the SG06 composite depth scale is generated through addition of the respective raw depth scales of the designated master core sections throughout the entire sediment profile. Although an effectively arbitrary unit, the composite depth is a 'pure' measurement – not manipulated in any way – and is the primary depth unit given throughout the Suigetsu Varves 2006 project. The hashed red lines of figure 4.2 reflect less certain correlations between bore-holes. Thus, the reliability of the composite depth model is less sound for such sections. Fortunately for radiocarbon calibration purposes, the Suigetsu Varves 2006 project team considers there to be no

correlation error for the laminated core sections (primarily, from the core top to 4601.4 cm, which covers the entire radiocarbon dating range; Nakagawa *et al*. 2011).

In addition to the composite core depth scale, an 'event-free' depth profile was also generated for SG06 (cf. the 'event-removed' SG3 sediment profile of Katsuta *et al*. 2007). This latter depth scale is based on the composite depth model, but excludes aberrant single event layers (representing individual flood, earthquake, or tephra events) in excess of 5 mm thickness (generated by T. Nakagawa). This event-free chronology has aided construction of the preliminary Lake Suigetsu age-depth profile, prior to completion of the independent varve-based chronology by project colleagues (achieved through Bayesian statistical modelling of the radiocarbon data; section 5.4.2), and is also used for modelling of the final radiocarbon data, free from varve count information, to provide an independent test of the latter (chapter 7).

4.2 Macrofossil Sub-Sampling

Terrestrially-originating macrofossils were picked by eye from study of the exposed surface of the sediment generated through longitudinal division of the cores (figure 4.4). The majority of samples are plant leaves, although small twigs, bark, seeds, and a few segments of insect are also present. Sampling was thus undertaken throughout the entirety of the sediment profile covering the time period of interest for radiocarbon calibration (i.e. back to *circa* 60,000 BP at approximately 42 m composite depth). For core depths bearing an apparently reduced density of plant macrofossils, the core was necessarily re-split longitudinally to expose a greater area of sediment such that it was hoped to fill such gaps. In this way, the aim was to provide datable- (i.e. large enough, reliable-) samples at regular intervals throughout the core depths encompassing the entire radiocarbon dating method.

Figure 4.4: Magnified view of a section of the SG06 sediment core (section B-18), demonstrating the identification of terrestrial macrofossils within the sediment profile. (Plant macrofossil highlighted, #336, is a small to medium deciduous broad leaf at a composite core depth of 3562.5 cm.)

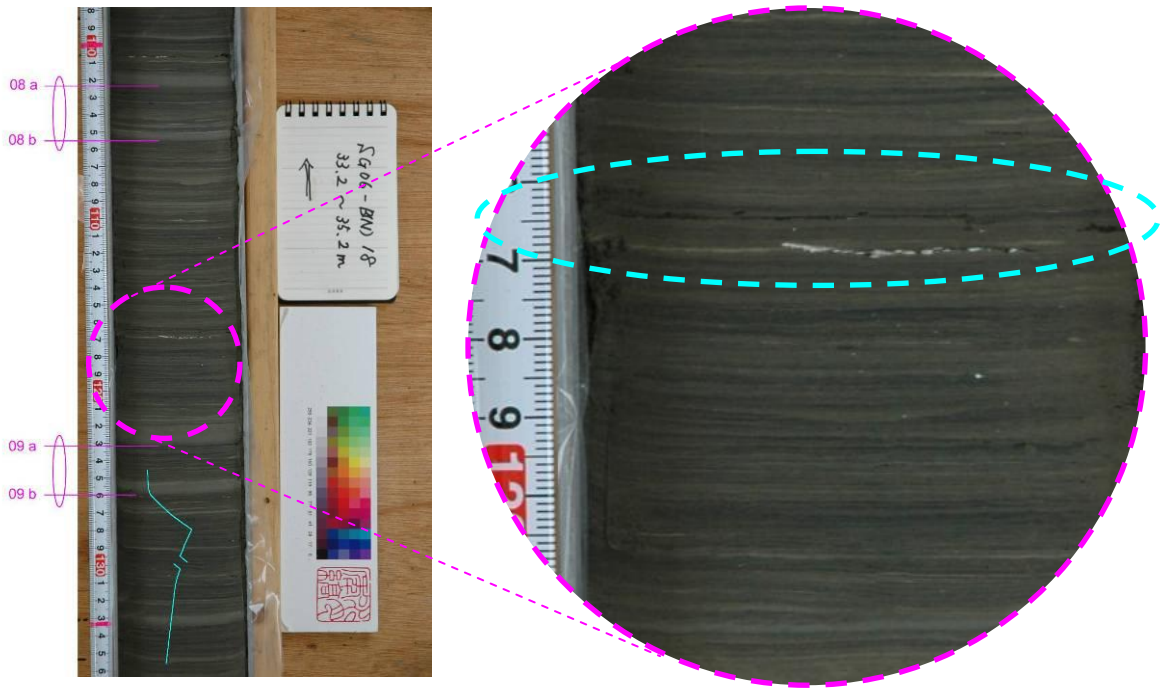

Although the aim of the project was to obtain radiocarbon-dated terrestrial macrofossils from throughout the required depths of the sediment column, particular sections of the core were preferentially avoided for sub-sampling, despite the fact that they might have contained quite tempting macrofossil samples. Event layers (section 3.2.2) were avoided since there is a reduced likelihood that samples retrieved from such laminae would represent material with a ^{14}C signal contemporaneous with the timing of the sedimentary event. Macrofossils washed into the lake at times of flooding bear an increased risk of being held longer *in situ* elsewhere in the lake catchment prior to in-wash, and would therefore contain an inbuilt age as compared to the date of the event layer formation itself. Similarly, samples contained within turbidite layers (whether caused by earthquake activity or otherwise) are likely to have been

re-worked from material previously stored in the upper littoral zone of the lake sediments, and could again provide material with an inbuilt age (Hajdas *et al*. 1995a).

Macrofossil samples were not analysed from where they lay close to the outside of the sediment core, as these samples might potentially have been moved up or down the sediment column during the coring process. Also, samples from the upper 5 cm of core sections were avoided because of the potential for these layers to have been compacted/disturbed during the core extraction process (section 4.1, above). Thus, only samples taken from a sound chronostratigraphic context were obtained for dating.

Single pieces of terrestrial macrofossils were chosen for analysis since a wholly intact individual entity is far less likely to have moved up or down the sedimentary profile as compared to an unidentifiable mixture of organic remains that, in general, would be far less reliable for dating. Such a mixture of sampling material might represent a range of differing radiocarbon ages, and therefore not be appropriate for combining into a single sample for dating (Hatté and Jull 2007).

Since the strength of the Lake Suigetsu macrofossil record for radiocarbon calibration purposes lies in the fact that samples are of terrestrially-growing species, samples identified as aquatic species (those growing within the lake itself) were necessarily avoided for dating. Such samples might be expected to demonstrate an offset from the contemporaneous atmospheric ^{14}C record as a result of the reservoir effects discussed previously (section 2.2.1).

Broad leaves were preferentially sampled over seeds, needles, twigs or bark on the assumption that since the leaf samples are generally much more fragile, they would be more likely to have been transported relatively quickly between their separation from the living organism and their deposition in the anoxic basal lake sediments if they were to remain intact enough to yield sufficient carbon (ideally >0.6 mg C) for radiocarbon dating (see appendix 4). Observation of the aerobic decomposition of leaves in the terrestrial

environment suggests that this time lag from host organism to deposition in the lake varves must be relatively short (i.e. well below the resolution of the calibration dataset being produced herein) if leaves are to survive intact enough to meet this minimum mass criterion. This approach of selecting "fragile macrofossils" is advocated by Hatté and Jull (2007), who suggest that such samples will also be damaged/destroyed by sediment re-working.

Although very scarce in the lake record in any case, insects were preferentially avoided for dating since the synthesis of ^{14}C via the trophic pathway into these organisms is not as direct (from that of the atmosphere) as is the case with photosynthesising terrestrial plants. Detrital feeders, for example, might feed on relatively old, decaying organic material, and assimilate this relatively older carbon (depleted in ^{14}C) into their tissue.

4.2.1 Depth Control

As with sub-sampling (or, indeed, direct data retrieval) from the sediment cores of other sites, depth control for the sub-sampling of SG06 is of paramount importance. Issues such as post-coring expansion/contraction of core sections should be accounted for, as must the issue of (slightly) differing deposition rates between the parallel bore-holes. Designed especially for the Suigetsu Varves 2006 project (but with the ability to transfer to other study sites), the 'Level Finder' software (developed by T. Nakagawa) enables such depth control issues to be accounted for and provides exceptionally high precision for all aspects of the project.

Level Finder incorporates the composite core depth model (and, if desired, the event-free depth model, an age-depth model, and varve count data), which includes depth information of all the numbered characteristic laminae from each core section. Figure 4.5 illustrates a 'screen grab' of this Level Finder software. The core sections from each of the four contributing bore-holes can be seen in parallel, with those contributing to the 'master'

(composite core) depth scale highlighted in light blue; depths of the characteristic laminae are shown in magenta, with the 'key' correlation layers (section 4.1.1) shown in red; the combined, composite core profile is additionally shown as the fifth column, with just the key correlation layers plotted. If the event-free model is included, event layers (> 5 mm in duration for the event-free model applied herein; section 4.1.1) are additionally shown in a 'sandy' colour. With an age-depth model included, depths that have contributed to the model implemented (for the present example of the SG06 core: the upper ≈ 42 m of which being based on radiocarbon determinations; the remainder being based upon tephra events and palynological data presently tied to a nearby marine core by project colleague R. Payne) are marked by darker blue circles.

Figure 4.5: A 'screen grab' of the Level Finder software (developed by T. Nakagawa) with a 2 m section of the SG06 core illustrated (150 to 350 cm composite depth). Core sections from the four contributing bore-holes, A, B, C and D, are shown, along with the master (composite) core depth profile. Characteristic laminae from the four bore-holes are shown in magenta, along with 'key' correlation layers shown in red. Event layers (> 5 mm in duration) are shown in the 'sandy' colour. Depths that have contributed to the age-depth model applied (here, depths from which samples have been radiocarbon dated) are marked with darker blue circles.

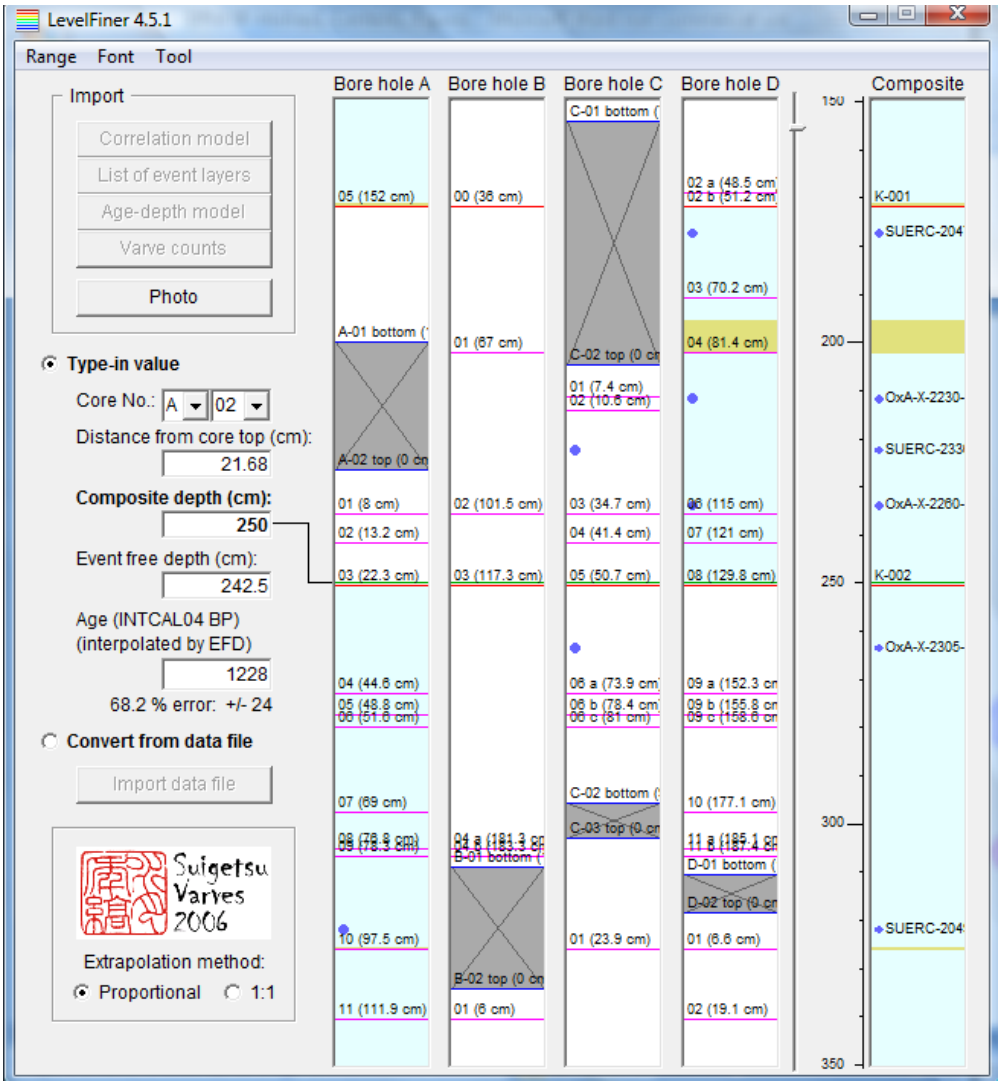

As has been reiterated, only the core section from one bore-hole contributes to the composite depth model at any given depth. Therefore, if the composite depth is required from one of the 'non-master' core sections (illustrated as the white core sections in Level Finder), for which the raw depth scale (at the time of extraction, as defined by the digital core photographs) is likely to differ slightly from that of the master core section (due to the random nature of the sediment deposition process), the program interpolates the depth of the master core section on to that of the non-master core section between the nearest two shared event layers. In a similar manner, post-extraction (i.e. since the time at which the depth scale was defined – when the digital photographs were taken) expansion/contraction of core sections is corrected for in Level Finder. Launching the 'Divider' function in another, sub-window (figure 4.6), the depths of the two adjacent characteristic laminae to the depth required (i.e. the nearest marker laminae above- and below the macrofossil sample/other datum point to be collected), as observed by the user at the time of sub-sampling, are fed into the program, as well as the observed depth of the intervening sample; Level Finder subsequently interpolates the original, 'master' depth scale on to that of the revised, observed depth scale and produces a 'true' (original) composite depth for the latter based on the former.

Additionally, Level Finder provides the ability to plot the results of any of the palaeoenvironmental proxies examined (by project members) from the core against SG06 composite core depth. In this way, the signals of the different proxy datasets can be visually compared, and thus the program facilitates the identification of broader trends/events of palaeoenvironmental/palaeoclimatic significance. Data from other sites can also be compared via matching of the calendar age chronology of such sites to that of SG06. The program (currently; version 4.5.1) has the capability to represent five such proxy datasets (from Lake Suigetsu or otherwise) at any one time.

Figure 4.6: A 'screen grab' of the Level Finder software (developed by T. Nakagawa) with a 2 m section of the SG06 core illustrated and the additional 'Divider' sub-window shown. The 'Divider' function allows for the post-extraction expansion/contraction of core sections by interpolating the original, master depth scale on to the revised (observed) depth scale at the time of sub-sampling.

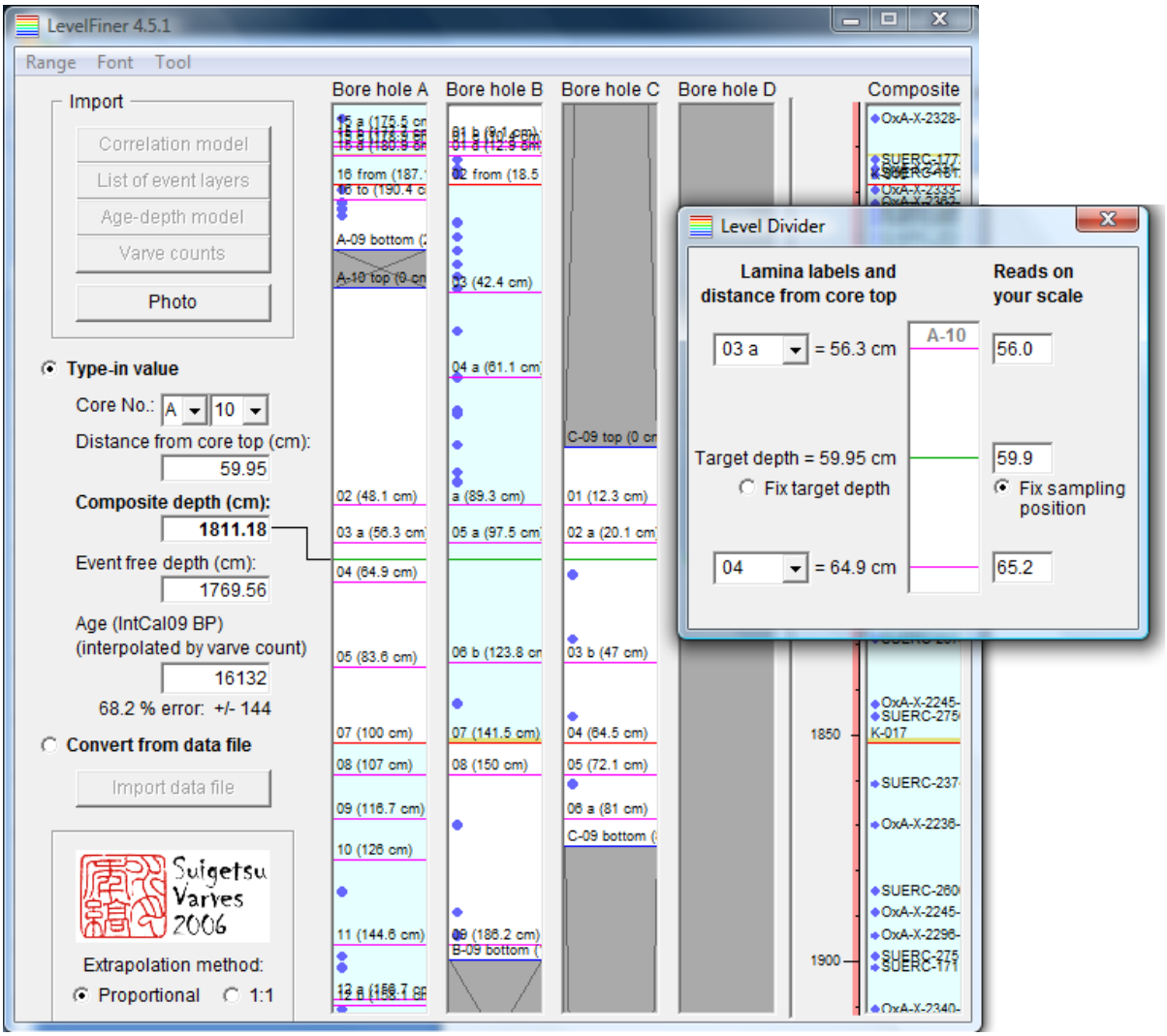

4.3 Radiocarbon Pre-Treatment, Combustion and Graphitisation

The terrestrial macrofossil samples were washed repeatedly with ultra-pure (MilliQ™, MILLIPORE, USA) water upon sub-sampling from the core, and subsequently stored in dilute

hydrochloric acid (HCl; approximately 0.2 M) to minimise the potential for contamination from modern atmospheric carbon during transport and storage. Samples were subsequently selected for radiocarbon dating according to their stratigraphic position, sample type and sample size (following the provisos outlined above). Those samples selected for dating were divided between the Oxford Radiocarbon Accelerator Unit (ORAU) and NERC Radiocarbon Facility-Environment (NRCF-E), East Kilbride laboratories such that the total number of samples to be dated at each lab (≈ 300) were evenly distributed across the time period represented by the radiocarbon dating method (*circa* 0 to 60,000 BP; SG06 composite core depths 0 to ≈ 42 m). As a method of quality assurance, ≈ 10% inter-laboratory duplication of (sufficiently large) samples was targeted as a means of demonstrating the lack of bias by either individual laboratory's protocols (section 4.5, below). Again, these samples were divided as regularly as possible down the sediment profile (based upon the size constraints imposed by the distribution of macrofossils).

Sample pre-treatment for accelerator mass spectrometry (AMS) radiocarbon dating followed standard acid-base-acid (ABA; occasionally referred to elsewhere as 'acid-alkali-acid', AAA) methodologies (after de Vries and Barendsen 1954), according to the regular laboratory protocols of both laboratories. The three main stages of this process (successive acid-, base-, and acid washes) are similar across most radiocarbon laboratories and are respectively intended to remove: (i) sedimentary- and other carbonate contaminants; (ii) organic (principally humic- and fulvic-) acid contaminants; and (iii) any dissolved atmospheric CO_2 that might have been absorbed during the preceding base wash (Brock *et al*. 2010). In this way, any potential secondary carbon contamination is removed, leaving the samples pure for combustion.

The specific ORAU laboratory pre-treatment protocols (Brock *et al*. 2010), for both delicate plant material (ORAU pre-treatment code 'VV') and sturdier wood samples (and

tree-ring lab standards; ORAU pre-treatment code 'UW'), are summarised in figure 4.7. The equivalent protocols at NRCF-E are essentially the same, but with the exceptions that: (i) the initial acid wash is performed for 30 minutes, rather than the 20 minutes at ORAU; and (ii) 0.2 M potassium hydroxide (KOH), rather than 0.2 M sodium hydroxide (NaOH), is used for the base wash. The respective pre-treatment protocols of the two labs were not altered to be identical but, rather, the usual laboratory procedures were followed, as are performed with all other samples (of the same material) submitted to the labs. Such a stance was taken, since the final calibration dataset produced from the project should be universally applicable, not only to samples that have undergone a specific (non-routine) pre-treatment procedure (see section 4.5, below).

At ORAU, the freeze-dried, pre-treated samples were weighed into tin capsules (≤ 5 mg of plant material) and subsequently combusted in an elemental analyser (EA; e.g. a CARLO-ERBA NA 2000) at a temperature of 1000 ˚C. Pure carbon dioxide (CO_2) and nitrogen (N_2) was bled off from the gas chromatograph (GC) into an isotope ratio mass spectrometer (IRMS; e.g. a SERCON 20/20) via a 50:1 splitter, where the quantities of carbon and nitrogen, as well as their stable isotopic compositions ($\delta^{13}C$ and $\delta^{15}N$, respectively), were determined. The remaining 98% of the CO_2 gas was collected cryogenically to a reactor 'rig' for graphitisation (Brock *et al*. 2010). For the largest samples, ≈ 1.7 mg C was collected to produce 'normal'-sized graphite ('G') targets, whilst for smaller samples ≈ 0.8 mg C was collected to yield 'small graphite' ('g') targets. For samples yielding even lower masses of carbon (so-called 'very small graphite-', 'vsg-', targets) the maximum mass of carbon possible was collected. An important aspect of this DPhil research (objective ii) was to investigate and improve the reliability of these vsg samples, and a more thorough discussion of these smallest samples is given in appendix 4.

Figure 4.7: Summary of the acid-base-acid (ABA) radiocarbon pre-treatment methodology applied to delicate plant macrofossils (the majority of samples from SG06; ORAU pre-treatment code 'VV') and sturdier wood material (tree ring standards and sturdier samples from SG06; ORAU pre-treatment code 'UW'), according to ORAU laboratory protocols (Brock *et al*. 2010).

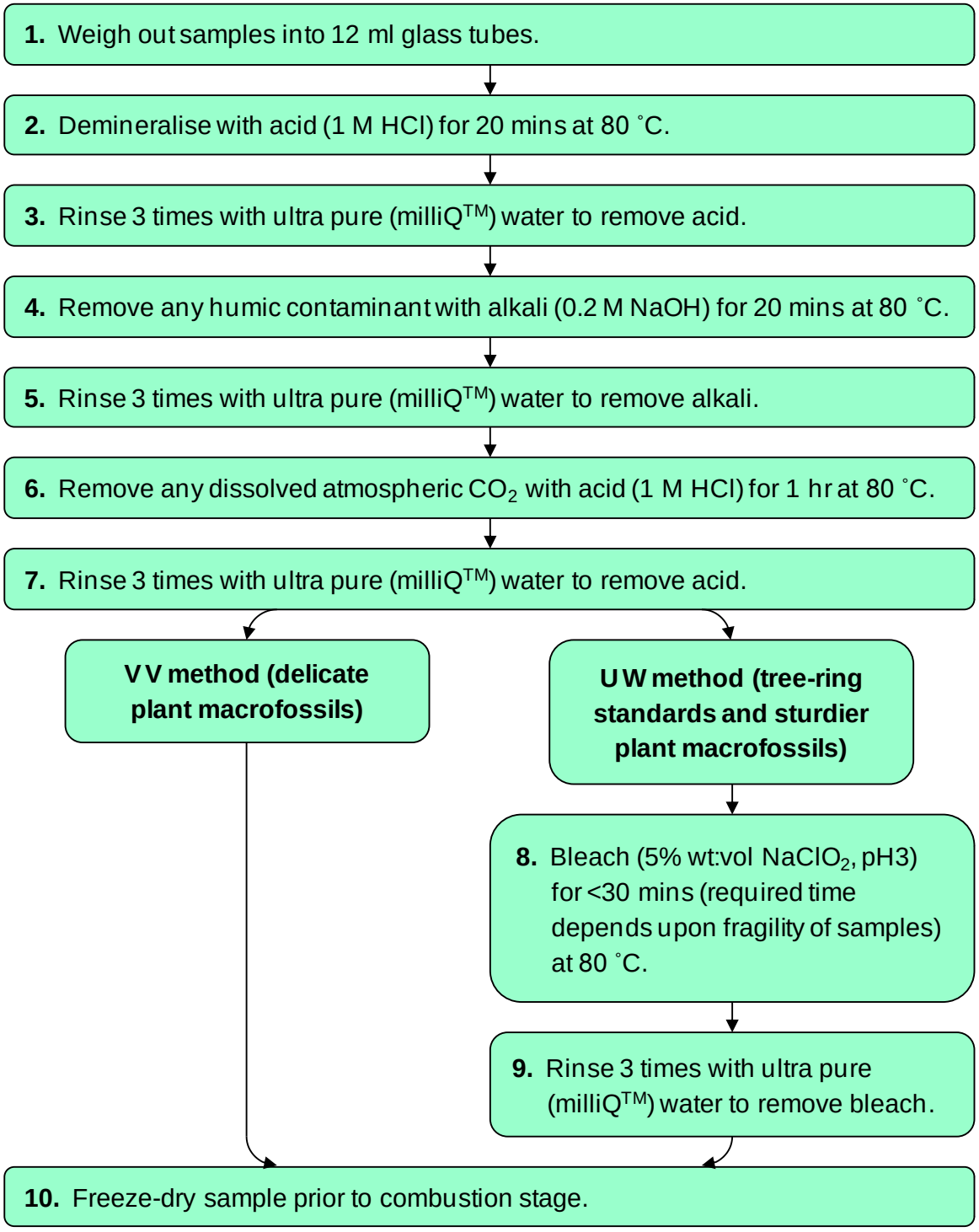

Subsequent to combustion, graphitisation was performed whereby the samples' CO_2 was reduced to pure C (graphite) over a powdered iron (Fe) catalyst (Vogel *et al*. 1984). ORAU protocol (Dee and Bronk Ramsey 2000) was followed such that the graphite rigs were heated at 560 ˚C for 6 hours. (A more detailed discussion of these parameters is again given in appendix 4). The residual- ('log-off') pressure of the remaining gas in the reactor rigs was measured to confirm that graphitisation had continued to completion (≥ 95% efficiency). Graphite was subsequently transferred- and pressed into aluminium targets for AMS at 350 kgf for 20 seconds.

A differing methodology subsequent to pre-treatment was applied at NRCF-E. The pre-treated macrofossil material was placed wet into silver foil, freeze-dried, and combusted in quartz tubes in the presence of copper oxide (Boutton *et al*. 1983; Vandeputte *et al*. 1996). $\delta^{13}C$ was measured using a VG SIRA 10 IRMS (Freeman *et al*. 2010). Aliquots of CO_2 (3 ml, where sample size was sufficient) were cryogenically collected and converted to an iron/ graphite mix through initial reduction to carbon monoxide (CO) over hot zinc (at 425 ºC), prior to further reduction over hot iron (at 610 ºC) to elemental graphite (Slota *et al*. 1987), with a typical reaction time of 18 hours.

4.3.1 Contamination

Contamination of samples is a result of the addition of either younger- or older material than the samples to be radiocarbon dated and leads to the generation of erroneous dates. Such contamination may occur both prior to sample collection and in the laboratory. Small samples are particularly prone to such contamination issues, since small quantities of carbon contaminant represent an increased proportional component of the total carbon measured. Table 4.1 summarises the effects of varying proportions of both modern- and 'dead' (inert) radiocarbon on the 'true' age of samples. Whilst the incorporation of a given proportion of

dead radiocarbon yields a consistent aging effect (as measured in 'radiocarbon years') on dated samples, the incorporation of modern contaminant yields an increasing 'rejuvenation' effect (in 'radiocarbon years') as the 'true' age of dated samples gets older. Such an effect is the result of the exponential nature of radioactive decay.

Table 4.1: The effects of: **(a)** modern-; and **(b)** 'dead'- (inert) carbon contamination on sample age.

(a):

True age (^{14}C years BP)	Measured age (^{14}C years BP) as a result of:				
	0.1% contamination by modern C	0.5% contamination by modern C	1% contamination by modern C	5% contamination by modern C	10% contamination by modern C
500	499	497	495	474	449
1,000	999	995	989	947	894
5,000	4,993	4,965	4,931	4,660	4,335
10,000	9,980	9,901	9,804	9,064	8,225
12,345	12,316	12,200	12,057	10,999	9,846
20,000	19,912	19,568	19,157	16,464	14,018
30,000	29,678	28,506	27,247	21,059	16,933
40,000	38,917	35,634	32,822	23,078	18,014
infinitely old	55,490	42,561	36,993	24,065	18,497

(b):

% of 'dead' C contamination	0.1	0.5	1.0	2.34	5	10
Effect on true age (^{14}C years older)	8	40	81	190	412	846

4.3.1a Contamination Related to the Study Site

A major strength of the present study is the integrity of the sedimentary régime from which the four Suigetsu sediment cores were collected (section 3.2). The anoxic conditions in the basal waters of Lake Suigetsu prevent disturbance of the sediment through bioturbation by benthic-dwelling organisms and so *in situ* contamination through upward/downward

movement of material in the sedimentary environment is negligible. One major caveat of the Lake Suigetsu site, however, is that the lake is tectonic in nature, and as such experiences regular earthquake activity (section 3.4). Such activity could disturb the lake's basal sediment deposits, but micro-facies analysis by project colleagues (A. Brauer, H. Lamb, M. Marshall and G. Schlolaut) should identify any such disturbance.

To examine the potential effects of contaminant on the macrofossil samples from the surrounding SG06 sediment matrix, a small selection of bulk sediments were dated from the same depths as dated macrofossil samples (section 7.2.6). At ORAU, the regular laboratory protocols for sediments are given the pre-treatment codes 'SRa' and 'SRb' for the humin- (base insoluble) and humic- (base soluble) sediment fractions, respectively (Brock *et al*. 2010). Again, these protocols represent an ABA methodology, but differ from those of the 'UW' or 'VV' protocols in that the initial acid- and base washes are both longer (1 hour), and five rinses with MilliQ^{TM} water (rather than three) are performed between each successive stage of the protocol. If the humic fraction is required, this is obtained by re-acidifiying the effluent from the base wash; the humin fraction is that which has remained in solution throughout the base wash.

4.3.1b Contamination from the Sampling Process

Contamination could have been incorporated during the coring process itself. Any such contamination should be confined to the core edge, however, and so such areas were avoided for macrofossil sub-sampling. Leaf material that could be clearly seen to lie along a given, yet distorted (through the coring process), sedimentary horizon was still considered for dating. Larger material, such as bark fragments, from the core edge that could not be identified to a specific sedimentary horizon was not considered for dating since such material

bears an increased likelihood of representing contamination that had slipped up- or down the sediment column during the coring process.

It has already been noted that macrofossil samples were not collected from either flood- or earthquake layers since such events could lead to the introduction of material into the sediment column that had potentially been held in the catchment/in the littoral lake sediments for an unknown period of time after separation from the atmospheric ^{14}C exchange reservoir (i.e. after the macrofossil material was severed from the host plant). Such samples therefore do not demonstrate the same strength of depositional integrity as do the other macrofossil samples.

The laboratory processes themselves could also have been responsible for the incorporation of contamination, with the very small sample sizes of material dated in the present project being even more susceptible to contamination from even very tiny quantities of contaminant. At ORAU (and similarly at NRCF-E), every care was taken throughout the laboratory process to minimise any such contamination. Fresh ultrapure (MilliQ™) water was used through all stages of pre-treatment, so as to minimise the chances of there being any dissolved atmospheric carbon added to samples. All glassware used for sample pre-treatment was thoroughly cleaned and baked out for a minimum of 3 hours at 500 ºC to ensure removal of any organic contamination before usage. The 60 to 90 μm polyethylene Ezee-filters™ (ELKAY, UK) used to aid the rinsing process were ultrasonicated in MilliQ™ water for 20 minutes, and subsequently passed through fresh MilliQ™ water, before use with samples (Brock *et al*. 2010). Separate Ezee-filters™ (ELKAY, UK) were used for each sample, and all samples covered with aluminium foil between rinsing, to avoid the potential for cross-contamination of samples, or addition of any other- (most likely to be modern) carbon source. The freeze-driers used (VaCo 5, ZIRBUS, Germany), both before- and after sample pre-

treatment, have scroll pumps (in preference to oil pumps) so as to avoid any back-migration of oil and subsequent contamination of samples (Brock *et al*. 2010).

4.3.2 Alternative Methodological Options

As described above, the sub-sampled SG06 macrofossils were stored in vials of dilute HCl in a cool, dark environment prior to chemical pre-treatment for radiocarbon dating. The sediment cores themselves were stored in air-tight, sealed (double-wrapped) polythene, in a dark, refrigerated (4 ºC) cold-store. This storage environment allowed the core sections to remain moist, avoiding desiccation and any resultant loss of sedimentary integrity of the cores. Both of these storage régimes therefore maintained long-term sample storage in wet conditions – a situation that Wohlfarth *et al*. (1998) highlight as being detrimental to reliable radiocarbon dating of macrofossils. Since the methodological process from sediment coring through to sub-sample storage cannot be performed in a sterile environment, modern micro-organisms and fungal spores can contaminate samples, with such organisms then able to grow (and hence add potentially significant contributions of modern ^{14}C), even in cool, dark, slightly acidic storage conditions (Geyh *et al*. 1974; Colman *et al*. 1996; Wohlfarth *et al*. 1995, 1998). More normal ORAU protocol would be to immediately freeze-dry samples submitted to the laboratory wet (Brock *et al*. 2010). However, the alternative sample storage in dilute acid was deemed appropriate to serve the same purpose, and since earlier (pilot) samples from the project had been treated in this way, for the purposes of consistency, this protocol was continued throughout the remainder of the project. This area might provide one potential refinement to the current protocol were the project to be repeated. However, the overall quality of the radiocarbon determinations achieved (chapter 7), and the lack of any observable relationship between sample storage time and erroneous- (younger than expected)

radiocarbon determinations, is suggestive of there being no detrimental effect on the quality of the radiocarbon data produced as a result of the sample storage approaches adopted.

Several authors have questioned the reliability of a straightforward ABA methodology for the pre-treatment of plant material for radiocarbon dating (e.g. Hatté *et al*. 2001; Kilian *et al*. 2002), suggesting that the final acid stage of the 'classical' ABA method is not always sufficient to remove any modern carbon incorporated during the previous base stage. Potential solutions to this laboratory rejuvenation issue include: reducing the time of the base wash stage (which must, nevertheless, be long enough to ensure removal of potential humic acid contamination); replacing the HCl used for the second acid wash with the stronger, sulphuric acid (H_2SO_4; Hatté *et al*. 2001); the addition of an oxidation stage after the regular ABA protocol (Bird *et al*. 1999; Hatté *et al*. 2001); or (the impractical) performance of the chemical pre-treatment under an inert atmosphere (Hatté and Jull 2007). Comparative data from two pilot samples from the current project did not produce any statistically significant difference in the radiocarbon ages of samples performed with either the standard HCl- or stronger-, H_2SO_4, second acid wash (section 7.2.5), and thus support the application of the standard ORAU protocols for the current project. This data was, admittedly, from a very small cohort (only two Suigetsu samples), but confirms the findings of on-going methodological testing on other, similar sample material at the ORAU lab.

Another methodological alternative is a more comprehensive procedure to reduce the 'bulk' plant material to more pure holocellulose or alpha-cellulose (e.g. Leavitt and Danzer 1993). Such a procedure removes alternative carbon-containing compounds, such as the potentially mobile lignin-, resin- or wax fractions, leaving a more pure carbohydrate substrate. This further purification is achieved through additional treatment after the initial ABA protocol, and includes subjecting the sample material to bleach (sodium chlorite, $NaClO_2$). The resultant reduction in mass of the purified substrate clearly necessitates a larger

starting weight of sample (> 30 mg of wood in some cases; Southon and Magana 2010) to yield sufficient carbon (≈ 1 mg) to produce a reliable AMS target, which is much larger than all but the biggest macrofossil samples retrieved from the SG06 sediments. Therefore, despite the suggested increased reliability of dates produced from these more rigorous pre-treatment methodologies, the simplified ABA protocol was maintained throughout the SG06 project. Several larger samples treated later in the progress of the project were, however, subjected to a more stringent methodology (ORAU pre-treatment protocol 'UW', incorporating an additional bleaching stage), generally duplicating samples pre-treated using the regular ('VV') ABA approach, to assess any differences thus generated in the radiocarbon measurements (section 7.2.5).

4.3.3 Method Development for Very Small Mass Samples

As at other radiocarbon laboratories, ORAU continues to hone its methodology to produce ever more robust radiocarbon determinations. However, the very small masses of the samples analysed in the current project required further methodological refinements specific to these significantly smaller sample sizes.

Initial sample preparation (figure 4.7) essentially followed the same laboratory protocols as with the 'normal', larger samples more regularly processed at ORAU. For the more delicate Suigetsu macrofossil samples, however, a final bleaching stage (which would normally be performed on plant material following the second acid rinse) was generally not performed. Although the more robust specimens would stand up to such treatment, the majority of samples, being far more delicate, would not, and, to maintain consistency of methodology to all samples, it was therefore decided not to include a bleaching stage for all-(but a few duplicated-) samples.

The most significant stage of the radiocarbon dating process that was more heavily tailored to the smaller mass samples was that of graphite target production for AMS. As with the regular mass samples, the aim was to maximise graphite yields from the quantities of carbon present. Therefore, an important aspect of the present project was to optimise the graphitisation process for very small mass samples before the majority of Suigetsu samples could be processed (DPhil objective ii). The exact nature of this problem, the various parameters examined, and the results obtained for this vsg target production is provided in appendix 4.

4.4 Accelerator Mass Spectrometry (AMS)

The proportion of ^{14}C in a sample can be measured by two differing means. These are: (i) measuring a sample's radioactivity by counting the emission rate of beta (β) particles per gram of carbon present; or (ii) directly measuring the ratio of ^{14}C:^{12}C atoms present in a sample (along with the ratio of ^{14}C:^{13}C atoms) through accelerator mass spectrometry (AMS).

The development of AMS for ^{14}C measurement in the late 1970s (Bennett *et al*. 1977; Nelson *et al*. 1977) and subsequent technological improvement through the 1980s allowed significantly smaller samples to be radiocarbon dated than with the 'conventional' β-counting technique, as well as speeding up the laboratory sample processing procedure. Whereas β-counting requires several grams of material (typically 1 to 2 g C) and count times on the order of days (to weeks), AMS laboratories are able to routinely process samples of < 1 mg organic carbon with measurements taken on the order of hours (Walker 2005, pp.20-23). Thus, AMS allows the dating of tiny samples such as individual leaves or seeds, and therefore enables radiocarbon dating at much greater stratigraphic resolution than was previously possible (Hatté and Jull 2007). Accordingly, the AMS method was necessarily utilised by both radiocarbon laboratories for the present study.

Samples at ORAU were dated on the HVEE AMS system (described in Bronk Ramsey *et al*. 2004), whilst samples at NRCF-E (hosted by the Scottish Universities Environmental Research Centre, SUERC) were dated on either of the NATIONAL ELECTROSTATICS CORPORATION (NEC) 5 MV tandem AMS- or NEC 250 kV single-stage AMS (SSAMS) systems (Xu *et al*. 2004; Freeman *et al*. 2010; Naysmith *et al*. 2010).

Radiocarbon dates issued by all radiocarbon laboratories are issued with unique sample identifiers: the ORAU lab issues dates with an 'OxA-' prefix, the NRCF-E lab issues dates with an 'SUERC-' prefix, and the Groningen AMS facility (utilised for the Suigetsu '93 study) issues dates with a 'GrA-' prefix. Additional non-standard/experimental research measurements obtained at ORAU are differentiated by use of an 'OxA-X-' prefix.

4.5 Quality Assurance

Approximately half of the ≈ 600 radiocarbon determinations generated for the Suigetsu Varves 2006 project were carried out at each of the ORAU and NRCF-E laboratories. As with the decision not to standardise pre-treatment chemistry specifically for the project (section 4.3), the purpose of not performing all ≈ 600 radiocarbon determinations at the one laboratory was to ensure that the final radiocarbon calibration dataset is universally applicable – not solely valid for use with unknown samples dated at one particular radiocarbon laboratory, using one particular lab protocol. By producing dates from the Lake Suigetsu samples from dual laboratories in this way, any systematic bias from either single lab's methodological protocols should become apparent. (Similarly, the Cariaco Basin radiocarbon calibration data were provided by three separate laboratories; Hughen *et al*. 2004b.) Any inter-lab divergence should anyway be avoided through the regular inter-laboratory quality assurance schemes implemented by the international radiocarbon community (e.g. International Study Group 1982; Scott *et al*. 1990, 2007, 2010; Scott 2003;

Bryant *et al*. 2001), which provide confidence in the reliability and inter-comparability of results amongst the differing radiocarbon laboratories worldwide. In addition, specific inter-laboratory comparisons were also made upon selected Suigetsu samples as a direct test of the comparability of laboratory- and analytical procedures applied throughout the present project (≤ 10% sample duplication between labs, cited in objective iv of this thesis).

Intra-lab quality assurance comes through the regular comparison of radiocarbon dates on samples with those of standard materials of known age. Specifically, these known-age standards are tree-ring samples, independently dated through dendrochronological methods, which were subjected to the same ABA radiocarbon pre-treatment methods as were the unknown age plant macrofossil samples. At ORAU, at least two such tree-ring standards were pre-treated with each batch of (usually 18) samples that underwent pre-treatment chemistry, with a similar protocol at NRCF-E. Further 'modern' standards run in each AMS 'wheel' (batch) at both labs were provided by the United States National Institute of Standards and Technology (NIST; formerly, the National Bureau of Standards, NBS) oxalic acid-II ('NOX') standard (comprising 1.34% fraction modern ^{14}C, $F^{14}C$). This is the primary standard used in the calculation of dates for all of the 'unknown' samples within an AMS wheel (four NOX samples per wheel of ≈ 45 to 50 unknown samples), which, although not subjected to pre-treatment chemistry, would incorporate the same (small) proportion of modern ^{14}C added to samples at the combustion stage. Background age laboratory standards were provided at ORAU (two per AMS wheel) by pre-combusted (bulk) anthracite CO_2 (sourced from the Groningen AMS facility) and in-house nylon- and alanine standards (usually, one per AMS wheel); at NRCF-E, equivalent standards were provided by pre-combusted (bulk) Icelandic spar calcite CO_2, and a bituminous coal standard. These background samples, run on each AMS wheel, serve the multiple purposes of: (i) confirming that the AMS is running optimally; (ii) providing the detection limit for that specific AMS

wheel (i.e. the point at which samples can no longer be defined with finite radiocarbon ages); and (iii) assessing the incorporation of any modern ^{14}C during the weighing out, combustion, graphitisation, target pressing, or AMS stages of the dating process (since all ^{14}C present in these samples would represent contamination). Additional background age material, specific to the Suigetsu Varves 2006 project, was provided by equivalent plant macrofossil- and peat samples retrieved from much lower down the SG06 core profile, well beyond the limit of radiocarbon detection (section 7.2.1).

At ORAU, the alanine standard (formerly the nylon standard, before mid-2009) was additionally used for quality assurance of the IRMS, with one standard run with every seven unknown samples combusted (Brock *et al*. 2010). Again, similar protocols were adopted at NRCF-E, utilising international standard materials.

One final in-house quality control measure is the auto-duplication of every 20th sample submitted to ORAU. Two separate aliquots of the same sample are independently pre-treated and AMS-dated, and compared for their consistency. Auto-duplication may be over-ridden if there is insufficient material for duplication, and the next suitable sample is duplicated in its place.

Throughout the entire laboratory and AMS process, batches of samples were selected at random depths from across the SG06 core profile. Such a procedure was designed to eliminate the potential for any non-random effects in the procedural blanks (cf. those cited by Hoffmann *et al*. 2010 in affecting the measurements of Beck *et al*. 2001).

5. Statistical Methods

Following on from the field- and laboratory methods described in chapter 4, chapter 5 describes the statistical methodological approaches applied to the data within this present DPhil thesis. The chapter opens with an introduction to the basic statistical considerations that are necessarily applied to all radiocarbon data. Following on from this, section 5.2 introduces the rôle of Bayesian statistics in refining the chronological information that can be gathered from these initial radiocarbon data. The chapter continues with an introduction to the OxCal calibration software (e.g. Bronk Ramsey 1995) used throughout the remainder of this thesis to implement these Bayesian statistical approaches. Finally, the chapter concludes with an introduction to the specific implementation of these statistical approaches for the radiocarbon data from the Suigetsu Varves 2006 project.

5.1 Initial Statistical Considerations

5.1.1 Presentation of Raw Radiocarbon Data

It is common practice amongst the radiocarbon dating community to convert initial radiocarbon determinations (calculated from measurements of the emission of β radiation, in the case of 'conventional' radiocarbon dating; calculated from the ratios of ^{14}C to ^{12}C or ^{13}C, in the case of AMS facilities; section 4.4) into 'radiocarbon years' (based upon the original Libby radiocarbon half-life of 5,568 years; section 2.1). The associated error term incorporates counting statistics (related to the inherently random nature of radioactive decay) and experimental uncertainties (including sample purity, fractionation effects and machine efficiencies).

However, the notion of publishing uncalibrated radiocarbon determinations as 'years' is misleading, since, as has been discussed earlier (section 2.3), the passing of 'radiocarbon

time' does not directly translate into the passing of 'true', calendar time. Uncalibrated radiocarbon data are essentially just measurements of isotopic ratios (rather than a strict chronological unit), and it would perhaps be preferable to publish raw data as such, rather than introducing the complicating concept of 'radiocarbon time'. Presenting raw data only in formats such as 'percent modern carbon' (pMC), or the better defined 'fraction modern carbon' ($F^{14}C$; Reimer *et al*. 2004b), would be a sound approach for the radiocarbon dating community (Bronk Ramsey 2008b), but once conventions have been adopted in a field, it is hard to effect such changes. The removal of 'radiocarbon years' might certainly clarify matters for non-specialist users of radiocarbon data, for whom the unit might easily be mistaken for authentic calendar time.

The term '$F^{14}C$' is equivalent to the term 'A/A_0' of equation 2.3, but explicitly stipulates that this value has been fractionation-corrected (whereas previous publication of the supposedly equivalent terms 'A/A_0', 'pMC', or 'Fm' were not always corrected, and therefore ambiguous; Reimer *et al*. 2004b). $F^{14}C$ and conventional radiocarbon age (t), are therefore related by:

[5.1] $t = -8{,}033 \ln F^{14}C$.

Whereas the uncertainties on $F^{14}C$ values are symmetrical, those on the conventional radiocarbon age are asymmetrical, due to the exponential derivation of t. This is unimportant at the younger end of the radiocarbon dating technique, but becomes increasingly significant at the older end, where uncertainties on conventional radiocarbon ages are sometimes given separately for '+' and '–' values. Thus, quoting data in terms of $F^{14}C$ is 'neater' (not requiring an estimated, equal '±' uncertainty value), and also much simpler for further statistical analysis of the data (i.e. the Bayesian statistical packages implemented for analysis of

radiocarbon data, introduced below, in any case perform their internal calculations in $F^{14}C$, rather than in terms of t).

Conversion of radiocarbon determinations into chronological data requires comparison of the results with those of known age material collected together in the form of a calibration curve. Calibration curves/datasets are typically presented with 'radiocarbon years' (for the time period preceding AD 1950) on the y-axis (with $F^{14}C$ used for the post-1950 'bomb curve'; Reimer *et al*. 2004b), and calibrated age on the x-axis. The calibration of these raw radiocarbon determinations generally leads to a decreased precision, because of the non-monotonic nature of the calibration curve, and additional uncertainties incorporated in the calibration curve itself (Bronk Ramsey *et al*. 2001; Galimberti *et al*. 2004).

5.1.2 Combination of Replicate Sample Data

As noted in section 4.5, ORAU laboratory protocol specifies that each 20th sample submitted to the lab is duplicated as a test of internal consistency. Statistically, such replicate measurements of individual samples are reduced to an individual weighted mean, $\overline{Y}$, defined by the equation:

$$[5.2] \quad \overline{Y} = \frac{Y_1 / S_1^{\,2} + Y_2 / S_2^{\,2} + \ldots}{1 / S_1^{\,2} + 1 / S_2^{\,2} + \ldots}$$

where: Y_i are the individual radiocarbon determinations for a given sample, with associated 1σ uncertainties S_i. Use of the weighted mean for combining radiocarbon results is a convention of the radiocarbon dating community and means that greater weight is applied to determinations with smaller uncertainties (in contrast to the arithmetic mean which gives all values equal weighting). The error limits of this weighted mean, $\overline{S}$, are given by:

[5.3] $$\bar{S} = \frac{1}{1/S_1^2 + 1/S_2^2 + \ldots}$$

Thus, the more replicate measurements obtained from the same sample, the lower the associated uncertainty value becomes.

As a test of whether it is appropriate to combine particular replicate radiocarbon dates in this way, the test statistic (T) is calculated:

[5.4] $$T = \frac{(Y_1 - \bar{Y})^2}{S_1^2} + \frac{(Y_2 - \bar{Y})^2}{S_2^2} + \ldots$$

The resulting values are compared with the χ^2 probability distribution and, generally, T values with a < 5% probability of being congruous (representative samples of one particular 'true' date, given the stated error terms) are considered to be erroneous (inconsistent). Where the T value exceeds this probability, one or more of the individual radiocarbon determinations should be excluded as being statistical outliers, since the measurement difference is too great to be attributed to chance alone. A table of the 5% points of the χ^2 distribution (the threshold for acceptable T values applied herein) is given in appendix 6.

So long as there is no systematic bias between different laboratories' measurements, the same statistics can be applied to inter-laboratory sample duplicates as for the intra-laboratory duplicates, above. If multiple samples come from the same context (i.e. the same SG06 sedimentary horizon in the present project), these samples can additionally be combined in the same way (but only if one assumes that the multiple samples represent the same calendar age, which is justified for the Lake Suigetsu material, since the assumption is made that the plant macrofossils' radiocarbon data are representative of the varve year in which they were deposited). However, there is a possibility in this latter instance that such samples might not represent the same calendar age event (in which case the T test would not

be valid; Christen 1994b), and so increased caution should be taken. Again, a χ^2 test will demonstrate whether the multiple dates are consistent with representing a single chronological episode.

5.2 Bayesian Statistical Methods

Bayesian data analysis across the broader physical- and social sciences has expanded dramatically over the last two decades, facilitated largely by advances in computer processing power that enable the multiplicity of calculations required in such methods, which would not have been possible before. The development of such freely available Bayesian statistical computing packages for radiocarbon calibration as 'OxCal' (Bronk Ramsey 1994, 1995, 1998, 2001, 2008a, 2009a, 2009b), 'BCal' (Buck *et al*. 1999), 'Datelab' (Jones and Nicholls 2002), 'BPeat' (Blaauw *et al*. 2003; Blaauw and Christen 2005) and 'Bacon' (Christen and Blaauw, forthcoming) has greatly advanced the science. These programs implement such random sampling procedures as Markov Chain Monte Carlo (MCMC) analysis, which generate accurate approximations of the required probability densities through computationally intensive, iterative means.

On-going development of such statistical tools is ever-refining both the accuracy and precision of questions that radiocarbon can be used to answer (Bronk Ramsey *et al*. 2010a). However, it is important to note that such modelling approaches cannot be used as a replacement for robust sampling procedures, with careful scrutiny and quality control of samples performed prior to any statistical analysis (Bronk Ramsey 1998; Bayliss 2009; Bronk Ramsey *et al*. 2010a).

Radiocarbon dating is an ideal field to implement Bayesian methodologies, since the raw determinations produced are (relatively) imprecise, are often numerically fewer than would be desirable (due to the expense of the method), and present complex statistical

distributions, yet are often combined with a wealth of instructive, additional information (such as relative stratigraphic ordering). This incorporation of Bayesian statistics into radiocarbon dating has had such a significant impact on the field that Bayliss (2009) has dubbed it "the third radiocarbon revolution" (the first- and second 'revolutions' being the initial discoveries of the radiocarbon dating method, and the need for calibration of radiocarbon data, respectively). (It should be noted, however, that previous authors have also described the advent of AMS as "the third radiocarbon revolution"; e.g. Taylor 1996.) The implementation of such methodologies has allowed for the significant reduction of uncertainty in the calibration of radiocarbon determinations; the relative imprecision of individual calibrated radiocarbon dates can be refined significantly through the incorporation of additional information, which is simply not possible through application of classical statistical methods (Bronk Ramsey 2000, 2005, 2008a).

5.2.1 Bayes' Theorem

Bayesian statistical approaches differ from those of classical (frequentist) statistics in that prior knowledge and assumptions about the data are included explicitly in the calculation of the dating probabilities. The 'prior model' (i.e. that information known about the system before taking actual radiocarbon measurements) is combined with the 'likelihood' (the radiocarbon data themselves in the form of probability density functions, PDFs) to produce a more tightly constrained set of 'posterior' probability densities (Bronk Ramsey 2008a). Mathematically, Bayes' theorem, posthumously published in 1763, states that:

[5.5] $p(t|y) \propto p(y|t)\ p(t)$

where: t is the set of parameters; and y is the set of measurements made. p(t) therefore represents the prior probability, p(y|t) is the likelihood, and p(t|y) is the posterior probability (Bronk Ramsey 2009a).

The likelihood distributions are composed of individually-calibrated radiocarbon determinations against the calibration curve, which give a series of PDFs for the calendar ages of the samples. An example of how an individual PDF is produced from a raw radiocarbon determination and its relationship with the complex radiocarbon calibration curve is shown in figure 5.1. As is illustrated in this example, the likelihood distributions are non-Normally-, often multi-modally-distributed. It is this complexity of statistical distributions that make classical statistical approaches impossible to apply, in practice, to complex radiocarbon datasets, and is why these new (Bayesian) statistical methods were developed for radiocarbon dating (e.g. Buck *et al*. 1991, 1992, 1994, 1996; Christen 1994a, 1994b; Christen and Litton 1995; Christen *et al*. 1995; Litton and Buck 1995, Nicholls and Jones 2001).

The model prior comprises any additional information about the data and is independent of the actual radiocarbon measurements (so should, theoretically, be constructed before the performance of any laboratory measurements at all). This might, for example, include any relative chronological information about a group of samples, such as the stratigraphic order of deposition (in a sedimentological context) or the relative order of archaeological phases (in an archaeological context).

Through implementation of Bayes' theorem, these likelihood distributions and the model prior are multiplied together to yield the posterior (modelled) distribution. Thus, Bayesian methods synthesise all available evidence together, providing "a powerful tool" in the interpretation of radiocarbon data (Bronk Ramsey 2000), and giving quantifiable conclusions with robust, statistically defined uncertainties.

Figure 5.1: An example of the generation of an individual probability density function (PDF; at the bottom of the figure, shown in dark grey) from a raw radiocarbon determination (2,520 ± 30 BP; demonstrated by the red Gaussian curve on the left of the figure) and its relationship with the complex radiocarbon calibration curve (IntCal09; shown here in blue; Reimer *et al*. 2009). The most probable range of the raw radiocarbon determination intersects with the calibration curve (the areas highlighted in yellow) to produce the highest probability density (HPD) range(s) of the posterior, calibrated date (2,727 to 2,697, 2,637 to 2,615, 2,593 to 2,539, and 2,528 to 2,507 cal. BP at 68.2% probability, as illustrated here).

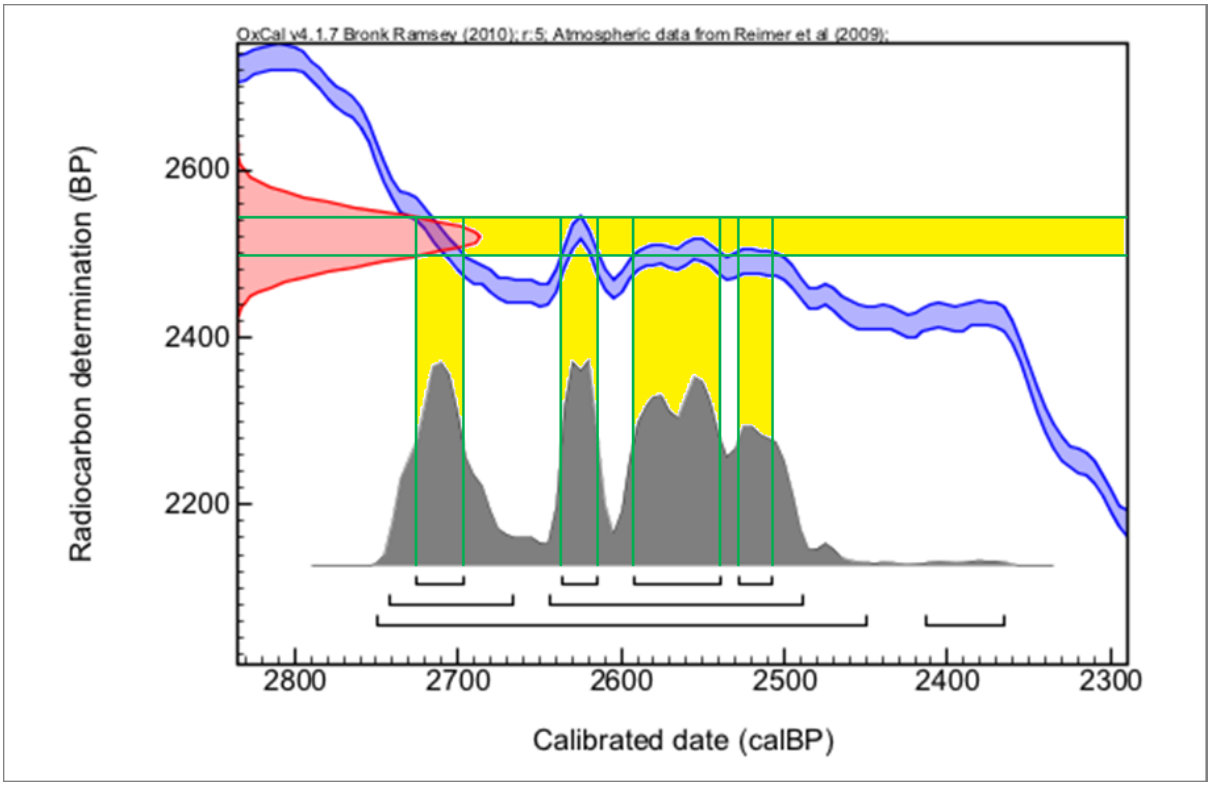

5.2.2 The Meaning of Model Outputs

It is of critical importance to be aware that the output of any data modelling (be it Bayesian, or otherwise) is contingent upon both the quality of the raw data entered into the model, as well as the construction of the model itself. A valid choice of model prior is crucial. Furthermore, the subsequent interpretation of "what the results of the Bayesian analysis actually mean" must be understood in light of this model construction (Bronk Ramsey 2000). A simple example of this (in relation to Bayesian analyses of radiocarbon data) is that the calibrated age of an individual radiocarbon determination might vary according to the choice of calibration dataset applied. It is therefore essential to state which calibration dataset has been used in determining all calibrated radiocarbon dates (Reimer *et al*. 2009), and, similarly, the model coding applied to determine more complex model outcomes should also be stated explicitly (ideally, published alongside the conclusions drawn from the exercise).

Although, as noted above, the choice of model prior is fundamental to the interpretation of the modelling output (the 'posterior' probability distributions), there is "no one correct prior for a given situation" (Bronk Ramsey 2000), which might necessitate some subjective choices on the part of the modeller. In practice, the alteration of certain prior parameters may make little difference to the modelling outcomes. It is therefore useful to run multiple models, with differing prior information, to determine the sensitivity of the modelling outcomes to particular prior parameters (Bronk Ramsey 2000, 2001).

The output of Bayesian modelling is generally quoted as a range of values at a given probability (e.g. at 95.4%), obtained by numerical integration (highest probability density, HPD) of the PDF histograms (Bronk Ramsey 2009a). This range describes the values that include the 95.4% most likely results, based upon the model prior applied. This does not imply that any result falling outside of this stated range has a 95.4% probability of being false (in contrast to classical statistical methods). Bayesian statistics gives us results that are

correct in 95.4% of all possible scenarios (based upon the prior information included), rather than giving us the 'correct result' 95.4% of the time (Bronk Ramsey 2000). Usually, data are presented at the 68.2%, 95.4%, or 99.7% ranges, providing comparability with the one-, two-, or three standard deviation (σ) ranges provided for Normally-distributed data. (Since the PDFs produced in radiocarbon analysis are not Normally-distributed, such ranges should not be quoted as '1σ', '2σ' or '3σ'; Bronk Ramsey 2009a.)

5.3 OxCal

Throughout the remainder of this DPhil thesis, the latest version (4.1) of the OxCal software (freely available online at https://c14.arch.ox.ac.uk/oxcal/OxCal.html; Bronk Ramsey 1994, 1995, 1998, 2001, 2008a, 2009a, 2009b) has been used for the implementation of Bayesian statistical modelling, however, other programs could equally have been applied. To aid the reader, commands specific to OxCal are given in '`Lucida Console`' font throughout. However, many of these features are also available in the alternative software packages, albeit perhaps with differing terminologies.

Since this DPhil thesis did not involve the development of programming for OxCal, the mathematical formulation of the model features implemented will not be reproduced herein. Rather, a users' introduction to the meaning and utility of these modelling elements will be described in the following sections. A full mathematical explanation of these model constructs is given in, *inter alia*, Bronk Ramsey (2008a, 2009b).

Having said this, some underlying mathematical principles of OxCal will nevertheless be introduced here. Firstly, all possible calendar ages are assumed, *a priori*, to be equally likely (whereas not all radiocarbon determinations are deemed equally likely, since some radiocarbon 'ages', notably those that fall on plateaux of the calibration curve, are more likely than others; Bronk Ramsey 2009a). Secondly, the 'Metropolis-Hastings' MCMC

algorithm (e.g. Gilks *et al*. 1996) is now implemented in OxCal (Bronk Ramsey 2009a; *cf*. the 'Gibbs sampling' algorithm applied in previous versions of the program). Each successive iteration provides a possible set of solutions for all of the stated parameters, with at least 10^5 to 10^6 iterations generally required to produce a "reasonably representative solution" (Bronk Ramsey 2009a). Models are generally left to run for longer than this, however, so as to fully reduce the 'noise' of the posterior PDFs generated. OxCal contains tests of model 'convergence' to assess the degree to which the modelled data provides a truly representative solution (Bronk Ramsey 2009a; i.e. convergence gives a measure of the model 'stability' between successive iterations). If this convergence is < 95%, the algorithm is probably unstable (Bronk Ramsey 1995), and the model results should be treated "with the utmost caution" (Bronk Ramsey 1998). The program automatically increases the number of iterations required for model completion, until the model convergence is reasonable (Bronk Ramsey 2001). Occasionally, this convergence may never occur and the model would run indefinitely. In such instances, the model run must be aborted. The convergence data of individual parameters within the model illustrate to the user which are the model elements that have caused poor overall convergence (Bronk Ramsey 2001).

Complex models are built up in modular fashion from simple elements of defined constraints and groupings, with the mathematics underlying these composite models essentially the same as the simpler components (Bronk Ramsey 2009a). For all of the models implemented herein, a 'uniform phase' model prior is implemented, which does not bias the span of events within a given model grouping to be either shorter or longer (although OxCal version 4.1 additionally allows ramped-, exponential-, or Normally-distributed phase priors to be implemented; Bronk Ramsey 2009a).

5.3.1 Chronological Query Language (CQL)

Data may be entered into OxCal using the chronological query language (CQL) coding, specifically designed for the software (Bronk Ramsey 1998, 2009a). The CQL commands used in the construction of any of the models applied in the present study, and any of the other commands referred to in the present thesis, are listed in table 5.1, along with a brief description of how these commands are applied. CQL provides a clear, unambiguous formalism for describing chronological models, in a simple, user-friendly way, based upon rigorous underlying mathematical formulae (Bronk Ramsey 1998).

The CQL coding of a given OxCal model is hierarchically-composed of different model elements of the form:

command (parameters) {additional information}

(Bronk Ramsey 2009a), where: 'commands' are the central program functions (e.g. `Sequences`, `Phases`, `Dates`); 'parameters' define the name of the command and, where applicable, include further information (such as laboratory measurements or statistical distributions); and 'additional information' may include supplementary prior mathematical information relating to the command (e.g. its prior `Outlier` probability, or associated stratigraphic information, `z`), specific aesthetic information pertaining to how the modelled data for the given command will be illustrated (e.g. `Color`), or further, nested command functions at a lower level of the overall model hierarchy (e.g. radiocarbon dates, `R_Dates`, within a `Sequence` or `Phase`).

Complex chronological models can be built up through interlinking of commands. For example, a specific sediment horizon in a given deposition sequence (e.g. a specific tephra horizon) might be equivalent to a given horizon within a second deposition sequence. The totality of the data contained within both separate sequences would inform the posterior

distribution of the age range for that given event (thereby increasing the reliability of the modelled age produced).

Additional query functions (such as the '`Difference`' or '`Interval`' commands) can be implemented to interrogate the chronological model for information pertaining to the specific questions that are of direct interest to the user. Such query functions do not affect the modelling outcomes in any way (other than providing an extra parameter, all other parameters remain unaffected by the query term), unless additional information is stipulated for the prior distributions of these functions (Bronk Ramsey 2009a).

If required, OxCal can be made to ignore particular sections of model code (that otherwise would be recognised by the program) by enclosing unwanted sections within the symbols: '/* [model coding] */'. Alternatively, individual lines of code are ignored through use of the prefix '//'.

Table 5.1: Selected Chronological Query Language (CQL) commands used in the radiocarbon calibration program OxCal (Bronk Ramsey 1998, 2009a).

CQL Command	Explanation
"=[name]"	Notation for cross-referencing parameters.
[name]&=	Provides additional information to a previously introduced parameter.
`Boundary`	Used as the start and end points within sequence modelling, as well as at mid-points to demark any changes in depositional régime.
`calBP`	An age given in calibrated years before present (BP), where 'present' is defined as the mid-point of AD 1950 according to the conventions of radiocarbon dating.
`Color`	Aesthetic function that defines the colour output of model elements (date distributions or calibration curves).
`Curve`	Inserts a calibration curve into the model, either for calibration of selected radiocarbon data within the model (more than one curve can be used for calibration within each model), or simply plotted for comparative purposes.
`Date`	Gives a probability density function (PDF) for the event described.
`D_Sequence`	A 'defined sequence' whereby adjacent model elements are separated by a known age gap (without uncertainties; see section 5.3.2, below).

Table 5.1 (continued):

CQL Command	Explanation
Delta_R	Defines the offset (in radiocarbon years) between the respective radiocarbon reservoirs from which the R_Date- and calibration curve samples have drawn their ^{14}C. Generally, Delta_R is entered as a Normal distribution, with μ and σ stated, and instructs the program to deal with all radiocarbon data as if their determinations were all higher/lower by the value stated.
Difference	Query function that calculates a PDF of the age difference between two stated parameters.
Gap	Placed within a D_Sequence (without an uncertainty stated) or V_Sequence (with an uncertainty stated) to define the age gap between adjacent events.
Interval	Query function that finds the time interval between adjacent events-, or groups of events-, within a sequence model.
kIterations	The number (in hundreds) of MCMC iterations performed by OxCal before an initial assessment of model convergence is made (default value = 30). If convergence isn't sufficiently high, the model run will abort at this stage. More complex models might require a higher value of kIterations to facilitate sufficient initial model convergence.
N	Defines a Normal PDF distribution with mean, μ, and standard deviation, σ, stated.
Outlier	Modifier function that defines the *a priori* probability of a given model event being rogue (erroneous; see section 5.3.3, below).
Outlier_Model	Defines the method of detecting and down-weighting erroneous samples within an OxCal model (see section 5.3.3, below).
P_Sequence	'Poisson process sequence' whereby the deposition rate of the sediment sequence varies from that of a constant deposition rate through time, according to the additional constraint of the specified 'k' parameter. (A higher value of k gives an increasingly linear deposition rate; lower values of k allow increasing flexibility away from a uniform deposition rate; see section 5.3.2, below).
Phase	A collection of model elements (such as R_Dates) whose chronological order cannot be further specified. More generally applicable to archaeological contexts than sediment deposition sequences.
R_Combine	Combines radiocarbon dates (taking their weighted averages, and performing a χ^2 test of congruence, according to section 5.1.2), prior to calculating their combined likelihood PDF calibrated age range.
R_Date	Calculates the likelihood PDF for a calibrated date from an individual radiocarbon date (and uncertainty) stated.
R_Simulate	Provides a simulated radiocarbon date for the calendar age specified. In combination, these can be applied to test for any inherent bias in a model prior, before the addition of the real (observed) radiocarbon data.

Table 5.1 (continued):

CQL Command	Explanation
Resolution	The 'bin' size used in PDF generation and interval definition. The default value = 5 (years). A lower value (higher modelling resolution) will result in the model run taking longer.
Sequence	Constrains the relative chronological order of model elements (see section 5.3.2, below).
T	Defines a Student's t PDF distribution.
U	Defines a uniform PDF distribution between the start and end points stated.
U_Sequence	A 'uniform sequence' whereby the deposition rate of the sediment sequence remains constant through time (see section 5.3.2, below).
V_Sequence	A 'variable sequence' whereby adjacent model elements are separated by a known age gap (with uncertainties specified; see section 5.3.2, below).
z=	Defines the stratigraphic position of elements within deposition models.

5.3.2 Deposition Modelling

In the present context of a sedimentary deposition sequence, the prior model incorporates information pertaining to the depths of samples within the sediment column and the relative order of their deposition. The present version of OxCal (4.1) includes five different deposition models, and these will be described briefly below. A more thorough mathematical description of these deposition models is provided by Bronk Ramsey (2008a).

The simplest deposition model is that of a '`Sequence`'. The `Sequence` model simply stipulates the relative chronological order of the events contained within it and, as with the more complex deposition models (below), is based upon the basic stratigraphic principle that older material will underlie younger material in the sedimentary régime. No further assumptions are made upon the relationship between samples (i.e. absolute depth- or chronological relationships aren't considered) beyond the relative ordering of events.

The '`D_Sequence`' ('defined sequence') is the most rigid deposition model and stipulates in absolute terms the age gap between adjacent model elements, defined in OxCal

by the 'Gap' function (without any uncertainty value applied). The most obvious application of a D_Sequence is in the case of dating wood, where the absolute age gap between successive radiocarbon-dated samples is defined by the counting of annually laid-down tree-rings (e.g. Christen and Litton 1995; Galimberti *et al*. 2004).

A 'V_Sequence' ('variable sequence') model is essentially the same as a D_Sequence in that the difference between dated samples in calendar years is defined in the model prior; the difference between the two models being that the V_Sequence allows for (Normally-distributed) uncertainty in these pre-defined absolute age gaps. The uncertainty applied to each Gap within the V_Sequence is defined individually, enabling the user to apply more- or less rigid constraints to the age gaps through the sequence depending upon how certain one is of these pre-defined gaps. V_Sequence deposition models are particularly suitable to annually-layered ice-core records, lacustrine- or marine varves, or (less secure) tree-ring records, where the uncertainty of the annual layering is well defined.

Like the D_Sequence model, a 'U_Sequence' ('uniform sequence') is very rigid in its construction – the difference being that whilst the D_Sequence stipulates the age difference between adjacent samples in chronological terms, the U_Sequence defines the difference between samples in sedimentological (i.e. depth) terms. As the name implies, the deposition rate is assumed to be uniform (constant) through time.

A 'P_Sequence' ('Poisson process sequence') model is similar to that of the U_Sequence model in that the stratigraphic position of samples is used to define the age difference between samples. Unlike the U_Sequence, however, the rigidity of the deposition rate of the P_Sequence can be adjusted. This is achieved through defining a 'k' parameter in the P_Sequence command. In the present context of sediment deposition, the P_Sequence model provides the most realistic depiction of sedimentation rate, with the complexity (randomness) of the underlying depositional process modelled according to a

Poisson process. The model rigidity essentially relates to the size of individual particles contributing to the sediment column, with the Poisson process describing the random nature of the accumulation of these particles. The smaller the particles (depositional increments) are, the closer the deposition rate through time comes to being constant. With larger increments, the overall deposition rate becomes more variable (with 'noise' on a larger scale). 'k' therefore provides 'the number of accumulation events per unit depth' (Bronk Ramsey 2008a), but can be thought of as simply the flexibility of the overall deposition rate (with higher values of k providing increased rigidity, and lower values of k providing increased flexibility).

Any abrupt changes in the modes of sedimentary deposition might often be expected to be visually recognisable in the sediment stratigraphy, or else might become apparent with initial statistical modelling, requiring refinement of the model prior. Such depositional transitions can be treated in OxCal through insertion of an additional internal 'Boundary' within the sequence model (allowing a change in the deposition rate within the context of the same overall sequence model type). If a hiatus is present, this can be modelled through insertion of a further internal 'Boundary', with an 'Interval' inserted between the two Boundaries. (This Interval is only required if one wants to find out the duration of the hiatus/time gap, and can include a prior distribution if additional information is known about the Interval *a priori*.) If a completely different deposition régime is invoked (e.g. a transition from a V_Sequence in the varved SG06 core section to a P_Sequence in the non-varved section), two separate sequences must be modelled, with the upper Boundary of the lower sequence cross-referenced to equal the lower Boundary of the upper sequence (unless an Interval is required between the respective sequences).

5.3.2a ‘Wiggle Matching’

The deposition modelling approaches described above are based upon ‘wiggle-matching’ of radiocarbon determinations to the calibration curve. The method takes advantage of the characteristic short-term fluctuations (‘wiggles’) in the calibration curve to fit series of radiocarbon determinations (related relatively to each other according to the assumptions of the respective sequence model priors) on to the calibrated timescale (figure 5.2). Such an approach yields more robust chronological information (as compared to the simple calibration of individual radiocarbon determinations), increasing both the accuracy and precision of the resultant posterior data (Bronk Ramsey *et al*. 2001). Wiggle-matching is best applied over relatively short sections of the calibration curve, as the increased uncertainties in the temporal relationship between the dated samples over longer core sections reduces the reliability of the overall modelled fit.

Although, in its broadest sense, the term ‘wiggle-matching’ applies to the modelling of data in all types of sequence models (Bronk Ramsey *et al*. 2001), the term is more readily applied to instances where the age difference between adjacent radiocarbon samples is precisely defined (i.e. ‘`D_Sequence`’ models in OxCal). Such models are able to provide the most precise fit to the calibration curve, since there is not an additional uncertainty parameter in the age gaps of samples relative to each other. The well-constrained, annually-resolved nature of wood samples (providing annual increments), allows such approaches to be readily applied to modelling of radiocarbon-dated tree-ring sequences (e.g. Pearson 1986; van der Plicht *et al*. 1995; Galimberti *et al*. 2004; Nishimoto *et al*. 2010). Ideally, several tens of tree-rings are required for such wiggle-match approaches. In the context of radiocarbon calibration curve development, such wiggle-matches have been performed to match elements of ‘floating’ tree-ring chronologies (i.e. those without sufficient overlap to enable robust dendrochronological matching of such sequences; e.g. Kromer and Spurk 1998; Schaub *et al*.

2008a, 2008b), or floating varve sequences (e.g. those from Lake Gościąż, Goslar *et al*. 1995; the Cariaco Basin, Hughen *et al*. 1998a, 1998b; Lake Suigetsu, Kitagawa and van der Plicht 1998a, 1998b, 2000, section 3.5; and Palaeolake Lisan, Prasad *et al*. 2009), to the pre-existing, absolutely-dated calibration curve.

Figure 5.2: Schematic representation of a generalised 'wiggle match' approach of a series of radiocarbon determinations on to the calibration curve. The entire dataset can be imagined to be moved horizontally across the calibration curve, until the optimal fit is established.

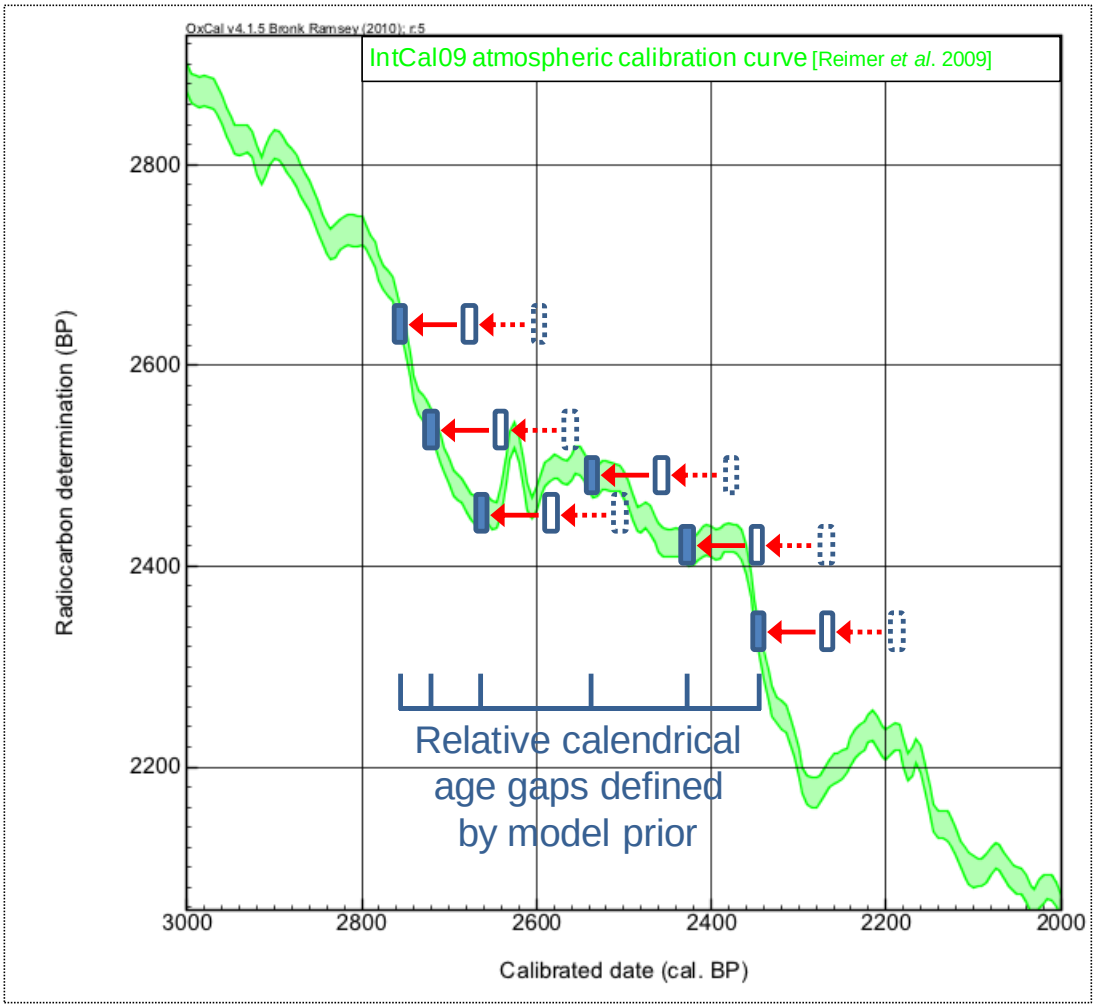

The ultimate precision of such 'wiggle-matching' techniques is provided by the accuracy of the calibration curve. Any modelling can only be as accurate as the calendar

dates within the calibration curve itself (with the calibration curve necessarily interpolated to perform such analyses; Bronk Ramsey *et al*. 2001). Sections of the calibration curve offering a high gradient provide a stronger influence on the modelled fit (as opposed to plateaux), since there is a much more restricted calendar age range for the potential fitting of such data (Bronk Ramsey *et al*. 2001).

5.3.2b Defining 'k'

As introduced above, the P_Sequence is the deposition model type that best represents the non-linearities inherent in real depositional régimes. However, in order to model such data as realistically as possible, the rigidity of the deposition rate (described in OxCal using the k parameter) must be suitably defined. This is not always a simple procedure (Bronk Ramsey 2008a) but, fortunately for the modelling to be described herein, the Lake Suigetsu sediments have the advantage of providing varve count information, which greatly aids the optimisation of k.

Most straightforwardly, varve count data can be directly incorporated into OxCal as the z unit (rather than using more 'pure' core depth units). When combined with a P_Sequence, this approach approximates a V_Sequence model (in that the prior gap between adjacent samples is defined in calendar years with uncertainties), but with the additional benefit that a constant bias (i.e. regular over- or under-counting of varves) is accounted for. When varve counts (or annually-layered ice cores or uncertain tree-ring counts) are modelled in this way, a suitable estimation of k is given by:

$$[5.6] \quad k = \frac{M}{m}$$

where: M represents the total number of counted years in a given section; and m represents the total number of 'uncertain years' contained within that same section (Bronk Ramsey 2008a, p.46).

In the OxCal models to be applied herein, varve count will not always provide the z unit. Most obviously, this is the case for the SG06 core section above 1250 cm composite depth, which is not annually laminated. A value of k can nevertheless be extracted from the varve-counted section of the core to provide an objective rigidity to the P_Sequence model applied. This is not a straightforward question of transforming the implied meaning of k from varves to depth (i.e. using the value of k as being the 'number of deposition events per varve' and using the mean varve thickness to obtain an equivalent 'number of deposition events per cm'), since the value of k for varves is simply a measure of the divergence from a linear relationship between the 'true' deposition rate and that determined from varve counting. The value of k when z reflects authentic depth units must also take into account the inter-annual variation in varve thickness. For P_Sequence models with depth as the z unit, k can be estimated through comparing the variability of varve counts over depth. Figure 5.3 demonstrates how k can thus be estimated from either an exposed sediment section, or multiple sediment cores, where three identifiable isochronous stratigraphic layers can be identified. The variability of the distances between these respective layers is then used to estimate k as follows:

[5.7] $$U_i = \frac{u_i}{(u_i + v_i)}$$

[5.8] $$V_i = \frac{v_i}{(u_i + v_i)}$$

[5.9] $$k = \frac{\mu_U \mu_V}{\sigma_U \sigma_V (p_i + q_i)}$$

where: u_i and v_i are the measured distances between the three stratigraphic horizons; μ_U and σ_U, and μ_V and σ_V are the mean- and unbiased standard deviation values of U_i and V_i, respectively; and $p_i + q_i$ represents the total temporal duration of the sequence (Bronk Ramsey 2008a, equations A.19 and A.20).

Figure 5.3: Method for estimating the k parameter of P_Sequence deposition models in OxCal from three identifiable stratigraphic horizons in an exposed sedimentary section or multiple sediment cores. The distances, u_i and v_i, between these stratigraphic layers are combined with equations 5.7 to 5.9 to yield k. (Adapted from Bronk Ramsey 2008a.)

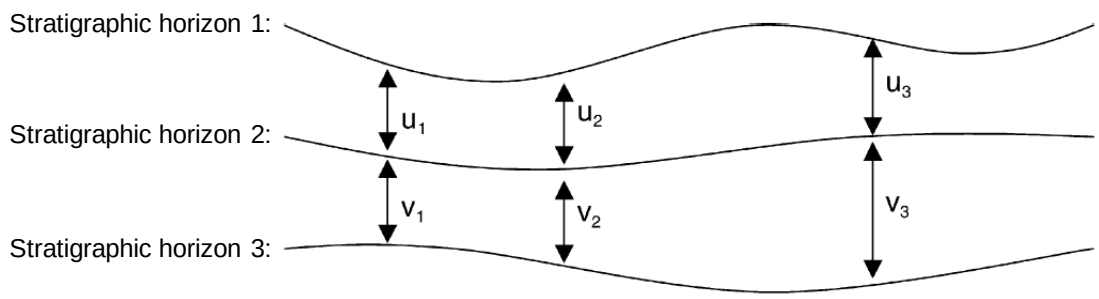

In the case of the SG06 core, the respective positions of these three stratigraphic horizons can be determined by their relative position in varve years and the intervening distance in depth utilised. For example, stratigraphic horizons 1 and 3 could be determined to be 1000 varve years apart, with stratigraphic horizon 2 at 400 varves from horizon 1. u_i and v_i would then be the composite- (or event-free) depth differences between these respectively defined points, with 'i' measurements made from successive sections of 1000 varve years' duration down-core. In this way, a reliable, 'objective' value of k can be estimated for sections of core that do not have varve information, via extrapolation from successive core sections that do. This method is not entirely 'objective', however, since the choice of horizons 1 to 3 and number of sections, i, must still be arbitrarily decided upon. If equivalent

stratigraphic horizons are identified from parallel bore-holes (as was initially noted above, and as was also described in Bronk Ramsey 2008a), a more reliable value of k is obtained for that specific time interval, but which is less reliable for taking into account the changes in deposition rate over a broader depth range, such as for the purpose of extrapolating to the non-varve-counted core sections, as was described subsequently.

Finally, in relation to defining k, it is noted that future developments of OxCal will allow for k to be ascertained through 'model averaging' techniques (Bronk Ramsey *et al*. 2010a; Bronk Ramsey and Lee, forthcoming). In this way, the program will model the optimal value of k from the radiocarbon and stratigraphic data fed into a model. Such a development would not affect the principal models of the present project (where k is determined from the varve count data), but would aid the supporting models (run as a test of, and supposedly totally independent of, the SG06 varve counting).

5.3.3 Outlier Analysis

Despite the precautions taken throughout the sampling and laboratory processes, a small proportion of radiocarbon determinations might be inconsistent within a model (i.e. with respect to the other radiocarbon determinations, within the framework of the applied model prior). Bronk Ramsey (2009b; Bronk Ramsey *et al*. 2010a) ascribes four potential causes of such outlying results (termed: 's-', 'r-', 'd-' or 't-type' outliers), which will be introduced below. All of these causes of erroneous data can be dealt with statistically in OxCal (version 4.1) using "essentially similar methods, but in slightly different ways", through application of the 'Outlier' functionality (Bronk Ramsey 2009b). (For a full mathematical description of the way that these different 'Outlier_Models' are applied in OxCal, see Bronk Ramsey 2009b).

'`s`-type' outliers are those where the radiocarbon determination obtained from a sample is simply incorrect. These outliers should, ideally, be encompassed within the quoted dating uncertainty, but there may be instances where this is not the case in reality. Such outliers are identified by OxCal through expansion of this quoted uncertainty by a certain factor (after Christen 1994a, 2003; Christen and Litton 1995; figure 5.4a).

'`r`-type' outliers arise where the radiocarbon measurement obtained is correct, but where the ^{14}C content of a sample is anomalously high or low, compared to that of the calibration curve for its associated calendar age (figure 5.4b). This might be the result of short-term fluctuations in the ^{14}C concentrations within the reservoirs from which the samples (or calibration curve samples) drew their carbon, or through the effects of contamination. Such outliers are similar to those of the `s`-type outliers introduced above, but are not related to the measurement uncertainty, and would not be improved by replicate measurement.

'`d`-type' outliers reflect a more systematic offset in radiocarbon determinations of samples relative to the calibration curve. This might be associated with environmental effects (such as 'reservoir effects', section 2.2.1, or geographic offsets, section 2.2.3), or with a consistent laboratory bias in the measurements produced (although the latter issue should be identified through the regular comparison with intra- and inter-laboratory standards; section 4.5). In such instances, the entire dataset (or a particular section of the dataset) may be temporally offset from the data contained within the chosen radiocarbon calibration dataset (figure 5.4c). Such outliers can be dealt with using the same methodology as is applied to ΔR offsets present in marine calibration (Stuiver and Braziunas 1993a; Jones and Nicholls 2001; section 2.2.1), since the outcomes of such effects are mathematically indistinguishable. This is implemented in OxCal through application of the '`Delta_R`' command.

'`t`-type' outliers arise where a sample's true age is not representative of the context from which it is taken. Rather than a shift in radiocarbon time, these outliers are the result of offsets in relation to the calendar timescale (figure 5.4d), and might reflect 'residuality' of samples or intrusion of younger material into an older context. In relation to the present study, such outlying samples might be the result of material that has moved stratigraphically up- or down the sediment profile (which is why samples from the core edge were preferentially avoided for dating; section 4.2), or where samples contain an inbuilt age as compared to the varve depth from which they were sampled (and is why the more fragile samples were selected for dating, and event layers avoided; section 4.2).

In previous versions of the OxCal software, the removal of outlying data had to be performed manually. This was not a wholly subjective process, however, as the 'agreement indices' ('A-values') displayed in the model output could be used to assist in this rejection process. These A-values demonstrate the goodness of fit between the likelihood- and posterior distributions for individual elements within a model (by means of an 'overlap integral', which offer a 'pseudo-Bayes factor'; Bronk Ramsey 1995; Bronk Ramsey *et al*. 2001), and therefore highlight those cases where the model prior is inconsistent with the measurement data (Bronk Ramsey 2000). A-values below 60.0% (which give a similar level of discrimination to the 5% confidence level of the non-Bayesian χ^2 test for simple combinations) are indicative of questionable data (Bronk Ramsey 1995), and so any `R_Dates` yielding agreement indices below this threshold could be excluded from the model, and the model re-run. (The fact that, statistically, the 'true' ages of approximately one third of radiocarbon determinations will fall outside the 68.2% probability range, and one in 20 outside the 95.4% probability range, means that exclusion of samples falling below this rejection criterion should, ideally, only be undertaken if there is additional supporting justification for doing so.)

Figure 5.4: Schematic representations of the treatment in OxCal of the differing causes of-, and treatment of-, outlying data for: **(a)** '`s`-type' outliers (under-estimated measurement uncertainties); **(b)** '`r`-type' outliers (individual radiocarbon offsets); **(c)** '`d`-type' outliers (systematic radiocarbon offsets); and **(d)** '`t`-type' outliers (due to uncertainties of context). In each case, the vertical extent of each rectangle represents the 1σ range of the raw radiocarbon determination, and the horizontal extent of each rectangle represents the 68.2% range for the modelled fit to the calendar timescale. The solid rectangles represent the placement of the data without consideration of the respective causes of outliers, and the dotted rectangles represent the 'true' fit of the data to the calibration curve (with outlier analysis having been performed to account for the outlying samples). (Sources: Bronk Ramsey 2009b; Bronk Ramsey *et al*. 2010a.)

(a):

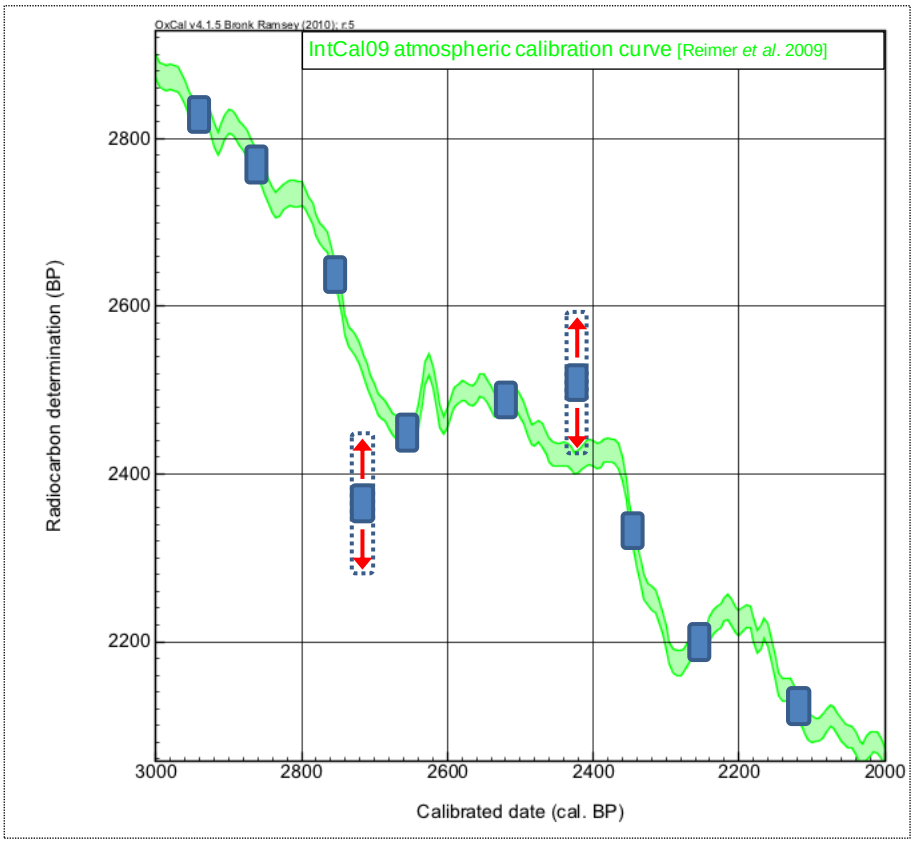

Figure 5.4 (continued):

(b):

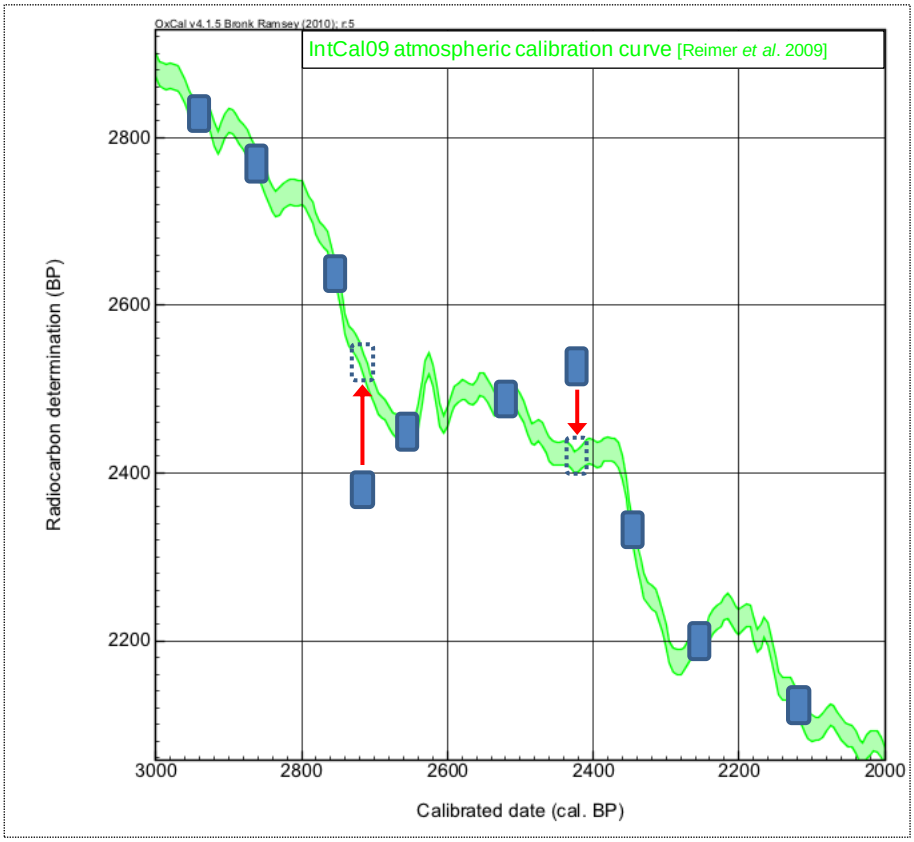

(c):

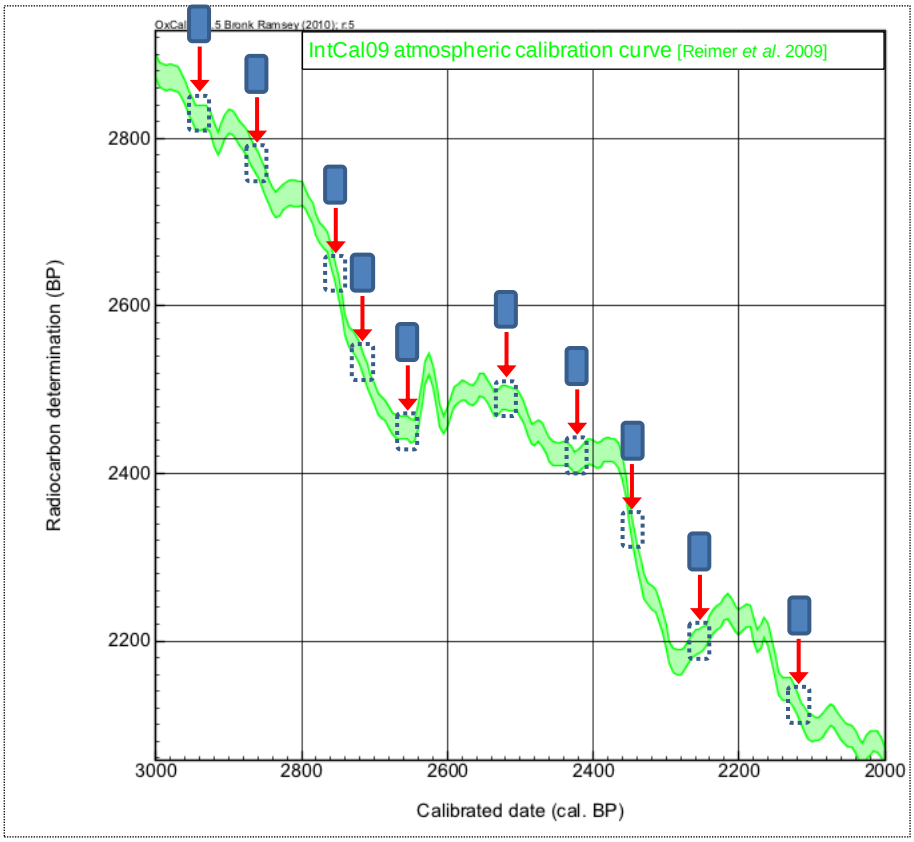

Figure 5.4 (continued):

(d):

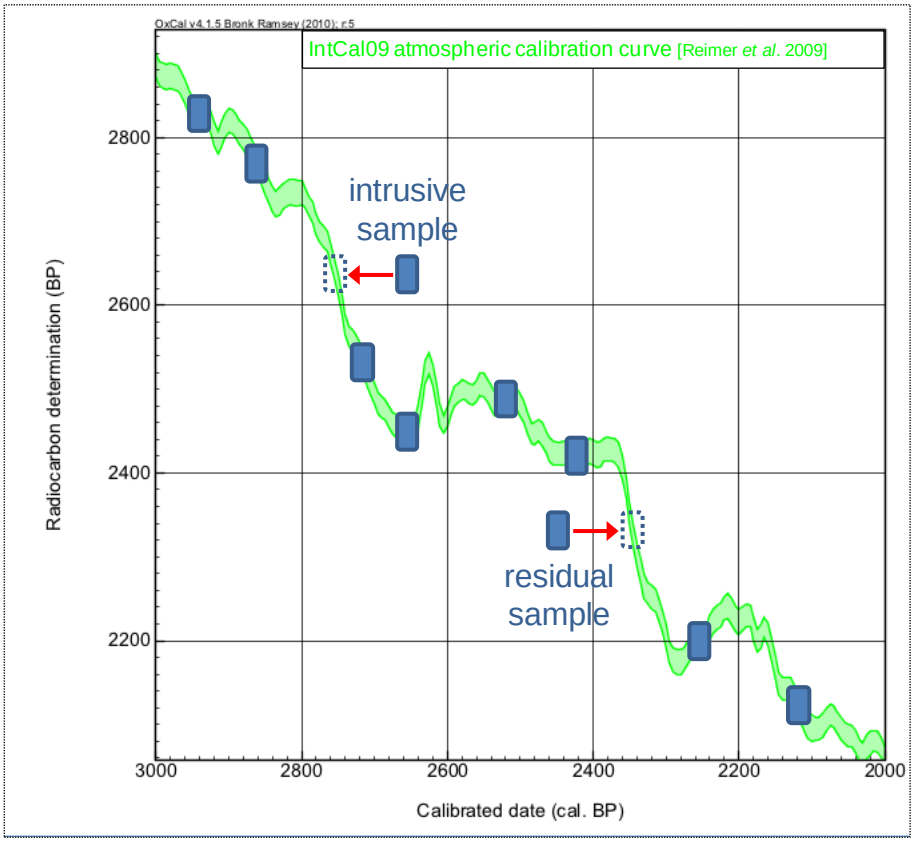

The newer outlier analysis functionality within OxCal can be utilised in a similar fashion, especially where `s`-type outliers have been identified. A particular probability threshold (of given samples being outliers) can be adopted, and all data falling below this threshold again excluded from the model, and the model re-run (without implementing a further `Outlier_Model`). This methodology has the advantage of showing clearly which samples are affecting the modelling outcome (since all remaining data contribute equally to the modelled fit).

Alternatively, implementation of the `Outlier_Model` function in OxCal enables a 'model averaging' methodology, whereby the program uses all sample data included within the model, but weighted according to how likely samples are to be 'correct'. The prior weighting is defined by the user, with a posterior weighting determined by the program,

generated through the iterative (MCMC) process underlying the program's functioning, and influenced by all of the available information within the model. Such an approach is preferable in examples, such as the present project, where one cannot be certain whether particular samples are truly outlying. (I.e. the premise of this project is that the marine-derived calibration curve is not reliable throughout the radiocarbon dating method, and so any outliers identified when modelling the Lake Suigetsu dataset against a marine-derived dataset might be considered to represent either a real deviation between the respective ^{14}C reservoirs, or genuinely outlying sample data.) Again, this implementation of an '`Outlier_Model`' explicitly in the modelling process, has the advantage of reducing the subjectivity in the identification of outliers, but both methods nevertheless contain a somewhat subjective judgement of what threshold is applied to outlier rejection.

In instances in the present project where there is no prior information to suggest which samples are more likely to be outlying, samples are not excluded from the model (if this is possible; i.e. if the program can nevertheless find a valid solution with such data included), as they still exert an influence (albeit, significantly down-weighted) on the overall modelled fit. Only if samples are found to be 100% outlying are such samples excluded from subsequent model runs (if further modelling is required), since samples identified as representing 100% outliers exert no influence on the final modelled fit, yet will slow down the model's convergence, inhibiting the program's progress.

The prior `Outlier` probability is applied to each radiocarbon determination individually, which allows for specific samples to be given an increased *a priori* probability of being an outlier, if there is reason to believe that this is the case. However, it is generally unlikely that such identification of particular outlying samples can be predicted before radiocarbon measurements have been obtained (so long as a robust sampling strategy has been undertaken). In the present study, all radiocarbon determinations were given an equal *a*

priori 5% `Outlier` probability. The choice of such prior probability values is somewhat arbitrary, but is made on the basis that since most radiocarbon scientists quote their findings at the 95% probability range (for calibrated ages; though at ±1σ for uncalibrated radiocarbon 'ages'), there should be an expected 5% of samples that would produce measurements not within this 95% range.

The '`Outlier_Model`' chosen is coded in OxCal along with an expected statistical distribution for the offsets, and for their likely order of magnitude. For all models in this present thesis, an '`r`-type' `Outlier_Model` was applied, which allows for transient fluctuations in the radiocarbon concentrations between the respective radiocarbon reservoirs of the sample data (from Lake Suigetsu) and the calibration curve (IntCal09) datasets (Bronk Ramsey *et al*. 2010a). The scale of each `Outlier_Model` was allowed to vary in the range 10^0 to 10^4 years, and a Student's t distribution (with five degrees of freedom) implemented, which allows for longer tales on the distribution of outliers, as compared to a Normal distribution. A longer-tailed distribution is advantageous, since this allows the posterior `Outlier_Model` distribution to not be so overly-dependent on a small number of extreme outliers (Bronk Ramsey 2009b), which might well be present in such a dataset.

It should be re-iterated that statistics cannot identify the reasons why samples might be outlying, but are useful for identifying those samples most likely to be erroneous. Outlier analysis is no replacement for a sound sampling strategy, and cannot account for datasets with a high proportion of erroneous data. Such outlier modelling is particularly advantageous in analysing datasets with a large number of radiocarbon determinations (such as those herein). Issues of 'over-precision' (which can arise where no consideration of outliers is considered) are also prevented (Bronk Ramsey 2009b).

5.3.4 Model Output

The output of model data in OxCal can be illustrated in a variety of formats. In addition to the principal results table, the formats illustrated herein are: the 'depth plot'; 'curve plot'; 'intervals' view; 'outliers' view; and 'single plot' (table 5.2). A variety of statistical parameters (68.2% range, 95.4% range, 99.7% range, mean, standard deviation and median) can be illustrated (if desired) with all of these output formats, with the ability to show both modelled- (posterior) and unmodelled- (likelihood) probability density functions (PDFs), providing ready visualisation of the effect of modelling.

Table 5.2: The OxCal model output formats utilised in the present thesis.

OxCal Model Output Format	Description
Depth plot	Illustrates the probability density functions (PDFs) on the x-axis, against the stratigraphic depth of the sample (defined by `z`) on the y-axis.
Curve plot	Demonstrates the fit of the radiocarbon determination (shown on the y-axis) against the chosen calibration dataset (with the x-axis reflecting the modelled, calibrated sample age). Additional calibration datasets can also be plotted to enable comparison of these respective datasets. For the present project, where a large, high resolution dataset is presented, it is clearer not to plot the PDF on the curve view, but, rather, a simple box plot of radiocarbon age versus modelled, calibrated age is shown. For clarity, these plots are shown at only the 68.2% probability range herein, due to the overall density of radiocarbon data obtained.
Intervals view	Plots the calibrated age of specific `intervals` described within the model. (Used herein for the statistical re-analysis of the Suigetsu '93 dataset; section 6.1.)
Outliers view	Where outlier analysis has been applied, the model output presents a revised estimate of the probability that a sample actually is outlying, in light of the body of evidence contained within the entirety of the model
Single plot	Demonstrates both the unmodelled- and modelled fit of an individual radiocarbon determination/event on the calibration curve, and is the optimal view for demonstrating the full statistical distribution (PDF) of the posterior age range of that sample/event.

5.4 Application to the Lake Suigetsu Datasets

5.4.1 'Wiggle Matching' to IntCal09

As has been described in chapter 3, the annual laminations of the Lake Suigetsu sediment profile do not continue through to the present day; i.e. the varve-counted chronology of the Suigetsu Varves 2006 project is necessarily floating, rather than absolute. Therefore, as with the timescale of the SG93 core (Kitagawa and van der Plicht 1998a, 1998b, 2000), the SG06 varve-counted timescale (given in 'SG06 vyr') is herein tied to the absolute timescale via wiggle-matching of radiocarbon determinations from a section of the core to an 'absolutely-dated' record (section 7.4). Where Kitagawa and van der Plicht (2000) used the datasets of Spurk *et al*. (1998) and Kromer and Spurk (1998) for this purpose, the latest international consensus calibration curve, that of IntCal09 (Reimer *et al*. 2009), is implemented for defining the SG06 'calendar' timescale.

As has been reiterated, the overarching aim of this DPhil thesis, and one of the principal aims of the Suigetsu Varves 2006 project, is to provide a 'wholly terrestrial' radiocarbon calibration dataset, free from the uncertainties incorporated from correcting for the temporally variable marine reservoir effect. Therefore, only the portion of IntCal09 based entirely on terrestrial- (i.e. tree-ring) data is used to perform this wiggle-match. The present terrestrial limit to the radiocarbon calibration curve (hereafter, referred to simply as 'the IntCal09 tree-ring limit') is 12,550 cal. BP (Reimer *et al*. 2009).

Although the U-Oki tephra (with a previously reported age of 10,250 to 10,200 SG93 vyr BP; H. Kitagawa, personal communication) is the reference ('zero') year for the floating Suigetsu Varves 2006 varve chronology, varve counting was actually undertaken from 1250 cm composite depth (≈ 36 cm above the U-Oki tephra). This, gives a period of approximately 2,600 (cal.) years for which the SG06 varve chronology overlaps the

dendrochronologically-derived portion of IntCal09, and is the time period utilised for the principal wiggle-match model herein (OCM-7.1; section 7.4.1).

As has been outlined above, there are differing statistical models that can be applied to perform such a wiggle-match. Several of these methods are also implemented herein, incorporating different radiocarbon data, and covering different SG06 depth ranges. The exact model specifications used to perform these wiggle-matches, along with their justifications and implications, are provided in section 7.4.2.

5.4.2 Comparison with the SG06 Varve Chronology

The primary age scale of the SG06 core is provided by the independent varve count data (section 3.6.3). This is the age scale against which the radiocarbon determinations from plant macrofossils is plotted herein (chapters 7 and 8), and that will constitute the final 'Suigetsu Varves 2006 radiocarbon calibration dataset'. However, as a means of testing this independent calendar age chronology, the radiocarbon measurements from the core, as calibrated against the existing radiocarbon calibration datasets (principally IntCal09), can be used, implementing the same modelling approaches as described above. Again, the specifics of these models are provided, along with their implications, in chapters 7 and 8.

Similar modelling approaches have also been utilised to provide interim age-depth models to Suigetsu Varves 2006 project members over the course of the project.

5.4.3 Updated Modelling of the Suigetsu '93 Dataset

Section 6.1 presents a statistical re-analysis of the Suigetsu '93 radiocarbon calibration dataset of Kitagawa and van der Plicht (2000). As with the Bayesian modelling applied to the SG06 data (described above), this application calibrated the SG93 data against the latest

international consensus calibration curve, IntCal09 (Reimer *et al*. 2009). The purpose of this exercise was to statistically estimate the durations of the inter-core section gaps in the SG93 sediment profile, and thereby provide a predictive model for the outcomes of the present, Suigetsu Varves 2006, project (DPhil objective i). Further details of this modelling exercise, along with the results generated, are provided in section 6.1, whilst an assessment of the accuracy of the findings of this exercise is provided through a visual comparison of archive SG93 core material with the composite (gap-free) sediment profile of SG06 (section 6.2).

6. Re-analysis of the Suigetsu ’93 Dataset

Early in the progress of the Suigetsu Varves 2006 project, a statistical exercise was undertaken on the original Suigetsu ’93 dataset of Kitagawa and van der Plicht (1998a, 1998b, 2000) to examine the potential extent of error in their original study. Accordingly, such an exercise provided a predictive age-depth model for the Suigetsu Varves 2006 project. Chapter 6 is divided into two principal sections, with the initial section detailing the findings of this modelling exercise.

The latter half of chapter 6 describes a physical matching of the SG93 core material against the SG06 composite core profile. This exercise, performed later in the Suigetsu Varves 2006 project, was enabled when we were granted access to archive sediment material from the original SG93 core. This physical core comparison therefore enabled both assessment of the accuracy of the preliminary statistical modelling exercise, as well as the more robust combination of the two Lake Suigetsu radiocarbon datasets, thus significantly enhancing the resolution of the final calibration dataset to be obtained from the present project. Provisional re-interpretations are made of the palaeoenvironmental reconstruction dataset from the Suigetsu ’93 project (sections 6.2.5), with comparison made between the Suigetsu ’93- and Suigetsu Varves 2006 radiocarbon datasets in the following chapter (section 7.6).

6.1 Bayesian Re-analysis of the Suigetsu ’93 Dataset

6.1.1 Introduction to the Exercise

In section 3.5.3, the methodological problems of the Suigetsu ’93 study were identified as being responsible for the offsets between this radiocarbon calibration record and those of the alternative, marine- and speleothem-based calibration datasets (figure 3.11). Principally,

these problems were cited as lying in the unknown age gaps between successive SG93 sediment core sections, and the reliability of the varve-counted 'absolute' age scale. Early in the progress of the present project, a purely statistical exercise was undertaken to quantitatively assess these uncertainties through comparison of the Suigetsu '93 calibration dataset with those of IntCal04 (Reimer *et al*. 2004a) and the Cariaco Basin marine sediment record (Hughen *et al*. 2006). This exercise, published in *Nuclear Instruments and Methods in Physics Research B* (Staff *et al*. 2010), is reproduced *in toto* in appendix 7. Since the undertaking of this exercise, however, the publication of the improved international consensus calibration curve, IntCal09 (Reimer *et al*. 2009), has provided a more reliable calibration curve with which to compare the SG93 data, and removes the need to choose an individual site's calibration dataset to apply to data beyond the previous (26,000 cal. BP) IntCal limit. Section 6.1, therefore, presents an updated working of this statistical exercise, now calibrating the SG93 data against IntCal09.

6.1.2 Model Construction

All 279 radiocarbon measurements from the varve-counted sections ('SG13' to 'SG34') of the original Suigetsu '93 dataset (Kitagawa and van der Plicht 2000) were entered into OxCal (section 5.3), with the IntCal09 (Reimer *et al*. 2009) calibration curve applied. Ten sampling depths bore duplicated measurements, which were combined prior to modelling, according to the protocols outlined in section 5.1.2, giving 269 separate radiocarbon-dated sediment horizons within the model.

Outlier analysis was implemented to objectively down-weight those determinations most likely to be suspect (section 5.3.3). An `r`-type `Outlier_Model` was implemented (Bronk Ramsey 2009b), allowing for any short-term fluctuations in the radiocarbon concentrations between the respective radiocarbon reservoirs of the Lake Suigetsu- and

calibration curve (IntCal09) datasets. The scale of this Outlier_Model was allowed to vary anywhere in the range 10^0 to 10^4 years, and the Student's t distribution (with five degrees of freedom) applied to allow for longer tails on the outlier distributions. This is necessary, because comparison of terrestrial- and marine archives in this way, must allow for occasionally significant deviation, since the marine dataset represents a temporally-smoothed signal (due to the residence time of ^{14}C in the ocean), compared to the short-term, potentially high magnitude, deviations of ^{14}C concentration present in the atmosphere (Bronk Ramsey *et al*. 2010a; chapter 2). Since none of the Suigetsu samples are from a questionable stratigraphic context, there is no *a priori* reason to suppose that particular determinations are more likely to be 'rogue' than others. Therefore, an equal prior Outlier probability of 5% was assigned to each of the 269 radiocarbon determinations entered.

The original varve-counted values of Kitagawa and van der Plicht were used as the z unit (so as to take account of such event layers as those relating to earthquakes or floods, as well as the regular inter-annual variations in sedimentation rate). Boundaries were applied at the top and bottom of each of the 22 core sections (labelled 'SG13' at the younger end through to 'SG34' at the older, as defined by the original authors) from which the 269 radiocarbon measurements were drawn, with intervals placed in between each Boundary pair. These intervals were given uniform prior distributions of between 0 and 5,000 years, such that none of the posterior probability distributions generated for these intervals was curtailed by this prior.

Additionally, the durations of each section of Suigetsu core were constrained to vary normally around the varve-counted values given by Kitagawa and van der Plicht. An arbitrary σ value of 10% was applied to this distribution to allow sufficient flexibility for divergence from these varve-counted values.

A P_Sequence deposition model was applied (Bronk Ramsey 2008a; section 5.3.2). Such a model was selected over the D_Sequence or V_Sequence specifications since these two alternatives require that the exact age differences between dates are known precisely, or at least that their uncertainties are very well-defined; since the varve-counted depth scale was one of the most likely sources of error in the original study, the application of a P_Sequence was deemed more appropriate. Use of either the D_Sequence or V_Sequence would also not allow for significant systematic over- or under-counting. A U_Sequence could be implemented, but would constrain such deviation to be constant across the entirety of the dataset (i.e. proportional to the varve-counted age gaps, though not necessarily with a 1:1 relationship between varve- and calendar- time), whereas, in reality, such issues might be expected to vary with depth, with the reliability of varve counting related to issues of differential varve preservation.

As described in section 5.3.2, the k value applied to a P_sequence can be altered to determine the rigidity of the modelled sedimentation rate. An alternative derivation of k is needed from that of equation 5.6, since that equation required that the number of uncertain years (varves) within a known duration core section is well-defined *a priori*. In relation to SG93 there is no independent estimation of such a value (although the ≈ 1.5% estimation of Kitagawa and van der Plicht could arguably be applied). Rather, the value of k was determined here to equal 0.4 (from equation A.17 of Bronk Ramsey 2008a), such that the uncertainty at the mid-point of a core section of duration 1,000 years (a representative value for these SG core sections) was ±5% (consistent with the arbitrary 10% uncertainty applied to the duration of an entire core section):

[6.1] $$\frac{\sigma_t}{M} = \frac{1}{2}\frac{1}{\sqrt{k(M)}}$$

[6.2] $$\sigma_t = 25 = \frac{1000}{2}\frac{1}{\sqrt{k(1000)}}$$

[6.3] $$k = \left(\frac{20}{\sqrt{1000}}\right)^2 = 0.4$$

where: M is the known duration of the core section in years (set to 1,000); and σ_t is the uncertainty at the mid-point of the core section (set to equal 5% at 500 years, = 25 years).

The full OxCal coding for this model (OCM-6.1) is given in appendix 8, whilst a truncated version is provided in figure 6.1.

Figure 6.1: A truncated version of the OxCal coding (OCM-6.1) applied for the statistical re-analysis of the original SG93 dataset (Kitagawa and van der Plicht 2000). (The full OxCal coding for this model specification is provided in appendix 8.)

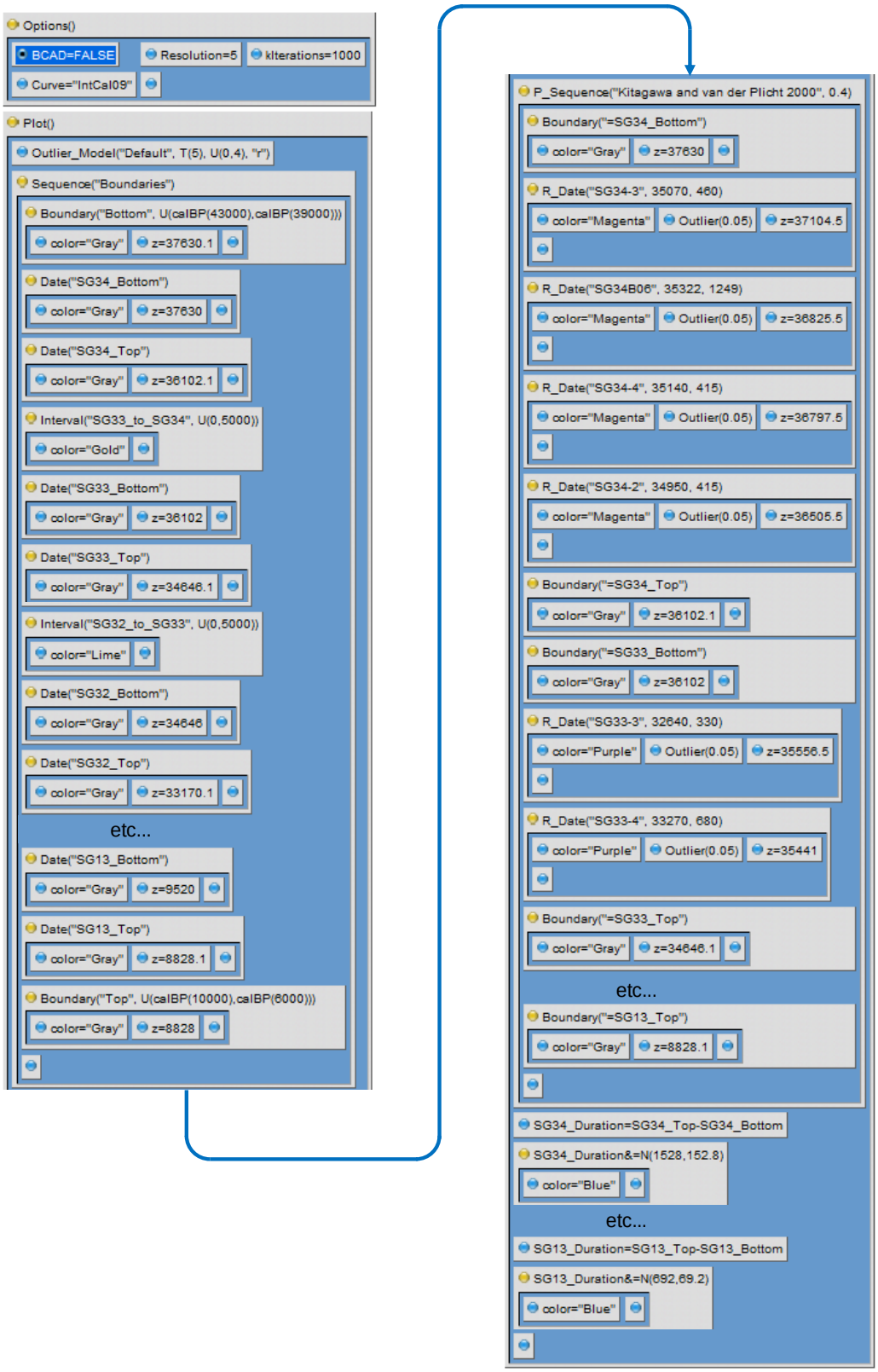

6.1.3 Modelling Results and Interpretation

With `intervals` of unknown duration inserted between adjacent core sections, the Suigetsu ’93 data can be ‘pulled’ to match far more tightly the IntCal09 calibration curve, to which the former data are calibrated (figure 6.2). It can be clearly seen (figure 6.3) that whilst some inter-core section `intervals` are minimal, others are much larger, with over 1,000 years’ gap predicted in one instance (between core sections SG26 and SG27). Such a gap, if real, would represent a depth of over 60 cm of missing material from the sedimentary record (based upon a mean annual deposition during the Glacial of ≈ 0.61 mm; Kitagawa and van der Plicht 1998a).

Figure 6.2: The re-modelled (OCM-6.1) data of Kitagawa and van der Plicht (2000) as calibrated against IntCal09 (Reimer *et al*. 2009), shown for the periods: **(a)** 18 to 8 cal. ka BP; **(b)** 26 to 16 cal. ka BP; **(c)** 34 to 24 cal. ka BP; and **(d)** 42 to 32 cal. ka BP. The modelled data are plotted with 1σ (BP)/68.2% (cal. BP) probability distributions shown, with successive core sections coloured alternately in magenta and purple. The calibration datasets of IntCal09 (Reimer *et al*. 2009; lime green), IntCal04 (Reimer *et al*. 2004a; dark green), Hughen *et al*. (2006; light blue), Fairbanks *et al*. (2005; gold) and the original, unaltered (i.e. without intervals inserted between core sections) Kitagawa and van der Plicht (2000) data (red) are plotted for comparison, all at 1σ uncertainty.

(a):

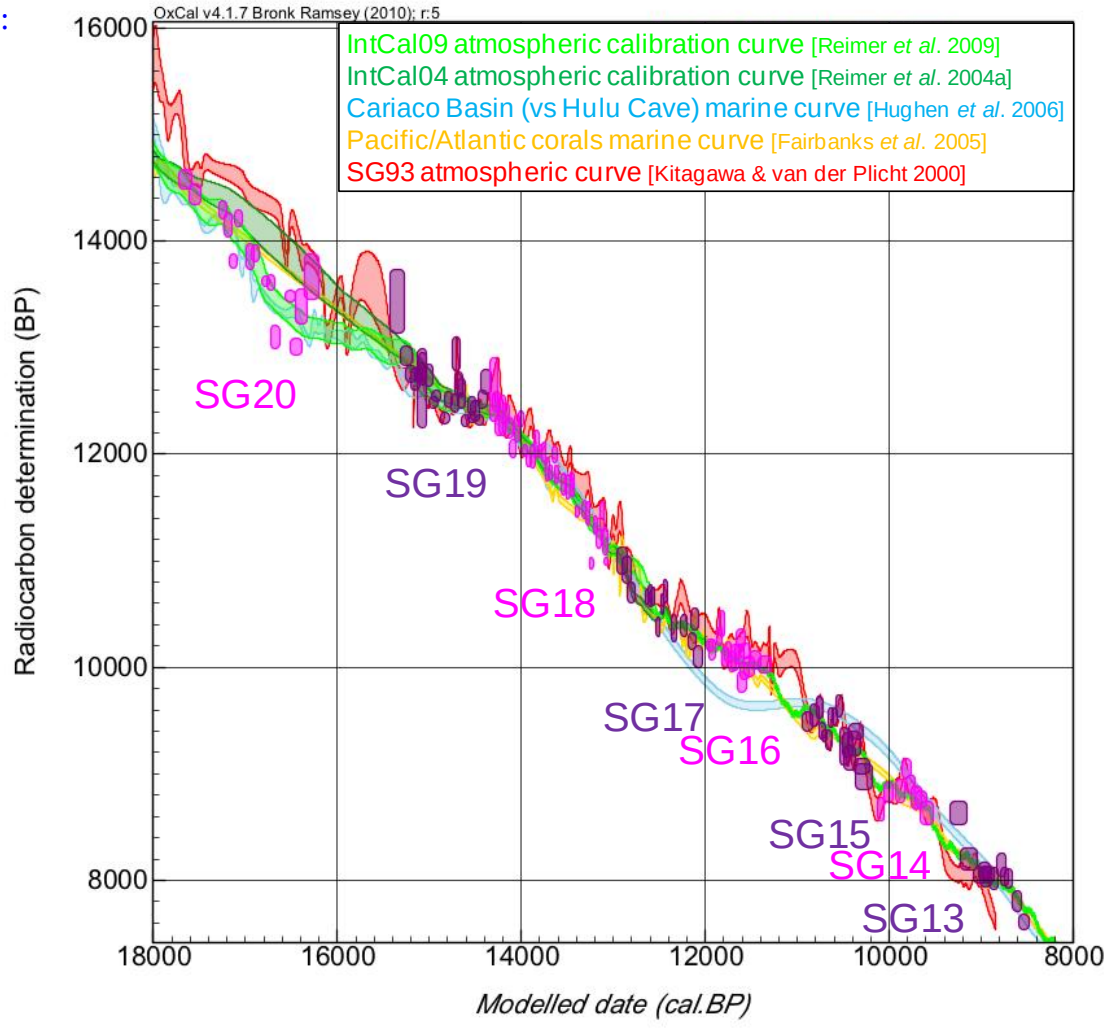

Figure 6.2 (continued):

(b):

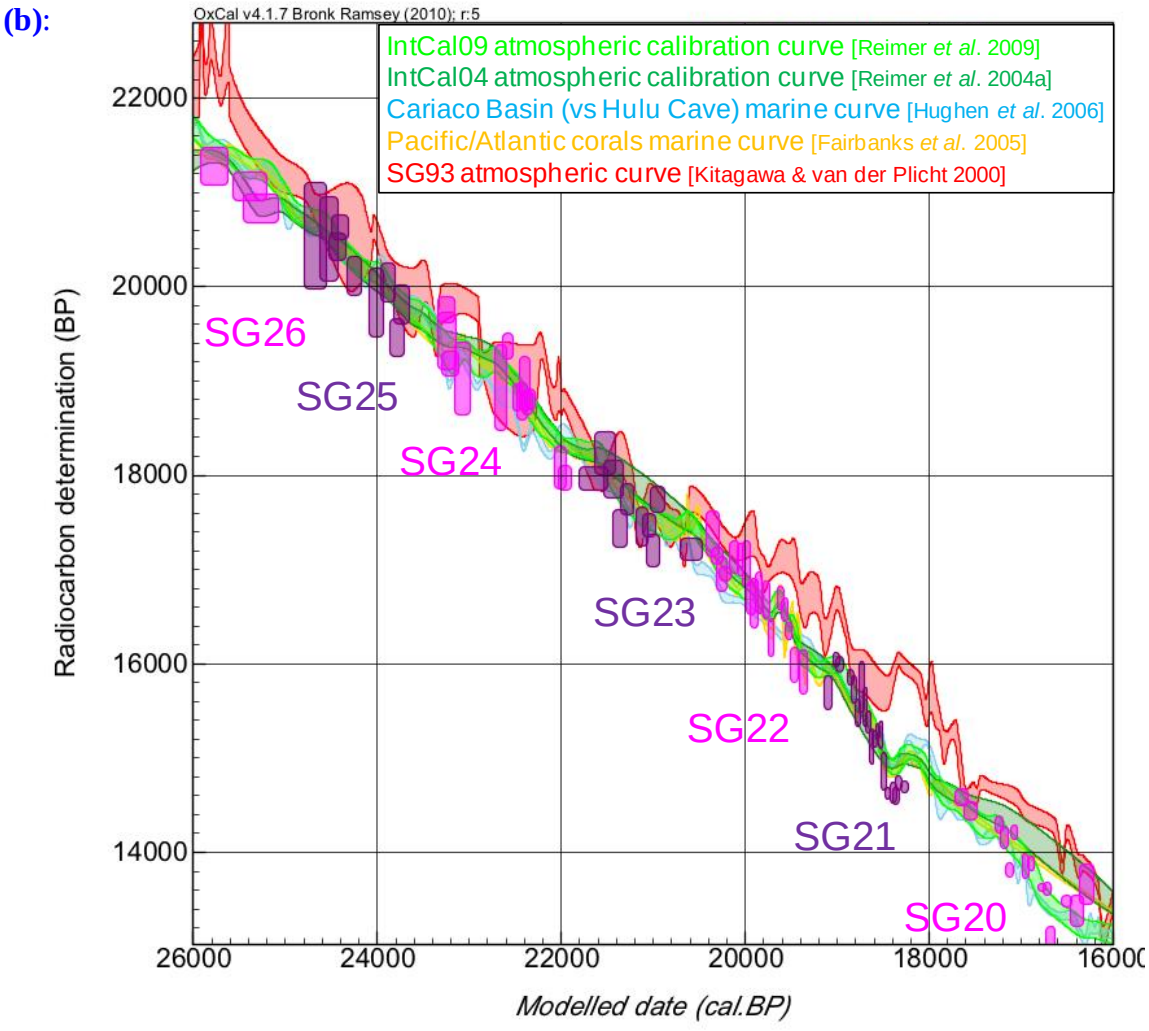

Figure 6.2 (continued):

(c):

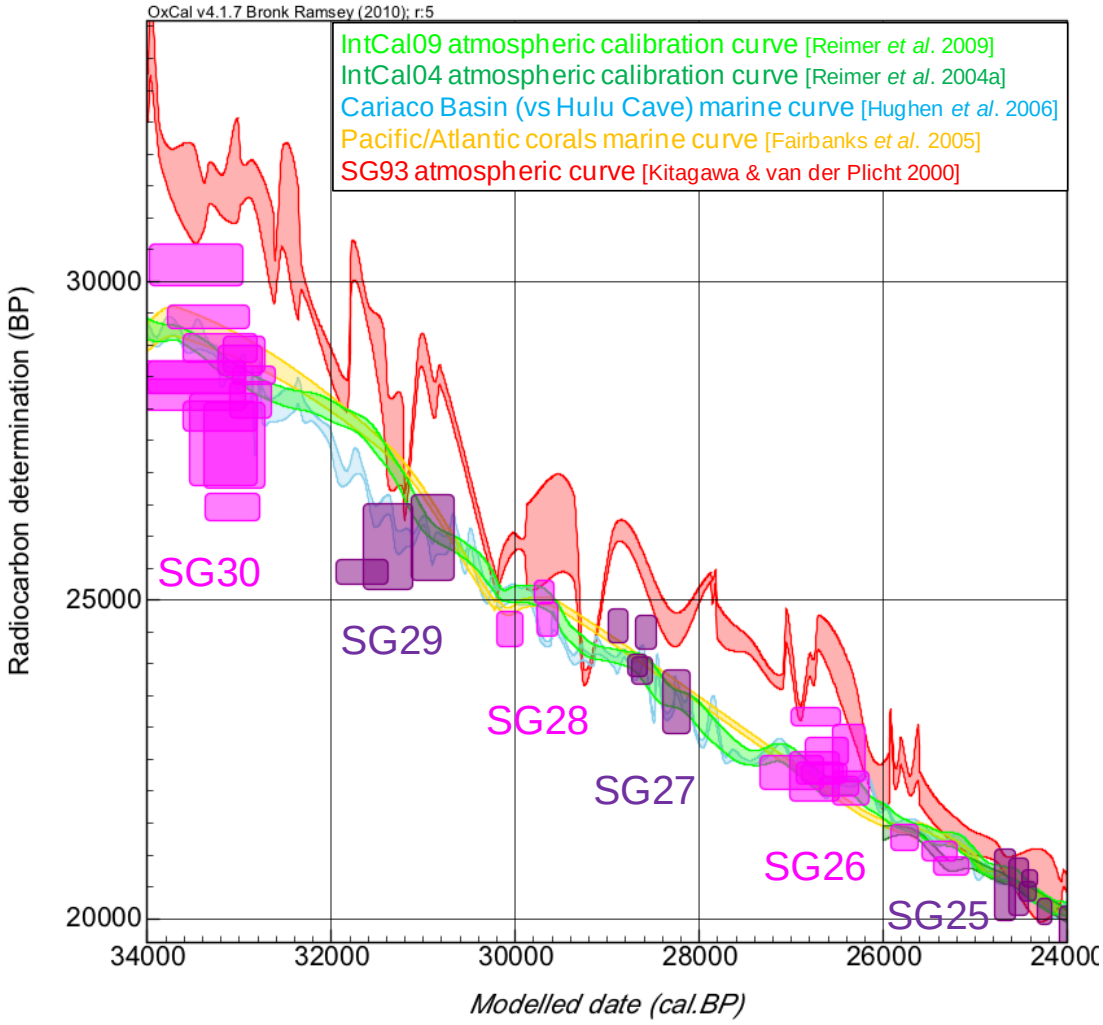

Figure 6.2 (continued):

(d):

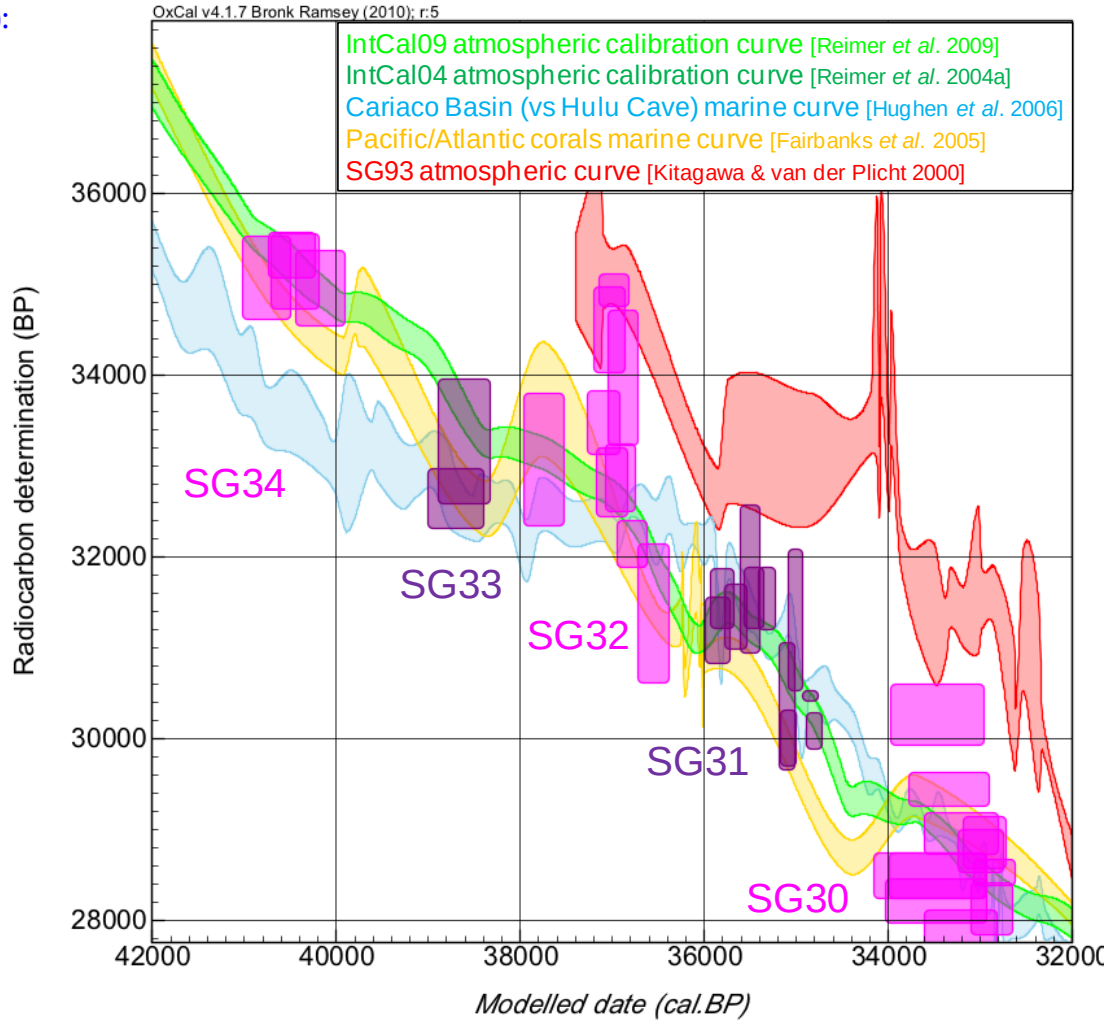

Figure 6.3: The inter-core section `intervals` identified in the Suigetsu '93 dataset (Kitagawa and van der Plicht 2000) by OCM-6.1. The prior distributions, given in the lighter shading, were constrained to be uniformly distributed between 0 and 5,000 years, whilst the darker shading shows the posterior distributions, which take into account the full gamut of information contained within the model. Whilst the majority of `intervals` are found to be short, several gaps are found to be longer (`intervals` with a median value in excess of 200 years highlighted in gold, and in excess of 400 years highlighted in red), with one such gap found to exceed 1,000 years' duration (between core sections SG26 and SG27). The horizontal bars below each probability distribution represent the posterior 68.2%, 95.4%, and 99.7% probability ranges, respectively. The median is also shown.

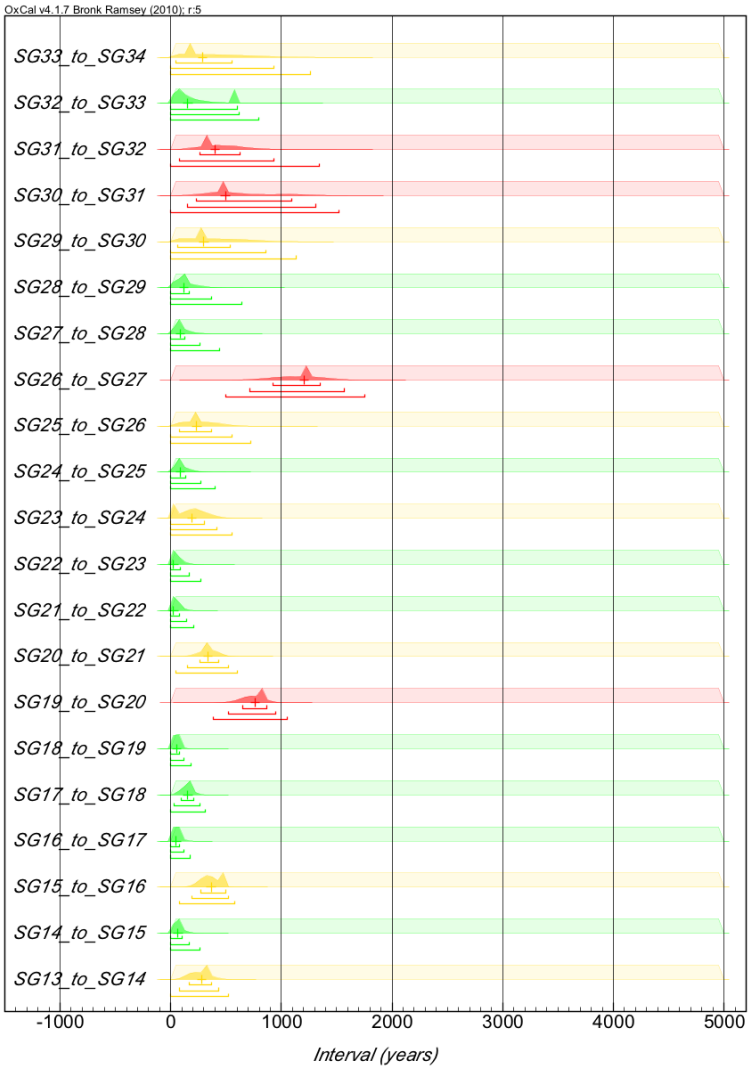

It was suggested by the original authors (H. Kitagawa, personal communication) that the more likely reason for the disagreement of the Suigetsu data with those of the other calibration datasets was error in the varve counting itself, rather than in there being significant missing sediment due to the core-drilling methodology applied. Agreement between the varve-counted core section durations and those predicted by OxCal, based upon the radiocarbon determinations of macrofossils within them (figure 6.4) is, however, generally very good and would tend towards support for the original varve counting. Having said this, five of the 22 core sections are, nevertheless, found to demonstrate poor agreement between the prior- and posterior information (as determined in OxCal by agreement indices, A, of < 60.0%; Bronk Ramsey 1995; section 5.3.3). In each of these instances, the modelled core section durations are found to be shorter than the varve-counted values, suggesting that errors in varve counting are tending towards the inclusion of additional 'years', perhaps through the inclusion of intra-annual laminations. Varve count errors of this nature would not be responsible for the divergence of the original Lake Suigetsu calibration dataset from the alternative records, however, since their correction would foreshorten the Suigetsu dataset yet further as compared with these records. From this purely statistical modelling exercise, therefore, it would appear that the explanation for the discordance of the Lake Suigetsu calibration dataset is that of missing sections of retrieved sediment.

Figure 6.4: Comparison of the prior distributions (lighter shading) for the duration of each SG93 core section (as based upon the original varve count data; Kitagawa and van der Plicht 2000), and the posterior distributions (darker shading) generated from OCM-6.1. Agreement indices (in parentheses) exceeding 60.0 represent a good fit, whilst those falling below this value represent ill-fitting data (Bronk Ramsey 1995). Here, such core section examples (sections SG17, SG19, SG21, SG22 and SG23, highlighted in red) are interpreted as areas where the reliability of the original varve counting should be questioned. The horizontal bars below each probability distribution represent the posterior 68.2%, 95.4%, and 99.7% probability ranges, respectively. The median is also shown.

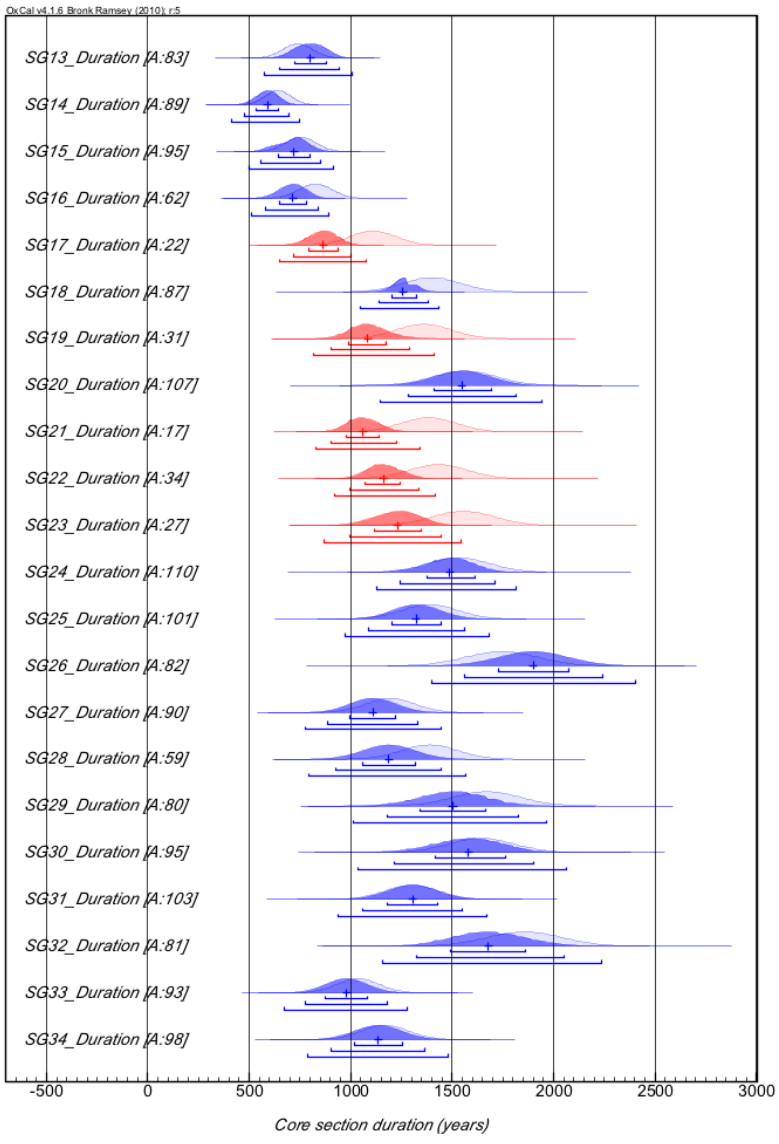

In terms of the outlier analysis applied, only three of the 269 radiocarbon dates were found to yield ≥ 95% probability of being outliers (and no further dates ≥ 90%), whilst 222 of the 269 dates were given a posterior probability of ≤ 5% of being outliers (as compared to the arbitrary 5% prior probability applied). Such findings support the validity of the individual radiocarbon determinations themselves, and do not suggest any systematic bias in the methodology of Kitagawa and van der Plicht. Prior to the examination of radiocarbon determinations from SG06 samples, this statistical finding added support for the reliability of the Lake Suigetsu site, and boded well for the radiocarbon determinations subsequently generated from the Suigetsu Varves 2006 project.

Whilst this modelling exercise undoubtedly contains significant circularity in the assumptions made, particularly since calibrating the one dataset on to the other should inevitably produce strong correspondence, the fact that the revised age-depth profile for the Suigetsu ’93 data (figure 6.5) remains generally linear (albeit with occasional ‘steps’, where OxCal has identified more significant inter-core section gaps), lends support for this profile being authentic, and therefore for the correspondence with IntCal09 to be genuine.

Figure 6.5: Age-depth profile of the re-modelled (OCM-6.1) Suigetsu ’93 dataset (Kitagawa and van der Plicht 2000), as calibrated against IntCal09 (Reimer *et al*. 2009), shown at 68.2% and 95.4% probability ranges.

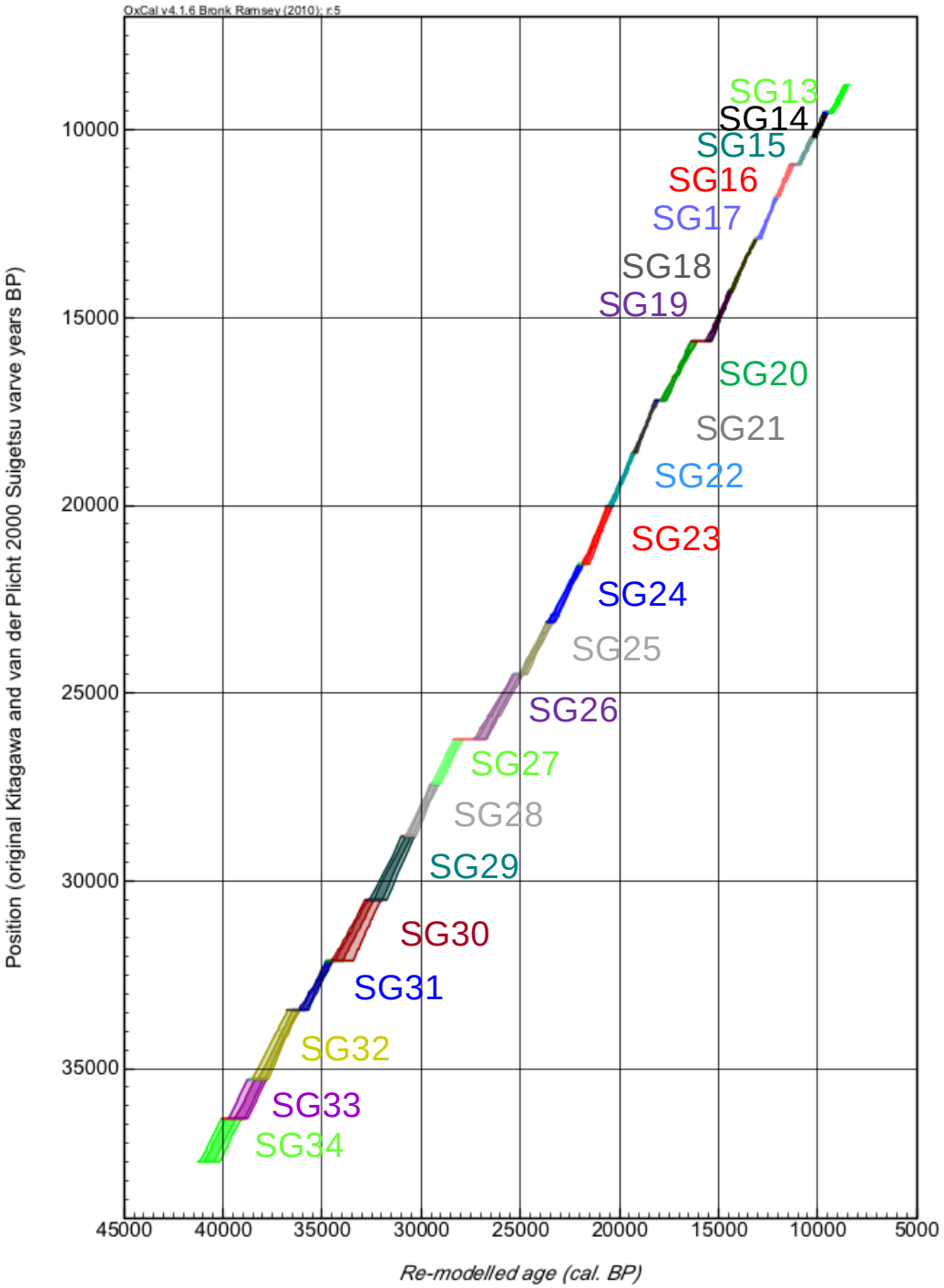

6.2 Physical Re-analysis of the Suigetsu'93 Sediment Core

6.2.1 Purpose of the Exercise

Although the above statistical exercise provided a linkage of the Suigetsu '93 chronology to that of IntCal09 (Reimer *et al*. 2009), the resultant revised SG93 chronology necessarily incorporated various assumptions. Most crucially, an assumption that the actual Lake Suigetsu radiocarbon calibration curve would fit precisely on to IntCal09 has been made. Since the fundamental premise of this thesis is that the IntCal curve, based on assumptions of corrected marine data beyond the present tree-ring limit, might not reliably represent the 'true' atmospheric radiocarbon concentration across the entirety of this time period (chapter 2), the modelling exercise should not be relied upon to firmly link the SG93 chronology to the IntCal09 timescale (or, via this process, to the SG06 chronology). A more direct linkage to the SG06 timescale would be through applying the same modelling process as outlined above to fit the SG93 data directly on to the now semi-complete SG06 varve chronology (chapter 7). This would not involve any assumed marine reservoir correction, and would be completely legitimate considering that the terrestrial macrofossils dated from both the SG93 and SG06 cores would obviously have drawn their ^{14}C from the same atmospheric ^{14}C reservoir. However, this process would assume the reliability of most samples dated, and would anyway incorporate a degree of uncertainty in the fit (as is generated from all radiocarbon PDFs).

Although not initially clear from correspondence with the original authors, archive 'U-channels' of original SG93 core material were kept in storage in Nagoya. Therefore, subsequent to the performing of the purely statistical modelling exercise described above, a more robust re-modelling of the SG93 data was made possible through matching of the SG93 sediment core to the composite SG06 sediment profile via direct matching of major event

horizons between the respective cores (sections 6.2.2 and 6.2.3, below). Not only does such a physical matching enable assessment of the findings of the statistical exercise (section 6.2.4), it also allows a thoroughly reliable incorporation of the ≈ 300 radiocarbon determinations from the original Suigetsu study into the ≈ 600 radiocarbon determinations from the present study (chapter 7), thus significantly enhancing the number/resolution of data points in the final Lake Suigetsu calibration dataset (section 7.6). Finally, examination of this revised SG93 chronology has implications for the palaeoenvironmental conclusions (e.g. Nakagawa *et al*. 2003) drawn from the original Suigetsu project (section 6.2.5).

6.2.2 Visual Matching Methodology

As noted above, a U-channel archive from the original SG93 sediment core was kept in storage at the University of Nagoya (Institute for Hydrospheric-Atmospheric Sciences) by the original principle investigator, Professor Hiroyuki Kitagawa. Comparison of this U-channel material with the high resolution core images of the SG06 project therefore enabled the matching of the original sediment core to that of the composite stratigraphy of the present project. Digital photographs made of this archive SG93 material were aligned to those of the SG06 project to support this matching process, an example of which can be seen in figure 6.6 (and the matching of the remaining core sections being given in appendix 9).

The original stratigraphic description of the SG93 sediment material by H. Kitagawa (personal communication) included depths marked of major event horizons (to 5 mm precision). These horizons were, where possible, identified in the archive SG93 sediment and used, along with the 'firm' visual correlations to SG06, to build a conversion model for the Level Finder software (T. Nakagawa; section 4.2.1) through which interpolated SG06 composite- (and 'event-free') depth equivalents could be derived for all original SG93 radiocarbon samples. Since the depths of the SG93 major event horizons, as well as the

depths from which the SG93 radiocarbon samples were taken, were recorded close to the time of the original coring, subsequent expansion/contraction of the archive core material is not a problem for the generation of this physical matching model.

Archive U-channel sediment was, however, only available for the SG11 to SG14 and SG20 to SG36 core sections. Remnant material for the core sections SG15 to SG19 was not available, and therefore recourse to the original SG93 core images (those used for the original SG93 varve counting) had to made (though these core photographs necessitated piece-wise matching, since images showed only ≈ 3 cm length core section intervals, with a resultant potential for errors in the compilation of these images).

Although not yet performed, correlation of microtephra horizons between the respective SG93 and SG06 sediment cores might add further weight to these visual correlations. To this end, 5 cm (or smaller) contiguous sub-samples were made of the archive SG93 U-channel material and might be analysed in future. Furthermore, it might be possible to compare the original SG93 XRF data with those of the present project, providing additional credence to the correlations drawn. However, having said this, the majority of the SG93 core sections could be matched fairly easily to SG06 through purely visual means (appendix 9), despite the fact that the SG93 sediment had obviously now oxidised and therefore lost much of its visible lamination. Only a handful of SG93 core sections were more difficult to place.

Figure 6.6: An example of the physical matching of the archive SG93 U-channel material to the composite SG06 sediment profile. The example shown is for SG93 core section SG11 (right), as compared to SG06 core sections C-07 and C-08 (left), and B-05 (centre). Firm linkages are illustrated in green, more questionable linkages in amber, and the (K-Ah) tephra layer in red. Numbered laminae from SG93 are those identified in the original stratigraphic description of H. Kitagawa (personal communication). (The turquoise lines reflect disturbance of the retrieved SG06 core segments, primarily shown here for the upper ≈11 cm of core section C-08, from which plant macrofossils were not sampled for the SG06 radiocarbon calibration dataset.)

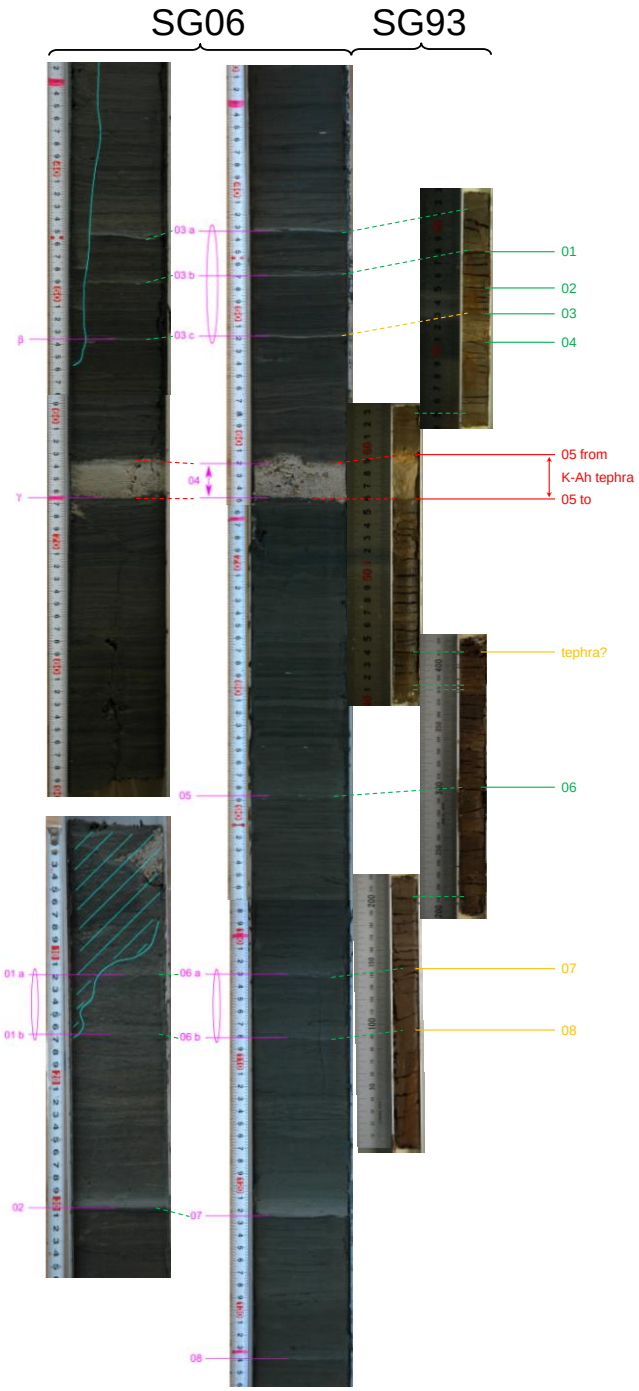

6.2.3 Results of Visual Matching

Table 6.1 gives the equivalent SG06 composite- and event-free depths for the top and bottom of each of the SG93 core sections (SG11 to SG36), as generated from the visual matching exercise described above. The 'real' span of missing sedimentary gaps between adjacent SG93 core sections is thus obtained through subtracting the equivalent SG06 composite core depth of the bottom of a given SG93 core section from that of the top of the underlying core section. These values are given in table 6.2.

Table 6.1: The equivalent depths of SG93 core sections (SG11 to SG36) in the SG06 sediment core, as achieved through visual matching of the respective core profiles.

Core section		Original SG93 depth (cm)	Original SG93 vyr BP	SG06 composite depth (cm)	SG06 event-free depth (cm)
SG11	Top	895.0	n/a	945.0	930.0
	Bottom	987.0	n/a	1029.6	1010.3
SG12	Top	987.0	n/a	1037.8	1018.5
	Bottom	1045.0	n/a	1091.8	1069.5
SG13	Top	1042.0	8,828	1095.0	1072.7
	Bottom	1133.0	9,520	1182.2	1159.9
SG14	Top	1133.0	9,520	1193.2	1170.9
	Bottom	1225.0	10,213	1280.7	1257.4
SG15	Top	1225.0	10,213	1285.1	1261.8
	Bottom	1317.0	10,880	1374.2	1343.0
SG16	Top	1317.0	10,880	1393.4	1362.2
	Bottom	1408.0	11,789	1474.2	1440.7
SG17	Top	1408.0	11,789	1490.6	1456.5
	Bottom	1498.0	12,864	1579.0	1544.9
SG18	Top	1498.0	12,864	1580.6	1546.5
	Bottom	1589.0	14,267	1672.4	1631.8
SG19	Top	1589.0	14,267	1681.1	1640.5
	Bottom	1680.0	15,713	1765.1	1723.5

Table 6.1 (continued):

Core section		Original SG93 depth (cm)	Original SG93 vyr BP	SG06 composite depth (cm)	SG06 event-free depth (cm)
SG20	Top	1680.0	15,713	1769.0	1727.4
	Bottom	1771.0	17,166	1853.5	1810.9
SG21	Top	1771.0	17,166	1858.2	1815.6
	Bottom	1855.0	18,572	1947.3	1898.7
SG22	Top	1855.0	18,572	1950.8	1902.2
	Bottom	1939.0	19,992	2036.9	1985.1
SG23	Top	1939.0	19,992	2035.3	1983.5
	Bottom	2028.0	21,566	2120.9	2064.2
SG24	Top	2028.0	21,566	2123.9	2067.2
	Bottom	2119.0	23,088	2219.1	2161.4
SG25	Top	2119.0	23,088	2217.9	2160.2
	Bottom	2210.0	24,630	2316.4	2247.6
SG26	Top	2210.0	24,630	2327.7	2258.9
	Bottom	2301.0	26,162	2427.2	2355.8
SG27	Top	2301.0	26,162	2429.5	2358.1
	Bottom	2393.0	27,601	2526.8	2453.4
SG28	Top	2393.0	27,601	2530.5	2457.1
	Bottom	2477.0	28,938	2609.0	2527.9
SG29	Top	2494.0	29,238	2643.5	2535.3
	Bottom	2586.0	30,521	2729.8	2614.3
SG30	Top	2586.0	30,521	2740.1	2624.6
	Bottom	2678.0	32,040	2830.9	2712.5
SG31	Top	2678.0	32,040	2833.3	2714.9
	Bottom	2770.0	33,470	2918.1	2798.9
SG32	Top	2770.0	33,470	2930.1	2810.9
	Bottom	2862.0	34,946	3015.3	2896.1
SG33	Top	2862.0	34,946	3027.0	2907.8
	Bottom	2953.0	36,402	3123.5	2992.2
SG34	Top	2953.0	36,402	3134.0	3002.7
	Bottom	3045.0	37,930	3203.1	3071.3
SG35	Top	3045.0	n/a	3217.8	3086.0
	Bottom	3136.0	n/a	3297.6	3163.5

Table 6.1 (continued):

Core section		Original SG93 depth (cm)	Original SG93 vyr BP	SG06 composite depth (cm)	SG06 'event-free' depth (cm)
SG36	Top	3136.0	n/a	3302.0	3167.9
	Bottom	3227.0	n/a	3385.1	3247.5

Table 6.2: The 'real' lengths of SG93 inter-core section gaps identified by the visual matching of the respective SG93 and SG06 core profiles. (Negative values reflect overlap between adjacent core sections.)

SG93 inter-core section gap	Length of missing sediment (cm)	SG93 inter-core section gap	Length of missing sediment (cm)
SG11 to SG12	8.2	SG24 to SG25	-1.2
SG12 to SG13	3.2	SG25 to SG26	11.3
SG13 to SG14	11.0	SG26 to SG27	2.3
SG14 to SG15	4.4	SG27 to SG28	3.7
SG15 to SG16	19.2	SG28 to SG29	34.5
SG16 to SG17	16.4	SG29 to SG30	10.3
SG17 to SG18	1.6	SG30 to SG31	2.4
SG18 to SG19	8.7	SG31 to SG32	12.0
SG19 to SG20	3.9	SG32 to SG33	11.7
SG20 to SG21	4.7	SG33 to SG34	10.5
SG21 to SG22	3.5	SG34 to SG35	14.7
SG22 to SG23	-1.6	SG35 to SG36	4.4
SG23 to SG24	3.0		

6.2.4 Re-modelling of the SG93 Data Using Equivalent SG06 Core Depths

Having generated an approximation of the 'true' depth profile of the SG93 sediment core, a more reliable comparison of the Suigetsu '93- and alternative radiocarbon calibration datasets could then be made. A second model was therefore run in OxCal (OCM-6.2), which

again calibrated the original Suigetsu '93 radiocarbon determinations against IntCal09 (Reimer *et al*. 2009), but this time using equivalent SG06 event-free depth (EFD) as the z unit. This model was much simpler in construction than OCM-6.1, lacking the need for the inclusion of (unknown duration) intervals (and hence giving increased robustness to the output of this model). Again, a P_Sequence model was applied, with the value of the k parameter (1.51) generated from an assessment of the varve count data from the present (Suigetsu Varves 2006) project (section 7.4.2). A truncated version of the OCM-6.2 model coding is given in figure 6.7, with the full coding again given in appendix 8. The only prior age information fed into this model was a constraint on the bottom (< 43,000 cal. BP) and top (> 7,000 cal. BP) of the sequence, which allowed OxCal to find a suitable starting point from which to run. These ages were conservatively old and young, respectively, such that they did not curtail the posterior distributions of the oldest- ('SG34_bottom') and youngest ('SG13_top') events in the model. A single additional internal boundary was included in the P_Sequence at a depth of 1695 cm EFD, reflecting the change in sedimentation rate in the lake at this time (section 7.3). This boundary required additional prior constraining information to facilitate the model's running. A uniform distribution of between 16,000 and 14,000 cal. BP was ascribed to this event, again chosen so as not to curtail the posterior age distribution of the event. For direct comparison of the outcomes of this model with those of OCM-6.1 (above), the same 269 radiocarbon determinations (from SG93 core sections SG13 to SG34) were included in OCM-6.2. Additional data from the other physically-matched core sections (SG11, SG12, SG35 and SG36) were therefore not included in OCM-6.2. (These data could not be included in OCM-6.1 since varve counting of these core sections was not possible in the Suigetsu '93 project, due to the poor quality of varve preservation over these core depths.)

Figure 6.7: A truncated version of the OxCal coding (OCM-6.2) calibrating the original SG93 dataset (Kitagawa and van der Plicht 2000) against IntCal09 (Reimer *et al*. 2009), using equivalent SG06 event-free depth as the `z` unit. (The full OxCal coding for this model specification is provided in appendix 8.)

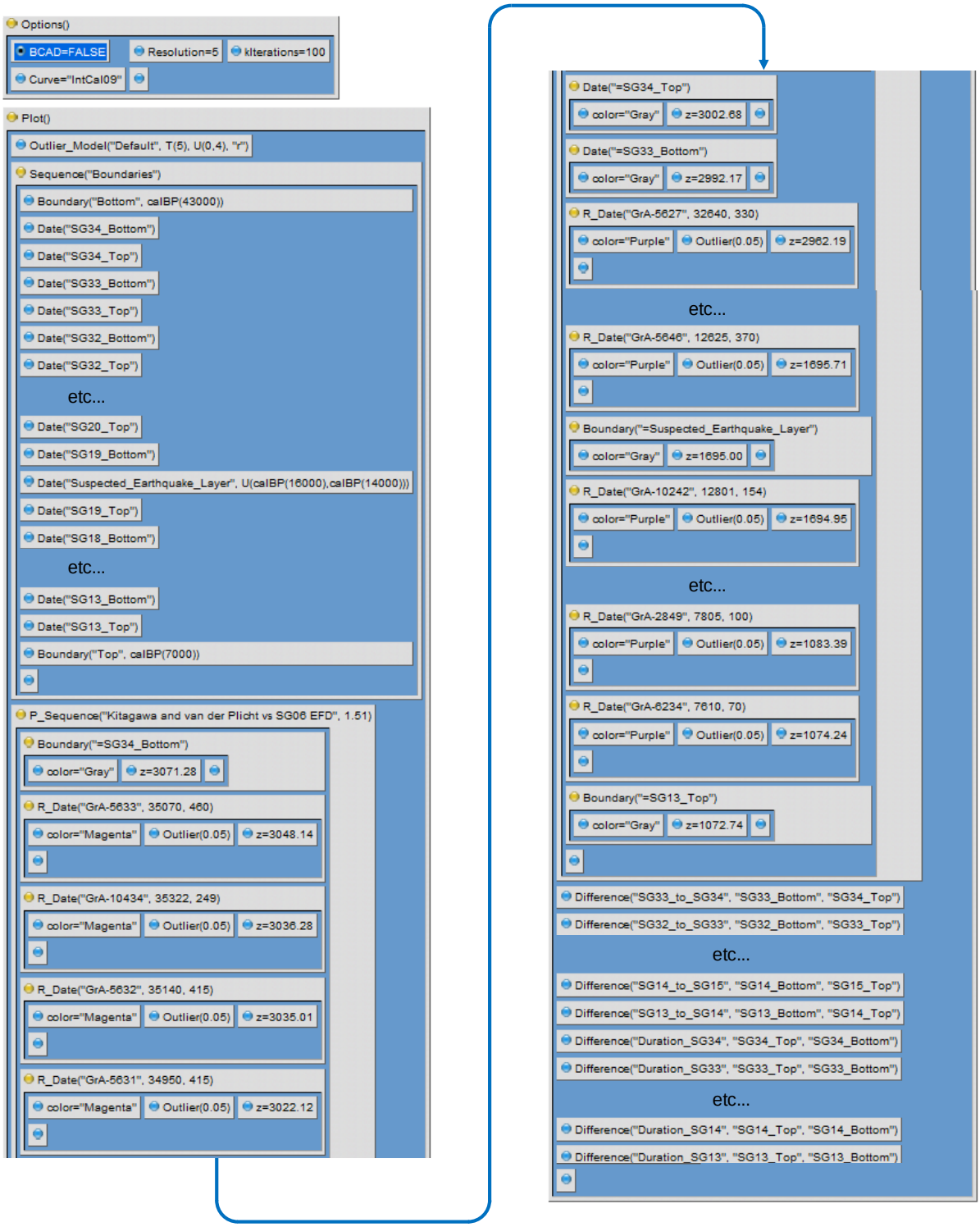

As with the purely statistical re-modelling exercise described above (section 6.1), the results of this latter re-modelling of the SG93 radiocarbon data, incorporating the SG06 event-free depth profile, produce excellent correspondence with the IntCal09 (Reimer *et al*. 2009) calibration curve against which the Suigetsu data were calibrated (figure 6.8). The resulting re-modelled SG93 age-depth profile (figure 6.9) is generally linear, with the single change in deposition rate specified at 1695 cm EFD.

In contrast to OCM-6.1, which allowed the individual contributory core sections of SG93 to shorten- or lengthen in duration separately, the construction of OCM-6.2 (a single `P_Sequence`, with only the one change in deposition rate) was such that the entire dataset would have to be shortened/lengthened in order to fit IntCal09. Therefore, the fact that the degree of correspondence between the SG93 data and IntCal09 remains so high is testament to the integrity of the Lake Suigetsu sediments. I.e., this suggests that there are no obvious (lengthy) hiatuses down the Suigetsu sediment profile, which had been previously suggested by several authors (e.g. Voelker *et al*. 2000; Bard 2001; Beck *et al*. 2001; Bard *et al*. 2004c), who rightly recognised the overall under-count of the SG93 chronology. Such a finding is hugely significant for the outcomes of the Suigetsu Varves 2006 project as it demonstrates that a robust chronology can be derived from SG06, providing the calendar age scale against which both palaeoenvironmental- and radiocarbon calibration datasets can be compared.

Tables 6.3 and 6.4, respectively, give the durations of the individual core sections and inter-core section gaps of SG93 as produced from OCM-6.2 (using SG06 EFD), and compare these to the purely statistical values generated by OCM-6.1 (using original SG93 varve count data). For comparison, the values of these durations are additionally given according to the SG06 varve count chronology (completed by both varve counting methods down to 1814.6 cm composite depth, and based solely on the XRF and X-radiography data for the remainder of the core), which will be more thoroughly introduced in section 7.3.

Figure 6.8: The re-modelled (OCM-6.2) data of Kitagawa and van der Plicht (2000) as calibrated against IntCal09 (Reimer *et al*. 2009), shown for the periods: **(a)** 18 to 8 cal. ka BP; **(b)** 26 to 16 cal. ka BP; **(c)** 34 to 24 cal. ka BP; and **(d)** 42 to 32 cal. ka BP. The data are plotted with 1σ/68.2% probability distributions shown, with successive core sections coloured alternately in magenta and purple. The calibration datasets of IntCal09 (Reimer *et al*. 2009; lime green), IntCal04 (Reimer *et al*. 2004a; darker green), Hughen *et al*. (2006; light blue), Fairbanks *et al*. (2005; gold) and the original, unaltered (i.e. without intervals inserted between core sections) SG93 data (Kitagawa and van der Plicht 2000; red) are plotted for comparison, all at 1σ uncertainty.

(a):

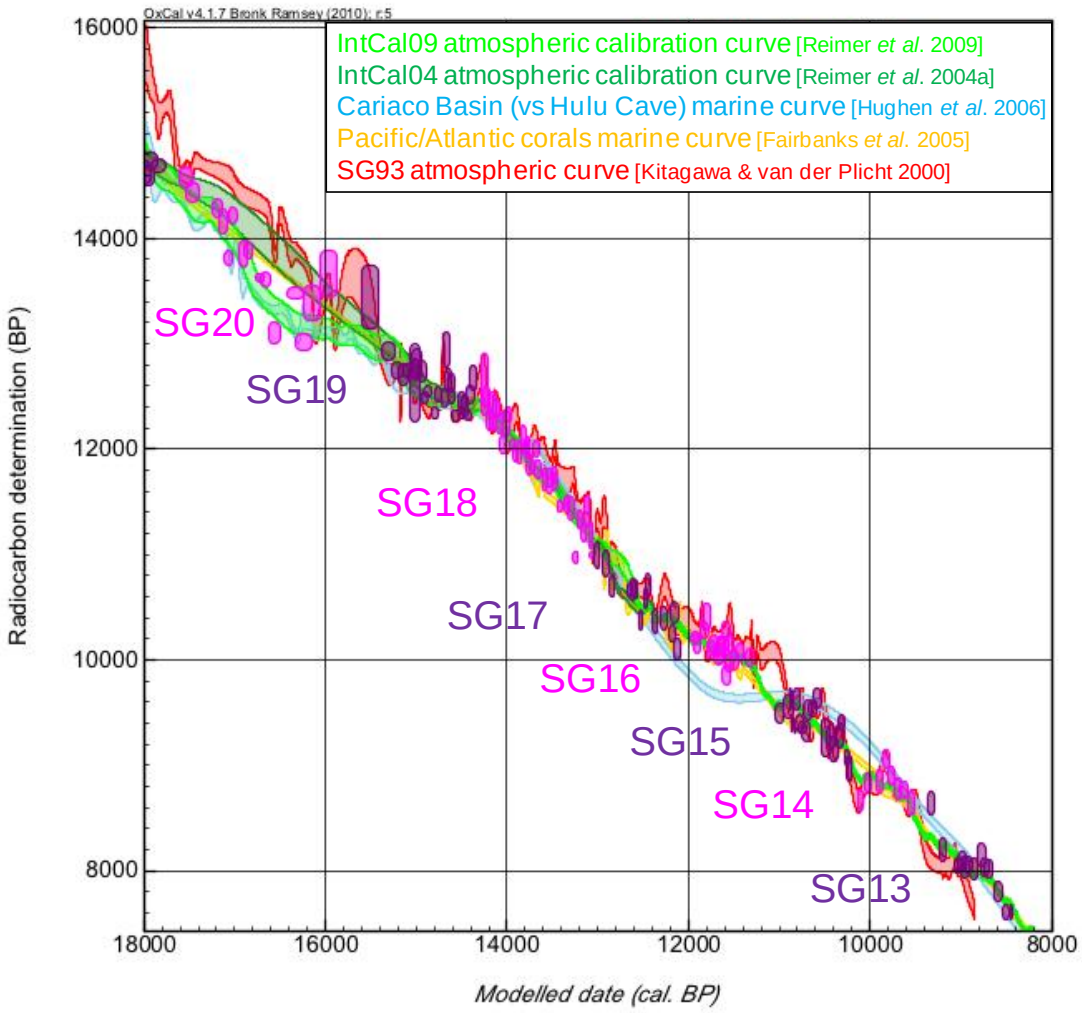

Figure 6.8 (continued):

(b):

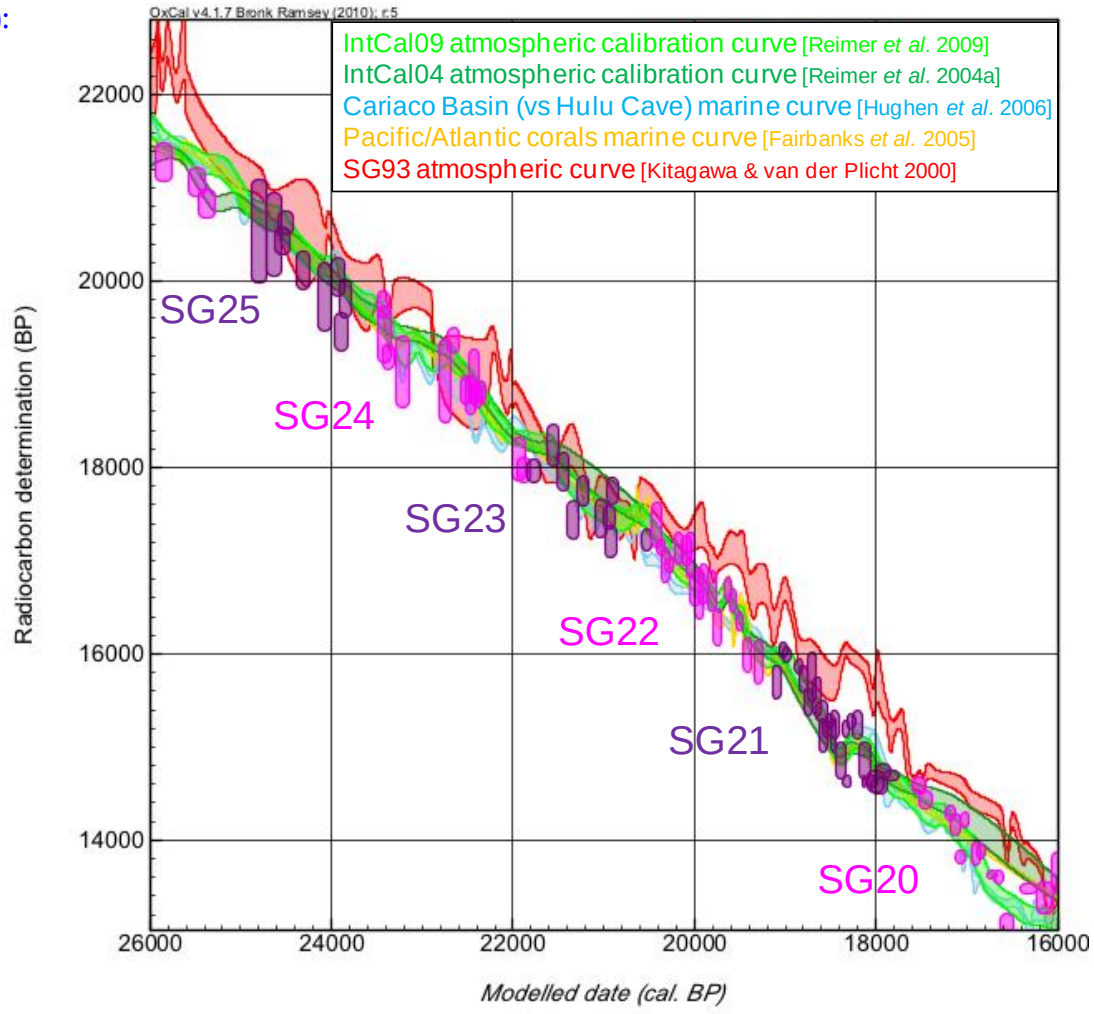

Figure 6.8 (continued):

(c):

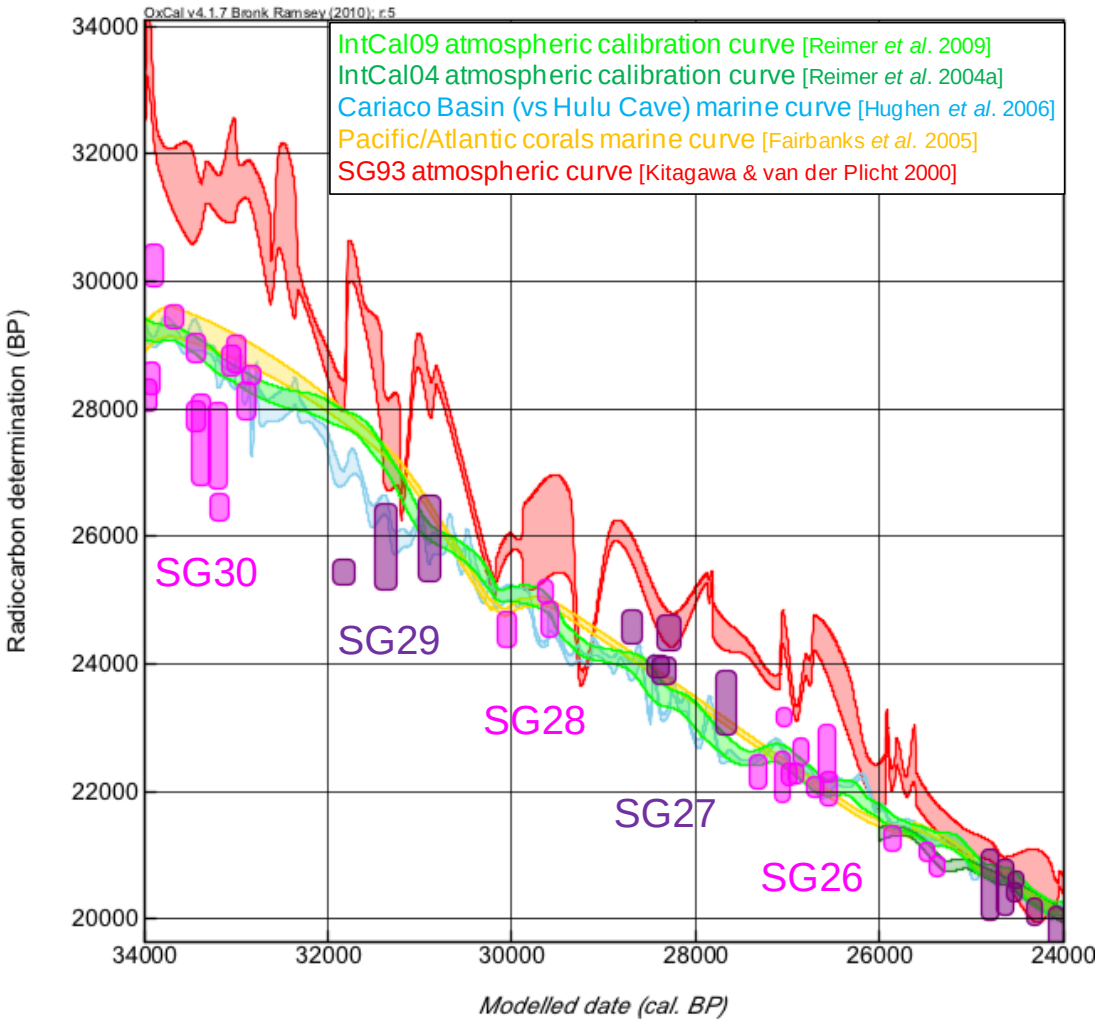

Figure 6.8 (continued):

(d):

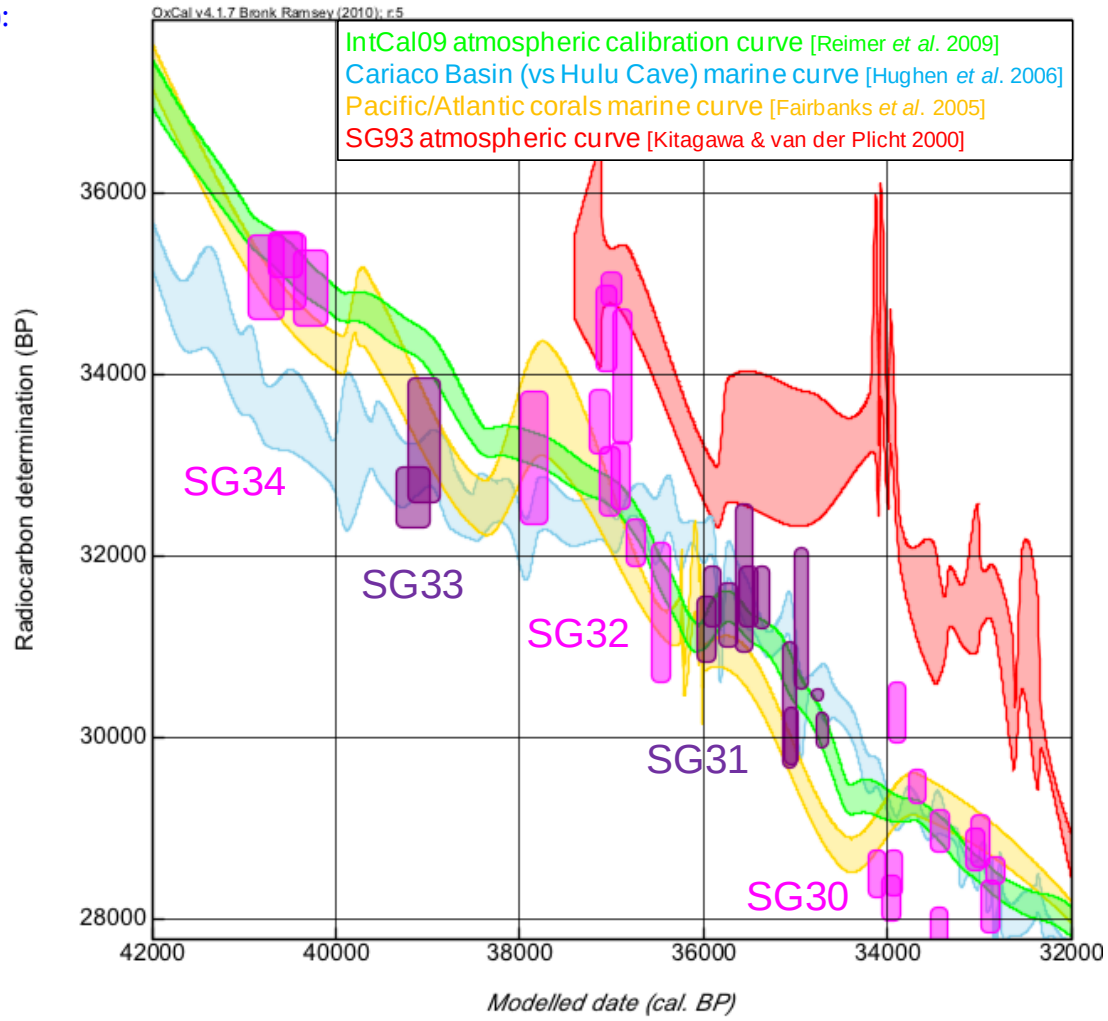

Figure 6.9: Age-depth profile of the re-modelled (OCM-6.2) Suigetsu '93 dataset, as calibrated against IntCal09 (Reimer *et al*. 2009), using SG06 event-free depth. Successive SG93 core sections are coloured alternately in purple and magenta, with the prior, unmodelled distributions shown in lighter fill, and the posterior, modelled distributions shown in darker fill. The top and bottom of individual core sections are additionally shown in grey.

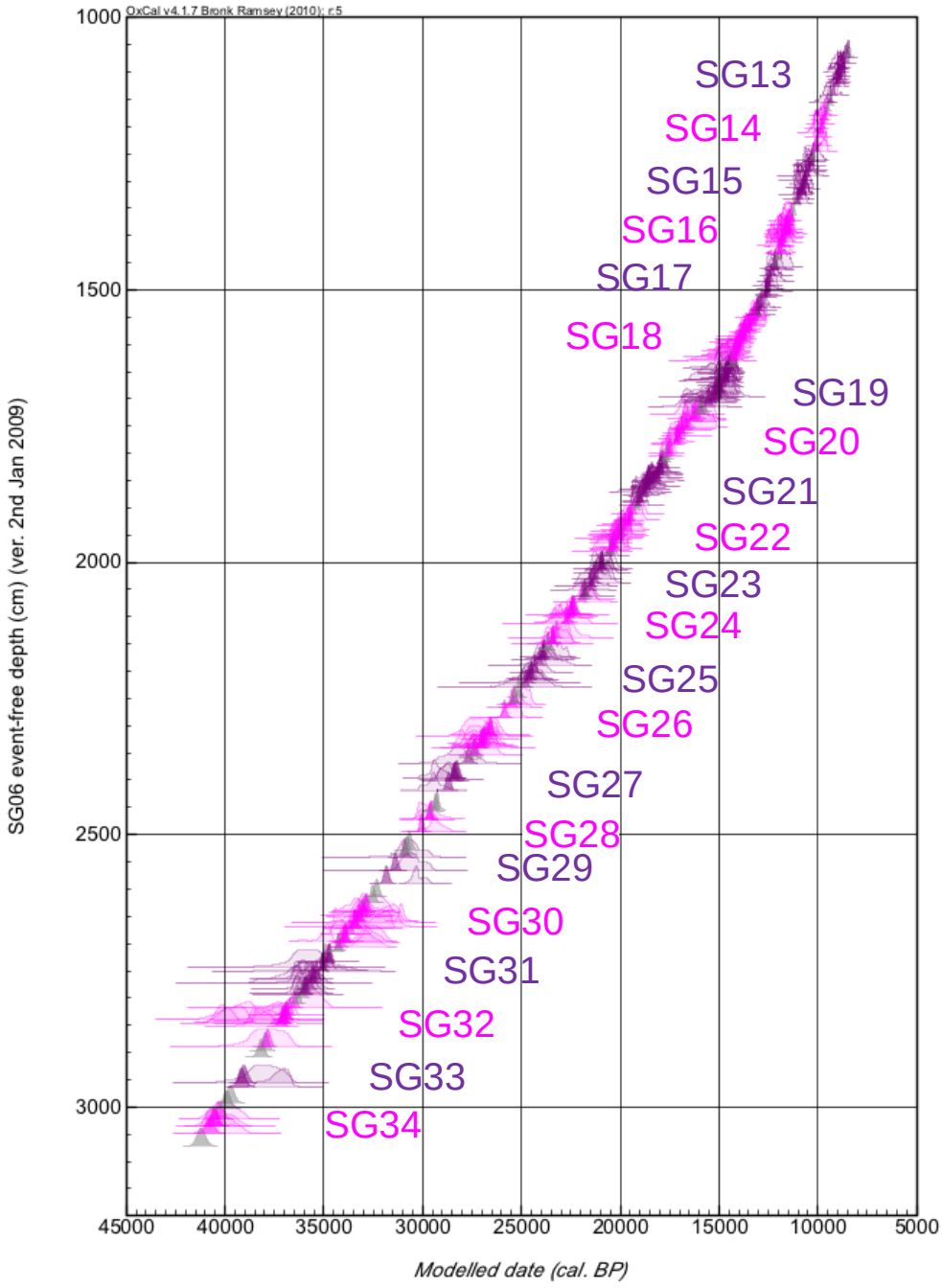

Table 6.3: Duration of SG93 inter-core section gaps as determined by: (i) statistical re-modelling (OCM-6.1) of the SG93 radiocarbon dataset against IntCal09 (Reimer *et al*. 2009); (ii) mean SG06 varve count, obtained through visual matching of archive SG93 core sections to the SG06 composite core profile; (iii) re-modelling (OCM-6.2) of the SG93 radiocarbon dataset against IntCal09, using equivalent SG06 event-free depth (EFD). Modelled data are given at both 68.2% and 95.4% probability ranges, with median values in parentheses.

SG93 inter-core section gaps	Duration of inter-core section gaps in calendar years as obtained by:		
	statistical re-modelling of SG93 dataset (OCM-6.1)	comparison with SG06 varve count	re-modelling of SG93 dataset utilising SG06 EFD (OCM-6.2)
SG13 to SG14	165 to 365; 75 to 435 (280)	n/a	77 to 125; 58 to 153 (103)
SG14 to SG15	0 to 105; 0 to 170 (65)	45	19 to 49; 11 to 67 (35)
SG15 to SG16	275 to 495; 190 to 520 (365)	198	169 to 243; 139 to 282 (208)
SG16 to SG17	0 to 80; 0 to 115 (50)	170	104 to 156; 84 to 186 (132)
SG17 to SG18	95 to 210; 30 to 265 (155)	18	5 to 31; 0 to 52 (20)
SG18 to SG19	0 to 80; 0 to 115 (55)	101	55 to 99; 40 to 125 (79)
SG19 to SG20	650 to 865; 520 to 945 (765)	64	54 to 131; 30 to 187 (98)
SG20 to SG21	265 to 430; 150 to 520 (335)	101	38 to 87; 23 to 121 (66)
SG21 to SG22	0 to 80; 0 to 140 (25)	54	23 to 61; 12 to 89 (45)
SG22 to SG23	0 to 85; 0 to 170 (25)	-28	-32 to -5; -60 to 0 (-22)
SG23 to SG24	0 to 305; 0 to 420 (190)	54	23 to 69; 11 to 106 (50)
SG24 to SG25	0 to 135; 0 to 270 (85)	-22	-29 to -2; -54 to 0 (-17)
SG25 to SG26	75 to 370; 0 to 550 (235)	220	154 to 249; 118 to 305 (205)
SG26 to SG27	925 to 1,350; 715 to 1,565 (1,205)	35	17 to 68; 6 to 110 (47)
SG27 to SG28	0 to 125; 0 to 265 (85)	59	33 to 85; 18 to 123 (63)
SG28 to SG29	0 to 170; 0 to 370 (120)	63	89 to 169; 62 to 218 (133)
SG29 to SG30	60 to 540; 0 to 860 (300)	205	147 to 248; 109 to 310 (201)
SG30 to SG31	235 to 1,095; 155 to 1,310 (495)	38	18 to 67; 7 to 108 (47)
SG31 to SG32	265 to 630; 75 to 930 (400)	215	179 to 287; 138 to 351 (237)
SG32 to SG33	0 to 600; 0 to 620 (155)	173	154 to 254; 117 to 314 (208)
SG33 to SG34	45 to 555; 0 to 930 (290)	140	140 to 237; 104 to 296 (192)

Table 6.4: Duration of SG93 core sections as determined by: (i) original SG93 varve counting (Kitagawa and van der Plicht 1998a, 1998b, 2000); (ii) statistical re-modelling (OCM-6.1) of the SG93 radiocarbon dataset against IntCal09 (Reimer *et al*. 2009); (iii) SG06 varve count, obtained through visual matching of archive SG93 core sections to the SG06 composite core profile; (iv) re-modelling of the SG93 radiocarbon dataset against IntCal09, using equivalent SG06 event-free depth (EFD). Modelled data are given at both 68.2% and 95.4% probability ranges, with median values in parentheses.

SG93 core section	Duration of core section in calendar years as obtained by:			
	original SG93 varve counting	statistical re-modelling of SG93 dataset (OCM-6.1)	comparison with SG06 varve count	re-modelling of SG93 dataset utilising SG06 EFD (OCM-6.2)
SG13	691	729 to 876; 657 to 938 (773)	n/a	839 to 954; 790 to 1,022 (898)
SG14	692	537 to 633; 482 to 686 (601)	n/a	674 to 766; 631 to 830 (722)
SG15	666	656 to 771; 556 to 833 (699)	790	726 to 828; 674 to 879 (776)
SG16	908	554 to 840; 553 to 904 (750)	799	699 to 809; 644 to 864 (754)
SG17	1,074	783 to 916; 721 to 982 (874)	987	850 to 950; 799 to 999 (900)
SG18	1,402	1,179 to 1,298; 1,141 to 1,356 (1,238)	1,028	1,126 to 1,214; 1,088 to 1,262 (1,171)
SG19	1,445	1,063 to 1,242; 984 to 1,354 (1,137)	1,168	1,522 to 1,707; 1,427 to 1,796 (1,613)
SG20	1,452	1,406 to 1,625; 1,265 to 1,743 (1,544)	1,532	1,494 to 1,715; 1,390 to 1,830 (1,606)
SG21	1,405	796 to 1,151; 796 to 1,239 (1,056)	1,414	1,364 to 1,532; 1,274 to 1,614 (1,447)
SG22	1,419	1,073 to 1,226; 1,000 to 1,322 (1,181)	1,638	1,248 to 1,389; 1,184 to 1,469 (1,321)
SG23	1,573	1,136 to 1,418; 1,011 to 1,445 (1,271)	1,578	1,244 to 1,404; 1,161 to 1,484 (1,324)
SG24	1,521	1,378 to 1,683; 1,241 to 1,698 (1,520)	1,706	1,719 to 1,909; 1,629 to 2,013 (1,816)
SG25	1,541	1,338 to 1,575; 1,201 to 1,711 (1,419)	1,786	1,380 to 1,581; 1,278 to 1,679 (1,480)

Table 6.4 (continued):

SG93 core section	Duration of core section in calendar years as obtained by:			
	original SG93 varve counting	statistical re-modelling of SG93 dataset (OCM-6.1)	direct comparison with SG06 varve count	modelling of SG93 dataset, but utilising SG06 EFD (OCM-6.2)
SG26	1,531	1,535 to 1,822; 1,356 to 1,971 (1,626)	1,868	1,902 to 2,144; 1,786 to 2,271 (2,025)
SG27	1,438	1,183 to 1,422; 1,048 to 1,570 (1,350)	1,574	1,748 to 1,973; 1,640 to 2,091 (1,862)
SG28	1,336	1,054 to 1,383; 924 to 1,425 (1,213)	942	1,195 to 1,419; 1,091 to 1,535 (1,309)
SG29	1,282	1,090 to 1,363; 946 to 1,448 (1,247)	1,180	1,409 to 1,634; 1,300 to 1,754 (1,524)
SG30	1,518	1,291 to 1,602; 1,122 to 1,755 (1,420)	1,547	1,598 to 1,838; 1,484 to 1,964 (1,720)
SG31	1,429	1,298 to 1,618; 1,168 to 1,689 (1,473)	1,449	1,654 to 1,900; 1,538 to 2,034 (1,780)
SG32	1,475	1,264 to 1,568; 1,118 to 1,726 (1,414)	1,419	1,494 to 1,764; 1,366 to 1,906 (1,632)
SG33	1,455	1,204 to 1,472; 1,066 to 1,620 (1,310)	1,474	1,401 to 1,655; 1,283 to 1,787 (1,530)
SG34	1,527	1,308 to 1,639; 1,196 to 1,783 (1,443)	1,134	1,150 to 1,401; 1,037 to 1,538 (1,279)

From table 6.3, it can be seen that the inter-core section gaps predicted by the purely statistical re-modelling exercise (OCM-6.1) are generally longer than the physical comparison of the SG93 and SG06 cores suggests in reality. This trend is illustrated more clearly in figure 6.10. The 'true' gaps between core sections are all < 20 cm (with the exception of SG28 to SG29 at 34.5 cm), with a mean sediment loss of 8.27 cm (from table 6.2) or 95.15 years (from table 6.3).

Table 6.4 indicates that the core section durations re-modelled in OCM-6.1 are generally shorter than is suggested by either the OCM-6.2 model or the actual SG06 varve count data. These trends are illustrated more clearly in figure 6.11.

Figure 6.10: Comparison of the durations of SG93 inter-core section gaps as determined by: (i) statistical re-modelling (OCM-6.1) of the SG93 radiocarbon dataset against IntCal09 (Reimer *et al*. 2009; magenta); (ii) SG06 varve count, obtained through visual matching of archive SG93 core sections to the SG06 composite core profile (blue); and (iii) re-modelling (OCM-6.2) of the SG93 radiocarbon dataset against IntCal09, using equivalent SG06 event-free depth (EFD; purple). The 68.2%, 95.4% and 99.5% posterior probability ranges are shown.

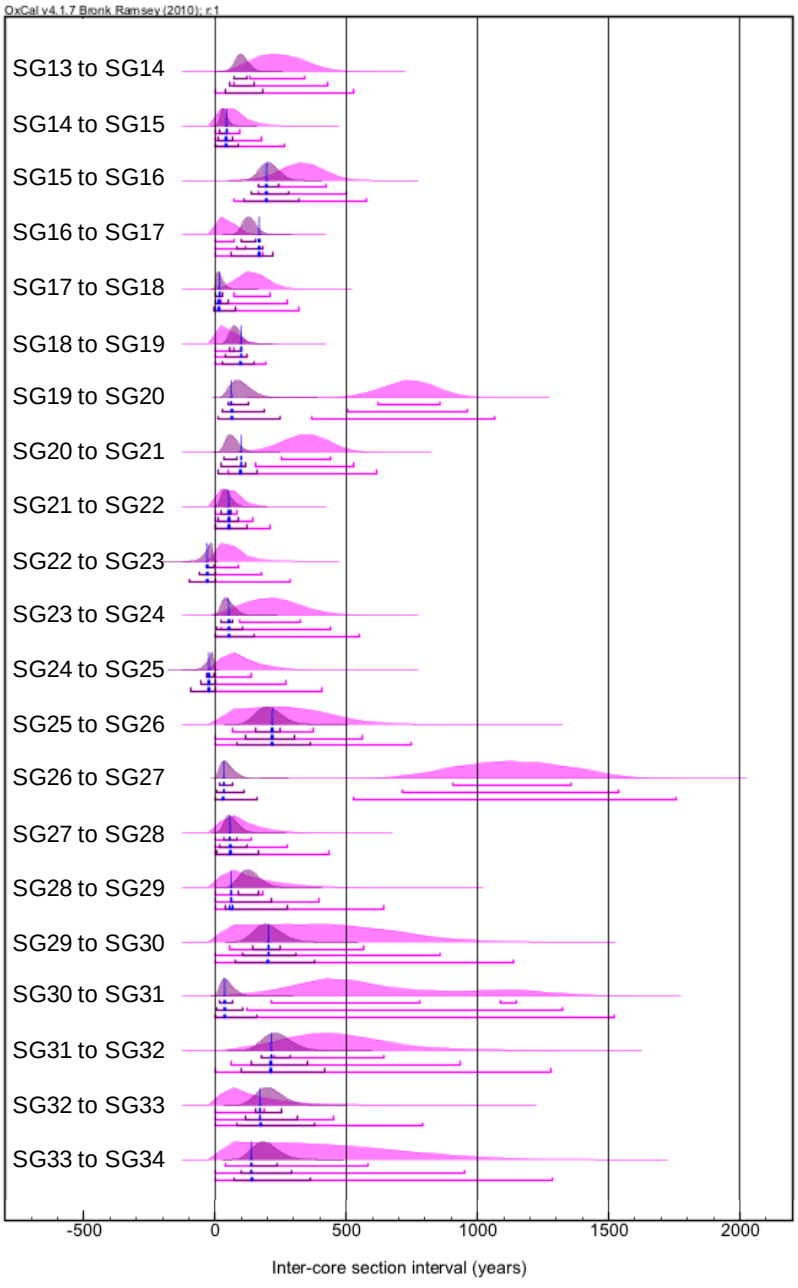

Figure 6.11: Comparison of the durations of SG93 core sections as determined by: (i) original SG93 varve counting (Kitagawa and van der Plicht 1998a, 1998b, 2000; red); (ii) statistical re-modelling (OCM-6.1) of the SG93 radiocarbon dataset against IntCal09 (Reimer *et al*. 2009; magenta); (iii) SG06 varve count, obtained through visual matching of archive SG93 core sections to the SG06 composite core profile (blue); (iv) re-modelling of the SG93 radiocarbon dataset against IntCal09, using equivalent SG06 event-free depth (EFD; purple). The 68.2% and 95.4% posterior probability ranges are shown.

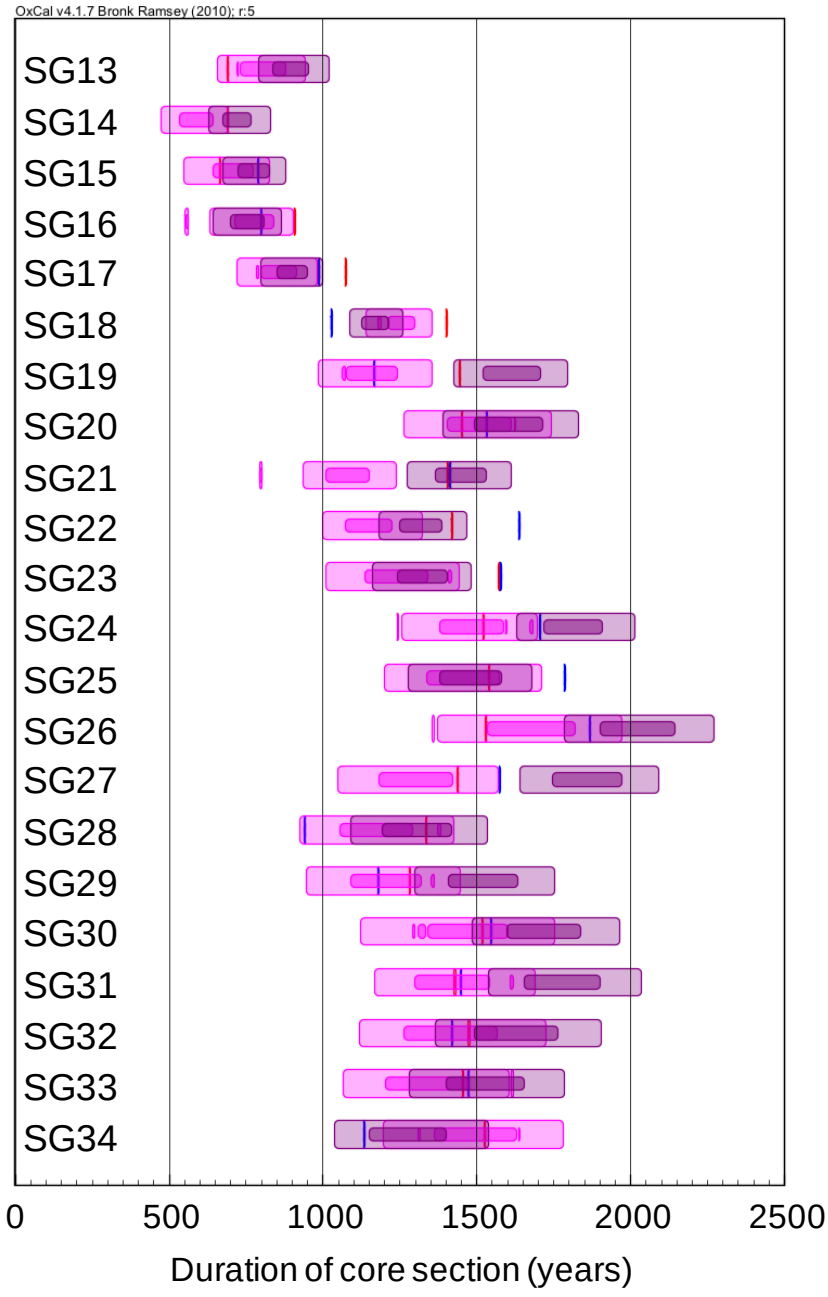

Taken in combination, tables 6.3 and 6.4 and figures 6.10 and 6.11 imply that OCM-6.1 is able to provide greater correspondence with IntCal09 by shortening individual core sections, which necessarily increases the duration of inter-core section age gaps. To avoid such an effect, the rigidity of the prior constraints to the durations of individual core sections could have been tightened (i.e. the arbitrary 10% σ value reduced, or the original varve-counted values taken as lacking uncertainty at all), but this would have limited the ability of the modelling exercise to assess any potential errors in the varve counting – one of the fundamental aims of the statistical exercise.

Such a modelling outcome might have been the result of unintended bias in the model prior of OCM-6.1, but further inspection of this model, using 'simulated' data (Bronk Ramsey 2009a; table 5.1), demonstrates this not to be the case. An alternative proposition is that OxCal is unable to find an optimal fit of the SG93 core sections to IntCal09 without shortening their durations in this way because of real disagreement between portions of the respective radiocarbon datasets. This suggestion will not be dwelt upon here, but will be returned to in chapter 8, having first introduced the ≈ 600 new radiocarbon determinations of the Suigetsu Varves 2006 project (in chapter 7), and compared the respective SG93 and SG06 datasets (section 7.6). Similarly, plotting of the SG93 data directly against SG06 varve age will be described in the following chapters.

6.2.5 Palaeoenvironmental Implications

Finally for the present chapter, the timing of the key palaeoclimatic events of the Late Glacial/Interglacial transition (LGIT) in Lake Suigetsu, as defined by Nakagawa *et al*. (2003; section 3.5.4), can be re-examined in light of the revised (OCM-6.2) chronology produced above. The onset of the Bølling-equivalent warming ('SGPI-1', as defined by Nakagawa *et al*. 2003) is shifted slightly younger, from ≈ 15,000 SG93 vyr BP to between 14,936 and

14,848 cal. BP (68.2% probability range). This is still earlier than suggested for the equivalent climatic event in North Atlantic records, however (14,692 b2k, 14,642 cal. BP in NGRIP, Rasmussen *et al*. 2006). Conversely, the cold reversal in Japan ('SGPS-1' *sensu* Nakagawa *et al*. 2003) is found to be slightly older (12,494 to 12,445 cal. BP, 68.2% probability range) than was previously suggested by the SG93 chronology (≈ 12,300 SG93 vyr BP), which is now much closer to-, though still younger than-, the ages suggested for the North Atlantic counterpart event, the Younger Dryas (12,896 b2k, 12,846 cal. BP in NGRIP, Rasmussen *et al*. 2006). Finally, the onset of the Holocene, as defined by SG93 pollen (Nakagawa *et al*. 2003) is also significantly older (11,592 to 11,496 cal. BP, 68.2% range) than was suggested for the original SG93 chronology (11,250 SG93 vyr BP), now roughly in line with the events of the circum North Atlantic (11,703 b2k, 11,653 cal. BP in NGRIP, Rasmussen et al. 2006).

Disappointing for such re-analysis, however, is the fact that these important climatic events fall in the core sections (SG15 to SG19) for which the physical matching was less reliable. Therefore no firm conclusions should be drawn from the suggested revised chronology presented here, despite the potentially significant implications that could be drawn from such data.

7. Radiocarbon Results from the Suigetsu Varves 2006 Project

Chapter 7 introduces the principal radiocarbon data obtained from the Suigetsu Varves 2006 project. The opening section, 7.1, commences with an introduction to the macrofossil samples picked from the SG06 sediment core. Section 7.2 then introduces the principal radiocarbon data obtained from these samples, describing specific aspects of these data, including: dating of 'background' samples; intra- and inter-laboratory sample duplication; choice of sample material; and choice of pre-treatment methodology. The following section, 7.3, introduces the preliminary SG06 varve count data, against which the Lake Suigetsu radiocarbon data described in this thesis are directly compared. Section 7.4 describes the principal Bayesian modelling exercise of the entire Suigetsu Varves 2006 project, describing the wiggle-match of the floating Suigetsu varve chronology to the absolutely-dated Intcal09 (Reimer *et al*. 2009) dendrochronological timescale. The subsequent section, 7.5, describes the protocol necessarily implemented to remove the most extreme statistically-outlying radiocarbon data. Finally, section 7.6 compares the revised Suigetsu '93 radiocarbon dataset (of the previous chapter) with that of the current project, and combines these respective datasets into a single, integrated 'Lake Suigetsu radiocarbon calibration dataset'. The following chapter, 8, then compares these calibration datasets with selected alternative radiocarbon calibration data (previously introduced in chapter 2), and discusses the potential implications of these comparisons.

7.1 Suigetsu Varves 2006 Macrofossil Samples

During the course of the Suigetsu Varves 2006 project, some 1,176 macrofossils were picked from the SG06 sediment core. A full description of these macrofossil samples is provided in appendix 10, whilst a visual archive of these samples is provided by the scanned

images of these samples within their storage vials, shown in appendix 11. For clarity, these 1,176 SG06 macrofossil samples are given a '#' prefix throughout this thesis, allowing differentiation from the individual radiocarbon determinations obtained from the samples selected for dating, which are given 'OxA-' and 'SUERC-' prefixes at the Oxford Radiocarbon Accelerator Unit (ORAU) and NERC Radiocarbon Facility-Environment (NRCF-E), East Kilbride, AMS laboratories, respectively.

Figure 7.1 demonstrates a selection of images of these SG06 macrofossil samples, exemplifying the different sample types present, and degree of differential sample preservation. Of the total 1,176 macrofossil samples, the vast majority (1,003) were terrestrial leaves – 831 of which were deciduous broad leaves (e.g. figures 7.1c, 7.1d, 7.1f and 7.1g), 96 were evergreen broad leaves (e.g. figure 7.1e) and 76 were conifer needles (e.g. figure 7.1h). Of the 212 'non-leaf' samples, 43 were bark fragments (e.g. figure 7.1a), 43 were small twig fragments (e.g. figure 7.1b), 34 were stem fragments, twelve were bud cases, and five were insect fragments. (N.b. 'leaves' plus 'non-leaves' is greater than the total number of sub-samples collected, 1,176, because certain samples incorporated two different sample types picked from the same sediment. Although plant macrofossils were not identified to species level, all dated samples – section 7.2 – were identified as being terrestrial. I.e. samples were not freshwater species, so would not have drawn their carbon from the lake water, and therefore would not suffer from lake reservoir effects – an important prerequisite for the 'wholly terrestrial' dataset being generated.)

Figure 7.1: A selection of images of the 1,176 SG06 macrofossil samples collected, demonstrating: **(a)**: #951 (a large, 'background age' bark sample); **(b)**: #1125 (a twig); **(c)**: #640 (a deciduous broad leaf); **(d)**: #1024 (a large deciduous broad leaf); **(e)**: #606 (an evergreen broad leaf); **(f)**: #398 (a fragile deciduous broad leaf vein network); **(g)**: #617 (a deciduous broad leaf); and **(h)**: #452 (a conifer needle).

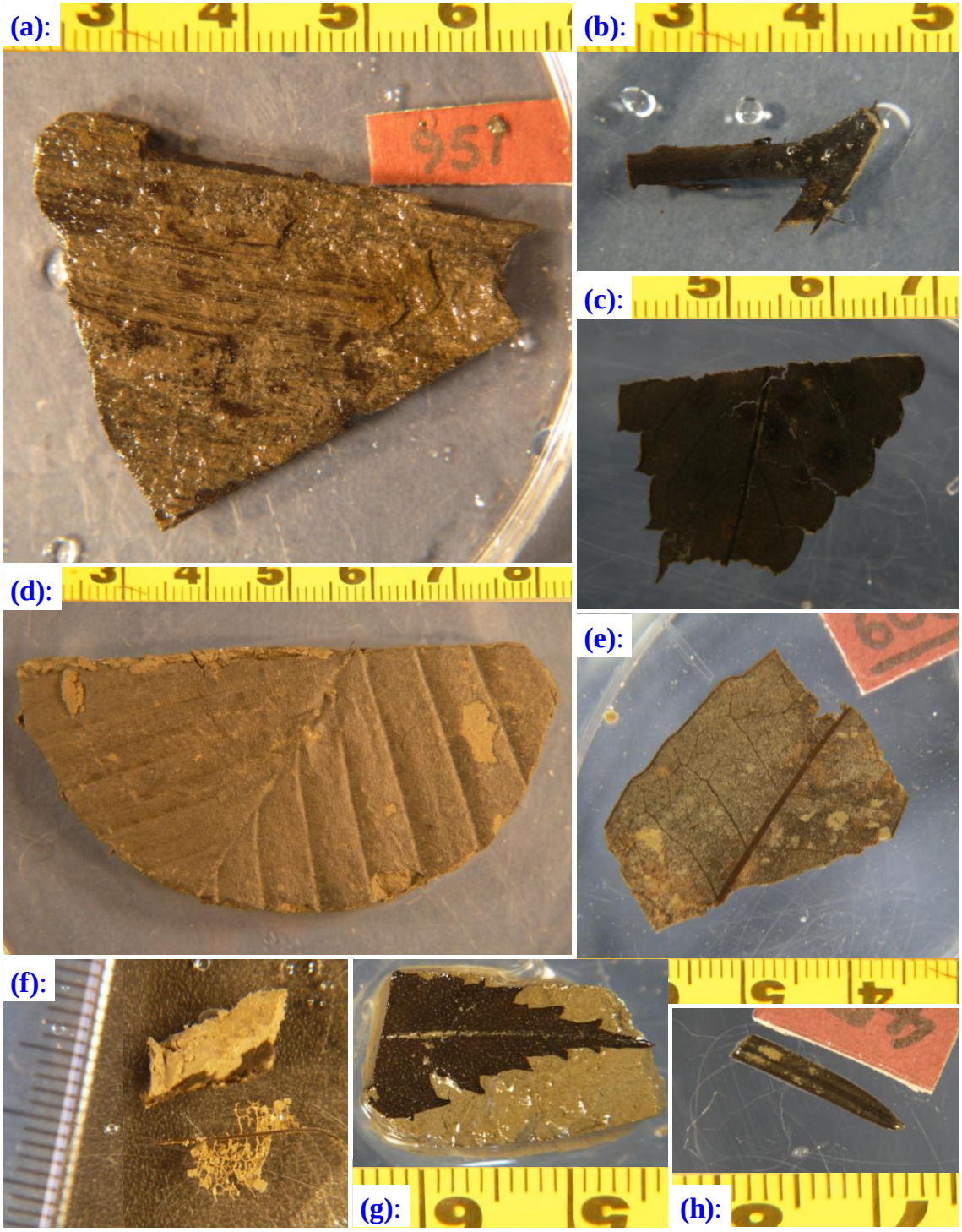

7.2 Suigetsu Varves 2006 Radiocarbon Determinations

In total, 647 radiocarbon determinations were obtained from SG06 sample material over the course of the Suigetsu Varves 2006 project – 361 from ORAU and 286 from NRCF-E. Of the ORAU measurements, 26 were of samples older than the radiocarbon detection limit (according to their stratigraphic position; section 7.2.1), eight were of sediment (rather than plant macrofossils; section 7.2.7), and eighteen were intra-laboratory 'auto-duplicates' (section 7.2.2). Of the NRCF-E measurements, ten were of samples beyond the radiocarbon detection limit (section 7.2.1), four were sediment samples (section 7.2.7), and three were intra-laboratory duplicates (section 7.2.2). To facilitate inter-laboratory comparability, 52 samples, spread across the radiocarbon dating range, were duplicated between the ORAU and NRCF-E laboratories (section 7.2.3). The remainder of section 7.2 describes these radiocarbon data in greater detail.

7.2.1 Background Subtraction

As described in chapter 4 (sections 4.3.1 and 4.5), the contribution of laboratory procedures to the background ^{14}C measurement of samples must be adequately defined to ensure both the precision and accuracy of radiocarbon determinations, especially towards the older end of the technique (Gillespie and Hedges 1984). To this end, specific macrofossil samples were picked from much lower down the SG06 sediment profile (from the Last Interglacial period, based upon palynological data; R. Payne, personal communication; i.e. well beyond the radiocarbon detection limit) to enable quantification of this laboratory contribution to background measurements. Both leaf (#976) and non-leaf (bark; #951; figure 7.1a) samples were used to assess these background determinations. These samples were selected for this purpose since they should be directly analogous to the overwhelming

majority of ‘non-background’ plant macrofossil samples contributing to the main SG06 radiocarbon dataset.

Additional, background peat material was also dated along with pilot samples of the project, but these data were deemed less directly comparable to the leaf and twig/bark samples comprising the majority of the SG06 calibration dataset. A second wood sample (#35) beyond the presumed detection limit was also dated along with pilot measurements, but, being chronologically much younger than the other material used for ‘background’ determination (i.e. only dating to *circa* 60,000 cal. BP), the data from this sample do not give such reliable background information. The radiocarbon determinations obtained from each of the five SG06 ‘background age’ samples are provided in tables 7.1 and 7.2 for the ORAU and NRCF-E laboratories, respectively. Additionally, these data can be compared to data from other background lab standards (as described in section 4.5) to further assess their reliability.

Figure 7.2 plots the raw (non-background-corrected) ^{14}C:^{13}C data of the ORAU sub-samples (given in table 7.1), compared with the mean ORAU laboratory combustion background (0.0007 ± 0.001 mg C) obtained from 136 measurements of directly-combusted nylon (i.e. background standards that have undergone combustion and graphitisation, but that have not undergone any pre-treatment chemistry; Wood *et al*. 2010). Through comparison of these data, it should be possible to establish the contribution of any additional ^{14}C introduced to the Suigetsu plant macrofossil samples through the sediment coring to chemical pre-treatment methodological stages (sections 4.1 to 4.3).

Table 7.1: The five SG06 plant macrofossil samples dated to determine background correction at ORAU. (Sample type 'Ev.br.leaf' is an evergreen broad leaf; 'SG06 CD' and 'SG06 EFD' refer to Suigetsu Varves 2006 composite depth and event-free depth, respectively; target types 'G', 'g' and 'vsg' refer to large-, small- and very small graphites, respectively; and 'C yield' is the mass of carbon combusted in the EA for each sub-sample; the 'VV' and 'UW' ORAU pre-treatment protocols are described in section 4.3, and the 'NRC' protocol in section 7.2.5. Conventional radiocarbon ages and $F^{14}C$ are already background-corrected, as compared to other background standards in the AMS wheel, whereas ^{14}C:^{13}C ratio reflects the uncorrected isotope ratios off the AMS, though normalised for NOX values.)

SG06 sample ID (#)	Sample type	SG06 CD (cm)	SG06 EFD (cm)	SG06 yr BP	Expected radiocarbon age (BP)	AMS target ID	ORAU pre-treatment protocol	Target type	C yield (mg)	Conventional radiocarbon date (± 1σ)	$F^{14}C$ (± 1σ)	$^{14}C/^{13}C$ e^{-10}	% error
35	Wood	4691.1	4528.8	-	Background	OxA-X-2213-20	WW	g	1.104	> 54,800	0.00043 ± 0.00033	0.001239	14.2
						OxA-X-2213-21	NRC	g	0.969	55,200 ± 2,900	0.00104 ± 0.00037	0.001953	9.6
						OxA-X-2215-50	WW	G	3.157	> 53,400	0.00000 ± 0.00065	0.002667	5.7
						OxA-X-2215-51	NRC	G	2.558	> 53,300	0.00000 ± 0.00065	0.002573	6.1
976	Ev.br.leaf	6444.2	6265.3	-	Background	OxA-X-2340-37	V V	g	2.000	> 60,300	0.00000 ± 0.00028	0.000084	266.9
						OxA-X-2340-38	V V	g	1.291	> 58,800	0.00000 ± 0.00033	0.000284	78.9
						OxA-X-2356-47	V V	G	2.925	> 57,700	0.00000 ± 0.00038	0.000011	1330.4
951	Bark	6591.7	6408.2	-	Background	OxA-X-2340-39	UW	g	1.229	> 58,500	0.00000 ± 0.00034	0.000473	49.5
						OxA-X-2345-16	V V	G	1.688	> 52,800	0.00011 ± 0.00065	0.000525	40.3
						OxA-X-2345-17	V V	g	1.148	> 50,600	0.00000 ± 0.00092	0.000063	306.8
						OxA-X-2345-18	V V	g	0.685	> 46,600	0.00000 ± 0.00152	0.000074	261.6
						OxA-X-2356-48	V V	G	2.702	> 57,300	0.00000 ± 0.00040	0.000011	1191.0
						OxA-X-2356-49	V V	G	2.203	> 55,700	0.00000 ± 0.00048	0.000011	1243.9
						OxA-X-2356-50	UW	G	2.340	> 56,200	0.00000 ± 0.00045	0.000011	1205.9
						OxA-X-2362-52	V V	vsg	1.714	> 44,300	0.00000 ± 0.00061	0.000011	1363.1

Table 7.1 (continued):

SG06 sample ID (#)	Sample type	SG06 CD (cm)	SG06 EFD (cm)	SG06 yr BP	Expected radiocarbon age (BP)	AMS target ID	ORAU pre-treatment protocol	Target type	C yield (mg)	Conventional radiocarbon date (± 1σ)	$F^{14}C$ (± 1σ)	$^{14}C/^{13}C$ e^{-10}	% error
B-43,05-22cm	Peat	6865.3	6602.9	-	Background	OxA-X-2203-40	NRC1	g	1.584	48,700 ± 1,000	0.00232 ± 0.00029	0.002856	7.3
						OxA-X-2203-41	UW	g	0.860	44,700 ± 900	0.00385 ± 0.00044	0.004841	5.1
						OxA-X-2204-50	NRC2	G	3.138	59,100 ± 2,300	0.00064 ± 0.00019	0.000924	16.8
						OxA-X-2204-51	WW	G	2.409	51,800 ± 1,100	0.00159 ± 0.00022	0.001953	9.3
						OxA-X-2207-39	WW	G	2.029	> 60,400	0.00011 ± 0.00022	0.000567	27.0
						OxA-X-2207-40	NRC1	G	2.118	> 62,300	0.00000 ± 0.00021	0.000399	38.9
						OxA-X-2207-41	NRC1	G	2.374	> 58,600	0.00026 ± 0.00021	0.000651	24.7
						OxA-X-2207-42	NRC	G	2.449	> 62,300	0.00002 ± 0.00020	0.000399	39.7
B43,50-70cm	Peat	6913.9	6650.1	-	Background	OxA-X-2203-42	NRC1	g	1.230	48,900 ± 1,200	0.00226 ± 0.00033	0.002961	7.2
						OxA-X-2203-43	UW	g	1.072	47,700 ± 1,100	0.00264 ± 0.00036	0.003444	6.4
						OxA-X-2204-52	NRC2	G	2.335	55,600 ± 1,700	0.00099 ± 0.00021	0.001376	11.7
						OxA-X-2204-53	WW	G	2.554	53,400 ± 1,300	0.00130 ± 0.00021	0.001649	10.3

Table 7.2: The four SG06 plant macrofossil samples dated to determine background correction at NRCF-E. (Sample type 'Ev.br.leaf' is an evergreen broad leaf; 'SG06 CD' and 'SG06 EFD' refer to Suigetsu Varves 2006 composite depth and event-free depth, respectively; target types 'g' and 'vsg' refer to regular (small)- and very small graphites, respectively; and 'C yield' is the mass of carbon combusted for each sub-sample. The 'uncorrected pMC', percent modern carbon, values presented have not been background-corrected – and hence the low uncertainty values – although they have been normalised to NOX values from the same AMS wheels.)

SG06 sample ID (#)	Sample type	SG06 CD (cm)	SG06 EFD (cm)	SG06 yr BP	Expected radiocarbon age (BP)	AMS target ID	Target type	C yield (mg)	Uncorrected pMC (± 1σ)
B43, 50-70 cm	Peat (humin fraction)	6913.9	6650.1	-	Background	SUERC-15705	g	10.446	0.310 ± 0.010
	Peat (raw material)					SUERC-15706	g	7.982	0.270 ± 0.010
	Peat (humic fraction)					SUERC-15707	g	3.214	0.340 ± 0.010
951	Bark (small sub-sample)	6591.7	6408.2	-	Background	SUERC-27525	g	0.964	0.199 ± 0.007
	Bark (medium sub-sample)					SUERC-27526	g	2.271	0.190 ± 0.005
	Bark (large sub-sample)					SUERC-27527	g	3.755	0.138 ± 0.005
976	Ev.br.leaf (small sub-sample)	6444.2	6265.3	-	Background	SUERC-27530	vsg	0.477	0.540 ± 0.011
	Ev.br.leaf (medium sub-sample)					SUERC-27531	g	1.661	0.146 ± 0.005
	Ev.br.leaf (large sub-sample)					SUERC-27532	g	2.775	0.176 ± 0.006
35	Wood fragment	4691.1	4528.8	-	Background	SUERC-13331	g	1.500	0.520 ± 0.010

Figure 7.2: **(a)** The five 'background age' Suigetsu samples dated at ORAU in the present project, as compared to the published ORAU combustion background nylon standard values (0.0007 ± 0.001 mg; Wood *et al.* 2010). Suigetsu samples are plotted with 'raw' (non-background-corrected) ^{14}C:^{13}C ratio (± 1σ uncertainty): #35 (wood) plotted in gold; #976 (evergreen broad leaf) in green; #951 (bark) in light blue; and peat samples from core section B-43, depths 0 to 22 cm and 50 to 70 cm, plotted in purple and red, respectively. The ORAU nylon background is shown in mauve (solid line for the mean, and hashed line for ± 1σ values); **(b)** identical plot to figure 7.2a, but zoomed in to show samples #951 and #976 only.

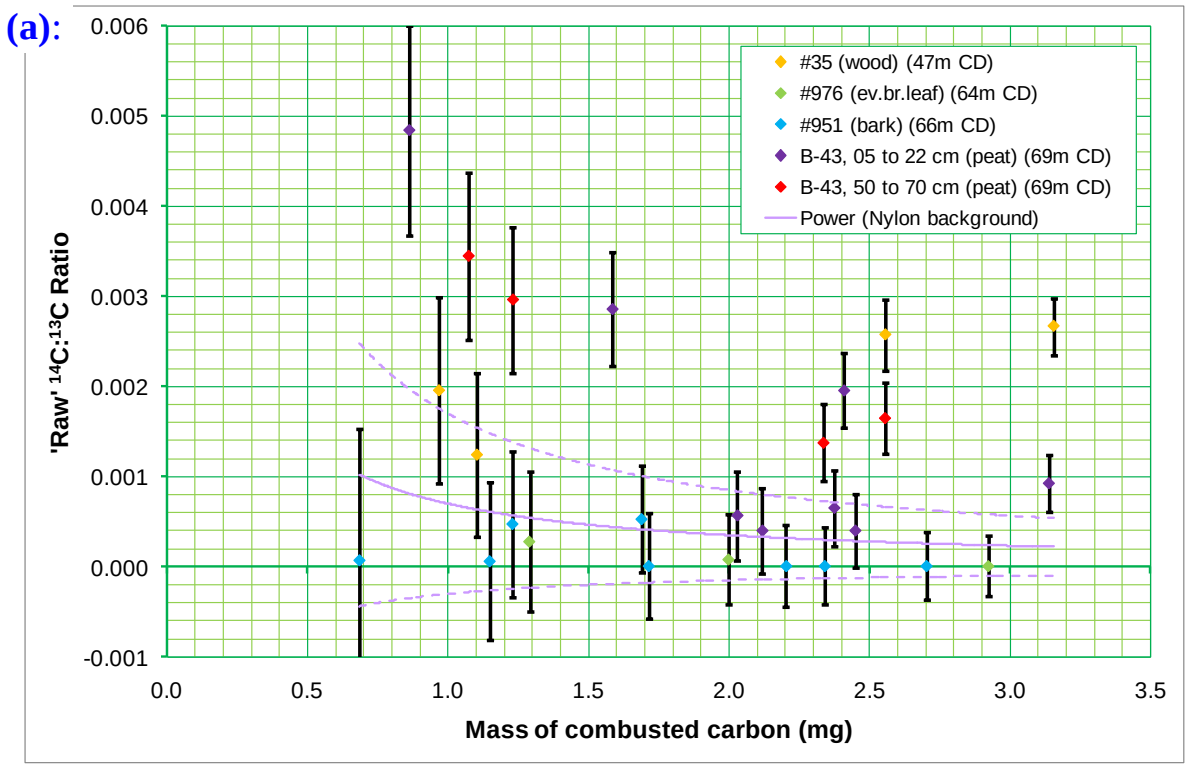

Figure 7.2 (continued):

(b):

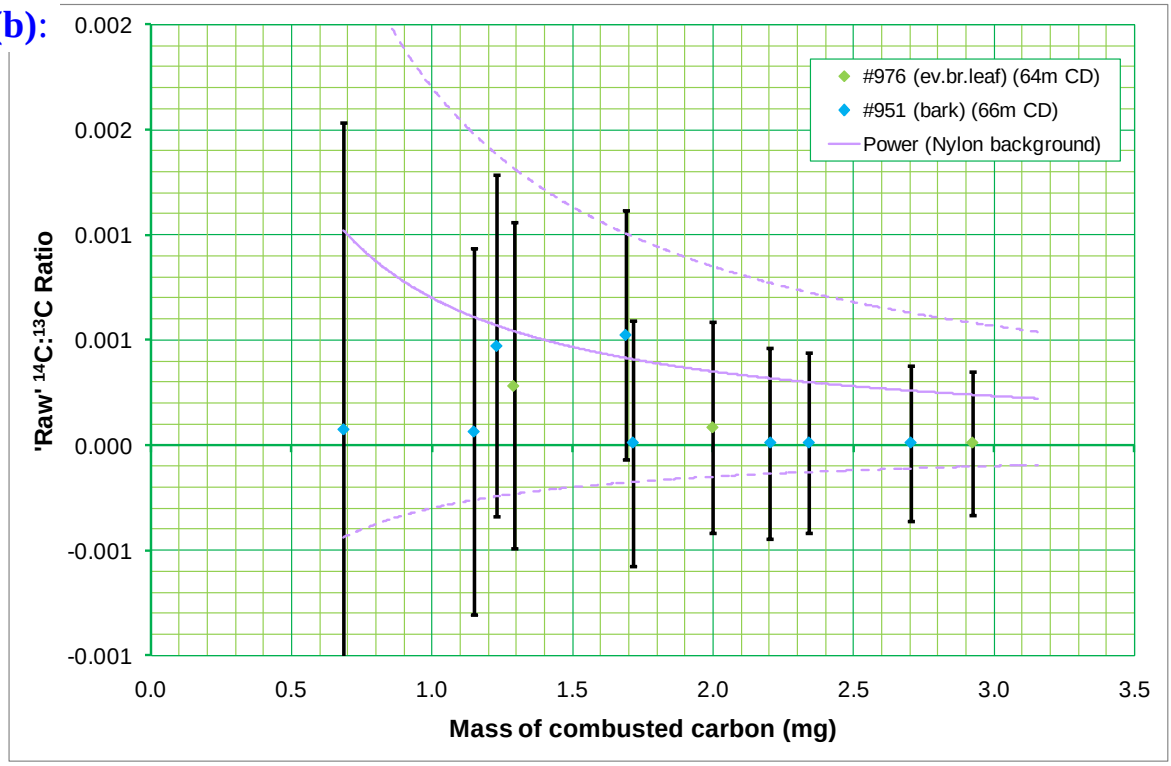

It can be seen that for the two most analogous SG06 background age samples (the bark sample, #951, and the evergreen broad leaf, #976; figure 7.2b), the contribution of modern ^{14}C contamination is not distinguishable from the nylon combustion background value. (If anything, these Suigetsu samples demonstrate lower contamination than the mean nylon value, but this is probably the result of the smaller subset of Suigetsu data, and the fewer AMS wheels represented by the Suigetsu data, which may have been operating more efficiently/stably for the few wheels including these Suigetsu samples, compared with the long-term average.)

In contrast, the two peat samples from the base of the core (SG06 core section B-43, depths 0 to 22 cm and 50 to 70 cm) demonstrate slightly greater ^{14}C:^{13}C ratios than the nylon standard, suggesting a modern contaminant at some stage through the field and laboratory processes (figure 7.2a). Since the bark and leaf samples (#951 and #976, above) underwent

essentially the same procedures throughout these stages (albeit with slightly differing chemical pre-treatment protocols), it is hypothesised that the younger ages for the background peat sub-samples are the result of modern carbon adsorbed on to the much larger surface area.

The data from the wood sample (#35) are also slightly 'younger' than for samples #951 and #976. Although this sample also provides analogous material to the remainder of the SG06 bark (and twig) samples, sample #35 is taken from ≈ 47 m composite depth (compared to the lowest alternative macrofossil dated from the current project at ≈ 42 m composite depth) and, although demonstrating only minute (statistically-indistinguishable from zero) quantities of remaining ^{14}C, might still contain sufficient remaining ^{14}C to influence this measurement. (Indeed, theoretically, there could be a real $\Delta^{14}C$ peak during this time period, although such a possibility is not pursued further in this thesis.) For comparison, samples #951 and #976 are from ≈ 66 and 64 m composite depth, respectively, markedly older (representing the Last Interglacial period) than sample #35 and, therefore, certainly 'dead' in terms of their ^{14}C values .

Figure 7.3 illustrates the data obtained from the five SG06 background samples at the NRCF-E laboratory (given in table 7.2). As with the ORAU data, the NRCF-E results suggest that the peat sub-samples experience additional laboratory ^{14}C contamination (more apparent here than for the ORAU samples, because a non-pre-treated peat sub-sample, SUERC-15706, actually gave a measurement slightly older than either of the pre-treated fractions, SUERC-15705 or 15707). The wood sample (#35), similarly gives a younger date than the determinations from the Last Interglacial samples, #951 and #976.

Figure 7.3: The four SG06 plant macrofossil samples dated to determine background correction at NRCF-E. The Suigetsu samples are plotted with their 'raw' (non-background-corrected) percent modern carbon (pMC) values (± 1σ uncertainty): #35 (wood) plotted in gold; #976 (evergreen broad leaf) in green; #951 (bark) in light blue; and peat samples from core section B-43, depths 50 to 70 cm, plotted in red. The applied NRCF-E background correction (f = 0.0015 ± 0.0006) is additionally shown in mauve (solid line for the mean, and hashed line for ± 1σ values).

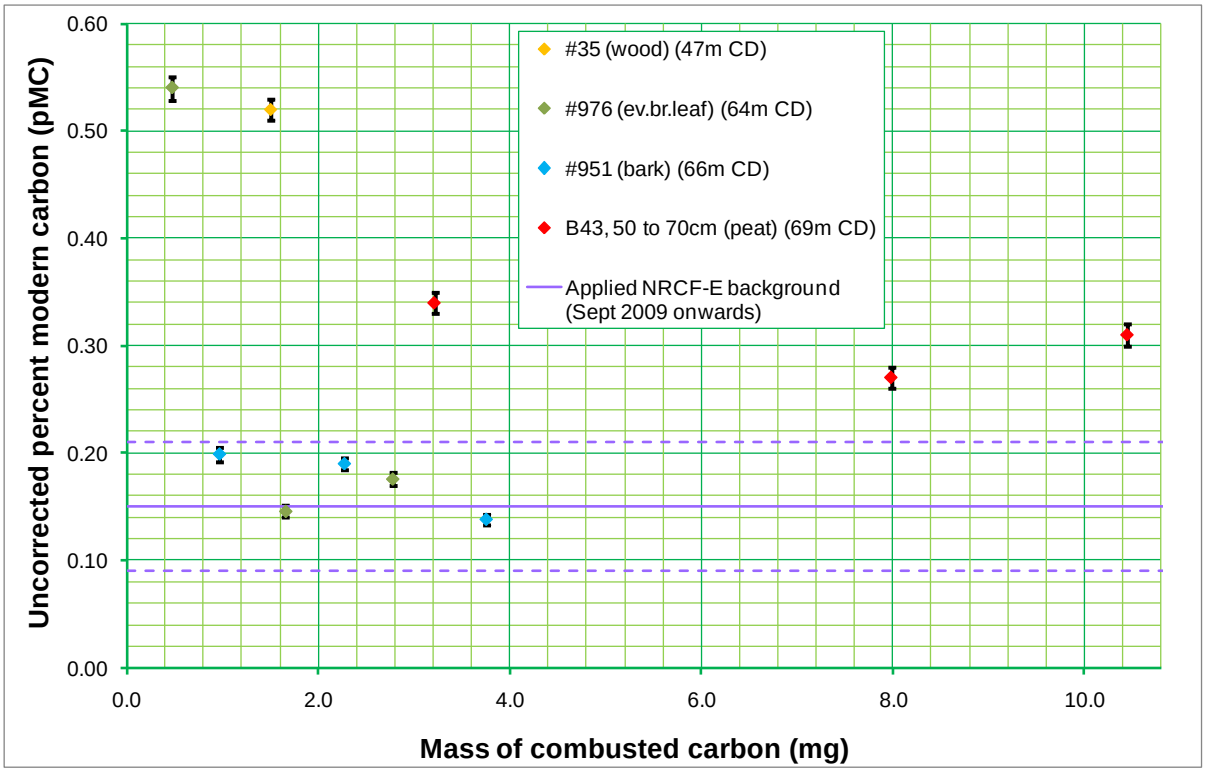

An initial background correction of f = 0.0015 ± 0.0006 was applied to the remainder of the NRCF-E SG06 macrofossil samples (from 1st September 2009 onwards), as generated from the 20 background age samples, which comprised fifteen bituminous coal sub-samples and five of the six 'deep' SG06 macrofossils (i.e. three measurements from #951 and two from #976, therefore excluding one determination from #976 that was < 0.5 mg C), obtained across all of the AMS wheels that included SG06 samples. Arguably, the mean value of only

the five Suigetsu determinations could have been applied (i.e. f = 0.0017 ± 0.0003), since this represents the contribution to background of the entirety of the lab process. However, the five contributing sub-samples were all pre-treated in the same chemistry batch, and measured on the same AMS wheel and therefore may not adequately describe the longer-term (between batch/wheel) variation of measurement through the NRCF-E laboratory. Since the mean value of these SG06 determinations is not statistically different from the bituminous coal lab standard, the incorporation of these additional fifteen data points provides a larger data cohort to provide a more realistic estimate of the expected uncertainty on the background measurement.

There is therefore a difference between the ORAU and NRCF-E laboratories in the initial generation of the background correction applied to the remainder of the SG06 plant macrofossil samples. The regular ORAU background corrections were applied (as generated from on-going AMS measurements from regular lab standards); whereas the NRCF-E lab implemented a specific background correction based upon only the background standards (SG06 and bituminous coal) that were measured on specific SG06 AMS wheels. This latter approach is the standard lab protocol for samples from similar, large-scale research projects going through the NRCF-E lab. Therefore, as with the non-inter-laboratory synchronisation of lab pre-treatment protocols (section 4.3), no alteration to regular laboratory protocol was adopted specifically for background-correction of the SG06 macrofossil samples. Since the radiocarbon determinations of these background SG06 samples (#951 and #976) do not demonstrate any marked deviation from alternative (nylon/bituminous coal) background standards through chemical pre-treatment and sample handling, the choices made as to the statistical treatment of these background measurements, in practice, make very little difference.

Examination of the final SG06 radiocarbon dataset (initially background-corrected as described above; appendix 12), however, suggested that there was a trend for the smallest samples (in terms of the mass of combusted carbon) to be outlying, and that the majority of outlying samples were to younger radiocarbon ages. Such an observation suggests sample size-related offsets that might need further correction. Independent statistical interrogation of each of the contributing laboratories' datasets revealed that an additional correction for 1.6 ± 0.8 μg of modern carbon contamination was needed to maximise the internal consistency of both datasets, whilst there was no evidence of any 'old' carbon contamination. A more detailed description of this second stage of the background correction is described in appendix 13.

The fact that the necessary correction for both ORAU and NRCF-E labs came out to be identical, adds credence to the empirically-derived values. It also provides insight into the likely causes of the contamination, suggesting addition of carbon prior to the pre-treatment stage, i.e. either in field sampling (during the core extraction, splitting and logging processes), or in sub-sampling from the core. The relative constancy of the observed background suggests that the input of particulate contaminant is less likely (although this might explain the several more severe outliers, described in section 7.5, below), but, rather, is atmosphere- or process-derived. The possibility of modern carbon addition from the growth of micro-organisms during sample storage (described in section 4.3.2; Wohlfarth *et al*. 1998) is not discounted.

The need for a second stage of background correction implies that the corrections originally-derived (from the SG06 background samples #951 and #976) were insufficient. It is therefore postulated that these samples, being relatively sturdier than the majority of the SG06 macrofossil samples (evident in the very large size of the bark sample, #951, and the fact that the smaller evergreen leaf sample, #976, could nevertheless be split into six separate

sub-samples for dating) were, conversely to the aforesaid statements, not wholly representative of the remainder of the SG06 macrofossils in terms of their susceptibility to modern carbon contamination. Whereas any contaminant would be easily removed from these robust samples, it might be more difficult to remove surface contaminant from the more fragile macrofossil samples by the physical cleaning applied prior to chemical pre-treatment. The pre-treatment itself would not necessarily remove such contamination if the carbon was organically-derived (from pollen or micro-organism growth) and physically integrated within the delicate macrofossil surfaces.

The application of the secondary correction greatly reduced the number of statistical outliers in the final dataset (section 7.5, below), and is applied prior to all of the radiocarbon data hereafter described.

7.2.2 Internal Reproducibility

Over the course of the project, eighteen plant macrofossil samples from SG06 were auto-duplicated at ORAU (section 4.5). These internal duplicates were in very good statistical agreement (table 7.3), with only a single sample (#307) not being acceptable as 'coeval' (producing a test statistic, T, exceeding the 5% probability threshold according to the χ^2 distribution). Curiously, this sample is actually the youngest of those duplicated at ORAU. Whilst it is usually expected that older (or smaller) samples are more problematic to date (because of the increased susceptibility of such samples to the effects of modern contamination; section 4.3.1), this is clearly not the case for sample #307. Whilst this sample was the earliest to be auto-duplicated (being part of the project's pilot results), this does not explain the anomalous result, since the laboratory procedures undertaken were no different from those regularly performed at ORAU with other such samples submitted to the lab. There are also no clues from other sources (e.g. questionable results from other samples/standards

in the same pre-treatment chemistry batch or AMS wheel). Since both dates cannot both represent a single radiocarbon age (the 'true' radiocarbon age) of the sample (due to their high T value), one (or both) of the radiocarbon determinations should be discarded for subsequent interpretation (section 7.5).

Statistically, one duplicate pair out of eighteen being non-coeval is what one would expect at the 2σ (95.4%) significance level, so the single discordant SG06 sample here does not indicate unexpectedly problematic data.

Unlike at ORAU, NRCF-E does not implement the intra-laboratory quality assurance protocol of auto-duplicating samples, instead just using known-age tree-ring material and other lab standards for this purpose. Therefore, only three depths from the SG06 sediment profile provided duplicated radiocarbon determinations from the NRCF-E lab (table 7.4). These samples were duplicated since their initial measurements (produced early on in the project's progress) appeared erroneously young (as compared to initial age-depth models built from the results obtained up to that time; section 5.4.2). The uppermost duplicated sampling horizon (SG06 samples #197 and #969, SG06 core depth 2190.6 cm CD) yielded data that were statistically coeval (albeit, only just – based upon the T value calculated), but only once the revised background correction (outlined in section 7.2.1, above) had been applied. The remaining two duplicated samples were found not to be in statistical agreement with each other, demonstrating that the initial data (AMS targets SUERC-17723, and 28910) were rightly questioned, and that the problem with these radiocarbon determinations lay in laboratory error (most probably incorporation of modern contamination at some stage during the dating process), rather than in the sample material (or core stratigraphy) itself.

Table 7.3: The eighteen SG06 plant macrofossil samples 'auto-duplicated' at ORAU. (Sample types 'Ev.br.leaf' and 'Dec.br.leaf' are evergreen- and deciduous broad leaves, respectively; 'SG06 CD' and 'SG06 EFD' refer to Suigetsu Varves 2006- composite depth and event-free depth, respectively; the 'VV' and 'UW' ORAU pre-treatment protocols are described in section 4.3; target types 'G' and 'g' refer to large- and small graphite AMS targets, respectively; and 'C yield' is the mass of carbon combusted in the EA for each sub-sample. The 'test statistic, T' is compared to the 5% probability of the χ^2 distribution, to assess whether the duplicate dates are- or are not statistically consistent with a single, coeval date.)

SG06 sample ID (#)	Sample type	SG06 CD (cm)	SG06 EFD (cm)	SG06 yr BP	Expected radiocarbon age (BP)	AMS target ID	ORAU pre-treatment protocol	Target type	C yield (mg)	Conventional radiocarbon date (± 1σ)	Weighted mean, $\bar{Y}$ (± $\bar{S}$)	Test statistic, T	Coeval at 5%?
307	Ev.br.leaf	108.4	107.9	371	444	OxA-24231	V V	G	3.000	505 ± 23	613 ± 17	45.814	no
						OxA-X-2248-48	V V	G	1.868	730 ± 24			
316	Ev.br.leaf	369.0	361.0	2,208	2,228	OxA-24243	V V	G	2.375	2,109 ± 27	2,116 ± 19	0.134	yes
						OxA-24244	V V	G	2.279	2,123 ± 27			
22	Ev.br.leaf (*Castanopsis*?)	413.9	405.9	2,581	2,501	OxA-24235	V V	G	2.887	2,426 ± 25	2,456 ± 18	3.051	yes
						OxA-24236	V V	G	2.896	2,489 ± 26			
319	Ev.br.leaf	439.9	430.9	2,794	2,697	OxA-X-2297-56	V V	G	2.120	2,493 ± 25	2,490 ± 18	0.027	yes
						OxA-X-2303-36	V V	g	0.875	2,487 ± 27			
4	Ev.br.leaf	635.2	623.7	4,357	3,930	OxA-24277	V V	G	2.811	3,895 ± 29	3,909 ± 21	0.450	yes
						OxA-24278	V V	G	2.900	3,923 ± 30			
381	Dec.br.leaf	1043.6	1024.3	8,051	7,266	OxA-24267	V V	G	2.634	7,284 ± 37	7,277 ± 27	0.080	yes
						OxA-24268	V V	G	3.133	7,269 ± 38			
1146	Dec.br.leaf	1400.9	1369.7	11,279	9,847	OxA-24446	V V	g	0.972	9,884 ± 50	9,878 ± 35	0.029	yes
						OxA-24447	V V	g	1.040	9,872 ± 49			

Table 7.3 (continued):

SG06 sample ID (#)	Sample type	SG06 CD (cm)	SG06 EFD (cm)	SG06 yr BP	Expected radiocarbon age (BP)	AMS target ID	ORAU pre-treatment protocol	Target type	C yield (mg)	Conventional radiocarbon date (± 1σ)	Weighted mean, $\bar{Y}$ (± $\bar{S}$)	Test statistic, T	Coeval at 5%?
1149	Dec.br.leaf	1451.6	1418.2	11,762	10,123	OxA-24448	V V	g	0.885	10,034 ± 50	10,045 ± 35	0.099	yes
						OxA-24449	V V	g	0.947	10,056 ± 49			
549	Twig	1714.0	1672.9	14,721	12,419	OxA-24323	V V	G	2.445	12,415 ± 50	12,454 ± 35	1.217	yes
						OxA-24324	V V	G	1.920	12,493 ± 50			
822	Dec.br.leaf	1999.4	1949.6	19,582	16,722	OxA-24311	V V	g	1.256	16,685 ± 74	16,624 ± 51	1.302	yes
						OxA-24312	V V	g	1.444	16,568 ± 71			
575	Dec.br.leaf	2058.3	2005.4	20,660	17,631	OxA-24303	V V	g	1.474	17,630 ± 80	17,553 ± 53	1.641	yes
						OxA-24368	V V	G	2.180	17,493 ± 71			
993	Bark (& some leaf material)	2477.9	2406.4	28,248	24,158	OxA-24422	V V	G	2.944	23,938 ± 169	23,928 ± 95	0.005	yes
						OxA-24423	V V	G	2.764	23,923 ± 115			
1024	Dec.br.leaf	2845.5	2726.3	33,285	30,562	OxA-24394	V V	g	0.902	29,697 ± 469	29,835 ± 244	0.120	yes
						OxA-24429	V V	G	1.610	29,887 ± 286			
903	Dec.br.leaf	2852.1	2732.9	33,369	30,279	OxA-24376	V V	g	1.024	31,056 ± 491	31,233 ± 346	0.257	yes
						OxA-24377	V V	g	1.085	31,407 ± 488			
912	Dec.br.leaf	2931.4	2812.2	34,765	32,123	OxA-24349	V V	g	1.018	33,072 ± 622	33,115 ± 417	0.009	yes
						OxA-24350	V V	g	1.162	33,150 ± 563			
887	Dec.br.leaf	3159.3	3027.4	38,352	35,676	OxA-24341	V V	g	0.814	34,158 ± 619	34,514 ± 457	0.726	yes
						OxA-24342	V V	g	0.828	34,940 ± 678			
1135a	Moss	3360.9	3226.8	41,616	38,475	OxA-24452	V V	g	1.168	36,349 ± 845	36,251 ± 613	0.028	yes
						OxA-24453	V V	g	1.000	36,142 ± 891			
746	Bark	3562.5	3423.4	44,838	42,516	OxA-24362	UW	g	0.999	39,455 ± 1,295	40,781 ± 1,039	2.947	yes
						OxA-24363	UW	g	1.145	43,181 ± 1,742			

Table 7.4: The three SG06 plant macrofossil samples duplicated at NRCF-E. (Sample type 'Dec.br.leaf' refers to deciduous broad leaves; 'SG06 CD' and 'SG06 EFD' refer to Suigetsu Varves 2006- composite depth and event-free depth, respectively; target types 'g' and 'vsg' refer to normal- and very small graphite AMS targets, respectively; and 'C yield' is the mass of carbon combusted in the EA for each sub-sample. The 'test statistic, T' is compared to the 5% probability of the χ^2 distribution, to assess whether the duplicate dates are- or are not statistically consistent with a single, coeval date.)

SG06 sample ID (#)	Sample type	SG06 CD (cm)	SG06 EFD (cm)	SG06 yr BP	Expected radiocarbon age (BP)	AMS target ID	Target type	C yield (mg)	Conventional radiocarbon date (± 1σ)	Weighted mean, $\overline{Y}$ (± $\overline{S}$)	Test statistic, T	Coeval at 5%?
197 969	Dec.br.leaf	2190.6	2132.8	23,055	19,762	SUERC-13333 SUERC-27788	g g	0.589 0.632	19,137 ± 123 19,481 ± 130	19,299 ± 89	3.695	yes
217 1000	Dec.br.leaf	2488.9	2417.5	28,425	24,315	SUERC-17723 SUERC-28910	g g	1.125 0.509	21,743 ± 165 23,912 ± 260	22,366 ± 139	49.613	no
247 743	Dec.br.leaf	3174.3	3042.5	38,604	35,161	SUERC-16527 SUERC-28890	vsg g	0.434 0.787	32,838 ± 885 35,660 ± 772	34,441 ± 582	5.774	no

7.2.3 Inter-Laboratory Reproducibility

Fifty two plant macrofossil samples were dated in duplicate between the ORAU and NRCF-E laboratories (table 7.5). This reflects exactly 10% duplication from the 518 dated horizons from SG06 (section 7.2.4, below), which is in line with the duplication proportion initially aimed for (DPhil objective iv). The stratigraphic distribution of these inter-laboratory duplicates is not as regular as would be preferable, however, with occasional, sizable intervals (most notably the 4.01 m gap between adjacent duplicate samples at 1652.7 cm and 2053.4 cm composite depth). This is a result of the limiting nature of the small sample size of the majority of SG06 macrofossils.

Of the total 52 duplicates, 43 are statistically consistent with representing a single radiocarbon age, whereas nine duplicates are not statistically coeval. There is a tendency for these non-consistent duplicates (six out of the nine) to be from older samples (> 30,000 BP), perhaps demonstrating the increased susceptibility of these older samples to modern ^{14}C contamination.

As with the intra-laboratory duplicates, either one or more of the individual radiocarbon determinations of the non-consistent inter-laboratory duplicates must be erroneous, and therefore excluded from further analysis (section 7.5). As in the previous section, certain sub-samples of these non-consistent duplicates can be identified as being more likely to be inaccurate. AMS targets SUERC-28906 (SG06 sample #847) and SUERC-19064 (#246) are of low carbon yield (0.520 and 0.482 mg C, respectively), and appear anomalously young compared to the alternative, duplicate ORAU targets (as well as the interpolated, 'expected', conventional radiocarbon age based upon the adjacent four samples in terms of their stratigraphic position; see section 7.5, below, for an explanation of how this 'expected age' was derived). It is therefore proposed that these targets contain more

significant contributions of modern carbon from the laboratory pre-treatment process than was derived as representing the standard laboratory background (section 7.2.1, above).

The discordance of targets OxA-X-2219-17, SUERC-13333, and SUERC-27788 (#197 and #969, both from SG06 composite depth 2190.6 cm), is also attributed to their being composed of relatively low carbon yields (between 0.480 and 0.632 mg C), with the younger than 'expected' NRCF-E targets again being ascribed to small quantities of modern contamination, and the slightly older than 'expected' ORAU sample perhaps being the result of an over-background correction.

Of the four AMS targets representing #1135 (3360.9 cm CD), the NRCF-E target (SUERC-29853) is clearly older than the three alternative ORAU targets, suggesting that this target is, for some reason, over-background-corrected. However, it is the NRCF-E target that is in better agreement with the 'expected age' (generated through interpolation of the adjacent four dated SG06 depth horizons; section 7.5), which complicates this interpretation. The three ORAU targets came from three separately-treated samples that underwent chemical pre-treatment at the same time, but there is no indication from the accompanying lab standards (section 4.5) that there were any problems with this chemistry batch. The AMS data were also produced on two separate AMS wheels (reducing the probability of an AMS-related issue), and the AMS standards also showed no apparent problem.

Of the remaining five non-coeval duplicates (#780, #1007, #747, #291, or #939), there is no similar *a priori* indication of the likely outliers, without performing more detailed comparison with the expected ages of these samples based upon their stratigraphic position in relation to the broader corpus of the SG06 radiocarbon data. Such evaluation (section 7.5, below) suggests that of these targets SUERC-28203 (#780), OxA-X-2357-20 (#1007), OxA-X-2360-43 (#747), SUERC-13334 (#291), and OxA-X-2360-48 (#939) are the more likely to be erroneous – all of which produced dates younger than expected.

Table 7.5: The 52 SG06 plant macrofossil samples duplicated between the ORAU and NRCF-E laboratories. (Sample types 'Ev.br.leaf' and 'Dec.br.leaf' are evergreen- and deciduous broad leaves, respectively; 'SG06 CD' and 'SG06 EFD' refer to Suigetsu Varves 2006- composite depth and event-free depth, respectively; the 'VV' and 'UW' ORAU pre-treatment protocols are described in section 4.3; target types 'G', 'g' and 'vsg' refer to large-, small- and very small graphite AMS targets, respectively; and 'C yield' is the mass of carbon combusted in the EA for each sub-sample. The 'test statistic, T' is compared to the 5% probability of the χ^2 distribution, to assess whether the duplicate dates are- or are not statistically consistent with a single, coeval date.)

SG06 sample ID (#)	Sample type	SG06 CD (cm)	SG06 EFD (cm)	SG06 yr BP	Expected radiocarbon age (BP)	AMS target ID	ORAU pre-treatment protocol	Target type	C yield (mg)	Conventional radiocarbon date (± 1σ)	Weighted mean, $\bar{Y}$ (± $\bar{S}$)	Test statistic, T	Coeval at 5%?
696	Ev.br.leaf	42.0	42.0	60	76	OxA-24328	V V	g	1.028	96 ± 27	110 ± 22	0.763	yes
						SUERC-26724	-	g	1.157	136 ± 37			
556	Ev.br.leaf	307.2	299.7	1,704	1,832	OxA-24379	V V	G	2.684	1,744 ± 24	1,754 ± 20	0.534	yes
						SUERC-26728	-	g	3.246	1,775 ± 35			
317	Ev.br.leaf	406.3	398.3	2,514	2,408	OxA-24183	V V	G	3.409	2,483 ± 28	2,472 ± 22	0.363	yes
						SUERC-13335	-	g	2.732	2,456 ± 35			
22	Ev.br.leaf (*Castanopsis*?)	413.9	405.9	2,581	2,501	OxA-24235	V V	G	2.887	2,426 ± 25	2,464 ± 16	4.129	yes
21						OxA-24236	V V	G	2.896	2,489 ± 26			
						SUERC-20472	-	g	4.393	2,499 ± 37			
2	Ev.br.leaf	631.6	620.1	4,327	3,893	OxA-24237	V V	G	2.103	3,906 ± 31	3,938 ± 23	2.559	yes
3						SUERC-23353	-	g	3.262	3,982 ± 36			
780	Ev.br.leaf	773.0	759.0	5,441	4,787	OxA-24351	V V	g	1.045	4,848 ± 35	4,737 ± 25	20.298	no
						SUERC-28203	-	g	2.030	4,625 ± 35			

Table 7.5 (continued):

SG06 sample ID (#)	Sample type	SG06 CD (cm)	SG06 EFD (cm)	SG06 yr BP	Expected radiocarbon age (BP)	AMS target ID	ORAU pre-treatment protocol	Target type	C yield (mg)	Conventional radiocarbon date (± 1σ)	Weighted mean, $\bar{Y}$ ($\pm \bar{S}$)	Test statistic, T	Coeval at 5%?
39	Ev.br.leaf	876.9	862.9	6,348	5,510	OxA-24181 OxA-24182 SUERC-13332	V V NRC -	G G g	3.161 3.067 6.268	5,500 ± 34 5,458 ± 35 5,465 ± 35	5,475 ± 20	0.858	yes
433	Dec.br.leaf	990.3	972.5	7,506	6,590	OxA-24419 SUERC-28207	V V -	G g	1.713 1.045	6,630 ± 34 6,715 ± 47	6,659 ± 28	2.147	yes
629	Ev.br.leaf	1097.9	1075.6	8,541	7,756	OxA-24424 SUERC-28229	V V -	G g	2.409 2.662	7,739 ± 41 7,781 ± 38	7,762 ± 28	0.564	yes
877 444	Dec.br.leaf	1198.0	1175.7	9,462	8,519	OxA-24420 SUERC-26366	V V -	G g	1.951 1.087	8,439 ± 38 8,422 ± 40	8,431 ± 28	0.095	yes
847	Dec.br.leaf	1259.6	1236.8	9,956	8,947	OxA-24440 SUERC-28906	V V -	g g	0.780 0.520	8,870 ± 47 8,730 ± 45	8,797 ± 33	4.629	no
1121 92	Twig	1383.1	1352.0	11,091	9,650	OxA-24431 OxA-24432 SUERC-20490	V V UW -	G G g	1.867 1.673 3.696	9,672 ± 40 9,678 ± 39 9,642 ± 42	9,665 ± 23	0.442	yes
99 1158	Dec.br.leaf	1420.7	1389.5	11,490	10,036	OxA-24200 SUERC-29521	V V -	g g	0.612 1.414	10,080 ± 55 10,094 ± 41	10,089 ± 33	0.042	yes
105 1155	Dec.br.leaf	1444.2	1410.8	11,689	10,055	OxA-24292 SUERC-29831	V V -	g g	0.834 1.329	9,992 ± 64 10,112 ± 40	10,078 ± 34	2.528	yes
136	Dec.br.leaf	1508.4	1474.3	12,355	10,420	OxA-24223 SUERC-20502	V V -	G g	2.337 1.393	10,494 ± 44 10,446 ± 46	10,471 ± 32	0.569	yes

Table 7.5 (continued):

SG06 sample ID (#)	Sample type	SG06 CD (cm)	SG06 EFD (cm)	SG06 yr BP	Expected radiocarbon age (BP)	AMS target ID	ORAU pre-treatment protocol	Target type	C yield (mg)	Conventional radiocarbon date (± 1σ)	Weighted mean, $\bar{Y}$ ($\pm \bar{S}$)	Test statistic, T	Coeval at 5%?
537	Dec.br.leaf	1612.7	1578.2	13,532	11,696	OxA-24421 SUERC-27505	V V -	G g	2.253 1.832	11,595 ± 46 11,706 ± 41	11,657 ± 31	3.245	yes
153	Dec.br.leaf	1652.7	1612.1	13,960	12,026	OxA-24211 SUERC-18126	V V -	g g	0.730 0.696	11,981 ± 64 11,870 ± 60	11,922 ± 44	1.601	yes
989 189	Dec.br.leaf	2053.4	2000.6	20,574	17,511	OxA-24380 SUERC-17125	V V -	G g	2.097 1.339	17,572 ± 73 17,597 ± 96	17,581 ± 58	0.043	yes
197 969	Dec.br.leaf	2190.6	2132.8	23,055	19,762	OxA-X-2219-17 SUERC-13333 SUERC-27788	V V - -	vsg g g	0.480 0.589 0.632	20,181 ± 189 19,137 ± 123 19,481 ± 130	19,461 ± 81	21.475	no
801	Dec.br.leaf	2418.4	2347.0	27,290	23,383	OxA-24345 SUERC-27514	V V -	g g	0.616 1.195	23,269 ± 302 23,315 ± 134	23,307 ± 122	0.019	yes
993	Bark (& some leaf material)	2477.9	2406.4	28,248	24,158	OxA-24422 OxA-24423 SUERC-27516	V V V V -	G G g	2.944 2.764 11.068	23,938 ± 169 23,923 ± 115 23,970 ± 104	23,947 ± 70	0.095	yes
701 689	Dec.br.leaf	2537.7	2463.7	29,207	24,742	OxA-24353 SUERC-28236	V V -	g g	1.093 0.584	24,875 ± 230 24,678 ± 258	24,788 ± 172	0.325	yes
888 221	Dec.br.leaf	2671.1	2555.5	30,325	25,735	OxA-24359 SUERC-20504	V V -	g g	0.809 0.643	26,402 ± 347 25,518 ± 316	25,919 ± 234	3.548	yes
521 890	Dec.br.leaf	2737.6	2622.1	31,437	28,042	OxA-24305 SUERC-28210	V V -	g g	0.888 1.104	27,953 ± 275 28,396 ± 256	28,190 ± 187	1.390	yes

Table 7.5 (continued):

SG06 sample ID (#)	Sample type	SG06 CD (cm)	SG06 EFD (cm)	SG06 yr BP	Expected radiocarbon age (BP)	AMS target ID	ORAU pre-treatment protocol	Target type	C yield (mg)	Conventional radiocarbon date (± 1σ)	Weighted mean, $\bar{Y}$ ($\pm \bar{S}$)	Test statistic, T	Coeval at 5%?
397	Dec.br.leaf	2800.9	2684.3	32,563	29,017	OxA-24325	V V	G	1.800	28,466 ± 187	28,572 ± 134	0.664	yes
1075						SUERC-29836	-	g	2.909	28,685 ± 193			
395&396	Dec.br.leaf	2816.4	2697.9	32,795	29,077	OxA-24360	V V	g	0.784	28,405 ± 451	29,098 ± 185	2.844	yes
1068						SUERC-29840	-	g	3.204	29,239 ± 203			
1024	Dec.br.leaf	2845.5	2726.3	33,285	30,562	OxA-24394	V V	g	0.902	29,697 ± 469	30,006 ± 215	2.312	yes
						OxA-24429	V V	G	1.610	29,887 ± 286			
394						SUERC-23351	-	g	1.441	30,604 ± 458			
912	Dec.br.leaf	2931.4	2812.2	34,765	32,123	OxA-24349	V V	g	1.018	33,072 ± 622	32,494 ± 249	3.438	yes
						OxA-24350	V V	g	1.162	33,150 ± 563			
						SUERC-27775	-	g	2.411	32,152 ± 310			
736	Dec.br.leaf	2965.3	2846.1	35,326	32,963	OxA-24361	V V	g	0.875	34,093 ± 797	33,533 ± 503	0.820	yes
733						SUERC-28216	-	g	0.761	33,163 ± 648			
1008	Dec.br.leaf	2991.6	2872.4	35,747	33,388	OxA-24395	V V	g	1.432	33,319 ± 484	33,621 ± 296	0.625	yes
						SUERC-29820	-	g	2.132	33,803 ± 375			
1021	Dec.br.leaf	2999.8	2880.6	35,896	33,794	OxA-24430	V V	G	1.906	32,925 ± 364	33,387 ± 258	3.239	yes
						SUERC-29821	-	g	2.448	33,854 ± 366			
1007	Dec.br.leaf	3051.1	2930.9	36,709	33,808	OxA-X-2357-20	V V	g	1.284	32,662 ± 487	33,418 ± 311	4.077	no
						SUERC-29824	-	g	1.746	33,941 ± 405			
1040	Bark	3125.2	2993.9	37,831	35,454	OxA-24434	V V	G	1.890	34,485 ± 427	34,900 ± 312	2.034	yes
						SUERC-29844	-	g	2.015	35,378 ± 458			

Table 7.5 (continued):

SG06 sample ID (#)	Sample type	SG06 CD (cm)	SG06 EFD (cm)	SG06 yr BP	Expected radiocarbon age (BP)	AMS target ID	ORAU pre-treatment protocol	Target type	C yield (mg)	Conventional radiocarbon date (± 1σ)	Weighted mean, $\bar{Y}$ ($\pm \bar{S}$)	Test statistic, T	Coeval at 5%?
246	Dec.br.leaf	3163.4	3031.6	38,420	35,141	OxA-24218 SUERC-19064	V V -	g vsg	0.803 0.482	34,213 ± 634 27,308 ± 402	29,288 ± 340	84.603	no
1047 247 743	Dec.br.leaf	3174.3	3042.5	38,604	35,161	OxA-24436 SUERC-16527 SUERC-28890	V V - -	G vsg g	1.726 0.434 0.787	34,287 ± 446 32,838 ± 885 35,660 ± 772	34,344 ± 354	5.818	yes
744	Dec.br.leaf	3191.0	3059.2	38,886	35,658	OxA-24356 SUERC-28217	V V -	g g	0.687 1.800	34,836 ± 1,067 34,858 ± 456	34,855 ± 419	0.000	yes
252 1049	Dec.br.leaf	3258.3	3126.4	40,015	36,247	OxA-24185 SUERC-29852	V V -	vsg g	0.435 0.793	40,788 ± 2,460 37,121 ± 917	37,568 ± 859	1.951	yes
1135a 1135b	Moss Bark	3360.9	3226.8	41,616	38,475	OxA-24452 OxA-24453 OxA-24437 SUERC-29853	V V V V UW -	g g G g	1.168 1.000 2.143 3.777	36,349 ± 845 36,142 ± 891 36,509 ± 485 38,721 ± 617	37,046 ± 324	10.306	no
266	Dec.br.leaf	3411.9	3274.3	42,464	38,666	OxA-24219 SUERC-20500	V V -	g g	0.681 0.964	38,158 ± 1,178 42,034 ± 1,852	39,274 ± 994	3.118	yes
272 1134	Dec.br.leaf	3467.0	3329.4	43,408	41,122	OxA-24252 SUERC-29855	V V -	g g	1.002 2.196	42,755 ± 1,419 40,567 ± 821	41,116 ± 711	1.781	yes
983	Dec.br.leaf	3486.7	3349.1	43,721	40,628	OxA-24383 SUERC-27779	V V -	G g	2.035 1.500	40,758 ± 812 39,716 ± 849	40,260 ± 587	0.787	yes
274 986	Dec.br.leaf	3506.6	3368.5	44,042	40,927	OxA-24205 SUERC-27780	V V -	g g	0.933 1.098	39,748 ± 1,060 40,012 ± 1,034	39,883 ± 740	0.032	yes

Table 7.5 (continued):

SG06 sample ID (#)	Sample type	SG06 CD (cm)	SG06 EFD (cm)	SG06 yr BP	Expected radiocarbon age (BP)	AMS target ID	ORAU pre-treatment protocol	Target type	C yield (mg)	Conventional radiocarbon date (± 1σ)	Weighted mean, $\bar{Y}$ ($\pm \bar{S}$)	Test statistic, T	Coeval at 5%?
747	Twig	3541.8	3403.7	44,545	41,546	OxA-X-2360-43 SUERC-28218	UW -	G g	1.835 7.232	38,751 ± 729 40,909 ± 777	39,761 ± 532	4.102	no
746	Bark	3562.5	3423.4	44,838	42,516	OxA-24362 OxA-24363 SUERC-28219	UW UW -	g g g	0.999 1.145 6.016	39,455 ± 1,295 43,181 ± 1,742 40,682 ± 757	40,716 ± 612	2.953	yes
283 675	Dec.br.leaf	3656.17	3509.66	46,137	43,743	OxA-24241 SUERC-27781	V V -	G g	2.634 0.836	42,425 ± 772 44,930 ± 2,239	42,691 ± 730	1.119	yes
762	Dec.br.leaf	3728.1	3578.3	47,250	46,398	OxA-24364 SUERC-28897	V V -	g g	0.698 0.787	47,265 ± 4,071 43,775 ± 2,045	44,478 ± 1,827	0.587	yes
291	Dec.br.leaf	3796.7	3646.9	48,351	44,162	OxA-24186 SUERC-13334	V V -	g g	1.381 1.286	49,142 ± 2,269 39,129 ± 844	40,346 ± 791	17.107	no
939	Dec.br.leaf	3977.9	3823.0	51,323	47,321	OxA-X-2360-48 SUERC-27787	V V -	G g	1.604 2.812	42,927 ± 1,294 47,785 ± 1,762	44,629 ± 1,043	4.938	no
943 296	Dec.br.leaf	4011.7	3856.9	51,951	47,634	OxA-24397 SUERC-17128	V V -	g g	1.107 1.071	45,178 ± 2,226 48,868 ± 3,663	46,173 ± 1,902	0.741	yes
944	Dec.br.leaf	4016.3	3861.4	52,040	46,550	OxA-24358 SUERC-27520	V V -	g g	0.678 0.654	44,138 ± 3,004 49,280 ± 4,663	45,646 ± 2,525	0.859	yes
947	Dec.br.leaf	4026.4	3871.6	52,223	47,771	OxA-24384 SUERC-27522	V V -	G g	2.303 2.041	47,886 ± 1,618 48,713 ± 2,066	48,200 ± 1,274	0.099	yes
32	*Phragmites* (?)	4064.5	3909.7	52,885	53,159	OxA-24282 SUERC-28902	V V -	G g	2.840 4.864	49,055 ± 1,278 50,261 ± 2,264	49,346 ± 1,113	0.215	yes

7.2.4 Complete SG06 Plant Macrofossil Radiocarbon Dataset

As already noted, a total of 647 radiocarbon determinations were obtained from the SG06 sediment core over the course of the Suigetsu Varves 2006 project. Of the 361 determinations obtained at ORAU, 26 were of 'background' samples (table 7.1) and eight were of sediment sub-samples (table 7.9), giving a total of 327 radiocarbon determinations performed on plant macrofossil samples to contribute to the SG06 radiocarbon calibration dataset. Of these 327 measurements, 112 were generated from 'large graphite' ('G'; ≈ 1.7 mg C) targets, 161 from 'small graphite' ('g'; ≈ 0.8 mg C) targets, and 54 from 'very small graphite' ('vsg'; < 0.7 mg C) targets (section 4.3). Excluding the eighteen intra-laboratory 'auto-duplicates' (table 7.3), and other (non-identical) duplicates (three methodological inter-comparisons, table 7.6; two comparisons of sample type, table 7.7; two experimental vsgs; and one replicate sample due to AMS malfunction, resulting in insufficient run-time), these 327 ORAU measurements represent 301 separate SG06 sampling horizons.

Of the 286 determinations performed at NRCF-E, ten were of background samples (table 7.2) and four were of sediment samples (table 7.9), giving a total of 272 determinations from plant macrofossil samples to contribute to the SG06 radiocarbon calibration dataset. Of these 272 measurements, 249 were generated from 'normal graphite' (≥ 0.5 mg C) targets (defined as 'g' targets herein, following the ORAU nomenclature), whilst 23 were from 'smaller than regulation' (< 0.5 mg C) targets (given the notation 'vsg' herein). Excluding the three intra-laboratory duplicates (table 7.4), 269 separate SG06 sampling horizons are represented by NRCF-E data. Taking into account the 52 inter-laboratory duplicates (table 7.5), a total of 518 separate SG06 sampling horizons are therefore represented by the combined radiocarbon dataset of both laboratories.

Figure 7.4 plots the 327 ORAU and 272 NRCF-E radiocarbon determinations from SG06 plant macrofossil samples, shown against SG06 event-free depth (EFD). From the overview plot (figure 7.4a) it can be seen that the consistency of these data look generally good, with the data from the two labs seeming to overlie each other well, providing no immediate evidence of inter-laboratory offsets (despite the slightly more 'non-coeval' direct duplicates than would have been optimal; section 7.2.3). As would be expected, the data show increasing uncertainty with age/depth, but there is no evidence of any obvious inversions or lengthy gaps (hiatuses) within the dataset. This is especially evident for the younger portion of the dataset (< *circa* 30,000 BP) because of the reduced uncertainties on these measurements. Another feature of the overall dataset is a change in deposition rate at approximately 17 m EFD. This corroborates the similar trend in deposition rate at Lake Suigetsu observed by Kitagawa and van der Plicht (1998a, 1998b; section 6.2.4).

The supporting plots, figures 7.4b to 7.4e, allow examination of the same data at increased resolution. In all of these plots, the smaller 'vsg' samples (those < 0.5 mg C) are plotted separately from the larger 'G' and 'g' (and ORAU 'vsgs' > 0.5 mg C) data. It can be clearly seen that such data tend to be less reliable (vary more from the overall trend line of the combined data) than those from the larger AMS targets, suggesting that the background corrections applied to these data do not adequately represent the true background subtraction required, or that these samples demonstrate more varying levels of modern contamination.

Figure 7.4: The raw (uncalibrated) ORAU and NRCF-E radiocarbon determinations produced from SG06 plant macrofossils, plotted against SG06 event-free depth (EFD), over the conventional radiocarbon age ranges: **(a)** 0 to 60,000 BP; **(b)** 0 to 11,000 BP; **(c)** 10,000 to 21,000 BP; **(d)** 20,000 to 36,000 BP; and **(e)** 35,000 to 60,000 BP. ORAU 'G' and 'g' data are plotted in dark blue; ORAU 'vsg' data are plotted in light blue; NRCF-E 'g' data are plotted in magenta; and NRCF-E 'vsg' samples are plotted in light pink. Radiocarbon measurement uncertainties are shown at 1σ.

(a):

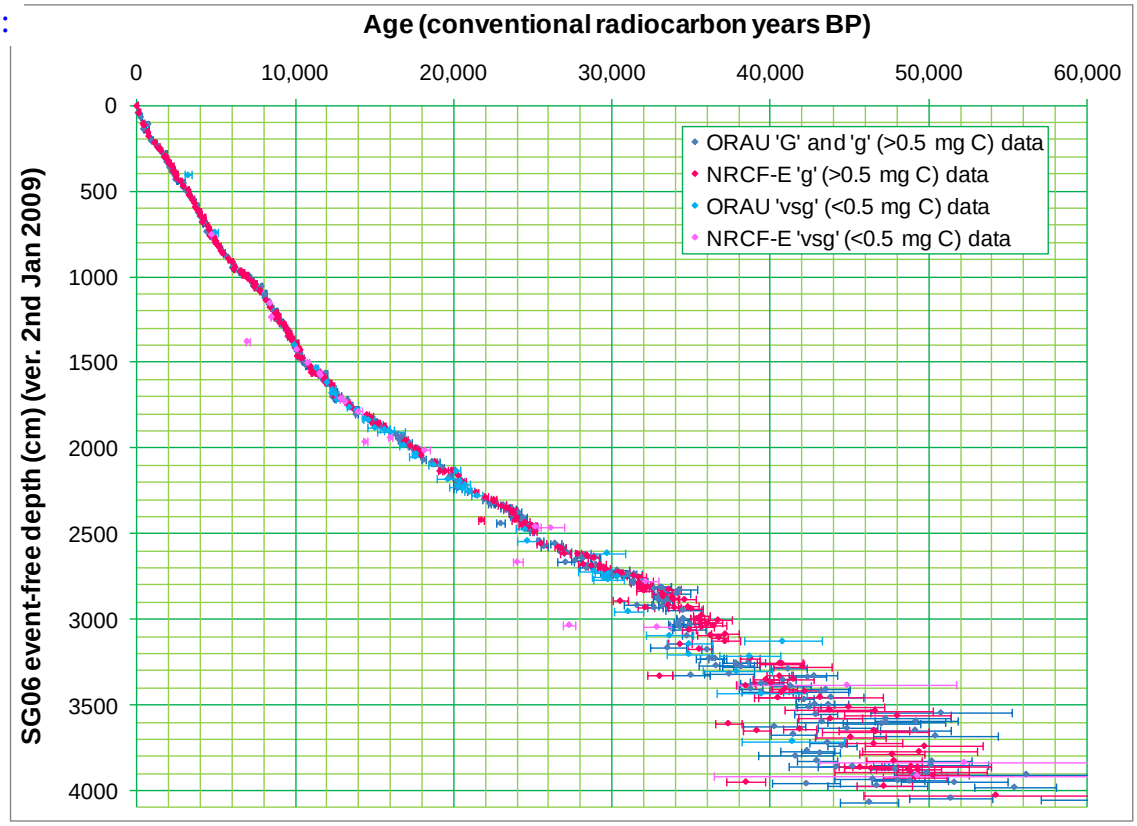

Figure 7.4 (continued):

(b):

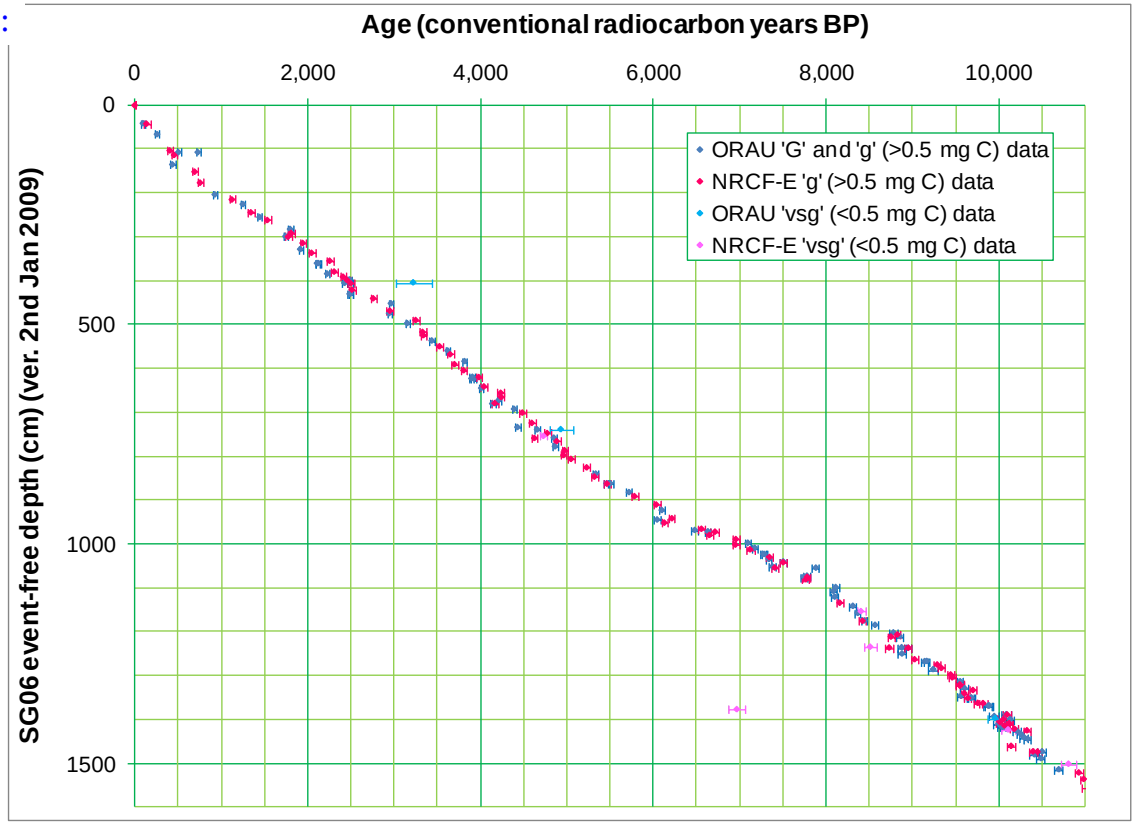

(c):

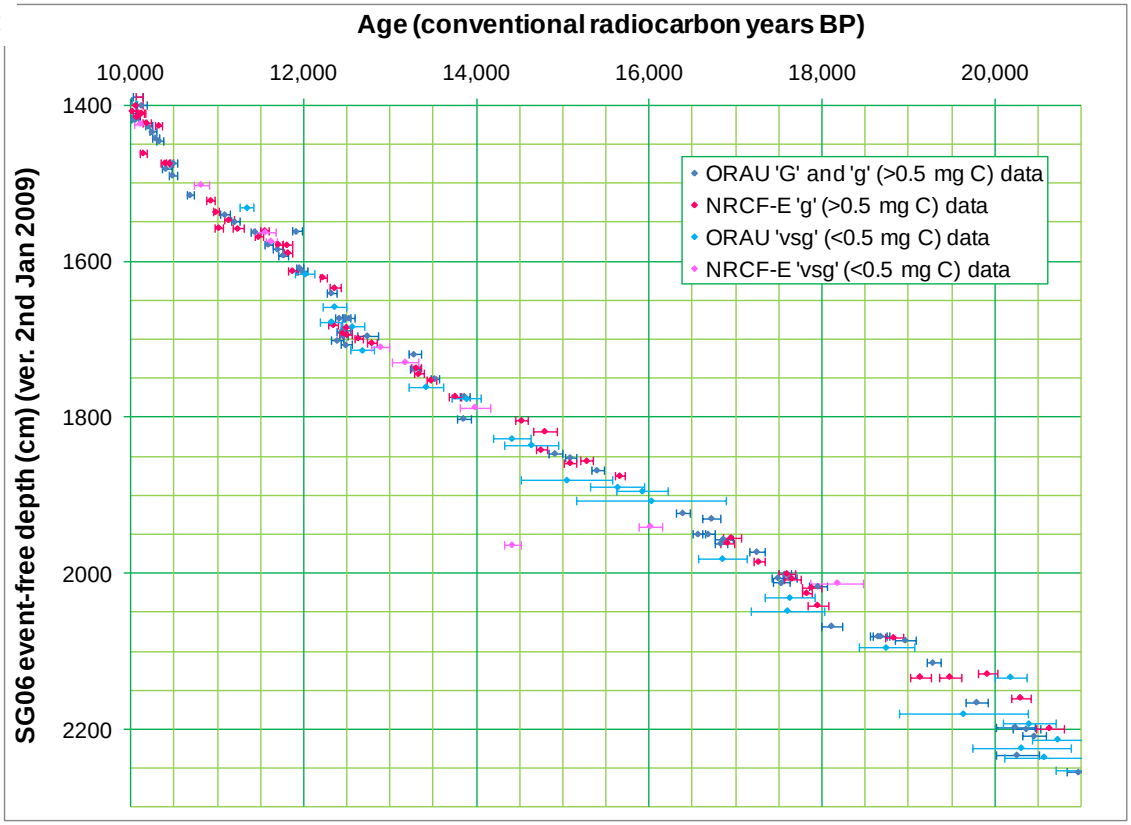

Figure 7.4 (continued):

(d):

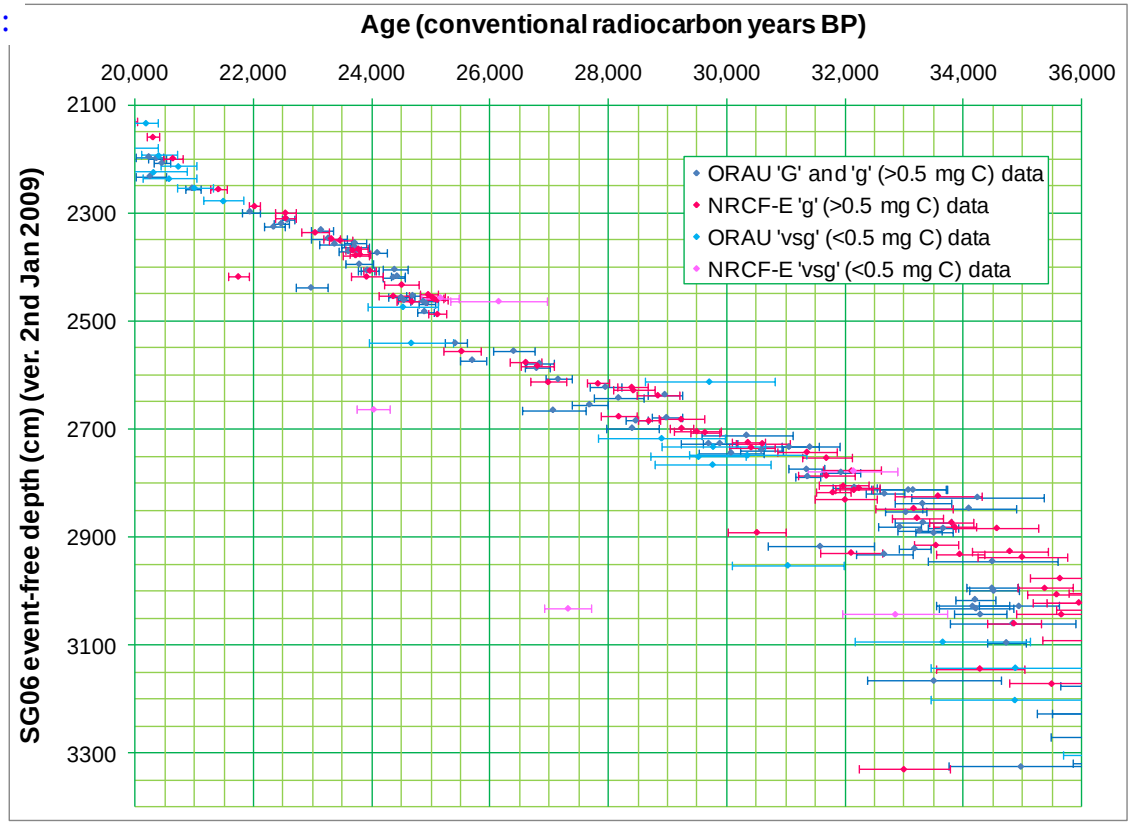

(e):

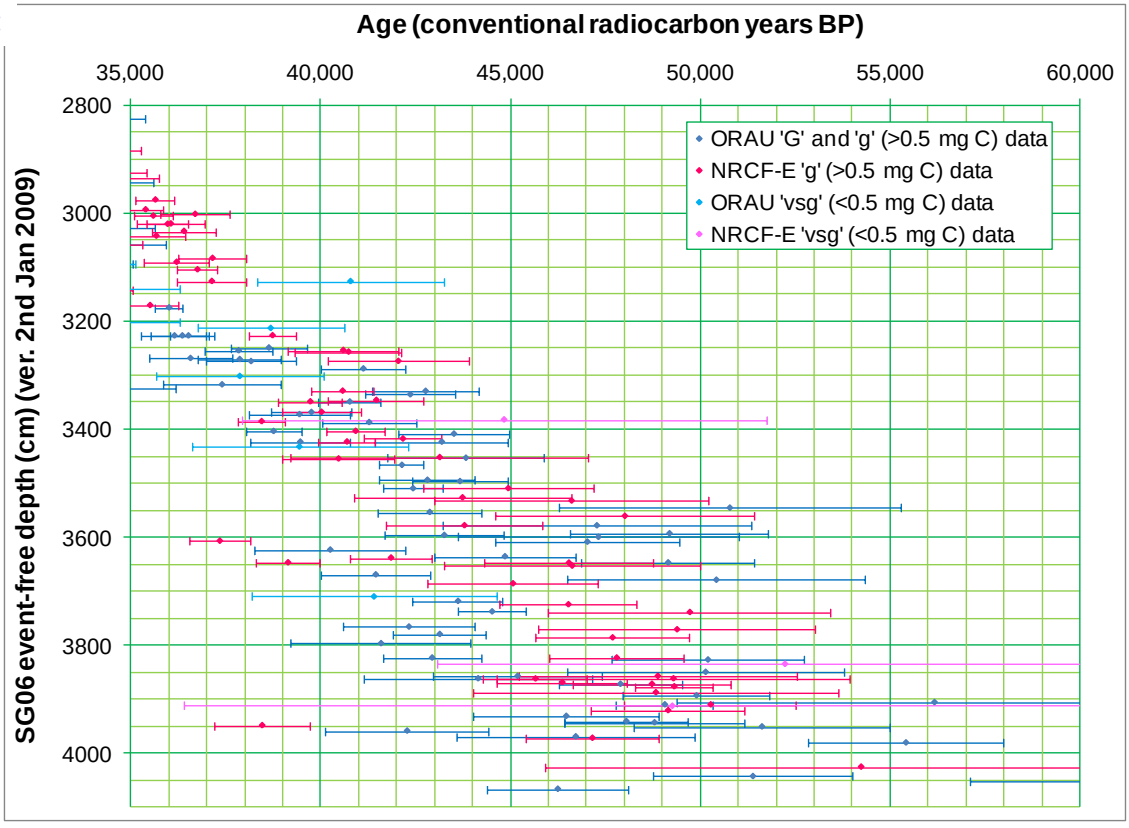

7.2.5 Methodological Inter-Comparison

Additional replicate measurements at ORAU were obtained from three further depth horizons in order to compare the effect of differing pre-treatment approaches (table 7.6). Two twig samples (#1121 and #595), which were treated by both 'VV' and 'UW' protocols (described in section 4.3), did not yield any statistically significant difference in the radiocarbon dates produced; indeed, the agreement between the two pairs of replicate dates is exceptionally good (with lower T values than most of the auto-duplicates that underwent the same pre-treatment protocols; table 7.3). Such a finding, although based upon only two samples, does support the choice of the less intensive VV method for the majority of the SG06 plant macrofossils, which, on this basis, would not benefit from the more thorough, yet detrimental to carbon yield, UW protocol.

Sample #39 (an evergreen broad leaf) was treated by both 'VV' and 'NRC' protocols. The latter ('non-routine chemistry') pre-treatment methodology involved a 1 M H_2SO_4 second acid wash (rather than the usual 1 M HCl). This experimental procedure was undertaken amongst the first (pilot) batch of SG06 samples in order to examine the robustness of the regular ORAU ABA protocol on the SG06 plant macrofossils (section 4.3.2). As with the two peat samples treated with the same NRC protocol (section 7.2.1, above), the coherence between the radiocarbon determinations produced from the dual methodological approaches was very good (indeed, the H_2SO_4-treated sub-sample produced a date slightly younger, though not statistically so, than that treated with the regular HCl wash), suggesting that the alternative, more severe, pre-treatment protocol was not necessary for the Lake Suigetsu macrofossils.

Table 7.6: The three SG06 plant macrofossil samples duplicated at ORAU as a test of differing pre-treatment methodologies. (Sample type 'Ev.br.leaf' refers to an evergreen broad leaf; 'SG06 CD' and 'SG06 EFD' refer to Suigetsu Varves 2006- composite depth and event-free depth, respectively; the 'VV' and 'UW' ORAU pre-treatment protocols are described in section 4.3, and the 'NRC' protocol on the previous page; target type 'G' refers to large graphite AMS targets; and 'C yield' is the mass of carbon combusted in the EA for each sub-sample. The 'test statistic, T' is compared to the 5% probability of the χ^2 distribution, to assess whether the duplicate dates are- or are not statistically consistent with a single, 'coeval' date.)

SG06 sample ID (#)	Sample type	SG06 CD (cm)	SG06 EFD (cm)	SG06 yr BP	Expected radiocarbon age (BP)	AMS target ID	ORAU pre-treatment protocol	Target type	C yield (mg)	Conventional radiocarbon date (± 1σ)	Weighted mean, $\bar{Y}$ (± $\bar{S}$)	Test statistic, T	Coeval at 5%?
39	Ev.br.leaf	876.9	862.9	6,348	5,510	OxA-24181	V V	G	3.161	5,500 ± 34	5,480 ± 24	0.741	yes
						OxA-24182	NRC	G	3.067	5,458 ± 35			
1121	Twig	1383.1	1352.0	11,091	9,650	OxA-24431	V V	G	1.867	9,672 ± 40	9,675 ± 28	0.012	yes
						OxA-24432	UW	G	1.673	9,678 ± 39			
595	Twig	2137.5	2080.3	22,123	18,695	OxA-24371	UW	G	2.392	18,681 ± 89	18,667 ± 64	0.052	yes
						OxA-24373	V V	G	2.114	18,652 ± 91			

As was noted in section 4.3.2, the discussion of these two methodological alternatives (additional bleaching stage, or H_2SO_4 second acid wash) to the (VV) protocol adopted for the remainder of the SG06 plant macrofossils is based upon a very small number of samples. However, such data are supported by the findings of on-going methodological testing on other, similar sample material at the ORAU laboratory.

7.2.6 Choice of Sample Type

Two sample depths yielded radiocarbon determinations upon two differing sample types picked from the same sedimentary horizon and, as such, might aid understanding of the choice of sample type from sample depths across the remainder of the SG06 sediment profile (table 7.7). Samples #548 (a deciduous broad leaf) and #549 (a small twig), picked from 1714.0 cm composite depth (core section A-09), yield no statistically significant difference in their radiocarbon determinations, although the leaf actually dates a little older than either of the (auto-duplicated) twig sub-samples.

Sample #1135 (sub-divided into separate ‘a’ and ‘b’ fractions immediately prior to pre-treatment, rather than upon initial sub-sampling from the core, and hence alternative nomenclature), picked from a composite core depth of 3360.9 cm (core section C-14), represents a sturdy fragment of bark with *Sphagnum* moss attached to it, which presumably grew on the bark sample either on the parent tree itself, or on the forest floor once the bark had been detached from the host plant. In the latter instance, *Sphagnum* would take its carbon from atmospheric CO_2 at the ground surface. At such levels, CO_2 represents a mixture of ambient atmospheric- and mineralised (i.e. decomposed) organic- CO_2 sources and may, therefore, represent a risk of inbuilt age (Hatté and Jull 2007). The results for sample #1135 do not show such a finding, however, with the ORAU bark sample slightly older (though not statistically so) than either of the moss sub-samples. The additional duplicated bark

measurement obtained from NRCF-E (discussed in section 7.2.3, above) would also suggest an older age for the bark, as compared to the two moss sub-samples. However, the lack of statistical agreement between the ORAU and NRCF-E determinations on these two bark sub-samples means that such analysis should be treated with caution.

In section 4.2, the preference for dating broad leaves, rather than sturdier samples (seeds, twigs or bark), was highlighted as being advantageous in decreasing the chances of selecting samples with a significant inbuilt age. On the basis of samples #548 and #549, this selection criterion would not be necessary, with the leaf sample slightly older than the twig. Conversely, on the basis of sample #1135, the older age of the bark, as compared to the moss, suggests that perhaps sturdier bark samples should indeed be avoided. Of course, neither of these samples yield statistically significant interpretations, and only represent two sampling horizons, and therefore such conclusions are indicative only.

To provide a more rigorous assessment of whether the sturdier (bark, twig, conifer needle, or even the evergreen broad leaf) samples do indeed bare an observable inbuilt age (as compared to the more fragile, deciduous broad leaf samples), the broader corpus of the complete SG06 radiocarbon dataset can be examined, using more robust statistical methods. Although not comparing equivalent depth horizons directly (as was the case for the two examples given above), such an approach can also be applied to identify such trends. Contingency tables were therefore constructed for subsets of the SG06 radiocarbon data, split up according to sample type, and compared for any systematic offset from the 'expected values' (section 7.5). These contingency tables are given in appendix 14, and summarised in table 7.8. These tests demonstrate that, as with the two direct comparisons made above, there is no observable offset between the respective sample types. Therefore, although leaves were preferentially dated over the sturdier (bark or twig) samples over the course of the project, there is no reason to question the data produced from the other sample types.

Table 7.7: The two SG06 sample depths from which radiocarbon determinations were obtained at ORAU from differing sample types. (Sample type 'Dec.br.leaf' refers to a deciduous broad leaf; 'SG06 CD' and 'SG06 EFD' refer to Suigetsu Varves 2006- composite depth and event-free depth, respectively; the 'VV' and 'UW' ORAU pre-treatment protocols are described in section 4.3; target types 'G' and 'g' refer to large- and small graphite AMS targets, respectively; and 'C yield' is the mass of carbon combusted in the EA for each sub-sample. The 'test statistic, T' is compared to the 5% probability of the χ^2 distribution, to assess whether the duplicate dates are- or are not statistically consistent with a single, coeval date.)

SG06 sample ID (#)	Sample type	SG06 CD (cm)	SG06 EFD (cm)	SG06 yr BP	Expected radiocarbon age (BP)	AMS target ID	ORAU pre-treatment protocol	Target type	C yield (mg)	Conventional radiocarbon date (± 1σ)	Weighted mean, $\overline{Y}$ (± $\overline{S}$)	Test statistic, T	Coeval at 5%?
548	Dec.br.leaf	1714.0	1672.9	14,721	12,419	OxA-24294	V V	g	1.339	12,528 ± 51	All 3 samples:		
549	Twig	1714.0	1672.9	14,721	12,419	OxA-24323	V V	G	2.445	12,415 ± 50	12,478 ± 29	2.639	yes
						OxA-24324	V V	G	1.920	12,493 ± 50			
1135a	Moss	3360.9	3226.8	41,616	38,475	OxA-24452	V V	g	1.168	36,349 ± 845	3 ORAU samples:		
						OxA-24453	V V	g	1.000	36,142 ± 891	36,410 ± 380	0.137	yes
1135b	Bark	3360.9	3226.8	41,616	38,475	OxA-24437	UW	G	2.143	36,509 ± 485	All 4 samples:		
						SUERC-29853	-	g	3.777	38,721 ± 617	37,046 ± 324	10.306	no

Table 7.8: Summary of the contingency tables derived to assess the potential offsets between the respective SG06 plant macrofossil sample types dated. (Full details of these tests are provided in appendix 14.)

SG06 sample type	Number of (non-background) radiocarbon determinations	$\Sigma (O_i - E_i)^2 / E_i$ (compared to χ^2_1 critical value of 3.841 at the 95% significance level)	Statistically significant?
Deciduous broad leaves	430	2.135	No
Evergreen broad leaves	73	0.000	No
Conifer needles	11	1.690	No
Bark	29	3.516	No
Twigs	27	0.026	No

7.2.7 Dating of Sediments

With the ability of the AMS technique to radiocarbon date individual plant macrofossil entities, it has become clear that the dating of such material is "inherently more reliable" than bulk dates obtained from the sediment matrix (Hatté and Jull 2007). The pathway of ^{14}C from atmosphere to sample is much simplified in the case of the former sample type, whereas the latter represents a heterogeneous mixing of carbonaceous material where this transfer of ^{14}C from the atmosphere to sample is far more convoluted. Thus, only macrofossil samples are utilised for the construction of the Lake Suigetsu calibration datasets (either from the Suigetsu '93- or Suigetsu Varves 2006 projects), since bulk dating of the sediment matrix would not yield a reliable depiction of the contemporaneous atmospheric ^{14}C concentration. However, early in the progress of the present project, pilot data were obtained on sediment samples from SG06 core depths that also bore datable plant macrofossil samples (table 7.9). The purpose of this exercise was to assess the potential for environmental contamination to the macrofossils dated (section 4.3.1).

The youngest depth horizon, sample #S39 (the 'S' prefix denoting 'sediment' picked from the same sampling horizon as the picked plant macrofossil), composite core depth 876.9 cm (core section A-05), is the only one to provide sediment samples (humin- and humic fractions from ORAU, humin only from NRCF-E) in statistical agreement with each other. The weighted mean of these samples, 5,823 ± 21 BP, is some 350 conventional radiocarbon years older than the weighted mean (5,475 ± 20 BP) of the three dated macrofossil sub-samples (#39). This depth probably provides the most reliable estimate of the reservoir age of the bulk sediment material (as compared to the contemporaneous atmospheric ^{14}C signal, represented by the terrestrial plant macrofossils), and therefore indicates the likely potential effect of any non-removed sediment contaminant from the SG06 plant macrofossils. Although the weighted means of #39 and #S39 are statistically different from each other, the reservoir age of the sediment is relatively small (as compared to the 1,000 ± 500 conventional radiocarbon year reservoir age of sediments from Lake Baikal, Siberia, for example; Colman *et al*. 1996). Since this offset is relatively small, and the chemical removal of any such material remaining after physical cleaning is deemed highly effective, it is therefore proposed that any environmental (as opposed to laboratory) contamination of the Suigetsu plant macrofossils would be negligible.

The subsequent sampling depth, (2190.6 cm CD, core section B-11) demonstrates a similar result (sediment dating older than macrofossil), but both the duplicate dates of the sediment (#S197) and leaf (#197 and #969) are not internally consistent – in the latter instance perhaps due to the small (≈ 0.6 mg C) sample sizes (section 7.2.3). Such issues complicate reliable quantification of the true age difference between these respective sample types at this sampling depth.

The two older sampling depths (2726.9 cm CD, core section B-14, and 3796.7 cm CD, core section A-20) provide an alternative finding. Although the sediment fractions of both

sampling depths (#S223 and #S291) are not internally consistent, the exclusion of the humin- (base insoluble) fractions dated at ORAU (which appear erroneously young as compared to the ORAU humic- and NRCF-E humin sediment fractions) provides dates that are statistically coeval in both instances, but that are still younger than the macrofossil samples (#223 and #291) dated from the equivalent sampling depths. Rather than this representing a 'real' offset between these respective sample types, it is most probable that this finding is a result of the less efficient laboratory pre-treatment of sediments, which might allow the incorporation of relatively more modern carbon contamination (as compared to more intact macrofossil samples) due to the relatively larger surface area to volume ratio for this contamination to adsorb. The reason identified here for the seemingly 'young' humin data is the exceptionally low proportion (< 3% by mass) of (humin) carbon within the bulk sediment, making these sub-samples far more susceptible to the effects of modern carbon contamination (section 4.3.1). It must be emphasised, therefore, that these erroneous SG06 humin data do not reflect unreliability of the ORAU pre-treatment protocol for humin dating more generally, as the proportion of carbon is often much higher in other sediments, and less prone to this modern carbon contamination.

The totality of these sediment/macrofossil comparison radiocarbon data demonstrate both the reduced reliability of dates produced from sediment (and therefore the necessity of using plant macrofossil samples for production of the Lake Suigetsu radiocarbon calibration dataset), and the approximate 'real' offset (lake water reservoir) between the bulk sediment material and plant macrofossils, thus reflecting the (very small) potential effect of any contamination upon the macrofossil samples from the sedimentary régime.

Table 7.9: The four SG06 sample depths from which radiocarbon determinations of sediment were obtained from both ORAU and NRCF-E labs, along with datable plant macrofossil samples. (Sample types 'Ev.br.leaf' and 'Dec.br.leaf' are evergreen- and deciduous broad leaves, respectively; 'SG06 CD' and 'SG06 EFD' refer to Suigetsu Varves 2006- composite depth and event-free depth, respectively; the 'VV' ORAU pre-treatment protocol is described in section 4.3, the 'SRa' and 'SRb' protocols in section 4.3.1, and the 'NRC' protocol in section 7.2.5; target types 'G', 'g' and 'vsg' refer to large-, small- and very small graphite AMS targets, respectively; 'C yield' is the mass of carbon combusted in the EA for each sub-sample; and '% C' reflects the carbon present in the sample, as a percentage of the starting mass. The 'test statistic, T' is compared to the 5% probability of the χ^2 distribution, to assess whether the duplicate dates are- or are not statistically consistent with a single, coeval date.)

SG06 sample ID (#)	Sample type	SG06 CD (cm)	SG06 EFD (cm)	SG06 yr BP	Expected radiocarbon age (BP)	AMS target ID	ORAU pre-treatment protocol	Target type	C yield (mg)	% C	Conventional radiocarbon date (± 1σ)	Weighted mean, $\bar{Y}$ (± $\bar{S}$)	Test statistic, T	Coeval at 5%?
39	Ev.br.leaf	876.9	862.9	6,348	5,510	OxA-X-2218-31	V V	G	3.161	57.5	5,500 ± 34			
						OxA-X-2218-32	NRC	G	3.067	55.1	5,458 ± 35	3 leaf samples:		
						SUERC-13332	-	g	6.268	63.0	5,465 ± 35	5,475 ± 20	0.858	yes
S39	Sediment (humic fraction)	876.9	862.9	6,348	5,510	OxA-X-2225-53	SRb	G	1.574	27.1	5,879 ± 34	3 sediment samples:		
	Sediment (humin fraction)					OxA-X-2236-08	SRa	g	0.812	4.3	5,782 ± 38	5,823 ± 21	4.428	yes
	Sediment (humin fraction)					SUERC-18047	-	g	-	10.8	5,797 ± 35			
197	Dec.br.leaf	2190.6	2132.8	23,055	19,762	OxA-X-2219-17	V V	vsg	0.480	54.5	20,181 ± 189			
						SUERC-13333	-	g	0.589	42.0	19,137 ± 123	3 leaf samples:		
969						SUERC-27788	-	g	0.632	-	19,481 ± 130	19,461 ± 81	21.475	no
S197	Sediment (humic fraction)	2190.6	2132.8	23,054	19,762	OxA-X-2226-43	SRb	g	0.978	11.5	20,080 ± 90	3 sediment samples:		
	Sediment (humin fraction)					OxA-X-2236-09	SRa	g	0.800	3.3	19,400 ± 90	19,862 ± 56	45.094	no
	Sediment (humin fraction)					SUERC-18911	-	g	-	2.1	20,289 ± 119			

Table 7.9 (continued):

SG06 sample ID (#)	Sample type	SG06 CD (cm)	SG06 EFD (cm)	SG06 yr BP	Expected radiocarbon age (BP)	AMS target ID	ORAU pre-treatment protocol	Target type	C yield (mg)	% C	Conventional radiocarbon date (± 1σ)	Weighted mean, $\bar{Y}$ (± $\bar{S}$)	Test statistic, T	Coeval at 5%?
223	Dec.br.leaf	2726.9	2611.4	31,232	27,270	OxA-X-2219-18	V V	vsg	0.249	60.7	29,703 ± 1,094			
S223	Sediment (humic fraction)	2726.9	2611.4	31,232	27,270	OxA-X-2226-44	SRb	g	0.769	10.8	27,190 ± 160	3 sediment samples:		
	Sediment (humin fraction)					OxA-X-2236-10	SRa	g	0.880	2.8	26,480 ± 150	26,847 ± 102	11.260	no
	Sediment (humin fraction)					SUERC-18046	-	g	-	2.3	27,080 ± 283			
291	Dec.br.leaf	3796.7	3646.9	48,351	44,162	OxA-X-2219-20	V V	g	1.381	53.7	49,142 ± 2,269	2 leaf samples:		
						SUERC-13334	-	g	1.286	93.0	39,129 ± 844	40,346 ± 791	17.107	no
S291	Sediment (humic fraction)	3796.7	3646.9	48,351	44,162	OxA-X-2226-22	SRb	g	1.356	26.5	43,750 ± 650	3 sediment samples:		
	Sediment (humin fraction)					OxA-X-2236-11	SRa	g	0.870	1.7	33,270 ± 270	34,952 ± 247	237.436	no
	Sediment (humin fraction)					SUERC-18912	-	g	-	1.5	41,832 ± 1,752			

7.3 Suigetsu Varves 2006 Varve Count Data

The dual methods of varve counting for the Suigetsu Varves 2006 project, those of XRF and X-radiography, and thin section microscopy, were introduced in section 3.6.3. As was noted, provisionally completed varve count data for SG06 are, at present, only available for the core section 1250.0 to 1814.6 cm composite depth. For the purposes of this thesis, the remainder of the annually laminated portion of SG06 (down to the limit of radiocarbon detection) must rely on data from the XRF and X-radiography method only. Figure 7.5 illustrates the varve count data for these upper- and lower core sections, respectively. It must be re-emphasised, therefore, that the radiocarbon calibration data presented against varve age below 1814.6 cm CD (in the coming sections) are only preliminary, and will be updated for publication once the remainder of the core has been counted by the thin section microscopy method (expected to be completed within ≈ 9 months from the submission of this thesis).

As can be seen in figure 7.5, there is a change in deposition rate evident at ≈ 1695 cm EFD. This finding is in good agreement with the change in deposition rate suggested by the uncalibrated radiocarbon data in figure 7.4. The varve count data do demonstrate longer-term increasing deposition rate through time, both below and above 1695 cm EFD, suggesting increased productivity in the catchment with associated increased in-wash to the lake through the transition from the Last Glacial Maximum (LGM) to the Bølling/Allerød interstadial (the placing of this transition being at either 1693.2 cm or 1686.5 cm EFD, according to SG06 palaeoenvironmental proxy data). However, the abruptness of the change in deposition rate (better demonstrated in figure 7.6), suggests that there might be a specific additional event superimposed – perhaps reflecting an increase in catchment size related to a single tectonic event. Since no significant event layers are evident in SG06 at this core depth (from direct observation of the core, or thin section analysis),

however, a dramatic climatic cause is not ruled out as having been responsible for affecting the lake sedimentation rate in this way.

Figure 7.5: The Suigetsu Varves 2006 varve count data plotted against SG06 event-free depth (EFD). For the core section 1250 cm to 1814.6 cm composite depth (CD; 1227.3 to 1773.0 cm EFD), provisionally completed data from the combined XRF and X-radiography, and thin section microscopy methods are presented; for the core section 1814.6 to 4497.7 cm CD (1773.0 to 4336.8 cm EFD) the preliminary data of only the XRF and X-radiography method are presented. The 'zero year' for this floating varve chronology is the U-Oki tephra layer, at 1286.1 to 1288.0 cm CD (1262.8 cm EFD). **(a)** illustrates varve count data across the entire data range (i.e. from 1227.3 to 4336.8 cm EFD); and **(b)** illustrates a higher resolution plot across the depth range 1400 to 1900 cm EFD. (Data supplied by project colleagues M. Marshall and G. Schlolaut.)

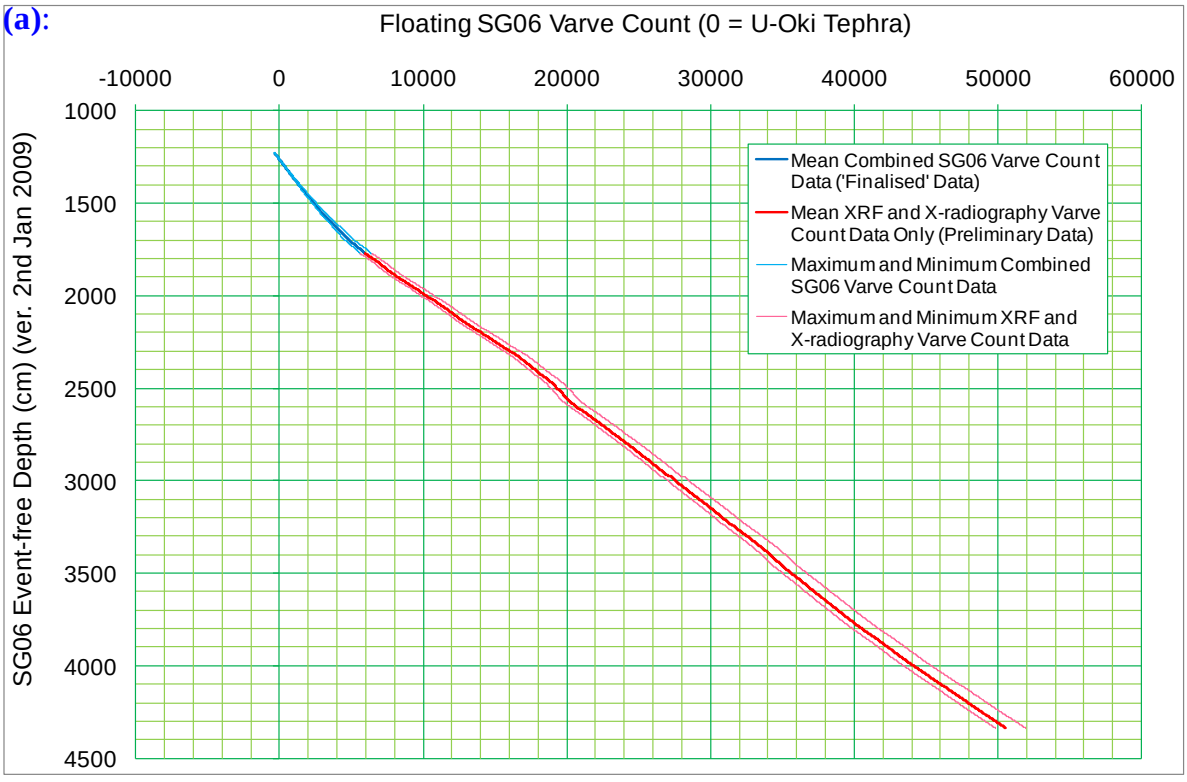

Figure 7.5 (continued):

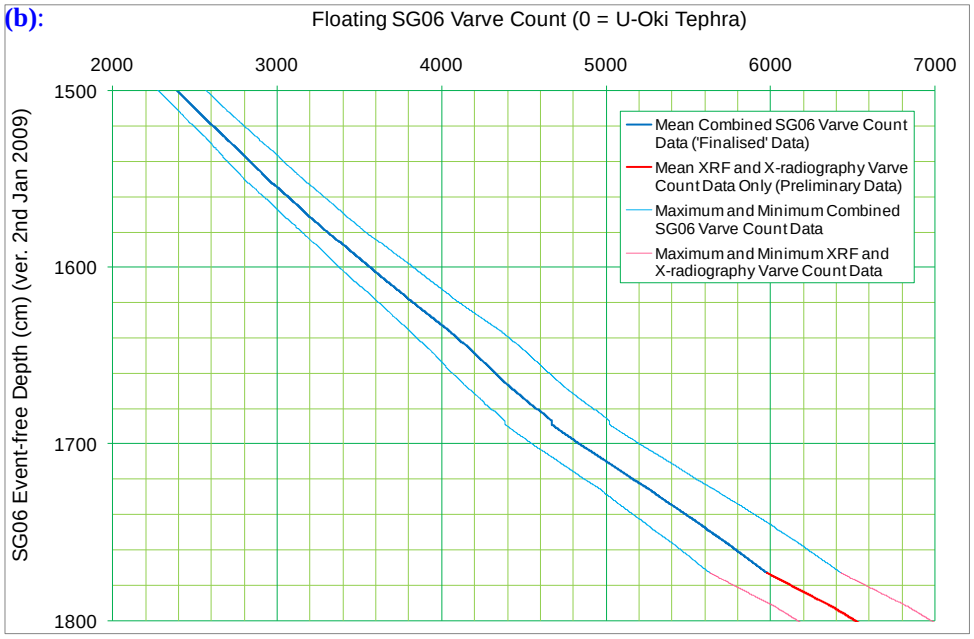

Figure 7.6: Alternative view of the provisionally completed portion of the Suigetsu Varves 2006 varve count data (1250 to 1814.6 cm event-free depth, EFD), with the mean number of varves in 10 cm EFD core sections plotted against SG06 EFD, highlighting the change in deposition rate at ≈ 1695 cm EFD.

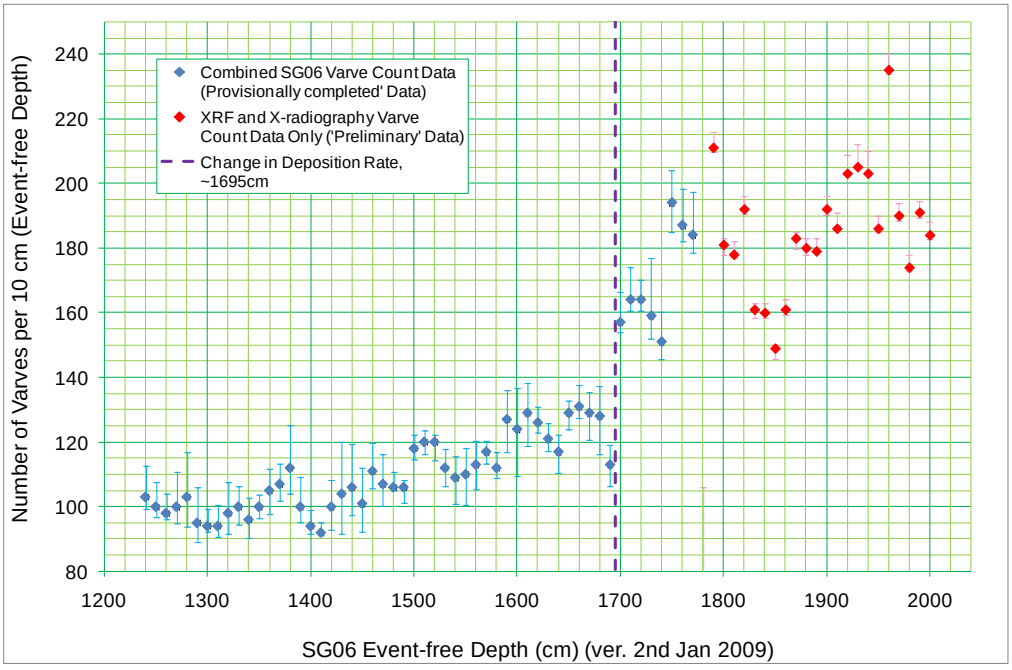

A second ‘kink’ in deposition rate implied at 1773.0 cm EFD (1814.6 cm CD) is an artefact of the transition between the combined-, and XRF and X-radiography only counting methods. Similarly, the reduced uncertainties on the latter data in figure 7.6 are a function of their being composed of the single counting method only.

Figure 7.6 also demonstrates the lack of coherence in the definition of varve counting uncertainties across the respective core sections. The upper core section presently demonstrates much greater uncertainties than the lower section, reflecting the comparison made between the dual varve counting methodologies. The uncertainties on the lower core section, generated from XRF and X-radiography counting only, are therefore an under-estimate of the final uncertainties that will be quoted, once the thin section microscopy counts have also been completed. It should be noted also, that the uncertainties given here for the provisionally completed core section represent the maximum uncertainty range (i.e. the maximum and minimum varve count values produced from the automated interpolation algorithm and dual method combination algorithms applied by project colleagues) rather than a more traditional 1σ or 2σ uncertainty approach, since the varve count data do not produce Normal probability distributions. (Such matters are discussed in much greater detail in Schlolaut *et al*. forthcoming.) For these reasons, the varve count data presented in the following sections are presented as the mean values, without data given for the uncertainty of these counts. An awareness of this is therefore necessary when examining the radiocarbon calibration datasets presented, but, for the majority of the time period covered by the data, which are represented by preliminary varve count data in any case, the quoting of the present uncertainty values would be essentially meaningless, with the final varve count from the project potentially falling outside this range anyway.

Independent support for the reliability of the SG06 varve counting can be provided through comparison with the radiocarbon data generated from the project. In order to avoid

any assumptions pertaining to marine- or DCF reservoir corrections, only the 'wholly reliable', terrestrial (i.e. dendrochronologically-derived) portion of IntCal09 (Reimer *et al*. 2009) should be used for this purpose. Calibrating the SG06 plant macrofossil data to IntCal09 therefore enables direct comparison between the 'SG06 vyr' and IntCal09 timescales. The principal (OCM-7.1) and supporting (OCM-7.2 to OCM-7.67) OxCal models that provide this corroboration for the reliability of the SG06 varve counting are discussed below in section 7.4, where the same models are used to provide 'wiggle matching' of the floating SG06 varve chronology to the absolute, IntCal09 timescale.

The time period of direct comparison between the SG06 vyr- and IntCal09 timescales is limited to 2,600 years, covering the time period between the top of the well-varved section of the SG06 sediment core (1250 cm CD) and the limit of tree-ring data in IntCal09 at 12,550 cal. BP. Therefore, this corroboratory support for the validity of the SG06 varve-counted timescale is limited to a relatively short period of the total (≈ 50,900 SG06 floating vyr) chronology. Although the use of the alternative, reservoir-corrected calibration datasets has been avoided thus far, these datasets, offering comparison data across the entirety of the radiocarbon dating range, can nevertheless provide support for the SG06 varve chronology further back in time. Chapter 8 will describe the comparison of the Lake Suigetsu radiocarbon calibration dataset with these alternative records. It will be argued in that chapter that, although there are shorter-term deviations evident between the Lake Suigetsu data and alternative radiocarbon calibration datasets (principally, IntCal09), the overall, long-term agreement between the datasets is generally good, providing increased credibility to the older portion of the SG06 varve-counted chronology (that is presently lacking in the thin section data).

7.4 'Wiggle Matching' to the IntCal09 Dendrochronological Timescale

Arguably the most important outcome of this DPhil thesis is the tying of the floating SG06 varve chronology to the absolute timescale (DPhil aim v). The securing of the independent, varve-counted SG06 timescale is fundamental to both of the over-riding aims of the Suigetsu Varves 2006 project, being necessary for both palaeoenvironmental reconstruction (including comparison to other sites) and radiocarbon calibration purposes (section 3.6). The present section details the radiocarbon wiggle-matching (sections 5.3.2 and 5.4.1) undertaken to achieve this outcome, describing the principal wiggle-match model (OCM-7.1), as well as a host of supporting models to verify this modelled fit.

7.4.1 Principal Model (OCM-7.1)

For the principal model applied to wiggle-match the floating SG06 varve chronology to that of the IntCal09 (Reimer *et al*. 2009) absolute, dendrochronological timescale (OCM-7.1), it was decided to utilise only radiocarbon determinations from the section of the SG06 sediment profile that is both varved, and that is represented by the portion of IntCal09 composed entirely of tree-ring data. No data older than this terrestrial limit were incorporated into the model, so as to totally avoid the inclusion of any uncertainties pertaining to reservoir corrections, and thereby allowing the final SG06 chronology to be truly, "wholly terrestrial" (*sensu* Staff *et al*. 2009). Therefore, all radiocarbon determinations from SG06 plant macrofossils from composite core depths 1250 cm (the 'varve count top') to ≈ 1519 cm (a conservative approximation of the 'IntCal09 tree-ring limit' at 12,550 cal. BP) were entered into a single `P_Sequence` model, with the exception of: (i) three 'vsg' samples from NRCF-E and one vsg sample from ORAU falling below 0.5 mg combusted carbon yield (see section 7.5, below); and (ii) one sample (SUERC-28906) from an inter-laboratory duplicate

pair that failed the χ^2 test of age equivalence (section 7.2.3, above). The P_Sequence model used mean varve count (from the combined, 'floating' SG06 varve chronology of project colleagues M. Marshall and G. Schlolaut; section 7.3, above) as the z unit, with the total uncertainty of these varve count data used explicitly in determining the rigidity of the model. Thus, the k parameter of this P_Sequence was calculated to equal 7.44 (using equation 5.6; Bronk Ramsey 2008a):

$$[7.1] \quad k = \frac{M}{m} = \frac{2{,}600}{349} = 7.44$$

where: M represents the total varve-counted duration of the core section, 2,600 years (from 1250 cm CD, mean SG06 floating vyr -354, to an approximation of the IntCal09 tree-ring limit, 1519.1 cm CD, mean SG06 floating vyr 2,246); and m represents the total number of 'uncertain years' contained within this section (349 years), generated through calculation of the difference between the maximum and minimum possible varve counts over this time period.

No additional prior chronological information was applied to either of the boundaries in the model. Other than the model resolution being set to 1 year, all modelling parameters were the same as the OxCal default settings. An 'r-type' outlier model was implemented, with all radiocarbon determinations (R_F14C) and R_Combines given an equal (0.05) prior probability of being outliers. In total, 49 radiocarbon determinations were included in OCM-7.1 (25 from ORAU and 24 from NRCF-E), representing 44 separate depth horizons.

Additionally, OCM-7.1 included a 'date' (query function) at the position of the Holocene onset in SG06 (1436.4 cm CD), as identified from the multiple palaeoenvironmental proxy data obtained by Suigetsu Varves 2006 project colleagues. A 'difference' (query) function was also included, giving a probability density function (PDF) for the posterior age difference between the varve count top and IntCal09 tree-ring

limit. Since neither this `difference`, nor the Holocene onset `date`, included any additional prior information, these functions did not affect the model fit in any way (simply providing additional output from the underlying model). A truncated version of the model coding for this principal wiggle-match model is provided in figure 7.7, with the full model coding provided in appendix 8.

The results of the model fit show excellent agreement between the SG06 data and the IntCal09 calibration curve. Figure 7.8 illustrates a depth plot (against SG06 floating varve years) of these SG06 data against modelled age, with figure 7.9 showing this fit on to the calibration curve. The wiggle-match thus performed provides a date for the U-Oki tephra of 10,230 to 10,209 cal. BP at the 68.2% probability range (10,239 to 10,197 cal. BP at the 95.4% probability range; figure 7.10), which is added to the '0 year' of the floating SG06 varve chronology to define the datum point for the 'absolute' SG06 timescale to be used in the remainder of the Suigetsu Varves 2006 project.

The modelled age for the Holocene onset (figure 7.11) is 11,651 to 11,637 cal. BP at the 68.2% probability range (11,660 to 11,629 cal. BP at the 95.4% probability range), which is in excellent agreement with data from other sites. Principally amongst these, the new GSSP for the Holocene onset, that of the NGRIP ice core, gives an age of 11,650 cal. BP (11,700 b2k) for this event (Walker *et al*. 2009). More detailed discussion relating to this, and other, palaeoclimatic events in SG06 is beyond the scope of this thesis (instead, see Nakagawa *et al*. forthcoming), but the modelled age is nevertheless presented here as additional support for both the original, floating, SG06 varve count data, and the wiggle-match fit to the absolute age scale applied herein.

Figure 7.7: A truncated version of the OxCal coding applied for the principal wiggle-match model (OCM-7.1) of the floating SG06 varve chronology on to the IntCal09 (Reimer *et al.* 2009) 'absolute' timescale. (The full OxCal coding for this model specification is provided in appendix 8.)

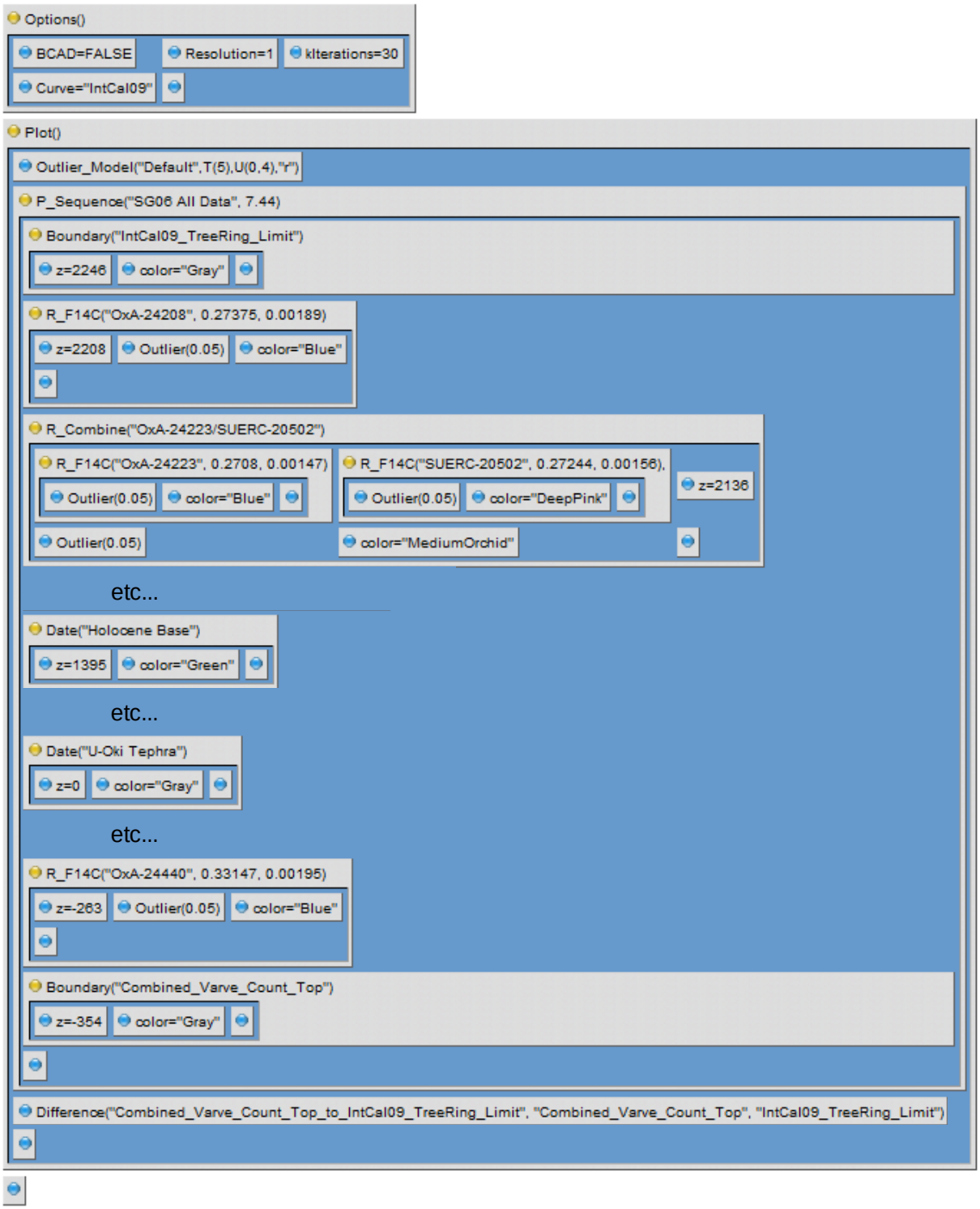

Figure 7.8: The modelled results of the principal wiggle-match model (OCM-7.1, calibrated against IntCal09; Reimer *et al*. 2009), as plotted against mean SG06 floating varve age. ORAU data are plotted in blue; NRCF-E data in magenta; and combined data, produced from inter-laboratory duplication, plotted in mauve. The posterior age-depth profile (the darker shading), overlies the prior, un-modelled probability density functions (lighter shading).

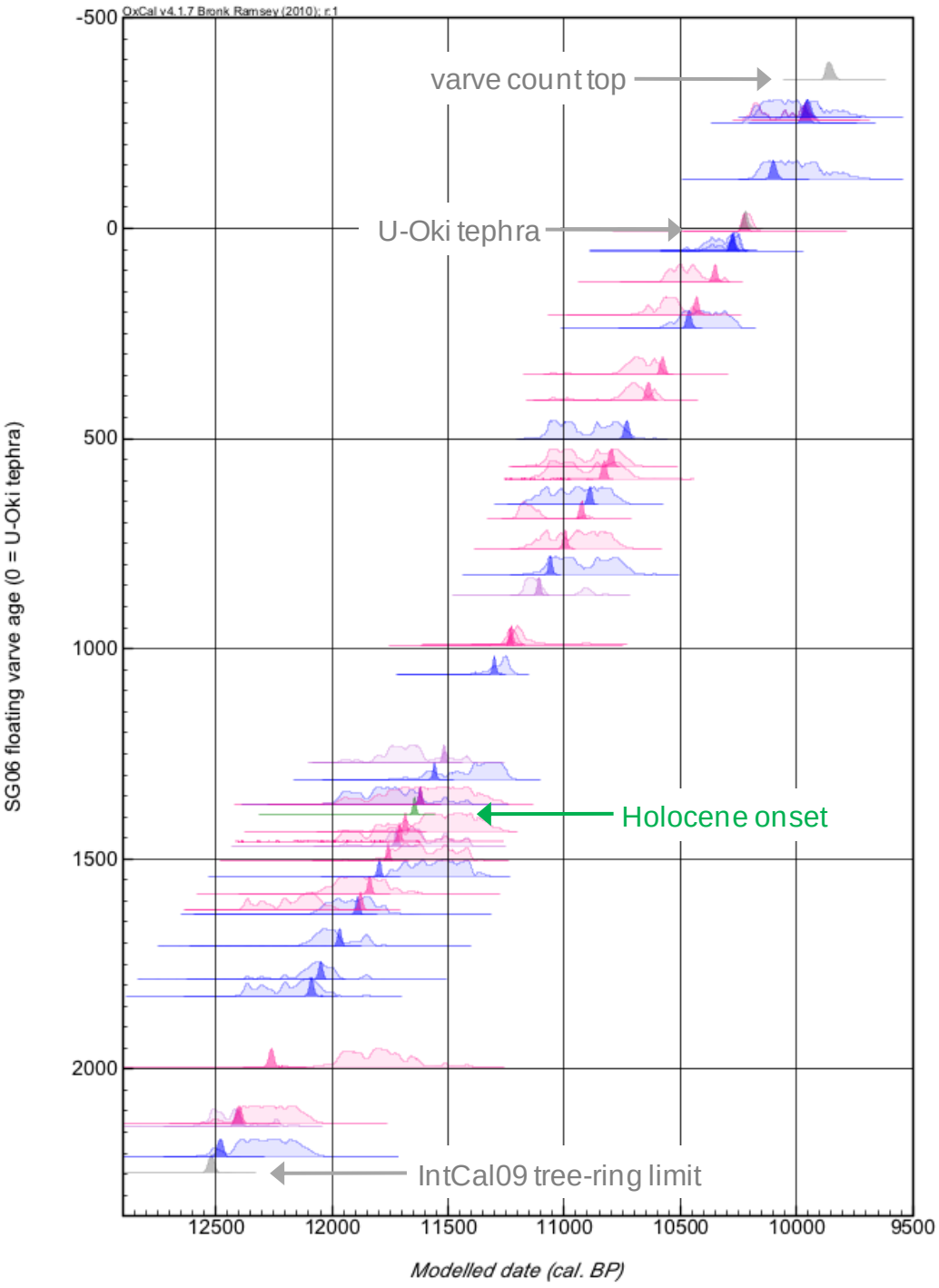

Figure 7.9: The modelled fit of the principal wiggle-match model (OCM-7.1) of the SG06 radiocarbon data on to the IntCal09 (Reimer *et al*. 2009) calibration curve (shown in lime green). ORAU data are plotted in blue; NRCF-E data in magenta; and combined data produced from inter-laboratory duplication plotted in mauve. For clarity, these data are shown at only the 1σ/68.2% confidence range. The alternative calibration datasets of IntCal04 (Reimer *et al*. 2004a; dark green), Hughen *et al*. (2006; light blue), and Fairbanks *et al*. (2005; gold) are also shown for reference. All calibration curves are plotted at 1σ uncertainty.

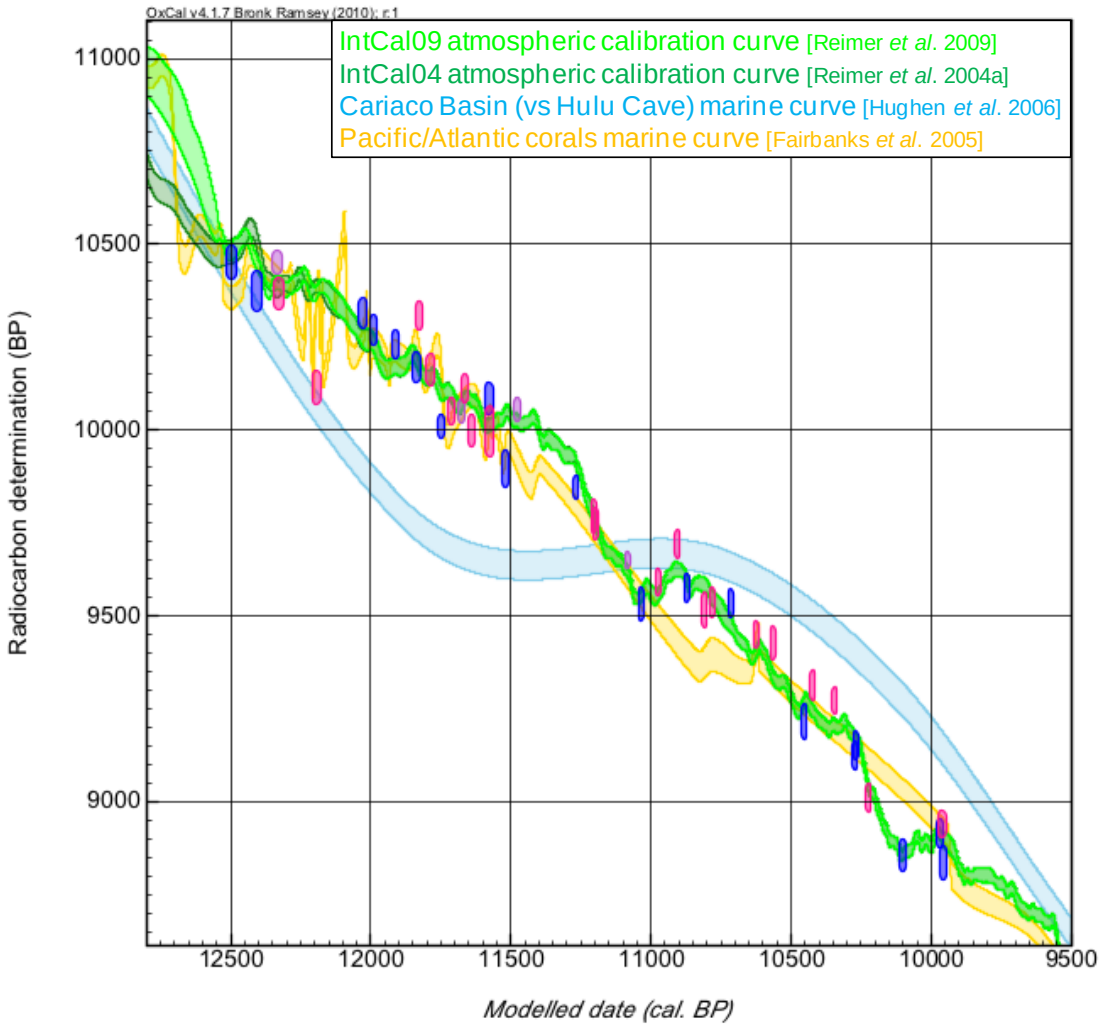

Figure 7.10: The modelled age of the U-Oki tephra, as generated by the principal wiggle-match model (OCM-7.1) of the SG06 radiocarbon data on to IntCal09 (Reimer *et al*. 2009).

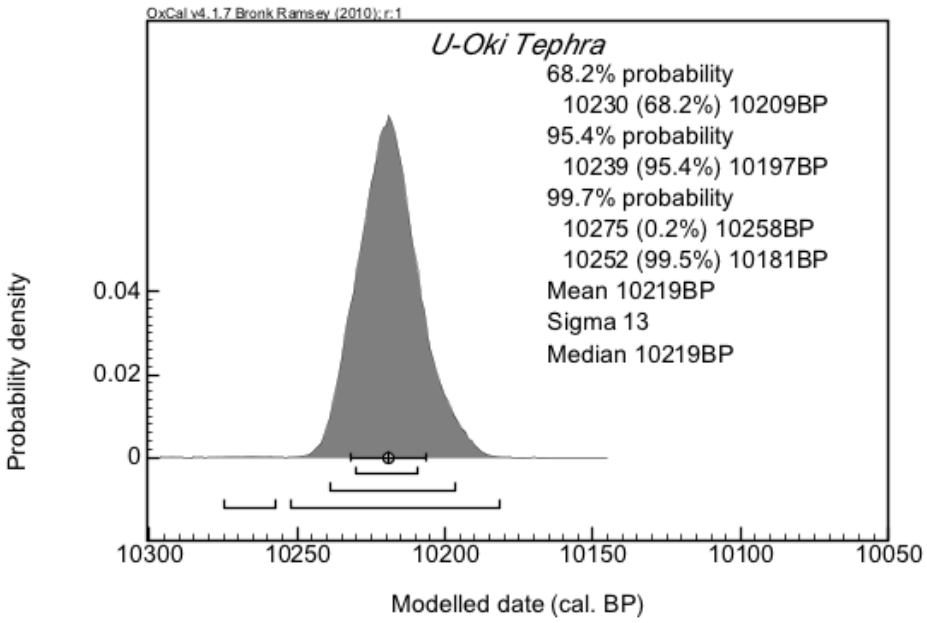

Figure 7.11: The modelled age of the Holocene onset at Lake Suigetsu (1436.4 cm composite depth), as generated by the principal wiggle-match model (OCM-7.1) of the SG06 radiocarbon data on to IntCal09 (Reimer *et al*. 2009).

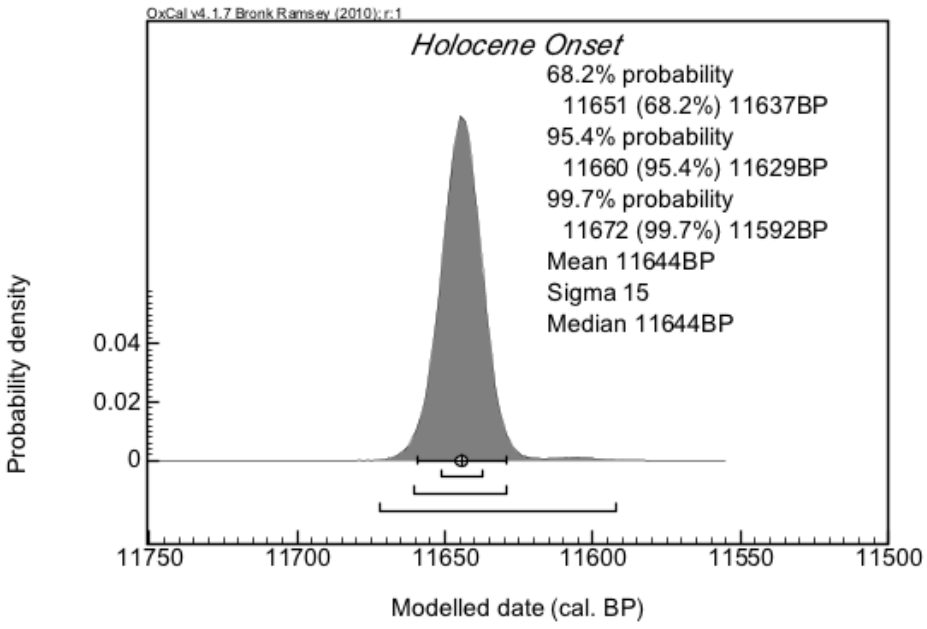

The modelled duration of the P_Sequence (between the varve count top and IntCal09 tree-ring limit) is 2,639 to 2,684 years at the 68.2% probability range (2,615 to 2,711 years at the 95.4% probability range; table 7.10), slightly longer than the original mean varve-counted duration of the core section (2,600 years), though well within the absolute minimum and maximum varve-counted values of 2,454 and 2,814 years, respectively.

7.4.2 Supporting Models

Due to the critical importance to the success of the broader Suigetsu varves 2006 project of tying the floating SG06 varve chronology to the absolute (IntCal09 dendrochronological) timescale, further models were run in OxCal, using different model specifications, to add weight to the findings of the principal wiggle-match model described above (OCM-7.1).

Firstly, a D_Sequence model (OCM-7.2) was run, using the same radiocarbon data and program settings as the principal model, but specifying (without uncertainties) the age gap between adjacent samples based upon the mean varve count data. A similar modelled fit to IntCal09 was obtained, with a bimodal 68.2% range for the age of the U-Oki tephra of 10,246 to 10,233 and 10,220 to 10,211 cal. BP (10,249 to 10,207 cal. BP at the 95.4% range). The total age range of this latter model (from the 'varve count top' to 'tree-ring limit') was 2,600 years (as defined by the varve count information), as opposed to the 2,639 to 2,684 year (68.2% probability range) duration generated from the P_Sequence model (OCM-7.1), where this value was not constrained *a priori*.

Other models, very similar in construction to OCM-7.1, were run with P_Sequence deposition models, but with varying values of k to test the modelling sensitivity to this parameter (OCM-7.4 to OCM-7.17). Sequence- (OCM-7.3) and U_Sequence- (OCM-7.18) models (equivalent to P_Sequences with 0 and infinite k values,

respectively) were also performed. An additional P_Sequence model (OCM-7.19), with a k value of 7.44 (like OCM-7.1), was run, but also including the five previously excluded measurements, so as to assess the effect of removing these samples. The results of all of these models, in terms of some of their key information (modelled age of the U-Oki tephra and duration of the SG06 core section between the varve count top and 1519.1 cm CD), are provided in table 7.10.

Table 7.10: The modelled age of the U-Oki tephra and modelled duration of the SG06 core depths ('varve count top' to 'IntCal09 tree-ring limit', 1250 to 1529.1 cm composite depth) utilised for the principal- and supporting wiggle-match models (OCM-7.1 to OCM-7.19) of the floating SG06 varve chronology on to the absolute (IntCal09; Reimer *et al*. 2009) timescale (as modelled against finalised SG06 varve depth). (* indicates a bimodal distribution.)

Model name	Model description	Modelled age of U-Oki tephra (cal. BP; 68.2%, and 95.4% probability ranges)	Modelled duration of sequence (varve count top to tree-ring limit; cal. years; 68.2%, and 95.4% probability ranges)
OCM-7.1	P_Sequence k = 7.44	10,230 to 10,209; 10,239 to 10,197	2,639 to 2,684; 2,615 to 2,711
OCM-7.2	D_Sequence	10,246 to 10,233 & 10,220 to 10,211*; 10,249 to 10,207	2,600
OCM-7.3	Sequence	10,215 to 10,135; 10,231 to 10,063	2,251 to 2,541; 2,136 to 2,697
OCM-7.4	P_Sequence k = 0.0744	10,229 to 10,197; 10,243 to 10,173	2,466 to 2,679; 2,359 to 2,762
OCM-7.5	P_Sequence k = 0.744	10,228 to 10,205; 10,238 to 10,192	2,626 to 2,699; 2,547 to 2,728
OCM-7.6	P_Sequence k = 1	10,228 to 10,207; 10,238 to 10,194	2,632 to 2,694; 2,564 to 2,726
OCM-7.7	P_Sequence k = 2.5	10,229 to 10,209; 10,238 to 10,196	2,638 to 2,689; 2,608 to 2,721

Table 7.10: (continued)**:**

Model name	Model description	Modelled age of U-Oki tephra (cal. BP; 68.2%, and 95.4% probability ranges)	Modelled duration of sequence (varve count top to tree-ring limit; cal. years; 68.2%, and 95.4% probability ranges)
OCM-7.8	P_Sequence k = 5	10,230 to 10,210; 10,240 to 10,196	2,637 to 2,683; 2,612 to 2,713
OCM-7.9	P_Sequence k = 6	10,230 to 10,209; 10,240 to 10,195	2,639 to 2,684; 2,617 to 2,711
OCM-7.10	P_Sequence k = 7	10,230 to 10,209; 10,239 to 10,196	2,637 to 2,683; 2,612 to 2,714
OCM-7.11	P_Sequence k = 8	10,230 to 10,209; 10,239 to 10,195	2,639 to 2,684; 2,617 to 2,712
OCM-7.12	P_Sequence k = 9	10,229 to 10,208; 10,238 to 10,195	2,640 to 2,685; 2,619 to 2,711
OCM-7.13	P_Sequence k = 10	10,230 to 10,209; 10,239 to 10,196	2,638 to 2,683; 2,616 to 2,710
OCM-7.14	P_Sequence k = 20	10,229 to 10,208; 10,238 to 10,195	2,639 to 2,683; 2,618 to 2,710
OCM-7.15	P_Sequence k = 50	10,228 to 10,207; 10,238 to 10,195	2,638 to 2,682; 2,618 to 2,708
OCM-7.16	P_Sequence k = 74.4	10,228 to 10,207; 10,238 to 10,195	2,640 to 2,683; 2,620 to 2,709
OCM-7.17	P_Sequence k = 744	10,227 to 10,206; 10,237 to 10,194	2,641 to 2,684; 2,621 to 2,710
OCM-7.18	U_Sequence	10,225 to 10,203; 10,235 to 10,191	2,645 to 2,690; 2,626 to 2,715
OCM-7.19	P_Sequence k = 7.44 5 additional samples included	10,223 to 10,201; 10,230 to 10,188	2,653 to 2,699; 2,633 to 2,723

The Sequence model (OCM-7.3), although including the varve count data as the z unit (as with all of the aforementioned models in section 7.4), does not actually make use of these data in performing its calculations, since the Sequence approach only utilises the relative order of the events within it (section 5.3). Therefore, OCM-7.3 is actually completely

independent of the varve count data (unlike all of the other preceding models). To obtain a more robust test of the varve count data, however, the additional stratigraphic information of core depth ('event-free'- rather than composite-; section 5.5) can be included in a model. The 'true test' of the varve count data entered into the principal wiggle-match model (OCM-7.1) is therefore obtained by running another P_Sequence model, but utilising EFD rather than varve count (OCM-7.20). As described in section 5.3.2a, a reliable value of k to be used with such 'pure depth' models can be calculated from the varve count data (equations 5.7 to 5.9). Thus, for OCM-7.20 k is found to equal 6.33 (table 7.11).

Clearly, this use of the varve count data in the calculation of k renders OCM-7.20 not 'truly independent' of the varve counting. Alternative supporting models were again run, therefore, utilising a Sequence (OCM-7.21), U_Sequence (OCM-7.33) and further P_Sequences with differing values for k (OCM-7.22 to OCM-7.32). An equivalent P_Sequence model to OCM-7.20 (k = 6.33) was also run, including the five otherwise excluded measurements (OCM-7.34). The key information from each of these models is summarised in Table 7.12.

In all of the above supporting models (OCM-7.2 to OCM-7.34), the modelled age of the U-Oki tephra is in excellent agreement with that of the principal model, OCM-7.1. Therefore strong support is provided for the placement of the floating SG06 varve chronology on to the absolute (IntCal09) timescale. This lack of sensitivity to the rigidity of these age-depth models is largely a function of the serendipitous coincidence of the eruption of the U-Oki tephra with the middle of a steep incline in the calibration curve between *circa* 10,300 and 10,125 cal. BP (illustrated in figure 7.9).

Table 7.11: Calculation of the optimal value of k for a P_Sequence model based upon event-free depth (EFD) units, using the varve count information from the same core section (the 'varve count top' to 'IntCal09 tree-ring limit', 1250 to 1529.1 cm composite depth). The total varve-counted section (2,600 SG06 vyr) is divided into eight equal sections, with equivalent EFD (cm) given for the top ('from'), bottom ('to'), and '150 varves from the top' ('through') of each of these contiguous eight sections (equivalent to stratigraphic horizons 1, 2 and 3 of figure 5.2). The differences (in EFD) between these respective horizons (u_i and v_i) are calculated, and equations 5.7 to 5.9 subsequently applied to yield k.

Section:	1	2	3	4	5	6	7	8
Varves in block ($p_i + q_i$)	325	325	325	325	325	325	325	325
EFD from:	1227.4	1260.0	1292.9	1326.4	1358.9	1389.5	1423.2	1453.8
EFD through:	1242.3	1274.9	1308.8	1342.0	1372.9	1405.7	1437.6	1468.2
EFD to:	1260.0	1292.9	1326.4	1358.9	1389.5	1423.2	1453.8	1485.0
$u_i + v_i$	32.6	32.9	33.5	32.5	30.6	33.7	30.6	31.2
u_i	14.9	14.9	15.9	15.6	14.0	16.2	14.4	14.4
v_i	17.7	18.0	17.6	16.9	16.6	17.5	16.2	16.8
$U_i = u_i / (u_i + v_i)$	0.457	0.453	0.475	0.48	0.458	0.481	0.471	0.462
$V_i = v_i / (u_i + v_i)$	0.543	0.547	0.525	0.52	0.542	0.519	0.529	0.538
$\mu_U = 0.467$; $\mu_V = 0.533$; $\sigma_U = 0.011$; $\sigma_V = 0.011$								
$k = \mu_U\mu_V / [\sigma_U\sigma_V\ (p_i + q_i)] = 6.330$								

Table 7.12: The modelled age of the U-Oki tephra and modelled duration of the SG06 core depths ('varve count top' to 'IntCal09 tree-ring limit', 1250 to 1529.1 cm composite depth) utilised for the supporting wiggle-match models (OCM-7.20 to OCM-7.34) of the floating SG06 varve chronology on to the absolute (IntCal09; Reimer *et al*. 2009) timescale (as modelled against SG06 event-free depth). (* indicates bimodal distributions.)

Model name	Model description	Modelled age of U-Oki tephra (cal. BP; 68.2%, and 95.4% probability ranges)	Modelled duration of sequence (varve count top to tree-ring limit; cal. years; 68.2%, and 95.4% probability ranges)
OCM-7.20	P_Sequence k = 6.33	10,226 to 10,202; 10,236 to 10,189	2,555 to 2,603 & 2,621 to 2,695*; 2,497 to 2,729
OCM-7.21	Sequence	10,215 to 10,136; 10,231 to 10,064	2,248 to 2,534; 2,130 to 2,708
OCM-7.22	P_Sequence k = 0.0633	10,233 to 10,188; 10,252 to 10,126	2,166 to 2,495; 2,020 to 2,721
OCM-7.23	P_Sequence k = 0.633	10,229 to 10,195; 10,243 to 10,170	2,413 to 2,650; 2,322 to 2,759
OCM-7.24	P_Sequence k = 1	10,228 to 10,196; 10,241 to 10,174	2,472 to 2,692; 2,371 to 2,766
OCM-7.25	P_Sequence k = 2.5	10,225 to 10,198; 10,237 to 10,182	2,543 to 2,706; 2,446 to 2,747
OCM-7.26	P_Sequence k = 5	10,225 to 10,201; 10,236 to 10,187	2,551 to 2,601 & 2,616 to 2,697*; 2,483 to 2,730
OCM-7.27	P_Sequence k = 7.5	10,226 to 10,203; 10,237 to 10,189	2,545 to 2,605 & 2,624 to 2,689*; 2,488 to 2,722
OCM-7.28	P_Sequence k = 10	10,226 to 10,204; 10,236 to 10,191	2,557 to 2,599 to 2,627 to 2,695*; 2,520 to 2,722
OCM-7.29	P_Sequence k = 25	10,227 to 10,206; 10,236 to 10,192	2,560 to 2,598 & 2,636 to 2,694*; 2,539 to 2,716
OCM-7.30	P_Sequence k = 50	10,229 to 10,209; 10,237 to 10,192	2,558 to 2,602 & 2,638 to 2,681; 2,538 to 2,706
OCM-7.31	P_Sequence k = 63.3	10,230 to 10,210; 10,238 to 10,193	2,553 to 2,606 & 2,641 to 2,671*; 2,533 to 2,703
OCM-7.32	P_Sequence k = 633	10,232 to 10,212; 10,238 to 10,190	2,555 to 2,611 & 2,650 to 2,662*; 2,539 to 2,698
OCM-7.33	U_Sequence	10,233 to 10,205; 10,236 to 10,185	2,562 to 2,607 & 2,650 to 2,687*; 2,549 to 2,707

Table 7.12 (continued):

Model name	Model description	Modelled age of U-Oki tephra (cal. BP; 68.2%, and 95.4% probability ranges)	Modelled duration of sequence (varve count top to tree-ring limit; cal. years; 68.2%, and 95.4% probability ranges)
OCM-7.34	P_Sequence k = 6.33 5 additional samples included	10,221 to 10,196; 10,231 to 10,184	2,631 to 2,735; 2,544 to 2,757

Further supporting models were run utilising the additional data provided by the radiocarbon determinations obtained from the non-varved portion of SG06 from the core top to 1250 cm composite depth. As with all preceding models in the present chapter, these data are free from any assumptions of reservoir corrections since this time period is entirely represented by the dendro-dated portion of IntCal09. As well as the five radiocarbon determinations excluded from analysis from the lower core section (1250 cm composite depth to the IntCal09 tree-ring limit), an additional six determinations were excluded from further analysis from the upper core section (0 to 1250 cm composite depth). These excluded samples comprised: (i) two experimental 'vsg' duplicates of previously dated 'G' samples at ORAU; (ii) two further 'vsg' samples from NRCF-E falling below the 0.5 mg C threshold; and (iii) two samples (OxA-X-2248-48 and OxA-X-2345-23) from duplicate pairs that failed the χ^2 test of age equivalence (sections 7.2.2 and 7.2.3, above). The first of these models (OCM-7.35) utilised a single P_Sequence (against event-free depth) through the entirety of this depth range, with an applied k value of 6.33, as determined from table 7.11, above. Again, additional models (OCM-7.36 to OCM-7.48) were run to assess the sensitivity of k (table 7.13), and a further model (OCM-7.49) to test the effect of removing the additional six excluded samples.

Table 7.13: The modelled age of the U-Oki tephra and modelled duration of the SG06 core depths ('varve count top' to 'IntCal09 tree-ring limit', 1250 to 1529.1 cm composite depth) utilised for the supporting wiggle-match models (OCM-7.35 to OCM-7.49) of the floating SG06 varve chronology on to the absolute (IntCal09; Reimer *et al*. 2009) timescale (as modelled against SG06 event-free depth). (* indicates bimodal distributions.)

Model name	Model description	Modelled age of U-Oki tephra (cal. BP; 68.2%, and 95.4% probability ranges)	Modelled duration of sequence (varve count top to tree-ring limit; cal. years; 68.2%, and 95.4% probability ranges)
OCM-7.35	P_Sequence k = 6.33	10,239 to 10,211; 10,286 to 10,256 & 10,252 to 10,200*	2,382 to 2,464; 2,321 to 2,508
OCM-7.36	Sequence	10,211 to 10,122; 10,230 to 10,052	2,376 to 2,655; 2,275 to 2,816
OCM-7.37	P_Sequence k = 0.0633	10,236 to 10,187; 10,260 to 10,108	2,266 to 2,524; 2,152 to 2,692
OCM-7.38	P_Sequence k = 0.633	10,230 to 10,196; 10,244 to 10,171	2,375 to 2,559; 2,318 to 2,660
OCM-7.39	P_Sequence k = 1	10,229 to 10,198; 10,245 to 10,174	2,388 to 2,550; 2,338 to 2,647
OCM-7.40	P_Sequence k = 2.5	10,231 to 10,203; 10,252 to 10,179	2,409 to 2,522; 2,361 to 2,587
OCM-7.41	P_Sequence k = 5	10,236 to 10,209; 10,286 to 10,194	2,392 to 2,489; 2,344 to 2,548
OCM-7.42	P_Sequence k = 7.5	10,243 to 10,210; 10,291 to 10,203	2,370 to 2,455; 2,311 to 2,484
OCM-7.43	P_Sequence k = 10	10,281 to 10,266 & 10,243 to 10,216*; 10,296 to 10,209	2,362 to 2,443; 2,309 to 2,472
OCM-7.44	P_Sequence k = 25	10,283 to 10,255 & 10,242 to 10,235*; 10,290 to 10,226	2,326 to 2,385; 2,306 to 2,418
OCM-7.45	P_Sequence k = 50	10,277 to 10,251; 10,284 to 10,234	2,328 to 2,364; 2,312 to 2,389
OCM-7.46	P_Sequence k = 63.3	10,273 to 10,250; 10,282 to 10,235	2,332 to 2,363; 2,312 to 2,391

Table 7.13 (continued):

Model name	Model description	Modelled age of U-Oki tephra (cal. BP; 68.2%, and 95.4% probability ranges)	Modelled duration of sequence (varve count top to tree-ring limit; cal. years; 68.2%, and 95.4% probability ranges)
OCM-7.47	P_Sequence k = 633	10,282 to 10,268 & 10,265 to 10,248*; 10,289 to 10,220	2,323 to 2,383; 2,308 to 2,468
OCM-7.48	U_Sequence	Model unable to find a solution.	
OCM-7.49	P_Sequence k = 6.33 11 additional samples included	Model unable to find a solution.	

Finally for the present section, additional models (OCM-7.50 to 7.67) were run that utilised the varve count data for the lower core section, and event-free depth data for the upper core section (where reliable varve counting could not be performed). These models consisted of two separate sequences, linked such that the upper boundary of the lower sequence (the 'varve count top') was equal to the lower boundary of the upper sequence. Such models would, arguably, provide the most rigorous age-depth modelling of the entire sequence, since the available SG06 dataset was much larger (174 radiocarbon determinations included, 88 from ORAU and 86 from NRCF-E, at 155 separate depth horizons), and relative varve age information (more precise in terms of accounting for the inter-annual variations in deposition rate than simply using event-free depth) are included. However, these models were not chosen to provide the principal wiggle-matching model since the position of the 'varve count top' boundary was found to be sensitive to the value of k implemented. The relative proximity of the U-Oki tephra to the varve count top meant that the posterior distribution for the former date was significantly influenced by the modelled age of the latter. Thus, data well above the U-Oki tephra stratigraphically, were imposing an undue influence on the age of the tephra. An interpretation drawn from these models, therefore, is that the deposition rate in

SG06 above the U-Oki tephra is not as regular as in the varve-counted section. (I.e. the upper core section requires a lower value of k than was extrapolated from the lower section.) The key information from these models is summarised in Table 7.14.

Table 7.14: The modelled age of the U-Oki tephra and modelled duration of the SG06 core depths ('varve count top' to 'IntCal09 tree-ring limit', 1250 to 1529.1 cm composite depth) utilised for the supporting wiggle-match models (OCM-7.50 to OCM-7.67) of the floating SG06 varve chronology onto the absolute (IntCal09; Reimer *et al*. 2009) timescale. Only the model specification of the upper core section (modelled against SG06 event-free depth) is altered, with the lower core section (modelled against finalised SG06 varve depth) using a P_Sequence, with k = 7.44. (* indicates bimodal distributions; † indicates trimodal distributions.)

Model name	Model description of upper core section	Modelled age of U-Oki tephra (cal. BP; 68.2%, and 95.4% probability ranges)	Modelled duration of sequence (varve count top to tree-ring limit; cal. years; 68.2%, and 95.4% probability ranges)
OCM-7.50	P_Sequence k = 7.44	10,237 to 10,219; 10,305 to 10,289, 10,270 to 10,263 & 10,248 to 10,206†	2,622 to 2,662; 2,551 to 2,686
OCM-7.51	D_Sequence	10,247 to 10,235; 10,253 to 10,215	2,600
OCM-7.52	P_Sequence k = 0.0744	10,230 to 10,197; 10,245 to 10,172	2,482 to 2,655; 2,378 to 2,698
OCM-7.53	P_Sequence k = 0.744	10,232 to 10,210; 10,249 to 10,192	2,596 to 2,672; 2,513 to 2,688
OCM-7.54	P_Sequence k = 1	10,234 to 10,211; 10,283 to 10,265 & 10,250 to 10,196*	2,601 to 2,672; 2,521 to 2,685
OCM-7.55	P_Sequence k = 2.5	10,237 to 10,215; 10,306 to 10,267 & 10,247 to 10,204*	2,617 to 2,666; 2,539 to 2,688

Table 7.14 (continued):

Model name	Model description of upper core section	Modelled age of U-Oki tephra (cal. BP; 68.2%, and 95.4% probability ranges)	Modelled duration of sequence (varve count top to tree-ring limit; cal. years; 68.2%, and 95.4% probability ranges)
OCM-7.56	P_Sequence k = 5	10,293 to 10,280 & 10,238 to 10,217; 10,310 to 10,270 & 10,245 to 10,209*	2,621 to 2,664; 2,558 to 2,686
OCM-7.57	P_Sequence k = 6	10,297 to 10,280 & 10,237 to 10,219; 10,308 to 10,270 & 10,244 to 10,211*	2,621 to 2,662; 2,559 to 2,686
OCM-7.58	P_Sequence k = 7	10,237 to 10,220; 10,268 to 10,263 & 10,248 to 10,207*	2,622 to 2,662; 2,552 to 2,686
OCM-7.59	P_Sequence k = 8	10,237 to 10,220; 10,295 to 10,288, 10,271 to 10,261 & 10,249 to 10,206†	2,621 to 2,661; 2,545 to 2,686
OCM-7.60	P_Sequence k = 9	10,296 to 10,273 & 10,231 to 10,230; 10,303 to 10,264 & 10,241 to 10,215*	2,621 to 2,661; 2,562 to 2,588 & 2,599 to 2,685*
OCM-7.61	P_Sequence k = 10	10,238 to 10,219; 10,299 to 10,285, 10,269 to 10,262 & 10,248 to 10,207†	2,622 to 2,662; 2,544 to 2,688
OCM-7.62	P_Sequence k = 20	10,300 to 10,285 & 10,238 to 10,221; 10,309 to 10,279 & 10,245 to 10,211*	2,621 to 2,660; 2,502 to 2,537, 2,544 to 2,584 & 2,596 to 2,685†
OCM-7.63	P_Sequence k = 50	10,297 to 10,273 & 10,236 to 10,213; 10,302 to 10,257 & 10,241 to 10,210*	2,626 to 2,662; 2,566 to 2,581 & 2,592 to 2,691*
OCM-7.64	P_Sequence k = 74.4	10,296 to 10,274 & 10,236 to 10,226; 10,299 to 10,269 & 10,243 to 10,213*	2,627 to 2,666; 2,569 to 2,694
OCM-7.65	P_Sequence k = 744	10,301 to 10,265 & 10,239 to 10,226; 10,305 to 10,264 & 10,245 to 10,214*	2,618 to 2,675; 2,553 to 2,703

Table 7.14 (continued):

Model name	Model description of upper core section	Modelled age of U-Oki tephra (cal. BP; 68.2%, and 95.4% probability ranges)	Modelled duration of sequence (varve count top to tree-ring limit; cal. years; 68.2%, and 95.4% probability ranges)
OCM-7.66	U_Sequence	Model unable to find a solution.	
OCM-7.67	P_Sequence k = 7.44 11 additional samples included	Model unable to find a solution.	

7.5 'Outlier' Detection and Removal

Inevitably the raw radiocarbon dataset produced from the SG06 plant macrofossil samples includes a number of erroneous, 'outlying' data points (illustrated in figure 7.4). Statistically, one might expect that ≈ 5% of the radiocarbon determinations would be outlying (at 2σ probability), based on AMS counting statistics alone. Rather than representing authentic variation in the radiocarbon calibration curve, we know that certain of these determinations must be erroneous (reflecting methodological error), since a number of measurements are of duplicate samples that were found not to be in statistical agreement (sections 7.2.2 and 7.2.3). By extrapolation, one would expect that such erroneous data would not be confined to duplicated samples, and so an objective means of identifying (and removing) such data was sought. Prior to presentation of the 'finalised' SG06 radiocarbon calibration dataset ('finalised' for the present thesis, rather than for the Suigetsu Varves 2006 project, which will require the completion of the dual varve counting across the entire range of the radiocarbon method), therefore, an objective means of screening the raw dataset for the most marked outliers was applied. The rationale behind the outlier detection method applied was that any significant deviations in the calibration curve would need to be supported by at

least two separate measurements (i.e. excluding all 'unsupported' data points). The outlier detection algorithm applied was therefore derived as follows:

- The 599 background-corrected SG06 plant macrofossil samples were arranged in stratigraphic order and an equivalent $\Delta^{14}C$ value obtained from the samples' $F^{14}C$ data ('$\Delta^{14}C_0$'). For samples obtained from below 1250 cm CD, the calendar age required for $\Delta^{14}C$ calculation was obtained directly from the SG06 vyr timescale (i.e. SG06 floating varve year plus the wiggle-matched age obtained for the U-Oki tephra from OCM-7.1). Above 1250 cm CD, the calendar age assigned to each dated horizon was obtained through calibration of the SG06 radiocarbon data from this uppermost core section on to the IntCal09 (Reimer *et al*. 2009) timescale (using a `P_Sequence` OxCal model, OCM-7.68, which is a truncation of OCM-7.35, but that does not continue below 1250 cm CD to the IntCal09 tree-ring limit).
- A weighted mean comparison $\Delta^{14}C$ value ('$\Delta^{14}C_{comp}$') was calculated for each dated sample based upon the values of the two adjacent dated depth horizons below, and two adjacent dated depth horizons above (weighted so that the nearer two sample depths contributed twice as much as the further two depths). As an aside, this $\Delta^{14}C_{comp}$ was what was used to define the 'expected age' of samples as quoted alongside the measured radiocarbon determinations throughout section 7.2, above.
- A test statistic, x, was subsequently calculated, by:

$$[7.2] \quad x = \frac{\Delta^{14}C_0 - \Delta^{14}C_{comp}}{\sqrt{(\sigma_0)^2 + (\sigma_{comp})^2}}$$

where: σ_0 is the uncertainty on the calculated $\Delta^{14}C$ value of the original sample measurement ($\Delta^{14}C_0$), and σ_{comp} is the uncertainty on the weighted mean comparison $\Delta^{14}C$ value ($\Delta^{14}C_{comp}$).

- The first samples to be excluded as outliers were those from duplicated depth horizons (either intra- or inter-laboratory duplicates, sections 7.2.2 and 7.2.3) that had failed the test of

age equivalence. The most outlying individual sample from each of these duplicated sampling depths was excluded on the basis of their demonstrating the highest value for x (i.e. the greatest difference in $\Delta^{14}C$ as compared to proximal dated samples). If more than two dated samples were obtained from a non-coeval duplicated sampling depth, the remaining contributing sub-samples, after the removal of the first, were again tested for age equivalence and, if still non-coeval, an additional sub-sample was excluded from that sampling horizon following the same exclusion procedure.

- With the non-coeval duplicated samples having been dealt with, the remaining dated depth horizons were subsequently examined. Firstly, those samples were excluded where both a $\Delta^{14}C$ shift of > 400‰ was demonstrated from the adjacent four dated sample horizons (again, two above and two below), and where the value of x exceeded four (i.e. where the $\Delta^{14}C$ value of the individual sample was > 4σ from the weighted mean of the adjacent four dated horizons, $\Delta^{14}C_{comp}$).
- Secondly, just those samples demonstrating a $\Delta^{14}C$ shift of > 400‰ from the adjacent four (two above and two below) dated depth horizons were excluded.
- And thirdly, those samples were excluded where x > 4 ($\Delta^{14}C_0$ was > 4σ from $\Delta^{14}C_{comp}$), and for which $\Delta^{14}C_0$ was the maximum or minimum of the samples from the adjacent four dated depth horizons. This latter criterion made sure that the excluded sample was 'unsupported' by any of the surrounding measurements, and was therefore more likely to be erroneous. (I.e. there were examples where x > 4, but where $\Delta^{14}C_0$ was not 'outside' of the range of the values from adjacent samples, and therefore these data points were retained on the basis of their being 'supported' by alternative measurements.)

The methodology thus derived was necessarily undertaken step-wise, with the most extreme outliers removed first, since these outlying data also influenced adjacent samples'

$\Delta^{14}C_{comp}$ values, and therefore caused additional data to appear 'erroneous'. Thus, excluding all apparent outliers in one sweep would have incorrectly removed too many data points.

In total, thirteen samples were excluded from non-coeval duplicated depth horizons; seven were excluded with both a $\Delta^{14}C$ shift of > 400‰ and > 4σ from adjacent samples; six were excluded with just a $\Delta^{14}C$ shift of > 400‰; and a further fifteen samples were excluded with data > 4σ from adjacent samples. These excluded samples are listed in table 7.15.

Thus, the outlier detection procedure is relatively conservative, attempting to only exclude the most obvious 'erroneous' data, and leaving in as much potentially authentic 'noise' in the $\Delta^{14}C$ record as would seem maximally reasonable. A harsher criterion was applied to the samples from duplicated depth horizons (excluding non-consistent samples at the 95.4% confidence level) since these are data that must represent the same original $\Delta^{14}C$ concentration. The more lenient 4σ (and 400‰) criteria for adjacent sampling depths are to allow for potentially real variation in the atmospheric radiocarbon concentration over time, although it is acknowledged that the remaining data almost certainly include some additional outlying values as compared to the theoretical 'true' atmospheric calibration curve.

It can additionally be seen that the smallest samples (vsgs) were preferentially represented amongst the excluded samples (statistically significant at the 90% significance level, but not at the 95% significance level; table 7.16). As has been reiterated, this is most likely due to the increased susceptibility of smaller samples to given quantities of contamination (section 4.3.1). This is a separate, though related, issue to the size-dependency of the background correction identified in section 7.2.1, and accounts for the more extreme outlying values, rather than the consistent size effects described previously. The slightly higher number of outliers at ORAU (22, compared to the 19 at NRCF-E), is also likely to be a result of the higher number of very small samples attempted at the ORAU facility (figure 7.12).

Table 7.15: The SG06 plant macrofossil radiocarbon measurements determined to be outliers, and removed from subsequent data analysis.

	SG06 sample ID (#)	Sample type	SG06 CD (cm)	SG06 EFD (cm)	SG06 yr BP	Expected radiocarbon age (BP)	AMS target ID	Target type	C yield (mg)	Conventional radiocarbon date (± 1σ)
Non-coeval duplicates:	307	Ev.br.leaf	108.4	107.9	371	444	OxA-X-2248-48	G	1.868	730 ± 24
	780	Ev.br.leaf	773.0	759.0	5,441	4,794	SUERC-28203	g	2.030	4,625 ± 35
	847	Dec.br.leaf	1259.6	1236.8	9,956	8,947	SUERC-28906	g	0.520	8,730 ± 45
	197	Dec.br.leaf	2190.6	2132.8	23,055	19,762	SUERC-13333	g	0.589	19,137 ± 123
	197	Dec.br.leaf	2190.6	2132.8	23,055	19,762	OxA-X-2219-17	vsg	0.480	20,181 ± 189
	217	Dec.br.leaf	2488.9	2417.5	28,425	24,315	SUERC-17723	g	1.125	21,743 ± 165
	1007	Dec.br.leaf	3051.1	2930.9	36,709	33,808	OxA-X-2357-20	g	1.284	32,662 ± 487
	246	Dec.br.leaf	3163.4	3031.6	38,420	35,141	SUERC-19064	vsg	0.482	27,308 ± 402
	247	Dec.br.leaf	3174.3	3042.5	38,604	35,161	SUERC-16527	vsg	0.434	32,838 ± 885
	1135b	Bark	3360.9	3226.8	41,616	38,475	SUERC-29853	g	3.777	38,721 ± 617
	747	Twig	3541.8	3403.7	44,545	41,546	OxA-X-2360-43	G	1.835	38,751 ± 729
	291	Dec.br.leaf	3796.7	3646.9	48,351	44,162	SUERC-13334	g	1.286	39,129 ± 844
	939	Dec.br.leaf	3977.9	3823.0	51,323	47,321	OxA-X-2360-48	G	1.604	42,927 ± 1,294
>400‰ and >4σ:	97	Dec.br.leaf	1408.7	1377.5	11,368	9,927	SUERC-19061	vsg	0.107	6,968 ± 94
	188	Dec.br.leaf	2015.5	1963.7	19,893	16,974	SUERC-19062	vsg	0.386	14,409 ± 94
	1067	Dec.br.leaf	2779.6	2664.1	32,197	28,167	SUERC-29834	vsg	0.471	24,023 ± 279
	238	Dec.br.leaf	3010.1	2890.9	36,081	33,452	SUERC-17724	g	1.018	30,514 ± 489
	270	Dec.br.leaf	3467.0	3329.4	43,408	41,122	SUERC-26008	g	0.536	32,998 ± 764
	759	Dec.br.leaf	3756.7	3606.9	47,697	44,253	SUERC-28898	g	1.002	37,332 ± 796
	302	Dec.br.leaf	4103.0	3948.1	53,539	49,161	SUERC-18131	g	0.964	38,448 ± 1,247
>400‰:	242	Dec.br.leaf	3071.7	2951.5	37,028	34,711	OxA-X-2374-11	vsg	0.482	31,029 ± 944
	1100	Dec.br.leaf	3461.7	3324.1	43,321	41,167	OxA-X-2362-50	g	0.602	34,975 ± 1,217
	497	Dec.br.leaf	3818.9	3669.1	48,718	46,294	OxA-X-2340-29	g	0.832	41,442 ± 1,445
	959	Dec.br.leaf	3861.7	3709.0	49,373	45,730	OxA-X-2374-18	vsg	0.440	41,404 ± 3,221
	936	Dec.br.leaf	3951.3	3796.5	50,827	46,635	OxA-X-2362-19	g	0.649	41,582 ± 2,367
	649	Dec.br.leaf	4113.0	3958.2	53,713	49,353	OxA-X-2362-20	g	0.798	42,269 ± 2,140

Table 7.15 (continued):

	SG06 sample ID (#)	Sample type	SG06 CD (cm)	SG06 EFD (cm)	SG06 yr BP	Expected radiocarbon age (BP)	AMS target ID	Target type	C yield (mg)	Conventional radiocarbon date (± 1σ)
>4σ (and 'outside'):	308	Twig	136.4	135.9	505	591	OxA-X-2270-49	G	2.769	436 ± 25
	528	Dec.br.leaf	392.9	384.9	2,396	2,337	OxA-X-2347-43	G	2.435	2,227 ± 24
	319	Ev.br.leaf	439.9	430.9	2,794	2,697	OxA-X-2297-56	G	2.120	2,493 ± 25
	319	Ev.br.leaf	439.9	430.9	2,794	2,697	OxA-X-2303-36	g	0.875	2,487 ± 27
	786	Dec.br.leaf	748.3	734.8	5,254	4,680	OxA-X-2360-44	G	1.993	4,427 ± 32
	429	Ev.br.leaf	960.5	945.5	7,209	6,311	OxA-X-2339-40	G	2.402	6,042 ± 34
	50	Ev.br.leaf	969.8	952.0	7,282	6,370	SUERC-17117	g	10.446	6,129 ± 38
	382	Dec.br.leaf	1077.5	1055.3	8,338	7,527	OxA-X-2297-53	g	1.000	7,878 ± 41
	76	Dec.br.leaf	1257.7	1234.9	9,937	8,931	SUERC-16524	vsg	0.204	8,512 ± 71
	135	Dec.br.leaf	1495.2	1461.1	12,213	10,391	SUERC-17726	g	1.179	10,141 ± 46
	124	Dec.br.leaf	1565.1	1531.0	13,002	10,962	OxA-X-2219-16	vsg	0.414	11,339 ± 80
	130	Dec.br.leaf	1591.4	1556.9	13,288	11,365	SUERC-17720	g	1.446	11,016 ± 49
	140	Dec.br.leaf	1596.4	1561.8	13,344	11,476	OxA-X-2297-42	g	0.901	11,916 ± 53
	174	Dec.br.leaf	1843.0	1801.4	16,895	14,352	OxA-X-2245-19	g	0.736	13,852 ± 78
	352	Dec.br.leaf	2512.2	2438.7	28,808	24,593	OxA-X-2362-11	g	0.673	22,980 ± 268

Table 7.16: Contingency table assessing the relationship between sample size (in terms of mass of combusted carbon) and the designation of radiocarbon determinations as outliers (according to the protocol described above). Cells are necessarily combined such that the expected values (E_i) ≥ 5 (Attwood *et al*. 2000, p.79.)

H_0: designation of radiocarbon determinations as outliers is independent of sample size (mass of combusted carbon).

H_1: designation of radiocarbon determinations as outliers is dependent upon sample size (mass of combusted carbon).

		Mass of combusted carbon (mg)					
		0 - 0.6	0.6 - 1.2	1.2 - 1.8	1.8 - 2.4	> 2.4	Total:
Targets designated as outliers	Observed, O_i	13	14	4	5	5	41
	Expected, E_i	6.44	14.82	6.58	5.68	7.48	
	$(O_i - E_i)^2 / E_i$	6.680	0.045	1.011	0.081	0.822	
Targets designated as non-outliers	Observed, O_i	80	200	91	77	103	551
	Expected, E_i	86.56	199.18	88.42	76.32	100.52	
	$(O_i - E_i)^2 / E_i$	0.497	0.003	0.075	0.006	0.061	
	Total:	93	214	95	82	108	592

Critical value, χ^2_4 (at the 95% significance level; 4 degrees of freedom) = 9.488 (see appendix 6).

Since $\Sigma (O_i - E_i)^2 / E_i$ (9.282) does not exceed χ^2_4 (9.488), there is insufficient evidence to reject the null hypothesis, H_0 (at the 95% significance level): sample size and designation of radiocarbon determinations as outliers are independent. (However, at the 90% significance level - critical value of χ^2_4 = 7.779 - H_0 would be rejected: sample size and designation of radiocarbon determinations as outliers would not be independent.)

Figure 7.12: Histogram illustrating the relative size distribution (in terms of mass of combusted C) of SG06 plant macrofossil radiocarbon determinations obtained at the ORAU and NRCF-E facilities. Non-outlying ORAU samples are plotted in blue; outlying ORAU data are plotted in light blue; non-outlying NRCF-E data are plotted in magenta; and outlying NRCF-E data are plotted in pink.

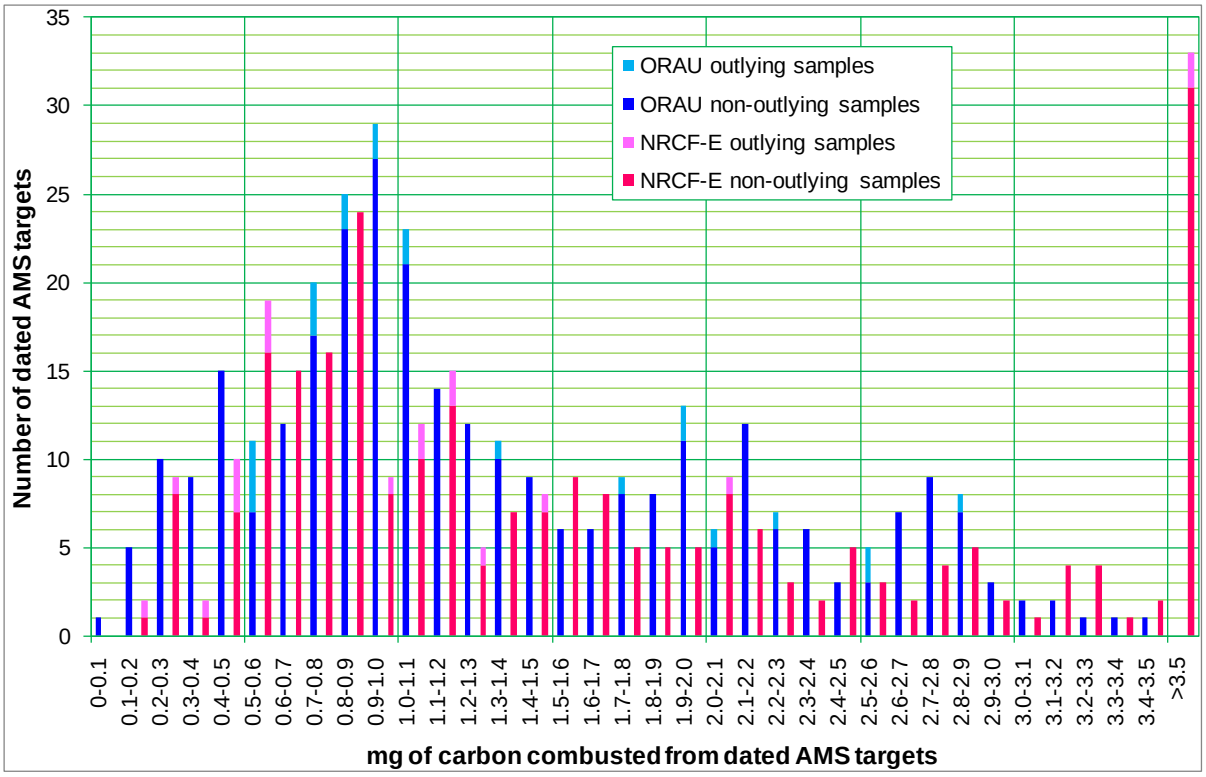

7.6 Integration of the SG93 and SG06 Radiocarbon Datasets

7.6.1 Comparison of the Individual Radiocarbon Datasets

Figure 7.13 illustrates the raw radiocarbon data of the SG93 core, as adjusted to equivalent SG06 event-free depth (using the visual core matching undertaken in section 6.2), and compared against the radiocarbon data from the SG06 plant macrofossil samples. It can be seen that the data from the two respective projects are in excellent agreement, with the Groningen laboratory's (SG93) data showing equally good agreement to the SG06 datasets as

between the ORAU and NRCF-E (SG06) datasets themselves. (As an aside, this close agreement between the respective datasets provides additional support for the placement of the respective core sections of SG93 against the composite SG06 core.)

Figure 7.13: Comparison of the raw (uncalibrated) SG93 and SG06 radiocarbon datasets, plotted against SG06 event-free depth (EFD), over the conventional radiocarbon age ranges: **(a)** 0 to 60,000 BP; **(b)** 6 to 17,000 BP; **(c)** 16,000 to 27,000 BP; and **(d)** 26,000 to 37,000 BP. ORAU 'G' and 'g' data are plotted in blue; ORAU 'vsg' data are plotted in light blue; NRCF-E 'g' data are plotted in magenta; NRCF-E 'vsg' samples are plotted in light pink; and Groningen (SG93) data are plotted in purple. Uncertainties are shown at 1σ.

(a):

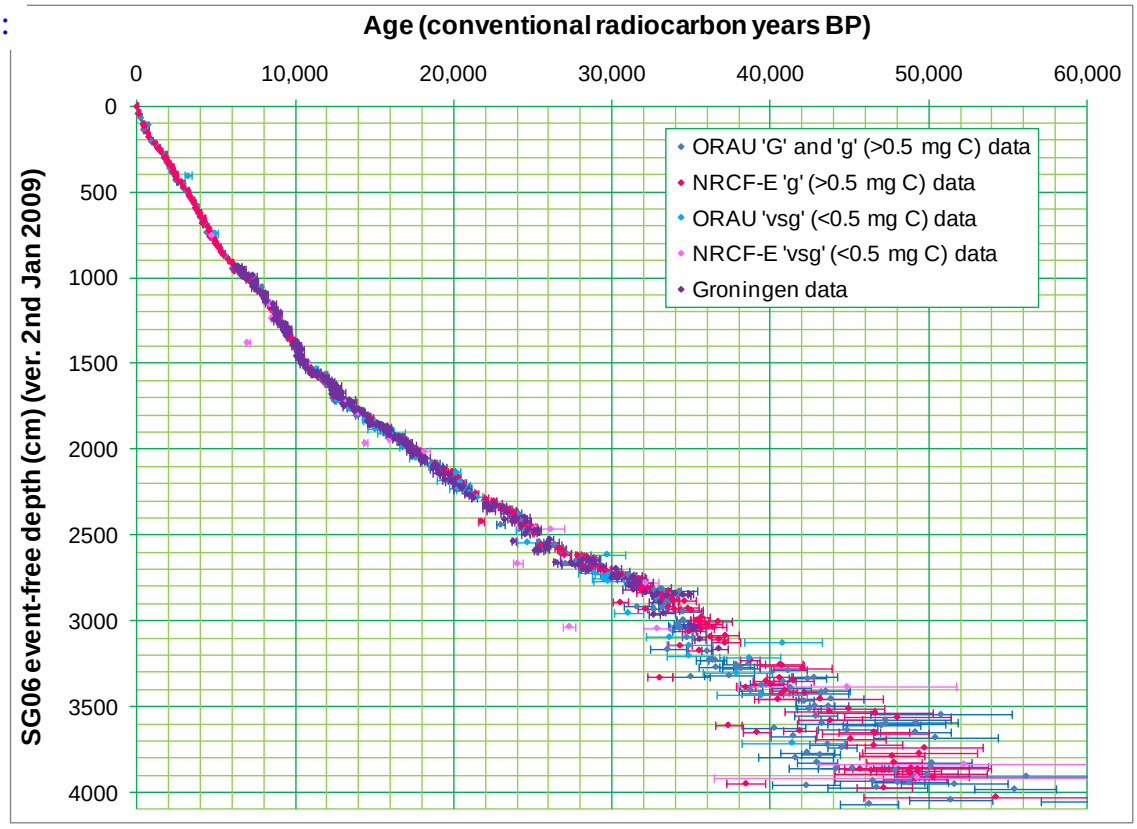

Figure 7.13 (continued):

(b):

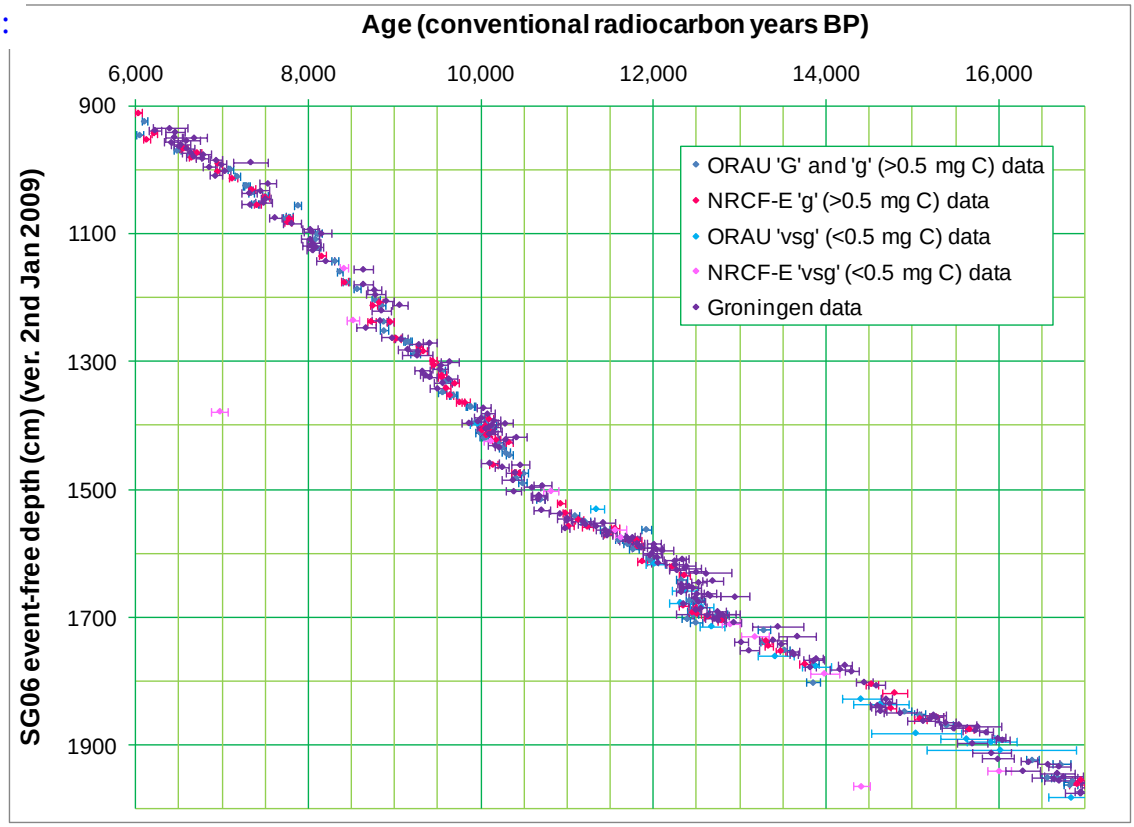

(c):

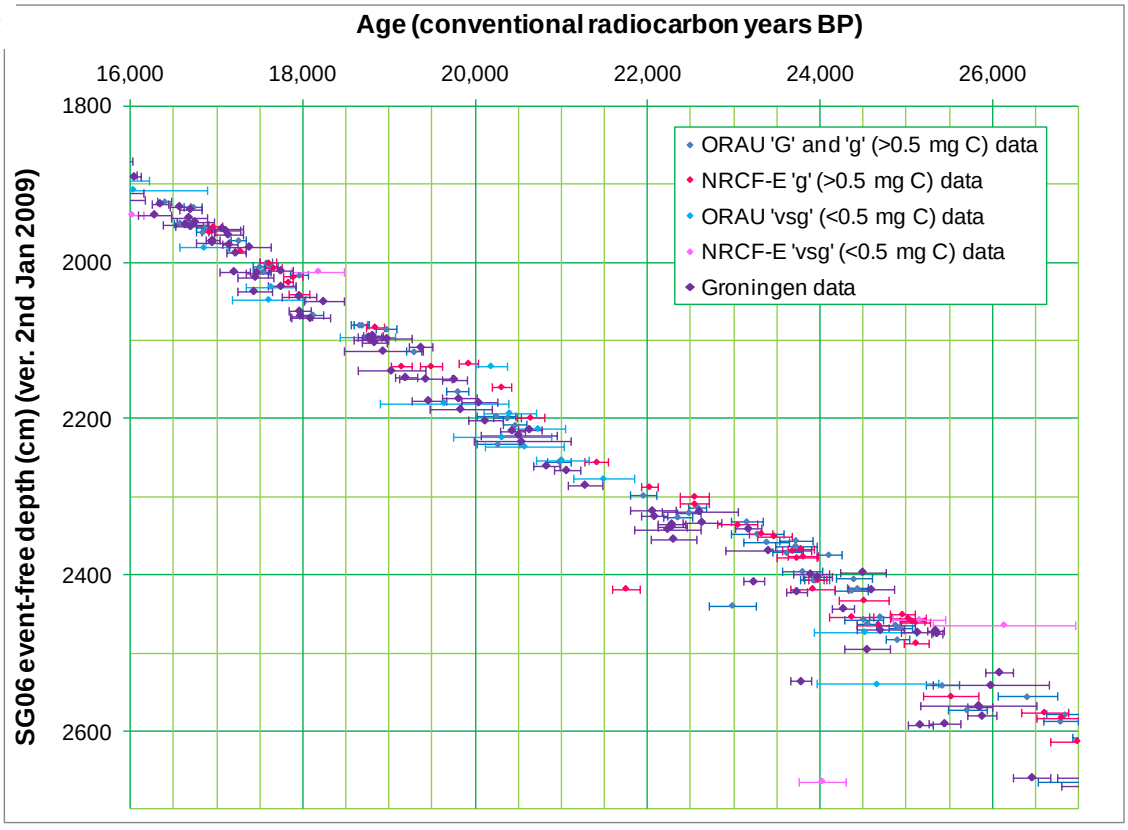

Figure 7.13 (continued):

(d):

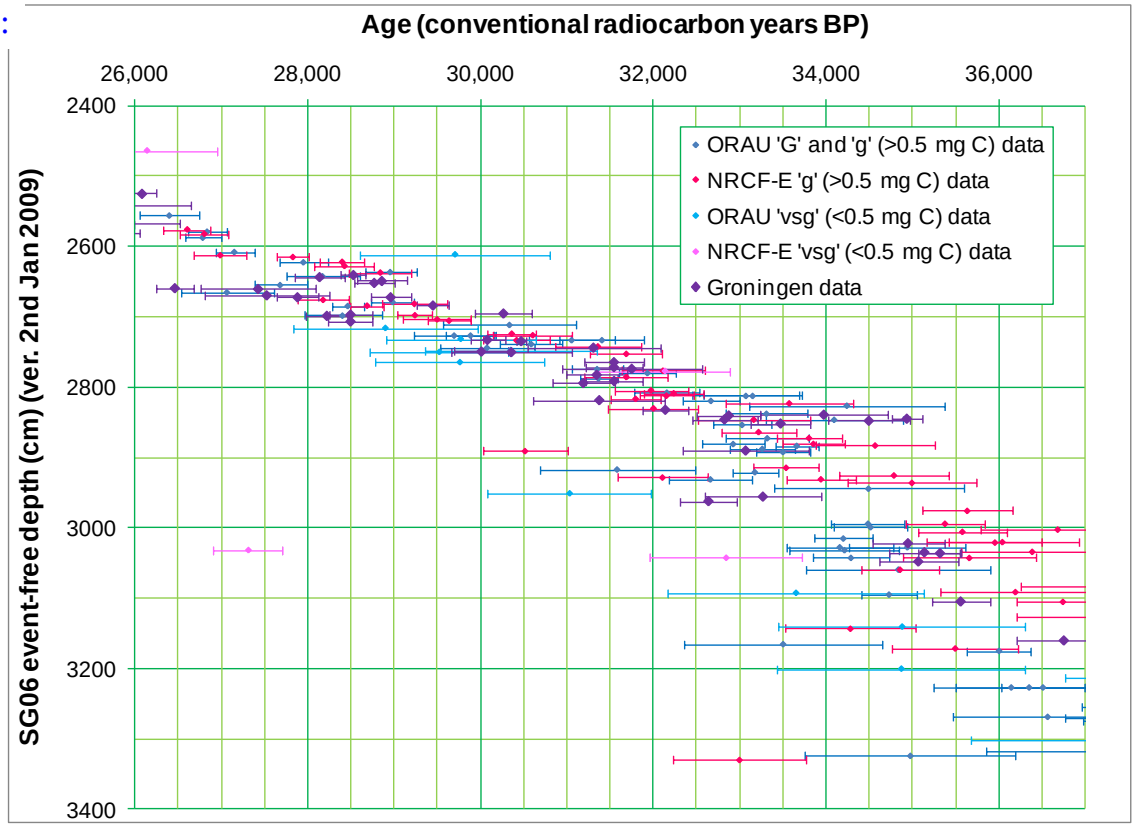

7.6.2 Combination of the Individual Radiocarbon Datasets

DPhil objective vi cited the aim of incorporating the original radiocarbon determinations from the Suigetsu ’93 project into the dataset of the Suigetsu Varves 2006 project, thereby greatly enhancing the resolution of the final ‘Lake Suigetsu radiocarbon calibration dataset’. The previous sub-section illustrated the close concordance between these respective datasets, suggesting that a composite dataset can certainly be generated. To this end, the data from both datasets were combined, in SG06-equivalent stratigraphic order, and the outlier removal methodology of section 7.5 repeated using this expanded dataset. In total, 48 samples were identified as being outliers from the combined 902 samples of the composite dataset (table 7.17). Of these outliers, 21 were from ORAU, seventeen were from NRCF-E,

and ten were from the Groningen laboratory. Four samples excluded by the previous (SG06 only) outlier removal are now no longer removed, whilst one additional sample is now excluded. The relatively small number of Groningen outliers, and lack of additional SG06 outliers when the SG93 data is included, provides additional confidence in the correspondence of the respective contributing datasets (and, therefore, of the core matching exercise of section 6.2). The higher proportion of outliers from the SG06 datasets is a result of the more stringent exclusion threshold applied to the duplicated sample depths (the first stage of the exclusion algorithm), as well as the fact that the SG06 data extend right back to the limit of the radiocarbon dating method (≈ 50,000 BP), whereas the SG93 data only extend to ≈ 37,000 BP, with the older SG06 samples more susceptible to small quantities of modern contamination (section 4.3.1), and therefore more likely to be erroneous.

Table 7.17: The SG06 and SG93 radiocarbon measurements determined to be outliers (and removed from subsequent data analysis) by the outlier identification algorithm when applied to the composite Lake Suigetsu radiocarbon calibration dataset.

	SG06/SG93 sample ID (# / 'SG...')	Sample type	SG06 CD (cm)	SG06 EFD (cm)	SG06 yr BP	Expected radiocarbon age (BP)	AMS target ID	Target type	C yield (mg)	Conventional radiocarbon date (± 1σ)
Non-coeval duplicates:	#307	Ev.br.leaf	108.4	107.9	371	444	OxA-X-2248-48	G	1.868	730 ± 24
	#780	Ev.br.leaf	773.0	759.0	5,441	4,794	SUERC-28203	g	2.030	4,625 ± 35
	#847	Dec.br.leaf	1259.6	1236.8	9,956	8,947	SUERC-28906	g	0.520	8,730 ± 45
	#197	Dec.br.leaf	2190.6	2132.8	23,055	19,762	SUERC-13333	g	0.589	19,137 ± 123
	#197	Dec.br.leaf	2190.6	2132.8	23,055	19,762	OxA-X-2219-17	vsg	0.480	20,181 ± 189
	#217	Dec.br.leaf	2488.9	2417.5	28,425	24,315	SUERC-17723	g	1.125	21,743 ± 165
	#1007	Dec.br.leaf	3051.1	2930.9	36,709	33,808	OxA-X-2357-20	g	1.284	32,662 ± 487
	#246	Dec.br.leaf	3163.4	3031.6	38,420	35,141	SUERC-19064	vsg	0.482	27,308 ± 402
	#247	Dec.br.leaf	3174.3	3042.5	38,604	35,161	SUERC-16527	vsg	0.434	32,838 ± 885
	#1135b	Bark	3360.9	3226.8	41,616	38,475	SUERC-29853	g	3.777	38,721 ± 617
	#747	Twig	3541.8	3403.7	44,545	41,546	OxA-X-2360-43	G	1.835	38,751 ± 729
	#291	Dec.br.leaf	3796.7	3646.9	48,351	44,162	SUERC-13334	g	1.286	39,129 ± 844
	#939	Dec.br.leaf	3977.9	3823.0	51,323	47,321	OxA-X-2360-48	G	1.604	42,927 ± 1,294
>400‰ and >4σ:	#97	Dec.br.leaf	1408.7	1377.5	11,368	9,927	SUERC-19061	vsg	0.107	6,968 ± 94
	#188	Dec.br.leaf	2015.5	1963.7	19,893	16,974	SUERC-19062	vsg	0.386	14,409 ± 94
	#1067	Dec.br.leaf	2779.6	2664.1	32,197	28,167	SUERC-29834	vsg	0.471	24,023 ± 279
	#238	Dec.br.leaf	3010.1	2890.9	36,081	33,452	SUERC-17724	g	1.018	30,514 ± 489
	#270	Dec.br.leaf	3467.0	3329.4	43,408	41,122	SUERC-26008	g	0.536	32,998 ± 764
	#759	Dec.br.leaf	3756.7	3606.9	47,697	44,253	SUERC-28898	g	1.002	37,332 ± 796
	#302	Dec.br.leaf	4103.0	3948.1	53,539	49,161	SUERC-18131	g	0.964	38,448 ± 1,247
>400‰:	#1100	Dec.br.leaf	3461.7	3324.1	43,321	41,167	OxA-X-2362-50	g	0.602	34,975 ± 1,217
	#497	Dec.br.leaf	3818.9	3669.1	48,718	46,294	OxA-X-2340-29	g	0.832	41,442 ± 1,445
	#959	Dec.br.leaf	3861.7	3709.0	49,373	45,730	OxA-X-2374-18	vsg	0.440	41,404 ± 3,221
	#936	Dec.br.leaf	3951.3	3796.5	50,827	46,635	OxA-X-2362-19	g	0.649	41,582 ± 2,367
	#649	Dec.br.leaf	4113.0	3958.2	53,713	49,353	OxA-X-2362-20	g	0.798	42,269 ± 2,140

Table 7.17 (continued):

	SG06/SG93 sample ID (# / 'SG...')	Sample type	SG06 CD (cm)	SG06 EFD (cm)	SG06 yr BP	Expected radiocarbon age (BP)	AMS target ID	Target type	C yield (mg)	Conventional radiocarbon date (± 1σ)
>4σ (and 'outside'):	#308	Twig	136.4	135.9	505	591	OxA-X-2270-49	G	2.769	436 ± 25
	#319	Ev.br.leaf	439.9	430.9	2,794	2,697	OxA-X-2297-56	G	2.120	2,493 ± 25
	#319	Ev.br.leaf	439.9	430.9	2,794	2,697	OxA-X-2303-36	g	0.875	2,487 ± 27
	#786	Dec.br.leaf	748.3	734.8	5,254	4,680	OxA-X-2360-44	G	1.993	4,427 ± 32
	#429	Ev.br.leaf	960.5	945.5	7,209	6,311	OxA-X-2339-40	G	2.402	6,042 ± 34
	#50	Ev.br.leaf	969.8	952.0	7,282	6,370	SUERC-17117	g	10.446	6,129 ± 38
	#382	Dec.br.leaf	1077.5	1055.3	8,338	7,527	OxA-X-2297-53	g	1.000	7,878 ± 41
	#124	Dec.br.leaf	1565.1	1531.0	13,002	10,962	OxA-X-2219-16	vsg	0.414	11,339 ± 80
	#130	Dec.br.leaf	1591.4	1556.9	13,288	11,365	SUERC-17720	g	1.446	11,016 ± 49
	SG18E05	-	1594.4	1559.8	13,321	11,361	GrA-4533	-	-	10,975 ± 55
	#140	Dec.br.leaf	1596.4	1561.8	13,344	11,476	OxA-X-2297-42	g	0.901	11,916 ± 53
	SG18B04	-	1648.8	1608.2	13,908	11,950	GrA-8147	-	-	12,333 ± 74
	#572	Dec.br.leaf	1748.8	1707.2	15,200	12,720	OxA-24392	g	0.927	12,490 ± 69
	SG20B01	-	1815.6	1773.9	16,356	13,791	GrA-6203/GrA-8142	-	-	14,217 ± 76
	#174	Dec.br.leaf	1843.0	1801.4	16,895	14,352	OxA-X-2245-19	g	0.736	13,852 ± 78
	SG27C06	-	2479.9	2408.5	28,280	24,168	GrA-15726	-	-	23,230 ± 120
	#352	Dec.br.leaf	2512.2	2438.7	28,808	24,593	OxA-X-2362-11	g	0.673	22,980 ± 268
	SG29D03	-	2650.8	2536.1	30,113	25,564	GrA-15725	-	-	23,780 ± 120
	SG29-1	-	2705.4	2589.8	30,851	26,965	GrA-6171	-	-	25,445 ± 190
	SG29B07	-	2706.8	2591.3	30,875	26,983	GrA-15732	-	-	25,160 ± 140
	SG30-5	-	2774.5	2659.0	32,104	28,114	GrA-6168	-	-	26,460 ± 215
	SG30A04	-	2812.6	2695.0	32,732	29,061	GrA-10390	-	-	30,265 ± 331
	SG32C01	-	2964.0	2844.8	35,304	32,955	GrA-10429	-	-	34,936 ± 180

8. Discussion: the Combined Lake Suigetsu Radiocarbon Calibration Dataset

The present chapter commences with a description of the combined (SG93 and SG06) Lake Suigetsu radiocarbon dataset, and a comparison with some of the alternative radiocarbon calibration datasets. This section (8.1) is broken down into distinct chronological sections and is discussed sequentially going back through time. The first sub-section (8.1.1) discusses the comparison of the dataset with the alternative records for the upper, non-varved portion of SG06, roughly equivalent to the time period representing the present interglacial, the Holocene. Section 8.1.2 describes the time period covering the Last Glacial/Interglacial transition (LGIT) for which 'provisional' varve counting by Suigetsu Varves 2006 project colleagues has now been completed. This section encompasses the time period overlapping the initial ≈ 2,600 years of the IntCal09 (Reimer *et al*. 2009) tree-ring record (previously introduced in section 7.4), but also includes the preceding ≈ 4,000 years, commencing mid-way through Heinrich event 1 (H1), a period for which there are known discrepancies between the IntCal09 calibration curve and alternative available calibration datasets (section 2.7). Section 8.1.3 describes the extension of the radiocarbon dataset back in time in to the Last Glacial, continuing the record back to the detection limit of the radiocarbon method. Finally, section 8.1.4 illustrates the reconstructed $\Delta^{14}C$ signal across the entirety of the Lake Suigetsu dataset, focussing particularly on the time period that encompasses the Laschamp and Mono Lake geomagnetic field excursions.

The following section, 8.2, notes the on-going work of the Suigetsu Varves 2006 project, which will be necessary to resolve some of the issues brought up through section 8.1, and also cites other potential future work to extend the scope of the over-arching project.

8.1 Comparison of the Lake Suigetsu Radiocarbon Calibration Dataset with Selected Alternative Datasets

8.1.1 Dating Through the Holocene (SG06 Core Top to Varve Count Top)

As described in section 7.4, the U-Oki tephra (SG06 composite core depth 1286.1 to 1288 cm) is dated to 10,230 to 10,209 cal. BP (68.2% probability range), and provides the tie-point to the absolute (calendar) timescale from which the 'Suigetsu Varves 2006 varve year' ('SG06 vyr') timescale is herein defined. The age of the top of the varve-counted portion of SG06 (1250 cm composite depth, CD; 1227.2 cm event-free depth, EFD) is therefore 9,876 to 9,855 SG06 vyr BP, several hundred years after the Holocene onset. Therefore, the actual Holocene base in SG06 falls within the subsequent section, 8.1.2. This present section, therefore, pertains to the vast majority of the Holocene, represented in SG06 by the uppermost 1250 cm of sediment, which, as previously described, is not clearly varved. Since no independent timescale is available through this period, the radiocarbon data from this uppermost SG06 core section were therefore fitted on to the IntCal09 (Reimer *et al*. 2009) 'absolute' timescale, according to the OxCal model (OCM-) 7.68, introduced in the previous chapter.

Unlike the present (Suigetsu Varves 2006) project, the previous (Suigetsu '93) study did not carry out as many radiocarbon measurements on Holocene macrofossils, since the primary aim of this project was the extension of the calibration curve back in time from the then limits of calibration (11,390 cal. BP from tree-ring data, extending to 21,950 cal. BP with lower resolution coral data; Stuiver and Reimer 1993; section 2.6.3). The additional radiocarbon analysis performed for the present project, extending through the later time period, serves to: (i) provide greater confidence in the stratigraphic integrity (lack of sedimentary hiatuses) of the Lake Suigetsu sediment profile (and, by extrapolation, across the

broader range of the entire radiocarbon dating range) through (intended) demonstration of coherence with the alternative calibration datasets across this more recent time period; and (ii) to provide the chronology required for the alternative, palaeoenvironmental aims of the Suigetsu Varves 2006 project.

Figure 8.1 illustrates the comparison between the SG06- and IntCal09 calibration datasets from this younger time period. Like Suigetsu, IntCal09 is entirely based upon terrestrial data through the entirety of this interval, and so one would expect the two respective datasets to be in good agreement throughout. Although the use of the IntCal09 curve to derive the SG06 'cal. BP' timescale through this period makes the comparison somewhat circular, the applied `P_Sequence` model bore a relatively high `k` value (6.33, as established through objective analysis of the varve count data from lower core depths; section 7.4.2), which would allow the preservation of shorter-term deviations between the respective datasets. The figures (8.1a to 8.1e) do indeed demonstrate a very good degree of concordance between the SG06 dataset and IntCal09, with some of the features of the calibration curve picked out nicely by the SG06 data (e.g. the plateau between *circa* 2,700 and 2,400 cal. BP, figure 8.1b, or the shape of the curve between *circa* 8,350 and 8,000 cal. BP, figure 8.1e). However, one must bear in mind the necessarily reduced resolution of the Suigetsu dataset over this time period (127 radiocarbon determinations from 108 separate depth horizons, therefore giving an average temporal resolution of ≈ 90 years), as compared to the decadal resolution of IntCal09, as well as the lack of an independent Suigetsu chronology, when assessing the SG06 data in this way. In terms of the latter point, figure 8.2 illustrates the linearity of the modelled (OCM-7.68) SG06 age-depth profile, which demonstrates the robustness of the derived calibrated timescale for SG06 above 1250 cm CD (i.e. shows that the age scale isn't 'fiddled' to match IntCal09 by allowing rapidly varying down-core deposition rates). This adds credence to the utility of the plant macrofossils picked

from the Lake Suigetsu benthic sediment as faithfully representing past variations in atmospheric radiocarbon concentration (i.e. fulfilling the initial aim, described above, for radiocarbon dating this time period). It is therefore believed that Lake Suigetsu, demonstrating annual laminations (varves) across the remainder of the radiocarbon dating technique, is capable of providing a reliable, direct record of atmospheric radiocarbon data back to the limit of the method.

Figure 8.1: The 127 radiocarbon determinations obtained from the uppermost 1250 cm (composite depth) of SG06, as plotted against (the median) calibrated age (derived from OCM-7.68) over the time period: **(a)** 2,100 to 0 cal. BP; **(b)** 4,100 to 2,000 cal. BP; **(c)** 6,100 to 4,000 cal. BP; **(d)** 8,100 to 6,000 cal. BP; and **(e)** 10,100 to 8,000 cal. BP. The 55 'non-outlying' ORAU measurements (as determined in section 7.5) are shown in blue, the eight 'outlying' ORAU measurements in light blue, the 62 'non-outlying' NRCF-E measurements in magenta, and the two 'outlying' NRCF-E data points in light pink. For comparison, the IntCal09 (Reimer *et al*. 2009) calibration curve is shown as the hashed red lines. Both the SG06 data and the IntCal09 curve are plotted at 1σ uncertainty.

(a):

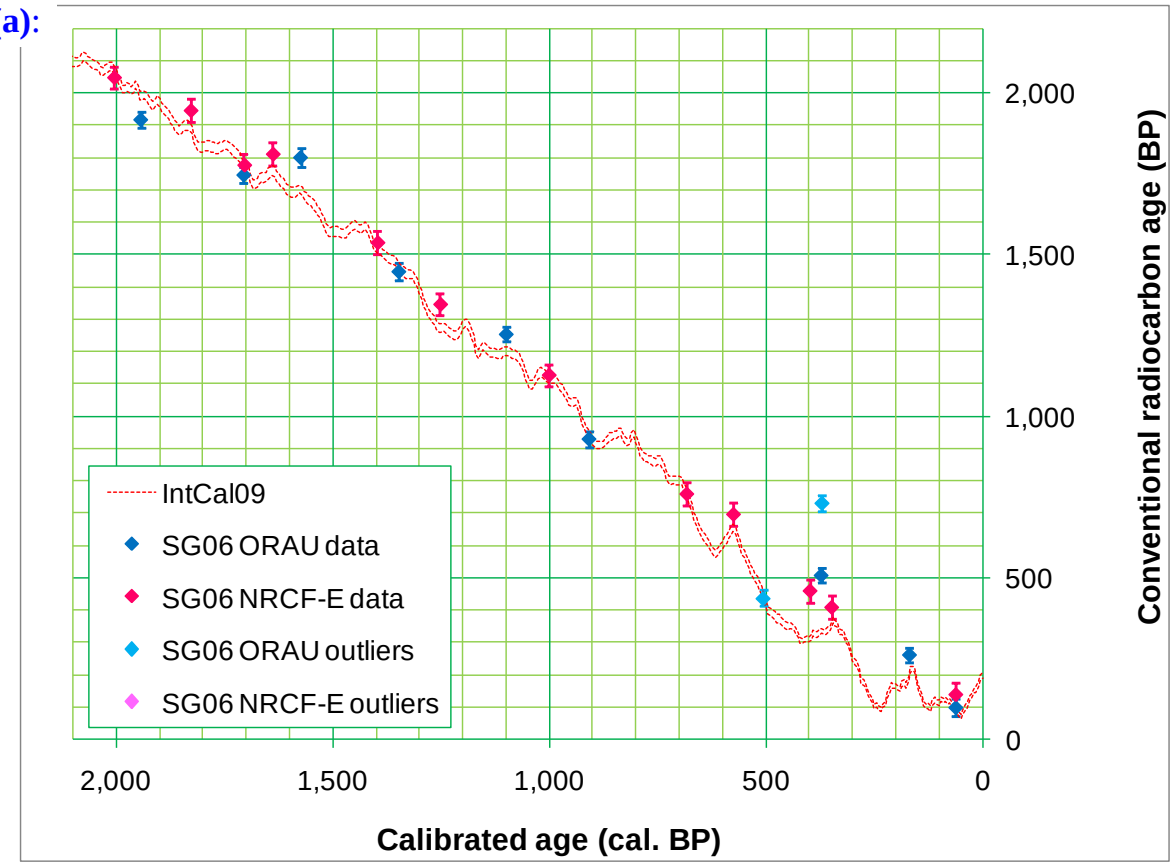

Figure 8.1 (continued):

(b):

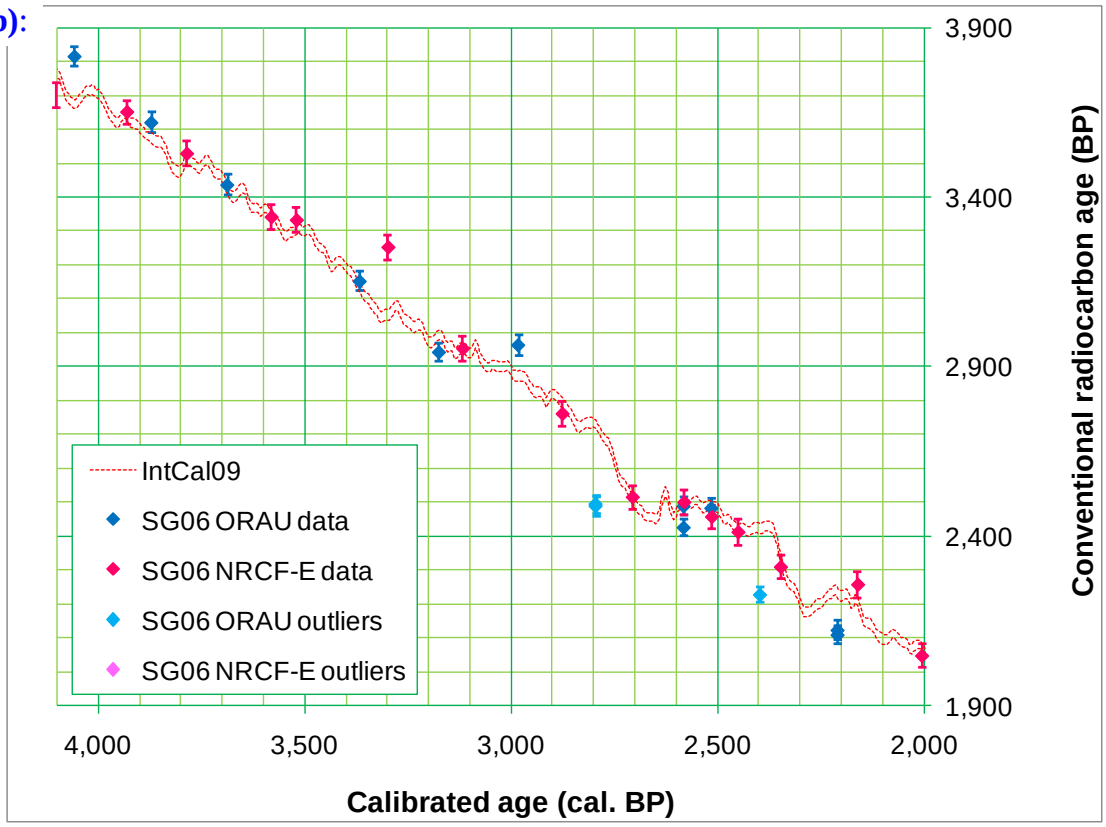

(c):

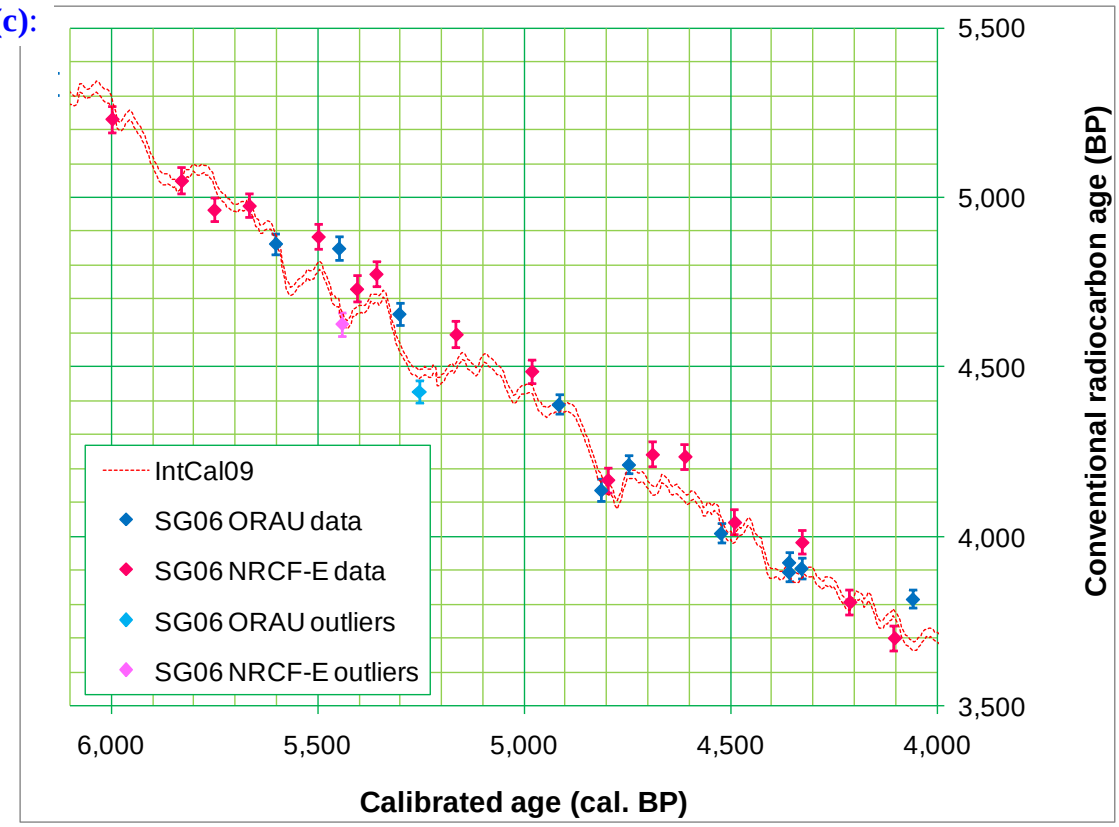

Figure 8.1 (continued):

(d):

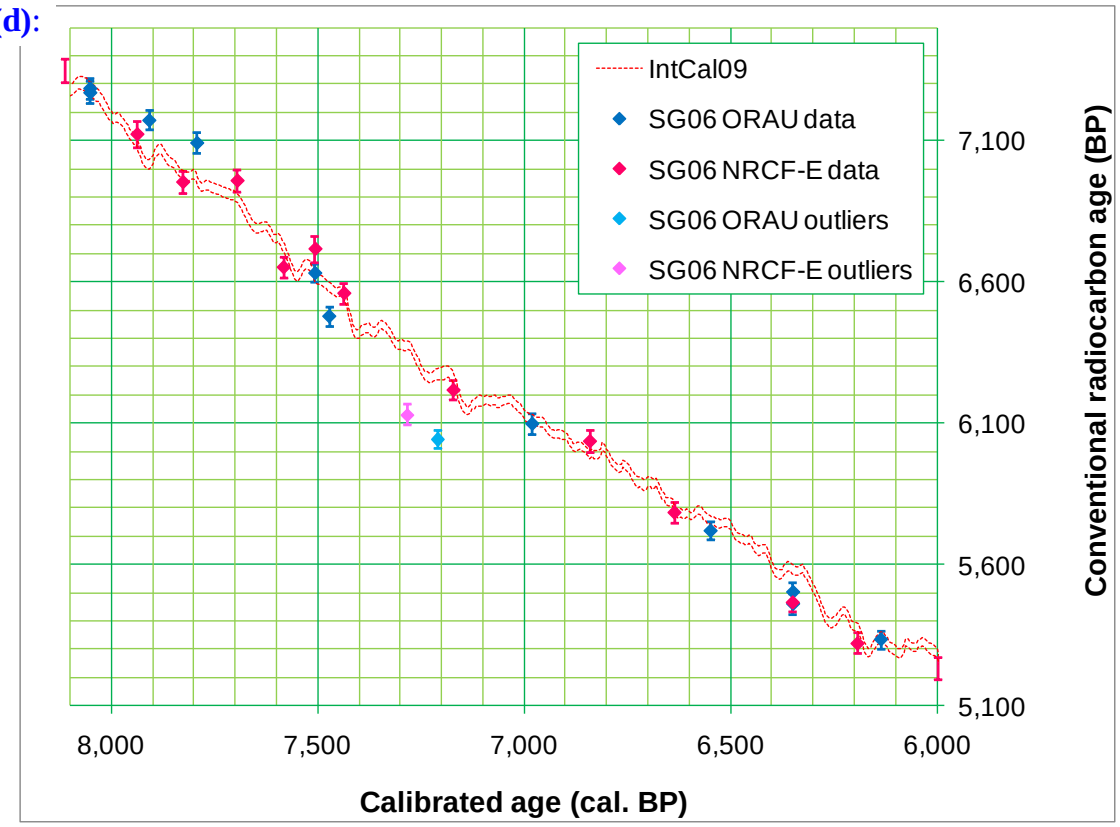

(e):

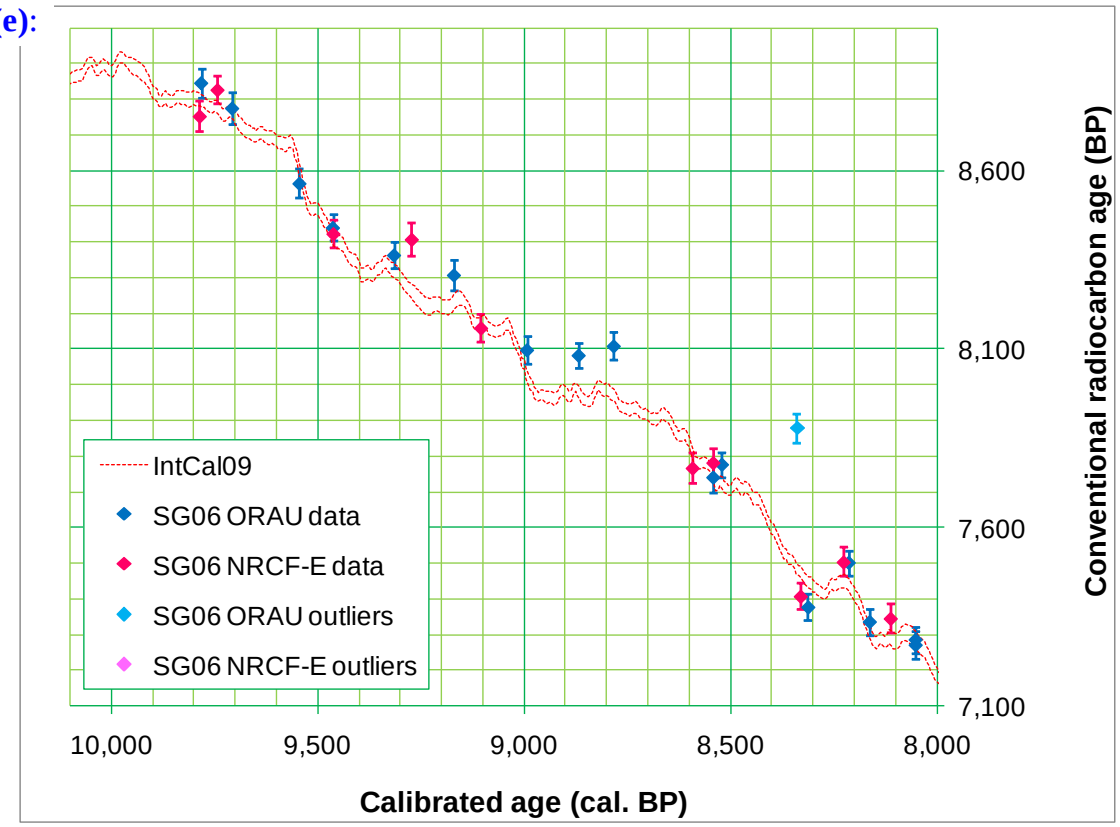

Figure 8.2: The age-depth profile of the uppermost 1250 cm (composite depth; 1227.2 cm event-free depth, EFD) of SG06, as derived from calibration of the SG06 radiocarbon data against IntCal09 (Reimer *et al*. 2009) according to OCM-7.68. The ORAU data are plotted in blue; NRCF-E data in magenta; and combined data produced from inter-laboratory duplication plotted in mauve. The posterior age-depth profile (the darker shading), overlies the prior, un-modelled probability density functions (lighter shading).

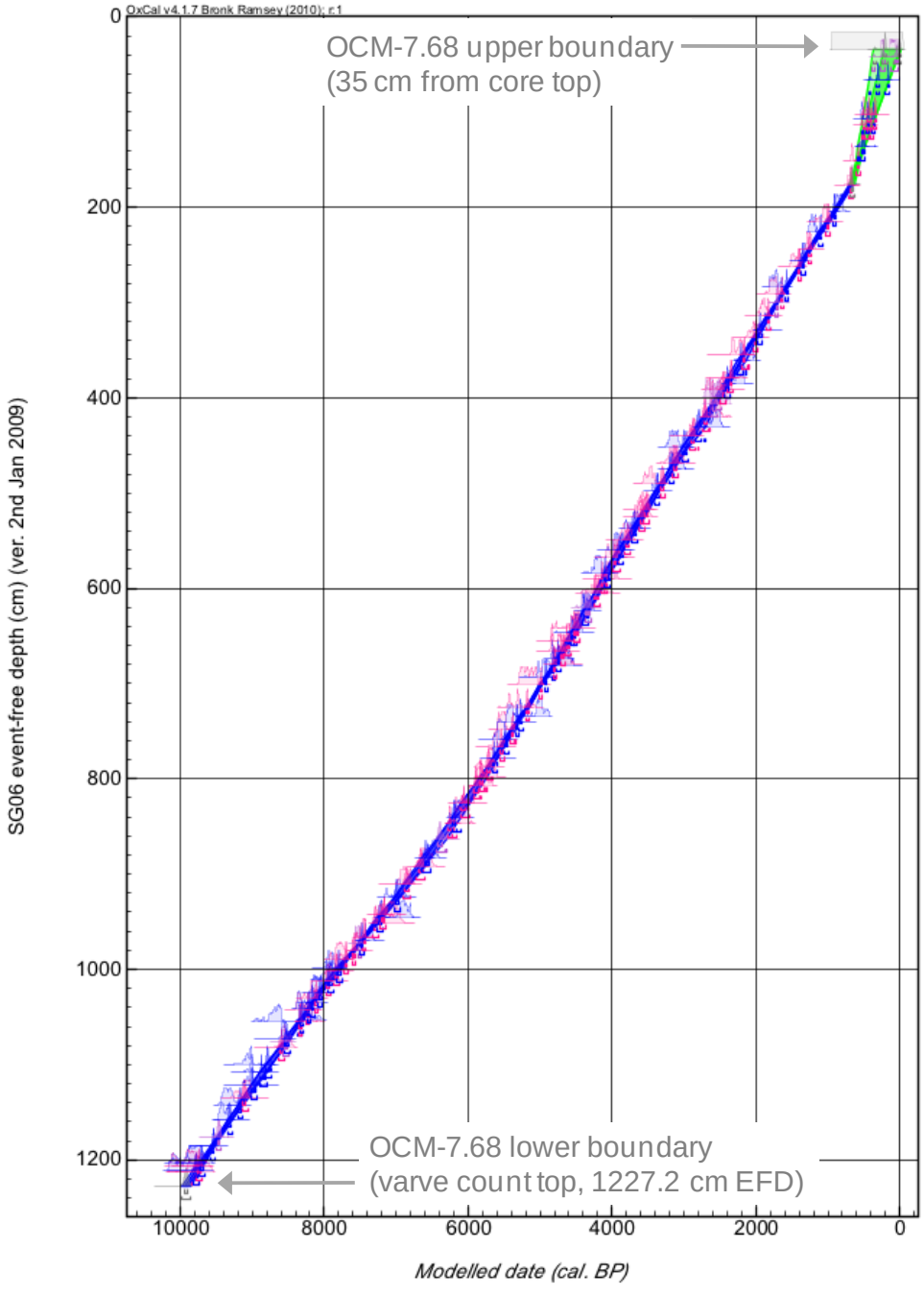

Additionally, figure 8.1 serves to illustrate the general reliability of the outlier detection methodology described in section 7.5. A summary of the prediction success of the outlier removal algorithm, as compared to that suggested by the `Outlier_Model` applied in OCM-7.68, is provided in table 8.1. This table demonstrates that six of the eight outliers identified in OCM-7.68 were correctly identified by the outlier removal algorithm, whilst 113 of the 115 non-outlying radiocarbon determinations (according to OCM-7.68) were also identified as such by the outlier detection protocol. (An additional AMS target, SUERC-19061, was so outlying as to not be included within the OxCal model.) This leaves two AMS targets (OxA-X-2248-47 at 505 BP, 371 cal BP; figure 8.1a; and SUERC-26729 at 3,251 BP, 3,298 cal. BP; figure 8.1b) as having not been identified as outlying, whereas they most probably are outliers in reality (100% posterior outlier probabilities in OCM-7.68). As described in the previous chapter, the outlier removal protocol was relatively conservative in nature, so as to allow as much authentic deviation to be preserved in the final dataset as possible. A higher removal threshold (than the '$> 4\sigma$' criterion applied) would have identified these samples as being outliers, but would have led to the erroneous removal by the protocol of more genuinely non-outlying samples than the two demonstrated in table 8.1. These two AMS targets (OxA-X-2270-49 at 436 BP, 505 cal. BP; figure 8.1a; and OxA-X-2360-44 at 4,427 BP, 5,254 cal. BP; figure 8.1c) seem to actually represent 'true' variation in the calibration curve (according to OCM-7.68) and have been identified as outliers due to a combination of both the high amplitude variability in the calibration curve through these time periods (creating deviation from the interpolated $\Delta^{14}C$ values of the four adjacent samples, according to the removal algorithm), as well as the low measurement uncertainty on these relatively young samples. Of the three AMS targets removed prior to modelling as a result of their being non-coeval duplicates, one target (SUERC-28203, at 4,625 BP, 5,441 cal. BP; figure 8.1c) is in closer agreement with IntCal09 than the alternative sample duplicate

(OxA-X-2345-23, 4,848 BP). Again, this is a result of the shape of the calibration curve at this time (an inversion in the curve).

Table 8.1: A summary of the prediction success of the outlier removal algorithm (of section 7.5), as compared to that suggested by the `Outlier_Model` applied in OCM-7.68.

		OCM-7.68 `Outlier_Model`	
		Outlying ^{14}C determinations (≥ 95% posterior outlier probability)	Non-outlying ^{14}C determinations (< 95% posterior outlier probability)
Outlier removal algorithm (section 7.5)	Predicted to be outlying	6 (OxA-X-2347-43; OxA-X-2297-56; OxA-X-2303-36; OxA-X-2339-40; SUERC-17117 & OxA-X-2297-53); An additional 3 determinations (OxA-X-2248-48; SUERC-28203 & SUERC-28906) from non-coeval duplicates (sections 7.2.2 & 7.2.3) were removed prior to inclusion in OCM-7.68, as was a single further determination (SUERC-19061) that was so outlying as to prevent the model from running)	2 (OxA-X-2270-49 & OxA-X-2360-44)
	Not predicted to be outlying	2 (OxA-X-2248-47 & SUERC-26729)	All of the remaining 113 ^{14}C determinations included within OCM-7.68

The outlier removal algorithm therefore seems to be generally reliable across this younger portion of the radiocarbon timescale, providing confidence in the ability of the methodology to have reliably removed the genuinely outlying radiocarbon determinations across the total range of the dataset (section 7.5).

Finally for this time period, the SG06 radiocarbon dataset can be bolstered by an additional 44 measurements from the revised stratigraphy of the SG93 dataset (figure 8.3).

Again, these data appear to be in good agreement with the IntCal09 calibration curve, with even the more outlying SG93 data points being consistent with IntCal at 2σ uncertainty.

Figure 8.3: Comparison between the 44 radiocarbon determinations from the Suigetsu '93 project ('Groningen data'; purple data points) and Suigetsu Varves 2006 data from SG06-equivalent core depths 950 to 1250 cm (composite depth), as plotted against the (median) calibrated age derived from OCM-7.68. The 20 'non-outlying' ORAU measurements are shown in blue, two 'outlying' ORAU measurements in light blue, seventeen 'non-outlying' NRCF-E measurements in magenta, and one 'outlying' NRCF-E data point in light pink. For comparison, the IntCal09 (Reimer *et al*. 2009) calibration curve is shown as the hashed red lines. Both the Lake Suigetsu data and the IntCal09 curve are plotted at 1σ uncertainty.

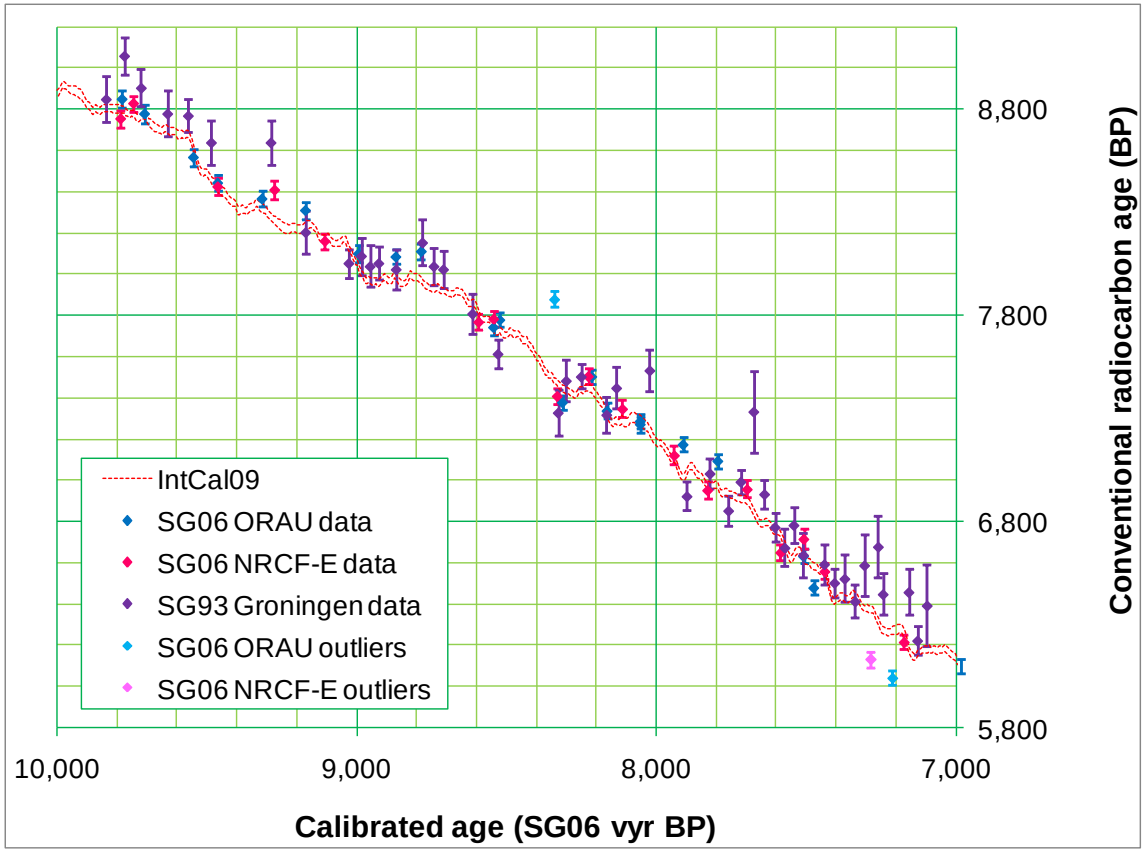

8.1.2 Dating through the Last Glacial/Interglacial transition

With the floating SG06 varve chronology having been tied to the absolute (IntCal09) timescale in section 7.4, the radiocarbon determinations across the Last Glacial/Interglacial Transition (LGIT) can be plotted directly against the SG06 vyr chronology to examine comparisons between the Suigetsu Varves 2006 calibration dataset and alternative radiocarbon calibration data. Unlike the previous section, this comparison is therefore free of any assumptions inherent in modelling of one dataset on to that of another. Figure 8.4 demonstrates this comparison from the varve count top (1250 cm CD, 9,865 SG06 vyr BP) to the present limit of the 'finalised' SG06 varve chronology (1814.6 cm CD, 16,337 SG06 vyr BP). From this figure, the apparent concordance between the SG06- and IntCal09 data through the majority of this time period seems excellent, implying both that the varve-counted SG06 age scale (and wiggle-matched fit to the absolute, IntCal timescale) is reliable, and that the assumed marine reservoir corrections applied to the IntCal data (beyond 12,550 cal. BP) are also sound. In the period before *circa* 15,300 SG06 vyr BP, however, there is a suggestion in this plot that the Lake Suigetsu data are beginning to diverge slightly from IntCal09 (i.e. to give systematically older conventional radiocarbon ages than the IntCal data from the equivalent calibrated ages). Since these data are at the older limit of this provisionally complete varve-counted core section, further discussion of this potential excursion will be discussed in the following section (8.1.3).

Figure 8.4: The 113 radiocarbon determinations obtained from the SG06 core section bearing a provisionally complete varve chronology, 1250 cm composite depth (9,865 SG06 vyr BP) to 1814.6 cm composite depth (16,337 SG06 vyr BP). The 55 'non-outlying' ORAU measurements are shown in blue, the two 'outlying' ORAU measurements in light blue, the 51 'non-outlying' NRCF-E measurements in magenta, and the five 'outlying' NRCF-E data points in light pink. For comparison, the IntCal09 (Reimer *et al*. 2009) calibration curve is shown as the hashed red lines. Both the SG06 data and the IntCal09 curve are plotted at 1σ uncertainty.

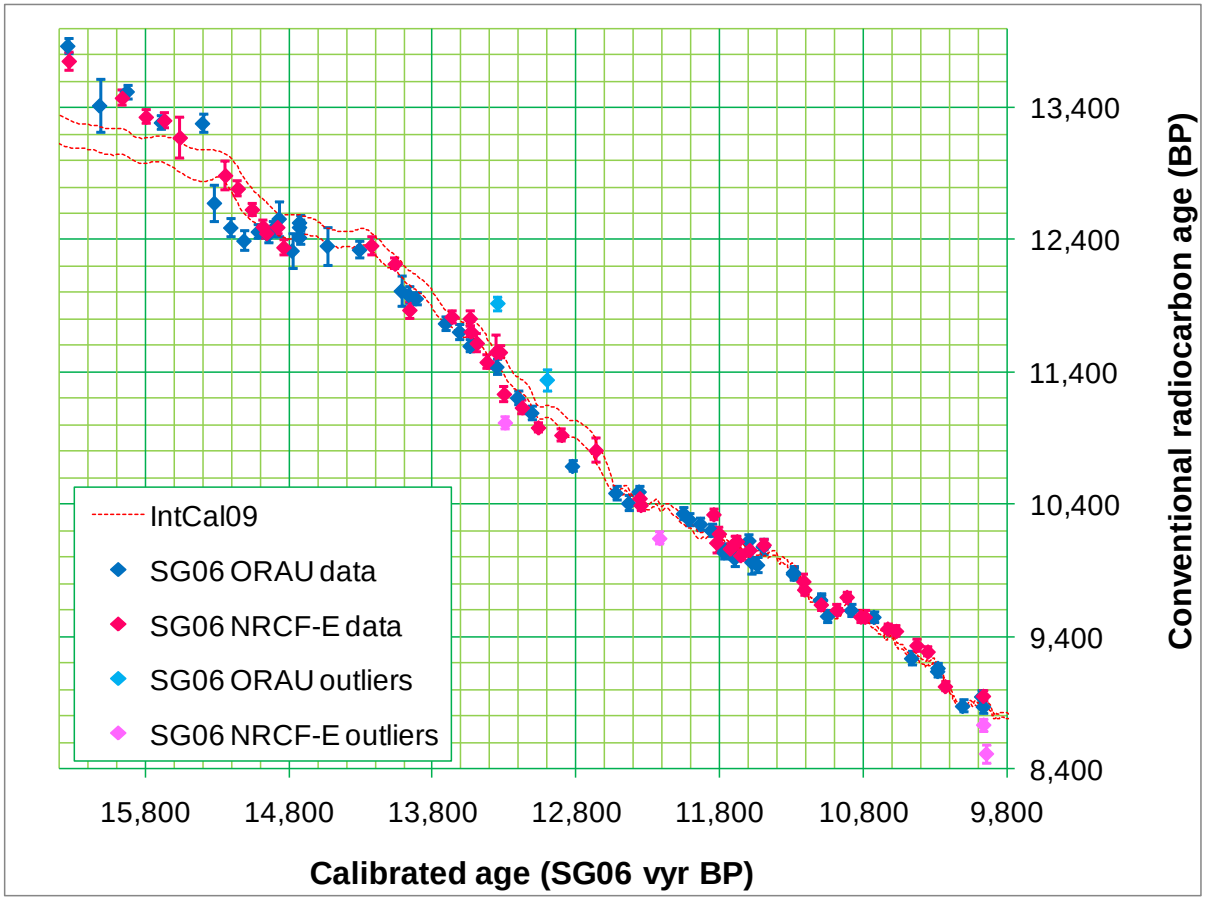

Through the time period represented by this section of the Lake Suigetsu sediment profile (SG06 core depths 1250 cm to 1814.6 cm CD), an additional 114 radiocarbon determinations can be incorporated into a combined Lake Suigetsu dataset from the original

Suigetsu ’93 project, doubling the total number of measurements and, accordingly, the average sampling resolution (to ≈ 30 years). The addition of these Groningen, SG93 measurements is illustrated in figure 8.5. As was previously demonstrated (section 7.6.1), the fit of the Suigetsu ’93 measurements with the Suigetsu Varves 2006 data seems excellent, adding belief in the matching of the respective projects’ core stratigraphies (section 6.2), which, for the majority of this time period (≈ 15,469 to 10,209 SG06 vyr BP) was achieved through the less reliable method of comparison with the original stratigraphic description, rather than with the archive U-channel material. The potential divergence of the Suigetsu data from IntCal09 before *circa* 15,300 SG06 vyr BP is again highlighted, but the addition of the SG93 data also suggests a second, relatively short-lived potential divergence between *circa* 13,200 and 12,600 SG06 vyr BP. This time period immediately precedes the present terrestrial limit of the radiocarbon calibration curve (12,550 cal. BP; Reimer *et al*. 2009), but is nevertheless represented in terrestrial archives by the, presently floating, central European pine chronology (Kromer *et al*. 2004; Friedrich *et al*. 2004; Schaub *et al*. 2008a, 2008b; section 2.5.1). This floating European dendrochronology was tentatively tied to the continuous IntCal tree-ring data by Hua *et al*. (2009), using Southern Hemisphere Huon pine samples (corrected for an assumed 40 year inter-hemispheric offset), and is reproduced in figure 8.6, with the Lake Suigetsu data superimposed. If one takes the Suigetsu data at face value, an argument could be made that Hua *et al*. have incorrectly joined the floating European pine data with their Huon pine dataset. Were this indeed the case, the resulting conclusion of these previous workers, that the Cariaco Basin dataset of Hughen *et al*. (2004b) requires a reduced marine reservoir correction through this time period, would seem invalid, with the Suigetsu data seeming to provide broad agreement for the original Cariaco data.

Figure 8.5: The 113 SG06 and 114 SG93 radiocarbon determinations obtained from the SG06 (or SG06-equivalent) core section bearing a provisionally complete varve chronology, 1250 cm composite depth (9,865 SG06 vyr BP) to 1814.6 cm composite depth (16,337 SG06 vyr BP). The 54 'non-outlying' ORAU measurements are shown in blue, the three 'outlying' ORAU measurements in light blue, the 53 'non-outlying' NRCF-E measurements in magenta, the three 'outlying' NRCF-E data points in light pink, the 112 'non-outlying' Groningen measurements in purple, and the two 'outlying' Groningen measurements in mauve. For comparison, the IntCal09 (Reimer *et al*. 2009) calibration curve is shown as the hashed red lines. Both the SG06 data and the IntCal09 curve are plotted at 1σ uncertainty.

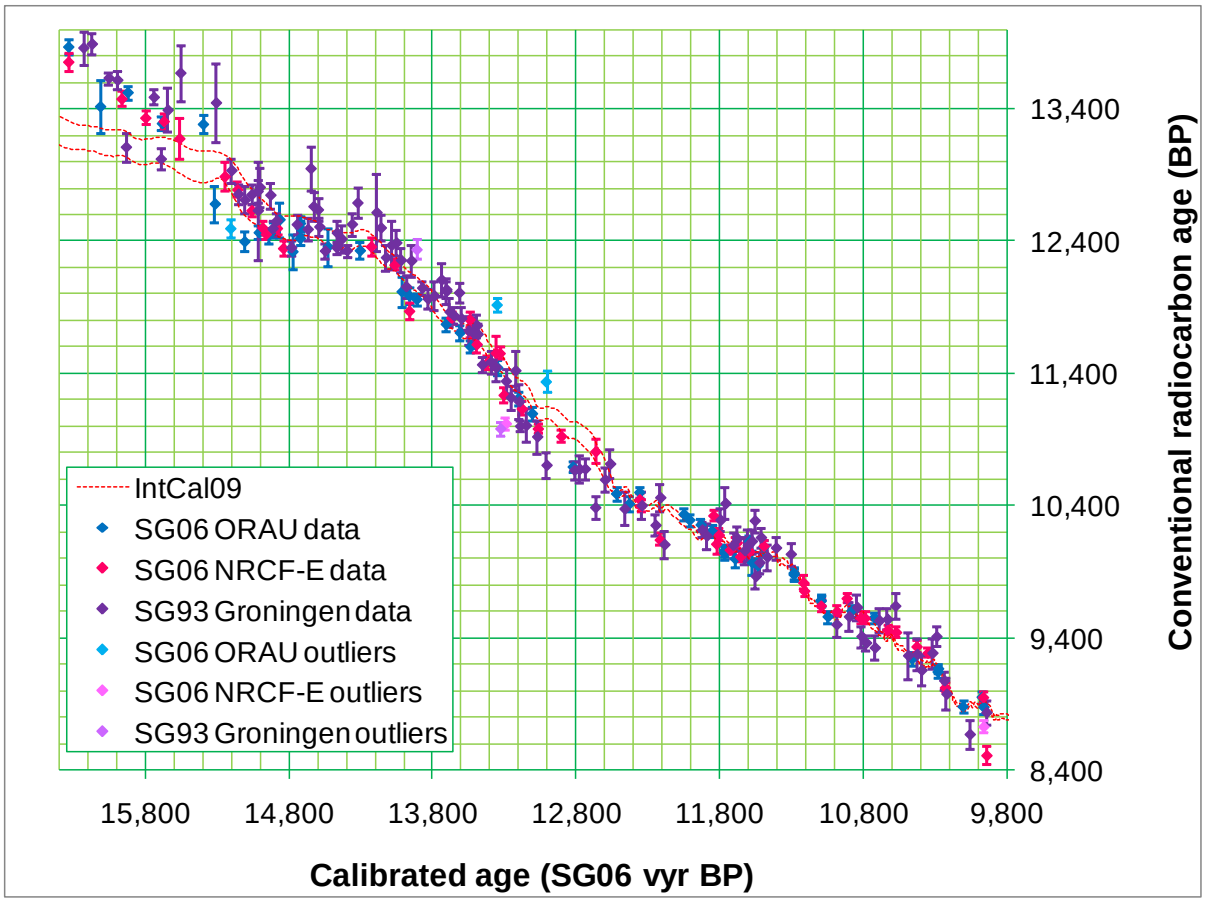

Figure 8.6: The placement of the Late-Glacial pine ('LCP'; green data points) radiocarbon calibration dataset on to the absolute, IntCal ('extended absolute TR'; black data points) timescale via the Southern Hemisphere Huon pine ('HP-40'; red data points) record, as derived by Hua *et al*. (2009). The 45 SG06 and 48 SG93 radiocarbon determinations through this time period (14,000 to 11,600 SG06 vyr BP) are overlain, with the contributing nineteen 'non-outlying' ORAU measurements shown in blue (with vertical error bars only), two 'outlying' ORAU measurements shown in light blue (solid circles), 23 'non-outlying' NRCF-E measurements in magenta, one 'outlying' NRCF-E data point in light pink, 46 'non-outlying' Groningen measurements in purple (or grey to highlight core section SG17), and two 'outlying' Groningen measurements shown in mauve. Additionally, data from the Cariaco Basin (Hughen *et al*. 2004b) are shown as light blue open circles, and Atlantic and Pacific coral data are plotted in blue and purple, respectively (with both vertical and horizontal error bars included; see Hua *et al*. 2009 for references). The IntCal09 (Reimer *et al*. 2009) calibration curve is also shown as the hashed red lines. All data are plotted at 1σ uncertainty.

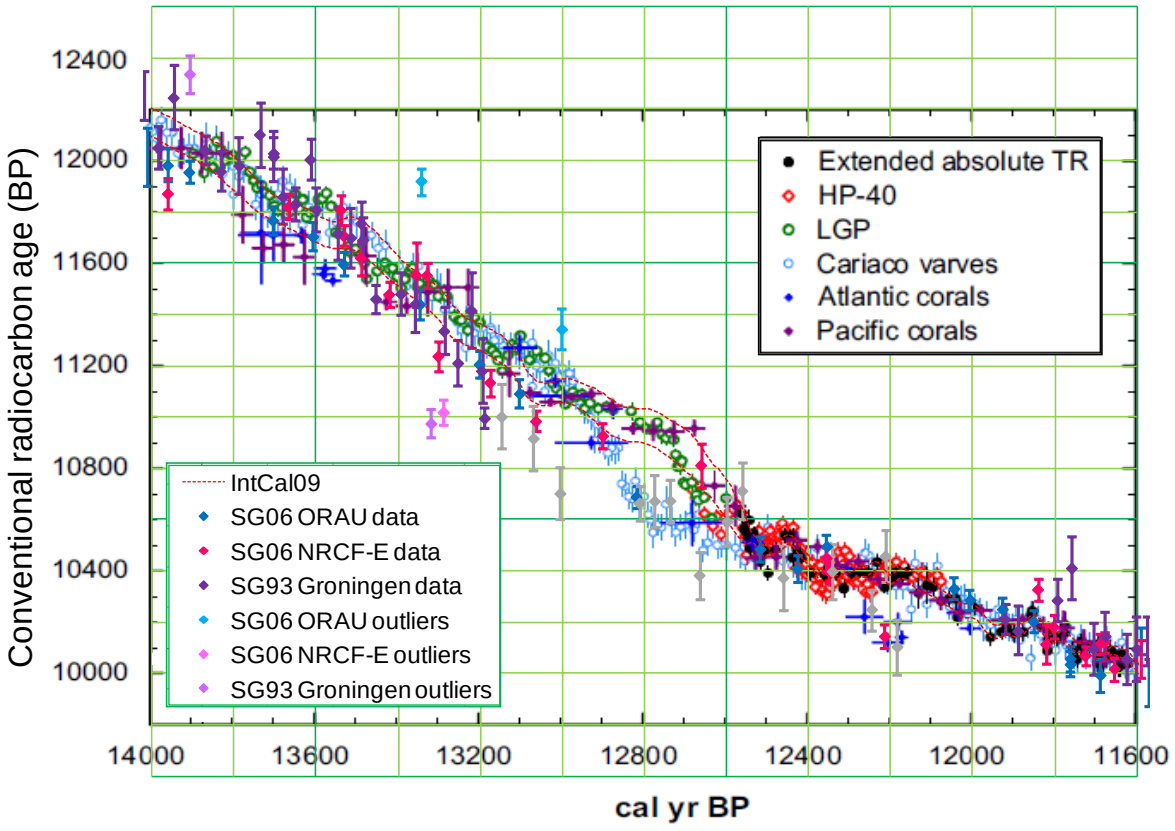

However, the agreement between the Lake Suigetsu and floating European pine data before *circa* 13,200 SG06 vyr BP is again good, implying that if a shift in the placement of the floating pine on the absolute timescale were applied at the younger end, the floating pine data would become discordant with Suigetsu (and IntCal) at the older end of the record. A possible scenario could be envisaged whereby only the younger end of the floating pine chronology could be moved significantly on the calendar age axis, if there were an internal problem within the dendrochronological matching of the pine tree-ring data, which is not beyond the bounds of probability. (For example, dendrochronological revision was required to the 1993 calibration curve following the errors identified by Kromer *et al*. 1996, and revision to the oldest portion of the calibration curve was required between the publication of IntCal04, Reimer *et al*. 2004a, and IntCal09; section 2.5.1. However, it should be noted that these floating tree-ring data are comprised of two independent chronologies that have been cross-matched, Schaub *et al*. 2008a, giving increased belief in the composite tree-ring dataset.) Alternatively, though more controversially, there could be a real regional offset between the European atmospheric carbon reservoir (from which the European tree-ring archives drew their carbon), and that of the atmospheric reservoir over the Japanese archipelago through this time interval. This latter suggestion would certainly require further evidence to be accepted, and it would be hard to envisage a feasible physical mechanism for this having been the case. Such a conclusion would require that the atmosphere over central Europe was depleted in ^{14}C relative to the atmosphere over Japan for several centuries. Potential, though unlikely, mechanisms could be significant ocean upwelling off the coast of western Europe (cf. Damon 1995; though it would be hard to envisage the trees of more distant central Europe being affected without producing a more widespread, circum-Hemispheric signal), or significant volcanic degassing (though, again, it would be difficult to imagine this affecting trees across central Europe – cf. Bruns 1980 – without the signal

having been propagated throughout the entire Northern Hemisphere). It has previously been proposed (Damon *et al*. 1996) that the radiocarbon concentration in central European tree-rings could have been depressed during deglaciation, as a result of significant quantities of dissolved, ^{14}C-deficient carbon being released from the melting European ice-sheets and depressing the ^{14}C signal of carbon assimilated into the trees from that dissolved in groundwater, or being released into the ambient atmosphere. However, the temporal coincidence with the Younger Dryas cooling contradicts such a theory, in this case, as any offsets from such a cause would presumably have been observed both prior to- and immediately after the Younger Dryas (i.e. at times of global climatic warming), rather than at a time of climatic cooling, as observed.

Closer inspection of the combined Lake Suigetsu data reveals that the specific time period in question is dominated by measurements from the Suigetsu '93 project, with the interval of *circa* 13,154 to 12,167 SG06 vyr BP represented by the single SG93 core section, 'SG17' (the data for which are highlighted in grey in figure 8.6). Inspection of the correlation model between SG93 and SG06 (table 6.1) reveals that there is presently a 16.4 cm gap between SG93 core sections SG16 and SG17, which could allow for the SG17 core section to be shifted by up to 170 SG06 varve years to younger ages (assuming no actual core overlap with the overlying SG16 core section, and that the matching of SG16 is in the right place, with either of these possibilities potentially allowing SG17 to shift slightly earlier still). The radiocarbon plateau demonstrated by the younger determinations from SG17 means that a shift in the placement of this core section is entirely feasible for these younger samples, and hinders the use of this younger time period to aid the resolution of this issue. A 170 year error would not entirely remove the discordance with the floating pine data, but would go a long way to resolving the matter (with the SG06 data sparse through this period, in comparison, due to low plant macrofossil abundance from this section of the core). Errors in the SG06

varve year timescale (either of systematic under- or over-counting, or of potential sedimentary hiatuses) should not be the principal cause of the offset shown, since agreement with the alternative calibration datasets is excellent for long time periods (> 1,500 SG06 varve years) both before- and after this interval.

The specific time period of potential deviation is critical to palaeoenvironmental reconstruction by Suigetsu Varves 2006 project colleagues, since it centres on the onset of the Younger Dryas (YD) cold reversal, which is defined by multi-proxy palaeoenvironmental reconstruction at 1554.5 cm CD in SG06, at *circa* 12,884 SG06 vyr BP (absolute maximum and minimum values of 13,082 and 12,741 SG06 vyr BP, respectively). As with the dating of the Holocene onset (section 7.4.1; figure 7.13), this globally significant palaeoclimatic event is in good temporal agreement with the onset of the YD in Greenland, being placed at 12,846 cal. BP (12,896 b2k) in NGRIP (total maximum counting error 138 years; Rasmussen *et al*. 2006). However, the necessity of a reliable chronology through this time period is reiterated, since the identification of potential palaeoclimatic leads or lags within the Earth's system (between Lake Suigetsu and more distant geographical regions) is critically reliant upon it. Were there indeed errors demonstrated in the SG06 varve chronology (through comparison of the project's radiocarbon data with those of other sites), this would then have ramifications for the placement of the YD-equivalent onset in SG06.

8.1.3 Dating into the Glacial

Below 1814.6 cm composite depth (16,337 SG06 vyr BP), the varve counting of SG06 remains un-finalised (being based entirely upon the Itrax™ XRF and X-radiography data only). The conclusions drawn for the present- and subsequent section therefore remain preliminary (in terms of the Suigetsu Varves 2006 project).

Figure 8.7 illustrates the extension of both the Suigetsu ’93 and Suigetsu Varves 2006 radiocarbon datasets, as compared to IntCal09 (Reimer *et al*. 2009), back into the Last Glacial. As was introduced in the previous section, the Lake Suigetsu radiocarbon data (both from SG93 and SG06) begin to diverge from IntCal09 before *circa* 15,300 SG06 vyr BP (figure 8.7a). Although these data come back into better agreement *circa* 17,600 SG06 vyr BP, the deviation continues further back in time, only coming back into full agreement *circa* 20,200 SG06 vyr BP (figure 8.7b).

Over the preceding time period, between *circa* 27,000 and 20,200 SG06 vyr BP, the respective datasets are in good agreement (figure 8.7c), but there again appears to be divergence in the time period before 27,000 SG06 vyr BP, and especially so between *circa* 39,000 and 33,000 SG06 vyr BP (figure 8.7d). Although the radiocarbon dating uncertainties become increasingly large beyond *circa* 40,000 SG06 vyr BP, the trend of the data seems to follow the smoothed IntCal09 curve and, by imagined extrapolation of the IntCal trend line beyond its present (50,000 cal. BP) limit, seems reasonable back to the *circa* 56,000 SG06 vyr BP limit of the Lake Suigetsu data (figure 8.7e).

Figure 8.7: Extension of the Lake Suigetsu radiocarbon calibration dataset into the Last Glacial, composed of the 352 SG06 and 149 SG93 radiocarbon determinations obtained from the SG06 (or SG06-equivalent) core depths below the present limits of the provisionally complete varve chronology, 1814.6 cm composite depth (16,337 SG06 vyr BP), plotted over the time periods: **(a)** 20,000 to 14,800 SG06 vyr BP; **(b)** 25,000 to 18,800 SG06 vyr BP; **(c)** 30,000 to 23,800 SG06 vyr BP; **(d)** 40,000 to 29,000 SG06 vyr BP; and **(e)** 56,000 to 39,000 SG06 vyr BP. The 189 'non-outlying' ORAU measurements (beyond 16,337 SG06 vyr BP) are shown in blue, the twelve 'outlying' ORAU measurements in light blue, the 139 'non-outlying' NRCF-E measurements in magenta, the twelve 'outlying' NRCF-E data points in light pink, the 141 'non-outlying' Groningen measurements in purple, and the eight 'outlying' Groningen measurements in mauve. For comparison, the IntCal09 (Reimer *et al*. 2009) calibration curve is shown as the hashed red lines. Both the SG06 data and the IntCal09 curve are plotted at 1σ uncertainty.

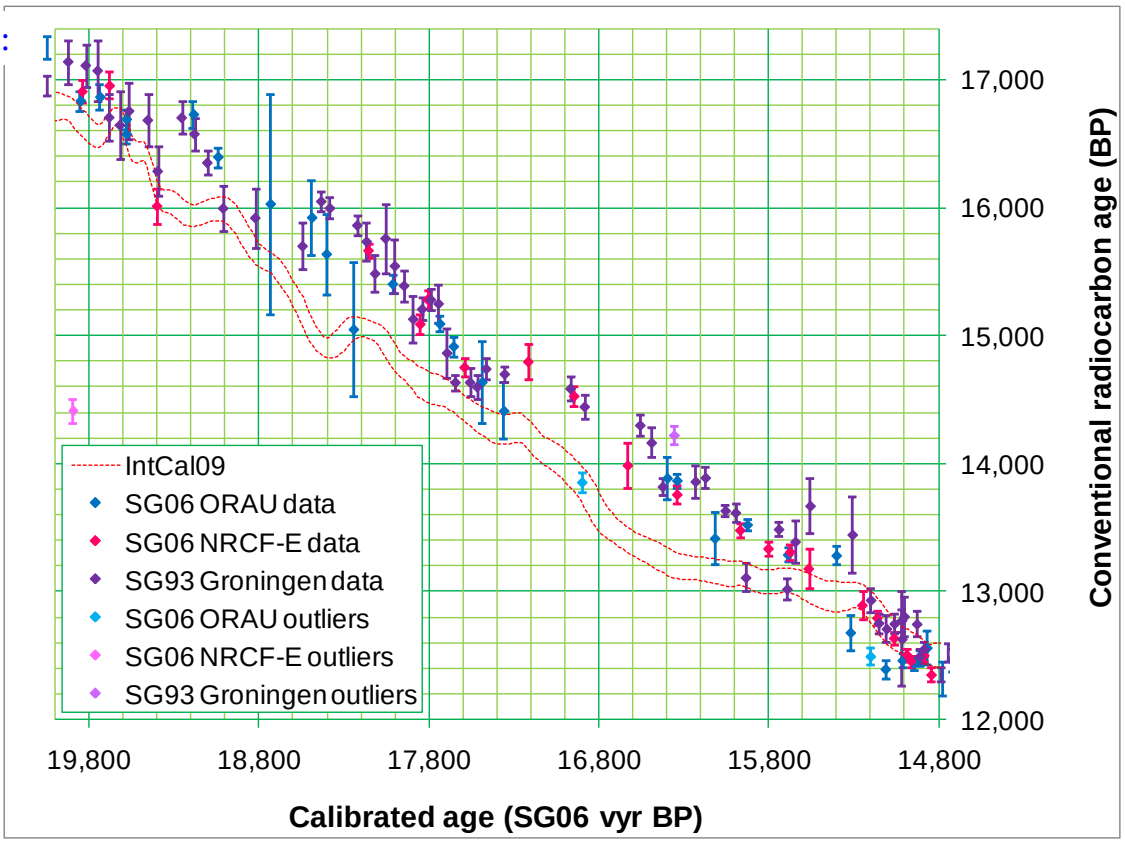

Figure 8.7 (continued):

(b):

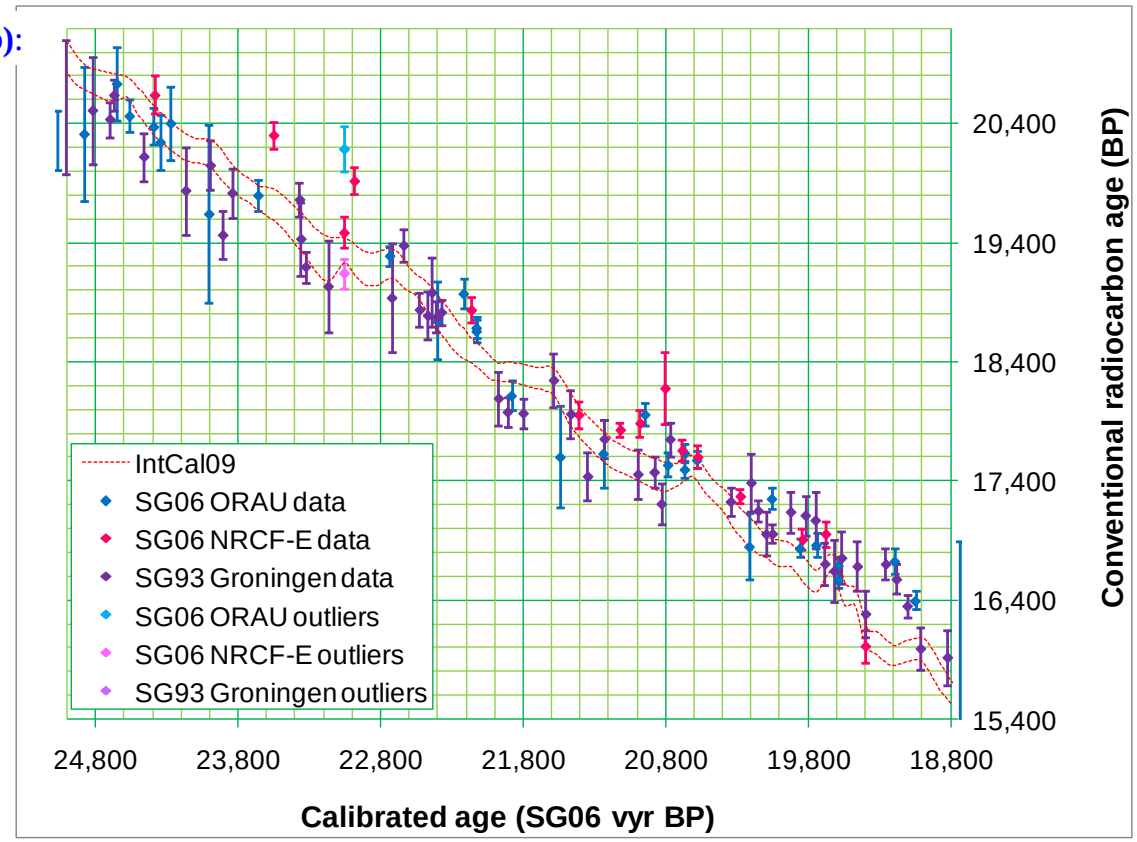

(c):

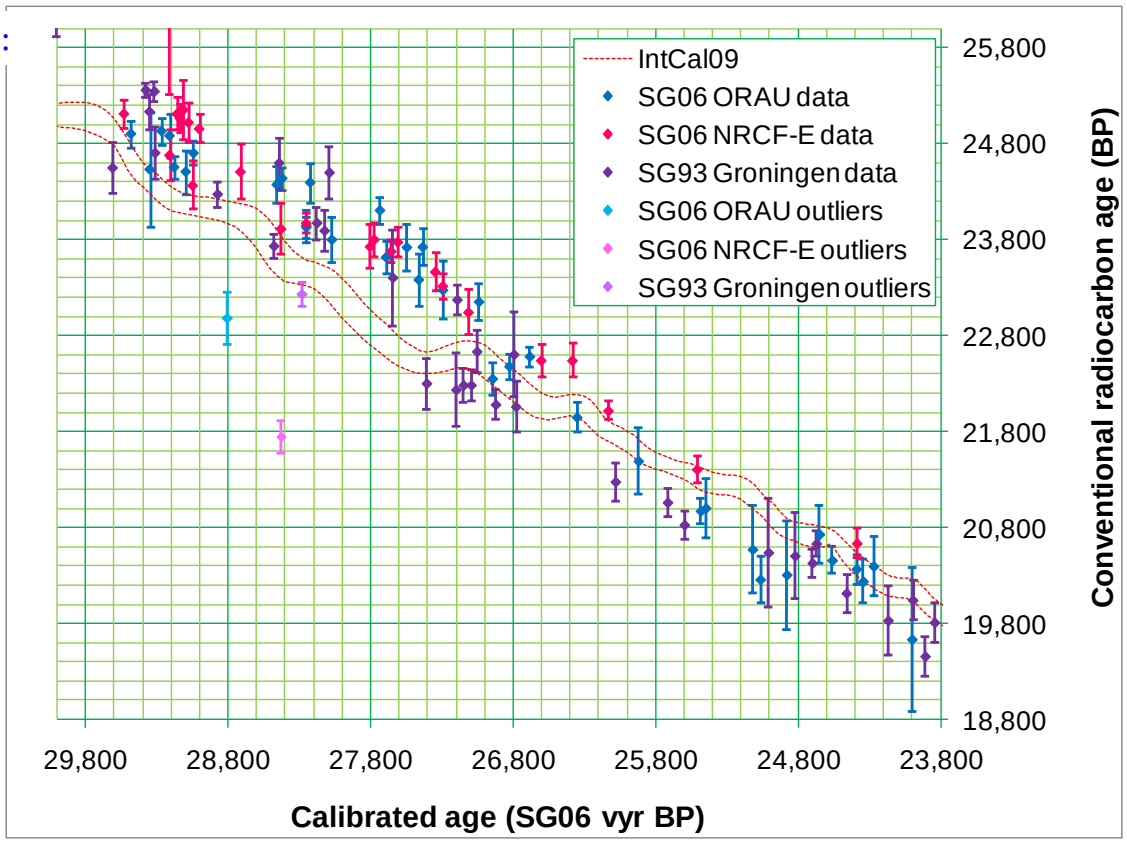

Figure 8.7 (continued):

(d):

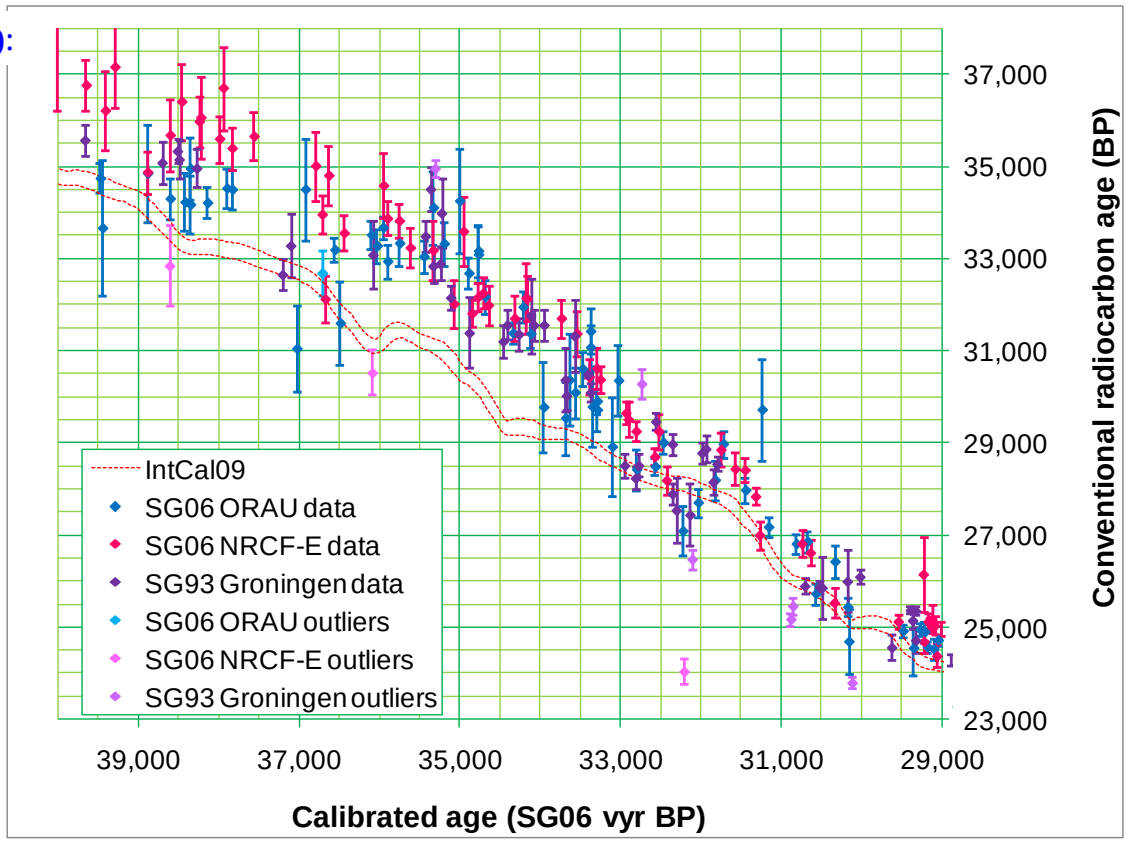

(e):

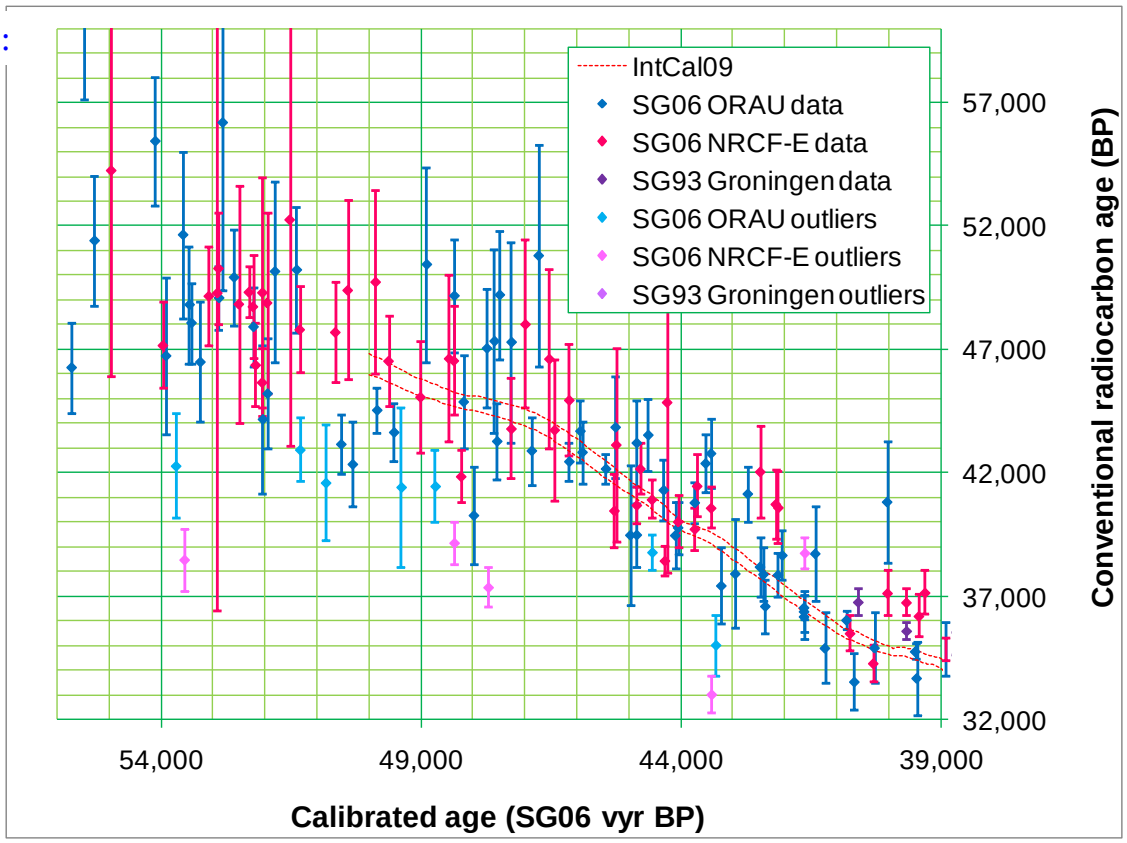

There are clearly several potential explanations for the periods of divergence between the Lake Suigetsu and IntCal09 datasets, which include both issues pertaining to the radiocarbon measurements themselves, as well as to the calendar timescales derived. The abundance and internal consistency of radiocarbon determinations from the three contributing laboratories to the Lake Suigetsu dataset rules out erroneous radiocarbon measurement (as it does for the data contributing to the IntCal curve), but there may be real reasons (including temporally varying reservoir corrections) why the observed radiocarbon determinations are offset between the two datasets. Alternatively, there may be inaccuracies in the SG06 varve year timescale caused by either systematic under- or over-counting, or due to hiatuses down the sediment profile. Additionally, the IntCal09 calendar age scale might not be wholly accurate throughout, due to the potential reasons discussed in section 2.5. However, unlike the previously mentioned period of discrepancy (between *circa* 13,200 and 12,600 SG06 vyr BP) for which the matching of SG93 to the SG06 composite depth scale was questioned, the matching of SG93 core sections is more robust through this time period, being based on the archive U-channel material (from the top of SG93 core section SG20 – 1769 cm CD, 15,533 SG06 vyr BP – and below), and so should not be the cause of such discrepancy.

Returning to the youngest period of divergence (20,200 to 15,300 SG06 vyr BP) specifically: the younger portion of this time period coincides with Heinrich event 1 (H1; ≈ 17,500 to 15,000 cal. BP), which was cited in section 2.7 as representing a 'questionable' interval within IntCal09, due to the previously demonstrated divergence between the Cariaco Basin record (Hughen *et al*. 2006), which forms the mainstay of the IntCal curve through this period, and the Bahamas speleothem and Iberian margin datasets of Beck *et al*. (2001) and Bard *et al*. (2004c), respectively. Figure 8.8 illustrates the same time period as figure 8.7a, but with the additional contributing data to IntCal09 plotted as raw data points. The IntCal09

curve is clearly dominated by the Cariaco Basin dataset (Hughen *et al*. 2006) through the period *circa* 18,000 to 15,500 cal. BP, but the alternative, low resolution data from the Iberian margin sediments (Bard *et al*. 2004c), as well as two supporting data points from marine corals (Bard *et al*. 1998), show good agreement with the Lake Suigetsu dataset. This suggests that the Suigetsu data might actually be representing the 'true' atmospheric radiocarbon calibration curve through this time period, which would be an important outcome of the Suigetsu Varves 2006 project in its own right. The proposed reason for this excursion in the Cariaco Basin dataset would be that the local marine reservoir correction applied (430 ± 50 years) is over-correcting the measured radiocarbon data through the Heinrich event, with altered surface ocean circulation patterns in the tropical North Atlantic allowing the reservoir correction to drop to near zero at this time. A similar observation has been made through H0 (the Younger Dryas), and is the reason for the exclusion of the Cariaco Basin data between 12,900 and 12,550 cal. BP from IntCal09 (Reimer *et al*. 2009).

Before 17,500 cal. BP, the Cariaco Basin dataset is supplemented in IntCal09 by the relatively high resolution Barbados coral data of Fairbanks *et al*. (2005), which seem to be in good agreement over the remainder of this time period. Both of these datasets therefore show discrepancy from the Lake Suigetsu data between *circa* 20,200 and 17,600 SG06 vyr BP. It is again possible that both the Cariaco Basin and Barbados coral data are demonstrating a similar marine reservoir over-correction, although the Bahamian speleothem data of Beck *et al*. (2001; not shown here) also support the marine data. Therefore, the SG06 varve year age scale before 17,600 SG06 vyr BP is questioned. If one assumes that the IntCal09 calibration is correct through this period, the Lake Suigetsu data can be calibrated against it to assess the scope for varve counting error. Both `P_Sequence` (with `k` = 7.44; section 7.4.1) and `D_Sequence` models were run in OxCal (OCM-8.1 and OCM-8.2, respectively), using just the Suigetsu data between 20,200 and 17,600 SG06 vyr BP (2032.5 and 1885.1 cm CD), as

well as including query (`difference`) functions to assess the degree of offset from IntCal09 at both the top and bottom of these deposition sequences. (As with all other OxCal models discussed in this thesis, the coding for these OxCal models is given in full in appendix 8.)

Figure 8.9 plots these two modelled fits of the Lake Suigetsu data against the IntCal09 calibration curve, and it can be clearly seen that the Suigetsu data can be 'pulled' to fit the calibration curve very well. Indeed, this high degree of concordance is demonstrated by the fact that none of the contributing 52 Suigetsu data points are identified as having ≥ 90% posterior probability of being outliers. A comparison of the original SG06 vyr ages of these Lake Suigetsu radiocarbon determinations against the modelled ages, derived through calibration against IntCal09, is given in figure 8.10, with figure 8.11 more clearly illustrating the modelled offsets between the respective timescales at the top and bottom of the modelled sequences.

The `D_Sequence` model (OCM-8.2) indicates a 389 to 452 year offset between the SG06 vyr timescale and the cal. BP timescale derived through the wiggle-match on to IntCal09 (at the 68.2% probability range; between 379 and 502 years at the 95.4% probability range). The closeness of fit between the datasets (including the lack of modelled outliers) supports the validity of the proposed model, which would represent a significant (389 to 452 year) hiatus in the Lake Suigetsu sediment profile at 17,600 SG06 vyr BP (1885.1 cm CD).

Figure 8.8: The 52 SG06 and 58 SG93 radiocarbon determinations obtained from between 20,000 and 14,800 SG06 vyr BP (1720.1 cm to 2021.0 cm composite depth). The 27 'non-outlying' ORAU measurements are shown in blue, the two 'outlying' ORAU measurements in light blue, the 22 'non-outlying' NRCF-E measurements in magenta, the single 'outlying' NRCF-E data point in light pink, the 57 'non-outlying' Groningen measurements in purple, and the single 'outlying' Groningen measurement in mauve. For comparison, the IntCal09 (Reimer *et al*. 2009) calibration curve is shown as the hashed red lines, with the contributory data points from the Cariaco Basin (Hughen *et al*. 2006) plotted in grey, Iberian margin (Bard *et al*. 2004c), and coral datasets of Bard *et al*. (1998, 2004a) and Fairbanks *et al*. (2005) plotted in dark- and light green, respectively. All data are plotted at 1σ uncertainty.

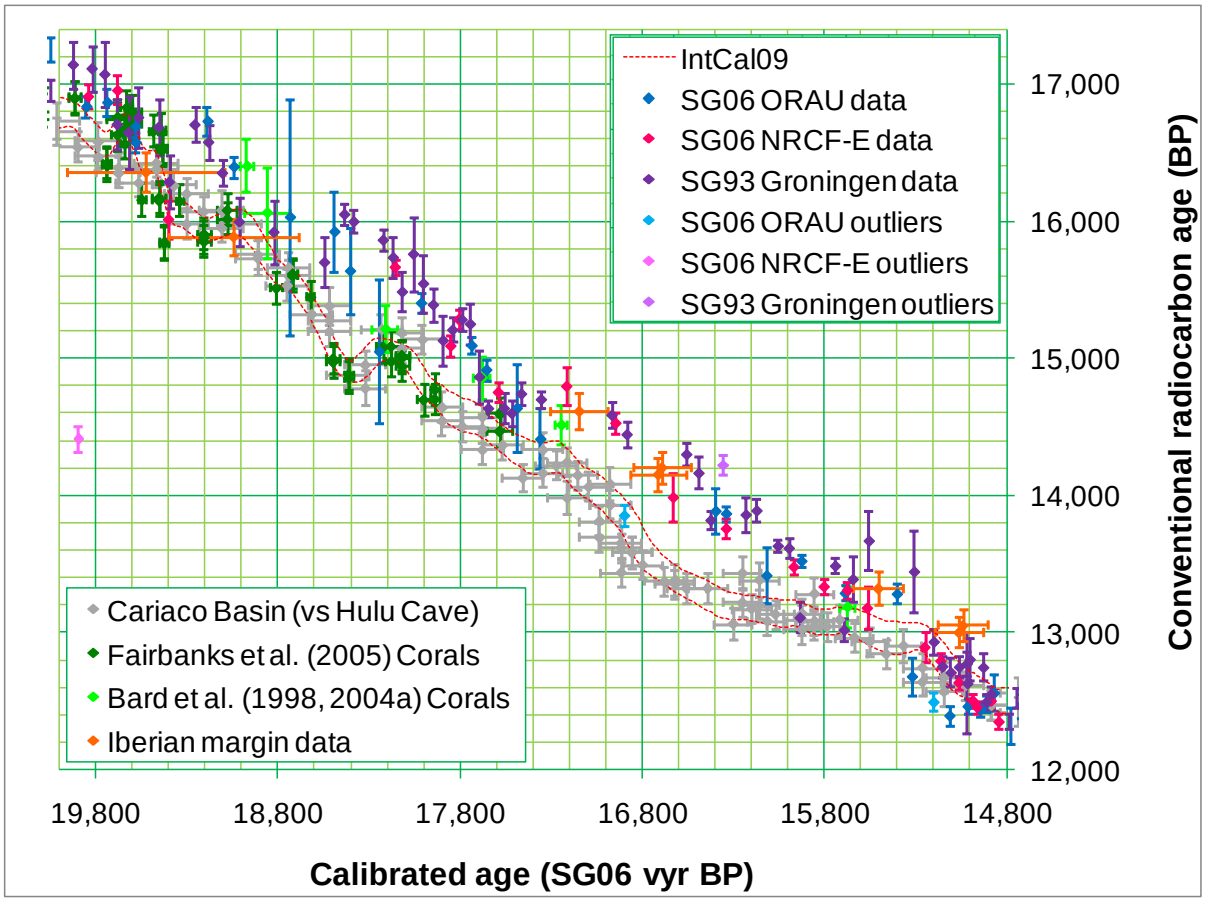

Figure 8.9: The placement of the Lake Suigetsu radiocarbon calibration dataset between 20,200 and 17,600 SG06 vyr BP when calibrated against IntCal09 (Reimer *et al*. 2009; lime green) using: **(a)** a `P_Sequence` model (OCM-8.1; k = 7.44); and **(b)** a `D_Sequence` model (OCM-8.2). ORAU data are plotted in blue, NRCF-E data in magenta, and Groningen data in purple, with all data points and the calibration curve plotted at 1σ uncertainty.

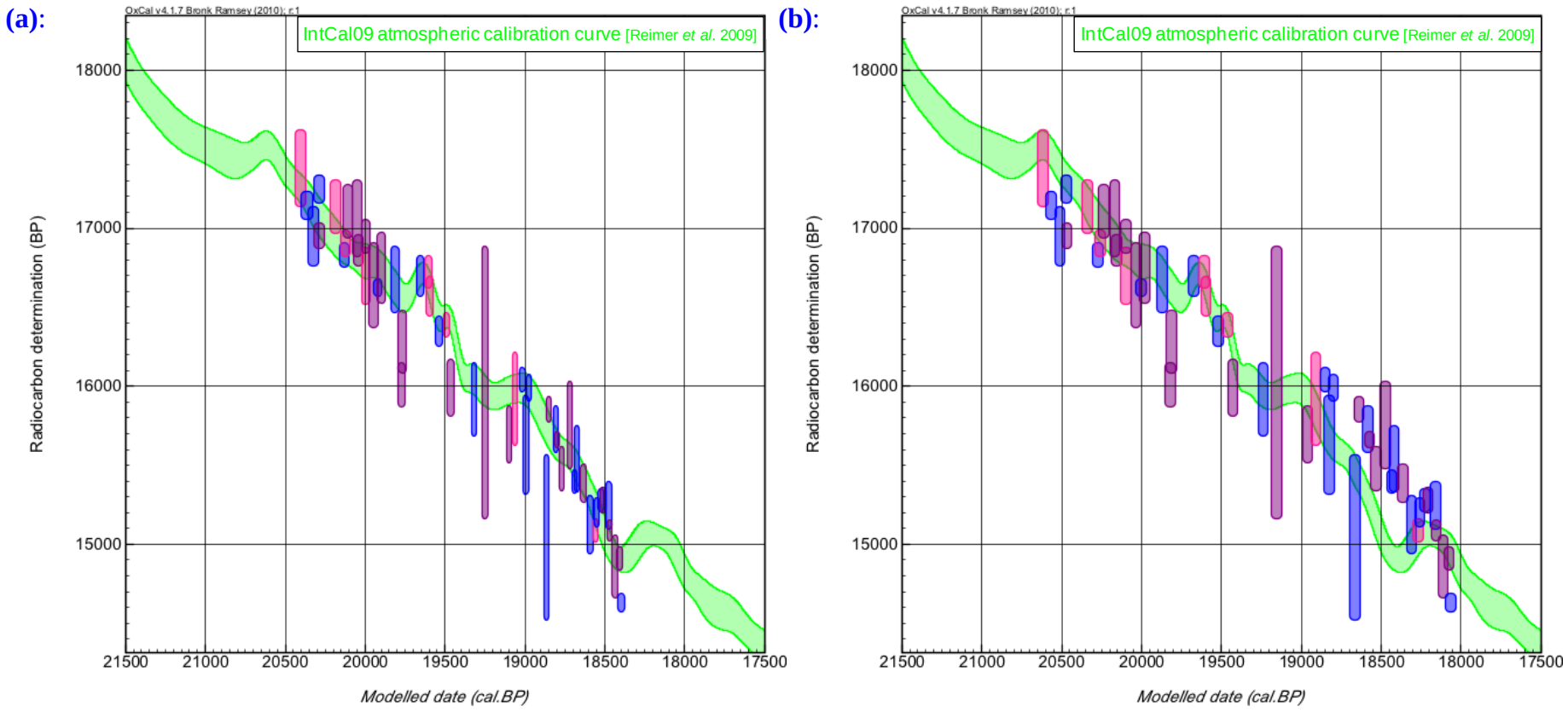

Figure 8.10: Plots to compare the 'un-manipulated' SG06 vyr- and modelled (calibrated against IntCal09; Reimer *et al*. 2009) ages of the Lake Suigetsu radiocarbon calibration dataset between 20,200 and 17,600 SG06 vyr BP. **(a)** is the output of a `P_Sequence` model (OCM-8.1; k = 7.44); and **(b)** is the output of a `D_Sequence` model (OCM-8.2). ORAU data are plotted in blue, NRCF-E data in magenta, and Groningen data in purple. The posterior age-depth profile (the darker shading), overlies the prior, un-modelled probability density functions (lighter shading).

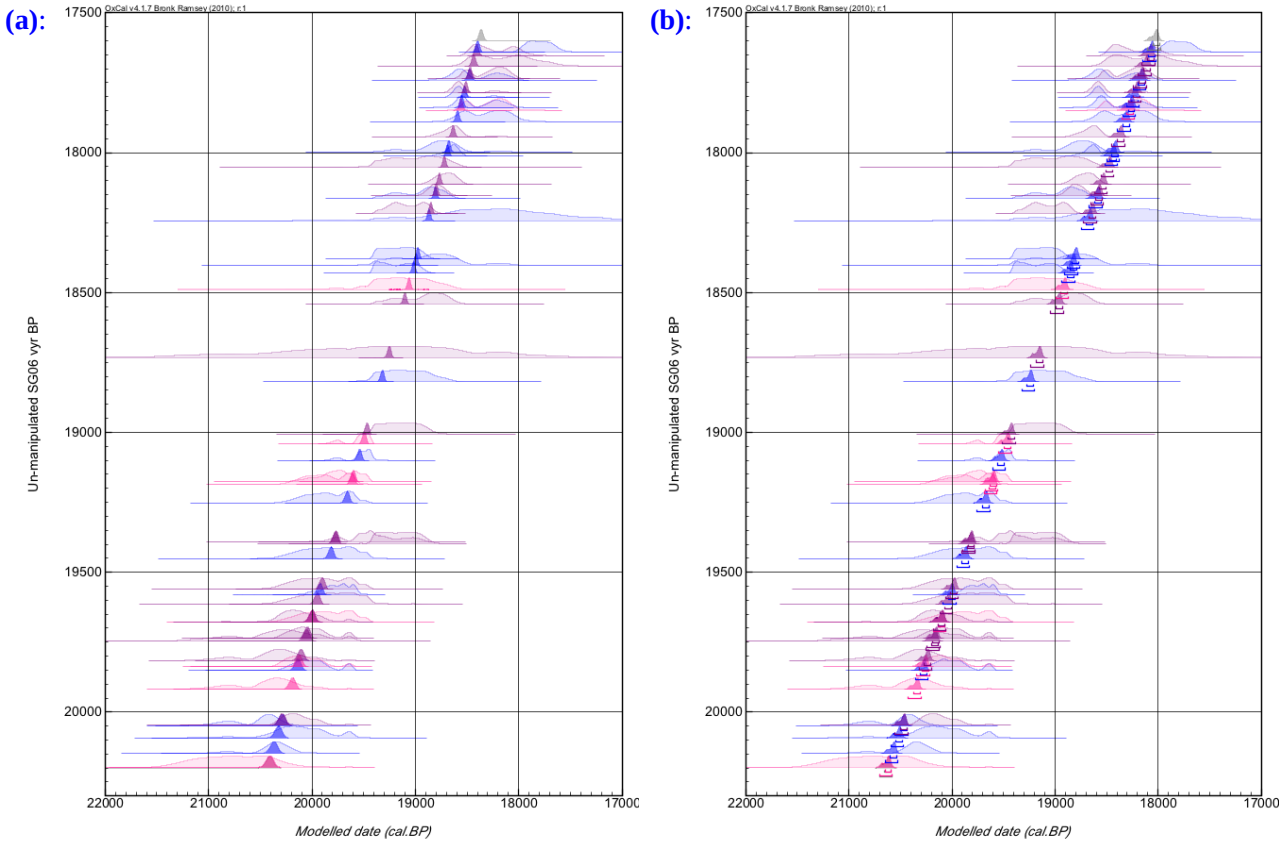

Figure 8.11: The modelled offset of the Lake Suigetsu radiocarbon calibration dataset, as calibrated against IntCal09 (Reimer *et al*. 2009), at 17,600 SG06 vyr BP using: **(a)** a `P_Sequence` model (OCM-8.1, k = 7.44); and **(b)** a `D_Sequence` model (OCM-8.2); and at 20,200 SG06 vyr BP using: **(c)** a `P_Sequence` model (OCM-8.1, k = 7.44); and **(d)** a `D_Sequence` model (OCM-8.2).

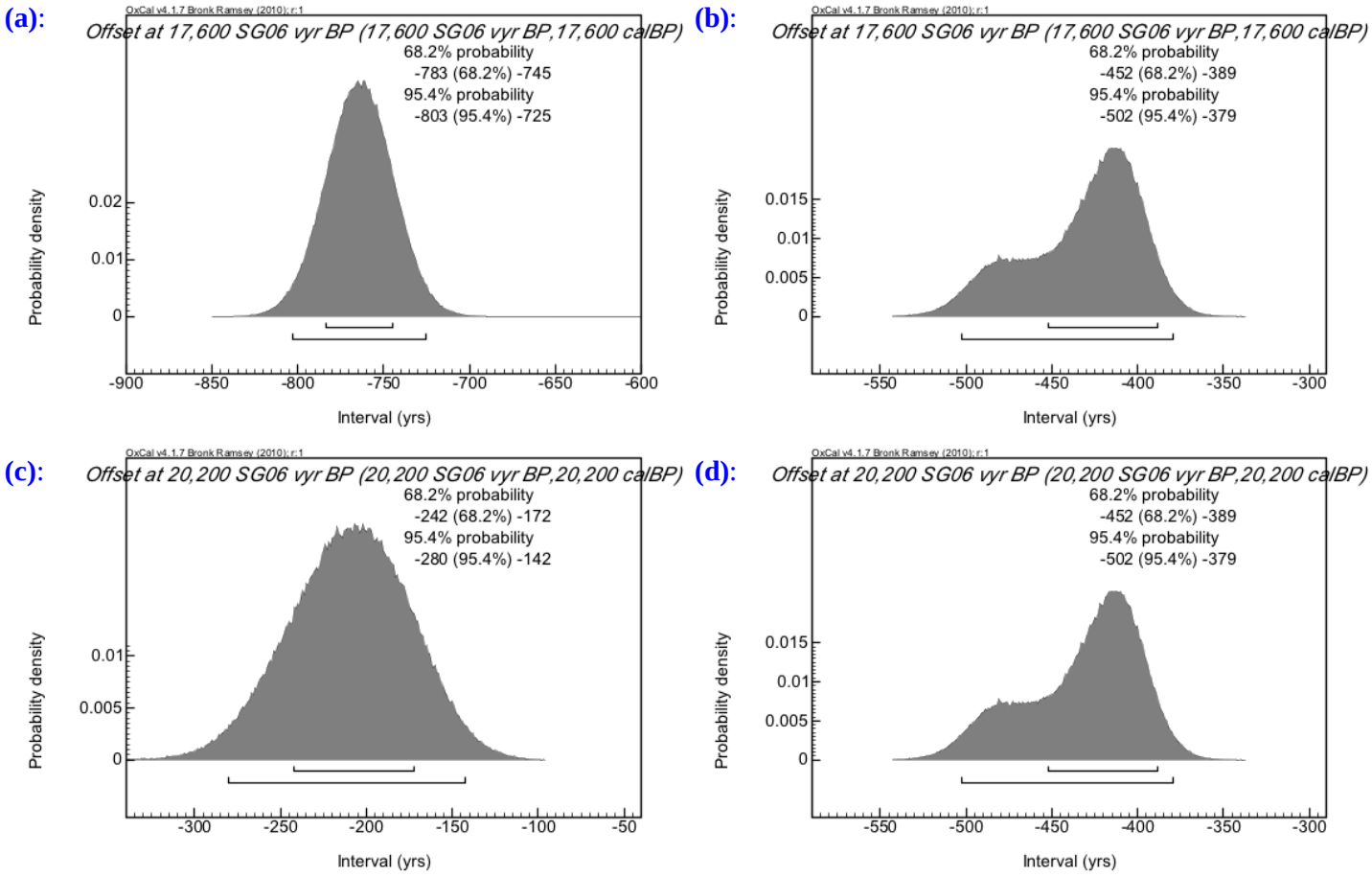

The results of the P_Sequence model (OCM-8.1), which does not constrain the overall duration of the modelled data *a priori*, suggests a closer fit to IntCal09 if the calibrated age scale is compressed, as compared to the original SG06 varve count. Accordingly, the modelled offset between the SG06 vyr and IntCal09 cal. BP timescales is 745 to 783 years at 17,600 SG06 vyr BP (68.2% probability range; 725 to 803 years at the 95.4% probability range), but reduced to 172 to 242 years (68.2% probability range; 142 to 280 years at the 95.4% probability range) at 20,200 SG06 vyr BP. For this model to represent the authentic situation would therefore require a large hiatus in the Lake Suigetsu sediment profile (representing the loss of ≈ 750 varves), followed by a systematic over-count across this modelled time period of ≈ 550 varves in 2,600 calendar years. Although the possibility of an over-count is certainly feasible (since the varve counting from this time period and earlier is based upon the XRF and X-radiography methodology only, and comparison with the thin section counting in the later time periods supports a slight over-count, due to the interpolation algorithm applied), an error of this magnitude certainly seems excessive. Such a scenario seems especially unlikely since the concordance between the Lake Suigetsu and IntCal09 datasets seems to be so good for the preceding time period, back to *circa* 27,000 SG06 vyr BP. It is therefore proposed that, even if there were a hiatus present, the offset in the Lake Suigetsu calibration dataset from IntCal would contain an element of authentic deviation.

The natural extension of this exercise is to produce similar modelled fits of the combined Lake Suigetsu data against IntCal09, but extended through the earlier time period also. P_Sequence (OCM-8.3) and D_Sequence (OCM-8.4) models were again run, therefore, covering the entire period of offset from IntCal09, 20,200 to 15,300 SG06 vyr BP. The modelled fits of the Suigetsu data on to the calibration curve according to these two

model specifications are illustrated in figure 8.12. The deviation between the SG06 vyr- and IntCal09 cal. BP timescales thus derived is illustrated in figures 8.13 and 8.14.

Again, the modelled fit of the Lake Suigetsu data against the calibration curve is very good, with only a single sample, GrA-4558, identified as having ≥ 95% posterior probability of being an outlier in OCM-8.3, and another single sample, SUERC-19063, identified as an outlier (≥ 95% posterior probability) in OCM-8.4. As with the shorter model sequences above (OCM-8.1 and OCM-8.2), the agreement between the Suigetsu data and IntCal09 is better with the `P_Sequence` model construction, again implying that a systematic varve over-count (≈ 450 extra varve years over 4,900 years of calendar time) would be required, following a sizable (≈ 750 year) hiatus in the Lake Suigetsu sediment profile. Again, such an over-count seems unrealistically large. Furthermore, this extended 'correction' to the SG06 vyr timescale would imply that the calibration curve through H1, based principally on the Cariaco Basin dataset (Hughen *et al*. 2006) is accurate, and that the alternative available data (including the datasets of Beck *et al*. 2001, Bard *et al*. 2004c, and Magana *et al*. 2009) are all in error.

Whether either of the scenarios (OCM-8.1 and OCM-8.2, or OCM-8.3 and OCM-8.4) is correct would require a sizable hiatus in the Lake Suigetsu sediment profile, for which there is no visible evidence, despite extensive searching by both thin section microscopy and XRF/X-radiography techniques. Such examination is by no means conclusive, however, with known hiatuses in the European maar lake records, for example, despite the lack of visible sedimentary evidence (A. Brauer, personal communication).

The position of any such hiatus in SG06, as suggested above, is determined *a priori* by the placement of the older- and particularly the younger boundaries in these four OxCal models. The purpose of the models is therefore to suggest how lengthy any such hiatus would be given the two possible scenarios for hiatus events (i.e. being placed at 17,600 cal. BP in

OCM-8.1 and 8.2, or at 15,300 cal. BP in OCM-8.3 and 8.4), rather than to determine precisely where in SG06 a hiatus event would be most likely to be placed. Modelling of the Suigetsu dataset on to IntCal09 across a broader time range is complicated by the genuine deviation believed to be present for at least the younger period (17,600 to 15,300 cal. BP) of the overall discrepancy between the two calibration datasets. Rather than there being genuine hiatus events in the Lake Suigetsu sediment profile, as discussed above, it is presently hypothesised that problems with the (non-finalised) varve-counted age scale are responsible for the offsets described (in addition to the 'real' deviation proposed above). It will be noted at this point, that there is a general decline in the quality of varve preservation below ≈ 1750 cm composite depth (i.e. back towards the Last Glacial Maximum, LGM), which might account for a large part of the deviation. With this difficulty of varve counting back into the Glacial, both under-counting or over-counting is possible because of the interpolation algorithm implemented.

Clearly, resolution of these potential issues with the SG06 vyr age scale is critical to disentangling the true nature of the calibration curve, and on-going work by Suigetsu Varves 2006 project colleagues seeks to achieve this goal. Additionally, funding has now been achieved to compare the Lake Suigetsu sediment profile over this 'problematic' time period with that of another Japanese varved lake, Ichi-no-Megata (section 8.2.1, below), to hopefully shed light on the above issues.

Figure 8.12: The placement of the Lake Suigetsu radiocarbon calibration dataset between 20,200 and 15,300 SG06 vyr BP when calibrated against IntCal09 (Reimer *et al*. 2009) using: **(a)** a `P_Sequence` model (OCM-8.3; `k` = 7.44); and **(b)** a `D_Sequence` model (OCM-8.4). ORAU data are plotted in blue, NRCF-E data in magenta, and Groningen data in purple, with all data points and the calibration curve plotted at 1σ uncertainty.

(a):

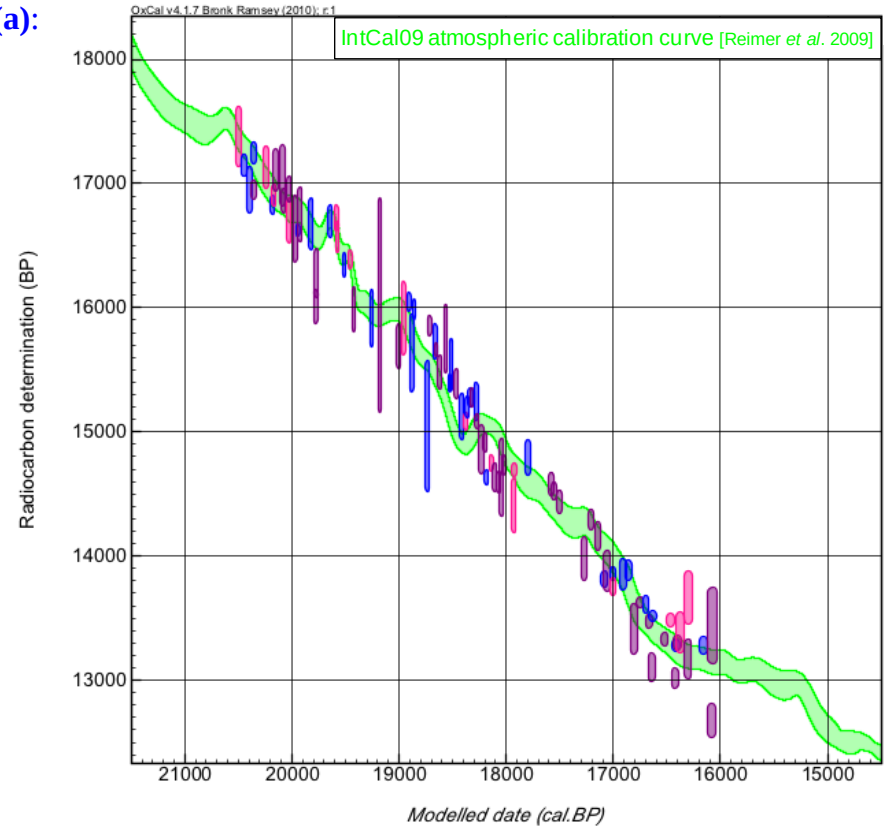

(b):

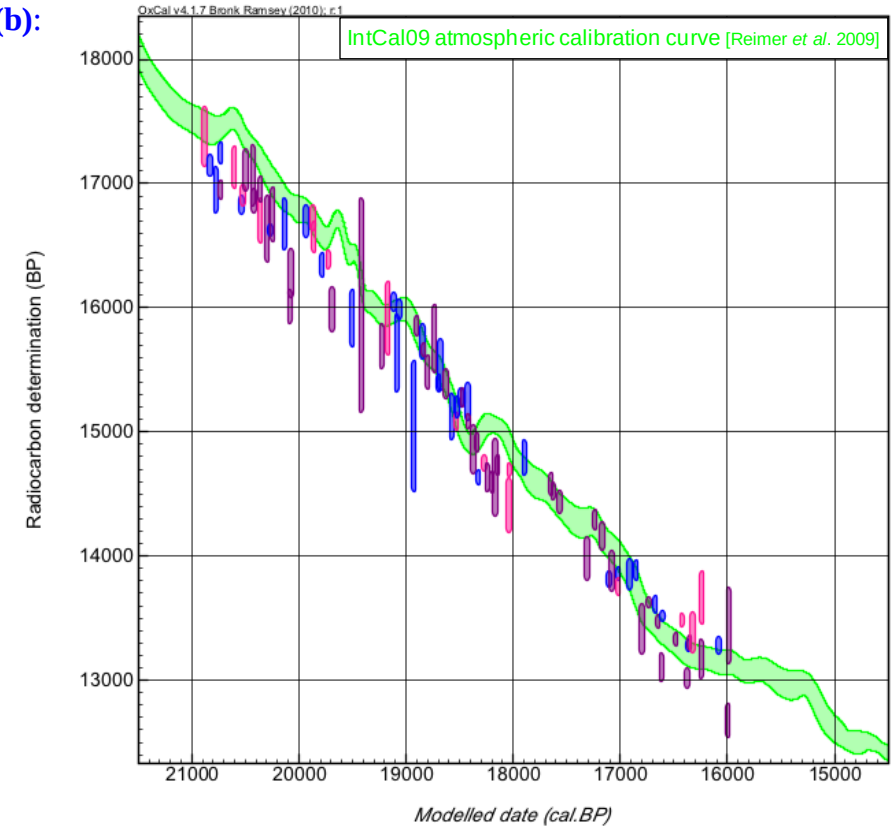

Figure 8.13: Plots to compare the 'un-manipulated' SG06 vyr- and modelled (calibrated against IntCal09; Reimer *et al*. 2009) ages of the Lake Suigetsu radiocarbon calibration dataset between 20,200 and 15,300 SG06 vyr BP. **(a)** is the output of a `P_Sequence` model (OCM-8.3; k = 7.44); and **(b)** is the output of a `D_Sequence` model (OCM-8.4). ORAU data are plotted in blue, NRCF-E data in magenta, and Groningen data in purple. The posterior age-depth profile (the darker shading), overlies the prior, un-modelled probability density functions (lighter shading).

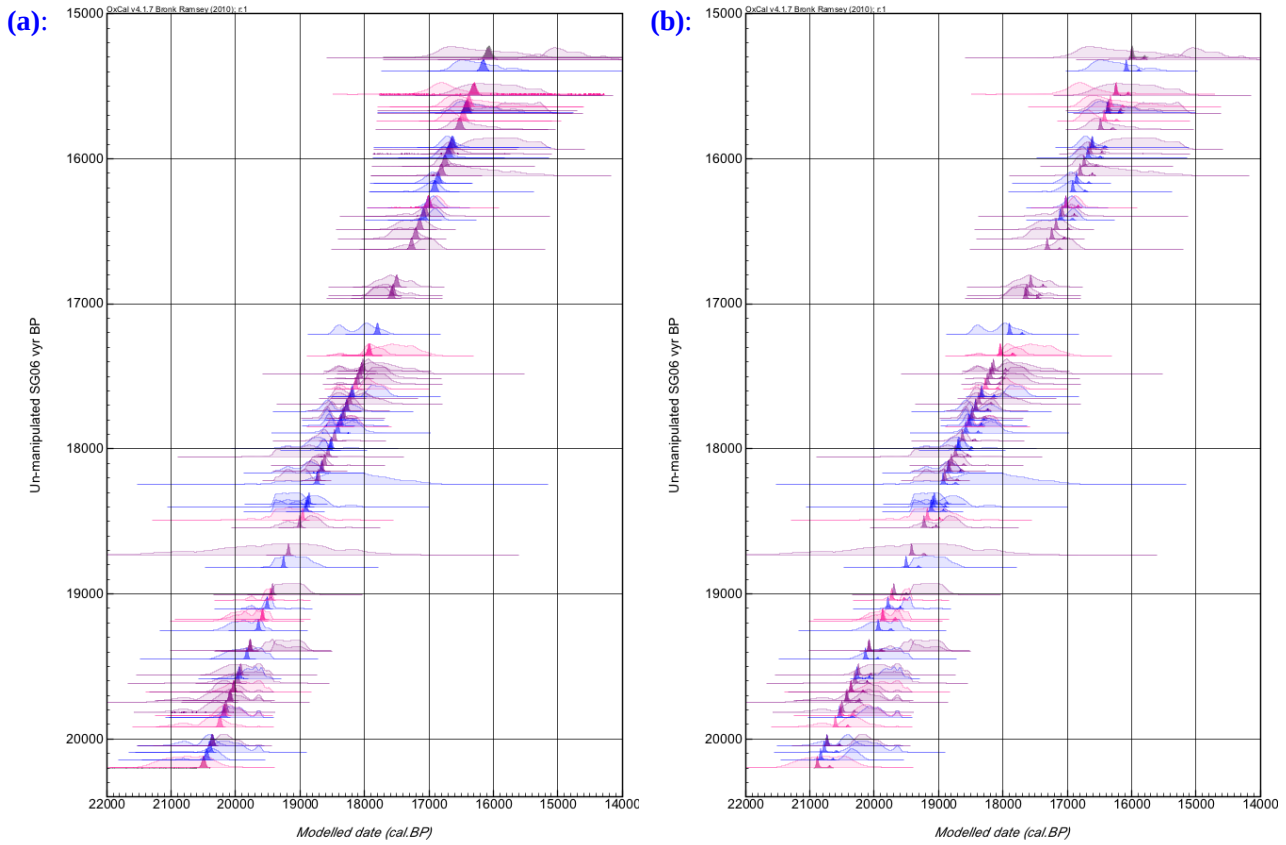

Figure 8.14: The modelled offset of the Lake Suigetsu radiocarbon calibration dataset, as calibrated against IntCal09 (Reimer *et al*. 2009), at 15,300 SG06 vyr BP using: **(a)** a `P_Sequence` model (OCM-8.3; `k` = 7.44); and **(b)** a `D_Sequence` model (OCM-8.4); and at 20,200 SG06 vyr BP using: **(c)** a `P_Sequence` model (OCM-8.3; `k` = 7.44); and **(d)** a `D_Sequence` model (OCM-8.4).

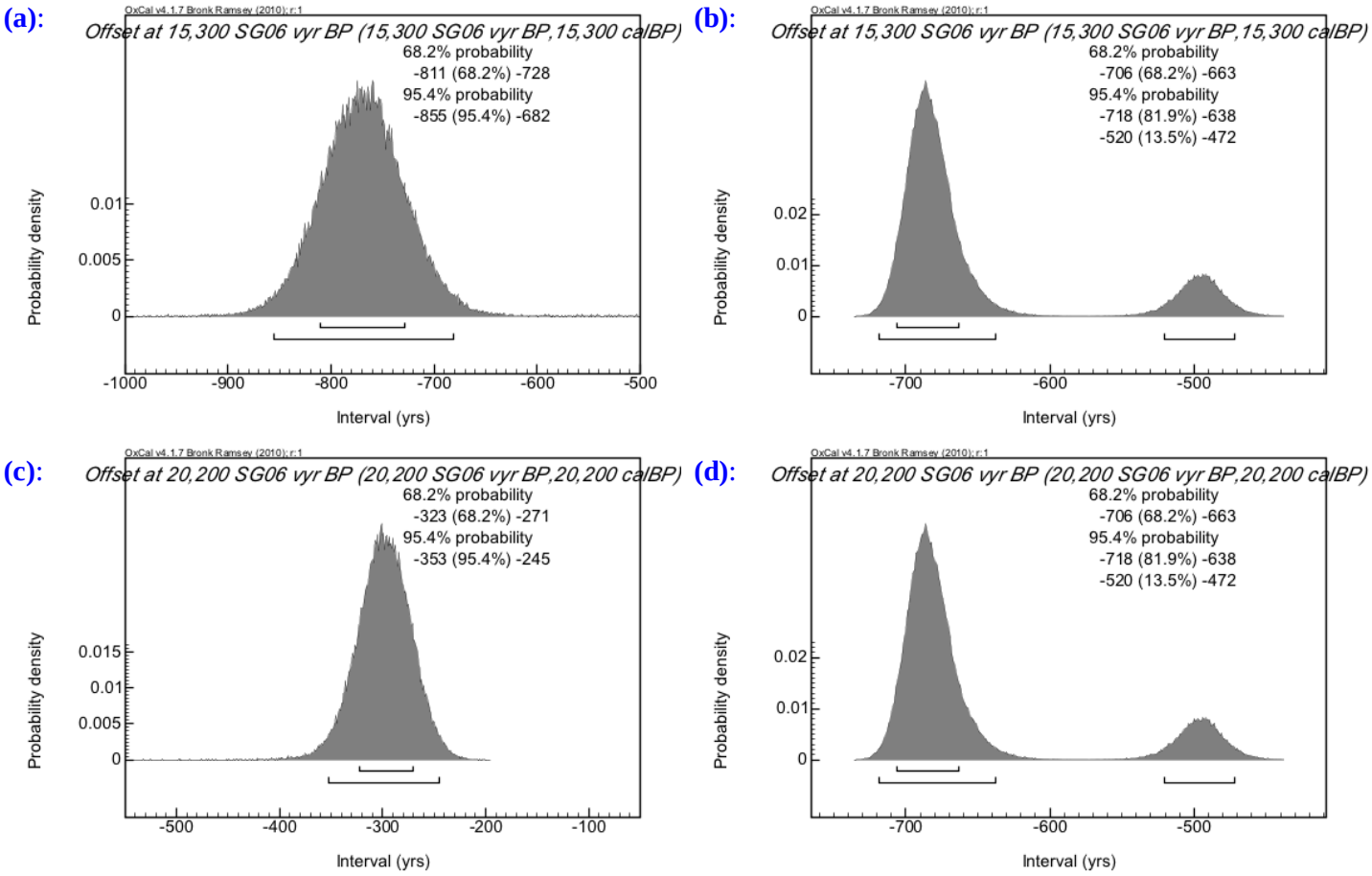

As was illustrated in figure 8.7, there is also a significant period of deviation between the Lake Suigetsu and IntCal09 calibration datasets between *circa* 39,000 and 27,000 SG06 vyr BP, which is greatest between *circa* 39,000 and 33,000 SG06 vyr BP (figure 8.7d). Before *circa* 40,000 SG06 vyr BP the general agreement between the respective datasets is good, although the radiocarbon dating uncertainties become increasingly large as the radiocarbon detection limit is approached (figure 8.7e).

The discordance between 39,000 and 27,000 SG06 vyr BP might again be the result of varve counting uncertainties (systematic under-counting at the younger end of the period of disagreement, coupled with systematic over-counting at the older end, due to the differential nature of varve preservation down the sediment profile), which might be resolved through completion of the dual varve counting methodology by Suigetsu Varves 2006 project colleagues. Alternatively, a single hiatus event (*circa* 27,000 SG06 vyr BP), or multiple hiatus events (perhaps *circa* 34,000 and 27,000 SG06 vyr BP) might be combined with systematic over-counting through the time period around 40,000 to 39,000 SG06 vyr BP, compensating for any later missing sediment. Unreliable radiocarbon data from the Suigetsu samples (i.e. due to over-background correction) is discounted, since the three respective laboratories' datasets remain consistent with each other, and the SG06 data beyond *circa* 39,000 SG06 vyr BP comes back into good agreement with the IntCal09 calibration curve. As has been discussed for the later time period, problems with the IntCal09 calendar timescale are perfectly feasible. Indeed, it is unlikely that the IntCal chronology is wholly accurate through the entirety of this preceding time period (as has been reiterated previously); some of this discordance is likely to be due to problems with the Hulu Cave speleothem timescale to which the non-varved portion of the Cariaco Basin chronology is tied (as suggested by an offset with the new Bahamas speleothem record; Hoffmann *et al*. 2010). However, the discordance with the Lake Suigetsu dataset seems to be too large through this interval for

problems with the consensus curve to be wholly responsible. It is, however, hypothesised that a proportion of the deviation between the Lake Suigetsu dataset and IntCal09 might be the result of over-correction of the marine datasets through H3 and H4 (*circa* 31 and 38 cal. ka BP, respectively), akin to the offset suggested through H1. It is hoped that such a hypothesis will become testable with the completion of the finalised SG06 vyr chronology, in due course. (For example, shared tephra horizons between Suigetsu and nearby marine records might demonstrate the concordance, or lack of concordance, of the marine Heinrich events with the suggested radiocarbon excursions.)

8.1.4 $\Delta^{14}C$

Taking the varve-counted SG06 vyr age scale at face value, $\Delta^{14}C$ can be calculated from the Lake Suigetsu radiocarbon determinations. Figure 8.15 illustrates the smoothed $\Delta^{14}C$ values (calculated as the weighted mean of five adjacent radiocarbon-dated depth horizons, as described in appendix 15), and compares this with the low resolution ^{10}Be analysis performed on SG06 (by project colleague Y. Yokoyama; section 3.6.4).

As was discussed in chapter 2, a major distinctive feature of the radiocarbon calibration curve is the Laschamp geomagnetic excursion, dated by ^{40}Ar-^{39}Ar to 40.4 ± 2.0 cal. ka BP (Guillou *et al*. 2004; section 2.7). As can be seen in figure 8.15, the ^{10}Be analysis from SG06 has yielded equivocal findings, however. Whilst a broad elevation in ^{10}Be flux, attributed to the Laschamp event, is identified in SG06 (composite core depths 3800 to 2950 cm; *circa* 48,000 to 35,000 SG06 vyr BP), the signal is complex, with a distinct 'double peak' in maximum ^{10}Be evident (between 3250 and 3000 cm CD; *circa* 39,900 to 35,900 SG06 vyr BP).

In contrast to the complex ^{10}Be signal, however, a prominent peak in $\Delta^{14}C$ (achieving the highest value across the entire radiocarbon dating range) is evident, and coincides very

well with the 40,400 ± 2,000 cal. BP ^{40}Ar-^{39}Ar age (with the main peak falling between *circa* 41,400 and 40,200 SG06 vyr BP). The multi-millennial rise in Δ^{14}C prior to the presumed Laschamp peak (from *circa* 47,000 SG06 vyr BP) is also in good agreement with the rise in ^{10}Be flux at this time. This could be taken as further support for the reliability of the contributing radiocarbon measurements across this time period, towards the older end of the radiocarbon method. Conversely, however, the clearer 'Laschamp' peak in Δ^{14}C occurs slightly before the earliest of the complex ^{10}Be peaks.

Figure 8.15: Comparison of the calculated (combined SG93 and SG06, five point-smoothed) Lake Suigetsu Δ^{14}C signal (purple line) with low resolution ^{10}Be data from SG06 (provided by project colleague Y. Yokoyama; light blue line).

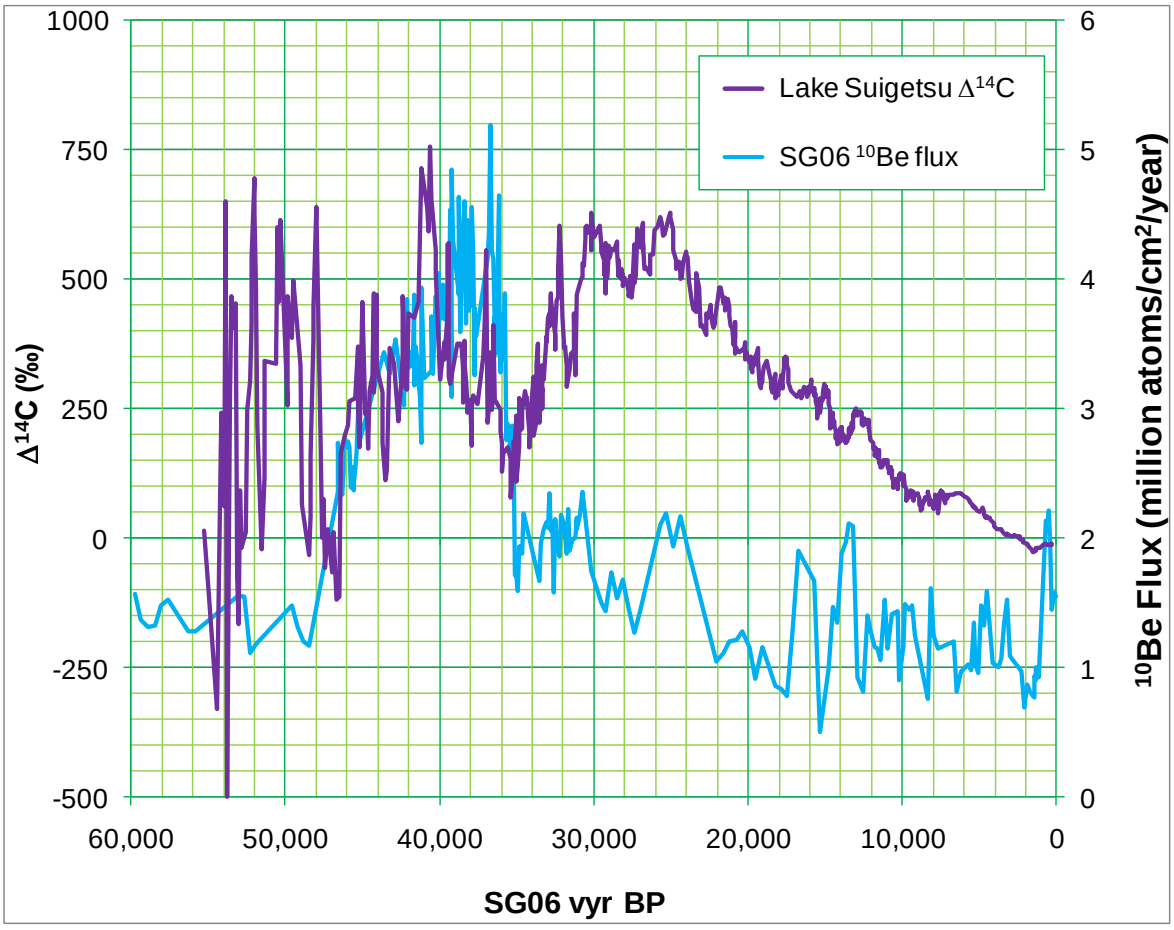

Unlike in ice cores, where ^{10}Be is simply a record of the isotope precipitated on to the snow *in situ*, ^{10}Be flux in lake sediment is also a function of the catchment area of the lake. Comparison of the positioning of the Laschamp ^{10}Be peak in SG06 in relation to the stratigraphy of the core is indicative of a potential change in catchment area around this time. I.e. a tectonic event may have changed the size of the catchment area, leading to in-wash of ^{10}Be from a broader catchment, making comparison of ^{10}Be flux before and after this event difficult. On-going geological study and provenance analysis of the geochemical data from SG06, and studies of the geochemistry of the broader Mikata-Suigetsu catchment (and even broader geographic range) is seeking to identify the precise changes in Lake catchment proposed at this time, to reliably re-quantify the ^{10}Be flux data (based upon revised catchment area data), and, ideally, gain a clearer signal of precisely when/where in SG06 the Laschamp event is placed.

A second prominent rise in Δ^{14}C occurs between *circa* 35,000 and 30,000 SG06 vyr BP. This rise is arguably separated into two separate periods by a brief interruption to rising Δ^{14}C levels between *circa* 32,000 and 31,000 SG06 vyr BP. If this reconstructed Δ^{14}C record is genuine (and the shape of the record should be fairly robust, even if the calendar age scale requires subsequent adjustment), this might provide an explanation for the range of dates attributed to the Mono Lake excursion (section 2.7), with the older ages of Voelker *et al*. (1998), Hughen *et al*. (2004b, 2006), and Hoffmann *et al*. (2010) perhaps picking up the main Δ^{14}C rise, whereas the younger ages of McHargue *et al*. (1995) and Benson *et al*. (2003) might be picking up the later peak in Δ^{14}C.

The Lake Suigetsu Δ^{14}C data can also be plotted against the Δ^{14}C record of IntCal09 (Reimer *et al*. 2009; figure 8.16). Such evaluation replicates the comparison made in ^{14}C space through the previous sections. The agreement between Suigetsu Δ^{14}C and IntCal09 Δ^{14}C is accordingly good back to *circa* 15,000 SG06 vyr BP, and beyond *circa*

39,000 SG06 vyr BP, but is offset to a greater- or lesser extent over the intervening time period. Using robust statistical means, one could try to match the Lake Suigetsu dataset to that of IntCal09 (and, indeed, such methods would be applied if the Suigetsu data were to be incorporated into a future revision of IntCal; Heaton *et al*. 2009), but, until the SG06 varve chronology has been finalised, such an approach will not be pursued herein. Whilst any deviation between *circa* 33,000 and 15,000 SG06 vyr BP could be accounted for by errors in the varve-counted age scale, with shorter-term, 'real' $\Delta^{14}C$ variations postulated as being the results of altered ocean circulation (perhaps associated with the North Atlantic Heinrich events), it is hard to envisage such reasons as being responsible for the extreme deviation between *circa* 39,000 and 33,000 SG06 vyr BP (centring on *circa* 35,000 SG06 vyr BP). Examination of the contributing data to IntCal09 through this time period (figure 8.17) demonstrates that the consensus curve is strongly influenced by the coral dataset of Fairbanks *et al*. (2005), with the $\Delta^{14}C$ signal of IntCal seemingly 'inflated' by this coral dataset, as compared to the alternative contributing Cariaco Basin (Hughen *et al*. 2006) or Iberian margin (Bard *et al*. 2004c) data. A further hypothesised conclusion of the present work would therefore be that the Fairbanks *et al*. (2005) dataset is recording erroneously low radiocarbon measurements through the 39,000 to 34,000 cal. BP time period. The extent of this offset would be too large to be the result of an over-corrected marine reservoir correction, so might be speculated as being the result of unrecognised diagenetic alteration of the corals, or small quantities of modern carbon contamination, which would exert more influence on the radiocarbon measurement of these older time periods. However, it should be emphasised that, even with the exclusion of the Fairbanks *et al*. (2005) dataset, there remains a major discrepancy between the IntCal09 and Lake Suigetsu datasets. It is therefore reiterated that, for the time being, such an offset is attributed to the preliminary SG06 vyr age scale being

utilised herein, and that more robust conclusions must await the finalisation of this varve chronology.

Figure 8.16: Comparison of the calculated (combined SG93 and SG06, five point-smoothed) Lake Suigetsu $\Delta^{14}C$ signal (purple line) with the $\Delta^{14}C$ signal of IntCal09 (Reimer *et al*. 2009; red line). The low resolution ^{10}Be data from SG06 (provided by project colleague Y. Yokoyama) are also provided (light blue line).

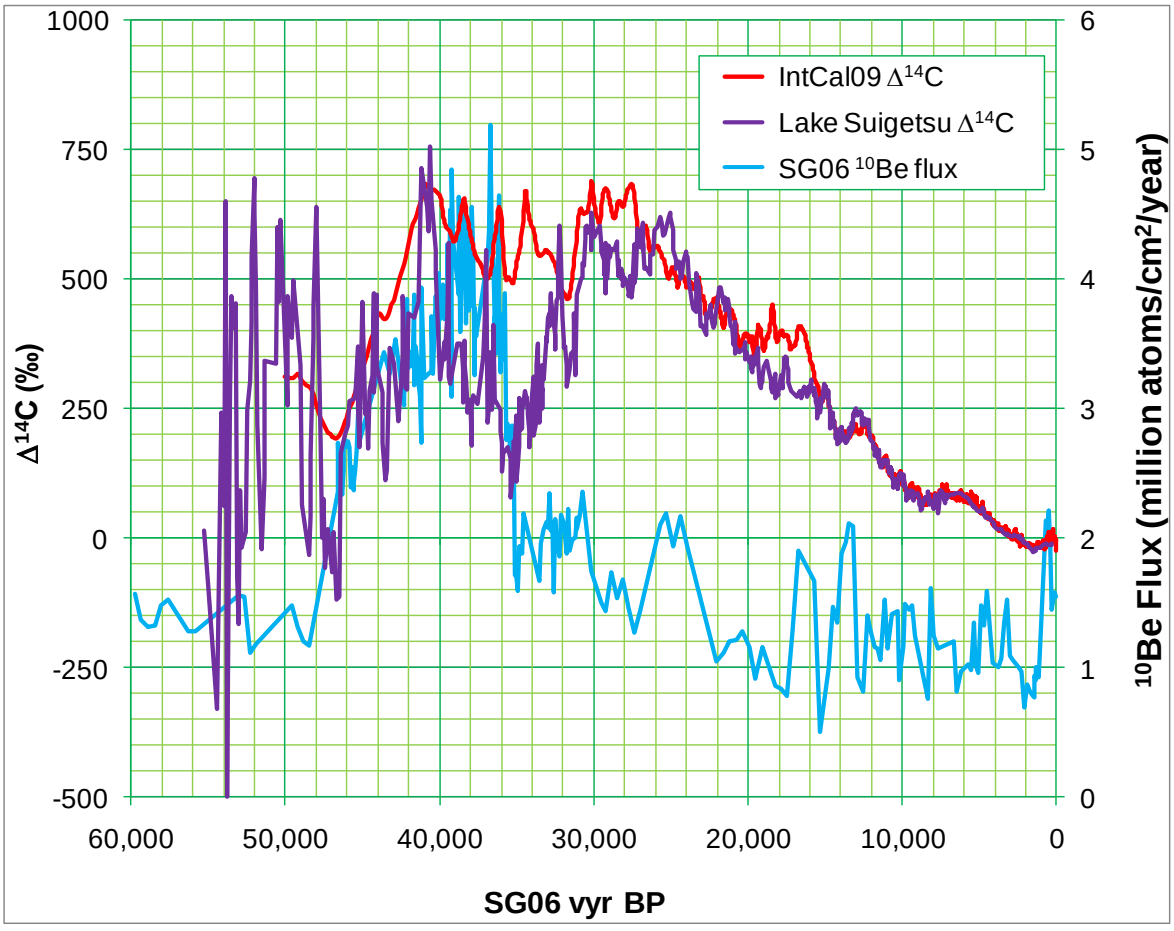

Figure 8.17: The IntCal09 $\Delta^{14}C$ signal (Reimer *et al*. 2009; red) between 40,000 and 30,000 cal. BP, separated out into its constituent datasets: the Cariaco Basin foraminifera (Hughen *et al*. 2006; orange), Iberian margin foraminifera (Bard *et al*. 2004c; dark green), Barbados coral (Bard *et al*. 1998; magenta; and Fairbanks *et al*. 2005; light blue), Araki (Pacific) coral (Fairbanks *et al*. 2005; navy blue), and Papua New Guinea coral (Cutler *et al*. 2004; mauve) records. For clarity, all data are plotted at 1σ uncertainty.

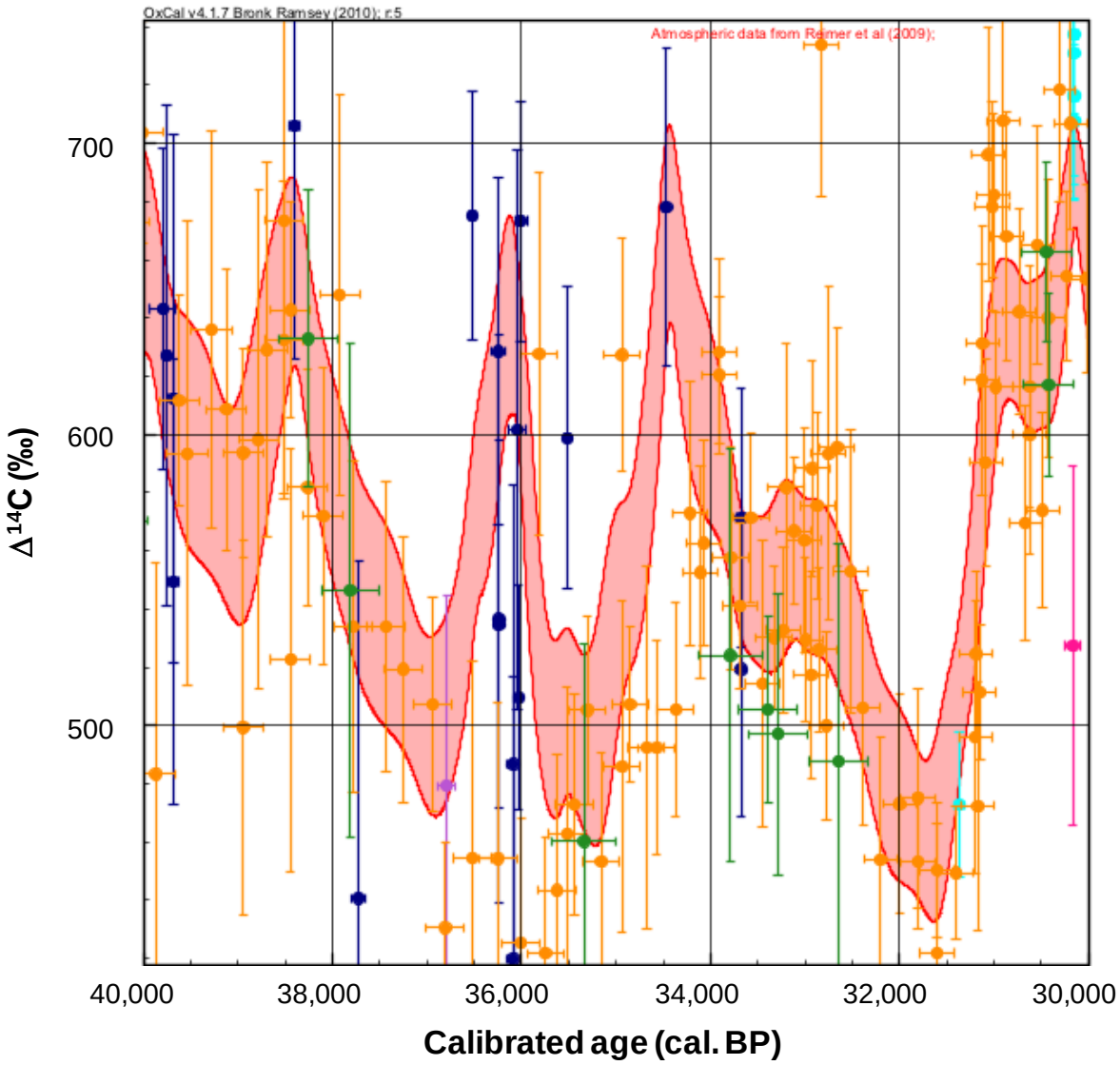

8.2 Future Developments

8.2.1 Comparison with Ichi-no-Megata Maar

Short-term funding has been obtained (from the 'Oxford University Press John Fell Fund', University of Oxford) to compare the Lake Suigetsu sediment profile with that of another varved lake core, 'IMG06' (Yamada *et al*., forthcoming), taken from Ichi-no-Megata maar, Akita prefecture, Honshu Island, north-eastern Japan (39° 57' 17" N, 139° 44' 22" E, 82.3 m a.s.l.; ≈ 600 km north-east of Lake Suigetsu). It is intended to link the respective varve chronologies via tephrostratigraphy over the time period *circa* 24,000 cal. BP (the base of continuous varving at this latter site) to 15,000 cal. BP, as well as doubling the present IMG06 radiocarbon dataset across this time range from 25 to 50 measurements. In this way it is hoped to demonstrate whether either: (i) the Lake Suigetsu sediment profile does indeed include a marked (multi-centennial) sedimentary hiatus at *circa* 17,000 SG06 vyr BP (the possibility of which was noted in section 8.1.3, above); (ii) there is a systematic bias in the varve counting of SG06 over this time period; or (iii) that the observed deviation from Intcal09 through this interval is real. The resolution of such issues may be crucial if the SG06 data through this period is to assume a central rôle in future revisions of the consensus calibration curve, IntCal.

8.2.2 'Suigetsu Varves 2006' – Phase 3

The Suigetsu Varves 2006 project clearly provides an excellent archive of multi-proxy palaeoenvironmental data, and it is hoped to extend the scope of the project (with a NERC consortium grant application presently in preparation). This continuation of the present project ('phase 3' – phases 1 and 2 being the initial sediment coring, and existing palaeoenvironmental analysis from SG06, respectively), will seek to dramatically expand its

geographical scope, using such isochronous markers as the numerous tephra horizons present in Suigetsu to tie the site's chronology to other terrestrial and marine sites in the region. The over-arching aim of this, much broader, project phase will be to tie the excellent chronology of the site to other significant records of palaeoenvironmental change with reliable chronological information, enabling more thorough identification of the leads and lags in the global climate system that might shed light on the underlying causal mechanisms of global climate changes.

If funded, phase 3 of the Suigetsu Varves 2006 project will also undertake further ^{40}Ar-^{39}Ar dating of sanidine-bearing tephra layers within the Lake Suigetsu sediment profile. As part of the pilot work undertaken on cryptotephra identification from the SG06 core, a second key Korean tephra horizon, the Ulleung-Yamato ('U-YM') tephra, has been provisionally identified at 3223.9 cm CD (by project colleague A. MacLeod). ^{40}Ar-^{39}Ar dating of the U-YM tephra would therefore provide a precise, independent chronological constraint to add accuracy to the already high precision SG06 varve chronology towards the older end of the radiocarbon method (the U-YM tephra provisionally being placed at 39,432 SG06 vyr BP). Additionally, optically-stimulated luminescence (OSL) dating from regular intervals across the entirety of the SG06 core would add further independent chronological constraints on the calendar age scale of the sediment profile.

8.2.3 Pollen dating

Whilst pollen concentrated from sediment offers an exciting potential material for radiocarbon dating of sediment profiles (or sections thereof) lacking in more advantageous plant macrofossil samples, previous studies (e.g. Zhou *et al*. 1997; Kilian *et al*. 2002) have failed to produce reliable chronologies from such an approach. The issues associated with such studies include the residence time of pollen in the catchment system and the apparent

age of re-worked pollen, as well as the problem of modern carbon contamination during the pollen extraction process. The method adopted for SG06 pilot pollen samples by project colleague F. Brock, and collaborator R. Jones (University of Exeter), is aiming to avoid the problems of sample handling and associated modern carbon contamination through use of a cytometer to concentrate the pollen grains sufficiently for radiocarbon dating (section 3.6.5). However, the pilot data thus far obtained are not yet reliable enough to be incorporated into the Lake Suigetsu radiocarbon calibration dataset presented herein. Since the dates produced are erroneously young, this suggests a methodological issue (incorporating modern carbon during the extraction process), rather than an inherent problem with the pollen grains themselves (which could be older – but never younger – than the timing of varve formation). On-going work to improve this methodology nevertheless offers the potential to provide reliable dates from concentrated SG06 pollen samples, which might, in future, further enhance the resolution of the radiocarbon calibration dataset.

8.2.4 Extension of the Lake Suigetsu Radiocarbon Calibration Dataset?

Although the radiocarbon determinations produced from the Lake Suigetsu sediments are limited to the core depths from which terrestrial plant macrofossil samples have been retrieved, and therefore provide a punctuated distribution of radiocarbon-dated material through calendar time, the benthic lake sediments nevertheless provide a potential archive of similar terrigenous material from every calendar year throughout the varve profile. If desired, Lake Suigetsu could be extensively re-cored, and similar plant macrofossils retrieved from these sediments, potentially providing a continuous record of atmospheric radiocarbon concentration across the entirety of the radiocarbon range (and potentially back further in time, if future methodological advancement could extend the present radiocarbon limit). As has been demonstrated for the multiple cores of the present project, as well as with the SG93

core (section 6.2), correlation of sedimentary facies is perfectly feasible, allowing for relatively easy integration of any such future lake corings. Of course, financial considerations might prevent such an undertaking, but if one weighs up the future expenses of extending the tree-ring record, or developing datasets from any of the other radiocarbon calibration archives (described in section 2.5), such an enterprise might be viewed as making good economic sense! Of the potential archives presently utilised, only tree-rings and terrestrial plant macrofossils picked from lacustrine sediments (varved or otherwise) provide a terrestrial record of past atmospheric radiocarbon concentration, and so one must also consider the enhanced credibility that can be given to such data, which are free from the need for any reservoir correction and the resultant additional uncertainty thus introduced.

Even if, in the future, it were possible to extend the reliable, dendrochronologically-dated tree-ring record across the entire range of the radiocarbon dating method, Lake Suigetsu could still provide an important contributory dataset to any future consensus calibration curve since, unlike the individual trees that contribute to the dendrochronological records (which only live for a few hundred- or, occasionally, up to several thousand years), Suigetsu provides a single, continuous record across the entire time period. In this way, Suigetsu would provide an ideal, similarly terrestrial, verification of the reliable compilation of the future tree-ring record. More realistically, in the short-term at least, the Lake Suigetsu radiocarbon calibration dataset can provide a continuous, though lower resolution, record to compliment the inevitably fragmented tree-ring record as suitable Glacial tree-ring datasets slowly emerge. For example, it might be difficult for intra- and inter-site cross-matching of the sub-fossil New Zealand kauri trees because of the low sample numbers found at most sites (Turney *et al*. 2007). The Lake Suigetsu record could be used as a low resolution, yet continuous record upon which the higher resolution tree-ring data could be pinned.

9. Synthesis and Conclusions

Since its inception in the mid-twentieth century (Libby *et al*. 1949; Libby 1955), radiocarbon dating has become a widely used method in such fields as archaeology and Quaternary (Earth) science, playing a central rôle in late Pleistocene geochronology. The technique was further enhanced with the development of accelerator mass spectrometry (AMS) from the late 1970s onwards (Bennett *et al*. 1977; Nelson *et al*. 1977), which dramatically increased the utility of radiocarbon dating, allowing significantly smaller sample sizes and increased laboratory throughput (van der Plicht 2004).

It soon became apparent (de Vries 1958; Suess 1970), however, that calibration was required if 'radiocarbon time' was to be translated into a more meaningful representation of the passing of 'real', calendar time. Such a calibration stage is necessary because of temporal variation in the ambient atmospheric concentration of ^{14}C ($\Delta^{14}C$), related to changes in the Earth's geomagnetic field intensity, changes in solar activity, and rearrangements of the distribution of carbon between the global carbon reservoirs.

In order to calibrate the radiocarbon timescale reliably, comparison must be made with the measured radiocarbon determinations of samples of known calendar age. To this end, a range of natural palaeoenvironmental archives has been exploited over recent decades, which act as records of natural $\Delta^{14}C$ variation through time. Such records must demonstrate a reliable, independent means of deriving calendar age, against which the radiocarbon determinations can be directly compared. Dendrochronologically-dated tree-rings (providing direct, terrestrial, non-reservoir-corrected atmospheric radiocarbon calibration) have been central to developing robust calibration datasets, but the scarcity of fossil trees dating from the Last Glacial period limits this dendro-calibration, at present, to the last ≈ 12,550 years (IntCal09; Reimer *et al*. 2009). This leaves approximately three quarters of the radiocarbon

timescale to be calibrated via less secure, marine records. Whilst extremely useful, these marine datasets (most extensively demonstrated by Hughen *et al*. 2004b, 2006 and Fairbanks *et al*. 2005) provide information on radiocarbon calibration in the oceans, rather than the atmosphere, and so these data must necessarily be corrected for the marine reservoir effect (section 2.2.1) if the contemporaneous atmospheric radiocarbon concentration is to be approximated from these archives. Since the marine reservoir effect is known to vary both temporally and spatially (Reimer and Reimer 2001), such approximations for $\Delta^{14}C$ therefore contain an additional tier of uncertainty. Similarly, speleothem data (demonstrated most extensively by Beck *et al*. 2001 and Hoffmann *et al*. 2010), require a reservoir correction (for the dead carbon fraction, DCF; section 2.5.3), which, like the marine correction, necessitates an assumption of temporal invariance, and therefore incorporates similar uncertainties.

A wholly terrestrial sequence of radiocarbon data across the entire radiocarbon dating method, beyond the existing limits of dendro-calibration, would remove the persisting uncertainties associated with the additional layer of complexity associated with the marine records, and therefore remains a fundamental aim of the radiocarbon community. The varved sedimentary record of Lake Suigetsu, Honshu Island, central Japan, provides "a natural timekeeper" and faithful recorder of environmental change (Fukusawa 1995), including "a very exciting record of atmospheric [radiocarbon] changes" spanning the complete range of the radiocarbon dating method (Kitagawa and van der Plicht 2000). In this way, Lake Suigetsu provides an ideal opportunity from which to extend the 'wholly terrestrial' radiocarbon calibration curve back to the limits of radiocarbon detection.

A former ("Suigetsu '93") study (Kitagawa and van der Plicht 1998a, 1998b, 2000) obtained ≈ 300 radiocarbon determinations from macrofossils (leaves, twigs and insect fragments) extracted from a ≈ 75 m sediment core ('SG93') taken from Lake Suigetsu. However, problems with the calendar age scale of the SG93 record resulted in disagreement

with alternative radiocarbon calibration datasets produced soon thereafter (e.g. Hughen *et al*. 1998, 2004b; Beck *et al*. 2001), precluding the widespread adoption of the Suigetsu dataset. A re-analysis of this SG93 data, performed as part of this DPhil thesis (chapter 6), highlights that gaps between successively-drilled sections of the SG93 sediment core were primarily responsible for the errors in the SG93 varve year age scale, whilst errors in the varve counting itself represented a more minor, secondary cause.

The problems associated with the former, Suigetsu '93, study were learnt from, with the recovery of multiple, overlapping sediment cores from Lake Suigetsu enabling "complete recovery" of the sediment profile for the present, 'Suigetsu Varves 2006' project (Nakagawa *et al*. 2011). Utilising the composite 73.19 m sediment core ('SG06') thus obtained, the Suigetsu Varves 2006 project therefore seeks to more fully exploit the excellent palaeoenvironmental archive provided by the annually-laminated sediment sequence, including an improved radiocarbon calibration dataset – the central objective of this present DPhil thesis.

In chapter 7, the 647 new radiocarbon determinations obtained from the SG06 sediment core were introduced. Excluding 'background' measurements and sediment samples, these radiocarbon determinations are composed of 327 measurements upon plant macrofossil samples at the Oxford Radiocarbon Accelerator Unit (ORAU) and 272 at the NERC Radiocarbon Facility-Environment (NRCF-E), East Kilbride. Collectively, these samples represent a total of 518 separate depth horizons from SG06 across the entire radiocarbon dating range, with approximately 10% duplication between the two laboratories.

One of the most important outcomes of this DPhil thesis was the tying of the floating SG06 varve year age scale, generated by a unique, dual methodology by project colleagues (Nakagawa *et al*. 2011; Marshall *et al*., forthcoming; Schlolaut *et al*., forthcoming), to the absolute timescale. To this end, Bayesian 'wiggle-matching' (section 5.3.2) was performed

on the radiocarbon data from the section of SG06 between the top of the varve counting (1250 cm composite depth, CD) and an approximation of the limit of terrestrial (tree-ring) data in the IntCal09 (Reimer *et al*. 2009) calibration curve (at 12,550 cal. BP; approximately 1529.1 cm CD). The principal model (OCM-7.1) provided an age for the 'zero year' of the floating SG06 varve year timescale (the clear marker horizon provided by the U-Oki tephra at 1286.1 to 1288 cm CD) of 10,219 cal. BP (mean age; 10,230 to 10,209 cal. BP at the 68.2% probability range). This tie-point to the absolute (IntCal09) calendar age scale was added to the floating SG06 varve chronology to provide the calendar age timescale for the remainder of this DPhil thesis. (A similar modelling approach will be performed for publication of the finalised SG06 vyr timescale, but will be updated to include a handful of additional radiocarbon determinations, performed following submission of this thesis, as well as using the project's finalised floating varve chronology.)

Physical comparison of archive U-channel core material from the Suigetsu '93 project with that of the composite SG06 sediment core was successfully undertaken for the majority of the original SG93 core sections (SG11 to SG14 and SG20 to SG36) from which radiocarbon determinations had been previously obtained by Kitagawa and van der Plicht (1998a, 1998b, 2000). However, a less secure match was necessarily required for several SG93 core sections (SG15 to SG19), which were missing from the SG93 archive. Once the SG93 depth profile had been revised to fit that of the complete SG06 record in this way, the radiocarbon measurements from the two respective Lake Suigetsu sediment cores were demonstrated to be in excellent agreement. Thus, the ≈ 600 radiocarbon measurements from the present project were bolstered to produce a combined Lake Suigetsu calibration dataset comprising ≈ 900 individual radiocarbon determinations.

For the past 12,550 years, the combined Lake Suigetsu calibration dataset demonstrates excellent agreement with the international consensus calibration curve, IntCal09 (Reimer *et*

al. 2009), which, across this time period, is composed of a reliable, terrestrial (tree-ring) record of past changes in atmospheric radiocarbon concentration. Although not adding anything to the present state of knowledge, this concordance of the 257 radiocarbon determinations produced from the combined SG93 and SG06 dataset with IntCal09 provides increased confidence in the integrity of the Lake Suigetsu sediment profile, and thereby in the remainder of the radiocarbon dataset produced from lower down the SG93 and SG06 sediment cores.

Across the remainder of the IntCal09 record, back to 50,000 cal. BP, the new Lake Suigetsu data show good agreement with IntCal over longer timescales (in contrast to the results of the former, Suigetsu '93 project, which demonstrate a systematic offset from IntCal09, especially before *circa* 26,000 cal. BP). However, there are particular, shorter-term time periods when the Lake Suigetsu data do seem to deviate quite significantly from the consensus calibration curve. The two most notable instances of deviation (described in detail in chapter 8) are those between *circa* 20,200 and *circa* 15,300 SG06 vyr BP, and between *circa* 39,000 and *circa* 27,000 SG06 vyr BP. At least the latter portion of the former interval (i.e. *circa* 17,600 to 15,300 SG06 vyr BP) is herein hypothesised as representing an authentic deviation from the IntCal09 curve. Such a belief is supported by alternative data from marine corals (Bard *et al*. 1998), Iberian margin sediments (Bard *et al*. 2004c), and the Hulu Cave speleothem (Magana *et al*. 2009). Such a finding would imply an over-correction for the marine reservoir of the Cariaco Basin radiocarbon record (Hughen *et al*. 2006; which dominates the IntCal09 curve through this time period), due to altered marine circulation patterns in the tropical North Atlantic, probably related to Heinrich event 1 (H1).

The reasons for the deviation of the Lake Suigetsu data from IntCal09 are less clear for the remaining periods of divergence. Similar changes to ocean circulation patterns through H3 and H4 (*circa* 32,000 and 38,000 cal. BP, respectively) could well provide a component of

the deviation in the earlier period of disagreement, but the size of the apparent discrepancy (approaching 2,000 radiocarbon years in places) is such that additional factors must also be responsible. At this stage, periods of systematic over- and under-counting of the SG06 varves is proffered as a likely cause of deviation, which should (hopefully) be improved upon by the completion of the dual counting methods beyond the present 1814.6 cm CD limit. Although explored theoretically in chapter 8, there is no sedimentary evidence of any hiatus events in the sediment profile that might be responsible for the deviations shown. Real discrepancy with IntCal09 prior to the present 12,550 cal. BP tree-ring limit might also be expected due to problems with the calendar age scales of the contributing datasets to the consensus calibration curve (discussed in chapter 2). However, before completion of the finalised SG06 varve counting, any such conclusions drawn from the present work remain speculative.

Using varved sediments for the extension of the wholly terrestrial radiocarbon calibration curve clearly requires a continuous, perfectly laminated sediment record. The Soppensee and Holzmaar datasets demonstrate the problems associated with varved records (section 2.5.4), exemplifying that, even where records are initially believed to be "perfectly laminated", later evidence may well be produced to show such assumptions to be erroneous (Hajdas *et al*. 2000). Whilst Suigetsu Varves 2006 project members have confidence in the radiocarbon (and palaeoenvironmental) datasets being produced from SG06, it has become increasingly evident over the last two decades, with the growth of alternative datasets and increased awareness of the multiplicity of potential problems associated with these datasets, that a *bona fide* calibration curve of past changes in atmospheric radiocarbon concentration can only be established through corroboration with alternative, independently-produced datasets (Pearson *et al*. 1986; Stuiver and Pearson 1986; Damon 1995b). It is therefore acknowledged that the Lake Suigetsu dataset can only represent a constituent part of a consensus calibration curve, rather than providing a 'stand-alone' 'comparison curve'

(van der Plicht *et al*. 2004; cf. Fairbanks *et al*. 2005). However, it is hoped that, upon completion of the Suigetsu Varves 2006 project, the Lake Suigetsu radiocarbon calibration dataset developed herein will indeed deliver upon the excellent potential of the site, and assume a central rôle in future revisions of IntCal.

References

Alley RB, Meese DA, Shuman CA, Gow AJ, Taylor KC, Grootes PM, White JWC, ram M, Waddington ED, Mayewski PA and Zielinski GA (1993) Abrupt increase in Greenland snow accumulation at the end of the Younger Dryas event. *Nature* **362**, 527-529.

Andersen KK, Svensson A, Johnsen SJ, Rasmussen SO, Bigler M, Röthlisberger R, Ruth U, Siggaard-Andersen M-L, Steffensen JP, Dahl-Jensen D, Vinther BM and Clausen A (2006) The Greenland Ice Core Chronology 2005, 15-42 ka. Part 1: constructing the time scale. *Quaternary Science Reviews* **25**, 3246-3257.

Anderson EC and Libby WF (1951) World-wide distribution of natural radiocarbon. *Physical Review* **81** (1), 64-69.

Andrews JT (1998) Abrupt changes (Heinrich events) in late Quaternary North Atlantic marine environments: a history and review of data and concepts. *Journal of Quaternary Science* **13** (1), 3-16.

Arnold JR and Libby WF (1949) Age determinations by radiocarbon content: checks with samples of known age. *Science* **110**, 678-680.

Arnold JR and Libby WF (1951) Radiocarbon dates. *Science* **113**, 111-120.

Attwood G, Dyer G and Skipworth G (2000) *Heinemann Modular Mathematics for Edexcel AS and A-level: Statistics 3*. Heinemann Educational Publishers, Oxford.

Bahrig B (1988) Paleoenvironment information from deepwater siderite (Lake of Laach, W. Germany). pp.153-158 in Fleet A, Kelts K and Talbot M (eds.) Lacustrine Petroleum Source Rocks. *Geological Society of London Special Publication* **40**.

Bard E (1997) Nuclide production by cosmic rays during the last ice age. *Science* **277**, 532-533.

Bard E (2001) Extending the calibrated radiocarbon record. *Science* **292**, 2443-2444.

Bard E, Hamelin B, Fairbanks RG and Zindler A (1990a) Calibration of the ^{14}C timescale over the past 30,000 years using mass spectrometric U-Th ages from Barbados corals. *Nature* **345**, 405-410.

Bard E, Hamelin B, Fairbanks RG, Zindler A, Mathieu G and Arnold M (1990b) U/Th and ^{14}C ages of corals from Barbados and their use for calibrating the ^{14}C time scale beyond 9,000 years BP. *Nuclear Instruments and Methods in Physics Research B* **52**, 461-468.

Bard E, Arnold M, Fairbanks RG and Hamelin B (1993) ^{230}Th-^{234}U and ^{14}C ages obtained by mass spectrometry on corals. *Radiocarbon* **35** (1), 191-199.

Bard E, Hamelin B, Arnold M, Montaggioni L, Cabioch G, Faure G and Rougerie F (1996) Deglacial sea-level record from Tahiti corals and the timing of global meltwater discharge. *Nature* **382**, 241-244.

Bard E, Arnold M, Hamelin B, Tisnerat-Laborde N and Cabioch G (1998) Radiocarbon calibration by means of mass spectrometric $^{230}Th/^{234}U$ and ^{14}C ages of corals: an updated database including samples from Barbados, Mururoa and Tahiti. *Radiocarbon* **40** (3), 1085-1092.

Bard E, Ménot-Combes G and Rostek F (2004a) Present status of radiocarbon calibration and comparison records based on Polynesian corals and Iberian margin sediments. *Radiocarbon* **46** (3), 1189-1202.

Bard E, Rostek F and Ménot-Combes G (2004b) A better radiocarbon clock. *Science* **303**, 178-179.

Bard E, Rostek F and Ménot-Combes G (2004c) Radiocarbon calibration beyond 20,000 ^{14}C yr BP by means of planktonic foraminifera of the Iberian margin. *Quaternary Research* **61**, 204-214.

Bayes T (communicated by R. Price, in a letter to J. Canton) (1763) An essay towards solving a problem in the doctrine of chances. *Philosophical Transactions* **53**, 370-418.

Bayliss A (2009) Rolling out revolution: using radiocarbon dating in archaeology. *Radiocarbon* **51** (1), 123-147.

Beavan-Athfield NR, McFadgen BG and Sparks RJ (2001) Environmental influences on dietary carbon and ^{14}C ages in modern rats and other species. *Radiocarbon* **43** (1), 7-14.

Beck JW, Richards DA, Edwards RL, Silverman BW, Smart PL, Donahue DJ, Hererra-Osterheld S, Burr GS, Calsoyas L, Jull AJT and Biddulph D (2001) Extremely large variations of atmospheric ^{14}C concentration during the last glacial period. *Science* **292**, 2453-2458.

Becker B (1980) Tree-ring dating and radiocarbon calibration in south-central Europe. *Radiocarbon* **22** (2), 219-226.

Becker B (1993) An 11,000-year German oak and pine dendrochronology for radiocarbon calibration. *Radiocarbon* **35** (1), 201-213.

Bennett CL, Beukens RP, Clover MR, Gove HE, Liebert RB, Litherland AE, Purser KH and Sondheim WE (1977) Radiocarbon dating using electrostatic accelerators: negative ions provide the key. *Science* **198**, 508-510.

Benson L, Liddicoat J, Smoot J, Sarna-Wojcicki, Negrini R and Lund S (2003) Age of the Mono Lake excursion and associated tephra. *Quaternary Science Reviews* **22**, 135-140.

Bird MI, Ayliffe LK, Fifield LK, Turney CSM, Cresswell RG, Barrows TT and David B (1999) Radiocarbon dating of 'old' charcoal using a wet oxidation, stepped-combustion procedure. *Radiocarbon* **41** (2), 127-140.

Björck S, Wohlfarth B and Possnert G (1995) 14C measurements from the Late Weichselian part of the Swedish time scale. *Quaternary International* **27**, 11-18.

Björck S, Kromer B, Johnsen S, Bennike O, Hammarlund D, Lemdahl G, Possnert G, Rasmussen TL, Wohlfarth B, Hammer CU and Spurk M (1996) Synchronised terrestrial-atmospheric deglacial records around the North Atlantic. *Science* **274**, 1155-1160.

Björck S, Walker MJC, Cwynar LC, Johnsen S, Knudsen K-L, Lowe JJ, Wohlfarth B and INTIMATE members (1998) An event stratigraphy for the Last Termination in the North Atlantic region based on the Greenland ice-core record: a proposal by the INTIMATE group. *Journal of Quaternary Science* **13** (4), 283-292.

Blaauw M and Christen JA (2005) Radiocarbon peat chronologies and environmental change. *Journal of the Royal Statistical Society, Series C (Applied Statistics)* **54** (4), 805-816.

Blaauw M and Christen JA (forthcoming) Flexible paleoclimate age-depth models using an auto-regressive gamma process.

Blaauw M, Heuvelink GBM, Mauquoy D, van der Plicht J and van Geel B (2003) A numerical approach to ^{14}C wiggle-match dating of organic deposits: best fits and confidence intervals. *Quaternary Science Reviews* **22**, 1485-1500.

Blais-Stevens A, Clague JJ, Bobrowsky T and Patterson RT (1997) Late Holocene sedimentation in Saanich Inlet, British Columbia, and its paleoseismic implications. *Canadian Journal of Earth Sciences* **34** (10), 1345-1357.

Blockley SPE and Housley RA (2009) Calibration commentary. *Radiocarbon* **51** (1), 287-290.

Blunier T, Chappellaz J, Schwander J, Dällenbach A, Stauffer B, Stocker TF, Raynaud D, Jouzel J, Clausen HB, Hammer CU and Johnsen SJ (1998) Asynchrony of Antarctic and Greenland climate change during the last glacial period. *Nature* **394**, 739-743.

Bond G, Heinrich H, Broecker W, Labeyrie L, McManus J, Andrews J, Huon S, Jantschik R, Clasen S, Simet C, Tedesco K, Klas M, Bonani G and Ivy S (1992) Evidence for massive discharges of icebergs into the North Atlantic ocean during the last glacial period. *Nature* **360**, 245-249.

Bond G, Broecker W, Johnsen S, McManus J, Labeyrie L, Jouzel J and Bonani G (1993) Correlations between climate records from North Atlantic sediments and Greenland ice. *Nature* **365**, 143-147.

Boutton TW, Wong WW, Hachey DL, Lee LS, Cabrera MP and Klein PD (1983) Comparison of quartz and pyrex tubes for combustion of organic samples for stable carbon isotope analysis. *Analytical Chemistry* **55**, 1832-1833.

Bowman S (1990) *Radiocarbon Dating*. British Museum, London.

Braziunas TF, Fung IY and Stuiver M (1991) Oceanic and solar forcing of natural geographic variations in atmospheric Δ^{14}C. *Radiocarbon* **33** (2), 180.

Braziunas TF, Fung IY and Stuiver M (1995) The preindustrial atmospheric $^{14}CO_2$ latitudinal gradient as related to exchanges among atmospheric, oceanic, and terrestrial reservoirs. *Global Biogeochemical Cycles* **9** (4), 565-584.

Brock F, Higham T, Ditchfield P and Bronk Ramsey C (2010) Current pre-treatment methods for AMS radiocarbon dating at the Oxford Radiocarbon Accelerator Unit (ORAU). *Radiocarbon* **52** (1), 103-112.

Broecker WS (1991) The great ocean conveyor. *Oceanography* **4** (2), 79-89.

Broecker WS, Gerard R, Ewing M and Heezen BC (1960) Natural radiocarbon in the Atlantic Ocean. *Journal of Geophysical Research* **65** (9), 2903-2931.

Broecker WS, Kennett JP, Flower BP, Teller JT, Trumbore S, Bonani G and Wolfli W (1989) Routing of meltwater from the Laurentide Ice Sheet during the Younger Dryas cold episode. *Nature* **341**, 318-321.

Bronk Ramsey C (1994) Analysis of chronological information and radiocarbon calibration: the program OxCal. *Archaeological Computing Newsletter **41***, 11-16.

Bronk Ramsey C (1995) Radiocarbon calibration and analysis of stratigraphy: the OxCal program. *Radiocarbon* **37** (2), 425-430.

Bronk Ramsey C (1998) Probability and dating. *Radiocarbon* **40** (1), 461-474.

Bronk Ramsey C (2000) Comment on 'the use of Bayesian statistics for ^{14}C dates of chronologically ordered samples: a critical analysis'. *Radiocarbon* **42** (2), 199-202.

Bronk Ramsey C (2001) Development of the radiocarbon calibration program. *Radiocarbon* **43** (2A), 355-363.

Bronk Ramsey C (2005) Improving the resolution of radiocarbon dating by statistical analysis. ch.5 in Levy TE and Higham T (eds.) *The Bible and Radiocarbon Dating: Archaeology, Test and Science*. Equinox Publishing Ltd., London.

Bronk Ramsey C (2008a) Deposition models for chronological records. *Quaternary Science Reviews* **27**, 42-60.

Bronk Ramsey C (2008b) Radiocarbon dating: revolutions in understanding. *Archaeometry* **50** (2), 249-275.

Bronk Ramsey C (2009a) Bayesian Analysis of Radiocarbon Dates. *Radiocarbon* **51** (1), 337-360.

Bronk Ramsey C (2009b) Dealing with outliers and offsets in radiocarbon dating. *Radiocarbon* **51** (3), 1023-1045.

Bronk Ramsey C and Lee S (forthcoming) Model averaging techniques for depositional sequences.

Bronk Ramsey C, van der Plicht J and Weninger B (2001) 'Wiggle matching' radiocarbon dates. *Radiocarbon* **43** (2A), 381-389.

Bronk Ramsey C, Higham T and Leach P (2004) Towards high-precision AMS: progress and limitations. *Radiocarbon* **46** (1), 17-24.

Bronk Ramsey C, Buck CE, Manning SW, Reimer PJ and van der Plicht J (2006) Developments in radiocarbon calibration for archaeology. *Antiquity* **80**, 783-798.

Bronk Ramsey C, Brenninkmeijer CAM, Jöckel P, Kjeldsen H and Masarik J (2007) Direct measurement of the radiocarbon production at altitude. *Nuclear Instruments and Methods in Physics Research B* **259**, 558-564.

Bronk Ramsey C, Dee M, Lee, S, Nakagawa T and Staff RA (2010a) Developments in the calibration and modeling of radiocarbon dates. *Radiocarbon* **52** (2-3), 953-961.

Bronk Ramsey C, Dee MW, Rowland JM, Higham TFG, Harris SA, Brock F, Quiles A, Wild EM, Marcus ES and Shortland AJ (2010b) Radiocarbon-based chronology for dynastic Egypt. *Science* **328**, 1554-1557.

Brown TA, Farwell GW, Grootes PM, Schmidt FH and Stuiver M (1993) Intra-annual variability of the radiocarbon content of corals from the Galapagos Islands. *Radiocarbon* **35** (2), 245-251.

Bruns M, Levin I, Münnich KO, Hubberten HW and Fillipakis S (1980) Regional sources of volcanic carbon dioxide and their influence on 14C content of present-day plant material. *Radiocarbon* **22** (2), 532-536.

Bryant C, Carmi I, Cook GT, Gulliksen S, Harkness DD, Heinemeier J, McGee E, Naysmith P, Possnert G, Scott EM, van der Plicht J and van Strydonck M (2001) Is comparability of 14C dates an issue? A status report on the fourth international radiocarbon intercomparisons. *Radiocarbon* **43** (2A), 321-324.

Buck CE and Blackwell PG (2004) Formal statistical models for estimating radiocarbon calibration curves. *Radiocarbon* **46** (3), 1093-1102.

Buck CE, Kenworthy JB, Litton CD and Smith AFM (1991) Combining archaeological and radiocarbon information: a Bayesian approach to calibration. *Antiquity* **65**, 808-821.

Buck CE, Litton CD and Smith AFM (1992) Calibration of radiocarbon results pertaining to related archaeological events. *Journal of Archaeological Science* **19**, 497-512.

Buck CE, Litton CD and Scott EM (1994) Making the most of radiocarbon dating: some statistical considerations. *Antiquity* **68**, 252-263.

Buck CE, Cavanagh W and Litton C (eds.) (1996) *Bayesian Approach to Interpreting Archaeological Data*. Wiley, Chichester.

Buck CE, Christen JA and James GN (1999) BCal: an on-line Bayesian radiocarbon calibration tool. *Internet Archaeology* **7** (http://intarch.ac.uk/journal/issue7/buck/toc.html).

Burr GS, Beck JW, Taylor FW, Récy J, Edwards RL, Cabioch G, Corrège T, Donahue DJ and O'Malley JM (1998) A high-resolution radiocarbon calibration between 11,700 and 12,400 calendar years BP derived from ^{230}Th ages of corals from Espirito Santo island, Vanuato. *Radiocarbon* **40** (3), 1093-1105.

Burr GS, Galang C, Taylor FW, Gallup C, Edwards RL, Cutler K and Quirk B (2004) Radiocarbon results from a 13-kyr BP coral from the Huon Peninsula, Papua New Guinea. *Radiocarbon* **46** (3), 1211-1224.

Cain WF and Suess HE (1976) Carbon 14 in tree rings. *Journal of Geophysical Research* **81** (21), 3688-3694.

Calvert SE (1966) Origin of diatom-rich, varved sediments from the Gulf of California. *Journal of Geology* **76**, 546-565.

Carcaillet J, Bourlès DL, Thouveny N and Arnold M (2004) A high resolution authigenic ^{10}Be/^{9}Be record of geomagnetic moment variations over the last 300 ka from sedimentary cores of the Portuguese margin. *Earth and Planetary Science Letters* **219**, 397-412.

Cato I (1985) The definitive connection of the Swedish geochronological time scale with the present, and the new date of the zero year in Döviken, northern Sweden. *Boreas* **14**, 117-122.

Chiu T-C, Fairbanks RG, Mortlock RA and Bloom AL (2005) Extending the radiocarbon calibration beyond 26,000 years before present using fossil corals. *Quaternary Science Reviews* **24**, 1797-1808.

Chiu T-C, Fairbanks RG, Mortlock RA, Cao L, Fairbanks TW and Bloom AL (2006) Redundant ^{230}Th/^{234}U/^{238}U, ^{231}Pa/^{235}U and ^{14}C dating of fossil corals for accurate radiocarbon age calibration. *Quaternary Science Reviews* **25**, 2431-2440.

Chiu T-C, Fairbanks RG, Cao L and Mortlock RA (2007) Analysis of the atmospheric ^{14}C record spanning the past 50,000 years derived from high-precision ^{230}Th/^{234}U/^{238}U, ^{231}Pa/^{235}U and ^{14}C dates on fossil corals. *Quaternary Science Reviews* **26**, 18-36.

Christen JA (1994a) Summarizing a set of radiocarbon determinations: a robust approach. *Journal of the Royal Statistics Society* **43** (3), 489-503.

Christen JA (1994b) Bayesian interpretation of radiocarbon results. Unpublished PhD thesis, University of Nottingham.

Christen JA (2003) Bwigg: an internet facility for Bayesian radiocarbon wiggle-matching. *Internet Archaeology* **13** (http://intarch.ac.uk/journal/issue13/christen_index.html).

Christen JA and Litton CD (1995) A Bayesian approach to wiggle-matching. *Journal of Archaeological Science* **22**, 719-725.

Christen JA, Clymo RS and Litton CD (1995) A Bayesian approach to the use of 14C dates in the estimation of the age of peat. *Radiocarbon* **37** (2), 431-442.

Clark RM (1975) A calibration curve for radiocarbon dates. *Antiquity* **49**, 251-266.

Clark PU, Pisias NG, Stocker TF and Weaver AJ (2002) The role of the thermohaline circulation in abrupt climate change. *Nature* **415**, 863-869.

Colman SM, Jones GA, Rubin M, King JW, Peck JA and Orem WH (1996) AMS radiocarbon analyses from Lake Baikal, Siberia: challenges of dating sediments from a large, oligotrophic lake. *Quaternary Science Reviews* **15**, 669-684.

Cook AC, Hainsworth LJ, Sorey ML, Evans WC and Southon JR (2001) Radiocarbon studies of plant leaves and tree rings from Mammoth Mountain, CA: a long-term record of magmatic CO_2 release. *Chemical Geology* **177**, 117-131.

Coplen TB (1994) Reporting of stable hydrogen, carbon, and oxygen isotopic abundances. *Pure and Applied Chemistry* **66** (2), 273-276.

Craig H (1953) The geochemistry of the stable carbon isotopes. *Geochimica et Cosmochimica Acta* **3**, 53-92.

Cutler KB, Gray SC, Burr GS, Edwards RL, Taylor FW, Cabioch G, Beck JW, Cheng H and Moore J (2004) Radiocarbon calibration and comparison to 50 kyr BP with paired ^{14}C and ^{230}Th dating of corals from Vanuatu and Papua New Guinea. *Radiocarbon* **46** (3), 1127-1160.

Dahl-Jensen D, Gundestrup NS, Miller O, Watanabe O, Johnson SJ, Steffensen JP, Clausen HB, Svensson A and Larsen LB (2002) The NorthGRIP deep drilling programme. *Annals of Glaciology* **35**, 1-4.

Damon PE (1995b) Note concerning "Intercomparison of high-precision ^{14}C measurements at the University of Arizona and the Queen's University of Belfast Radiocarbon Laboratories" by Kalin *et al*. (1995) and the regional effect. *Radiocarbon* **37** (3), 955-959.

Damon PE, Long A and Grey DC (1966) Fluctuation of atmospheric C^{14} during the last six millennia. *Journal of Geophysical Research* **71** (4), 1055-1063.

Damon PE, Ferguson CW, Long A and Wallick EI (1974) Dendrochronologic calibration of the radiocarbon time scale. *American Antiquity* **39** (2), 350-366.

Damon PE, Lerman JC and Long A (1978) Temporal fluctuations of atmospheric ^{14}C: causal factors and implications. *Annual Review of Earth and Planetary Science* **6**, 457-494.

Damon PE, Burr G, Cain WJ and Donahue DJ (1992) Anomalous 11-year $\Delta^{14}C$ cycle at high latitudes? *Radiocarbon* **34** (2), 235-238.

Dansgaard W, Johnsen SJ, Clausen HB, Dahl-Jensen D, Gundestrup NS, Hammer CU, Hvidberg CS, Steffensen JP, Sveinbjörnsdottir AE, Jouzel J and Bond G (1993) Evidence for general instability of past climate from a 250-kyr ice-core record. *Nature* **364**, 218-220.

de Geer (1912) A geochronology of the past 12,000 years. *XI Congrès de Géologie International, Comptes Rendues*, 241-253.

de Vries HL (1958) Variation in concentration of radiocarbon with time and location on Earth. *Proceedings of the Koninklijke Nederlandse Akademie van Wetenschappen* **B61**, 94-102.

de Vries HL and Barendsen GW (1954) Measurements of age by the carbon-14 technique. *Nature* **174**, 1138-1141.

Dee MW and Bronk Ramsey C (2000) Refinement of graphite target production at ORAU. *Nuclear Instruments and Methods in Physics Research B* **172**, 449-453.

Dee MW, Brock F, Harris SA, Bronk Ramsey C, Shortland AJ, Higham TFG and Rowland JM (2009) Investigating the likelihood of a reservoir offset in the radiocarbon record for ancient Egypt. *Journal of Archaeological Science* **37**, 687-693.

Deevey ES Jr., Gross MS, Hutchinson GE and Kraybill HL (1954) The natural C14 contents of materials from hard-water lakes. *Proceedings of the National Academy of Science* **40**, 285-288.

Douglass AE (1941) Crossdating in dendrochronology. *Journal of Forestry* **39**, 825-831.

Edwards RL, Chen JH, Ku T-L and Wasserburg GJ (1987a) Precise timing of the last interglacial period from mass spectrometric determination of thorium-230 in corals. *Science* **236**, 1547-1553.

Edwards RL, Chen JH and Wasserburg GJ (1987b) ^{238}U-^{234}U-^{230}Th-^{232}Th systematics and the precise measurement of time over the past 500,000 years. *Earth and Planetary Science Letters* **81** (2-3), 175-192.

Edwards RL, Beck JW, Burr GS, Donahue DJ, Chappell JMA, Bloom AL, Druffel ERM and Taylor FW (1993) A large drop in atmospheric ^{14}C/^{12}C and reduced melting in the Younger Dryas, documented with ^{230}Th ages of corals. *Science* **260**, 962-968.

Elsasser W, Ney EP and Winckler JR (1956) Cosmic ray intensity and geomagnetism. *Nature* **178**, 1226-1227.

Ertunç T, Xu S, Bryant CL, Maden C, Murray C, Currie M and Freeman SPHT (2005) Progress in AMS target production of sub-milligram samples at the NERC Radiocarbon Laboratory. *Radiocarbon* **47** (3), 453-464.

Fairbanks RG (1989) A 17,000-year glacio-eustatic sea level record: influence of glacial melting rates on the Younger Dryas event and deep-ocean circulation. *Nature* **342**, 637-642.

Fairbanks RG (1990) The age and origin of the "Younger Dryas climate event" in Greenland ice cores. *Paleoceanography* **5** (6), 937-948.

Fairbanks RG, Mortlock RA, Chiu T-C, Cao L, Kaplan A, Guilderson TP, Fairbanks TW, Bloom AL, Grootes PM and Nadeau M-J (2005) Radiocarbon calibration curve spanning 0 to 50,000 years BP based on paired ^{230}Th/^{234}U/^{238}U and ^{14}C dates on pristine corals. *Quaternary Science Reviews* **24**, 1781-1796.

Ferguson CW and Graybill DA (1983) Dendrochronology of bristlecone pine: a progress report. *Radiocarbon* **25** (2), 287-288.

Francus P, Lamb H, Nakagawa T, Marshall M, Brown E and Suigetsu 2006 project members (2009) The potential of high-resolution X-ray fluorescence core scanning: applications in paleolimnology. *PAGES news* **17** (3), 93-95.

Freeman SPHT, Cook GT, Dougans AB, Naysmith P, Wilcken KM and Xu S (2010) Improved SSAMS performance. *Nuclear Instruments and Methods in Physics Research B* **268**, 715-717.

Friedrich M, Remmele S, Kromer B, Hofmann J, Spurk M, Kaiser KF, Orcel C and Küppers M (2004) The 12,460-year Hohenheim oak and pine tree-ring chronology from central Europe – a unique annual record for radiocarbon calibration and paleoenvironment reconstructions. *Radiocarbon* **46** (3), 1111-1122.

Fritts HC (1976) *Tree rings and climate*. Academic Press, London.

Fromm E (1970) An estimation of errors in the Swedish varve chronology. pp.163-172 in Olsson IU (ed.) *Radiocarbon Variations and Absolute Chronology, Twelfth Nobel Symposium, Uppsala 1969*. John Wiley and Sons, New York, USA.

Fukui T (ed.) (1977) *The Climate of Japan*. Elsevier, Amsterdam, Netherlands.

Fukusawa H (1995) Non-glacial varved lake sediment as a natural timekeeper and detector on environmental changes. *The Quaternary Research* **34** (3) 135-149. In Japanese, with English abstract.

Fukusawa H (1999) Varved lacustrine sediments in Japan: recent progress. *The Quaternary Research* **38** (3) 237-243. In Japanese, with English abstract.

Fukusawa H, Koizumi I, Okamura M and Yasuda Y (1994) Historical earthquake, flood and human activity events recorded in the Holocene sediments of Lake Suigetsu, Fukui Prefecture, central Japan. *Journal of Geography* **103**, 127-139. In Japanese, with English abstract.

Fukusawa H, Kato M and Fujiwara O (2002) Changes of eco-systems in the last 500 years caused by human impacts in Lake Suigetsu, cantral Japan. *Geographical Reports of Tokyo Metropolitan University* **37**, 41-49.

Galimberti M, Bronk Ramsey C and Manning SW (2004) Wiggle-match dating of tree-ring sequences. *Radiocarbon* **46** (2), 917-924.

Genty D, Massault M, Gilmour M, Baker A, Verheyden S and Kepens E (1999) Calculation of past dead carbon proportion and variability by the comparison of AMS ^{14}C and TIMS U/Th ages on two Holocene stalagmites. *Radiocarbon* **41** (3), 251-270.

Geyh MA, Krumbein WE and Kudrass H-R (1974) Unreliable ^{14}C dating of long-stored deep-sea sediments due to bacterial activity. *Marine Geology* **17**, M45-M50.

Gilks WR, Richardson S and Spiegelhalter DJ (1996) *Markov Chain Monte Carlo in Practice*. Chapman & Hall, London.

Gillespie R and Hedges REM (1984) Laboratory contamination in radiocarbon accelerator mass spectrometry. *Nuclear Instruments and Methods in Physics Research B* **5**, 294-196.

Godwin H (1962) Radiocarbon dating: fifth international conference. *Nature* **195**, 943-945.

Goslar T and Mądry W (1998) Using the Bayesian method to study the precision of dating by wiggle-matching. *Radiocarbon* **40** (1), 551-560.

Goslar T, Pazdur A, Pazdur MF and Walanus A (1989) Radiocarbon and varve chronologies of annually laminated lake sediments of Gościąż Lake, central Poland. *Radiocarbon* **31** (3), 940-947.

Goslar T, Kuc T, Pazdur MF, Ralska-Jasiewiczowa M, Różański K, Szeroczyńska K, Walanus A, Wicik B, Więckowski K, Arnold M and Bard E (1992) Possibilities for reconstructing radiocarbon level changes during the Late Glacial by using a laminated sequence of Gościąż Lake. *Radiocarbon* **34** (3), 826-832.

Goslar T, Kuc T, Ralska-Jasiewiczowa M, Różański K, Arnold M, Bard E, van Geel B, Pazdur MF, Szeroczyńska K, Wicik B, Więckowski K and Walanus A (1993) High-resolution lacustrine record of the Late Glacial/Holocene transition in central Europe. *Quaternary Science Reviews* **12**, 287-294.

Goslar T, Arnold M, Bard E, Kuc T, Pazdur MF, Ralska-Jasiewiczowa M, Różański K, Tisnerat N, Walanus A, Wicik B and Więckowski K (1995) High concentration of atmospheric ^{14}C during the Younger Dryas cold episode. *Nature* **377**, 414-417.

Goslar T, Arnold M, Tisnerat-Laborde N, Czernik J and Więckowski K (2000a) Variations of Younger Dryas atmospheric radiocarbon explicable without ocean circulation changes. *Nature* **403**, 877-880.

Goslar T, Arnold M, Tisnerat-Laborde N, Hatté C, Paterne M and Ralska-Jasiewiczowa M (2000b) Radiocarbon calibration by means of varves versus ^{14}C ages of terrestrial macrofossils from Lake Gościąż and Lake Perespilno, Poland. *Radiocarbon* **42** (3), 335-348.

Gotanda K and Yasuda Y (2008) Spatial biome changes in southwestern Japan since the Last Glacial Maximum. *Quaternary International* **184**, 84-93.

Gotanda K, Nakagawa T, Tarasov P, Kitagawa J, Inoue Y and Yasuda Y (2002) Biome classification from Japanese pollen data: application to modern-day and Late Quaternary samples. *Quaternary Science Reviews* **21**, 647-657.

Gotanda K, Nakagawa T, Tarasov P and Yasuda Y (2008) Disturbed vegetation reconstruction using the biomization method from Japanese pollen data: modern and Late Quaternary examples. *Quaternary International* **184**, 56-74.

Guilderson TP, Schrag DP, Kashgarian M and Southon J (1998) Radiocarbon variability in the western equatorial Pacific inferred from a high-resolution coral record from Nauru Island. *Journal of Geophysical Research* **103** (C11), 24641-24650.

Guillou H, Singer BS, Laj C, Kissel C, Scaillet S and Jicha BR (2004) On the age of the Laschamp geomagnetic excursion. *Earth and Planetary Science Letters* **227**, 331-343.

Guyodo Y and Valet J-P (1996) Relative variations in geomagnetic intensity from sedimentary records: the past 200,000 years. *Earth and Planetary Science Letters* **143**, 23-36.

Guyodo Y and Valet J-P (1999) Global changes in intensity of the Earth's magnetic field during the past 800 kyr. *Nature* **399**, 249-252.

Haase-Schramm A, Goldstein SL, Stein M (2004) U-Th dating of Lake Lisan (late Pleistocene Dead Sea) aragonite and implications for glacial East Mediterranean climate change. *Geochimica et Cosmochimica Acta* **68** (5), 985-1005.

Hajdas I, Ivy SD, Beer J, Bonani G, Imboden D, Lotter AF, Sturm M and Suter M (1993) AMS radiocarbon dating and varve chronology of Lake Soppensee: 6,000 to 12,000 ^{14}C years BP. *Climate Dynamics* **9**, 107-116.

Hajdas I, Bonani G and Goslar T (1995a) Radiocarbon dating the Holocene in the Gościąż Lake floating varve chronology. *Radiocarbon* **37** (1), 71-74.

Hajdas I, Ivy-Ochs SD and Bonani G (1995b) Problems in the extension of the radiocarbon calibration curve (10-13 kyr BP). *Radiocarbon* **37** (1), 75-79.

Hajdas I, Zolitschka B, Ivy-Ochs SD, Beer J, Bonani G, Leroy SAG, Negendank JW, Ramrath M and Suter M (1995c) AMS radiocarbon dating of annually laminated sediments from Lake Holzmaar, Germany. *Quaternary Science Reviews* **14**, 137-143.

Hajdas I, Bonani G and Zolitschka B (2000) Radiocarbon dating of varve chronologies: Soppensee and Holzmaar Lakes after ten years. *Radiocarbon* **42** (3), 349-353.

Hatté C and Jull AJT (2007) Radiocarbon dating: plant macrofossils. pp.2958-2965 in Elias S (ed.) *Encyclopedia of Quaternary Science*. Elsevier, Amsterdam, Netherlands.

Hatté C, Morvan J, Noury C and Paterne M (2001) Is classical acid-alkali-acid treatment responsible for contamination? An alternative proposition. *Radiocarbon* **43** (2A), 177-182.

Heaton TJ, Blackwell PG and Buck CE (2009) A Bayesian approach to the estimation of radiocarbon calibration curves: the IntCal09 methodology. *Radiocarbon* **51** (4), 1151-1164.

Heinrich H (1988) Origin and consequences of cyclic ice rafting in the Northeast Atlantic Ocean during the past 130,000 years. *Quaternary Research* **29**, 142-152.

Hoffmann DL, Beck JW, Richards DA, Smart PL, Singarayer JS, Ketchmark T and Hawkesworth CJ (2010) Towards radiocarbon calibration beyond 28 ka using speleothems from the Bahamas. *Earth and Planetary Science Letters* **289**, 1-10.

Hogg AG, McCormac FGM, Higham TFG, Reimer PJ, Baillie MGL and Palmer JG (2002) High-precision radiocarbon measurements of contemporaneous tree-ring dated wood from the British Isles and New Zealand: AD 1850-950. *Radiocarbon* **44** (3), 633-640.

Hogg AG, Fifield LK, Turney CSM, Palmer JG, Galbraith R and Baillie MGL (2006) Dating ancient wood by high sensitivity liquid scintillation counting and accelerator mass spectrometry – pushing the boundaries. *Quaternary Geochronology* **1** (4), 241-248.

Hogg A, Palmer J, Boswijk, Reimer P and Brown D (2009) Investigating the interhemispheric ^{14}C offset in the 1st millennium AD and assessment of laboratory bias and calibration errors. *Radiocarbon* **51** (4), 1177-1186.

Hua Q (2009) Radiocarbon: a chronological tool for the recent past. *Quaternary Geochronology* **4**, 378-390.

Hua Q, Barbetti M, Fink D, Kaiser KF, Friedrich M, Kromer B, Levchenko VA, Zoppi U, Smith AM and Bertuch F (2009) Atmospheric 14C variations derived from tree rings during the early Younger Dryas. *Quaternary Science Reviews* **28**, 2982-2990.

Hughen KA and Zolitschka B (2007) Varved marine sediments. pp.3114-3123 in Elias S (ed.) *Encyclopedia of Quaternary Science*. Elsevier, Amsterdam, Netherlands.

Hughen KA, Overpeck JT, Peterson LC and Anderson RF (1996a) The nature of varved sedimentation in the Cariaco Basin, Venezuela, and its palaeoclimatic significance. *Geological Society, London, Special Publications* **116**, 171-183.

Hughen KA, Overpeck JT, Peterson LC and Trumbore S (1996b) Rapid climate changes in the tropical Atlantic region during the last deglaciation. *Nature* **380**, 51-54.

Hughen KA, Overpeck JT, Lehman SJ, Kashgarian M, Southon JR and Peterson LC (1998a) A new ^{14}C calibration data set for the last deglaciation based on marine varves. *Radiocarbon* **40** (1), 483-494.

Hughen KA, Overpeck JT, Lehman SJ, Kashgarian M, Southon JR, Peterson LC, Alley R and Sigman DM (1998b) Deglacial changes in ocean circulation from an extended radiocarbon calibration. *Nature* **391**, 65-68.

Hughen KA, Southon JR, Lehman SJ and Overpeck JT (2000) Synchronous radiocarbon and climate shifts during the last deglaciation. *Science* **290**, 1951-1954.

Hughen KA, Baillie MGL, Bard E, Beck JW, Bertrand CJH, Blackwell PG, Buck CE, Burr GS, Cutler KB, Damon PE, Edwards RL, Fairbanks RG, Friedrich M, Guilderson TP, Kromer B, McCormac G, Manning S, Bronk Ramsey C, Reimer PJ, Reimer RW, Remmele S, Southon JR, Stuiver M, Talamo S, Taylor FW, van der Plicht J and Weyhenmeyer CE (2004a) Marine04 marine radiocarbon age calibration, 0-26 cal kyr BP. *Radiocarbon* **46** (3), 1059-1086.

Hughen KA, Lehman SJ, Southon JR, Overpeck JT, Marchal O, Herring C and Turnbull J (2004b) ^{14}C activity and global carbon cycle changes over the past 50,000 years. *Science* **303**, 202-207.

Hughen KA, Southon JR, Lehman SJ, Bertrand C and Turnbull J (2006) Marine-derived ^{14}C calibration and activity record for the past 50,000 years updated from the Cariaco Basin. *Quaternary Science Reviews* **25**, 3216-3227.

Inoue N, Horiuchi T, Ikeda S, Nishikawa T, Gotanda K, Takemura K and Nakagawa T (2007) Image processing for continuous digital borehole core images from Lake Suigetsu, Japan. *Quaternary International* **167-168** (Supplement: INQUA 2007 Abstracts), 187.

International Study Group (1982) An inter-laboratory comparison of radiocarbon measurements in tree rings. *Nature* **298**, 619-623.

Japan Meteorological Agency (1998a) Daily and every 3-hours meteorological data at the ground surface (1961-1970). Japan Meteorological Agency, CD-ROM.

Japan Meteorological Agency (1998b) Daily and every 3-hours meteorological data at the ground surface (1971-1990). Japan Meteorological Agency, CD-ROM.

Johnsen SJ, Dahl-Jensen D, Gundestrup N, Steffensen JP, Clausen HB, Miller H, Masson-Delmotte V, Sveinbjörnsdottir AE and White J (2001) Oxygen isotope and palaeotemperature records from six Greenland ice-core stations: Camp Century, Dye-3, GRIP, GISP2, Renland and NorthGRIP. *Journal of Quaternary Science* **16** (4), 299-307.

Jones M and Nicholls G (2001) Reservoir offset models for radiocarbon calibration. *Radiocarbon* **43** (1), 119-124.

Jones M and Nicholls G (2002) New radiocarbon calibration software. *Radiocarbon* **44** (3), 663-674.

Kato M, Tanimura Y and Fukusawa H (2004) Survival strategy of diatom species living on now-depositing non-glacial varves. *Quaternary International* **123-125**, 21-26.

Katsuta N, Takano M, Kawakami S-I, Togami S, Fukusawa H, Kumuzawa M and Yasuda Y (2007) Advanced micro-XRF method to separate sedimentary rhythms and event layers in sediments: its application to lacustrine sediment from Lake Suigetsu, Japan. *Journal of Paleolimnology* **37**, 259-271.

Kaufman A and Broecker W (1965) Comparison of Th^{230} and C^{14} ages for carbonate materials from Lakes Lahontan and Bonneville. *Journal of Geophysical Research* **70** (16), 4039-4054.

Kawakami S-I, Fukusawa H and Kanaori Y (1996) A new opportunity to detect paleo-earthquake events dating back to the past 10 millennia: a record from lacustrine sediment. *Engineering Geology* **43**, 177-188.

Kilian MR, van der Plicht J, van Geel B and Goslar T (2002) Problematic ^{14}C-AMS dates of pollen concentrates from Lake Gosciaz (Poland). *Quaternary International* **88**, 21-26.

Kirner DL, Southon JR, Hare PE and Taylor RE (1996) Accelerator mass spectrometry radiocarbon measurement of submilligram samples. Ch.31 in Orna MV (ed.) *Archaeological Chemistry: Organic, Inorganic, and Biochemical Analysis* (American Chemical Society, Washington DC, USA).

Kitagawa H (forthcoming) Lacustrine varve counting as a dating technique: advantages and disadvantages. Ch.39 in Menotti F (ed.) *The Oxford Handbook of Wetland Archaeology*. Oxford University Press.

Kitagawa H and van der Plicht J (1998a) Atmospheric radiocarbon calibration to 45,000 yr B.P.: late glacial fluctuations and cosmogenic isotope production. *Science* **279**, 1187-1190.

Kitagawa H and van der Plicht J (1998b) A 40,000-year varve chronology from Lake Suigetsu, Japan: extension of the ^{14}C calibration curve. *Radiocarbon* **40** (1), 505-515.

Kitagawa H and van der Plicht J (2000) Atmospheric radiocarbon calibration beyond 11,900 cal BP from Lake Suigetsu laminated sediments. *Radiocarbon* **42** (3), 369-380.

Kitagawa H, Fukuzawa H, Nakumura T, Okamura M, Takemura K, Hayashida A and Yasuda Y (1995) AMS ^{14}C dating of varved sediments from Lake Suigetsu, Central Japan and atmospheric ^{14}C change during the Late Pleistocene. *Radiocarbon* **37** (2), 371-378.

Klein J, Lerman JC, Damon PE and Ralph EK (1982) Calibration of radiocarbon dates: tables based on the consensus data of the 'Workshop on Calibrating the Radiocarbon Time Scale'. *Radiocarbon* **24** (2), 103-150.

Kondo R and Butani J (2007) Comparison of the diversity of sulfate-reducing bacterial communities in the water column and the surface sediments of a Japanese meromictic lake. *Limnology* **8**, 131-141.

Kondo R, Kasashima N, Matsuda H and Hata Y (2000) Determination of thiosulfate in a meromictic lake. *Fisheries Science* **66**, 1076-1081.

Kondo R, Osawa K, Mochizuki L, Fujioka Y and Butani J (2006) Abundance and diversity of sulphate-reducing bacterioplankton in Lake Suigetsu, a meromictic lake in Fukui, Japan. *Plankton and Benthos Research* **1** (4), 165-177.

Kondo R, Nakagawa A, Mochizuki L, Osawa K, Fujioka Y and Butani J (2009) Dominant bacterioplankton populations in the meromictic Lake Suigetsu as determined by denaturing gradient gel electrophoresis of 16S rRNA gene fragments. *Limnology* **10**, 63-69.

Kromer B and Becker B (1993) German oak and pine ^{14}C calibration, 7200-9439 BC. *Radiocarbon* **35** (1), 125-135.

Kromer B and Spurk M (1998) Revision and tentative extension of the tree-ring based ^{14}C calibration, 9,200-11,855 cal. BP. *Radiocarbon* **40** (3), 1117-1125.

Kromer B, Rhein M, Bruns M, Schoch-Fischer H and Münnich KO (1986) Radiocarbon calibration data for the 6th to the 8th millennia BC. *Radiocarbon* **28** (2B), 954-960.

Kromer B, Ambers J, Baillie MGL, Damon PE, Hesshaimer V, Hofmann J, Jöris O, Levin I, Manning SW, McCormac FG, van der Plicht J, Spurk M, Stuiver M and Weninger B (1996) Report: summary of the workshop "Aspects of high-precision radiocarbon calibration". *Radiocarbon* **38** (3), 607-610.

Kromer B, Manning SW, Kuniholm PI, Newton MW, Spurk M and Levin I (2001) Regional $^{14}CO_2$ offsets in the troposphere: magnitude, mechanisms and consequences. *Science* **294**, 2529-2532.

Kromer B, Friedrich M, Hughen KA, Kaiser F, Remmele S, Schaub M and Talamo S (2004) Late Glacial ^{14}C ages from a floating, 1382-ring pine chronology. *Radiocarbon* **46** (3), 1203-1209.

Kromer B, Manning SW, Friedrich M, Talamo S and Trano N (2010) ^{14}C calibration in the 2nd and 1st millennia BC – Eastern Mediterranean radiocarbon comparison project (EMRCP). *Radiocarbon* **52** (2-3), 875-886.

Laj C, Kissel C, Mazaud A, Channell JET and Beer J (2000) North Atlantic palaeointensity stack since 75 ka (NAPIS-75) and the duration of the Laschamp event. *Philosophical Transactions of the Royal Society of London A* **358**, 1009-1025.

Laj C, Kissel C and Beer J (2004) High resolution global paleointensity stack since 75 kyr (GLOPIS-75) calibrated to absolute values. *Geophysical Monograph Series* **145**, 255–265.

Lal D and Peters B (1967) Cosmic ray produced radioactivity on the Earth. pp. 551-612 in Flügge S (ed.) Handbuch für Physik. Springer, Berlin, Germany.

Leavitt SW and Danzer SR (1993) Method for batch processing small wood samples to holocellulose for stable-carbon isotope analysis. *Analytical Chemistry* **65**, 87-89.

Leduc G, Thouveny N, Bourlès DL, Blanchet CL and Carcaillet JT (2006) Authigenic $^{10}Be/^{9}Be$ signature of the Laschamp excursion: a tool for global synchronisation of paleoclimate archives. *Earth and Planetary Science Letters* **245**, 19-28.

Lerman JC, Mook WG and Vodel JC (1970) 14C in tree-rings from different localities. pp.275-301 in Olsson IU (ed.) *Radiocarbon Variations and Absolute Chronology, Twelfth Nobel Symposium, Uppsala 1969*. John Wiley and Sons, New York, USA.

Leroy SAG, Zolitschka B, Negendank JFW and Seret G (2000) Palynological analyses in the laminated sediment of Lake Holzmaar (Eifel, Germany): duration of Lateglacial and Preboreal biozones. *Boreas* **29**, 52-71.

Leuschner HH (1992) Subfossil trees. pp.193-197 in Bartholin TS, Berglund BE, Eckstein D and Schweingruber FH (eds.) Tree rings and environment. Proceedings of the International Dendrochronological Symposium. *LUNDQUA report* **34**, Ystad, Sweden.

Libby WF (1951) Radiocarbon dates, II. *Science* **114**, 291-296.

Libby WF (1955) *Radiocarbon Dating* (second edition). University of Chicago Press, USA.

Libby WF, Anderson EC and Arnold JR (1949) Age determination by radiocarbon content: world-wide assay of natural radiocarbon. *Science* **109**, 227-228.

Lingenfelter RE (1963) Production of carbon 14 by cosmic-ray neutrons. *Reviews of Geophysics* **1,** 35-55.

Linick TW, Suess HE and Becker B (1985) La Jolla measurements of radiocarbon in south German oak tree-ring chronologies. *Radiocarbon* **27** (1), 20-32.

Linick TW, Long A, Damon PE and Ferguson CW (1986) High-precision radiocarbon dating of bristlecone pine from 6,554 to 5,350 BC. *Radiocarbon* **28** (2B), 943-953.

Litton CD and Buck CE (1995) The Bayesian approach to the interpretation of archaeological data. *Archaeometry* **37** (1), 1-24.

Lowe DJ (2011) Tephrochronology and its application: a review. *Quaternary Geochronology* **6**, 107-153.

Lowe JJ and Walker MJC (1997) *Reconstructing Quaternary Environments*. Prentice Hall, Harlow.

Lowe JJ, Hoek WZ and the INTIMATE group (2001) Inter-regional correlation of palaeoclimatic records from the Last Glacial-Interglacial Transition: a protocol for improved precision recommended by the INTIMATE project group. *Quaternary Science Reviews* **20**, 1175-1187.

Lowe JJ, Rasmussen SO, Björck S, Hoek WZ, Steffensen JP, Walker MJC, Yu ZC and the INTIMATE group (2008) Synchronisation of palaeoenvironmental events in the North Atlantic region during the Last Termination: a revised protocol recommended by the INTIMATE group. *Quaternary Science Reviews* **27**, 6-17.

Machida H (2002) Volcanoes and tephras in the Japan area. *Global Environmental Research* **6** (2), 19-28.

Machida H and Arai F (1992) *Atlas of Tephra in and around Japan*. University of Tokyo Press, Tokyo, Japan. In Japanese.

Machida H and Arai F (2003) *Atlas of Tephra in and around Japan* (revised edition). University of Tokyo Press, Tokyo, Japan. In Japanese.

Magana AL, Southon JR, Cheng H, Edwards RL and Wang Y (2009) A record of deglacial atmospheric ^{14}C from Hulu Cave speleothem H82. *Poster presentation, AGU Fall Meeting*, San Francisco, USA (14th to 18th December 2009).

Mangerud J (1972) Radiocarbon dating of marine shells, including a discussion of apparent age of recent shells from Norway. *Boreas* **1**, 143-172.

Marshall M and Schlolaut G (2010) Suigetsu Varves 2006: utilising μXRF and X-radiography for varve counting. *Oral presentation, PAGES Meeting*, Lahemaa National Park, Estonia (7th to 9th April 2010).

Marshall M, Schlolaut G, Nakagawa T, Lamb H, Brauer A, Bronk Ramsey C, Yokoyama Y and Suigetsu 2006 project members (2009) Suigetsu Varves 2006: varve counting by XRF core scanning. *Poster presentation, QRA Annual Discussion Meeting*, Oxford (5th to 7th January 2009).

Marshall M, Schlolaut G, Brauer A, Nakagawa T, Staff RA, Bronk Ramsey C, Lamb H, Yokoyama Y and Suigetsu 2006 project members (forthcoming) A novel approach to varve counting for the Lake Suigetsu 2006 Varved Sediment Core project: combining μ-XRF and X-radiography with thin section microscopy.

Masuzawa T and Kitano Y (1982a) Sulfate reduction and sulfur fixation in sediment of a historically meromictic lake, Lake Suigetsu, Japan. *Journal of the Oceanographical Society of Japan* **38**, 21-27.

Masuzawa T and Kitano Y (1982b) Diagenetic deposition of manganese in sediment of a historically meromictic lake, Lake Suigetsu, Japan. *Journal of the Oceanographical Society of Japan* **38**, 73-80.

Matsumoto A and Ui T (1997) K-Ar Age of Ata Pyroclastic Flow Deposit, Southern Kyushu, Japan. *Kazan* **42**, 223-225. In Japanese.

Matsuyama M (1973a) Some physiochemical features of a meromictic Lake Suigetsu. *Journal of the Oceanographical Society of Japan* **29** (2), 47-52.

Matsuyama M (1973b) Organic substances in sediment and settling matter during spring in a meromictic Lake Suigetsu. *Journal of the Oceanographical Society of Japan* **29** (2), 53-60.

Matsuyama M (1973c) Changes in the limnological features of a meromictic Lake Suigetsu during the years, 1926-1967. *Journal of the Oceanographical Society of Japan* **29** (4), 131-139.

Matsuyama M (1974) Vertical distribution of some chemical substances in surface sediments of a meromictic Lake Suigetsu. *Journal of the Oceanographical Society of Japan* **30** (5), 209-215.

Matsuyama M and Saijo Y (1971) Studies on biological metabolism in a meromictic Lake Suigetsu. *Journal of the Oceanographical Society of Japan* **27** (5), 197-206.

Mazaud A, Laj C, Bard E, Arnold M and Tric C (1991) Geomagnetic field control of ^{14}C production over the last 80 ky: implications for the radiocarbon time-scale. *Geophysical Research Letters* **18** (10), 1885-1888.

McCormac FG, Baillie MGL, Pilcher JR and Kalin RM (1995) Location-dependent differences in the ^{14}C content of wood. *Radiocarbon* **37** (2), 395-407.

McCormac FG, Hogg AG, Higham TFG, Baillie MGL, Palmer JG, Xiong L, Pilcher JR, Brown D and Hoper ST (1998a) Variations of radiocarbon in tree rings: Southern Hemisphere offset preliminary results. *Radiocarbon* **40** (3), 1153-1159.

McCormac FG, Hogg AG, Higham TFG, Lynch-Stieglitz J, Broecker WS, Baillie MGL, Palmer J, Xiong L, Pilcher JR, Brown D, Hoper ST (1998b) Temporal variation in the interhemispheric ^{14}C offset. *Geophysical Research Letters* **25** (9), 1321-1324.

McCormac FG, Reimer PJ, Hogg AG, Higham TFG, Baillie MGL, Palmer J and Stuiver M (2002) Calibration of the radiocarbon time scale for the Southern Hemisphere: AD 1850-950. *Radiocarbon* **44** (3), 641-651.

McCormac FG, Hogg AG, Blackwell PG, Buck CE, Higham TFG and Reimer PJ (2004) SHCal04 Southern Hemisphere calibration, 0-11.0 cal kyr BP. *Radiocarbon* **46** (3) 1087-1092.

McHargue LR and Damon PE (1991) The global beryllium 10 cycle. *Reviews of Geophysics* **29** (2), 141-158.

McHargue LR, Damon PE and Donahue DJ (1995) Enhanced cosmic ray production of ^{10}Be coincident with the Mono Lake and Laschamp geomagnetic excursions. *Geophysical Research Letters* **22** (5), 659-662.

Meese DA, Gow AJ, Alley RB, Zielinski GA, Grootes PM, Ram M, Taylor KC, Mayewski PA, and Bolzan JF (1997) The Greenland Ice Sheet Project 2 depth-age scale: methods and results. *Journal of Geophysical Research* **102** (C12), 26411-26423.

Mellars P (2006a) A new radiocarbon revolution and the dispersal of modern humans in Eurasia. *Nature* **439**, 931-935.

Mellars P (2006b) Mellars replies: replying to CSM Turney, RG Roberts and Z Jacobs, Nature 443, doi:10.1038/nature05214 (2006). *Nature* **443**, doi:10.1038/nature05215.

Montgomery CG and Montgomery DD (1939) The intensity of neutrons of thermal energy in the atmosphere at sea level. *Physical Review* **56**, 10-12.

Mook WG (1986) Recommendations/resolutions adopted by the twelfth international radiocarbon conference. *Radiocarbon* **28** (2A), 799.

Murayama M, Matsumoto E, Nakamura T, Okamura M, Yasuda H and Taira A (1993) Re-examination of the eruption age of the Aira-Tn Ash (AT) obtained from a piston core off Shikoku – determined by AMS ^{14}C dating of planktonic foraminifera. *Journal of the Geological Society of Japan* **99** (10), 787-798. In Japanese, with English abstract.

Muscheler R, Beer J, Wagner G and Finkel RC (2000) Changes in deep-water formation during the Younger Dryas event inferred from ^{10}Be and ^{14}C records. *Nature* **408**, 567-570.

Muscheler R, Beer J, Wagner G, Laj C, Kissel C, Raisbeck GM, Yiou F and Kubik PW (2004) Changes in the carbon cycle during the last deglaciation as indicated by the comparison of ^{10}Be and ^{14}C records. *Earth and Planetary Science Letters* **219**, 325-340.

Muscheler R, Beer J, Kubik PW and Synal H-A (2005) Geomagnetic field intensity during the last 60,000 years based on ^{10}Be and ^{36}Cl from the Summit ice cores and ^{14}C. *Quaternary Science Reviews* **24**, 1849-1860.

Muscheler R, Kromer B, Björck S, Svensson A, Friedrich M, Kaiser KF and Southon J (2008) Tree rings and ice cores reveal ^{14}C calibration uncertainties during the Younger Dryas. *Nature Geoscience* **1**, 263-267.

Nakagawa T (2007) Double-L channel: an amazingly non-destructive method of continuous sub-sampling from sediment cores. *Quaternary International* **167-168**, 268.

Nakagawa T, Tarasov PE, Nishida K, Gotanda K and Yasuda Y (2002) Quantitative pollen-based climate reconstruction in central Japan: application to surface and Late Quaternary spectra. *Quaternary Science Reviews* **21**, 2099-2113.

Nakagawa T, Kitagawa H, Yasuda Y, Tarasov PE, Nishida K, Gotanda K, Sawai Y and Yangtze River Civilization Program Members (2003) Asynchronous climate changes in the North Atlantic and Japan during the Last Termination. *Science* **299**, 688-691.

Nakagawa T, Kitagawa H, Yasuda Y, Tarasov PE, Gotanda K and Sawai Y (2005) Pollen/event stratigraphy of the varved sediment of Lake Suigetsu, central Japan from 15,701 to 10,217 SG vyr BP (Suigetsu varve years before present): description, interpretation, and correlation with other regions. *Quaternary Science Reviews* **24**, 1691-1701.

Nakagawa T, Tarasov PE, Kitagawa H, Yasuda Y and Gotanda K (2006) Seasonally specific responses of the East Asian monsoon to deglacial climate changes. *Geology* **34** (7), 521-524.

Nakagawa T, Gotanda K, Haraguchi T, Danhara T, Yonenobu H, Yokoyama Y, Brauer A, Tada R, Takemura K, Staff RA, Payne R, Bronk Ramsey C and Suigetsu 2006 project members (2011) SG06, a perfectly continuous varved sediment core from Lake Suigetsu, Japan: stratigraphy and potential for improving radiocarbon calibration model and understanding of climate changes. *Quaternary Science Reviews*, in press.

Nakagawa T, Gotanda K, Haraguchi T, Danhara T, Yonenobu H, Yokoyama Y, Brauer A, Tada R, Takemura K, Staff RA, Payne R, Bronk Ramsey C and Suigetsu 2006 project members (forthcoming) High precision palaeoclimatic reconstruction of the East Asian monsoon across the Last Glacial/Interglacial transition.

Naysmith P, Cook GT, Freeman SPHT, Scott EM, Anderson R, Xu S, Dunbar E, Muir GKP, Dougans A, Wilcken K, Schnabel C, Russell N, Ascough PL and Maden C (2010) ^{14}C AMS at SUERC: improving QA data with the 5MV tandem and 250kV SSAMS. *Radiocarbon* **52** (2-3), 263-271.

Nelson DE, Korteling RG and Stott WR (1977) Carbon-14: direct detection at natural concentrations. *Science* **198**, 507-508.

Nicholls G and Jones M (2001) Radiocarbon dating with temporal order constraints. *Journal of the Royal Statistical Society C* **50** (4), 503-521.

Nishimoto H, Nakamura T and Takeda H (2010) Radiocarbon dating and wiggle matching of wooden poles forming circular structures in the 1st millennium BC at the Mawaki archaeological site, central Japan. *Nuclear Instruments and Methods in Physics Research B* **268**, 1026-1029.

North Greenland Ice Core Project members (2004) High-resolution record of Northern Hemisphere climate extending into the last interglacial period. *Nature* **431**, 147-151.

Oeschger H, Siegenthaler U, Schotterer U and Gugelmann A (1975) A box diffusion model to study the carbon dioxide exchange in nature. *Tellus* **27** (2), 168-192.

Okada M, Taniuchi Y, Murakami A, Takaichi S, Ohtake S and Ohki K (2007) Abundance of picophytoplankton in the halocline of a meromictic lake, Lake Suigetsu, Japan. *Limnology* **8**, 271-280.

Okuno M, Shiihara M, Torii M, Nakamura T, Kim KY, Domitsu H, Moriwaki H and Oda M (2010) AMS radiocarbon dating of Holocene tephra layers on Ulleung Island, South Korea. *Radiocarbon* **52** (2-3), 1465-1470.

Olsson IU (ed.) (1970) *Radiocarbon Variations and Absolute Chronology, Twelfth Nobel Symposium, Uppsala 1969*. John Wiley and Sons, New York, USA.

O'Sullivan PE (1983) Annually-laminated lake sediments and the study of Quaternary environmental changes – a review. *Quaternary Science Reviews* **1**, 245-313.

Palmer J, Lorrey A, Turney CSM, Hogg A, Baillie M, Fifield K and Ogden J (2006) Extension of New Zealand kauri (*Agathis australis*) tree-ring chronologies into Oxygen Isotope Stage (OIS) 3. *Journal of Quaternary Science* **21** (7), 779-787.

Pasquier-Cardin A, Allard P, Ferreira T, Hatté C, Coutinho R, Fontugne M and Jaudon M (1999) Magma-derived CO_2 emissions recorded in ^{14}C and ^{13}C content of plants growing in Furnas caldera, Azores. *Journal of Volcanology and Geothermal Research* **92**, 195-207.

Pearson GW (1986) Precise calendrical dating of known growth-period samples using a 'curve fitting' technique. *Radiocarbon* **28** (2A), 292-299.

Pearson GW and Baillie MGL (1983) High-precision ^{14}C measurement of Irish oaks to show the natural atmospheric ^{14}C variations of the AD time period. *Radiocarbon* **25** (2), 187-196.

Pearson GW and Pilcher JR (1978) Absolute radiocarbon dating by low-altitude European tree-ring calibration. *Nature* **272**, 650.

Pearson GW and Qua F (1993) High-precision ^{14}C measurement of Irish oaks to show the natural ^{14}C variations from AD 1840-5000 BC: a correction. *Radiocarbon* **35** (1), 105-123.

Pearson GW and Stuiver M (1986) High-precision calibration of the radiocarbon time scale, 500-2500 BC. *Radiocarbon* **28** (2B), 839-862.

Pearson GW and Stuiver M (1993) High-precision calibration of the radiocarbon time scale, 500-2500 BC. *Radiocarbon* **35** (1), 25-33.

Pearson GW, Pilcher JR, Baillie MGL and Hillam J (1977) Absolute radiocarbon dating using a low altitude European tree-ring calibration. *Nature* **270**, 25-28.

Pearson GW, Pilcher JR, Baillie MGL, Corbett DM and Qua F (1986) High-precision ^{14}C measurement of Irish oaks to show the natural ^{14}C variations from AD 1840 to 5210 BC. *Radiocarbon* **28** (2B), 911-934.

Pearson GW, Becker B and Qua F (1993) High-precision ^{14}C measurement of German and Irish oaks to show the natural ^{14}C variations from 7890 to 5000 BC. *Radiocarbon* **35** (1), 93-104.

Peterson LC, Overpeck JT, Kipp NG and Imbrie J (1991) A high-resolution Late Quaternary upwelling record from the anoxic Cariaco Basin, Venezuela. *Paleoceanography* **6** (1), 99-119.

Peterson LC, Haug GH, Hughen KA and Röhl U (2000) Rapid changes in the hydrologic cycle of the tropical Atlantic during the Last Glacial. *Science* **290**, 1947-1951.

Pilcher JR, Baillie MGL, Schmidt B and Becker B (1984) A 7,272-year tree-ring chronology for western Europe. *Nature* **312**, 150-152.

Prasad S, Negendank JFW and Stein M (2009) Varve counting reveals high resolution radiocarbon reservoir age variations in palaeolake Lisan. *Journal of Quaternary Science* **24** (7), 690-696.

Raisbeck GM, Yiou F, Freneua M, Loiseaux JM, Lieuvin M, Ravel JC and Lorius C (1981) Cosmogenic ^{10}Be concentrations in Antarctic ice during the past 30,000 years. *Nature* **292**, 825-826.

Raisbeck GM, Yiou F, Bourles D, Lorius C, Jouzel J and Barkov NI (1987) Evidence for two intervals of enhanced ^{10}Be deposition in Antarctic ice during the last glacial period. *Nature* **326**, 273-277.

Raisbeck GM, Yiou F, Jouzel J and Stocker TF (2007) Direct north-south synchronization of abrupt climate change record in ice cores using beryllium 10. *Climate of the Past* **3**, 541-547.
Ralph EK and Michael HN (1967) Problems of the radiocarbon calendar. *Archaeometry* **10** (1), 3-11.

Rasmussen SO, Andersen KK, Svensson AM, Steffensen JP, Vinther BM, Clausen HB, Siggaard-Andersen M-L, Johnsen SJ, Larsen LB, Dahl-Jensen D, Bigler M, Röthlisberger R, Fischer H, Goto-Azuma K, Hansson ME and Ruth U (2006) A new Greenland ice core chronology for the last glacial termination. *Journal of Geophysical Research* **111**, D06102.

Reimer PJ (ed.) (2004) IntCal04: calibration issue. *Radiocarbon* **46** (3), 1029-1333.

Reimer PJ (ed.) (2009) IntCal09. *Radiocarbon* **51** (4), 1111-1211.

Reimer PJ and Reimer RW (2001) A marine reservoir correction database and on-line interface. *Radiocarbon* **43** (2A), 461-463.

Reimer PJ, Hughen KA, Guilderson TP, McCormac G, Baillie MGL, Bard E, Barratt P, Beck JW, Buck CE, Damon PE, Friedrich M, Kromer B, Bronk Ramsey C, Reimer RW, Remmele S, Southon JR, Stuiver M and van der Plicht J (2002) Preliminary report of the first workshop of the IntCal04 radiocarbon calibration/comparison working group. *Radiocarbon* **44** (3), 653-661.

Reimer PJ, Baillie MGL, Bard E, Bayliss A, Beck JW, Bertrand CJH, Blackwell PG, Buck CE, Burr GS, Cutler KB, Damon PE, Edwards RL, Fairbanks RG, Friedrich M, Guilderson TP, Hogg AG, Hughen KA, Kromer B, McCormac G, Manning S, Bronk Ramsey C, Reimer RW, Remmele S, Southon JR, Stuiver M, Talamo S, Taylor FW, van der Plicht J and Weyhenmeyer CE (2004a) IntCal04 terrestrial radiocarbon age calibration, 0-26 cal kyr BP. *Radiocarbon* **46** (3), 1029-1058.

Reimer PJ, Brown TA and Reimer RW (2004b) Discussion: reporting and calibration of post-bomb 14C data. *Radiocarbon* **46** (3), 1299-1304.

Reimer PJ, Baillie MGL, McCormac G, Reimer RW, Bard E, Beck JW, Blackwell PG, Buck CE, Burr GS, Edwards RL, Friedrich M, Guilderson TP, Hogg AG, Hughen KA, Kromer B, Manning S, Southon JR, Stuiver M, van der Plicht J and Weyhenmeyer CE (2006) Comment on "Radiocarbon calibration curve spanning 0 to 50,000 years BP based on paired $^{230}Th/^{234}U/^{238}U$ and ^{14}C dates on pristine corals" by RG Fairbanks et al. (Quaternary Science Reviews 24 (2005) 1781-1796) and "Extending the radiocarbon calibration beyond 26,000 years before present using fossil corals" by T-C Chiu et al. (Quaternary Science Reviews 24 (2005) 1797-1808). *Quaternary Science Reviews* **25**, 855-862.

Reimer PJ, Baillie MGL, Bard E, Bayliss A, Beck JW, Blackwell PG, Bronk Ramsey C, Buck CE, Burr GS, Edwards RL, Friedrich M, Grootes PM, Guilderson TP, Hajdas I, Heaton TJ, Hogg AG, Hughen KA, Kaiser KF, Kromer B, McCormac FG, Manning SW, Reimer RW, Richards DA, Southon JR, Talamo S, Turney CSM, van der Plicht J and Weyhenmeyer CE (2009) IntCal09 and Marine09 radiocarbon age calibration curves, 0-50,000 years cal. BP. *Radiocarbon* **51** (4), 1111-1150.

Roberts ML and Southon JR (2006) A determination of the absolute $^{14}C/^{12}C$ ratio of OX-I. *Poster presentation, 19th International Radiocarbon Conference*, Oxford (3rd–7th April 2006).

Robinson C, Raisbeck GM, Yiou F, Lehman B and Laj C (1995) The relationship between ^{10}Be and geomagnetic field strength records in central North Atlantic sediments during the last 80 ka. *Earth and Planetary Science Letters* **136**, 551-557.

Sakamoto M, Imamura M, van der Plicht J, Mitsutani T and Sahara M (2003) Radiocarbon calibration for Japanese wood samples. *Radiocarbon* **45** (1), 81-89.

Santos GM, Southon JR, Griffin S, Beaupre SR and Druffel ERM (2007) Ultra small-mass AMS ^{14}C sample preparation and analyses at KCCAMS/UCI Facility. *Nuclear Instruments and Methods in Physics Research B* **259**, 293-302.

Schaub M, Büntgen U, Kaiser KF, Kromer B, Talamo S, Andersen KK and Rasmussen (2008a) Lateglacial environmental variability from Swiss tree rings. *Quaternary Science Reviews* **27**, 29-41.

Schaub M, Kaiser KF, Frank DC, Büntgen U, Kromer B and Talamo S (2008b) Environmental change during the Allerød and Younger Dryas reconstructed from Swiss tree-ring data. *Boreas* **37**, 74-86.

Schlolaut G, Marshall M, Brauer A, Nakagawa T, Lamb H, Staff RA, Bronk Ramsey C, Bryant C, Brock F, Kossler A, Tarasov P, Yokoyama Y, Tada R, Haraguchi T and Suigetsu 2006 project members (forthcoming) A novel, automated method for varve interpolation using varve frequency distributions and its application to the Late Glacial Chronology from Lake Suigetsu, Japan.

Schramm A, Stein M and Goldstein SL (2000) Calibration of the ^{14}C time scale to >40 ka by ^{234}U-^{230}Th dating of Lake Lisan sediments (last glacial Dead Sea). *Earth and Planetary Science Letters* **175**, 27-40.

Scott EM (2003) The third international radiocarbon intercomparison (TIRI) and the fourth international radiocarbon intercomparison (FIRI). *Radiocarbon* **45** (2), 135-408.

Scott EM, Aitchison TC, Harkness DD, Cook GT and Baxter MS (1990) An overview of all three stages of the international radiocarbon intercomparison. *Radiocarbon* **32** (3), 309-319.

Scott EM, Cook GT, Naysmith P, Bryant C and O'Donnell D (2007) A report on phase 1 of the fifth international radiocarbon intercomparison (VIRI). *Radiocarbon* **49** (2), 409-426.

Scott EM, Cook GT and Naysmith P (2010) A report on phase 2 of the fifth international radiocarbon intercomparison (VIRI). *Radiocarbon* **52** (2-3), 846-858.

Shackleton NJ, Fairbanks RG, Chiu T-C and Parrenin F (2004) Absolute calibration of the Greenland time scale: implications for Antarctic time scales, and for Δ^{14}C. *Quaternary Science Reviews* **23**, 1513-1522.

Shigematsu T, Tabushi M, Nishikawa Y, Muroga T and Matsunaga Y (1961) Geochemical study on Lakes Mikata. *Bulletin of the Institute for Chemical Research, Kyoto University* **39** (1), 43-56.

Siegenthaler U, Heimann M and Oeschger H (1980) ^{14}C variations caued by changes in the global carbon cycle. *Radiocarbon* **22** (2), 177-191.

Simola H (1979) Micro-stratigraphy of sediment laminations deposited in a chemically stratifying eutrophic lake during the years 1913-1976. *Holarctic Ecology* **2** (3), 160-168.

Singarayer JS, Richards DA, Ridgwell A, Valdes PJ, Austin WEN and Beck JW (2008) An oceanic origin for the increase of atmospheric radiocarbon during the Younger Dryas. *Geophysical Research Letters* **35**, L14707 (doi:10.1029/2008GL034074).

Slota PJ Jr, Jull AJT, Linick TW and Toolin LJ (1987) Preparation of small samples for ^{14}C accelerator targets by catalytic reduction of CO. *Radiocarbon* **29** (2), 303-306.

Smith VC, Mark DF, Staff RA, Blockley SPE, Bronk Ramsey C, Bryant CL, Nakagawa T, Han KK, Weh A, Takemura K, Danhara T and Suigetsu 2006 Project Members (2011) Toward establishing precise $^{40}Ar/^{39}Ar$ chronologies for Late Pleistocene palaeoclimate archives: an example from the Lake Suigetsu (Japan) sedimentary record. *Quaternary Science Reviews* **30** (21-22), 2845-2850.

Sonnett CP, Morfill GE and Jokipii JR (1987) Interstellar shock waves and ^{10}Be from ice cores. *Nature* **330**, 458-460.

Southon JR and Magana AL (2010) A comparison of cellulose extraction and ABA pretreatment methods for AMS ^{14}C dating of ancient wood. *Radiocarbon* **52** (2-3), 1371-1379.

Spurk M, Friedrich M, Hofmann J, Remmele S, Frenzel B, Leuschner HH and Kromer B (1998) Revisions and extension of the Hohenheim oak and pine chronologies: new evidence about the timing of the Younger Dryas/Preboreal transition. *Radiocarbon* **40** (3), 1107-1116.

Staff RA, Bronk Ramsey C, Bryant C, Brock F, Lamb H, Marshall M, Brauer A, Schlolaut G, Tarasov P, Payne R, Pearson E, Yokoyama Y, Tyler J, Haraguchi T, Gotanda K, Yonenobu H, Nakagawa T. 2009. Suigetsu 2006: a wholly terrestrial radiocarbon calibration curve. *Oral presentation, 20th International Radiocarbon Conference*, Kona, Hawai'i, USA (31st May–5th June 2009).

Staff RA, Bronk Ramsey C, Nakagawa T and Suigetsu 2006 project members (2010) A re-analysis of the Lake Suigetsu terrestrial radiocarbon dataset. *Nuclear Instruments and Methods in Physics Research B* **268**, 960-965.

Stein M, Goldstein SL and Schramm A (2000) Radiocarbon calibration beyond the dendrochronology range. *Radiocarbon* **42** (3), 415-422.

Strömberg B (1985) Revision of the lateglacial Swedish varve chronology. *Boreas* **14**, 101-105.

Stuiver M (1961) Variations in radiocarbon concentration and sunspot activity. *Journal of Geophysical Research* **66** (1), 273-276.

Stuiver M (1982) A high-precision calibration of the AD radiocarbon time scale. *Radiocarbon* **24** (1), 1-26.

Stuiver M and Becker B (1993) High-precision decadal calibration of the radiocarbon time scale, AD 1950-6000 BC. *Radiocarbon* **35** (1), 35-65.

Stuiver M and Braziunas T (1993a) Modeling atmospheric ^{14}C influences and ^{14}C ages of marine samples to 10,000 BC. Radiocarbon 35 (1), 137-189.

Stuiver M and Braziunas T (1993b) Sun, ocean, climate and atmospheric $^{14}CO_2$: an evaluation of causal and spectral relationships. *The Holocene* **3**, 289-305.

Stuiver M and Braziunas T (1998) Anthropogenic and solar components of hemispheric ^{14}C. *Geophysical Research Letters* **25** (3), 329-332.

Stuiver M and Kra RS (eds.) (1986) Calibration issue. *Radiocarbon* **28** (2B), 805-1030.

Stuiver M and Pearson GW (1986) High-precision calibration of the radiocarbon time scale, AD 1950-500 BC. *Radiocarbon* **28** (2B), 805-838.

Stuiver M and Pearson GW (1993) High-precision bidecadal calibration of the radiocarbon time scale, AD 1950-500 BC and 2500-6000 BC. *Radiocarbon* **35** (1), 1-23.

Stuiver M and Polach HA (1977) Reporting of ^{14}C Data. *Radiocarbon* **19** (3), 355-263.

Stuiver M and Quay PD (1980) Changes in atmospheric carbon-14 attributed to a variable sun. *Science* **207**, 11-19.

Stuiver M and Quay PD (1981) Atmospheric ^{14}C changes resulting from fossil fuel CO_2 release and cosmic ray flux variability. *Earth and Planetary Science Letters* **53**, 349-362.

Stuiver M and Reimer PJ (1986) A computer program for radiocarbon age calibration. *Radiocarbon* **28** (2B), 1022-1030.

Stuiver M and Reimer PJ (1993) Extended ^{14}C data base and revised Calib 3.0 ^{14}C age calibration program. *Radiocarbon* **35** (1), 215-230.

Stuiver M and Suess HE (1966) On the relationship between radiocarbon dates and true sample ages. *Radiocarbon* **8**, 534-540.

Stuiver M and van der Plicht J (eds.) (1998) IntCal98: calibration issue. *Radiocarbon* **40** (3), 1041-1164.

Stuiver M, Kromer B, Becker B and Ferguson CW (1986a) Radiocarbon age calibration back to 13,300 years BP and the ^{14}C age matching of the German oak and US bristlecone pine chronologies. *Radiocarbon* **28** (2B), 980–1021.

Stuiver M, Pearson G and Braziunas T (1986b) Radiocarbon age calibration of marine samples back to 9,000 cal. yr BP. *Radiocarbon* **28** (2B), 980–1021.

Stuiver M, Braziunas TF, Becker B and Kromer B (1991) Climate, solar, oceanic, and geomagnetic influences on late-glacial and Holocene atmospheric $^{14}C/^{12}C$ change. *Quaternary Research* **35**, 1-24.

Stuiver M, Long A and Kra RS (eds.) (1993) Calibration 1993. *Radiocarbon* **35** (1), 1-244.

Stuiver M, Reimer PJ, Bard E, Beck JW, Burr GS, Hughen KA, Kromer B, McCormac G, van der Plicht J and Spurk M (1998a) IntCal98 radiocarbon age calibration, 24,000-0 cal BP. *Radiocarbon* **40** (3), 1041-1083.

Stuiver M, Reimer PJ and Braziunas TF (1998b) High-precision radiocarbon age calibration for terrestrial and marine samples. *Radiocarbon* **40** (3), 1127-1151.

Suess HE (1955) Radiocarbon concentration in modern wood. *Science* **122**, 415-417.

Suess HE (1965) Secular variations of the cosmic-ray-produced carbon 14 in the atmosphere and their interpretations. *Journal of Geophysical Research* **70** (23), 5937-5952.

Suess HE (1970) The three causes of secular C14 fluctuations, their amplitudes and time constants. pp.595-606 in Olsson IU (ed.) *Radiocarbon Variations and Absolute Chronology, Twelfth Nobel Symposium, Uppsala 1969*. John Wiley and Sons, New York, USA.

Suess HE (1978) Absolute radiocarbon dating by low-altitude European tree-ring calibration. *Nature* **272**, 649-650.

Suess HE (1980) The radiocarbon record in tree rings of the last 8,000 years. *Radiocarbon* **22** (2), 200-209.

Svensson A, Andersen KK, Bigler M, Clausen HB, Dahl-Jensen D, Davies SM, Johnsen SJ, Muscheler R, Rasmussen SO, Röthlisberger R, I, Steffensen JP and Vinther BM (2006) The Greenland Ice Core Chronology 2005, 15-42 ka. Part 2: comparison to other records. *Quaternary Science Reviews* **25**, 3258-3267.

Svensson A, Andersen KK, Bigler M, Clausen HB, Dahl-Jensen D, Davies SM, Johnsen SJ, Muscheler R, Parrenin F, Rasmussen SO, Röthlisberger R, Seierstad I, Steffensen JP and Vinther BM (2008) A 60,000 year Greenland stratigraphic ice core chronology. *Climate of the Past* **4**, 47-57.

Takahashi M and Ichimura S-E (1968) Vertical distribution and organic matter production of photosynthetic sulfur bacteria in Japanese lakes. *Limnology and Oceanography* **13** (4), 644-655.

Takemura K, Kitagawa H, Hayashida A and Yasuda Y (1994) Sedimentary facies and chronology of core samples from Lake Mikata, Lake Suigetsu and Kurota Lowland, central Japan – Sedimentary environment in Mikata Lowland since the last interglacial time. *Journal of Geography* **103** (3), 233-242. In Japanese, with English abstract.

Tauber H (1970) The Scandinavian varve chronology and C14 dating. pp.173-196 in Olsson IU (ed.) *Radiocarbon Variations and Absolute Chronology, Twelfth Nobel Symposium, Uppsala 1969*. John Wiley and Sons, New York, USA.

Turney CSM, Roberts RG and Jacobs Z (2006) Progress and pitfalls in radiocarbon dating: arising from P. Mellars, Nature 439, 931-935 (2006). *Nature* **443**, doi:10.1038/nature05214.

Turney CSM, Fifield LK, Palmer JG, Hogg AG, Baillie MGL, Galbraith R, Ogden J, Lorrey A and Tims SG (2007) Towards a radiocarbon calibration for oxygen isotope stage 3 using New Zealand kauri (*Agathis australis*). *Radiocarbon* **49** (2), 447-457.

Tyler J, Kashiyama Y, Ohkouchi N, Ogawa N, Yokoyama Y, Chikaraishi Y, Staff RA, Ikehara M, Bronk Ramsey C, Bryant C, Brock F, Gotanda K, Haraguchi T, Yonenobu H and Nakagawa T (2010) Tracking aquatic change using chlorine-specific carbon and nitrogen isotopes: the last glacial-interglacial transition at Lake Suigetsu, Japan. Geochemistry, Geophysics, Geosystems 11 (9).

van der Borg K, Stein M, de Jong AFM, Waldmann N and Goldstein SL (2004) Near-zero $\Delta^{14}C$ values at 32 kyr cal. BP observed in the high-resolution ^{14}C record from U-Th dated sediment of Lake Lisan. *Radiocarbon* **46** (2), 785-795.

van der Plicht (ed.) (2000a) The 2000 radiocarbon/varve comparison issue. *Radiocarbon* **42** (3), 313-452.

van der Plicht (2000b) Introduction: the 2000 radiocarbon/varve comparison issue. *Radiocarbon* **42** (3), 313-322.

van der Plicht J (2004) Radiocarbon calibration – past, present and future. *Nuclear Instruments and Methods in Physics Research B* **223-224**, 353-358.

van der Plicht J, Jansma E and Kars H (1995) The 'Amsterdam Castle': a case study of wiggle-matching and the proper calibration curve. *Radiocarbon* **37** (3), 965-968.

van der Plicht J, Beck JW, Bard E, Baillie MGL, Blackwell PG, Buck CE, Friedrich M, Guilderson TP, Hughen KA, Kromer B, McCormac FG, Bronk Ramsey C, Reimer PJ, Reimer RW, Remmele S, Richards DA, Southon JR, Stuiver M and Weyhenmeyer CE (2004) NotCal04-comparison/calibration ^{14}C records 26-50 cal. kyr BP. *Radiocarbon* **46** (3), 1225-1238.

van Geel B, van der Plicht J and Renssen H (2003) Major $\Delta^{14}C$ excursions during the late glacial and early Holocene: changes in ocean ventilation or solar forcing of climate change? *Quaternary International* **105**, 71-76.

Vandeputte K, Moens L and Dams R (1996) Improved sealed-tube combustion of organic samples to CO2 for stable carbon isotope analysis, radiocarbon dating and percent carbon determinations. *Analytical Letters* **29** (15), 2761-2773.

Vinther BM, Clausen HB, Johnsen SJ, Rasmussen SO, Andersen KK, Buchardt SL, Dahl-Jensen D, Seierstad IK, Siggaard-Andersen M-L, Steffensen JP, Svensson A (2006) A synchronized dating of three Greenland ice cores throughout the Holocene. *Journal of Geophysical Research* **111**, D13102.

Voelker AHL, Sarnthein M, Grootes PM, Erlenkeuser H, Laj C, Mazaud A, Nadeau M-J and Schleicher M (1998) Correlation of marine 14C ages from the Nordic Seas with the GISP2 isotope record: implications for 14C calibration beyond 25 ka BP. *Radiocarbon* **40** (1), 517-534.

Voelker AHL, Grootes PM, Nadeau M-J and Sarnthein M (2000) Radiocarbon levels in the Iceland Sea from 25-53 kyr and their link to the Earth's magnetic field intensity. *Radiocarbon* **42** (3), 437-452.

Vogel JC (1983) ^{14}C variations during the Upper Pleistocene. *Radiocarbon* **25** (2), 213-218.

Vogel JC and Kronfeld J (1997) Calibration of radiocarbon dates for the Late Pleistocene using U/Th dates on stalagmites. *Radiocarbon* **39** (1) 27-32.

Vogel JC and van der Plicht J (1993) Calibration curve for short-lived samples, 1900-3900 BC. *Radiocarbon* **35** (1), 87-89.

Vogel JS, Southon JR, Nelson DE and Brown TA (1984) Performance of catalytically condensed carbon for use in accelerator mass spectrometry. *Nuclear Instruments and Methods in Physics Research B* **5**, 289-293.

Vogel JC, Fuls A, Visser E and Becker B (1986) Radiocarbon fluctuations during the third millennium BC. *Radiocarbon* **28** (2B), 935-938.

Vogel JS, Nelson DE and Southon JR (1987) ^{14}C background levels in an accelerator mass spectrometry system. *Radiocarbon* **29** (3), 323-333.

Vogel JC, Fuls A, Visser E and Becker B (1993) Pretoria calibration curve for short-lived samples, 1930-3350 BC. *Radiocarbon* **35** (1), 73-85.

Walker MJC (2005) *Quaternary Dating Methods*. John Wiley & Sons Ltd, Chichester.

Walker MJC, Björck S and Lowe JJ (2001) Integration of ice core, marine and terrestrial records (INTIMATE) from around the North Atlantic region: an introduction. *Quaternary Science Reviews* **20**, 1169-1174.

Walker M, Johnsen S, Rasmussen SO, Popp T, Steffensen J-P, Gibbard P, Hoek W, Lowe J, Andrews J, Björck S, Cwynar L, Hughen K, Kershaw P, Kromer B, Litt T, Lowe DJ, Nakagawa T, Newnham R and Schwander J (2009) Formal definition and dating of the GSSP (Global Stratotype Section and Point) for the base of the Holocene using the Greenland NGRIP ice core, and selected auxiliary records. *Journal of Quaternary Science* **24** (1), 3-17.

Wang YJ, Cheng H, Edwards RL, An ZS, Wu JY, Shen C-C and Dorale JA (2001) A high-resolution absolute-dated Late Pleistocene monsoon record from Hulu Cave, China. *Science* **294**, 2345-2348.

Weyhenmeyer CE, Burns SJ, Fleitmann D, Kramers JD, Matter A, Waber HN and Reimer PJ (2003) Changes in atmospheric ^{14}C between 55 and 42 ky BP recorded in a stalagmite from Socotra Island, Indian Ocean. *EOS Transactions* **84** (46: Fall Meeting Supplement), abstract PP32B-0298.

Willis EH, Tauber H and Münnich KO (1960) Variations in the atmospheric radiocarbon concentration over the past 1,300 years. *American Journal of Science Radiocarbon Supplement* **2**, 1-4.

Wohlfarth B (1996) The chronology of the Last Termination: a review of radiocarbon-dated, high-resolution terrestrial stratigraphies. *Quaternary Science Reviews* **15**, 267-284.

Wohlfarth B and Possnert G (2000) AMS radiocarbon measurements from the Swedish varved clays. *Radiocarbon* **42** (3), 323-333.

Wohlfarth B, Björck S, Possnert G, Lemdahl G, Brunnberg L, Ising J, Olsson S and Svensson N-O (1993) AMS dating Swedish varved clays of the last glacial/interglacial transition and the potential/difficulties of calibrating Late Weichselian 'absolute' chronologies. *Boreas* **22**, 113-128.

Wohlfarth B, Björck S, Holmqvist B, Lemdahl G and Ising J (1994) Ice recession and depositional environment in the Blekinge archipelago of the Baltic Ice Lake. *GFF* **116** (1), 3-12.

Wohlfarth B, Björck S and Possnert G (1995) The Swedish time scale: a potential calibration tool for the radiocarbon time scale during the Late Weichselian. *Radiocarbon* **37** (2), 347-359.

Wohlfarth B, Björck S, Cato I and Possnert G (1997) A new middle Holocene varve diagram from the river Ångermanälven, northern Sweden: indications for a possible error in the Holocene varve chronology. *Boreas* **26**, 347-353.

Wohlfarth B, Skog G, Possnert G and Holmquist B (1998) Pitfalls in the AMS radiocarbon-dating of terrestrial macrofossils. *Journal of Quaternary Science* **13** (2), 137-145.

Wood RE, Bronk Ramsey C and Higham TFG (2010) Refining background corrections for radiocarbon dating of bone collagen at ORAU. *Radiocarbon* **52** (2-3), 600-611.

Wulf S, Kraml M, Brauer A, Keller J, Negendank JFW (2004) Tephrochronology of the 100ka lacustrine sediment record of Lago Grande di Monticchio (southern Italy). *Quaternary International* **122**, 7-30.

Wulf S, Kraml M and Keller J (2008) Towards a detailed distal tephrostratigraphy in the central Mediterranean: the last 20,000 yrs record of Lago Grande di Monticchio. *Journal of Volcanology and Geothermal Research* **177**, 118-132.

Xu S, Anderson R, Bryant C, Cook GT, Dougans A, Freeman S, Naysmith P, Schnabel C and Scott EM (2004) Capabilities of the new SUERC 5MV AMS facility for ^{14}C dating. *Radiocarbon* **46** (1), 59-64.

Yamada K, Gotanda K, Yonenobu H, Schwab MJ, Shinozuka Y, Okuno M, Kitagawa J, Oda H, Saito-Kato M, Haraguchi T, Hayashida A, Saarinen TJ, Makohonienko M, Goslar T and Yasuda Y (forthcoming) Annually laminated sediments for the last 30,000 years from Lake Ichi-no-Megata, northeastern Japan and its potential for high-resolution reconstruction of past environmental changes.

Yasuda Y, Yamaguchi K, Nakagawa T, Fukusawa H, Kitagawa J and Okamura M (2004) Environmental variability and human adaption during the Lateglacial/ Holocene transition in Japan with reference to pollen analysis of the SG4 core from Lake Suigetsu. *Quaternary International* **123-125**, 11-19.

Yiou F, Raisbeck GM, Baumgartner S, Beer J, Hammer C, Johnsen S, Jouzel J, Kubik PW, Lestringuez J, Stiévenard M, Suter M and Yiou P (1997) Beryllium 10 in the Greenland ice core project ice core at Summit, Greenland. *Journal of Geophysical Research* **102** (C12), 26783-26794.

Yokoyama Y, Esat TM, Lambeck K and Fifield LK (2000) Last ice age millennial scale climate changes recorded in Huon Peninsula corals. *Radiocarbon* **42** (3), 383-401.

Zhou W, Donahue D and Jull AJT (1997) Radiocarbon AMS dating of pollen concentrated from eolian sediments: implications for monsoon climate change since the Late Quaternary. *Radiocarbon* **39** (1), 19-26.

Zimmerman S, Guilderson T, Buckley B and Cook E (2010) Extension of the Southern Hemisphere atmospheric radiocarbon curve, 2120-850 years BP: results from Tasmanian Huon pine. *Radiocarbon* **52** (2-3), 887-894.

Zolitschka B (2007) Varved lake sediments. pp.3105-3114 in Elias S (ed.) *Encyclopedia of Quaternary Science*. Elsevier, Amsterdam, Netherlands.

Internet references:

http://dendro.naruto-u.ac.jp/~nakagawa – freely available PeakCounter software (T. Nakagawa).

http://www.calib.org – online marine reservoir correction database (Reimer and Reimer 2001).

http://www.suigetsu.org – 'Suigetsu Varves 2006' external project website.

http://www.wakasa-mikatagoko.jp (viewed 13/04/2010) – tourist information for the Wakasa region (including the *Mikata-goko*).

https://c14.arch.ox.ac.uk/oxcal/OxCal.html – OxCal Bayesian calibration software (Bronk Ramsey 1994, 1995, 1998, 2001, 2008a, 2009a, 2009b).